A Metathesis Route to Light Harvesting Polymers for Organic Solar Cells

A DISSERTATION
SUBMITTED TO THE FACULTY OF THE GRADUATE SCHOOL
OF THE UNIVERSITY OF MINNESOTA
BY

Joshua Cole Speros

IN PARTIAL FULFILLMENT OF THE REQUIREMENTS
FOR THE DEGREE OF
Doctor of Philosophy

Marc A. Hillmyer, Advisor
C. Daniel Frisbie, Advisor

May 2013

Acknowledgements

Most importantly, I would like to thank my advisors, Marc Hillmyer and Dan Frisbie. While here they fostered my creativity and showed me the beauty of elegant scientific communication. Their guidance and support during my graduate school experience helped me become a far better scientist, and person, than I could have ever hoped for. I am especially grateful for the opportunity to mentor an undergraduate researcher, Brad Slowinski (UMN), whose hard work resulted in two publications. I consider myself lucky to count him as a friend.

I have been fortunate to share time and space with several graduate students and post-doctoral associates. The importance of their intellectual and emotional support is beyond measure and my time here would have been difficult without them. Several of these people deserve recognition: Dr. Louis Pitet, Dr. Yang Qin, Dr. Bryan Paulsen, Dr. Bryan Boudouris, Dr. Derek Stevens, Dr. Elizabeth Jackson, Dr. Grayce Theryo, Dr. Ligeng Yin, Dr. Jihoon Shin, Dr. Mark Martello, Dr. Henry Martinez, Dr. Paula Delgado, Dr. Justin Kennemur, Dr. Myung Seo, Dr. Jonathan Zhang, Dr. William Gramlich, Dr. Jennifer Lowe, Dr. Mark Amendt, Dr. Shingo Kobayashi, Dr. Agostino Pietrangelo, Maria Miranda, Can Zhou, and Morgan Schulze.

I have had the pleasure to collaborate with and learn from many outstanding researchers while at the University of Minnesota. These people include: Dr. Timothy Anglin and Prof. Aaron Massari (UMN); Philip Goff and Prof. David Blank (UMN); and Dr. Ye Huang (ICCAS). In addition, I would like to thank the past, current, and future members of the Graduate Student Workshop Committee who taught me the value of giving back. I also thank my high school chemistry teacher (Dave Eckstrom, Hayward High School), my undergraduate advisor (Dr. Tom Ippoliti, University of St. Thomas),

and my intership supervisor (Matthew Valli, Eli Lilly & Co.) who all taught me the beauty of science, the importance of enthusiasm, and set me on my path.

Lastly, it is with deepest love that I acknowledge my wife, Ashley, my parents, Jason and Mary, and my brother, Jordan, for their constant support. Words cannot express my gratitude.

Financial support is gratefully acknowledged. The Krogh Endowed Fellowship from the Department of Chemistry supported my first year of graduate studies and funding from the Initiative for Renewable Energy and the Environment supported the research described herein.

Dedication

To my wife, Ashley, whose love, support, humor, and patience made this possible.

Abstract

Conjugated polymers (CPs), macromolecules consisting of alternating single and double bonds, are of tremendous interest to the scientific community considering their applications in field-effect transistors, light-emitting diodes, sensors, and organic photovoltaics (OPVs). OPVs are an area of particular interest because cost-effective solution processing techniques can be employed to prepare flexible large-area light harvesting devices. In addition, light absorption and charge transport characteristics may be tuned by synthetically altering the CP scaffold. This dissertation describes the synthesis of a variety of CPs prepared by acyclic diene metathesis (ADMET) polymerization using versatile ruthenium-based Grubbs catalysts. All polymers were based on the low band gap poly(thienylene vinylene) (PTV) scaffold. The influence of polymer molecular weight, composition, and repeat unit architecture on both individual polymer behavior and OPV performance was investigated systematically.

Table of Contents

List of Tables

List of Figures

List of Schemes

Chapter 1

Background: Conjugated Polymers for Organic Solar Cells

This chapter introduces organic solar cells (OSCs), often called organic photovoltaics (OPVs), and the conjugated polymers (CPs) that make their operation possible. The basic architecture, operation, and characterization of these devices is discussed. Additionally, particular care is taken to highlight the various classes of CPs and their diverse syntheses.

1.1 Motivation

Having recently surpassed seven billion,[1] the increasing global population demands more and more of the planet's resources. Managing these resources is a daunting task, and the availability of food,[2,3] water,[4] and healthcare[5-8] are serious concerns. However, the greatest of these challenges may be providing the almost 13.5 terawatts (TW) of energy annually consumed by humankind.[9,10] This has traditionally been accomplished by relying on rich fossil fuel reserves, but this approach has two obvious shortcomings. First, these resources are not renewable within a reasonable time period. Second, the effects of burning vast quantities of fossil fuels, though hotly debated,[11] are likely negative. This has not gone unrecognized by the scientific community, and a tremendous variety of alternative energy strategies (some mentioned below) have been explored. Emerging biological fuel sources have been investigated as promising fossil fuel alternatives.[12] However, their production often requires large amounts of fresh water, and their consumption generates greenhouse gases. Nuclear power is promising, but it generates hazardous byproducts, and meltdowns, though infrequent, threaten human safety.[13,14] Hydroelectric power is both clean and safe, but the damming of rivers threatens ecosystems and the communities that rely on them.[15,16] Harnessing the power of geothermal hotspots, the wind, and/or the tides is both clean, and renewable. However, these resources are geography-specific and do not always promise enough energy to warrant investment in collection.[9] Solar power is perhaps the most promising alternative energy technology for two reasons. First, relatively direct sunlight reaches most regions of high population density. Second, and more importantly, the sun provides the earth with 120,000 TW (nearly 9,000 times global demand) of incident light.[10] Additionally, this clean and abundant resource is extraterrestrial, and its collection places minimal stress our planet's precious resources.

Attempting to harness the sun's tremendous energy is not a new concept. In fact, Becquerel observed that a photovoltage resulted from the action of light on an electrode

in 1839.[17] More than one hundred years later in 1953, Gerald Pearson, Calvin Fuller, and Daryl Chapin successfully developed the first functioning silicon solar cell while working at Bell Laboratories.[18] Recently, inorganic solar cells (ISCs) have achieved power conversion efficiencies upwards of 40%.[19] Despite these efficiencies ISCs require energy-intensive processing and high purity materials. In fact, the production cost of a typical silicon solar cell is approximately $3.50/W, while fossil fuels are only $1/W.[20] Given the high energy and monetary costs it is no surprise that alternative solar cell technologies have been investigated. OSCs have emerged as one of the most popular and promising of these technologies.

Solar cells utilizing carbon-based conjugated polymers (CPs) serve to address the deficiencies of their inorganic counterparts. They are relatively inexpensive to manufacture as they can be processed from solution at room temperature using large-scale printing techniques such as ink jet,[21] screen,[22] and roll-to-roll printing.[23,24] ISCs require high temperature processing and thus an inherently larger energetic and monetary commitment. Finally, many of the compounds employed benefit from large absorption coefficients allowing for production of thin (ca. 100 nm) and mechanically flexible devices.[25,26] Despite substantial improvements in ISC efficiencies, it has been suggested that the minimum production cost may plateau at ~$1/W.[20] Although this value is comparable to fossil fuel costs, it is significantly higher than the $0.33/W goal set by the Department of Energy.[27] However, OSC theoretical efficiencies (15–24%[28]) are comparable to ISCs, and could therefore achieve an economy of scale warranting a transition away from dwindling fossil fuels.

1.2 Organics Solar Cells

1.2.1 Introduction

An organic solar cell (OSC) can be described simply as a device, in which the main or active component is a small molecule or polymer semiconductor capable of generating a current when irradiated with light. OSCs encompass a large set of varied and creative device designs.[29] Although they all rely on a similar operating principle, their materials, geometries, and fabrication can differ greatly. The purely organic active layer devices include bilayer[30-33] and bulk-heterojunction (BHJ)[34,35] OSCs. These devices typically take advantage of π-conjugated polymer donors,[36,37] and soluble fullerene acceptors.[38-40] Alternative devices exist that utilize inorganic active layer components. Two examples are dye-sensitized[41,42] and inorganic–organic hybrid solar cells.[43] Despite the various device architectures, the BHJ geometry will be described as it offers simplified processing, and the promise of efficiencies justifying large-scale production.[44]

1.2.2 OSC Operation

Three steps can broadly describe the process of converting solar radiation into electricity by an OSC.[45,46] First, a photon is absorbed by the active layer (semiconducting material) generating a coulombically bound electron–hole pair (exciton). The electron resides on the lowest unoccupied molecular orbital (LUMO), the hole on the highest occupied molecular orbital (HOMO), and the difference in energy between the two is known as the band gap (E_g). The neutral exciton diffuses to the donor-acceptor interface where the charge separation, or exciton dissociation, occurs. A donor is named for its ability to relinquish electrons while leaving positive holes behind. Complementary to the donor, the acceptor acquires electrons or releases holes to the donor. The donor and acceptor develop an overall positive (p-type) and negative (n-type) nature, respectively.

Finally, the separated charges are transported to their respective electrodes to complete the circuit. Figure 1.1 outlines this process in a simplified energy level diagram. However, more rigorous charge transfer models have been developed.[47,48]

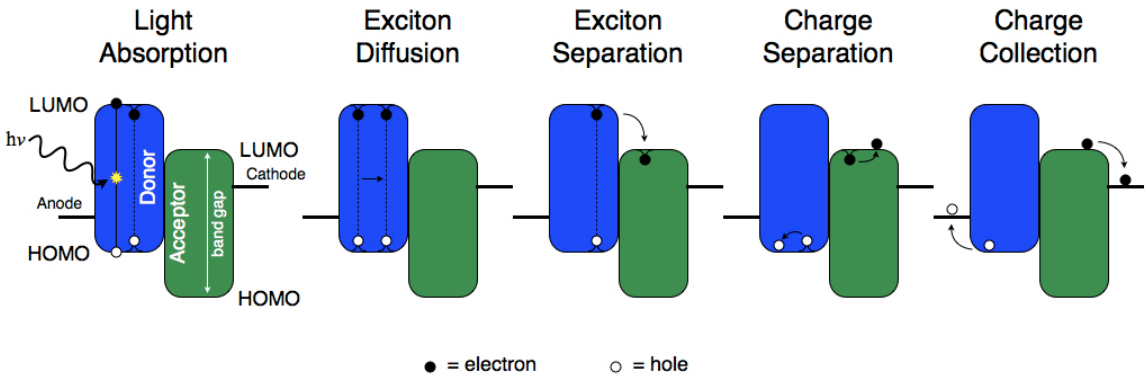

Figure 1.1
Free charge generation and collection mechanism in OSC. The lines denoting the anode and cathode are a generic representation of electrode work function (in eV).

Given the numerous steps involved in converting a photon into collected charges, it comes as no surprise that there are many losses in energy along the way.[49] These losses combine to render most OSCs relatively inefficient. To begin with, the E_g of most organic donors is too large (ca. 2 eV) to utilize the solar spectrum effectively.[50] In fact, an E_g of this size limits the solar absorption to a region of high-energy photons (ca. 30% of the total solar spectrum). Therefore, low E_g OSCs, where the optimum is about 1.4–1.8 eV, have recently become a promising target.[51] Once generated, an exciton must be separated into free charges. The coulombic interaction between the electron and hole requires strong electric fields to be overcome. This is accomplished because the acceptor LUMO level is lower in energy than the donor level and presents a thermodynamically favorable pathway for the electron (Figure 1.1). The gradient in chemical potential established immediately after charge separation drives current flow in OSCs. In contrast, ISC current flow requires an internal electric field along with a chemical potential gradient to efficiently separate and drive charges.[52-54] Once separated, an electron or hole

may become trapped within the active layer and recombine by radiative (photons)[55] or nonradiative (bond vibrations or rotations)[56] routes. Other factors impacting charge transport include ambient temperature and pressure, electric field, active layer crystallinity, impurities, donor molar mass, and molecular packing.[57]

Exciton recombination accounts for additional reduction in device efficiency. An exciton, being electrically neutral, is unaffected by electric fields and thus diffuses randomly in three dimensions. Also, short exciton lifetime and/or slow diffusion typically limit the diffusion length to about 5–15 nm prior to recombination.[58-60] The active layer thickness in bilayer designs must be comparable to the diffusion length in order to effectively dissociate the majority of bound charges. However, reducing device thickness prevents adequate absorption of the solar spectrum, and an intermediate thickness that balances these opposing forces must be sought.[48] BHJ devices have arisen as a possible solution to this intrinsic bilayer issue.[34]

1.2.3 Bulk-Heterojunction OSCs

A BHJ device is defined as such due to the morphology of the active layer. A typical bilayer device consists of an active layer, which is actually two distinct domains of donor and acceptor materials. These devices are capable of appreciable efficiencies,[61,62] but are largely limited by recombinative processes.[63] The effectiveness of a BHJ device relies on the morphology adopted by the donor and acceptor when solution casting from a cosolvent. Ideally, upon removal of the solvent the two materials will phase separate into domains on the exciton diffusion length scale (ca. 5–15 nm).[64] This device design can help overcome the exciton diffusion bottleneck[63] because making a thicker device for increased absorption should not theoretically increase exciton loss before separation. However, controlling the phase separation process, and in turn active layer morphology,

is still a topic of intense investigation.[65] Figure 1.2 illustrates a generic OSC with both bilayer and BHJ active layers.

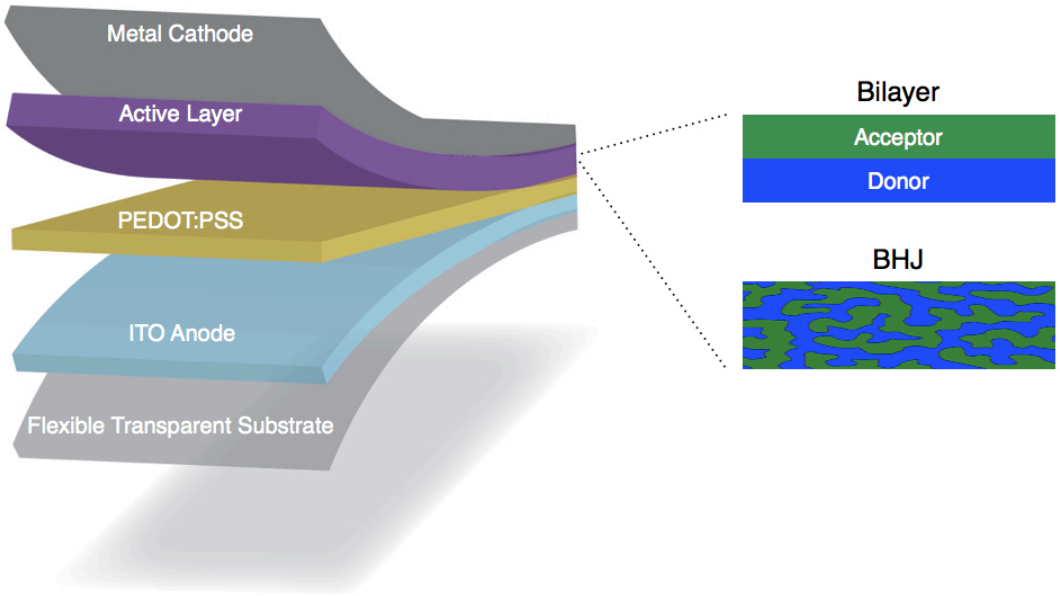

Figure 1.2
Generic OSC with bilayer and BHJ active layers.

A BHJ device is prepared by solution casting a donor–acceptor mixture (active layer) onto a transparent conducting anode, usually glass or a transparent flexible substrate coated with indium tin oxide (ITO).[66] Poly(3,4-ethylenedioxythiophene) doped with poly(styrenesulfonate) (PEDOT:PSS) is often cast on the anode before the active layer. This conducting polymer improves the surface of the ITO, by enhancing energy level alignment and reducing the probability of shorts. More recently, the high cost of indium and the mechanical rigidity of ITO have motivated efforts to prepare ITO-free OSCs.[67] A thin cathode layer (e.g., Ca, Al, Ag) is then deposited on the active layer via vacuum deposition to provide the cathode (Figure 1.2).[68] Completed devices are often annealed; heating has been shown to improve device quality and homogeneity in the active layer.[69,70] Along with annealing conditions, it has been shown that solvent choice,[50] donor-acceptor

blend ratio,[71] and additives[72] can all significantly impact active layer morphology.

Accompanying nanoscale morphology optimization, BHJ devices also require electrodes of different work functions to operate optimally. The intimate mixing of donor and acceptor means that the internal fields of separated charges have no preferred direction of flow. A bilayer cell does not have this problem as the separate donor and acceptor layers create an asymmetry that can effectively direct charge flow. Without different electrodes to induce drift by breaking electric field symmetry,[73] concentration gradients[53] or differences in chemical potential[46] are the only drivers for charge flow in BHJ cells.

1.2.4 OSC Characterization

The most typical means of OSC characterization is obtained in the form of a current density–voltage (*J*–*V*) curve (Figure 1.3).[74] Whether in the dark or under illumination, a voltage is swept through the device and the current response is measured. In the dark there is a linear current response for any applied bias below the open circuit voltage (V_{oc}). However, when the bias exceeds V_{oc} the contacts begin to inject significant charge and an exponential increase in current is observed.[50] When irradiated the device generates a photocurrent, which at zero applied voltage is known as the short circuit current (J_{sc}).[45] Eventually, the applied bias will offset the photocurrent ($J = 0$) and V_{oc} is determined. Along the illuminated curve exists a current and voltage whose product yields the largest power. This point, called the maximum power point (M), is crucial to determining the fill factor (Figure 1.3).[74] The FF (FF = $V_M J_M / V_{oc} J_{sc}$) is a measure of how well the device performs compared to how well it could theoretically perform. The overall solar cell efficiency, or power conversion efficiency (PCE), is the product of J_{sc}, V_{oc}, and FF divided by the incident light power density (P_{in}, Figure 1.3). To ensure photovoltaics are tested under similar conditions, P_{in} is standardized at 100 mW cm^{-2}. Also, the spectral intensity

distribution is set to match that of the sun at an angle of 48.2° incident to the earth's surface. This is often referred to as the air mass (AM) 1.5 spectrum.[75]

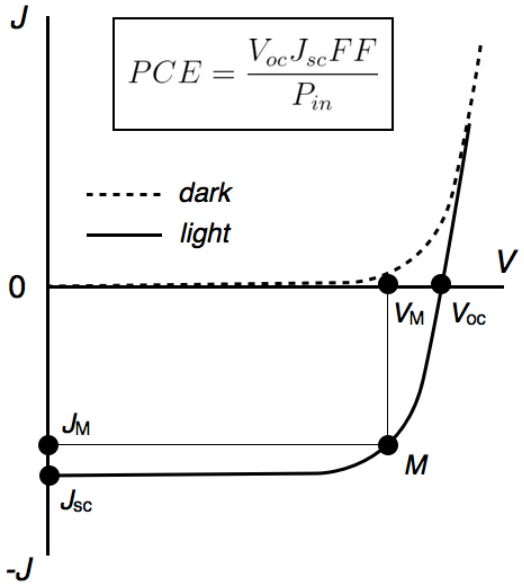

Figure 1.3
J–V plot illustrating dark and light curves and other key features. PCE equation is inset.

As is clear from Figure 1.3, PCE can be improved by increasing V_{oc}, J_{sc}, and/or FF. Research has shown V_{oc} to be directly correlated to the energy gap between the HOMO level of the donor and the LUMO level of the acceptor.[76] A larger gap results in increased V_{oc}. Also, V_{oc} is dependent on the energy match between Fermi level of the electrodes and their respective donor or acceptor material. The closer the match the more effectively separated charges enter the circuit. Coatings or surface modifications to both cathode and anode are often employed to improve these interfaces.[77]

J_{sc} is mainly a function of charge carrier mobility, while charge carrier density and electric field can all be considered constant. Mobility is dependent on nanoscale morphology and may be controlled by self-assembly strategies[78] or through previously mentioned fabrication techniques (Section 1.2.3). Another useful device quantifier is called incident photon to current efficiency (IPCE), or external quantum efficiency

(EQE). IPCE is essentially the number of carriers collected at the electrodes divided by the number of incident photons.[18]

Fill factor depends on many variables, and embodies the overall solar cell quality and optimization. In preparing a device, the series resistance should be minimized while the parallel (shunt) resistance should be maximized.[18] Series resistance is the deviation from perfect diode behavior and is intrinsic to all devices. High material conductivities and optimized interfaces can work to decrease series resistance and, according to Ohm's law, increase current.[79] Shunt resistance is representative of alternate pathways for current flow (i.e., leakage current). This might be represented by physical holes in the active layer of a device, allowing electrode–electrode contact.[80] Such pathways of lower resistance reduce photocurrent. Thus, a high shunt resistance ensures charge carriers move through the desired circuit. The competition between charge recombination and transport also directly influences FF.

A final parameter crucial to device performance is stability. An OCS needs to be prepared in such a way that it resists any environmental conditions that may be encountered. Moisture, oxygen, heat, and even light can all combine to quickly render a device worthless.[81] Therefore, protection from photooxidation/degradation represents a significant challenge.

1.3 Classes of CPs

1.3.1 Introduction

Most common polymer backbones are fully saturated and insulating. This is because all the valence electrons of carbon are used to form covalent bonds. However, conjugated (conducting) polymers (CPs) contain units of unsaturation. In fact, strictly speaking, these polymers consist of alternating carbon double and single bonds. This type of chemical bonding gives rise to a lone π electron for each carbon atom. In addition,

neighboring π orbitals overlap (π bonding) giving rise to electron delocalization. This provides a path for charge mobility along the CP backbone and is the reason why these materials are often referred to as "molecular wires." It should be noted that if the carbon-carbon bond length were the same in CPs these materials would be metallic. However, bond length alternation splits the π band into the filled π (i.e., HOMO) and unfilled π* (i.e., LUMO) bands. The π-π* difference is E_g and decreases with increasing conjugation length.[82] A molecular orbital interpretation of band construction is shown in Figure 1.4. Delocalized π electrons and bond length alternation are features that both define CPs and give rise to their interesting optical, electronic, and morphological properties.

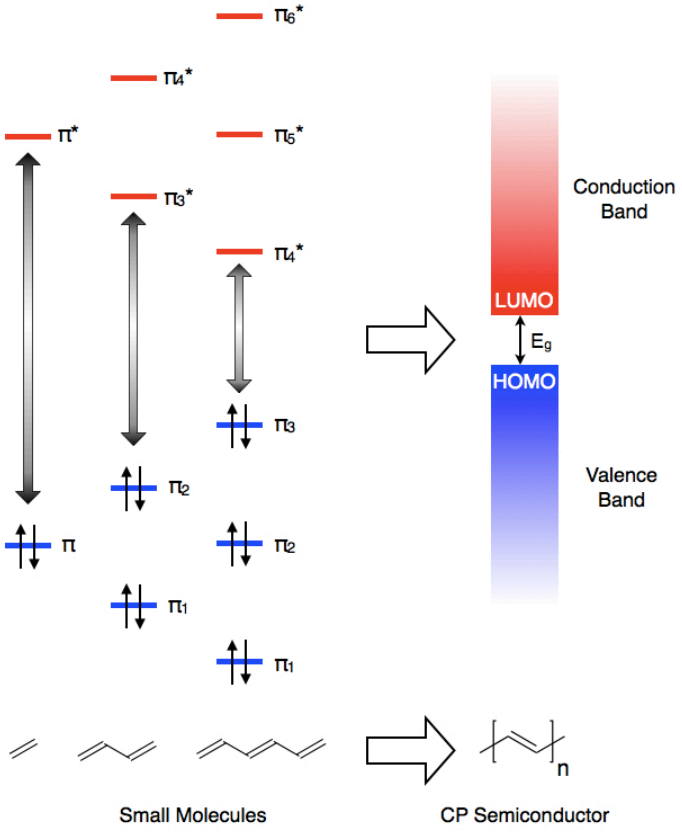

Figure 1.4
Molecular orbital representation of CP band development.

Although OSCs consist of many materials, it is the materials comprising the active layer that are of utmost importance. As stated, the active layer often consists of an electron-rich CP donor and an electron-poor acceptor (traditionally a soluble fullerene derivative[83]). Figure 1.5 highlights some common acceptor materials. OSCs with this architecture have recently achieved efficiencies of 8% and greater.[84-90] Solar cells employing conjugated small molecules are also of interest. The small molecule donors benefit from high batch-to-batch reproducibility and crystallinity,[91] and efficiencies of ca. 7% have been realized.[92,93] However, processing small molecules for use in OSCs often requires expensive and slow vacuum deposition techniques. CPs, though less uniform (i.e., disperse molar masses), are highly amenable to solution processing under mild conditions (i.e. room temperature and atmospheric pressure). In addition to optimizing OSC design and active layer morphology, higher efficiencies can be achieved by exploiting organic synthesis and the abundance of CP scaffolds (see following sections). This synthetic flexibility allows for tunability in CPs, but care must be taken to keep CP architectures relatively simple if they are to achieve commercial relevance.

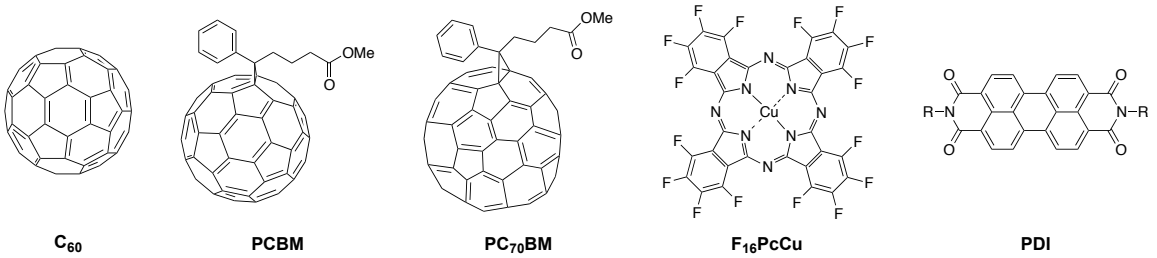

Figure 1.5

Small sample of acceptor materials.

Perhaps one of the most sought after CP properties is a low E_g. Both intra- and intermolecular interactions influence E_g. In fact, it is generally understood that four characteristics influence E_g.[63] Peierls predicted that polymeric structures capable of bond length alternation would yield two non-degenerate energetic minima (i.e., resonance

structures).[94] Brédas and Heeger used polythiophene and polyisothianaphthene as model systems for explaining this resonance contribution to band gap. Their calculations concluded that the quinoid form has a lower E_g. Therefore, increasing the quinoid resonance contribution will lead to a reduced E_g.[95] Aromatic monomer units also influence the magnitude of E_g. Although aromatic repeat units impart chemical stability to conjugated polymers, aromaticity tends to confine π-electrons to the ring and compete with delocalization. E_g decreases with increasing conjugation length, but torsion between adjacent monomer units can disrupt this conjugation and effectively increase E_g.[96] Methine spacers have been chemically introduced between aromatic repeat units to combat torsion. The double bond character of these "spacers" serves to prevent angular rotation between rings.[63] Finally, chemical functionalization of conjugated polymers has proven a highly effective means of tailoring E_g. An electron-withdrawing group (EWG) can lower both the HOMO and LUMO levels,[97] while an electron-donating group (EDG) would be expected to do the opposite. Implementation of EWGs is the preferred route, as lowering the HOMO typically reduces E_g and slows oxidative degradation.[98] Figure 1.6 illustrates the concepts of bond length alternation, aromaticity, conjugation length, and substituents. Intermolecular interactions in the solid state including substituent group interactions or regio-/stereochemical properties have also been shown directly influence E_g.[99]

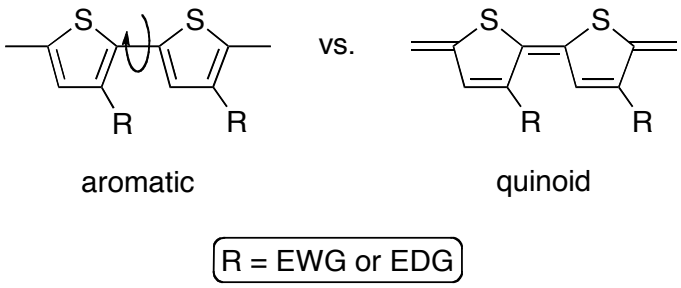

Figure 1.6
Bond length alternation is indicated by the two resonance forms (aromatic and quinoid). Aromaticity is dependent on monomer choice (thiophene in this case). Conjugation length depends on rotation about bonds (curved arrow). Indicated substituents could also be alkyl groups to aid in solubility and processing. Figure adopted from Winder et al.[63]

1.3.2 Poly(acetylene)

The first synthesis of poly(acetylene) (PA), the simplest CP, from gaseous acetylene dates back to 1958.[100] However, characterization was virtually impossible, as these PAs were isolated as black intractable powders with no clear melting points that decomposed at elevated temperatures and oxidized in air. In fact, thorough characterization of PA was not accomplished until nearly twenty years later when Shirakawa and coworkers successfully prepared PA films using (by accident) highly concentrated Ziegler-Natta catalysts (Scheme 1.1a).[101] The authors also found that the *cis*/*trans* ratio of the PA backbone could be controlled simply by controlling reaction temperature. The ability to form films opened PA up to a variety of studies—most notably, conductivity quantification. MacDiarmid and Heeger found that *trans*-PA behaved as a semiconductor until chemically or electrochemically doped, after which it demonstrated conductivities comparable to that of metallic silver.[82,102] In fact, the research by Shirakawa, MacDiarmid, and Heeger laid the foundation for CPs and earned them the Nobel Prize in 2000.[103]

Scheme 1.1

PA synthesis.

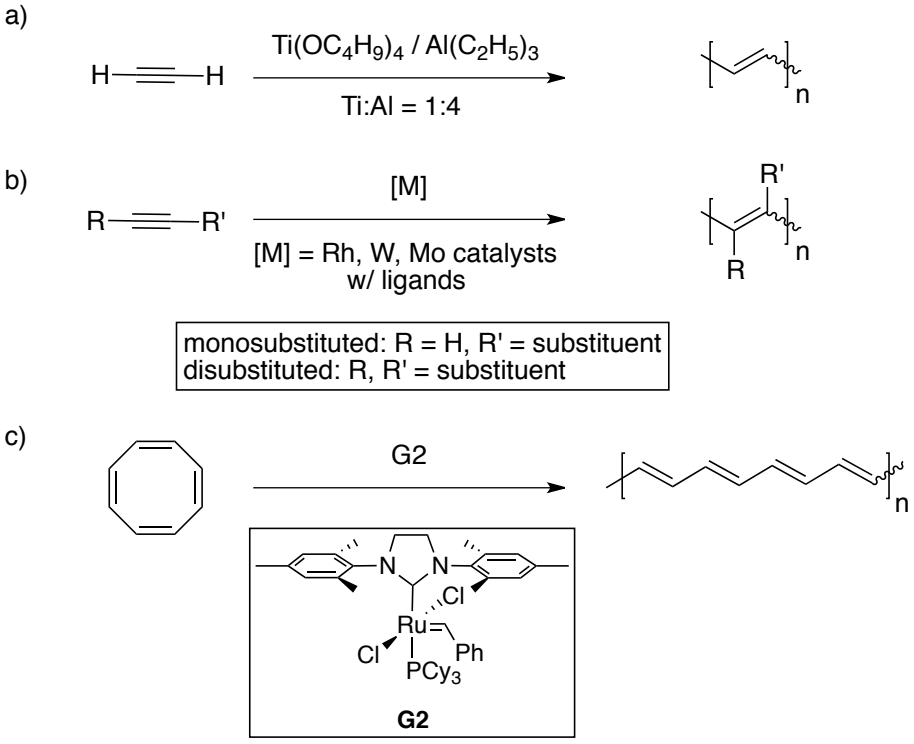

Interest in PA has extended beyond preparing "synthetic metals." In fact, more recent research has focused on functionalizing the backbone (Scheme 1.1b) to yield PAs demonstrating liquid crystallinity, photoconductivity, luminescence, helical chirality, optical nonlinearity, self-assembly, and bioactivity.[104] Also, because of the dangers associated with polymerizing acetylene, a highly flammable gas, alternative approaches to PA have been explored. For example, Klavetter and Grubbs demonstrated the ring-opening metathesis polymerization (ROMP) of 1,3,5,7-cyclooctatetraene using tungsten metathesis catalysts.[105] Although highly reactive, these tungsten catalysts were sensitive to air and moisture. Scherman and Grubbs addressed this by employing a robust

ruthenium-based catalyst (G2, Scheme 1.1c).[106] Additionally, they employed specialized chain transfer agents to generate PA block copolymers.[107]

1.3.3 Poly(phenylene vinylene)

Although PA has a suitable E_g (ca. 1.8 eV) for use in OSCs, the challenges associated with its synthesis and processing have compelled researchers to investigate alternative CPs. Facile and high yielding preparation makes poly(phenylene vinylenes) (PPVs) one such alternative. PPVs are of particular interest because their high electroluminescence values makes them ideal candidates for use in light-emitting electronics.[108] It is worth noting that unsubstituted PPVs, like PA, are highly insoluble in common solvents. Therefore, substitution (typically with linear or branched alkyl chains) of the CP backbone serves to disrupt chain aggregation and increase polymer solubility. For example, poly(2-methoxy-5-(2-ethylhexyloxy)-1,4-phenylene vinylene) (MEH-PPV) and poly(2-methoxy-5-(3',7'-dimethyloctyloxy)-1,4-phenylene vinylene) (MDMO-PPV) (Figure 1.7) are two highly soluble PPVs that, despite wide band gaps (ca. 2.2 eV), have achieved OSC efficiencies of 2.5–3.0%.[109-111]

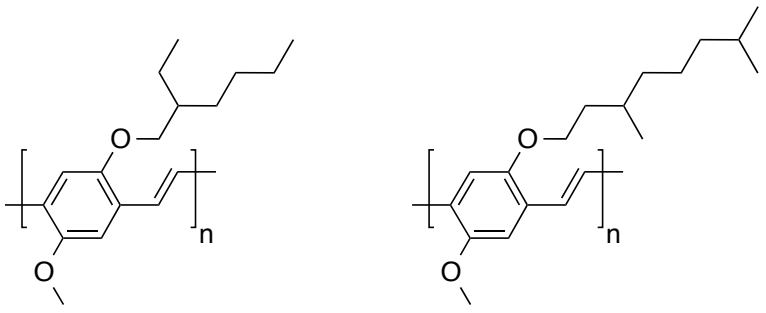

Figure 1.7
Structures of MEH-PPV and MDMO-PPV.

Preparation of PPVs can be accomplished by step (condensation) or chain (addition) growth approaches. In theory, any reaction that forms a carbon-carbon double bond could be used in the step approach. Although it has not been employed for PPV synthesis, McMurry coupling of a dialdehyde is one example (Scheme 1.2). Other examples of PPV step synthesis include Wittig, Horner-Wadsworth-Emmons (HWE), and Stille coupling chemistry (Scheme 1.2).[112,113] All polycondensation routes to PPV benefit from ease of synthesis. However, achieving high molar mass and exacting control over the *cis*/*trans* ratio is difficult. Consequently, precursor routes are far more popular for PPV preparation.[114]

Scheme 1.2

Polycondensation (non-precursor) routes to PPV.

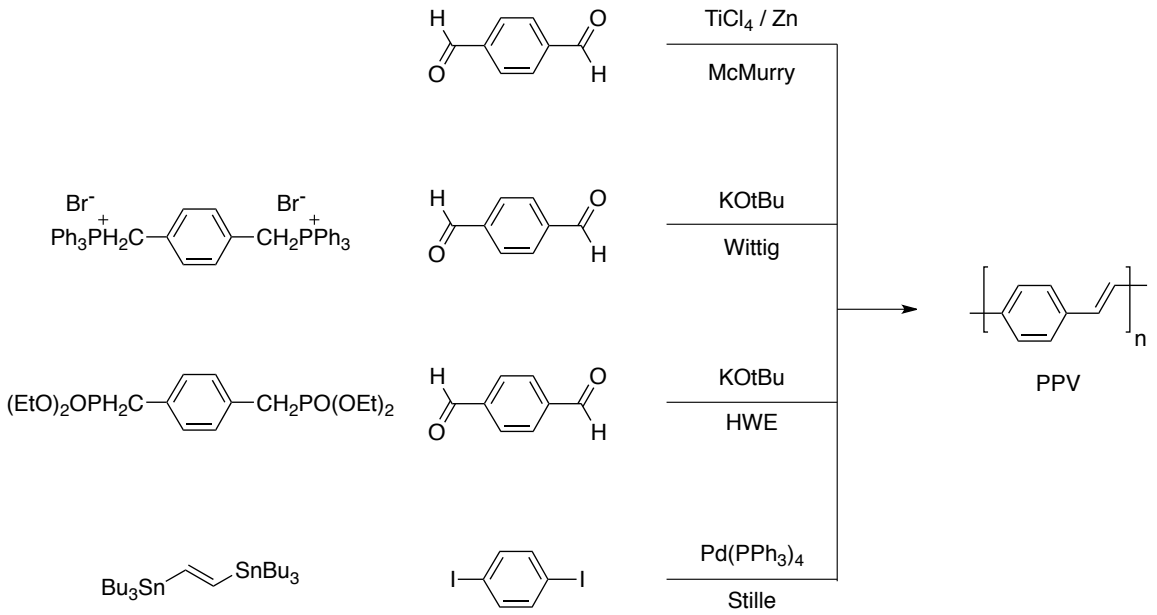

All precursor routes to PPV rely on generation of the same *p*-quinodimethane monomer species (red in Scheme 1.3). This is generated by adding base to a disubstituted precursor monomer, which affects the removal of a leaving group (L). The other substituent, referred to as the polarizer (P), remains and is built into the resulting polymer. As shown in Scheme 1.3, L and P are often, but not always, the same. Following initial polymerization, P is removed (often by heating) from the soluble "precursor" polymer to generate the desired PPV.[114]

Scheme 1.3

Precursor routes to PPV.

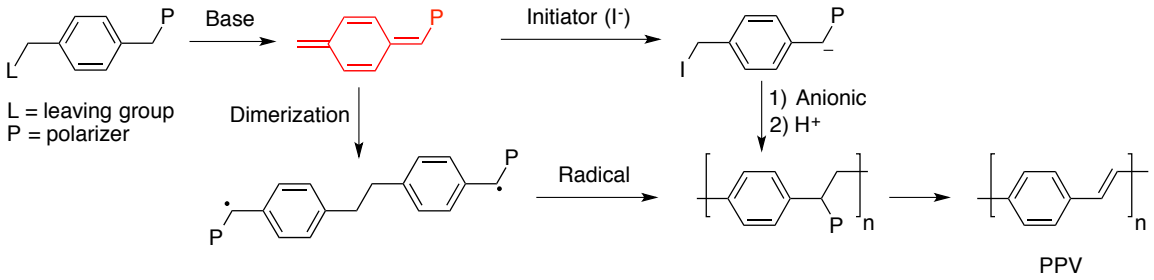

Route:	Gilch	Wessling	Sulfinyl	Xanthate	Dithiocarbamate
L ≡	Cl		Cl	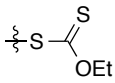	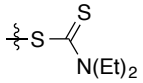
P ≡	Cl		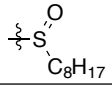	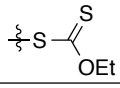	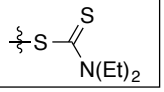

After generation of the *p*-quinodimethane monomer, polymerization can proceed in one of two ways. The first occurs after dimerization and formation of a diradical species, which initiates radical polymerization. This method of polymerization can give very high molar masses, but because the initiator is not fully conjugated the resulting PPV will have breaks in conjugation. The second polymerization is anionic, where the same base used to generate the *p*-quinodimethane can behave as an anionic initiator (I^-). Although regioregular (i.e., each monomer is added to the next in the same orientation) polymers are possible by this method, it suffers from reduced molecular weights because a relatively large amount of base must be employed to form the monomer, which ultimately results in a high number of initiated chains.[114]

The first precursor route to PPVs, reported by Gilch and Wheelwright, made use of a symmetric *α*,*α*'-dichloro *p*-xylylene monomer.[115] However, the most popular of the precursor routes is perhaps that developed by Wessling and Zimmerman in late 1960s.[116] The Wessling approach makes use of sulfonium salts in the monomer.[117] Other precursor

methods have expanded the sulfur-based polarizer concept to include sulfinyls,[118] xanthates,[119] and dithiocarbamates.[120] The L and P functionalities associated with each precursor route are shown in Scheme 1.3. In addition to the precursor routes, Turner et al. demonstrated the preparation of PPV homopolymers and block polymers by ring opening metathesis polymerization (ROMP, Scheme 1.4).[121-124] Although this method is capable of achieving high molar masses and an alternating *cis*/*trans* PPV backbone, the complexity of the monomers ultimately limits this approach.

Scheme 1.4

MEH-PPV by ROMP.

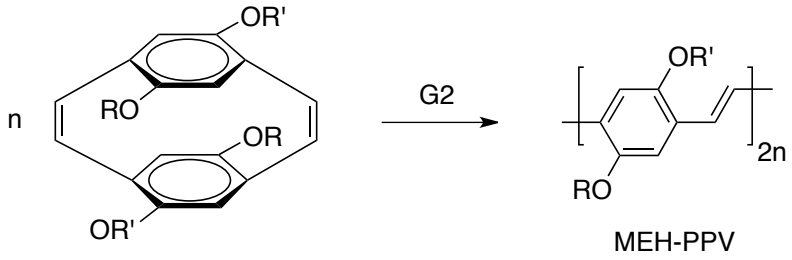

1.3.4 Poly(thiophene)

Perhaps one of the most commonly employed CPs is poly(thiophene) (PT). PTs have a lower E_g (ca. 1.9–2.0 eV) and are stronger absorbers (absorption coefficient ~ 1×10^5 M^{-1} cm^{-1}) than PPVs. Also, regioregular PTs, of which poly(3-hexylthiophene) (P3HT) is the most common, are capable of impressive hole mobilities (ca. 0.1 cm^2 V^{-1} s^{-1}).[125] This coupled with their strong photoluminescence (quantum yields = 40%)[126] suggests that excitons generated in the PT are long-lived and can dissociate with relatively high efficiency. Additionally, the high solubility, processibility, and environmental stability of substituted PTs have made them one of the most popular donor materials in OSCs.[50] In fact, P3HT-based OSCs have achieved record-setting efficiencies of 5%.[127]

Because PT properties are ideal for use in OSCs, it comes as no surprise that a variety of synthetic techniques have been employed to prepare these polymers. Although unsubtituted PTs have been prepared, these materials are insoluble, difficult to characterize, and non-ideal for OSCs. Scientists recognized early on that substituting the PT backbone with alkyl functionalities reduced the planarity of the polymer backbone and weakened intermolecular π-π interactions (i.e., π-stacking). This serves to prevent polymer aggregation and precipitation from solution without seriously affecting optical or electronic properties. Early polymerization techniques for PTs included anodic or cathodic electropolymerization,[128] oxidative polymerization with iron(III) chloride,[129] and metal catalyzed Kumada coupling (Scheme 1.5).[130,131] These syntheses generate sterically twisted regiorandom PTs with diminished optoelectronic properties. Therefore, research has since focused on regioregular PTs and the synthetic techniques used to produce them.[132]

Scheme 1.5

Regiorandom PT synthesis.

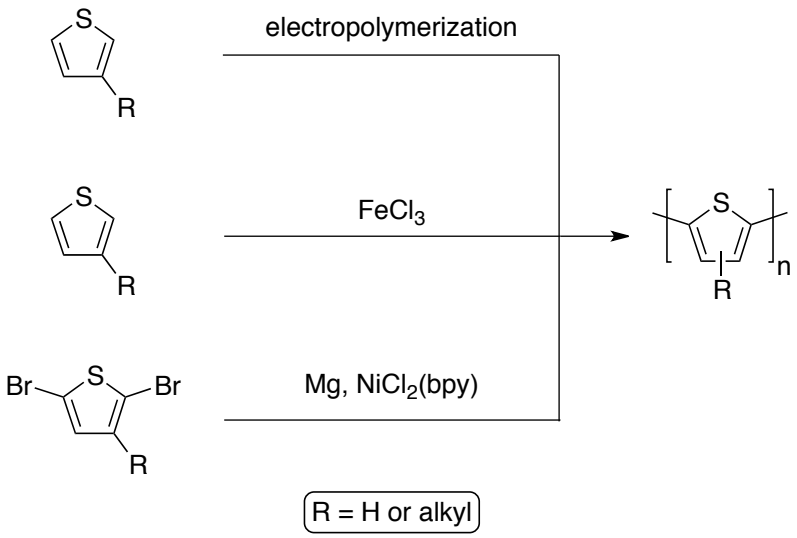

In 1992, McCullough and Rieke developed two slightly different methods for the synthesis of highly regioregular (head-to-tail coupling ≥97%) PTs.[133,134] The McCullough route involved the generation of 2-bromo-5-bromomagnesio-3-alkylthiophene by treating 2-bromo-3-alkylthiophene sequentially with lithium diisopropylamide (LDA) and magnesium bromide ethyl etherate. The Grignard intermediate was then treated with a nickel catalyst ($Ni(dppp)Cl_2$) to affect polymer formation. The Rieke method begins by treating 2,5-dibromo-3-alkylthiophene with an activated zinc reagent ("Rieke zinc" = Zn*) before addition of a nickel catalyst. These and other regioregular PT syntheses are summarized in Scheme 1.6.

Scheme 1.6

Regioregular PT synthesis.

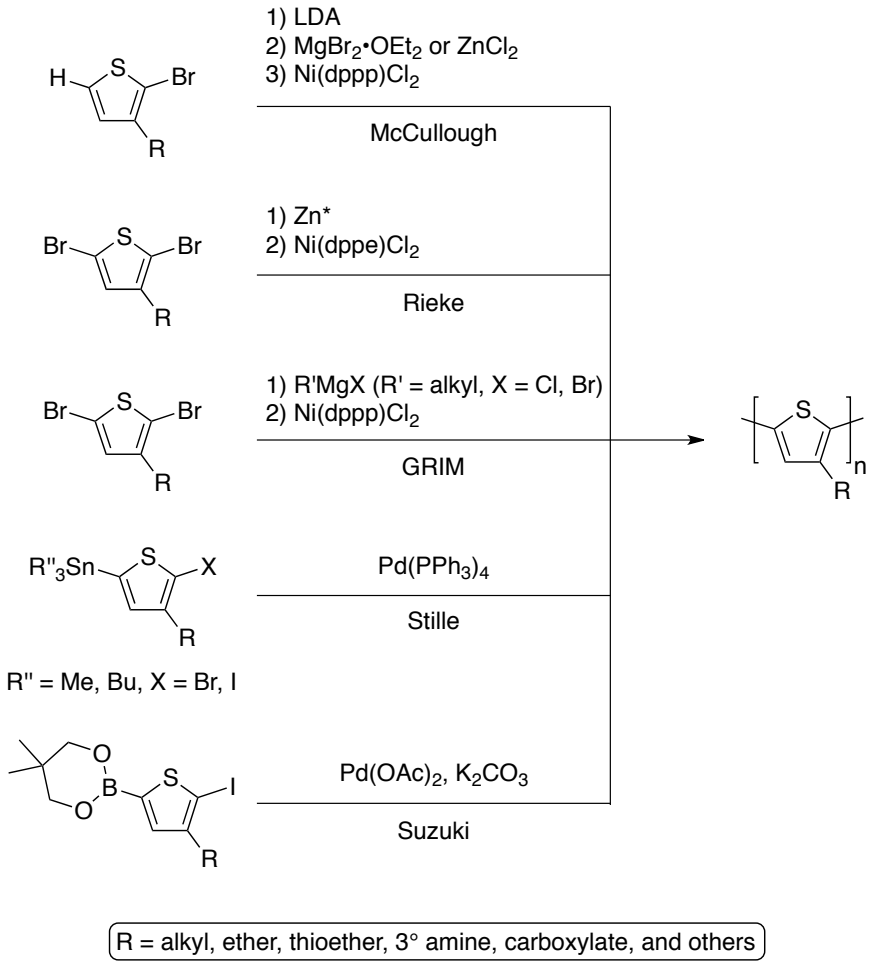

The original McCullough method was later modified to the Grignard metathesis (GRIM) method to avoid the use of highly reactive organometallic reagents and cryogenic temperatures.[135] The GRIM method employs the same nickel catalyst, but the reactive intermediate is generated by the addition of a less reactive Grignard reagent. The GRIM approach is additionally versatile because it is quasi-living[136] and can be selectively terminated with reactive functional groups[137] allowing for post-polymerization block polymer (i.e., rod-coil) formation (Scheme 1.7).[138-141] Additionally, all-conjugated block

polymers (i.e., rod-rod)[142-144] or even gradient copolymers[145] of PT can be synthesized with the GRIM method if monomer addition is carefully controlled (Scheme 1.8).

Scheme 1.7

Post-polymerization synthesis of PT block polymers.

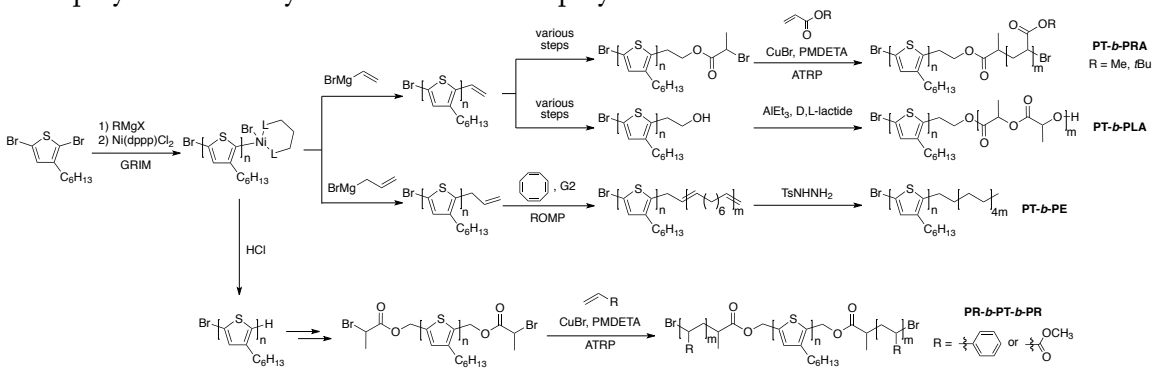

Scheme 1.8

PT copolymer synthesis by controlled monomer addition.

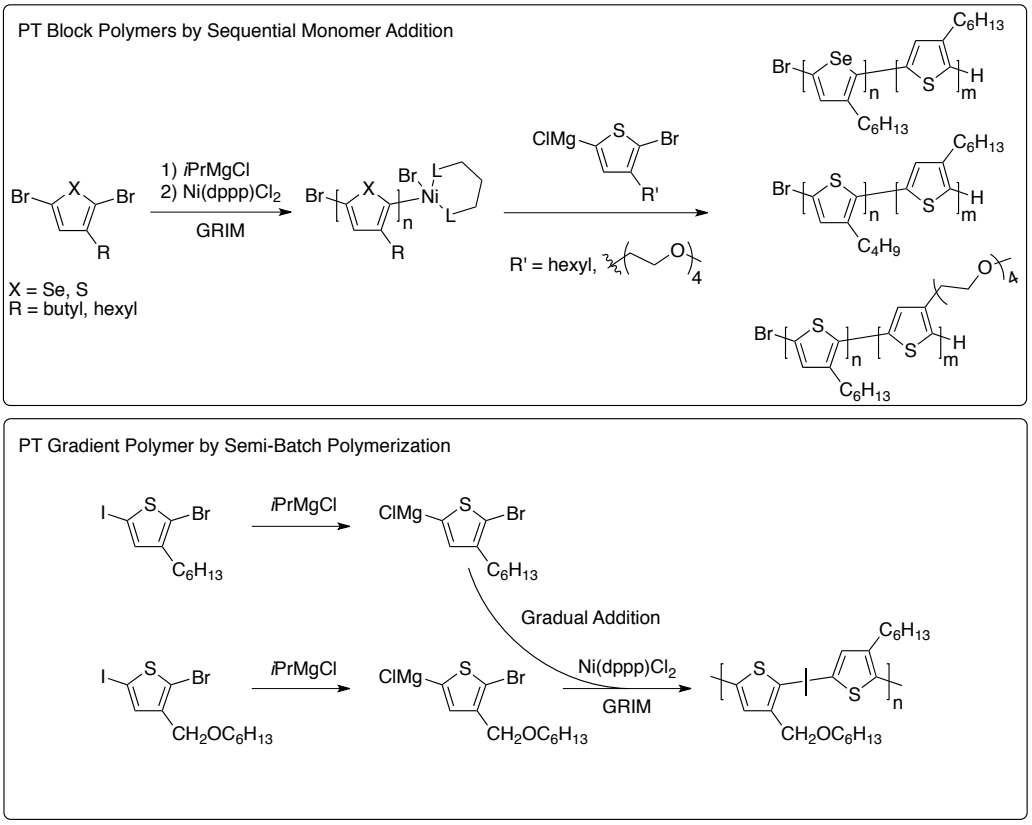

The synthesis of regioregular PTs has extended beyond the McCullough, Rieke, and GRIM methods to include palladium catalyzed Stille and Suzuki reactions.[146,147] These syntheses, although successful, require the challenging preparation of asymmetric organotin (Stille) or oganoboron (Suzuki) monomers. Because of ideal optoelectronic properties and relative ease of synthesis, PTs have been the subject of systematic regioregularity,[148] molar mass,[149] and alkyl chain length[150] studies.

1.3.5 Poly(thienylene vinylene)

Poly(2,5-thienylene vinylenes) (PTVs), are structurally similar to PTs with the exception of an olefinic "spacer." This additional functionality serves to minimize the steric interaction of neighboring thiophene rings without sacrificing conjugation (Figure 1.8a). The result is a CP with increased π orbital overlap (i.e., greater backbone planarity) and longer conjugation length. This increase in planarity manifests as a lower E_g (ca. 1.6–1.8) compared to PTs (ca. 1.9–2.0), which allows for absorption of light in a more optimal region of the solar spectrum (Figure. 1.8b). PTVs have found use in all manner of organic electronic devices including BHJ OSCs (PCE = 0.25–4.0%),[151-154] organic light-emitting diodes (OLEDs),[155] organic field-effect transistors (OFETs),[156] and nonlinear optics.[157]

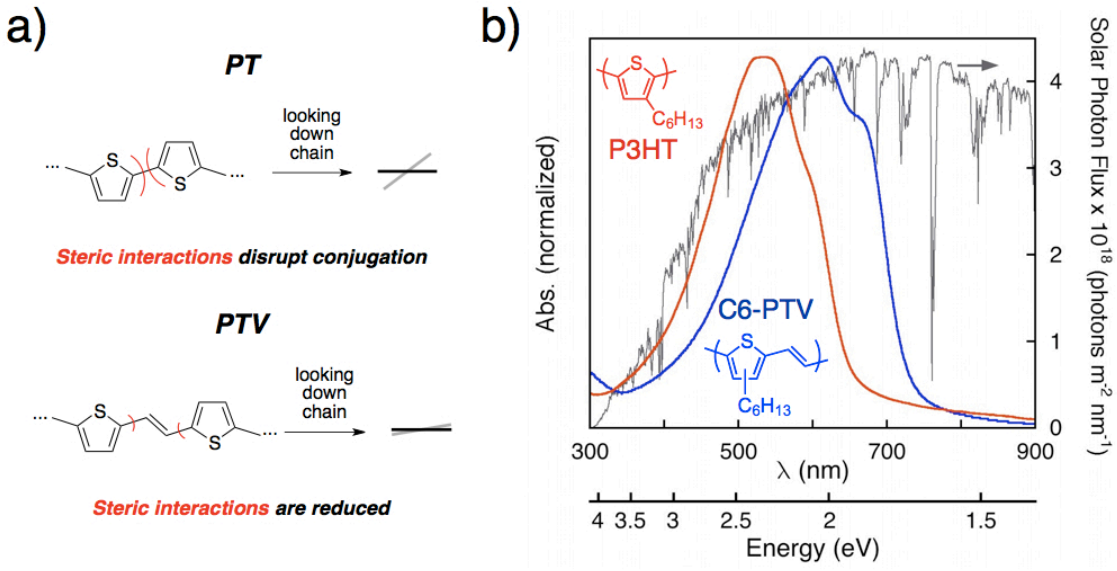

Figure 1.8

(a) Schematic representation of the thiophene-thiophene steric interactions in PT and PTV. (b) Thin film ultraviolet–visible absorption spectra of P3HT and C6-PTV compared to the solar photon flux.

The first synthesis of PTV was reported by Kossmehl in 1970 and was accomplished via a Wittig-like condensation reaction.[158] Other condensation approaches to PTVs have included the Horner-Wadsworth-Emmons (HWE) reaction[159] and McMurry coupling.[160,161] PTVs have also been prepared by the same soluble precursor methods used for PPVs[162-164] and by transition metal catalyzed reactions including Kumada, Stille, and Heck coupling.[165,166] More recently, ruthenium-catalyzed ROMP[167] and acyclic diene metathesis (ADMET) polymerization (discussed below), were employed in PTV synthesis. Scheme 1.9 summarizes these various synthetic methodologies.

Scheme 1.9

PTV synthesis. Condensation routes in blue, precursor routes in red, and transition metal catalyzed routes in green.

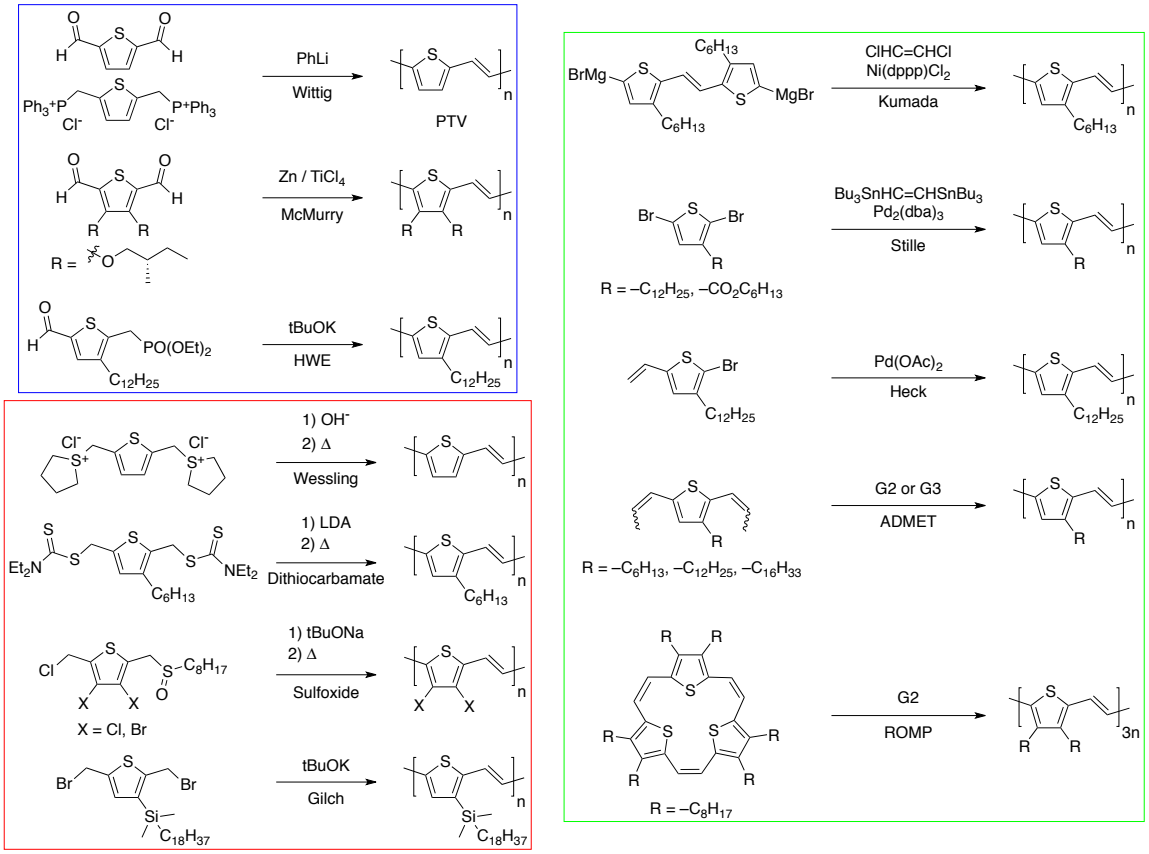

ADMET polymerization generates discrete units of unsaturation in a polymer backbone making it ideal for CP synthesis.[168-170] This polymerization, like ROMP,[171] makes use of the metathesis family of organometallic catalysts, a few of which are shown in Figure 1.9. However, unlike ROMP, a chain polymerization that is "living" under ideal and controlled conditions, ADMET is a step condensation polymerization. Therefore, taking advantage of Le Chatelier's principle, high molecular weights are reached through removal of the small molecule condensate, usually a low boiling point olefin (Scheme 1.10).[172] It should be noted that undesirable ring closing reactions are typically avoided by performing the polymerization in the bulk or at high concentration. Also, according to the Carothers equation ($X_n = 1/(1-p)$), significant degrees of polymerization (X_n) cannot be achieved without high conversions (p), and as the high conversion limit (p→100%) is approached the polydispersity index ($Đ$) should approach 2 ($Đ = X_w/X_n = 1 + p$, where X_w = weight-average degree of polymerization).

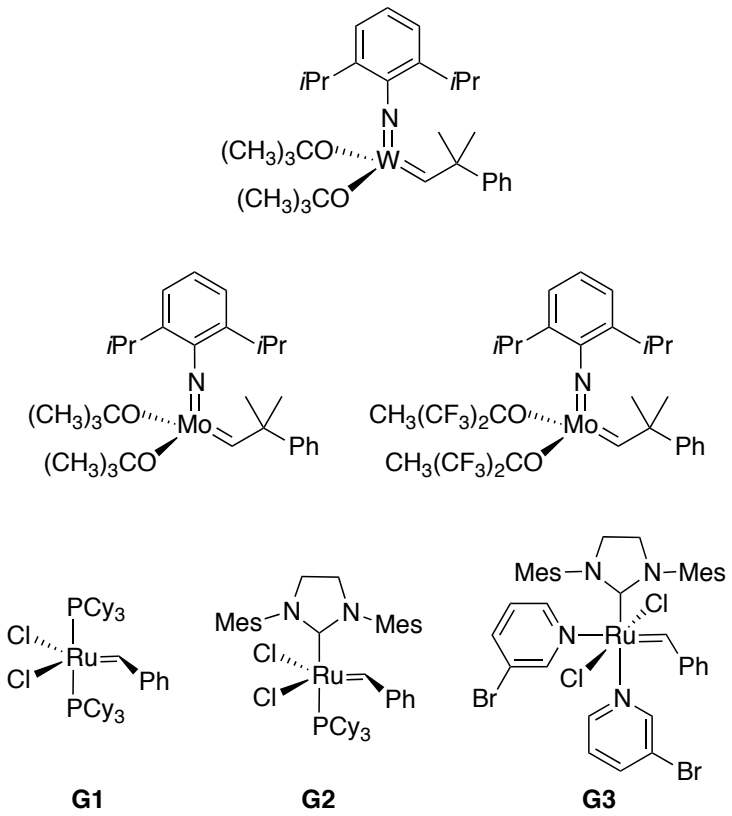

Figure 1.9

A sample of highly efficient metathesis catalysts based on tungsten, molybdenum, and ruthenium.

Scheme 1.10

ROMP and ADMET mechanisms.

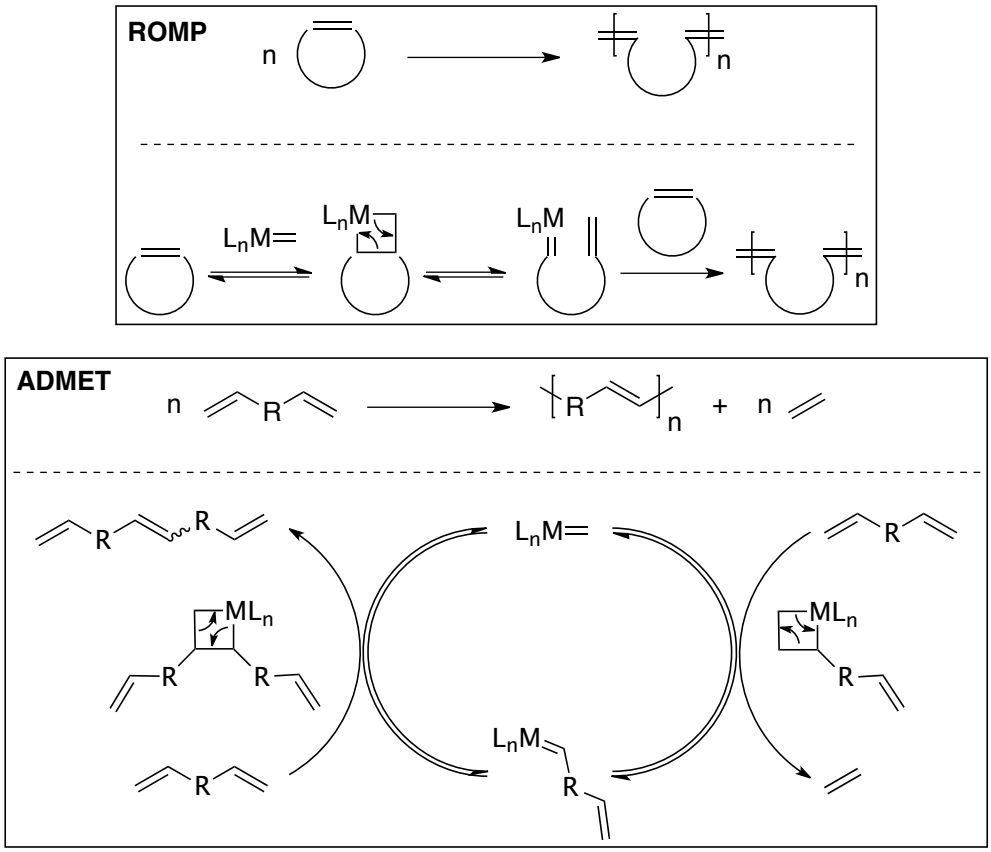

The classic metathesis mechanism proposed by Chauvin[173] is shown in Figure 1.10. Notably, each metathesis reaction begins with a 2+2 cycloaddition involving a metal-carbene complex and olefin species to form a metallacyclobutane. This is immediately followed by a 2+2 retrocycloaddition. When the retrocycloaddition proceeds degenerately, or the same starting materials are reformed, the reaction is termed "nonproductive." However, if the metallacyclobutane decomposition generates two new species the reaction is considered "productive." It should be noted that significant "scrambling" of substituents and stereochemistry occurs due

to the reversibility of metathesis reactions. Recently, scientists have demonstrated the metathesis preparation of regio-, stereo-, and syndiospecific materials by employing highly engineered catalysts[174-178] or starting materials.[179,180]

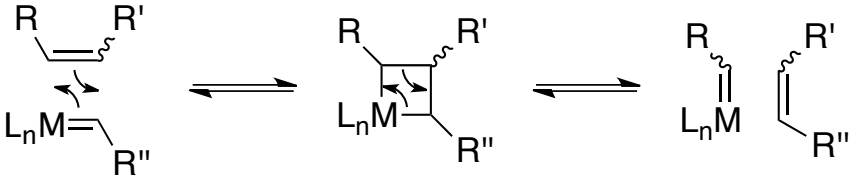

Figure 1.10
Metathesis mechanism proposed by Chauvin.

The feature distinguishing ADMET from other metathesis routes is the wide array of metal alkylidenes that can arise during the course of the reaction. Given the many possible intermediates and equilibria, a perceivable number of undesirable side reactions exist along the ADMET pathway. One such reaction is depolymerization, which occurs if the small molecule byproduct is allowed to reach a concentration that reverses equilibrium. Another reaction is cyclization, but this is avoided by keeping monomer concentration high during polymerization. A final reaction possibility is that of interchange. Interchange will occur if a functional group in the polymer (e.g., double bond) remains active to the catalyst, which usually is the case for ADMET. However, average polymer molecular weights remain unchanged by such interchange pathways.

ADMET has been employed to generate oligomeric PPVs[181] and PTVs. In the first reported PTV example, Tsuie et al. showed the polymerization of 2,5-divinyl-3-dodecylthiophene using a molybdenum-based Schrock catalyst.[182] A poorly soluble product was formed in low yield. Higher conversions and quantifiable molar masses were achieved by Qin et al. using G2 and a dipropenyl thiophene monomer.[183] More contemporary examples of PTVs prepared by ADMET include a solid state polymerization approach[184] and use of a more active ruthenium catalyst (i.e., G3).[185,186]

1.3.6 Donor–Acceptor Polymers

The desire to improve OSC efficiencies beyond the 5% achieved by PT containing devices has compelled scientists to investigate new CP architectures. Considering the wide array of conjugated small molecules, the numerous means of preparing and functionalizing them, and the various options for polymer synthesis, it should come as no surprise that the number of potential CPs is virtually limitless. Therefore, researchers have used this synthetic flexibility to prepare CPs with high molar masses, narrow band gaps, high charge mobilities, high absorption coefficients, and high solubility. The hope is that by balancing and maximizing these properties high OSC efficiency will follow. The contemporary method for preparing such high performance materials is known as the donor–acceptor (D-A) approach.[187]

D-A polymers, first introduced by Havinga and coworkers,[188] are named as such because the polymer backbone consists of an alternating sequence of electron-rich (donor) and electron-poor (acceptor) moieties. The space charge effects induced by alternation cause the valence (HOMO) and conduction (LUMO) bands of each moiety to curve. This band "bending" ultimately gives rise to a narrower E_g (Figure 1.11). This concept has since been expanded upon to include a tremendous variety D-A materials.[37,187]

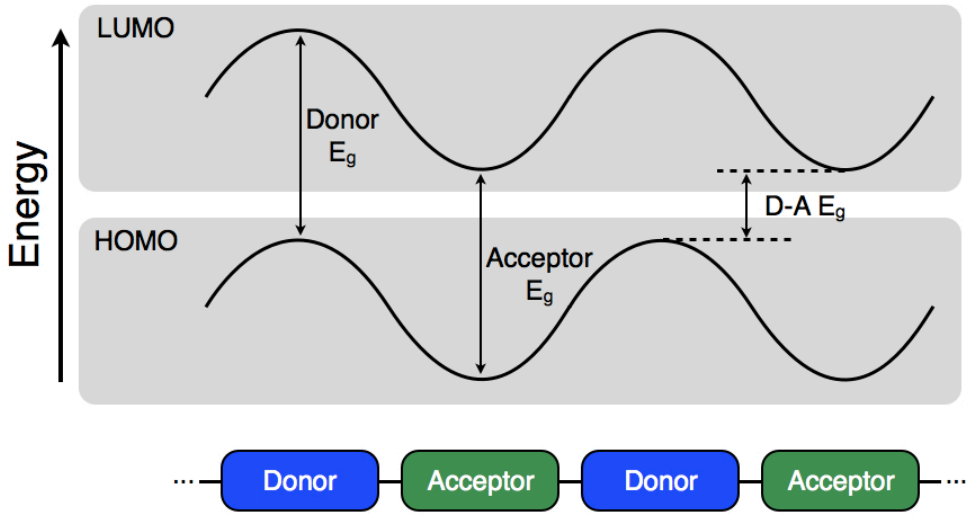

Figure 1.11
Schematic illustration of band structure in generic D-A polymer.

Many synthetic methods have been employed in the preparation of D-A polymers, but perhaps the most widely used are palladium-catalyzed polycondensations of which Stille, Suzuki, and direct (hetero)arylation routes are the most popular (Scheme 1.11). The Stille methodology employs dihalogenated and distannylated conjugated building blocks.[189] This reaction is highly effective, but generates toxic organotin byproducts. Therefore, Suzuki coupling is often favored because the diboronic acids/esters employed are far less toxic.[190] More recently, scientists have worked to simplify D–A synthesis and have developed direct (hetero)arylation as a potential solution.[191] This technique avoids additional synthetic steps by coupling a disubstituted species with the C–H bonds of an unsubstituted species. These polymerizations are often regioselective depending on the arene systems used. Additionally, a base is necessary to neutralize the acid that forms during reaction.

Scheme 1.11

Stille, Suzuki, and direct (hetero)arylation polymerizations.

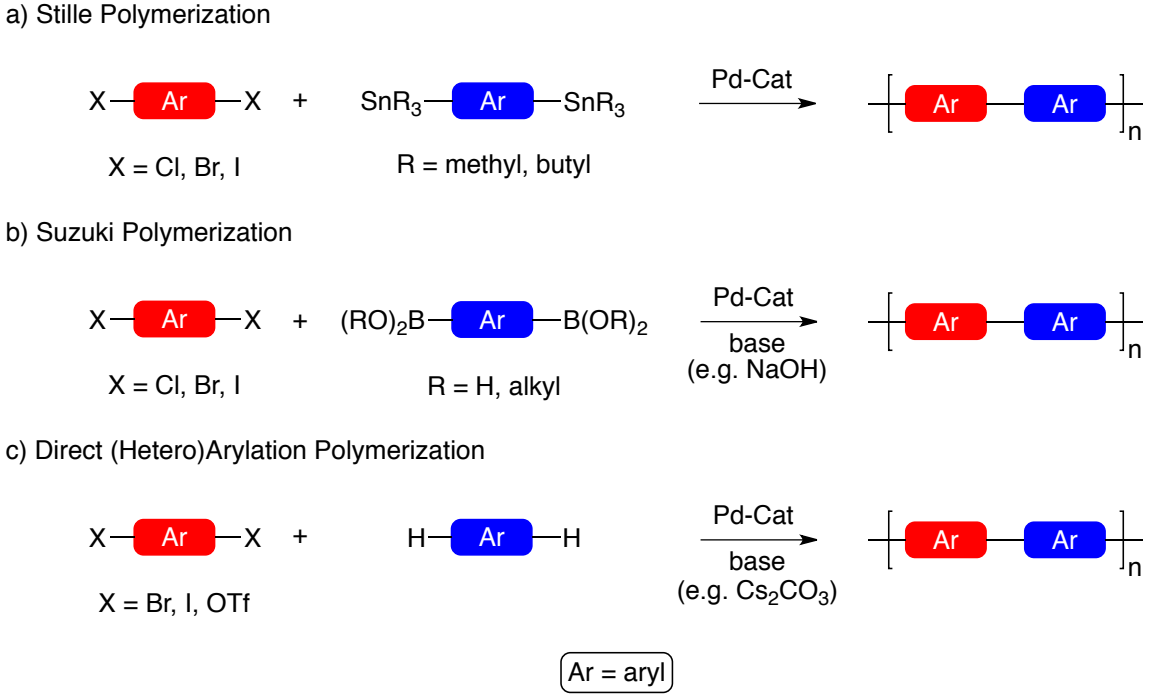

Although D-A polymers have enjoyed widespread use in devices like OFETs and OLEDs, they have been responsible for significant and rapid increases in OSC efficiency.[192] Recall, that in 2005 Ma et al. reported a record-breaking OSC (PCE = 5%) based on regioregular P3HT.[127] This record remained unbroken until 2009 when Leclerc and Heeger reported a 6.1% device based on a carbazole-benzothiadiazole D-A polymer.[193] The next big increase in efficiency was realized when Yu and coworkers developed D-A polymers composed of thieno[3,4-*b*]-thiophene and benzodithiophene. OSCs prepared from these materials gave efficiencies in excess of 7%.[194] In fact, He et al. used these same D-A polymers to prepare the current record holding OSC (PCE = 9.2%).[88] In addition to those discussed, Figure 1.12 illustrates several other high performance D-A polymers.

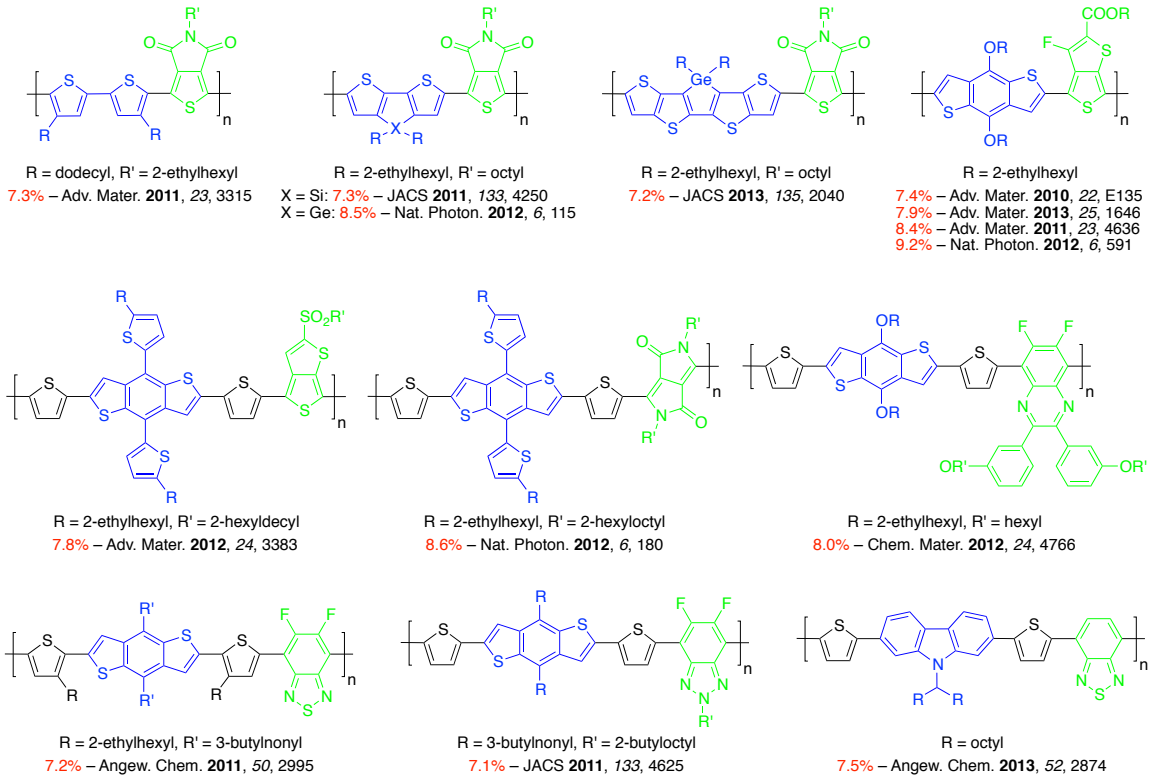

Figure 1.12
A sample of high performance D-A polymers. Electron-rich donors are in blue, electron-poor acceptors are in green, and OSC efficiencies are in red.

1.4 Conclusions

The design, operation, and characterization of OSCs was described briefly. Additionally, a wide variety of CPs and their syntheses were introduced semi-chronologically. The survey of these various polymers was meant to illustrate the diversity of these systems and to demonstrate the need for continued optimization. Synthetic polymer chemists are therefore necessary to the ongoing progress of the rapidly growing OSC field. Although many polymerization techniques have been used in CP synthesis, the examples of metathesis polymerization are relatively scarce. The remainder of this

dissertation will address this deficiency by employing ADMET in the preparation of novel PTV architectures. The studies described herein use results from the systematic variation of the PTV scaffold to build upon concepts central to all CPs.

1.5 References

[1] Bloom, D. E. *Science* **2011**, *333*, 562–569.

[2] Tilman, D.; Cassman, K. G.; Matson, P. A.; Naylor, R.; Polasky, S. *Nature* **2002**, *418*, 671–677.

[3] Foley, J. A.; Ramankutty, N.; Brauman, K. A.; Cassidy, E. S.; Gerber, J. S.; Johnston, M.; Mueller, N. D.; O'Connell, C.; Ray, D. K.; West, P. C.; Balzer, C.; Bennett, E. M.; Carpenter, S. R.; Hill, J.; Monfreda, C.; Polasky, S.; Rockström, J.; Sheehan, J.; Siebert, S.; Tilman, D.; Zaks, D. P. M. *Nature* **2011**, *478*, 337–342.

[4] Jackson, R. B.; Carpenter, S. R.; Dahm, C. N.; McKnight, D. M.; Naiman, R. J.; Postel, S. L.; Running, S. W. *Ecol. Appl.* **2001**, *11*, 1027–1045.

[5] Cohen, M. L. *Nature* **2000**, *406*, 762–767.

[6] Kopelman, P. G. *Nature* **2000**, *404*, 635–643.

[7] Parkin, D. M.; Bray, F.; Ferlay, J.; Pisani, P. *CA-Cancer J. Clin.* **2005**, *55*, 74–108.

[8] Jones, K. E.; Patel, N. G.; Levy, M. A.; Storeygard, A.; Balk, D.; Gittleman, J. L.; Daszak, P. *Nature* **2008**, *451*, 990–993.

[9] Lewis, N. S.; Nocera, D. G. *Proc. Natl. Acad. Sci. USA* **2006**, *103*, 15729–15735.

[10] Lewis, N. S. *MRS Bull.* **2007**, *32*, 808–820.

[11] Scheffran, J.; Brzoska, M.; Kominek, J.; Link, P. M.; Schilling, J. *Science* **2012**, *336*, 869–871.

[12] Ragauskas, A. J.; Williams, C. K.; Davison, B. H.; Britovsek, G.; Cairney, J.; Eckert, C. A.; Frederick Jr., W. J.; Hallett, J. P.; Leak, D. J.; Liotta, C. L.; Mielenz, J. R.; Murphy, R.; Templer, R.; Tschaplinski, T. *Science* **2006**, *311*, 484–489.

[13] Winograd, I. J.; Roseboom Jr., E. H. *Science* **2008**, *320*, 1426–1427.

[14] Normile, D. *Science* **2012**, *336*, 1220–1221.

[15] Malmqvist, B.; Rundle, S. *Environ. Conserv.* **2002**, *29*, 134–153.

[16] Dudgeon, D.; Arthington, A. H.; Gessner, M. O.; Kawabata, Z.-I.; Knowler, D. J.; Lévêque, C.; Naiman, R. J.; Prieur-Richard, A.-H.; Soto, D.; Stiassny, M. L. J.; Sullivan, C. A. *Biol. Rev.* **2006**, *81*, 163–182.

[17] Williams, R. *J. Chem. Phys.* **1960**, *32*, 1505–1514.

[18] Sun, S.-S.; Sariciftci, N. S. *Organic Photovoltaics*; Taylor & Francis: Boca Raton, FL, 2005.

[19] King, R. R.; Law, D. C.; Edmondson, C. M.; Fetzer, C. M.; Kinsey, G. S.; Yoon, H.; Sherif, R. A.; Karam, N. H. *Appl. Phys. Lett.* **2007**, *90*, 183516.

[20] Shaheen, S. E.; Ginley, D. S.; Jabbour, G. E. *MRS Bull.* **2005**, *30*, 10–19.

[21] Chang, S.-C.; Liu, J.; Bharathan, J.; Yang, Y.; Onohara, J.; Kido, J. *Adv. Mater.* **1999**, *11*, 734–737.

[22] Shaheen, S. E.; Radspinner, R.; Peyghambarian, N.; Jabbour, G. E. *Appl. Phys. Lett.* **2001**, *79*, 2996–2998.

[23] Logothetidis, S. *Mater. Sci. Eng. B-Adv.* **2008**, *152*, 96–104.

[24] Sommer-Larsen, P.; Jørgensen, M.; Søndergaard, R. R.; Hösel, M.; Krebs, F. C. *Energy Technol.* **2013**, *1*, 15–19.

[25] Peumans, P.; Bulovic, V.; Forrest, S. R. *Appl. Phys. Lett.* **2000**, *76*, 2650–2652.

[26] Kaltenbrunner, M.; White, M. S.; Glowacki, E. D.; Sekitani, T.; Someya, T.; Sariciftci, N. S.; Bauer, S. *Nature Commun.* **2012**, *3*, 1–7.

[27] Solar Energy Technologies Program. National Renewable Energy Laboratory. http://www.nrel.gov/docs/fy04osti/33875.pdf (accessed May 2013).

[28] Janssen, R. A. J.; Nelson, J. *Adv. Mater.* **2012**, *25*, 1847–1858.

[29] Kumar, P.; Chand, S. *Prog. Photovoltaics* **2012**, *20*, 377–415.

[30] Tang, C. W. *Appl. Phys. Lett.* **1986**, *48*, 183–185.

[31] Sariciftci, N. S.; Braun, D.; Zhang, C.; Srdanov, V. I.; Heeger, A. J.; Stucky, G.; Wudl, F. *Appl. Phys. Lett.* **1993**, *62*, 585–587.

[32] Tsuzuki, T.; Shirota, Y.; Rostalski, J. K.; Meissner, D. *Sol. Energ. Mat. Sol. C.* **2000**, *61*, 1–8.

[33] Xue, J.; Uchida, S.; Rand, B. P.; Forrest, S. R. *Appl. Phys. Lett.* **2004**, *85*, 5757–5759.

[34] Roncali, J. *Acc. Chem. Res.* **2009**, *42*, 1719–1730.

[35] Peet, J.; Heeger, A. J.; Bazan, G. C. *Acc. Chem. Res.* **2009**, *42*, 1700–1708.

[36] Hoeben, F. J. M.; Jonkheijm, P.; Meijer, E. W.; Schenning, A. P. H. J. *Chem. Rev.* **2005**, *105*, 1491–1546.

[37] Cheng, Y.-J.; Yang, S.-H.; Hsu, C.-S. *Chem. Rev.* **2009**, *109*, 5868–5923.

[38] Wudl, F. *Acc. Chem. Res.* **1992**, *25*, 157–161.

[39] Backer, S. A.; Sivula, K.; Kavulak, D. F.; Fréchet, J. M. J. *Chem. Mater.* **2007**, *19*, 2927–2929.

[40] Anthony, J. E.; Facchetti, A.; Heeney, M.; Marder, S. R.; Zhan, X. W. *Adv. Mater.* **2010**, *22*, 3876–3892.

[41] O'Regan, B.; Grätzel, M. *Nature* **1991**, *353*, 737–740.

[42] Hagfeldt, A.; Boschloo, G.; Sun, L.; Kloo, L.; Pettersson, H. *Chem. Rev.* **2010**, *110*, 6595–6663.

[43] Helgesen, M.; Søndergaard, R.; Krebs, F. C. *J. Mater. Chem.* **2010**, *20*, 36–60.

[44] Dennler, G.; Scharber, M. C.; Brabec, C. J. *Adv. Mater.* **2009**, *21*, 1323–1338.

[45] Nunzi, J. M. *CR Phys.* **2002**, *3*, 523–542.

[46] Gregg, B. A. *MRS Bull.* **2005**, *30*, 20–22.

[47] Veldman, D.; Meskers, S. C. J.; Janssen, R. A. J. *Adv. Funct. Mater.* **2009**, *19*, 1939–1948.

[48] Brédas, J.-L.; Norton, J. E.; Cornil, J.; Coropceanu, V. *Acc. Chem. Res.* **2009**, *42*, 1691–1699.

[49] Forrest, S. R. *MRS Bull.* **2005**, *30*, 28-32.

[50] Günes, S.; Neugebauer, H.; Sariciftci, N. S. *Chem. Rev.* **2007**, *107*, 1324–1338.

[51] Kroon, R.; Lenes, M.; Hummelen, J. C.; Blom, P. W. M.; de Boer, B. *Polym. Rev.* **2008**, *48*, 531–582.

[52] Gregg, B. A.; Hanna, M. C. *J. Appl. Phys.* **2003**, *93*, 3605–3614.

[53] Gregg, B. A. *J. Phys. Chem. B* **2003**, *107*, 4688–4698.

[54] Gregg, B. A. *MRS Bull.* **2005**, *30*, 20–22.

[55] Tvingstedt, K.; Vandewal, K.; Gadisa, A.; Zhang, F.; Manca, J.; Inganäs, O. *J. Am. Chem. Soc.* **2009**, *131*, 11819–11824.

[56] Ohkita, H.; Cook, S.; Astuti, Y.; Duffy, W.; Tierney, S.; Zhang, W.; Heeney, M.; McCulloch, I.; Nelson, J.; Bradley, D. D. C.; Durrant, J. R. *J. Am. Chem. Soc.* **2008**, *130*, 3030–3042.

[57] Coropceanu, V.; Cornil, J.; da Silva Filho, D. A.; Olivier, Y.; Silbey, R.; Brédas, J.-L. *Chem. Rev.* **2007**, *107*, 926–952.

[58] Theander, M.; Yartsev, A.; Zigmantas, D.; Sundström, V.; Mammo, W.; Andersson, M. R.; Inganäs, O. *Phys. Rev. B* **2000**, *61*, 12957–12963.

[59] Haugeneder, A.; Neges, M.; Kallinger, C.; Spirkl, W.; Lemmer, U.; Feldmann, J.; Scherf, U.; Harth, E.; Gügel, A.; Müllen, K. *Phys. Rev. B* **1999**, *59*, 15346–15351.

[60] Stübinger, T.; Brütting, W. *J. Appl. Phys.* **2001**, *90*, 3632–3641.

[61] Jenekhe, S. A.; Yi, S. *Appl. Phys. Lett.* **2000**, *77*, 2635–2637.

[62] Alam, M. M.; Jenekhe, S. A. *Chem. Mater.* **2004**, *16*, 4647–4656.

[63] Winder, C.; Sariciftci, N. S. *J. Mater. Chem.* **2004**, *14*, 1077–1086.

[64] Brabec, C. J.; Sariciftci, N. S.; Hummelen, J. C. *Adv. Funct. Mater.* **2001**, *11*, 15–26.

[65] Yang, X.; Loos, J. *Macromolecules* **2007**, *40*, 1353–1362.

[66] Armstrong, N. R.; Veneman, P. A.; Ratcliff, E.; Placencia, D.; Brumbach, M. *Acc. Chem. Res.* **2009**, *42*, 1748–1757.

[67] Manceau, M.; Angmo, D.; Jørgensen, M.; Krebs, F. C. *Organic Electronics* **2011**, *12*, 566–574.

[68] Eo, Y. S.; Rhee, H. W.; Chin, B. D.; Yu, J.-W. *Synth. Met.* **2009**, *159*, 1910–1913.

[69] Nguyen, L. H.; Hoppe, H.; Erb, T.; Günes, S.; Gobsch, G.; Sariciftci, N. S. *Adv. Funct. Mater.* **2007**, *17*, 1071–1078.

[70] Verploegen, E.; Mondal, R.; Bettinger, C. J.; Sok, S.; Toney, M. F.; Bao, Z. A. *Adv. Funct. Mater.* **2010**, *20*, 3519–3529.

[71] Parlak, E. A. *Sol. Energ. Mater. Sol. C.* **2012**, *100*, 174–184.

[72] Pivrikas, A.; Neugebauer, H.; Sariciftci, N. S. *Sol. Energy* **2011**, *85*, 1226–1237.

[73] Parker, I. D. *J. Appl. Phys.* **1994**, *75*, 1656–1666.

[74] Photovoltaic Research: Measurements & Characterization. National Renewable Energy Laboratory. www.nrel.gov/pv/measurements/current_vs_voltage.html (accessed May 2013).

[75] Rostalski, J.; Meissner, D. *Sol. Energ. Mater. Sol. C.* **2000**, *61*, 87–95.

[76] Scharber, S. C.; Muhlbacher, D.; Koppe, M.; Denk, P.; Waldauf, C.; Heeger, A. J.; Brabec, C. J. *Adv. Mater.* **2006**, *18*, 789–794.

[77] Koch, N. *ChemPhysChem* **2007**, *8*, 1438–1455.

[78] Segalman, R. A.; McCulloch, B.; Kirmayer, S.; Urban, J. J. *Macromolecules* **2009**, *42*, 9205–9216.

[79] Xue, J.; Uchida, S.; Rand, B. P.; Forrest, S. R. *Appl. Phys. Lett.* **2004**, *84*, 3013–3015.

[80] Ltaief, A.; Bouazizi, A.; Davenas, J. *Materials* **2009**, *2*, 710–718.

[81] Jørgensen, M.; Norrman, K.; Krebs, F. C. *Sol. Energ. Mater. Sol. C.* **2008**, *92*, 686–714.

[82] Heeger, A. J. *Angew. Chem., Int. Ed.* **2001**, *40*, 2591–2611.

[83] Thompson, B. C.; Fréchet, J. M. J. *Angew. Chem. Int. Ed.* **2008**, *47*, 58–77.

[84] He, Z.; Zhong, C.; Huang, X.; Wong, W.-Y.; Wu, H.; Chen, L.; Su, S.; Cao, Y. *Adv. Mater.* **2011**, *23*, 4636–4643.

[85] Service, R. F. *Science* **2011**, *332*, 293.

[86] Small, C. E.; Chen, S.; Subbiah, J.; Amb, C. M.; Tsang, S.-W.; Lai, T.-H.; Reynolds, J. R.; So, F. *Nat. Photonics* **2011**, 1-6.

[87] Dou, L.; You, J.; Yang, J.; Chen, C.-C.; He, Y.; Murase, S.; Moriarty, T.; Emery, K.; Li, G.; Yang, Y. **2012**, 1-6.

[88] He, Z.; Zhong, C.; Su, S.; Xu, M.; Wu, H.; Cao, Y. **2012**, *6*, 115–120.

[89] Chen, H.-C.; Chen, Y.-H.; Liu, C.-C.; Chien, Y.-C.; Chou, S.-W.; Chou, P.-T. *Chem. Mater.* **2012**, *24*, 4766–4772.

[90] Zhou, H.; Zhang, Y.; Seifter, J.; Collins, S. D.; Luo, C.; Bazan, G. C.; Nguyen, T.-Q.; Heeger, A. J. *Adv. Mater.* **2013**, *25*, 1646-1652.

[91] Mishra, A.; Bäuerle, P. *Angew. Chem. Int. Ed.* **2012**, *51*, 2020–2067.

[92] Sun, Y.; Welch, G. C.; Leong, W. L.; Takacs, C. J.; Bazan, G. C.; Heeger, A. J. *Nat. Mater.* **2011**, *11*, 44–48.

[93] van der Poll, T. S.; Love, J. A.; Nguyen, T.-Q.; Bazan, G. C. *Adv. Mater.* **2012**, *24*, 3646–3649.

[94] Peierls, R. E. *Quantum Theory of Solids*; Oxford University Press: London, 1955.

[95] Brédas, J.-L.; Heeger, A. J.; Wudl, F. *J. Chem. Phys.* **1986**, *85*, 4673–4678.

[96] Roncali, J. *Chem. Rev.* **1997**, *97*, 173–206.

[97] Li, Y. *Acc. Chem. Res.* **2012**, *45*, 723–733.

[98] Wan, M.; Wu, W.; Sang, G.; Zou, Y.; Liu, Y.; Li, Y. *J. Polym. Sci., Polym. Chem.* **2009**, *47*, 4028–4036.

[99] McCullough, R. D.; Lowe, R. D.; Jayaraman, M.; Anderson, D. L. *J. Org. Chem.* **1993**, *58*, 904–912.

[100] Natta, G.; Mazzanti, G.; Corradini, P. *Atti. Acad. Nazl. Lincei, Rend. Classe Sci. Fis. Mat. Nat.* **1958**, *25*, 3.

[101] Ito, T.; Shirakawa, H.; Ikeda, S.; *J. Polym. Sci. Chem. Ed.* **1974**, *12*, 11.

[102] MacDiarmid, A. G. *Angew. Chem. Int. Ed.* **2001**, *40*, 2581–2590.

[103] The Nobel Prize in Chemistry 2000. Nobel Prize site. www.nobelprize.org/nobel_prizes/chemistry/laureates/2000/ (accessed May 2013).

[104] Lam, J. W. Y.; Tang, B. Z. *Acc. Chem. Res.* **2005**, *38*, 745–754.

[105] Klavetter, F. L.; Grubbs, R. H. *J. Am. Chem. Soc.* **1988**, *110*, 7807–7813.

[106] Scherman, O. A.; Grubbs, R. H. *Synth. Met.* **2002**, *124*, 431–434.

[107] Scherman, O. A.; Rutenberg, I. M.; Grubbs, R. H. *J. Am. Chem. Soc.* **2003**, *125*, 8515–8522.

[108] Burroughes, J. H.; Bradley, D. D. C.; Brown, A. R.; Marks, R. N.; Mackay, K.; Friend, R. H.; Burns, P. L.; Holmes, A. B. *Nature* **1990**, *347*, 539–541.

[109] Yu, G.; Gao, J.; Hummelen, J. C.; Wudl, F.; Heeger, A. J. *Science* **1995**, *270*, 1789–1791.

[110] Shaheen, S.; Brabec, C.; Sariciftci, N. S. *Appl. Phys. Lett.* **2001**, *78*, 841–843.

[111] Wienk, M. M.; Kroon, J. M.; Verhees, W. J. H.; Knol, J.; Hummelen, J. C.; van Hal, P. A.; Janssen, R. A. J. *Angew. Chem. Int. Ed.* **2003**, *42*, 3371–3375.

[112] Babudri, F.; Cicco, S. R.; Farinola, G. M.; Naso, F.; Bolognesi, A.; Porzio, W. *Macromol. Rapid Comm.* **1996**, *17*, 905–911.

[113] Davey, A. P.; Drury, A.; Maier, S.; Byrne, H. J.; Blau, W. J. *Synth. Met.* **1999**, *103*, 2478–2479.

[114] Junkers, T.; Vandenbergh, J.; Adriaensens, P.; Lutsen, L.; Vanderzande, D. *Polym. Chem.* **2012**, *3*, 275–285.

[115] Gilch, H. G.; Wheelwright, W. L. *J. Polym. Sci., Polym. Chem.* **1966**, *4*, 1337–1349.

[116] Wessling, R. A. *J. Polym. Sci., Polym. Sym.* **1985**, 55–66.

[117] Akcelrud, L. *Prog. Polym. Sci.* **2003**, *28*, 875–962.

[118] Louwet, F.; Vanderzande, D.; Gelan, J. *Synth. Met.* **1992**, *52*, 125–130.

[119] Son, S.; Dodabalapur, A.; Lovinger, A. J.; Galvin, M. E. *Science* **1995**, *269*, 376–378.

[120] Henckens, A.; Duyssens, I.; Lutsen, L.; Vanderzande, D.; Cleij, T. J. *Polymer* **2006**, *47*, 123–131.

[121] Yu, C.-Y.; Turner, M. L. *Angew. Chem. Int. Ed.* **2006**, *45*, 7797–7800.

[122] Spring, A. M.; Yu, C.-Y.; Horie, M.; Turner, M. L. *Chem. Commun.* **2009**, 2676–2678.

[123] Yu, C.-Y.; Kingsley, J. W.; Lidzey, D. G.; Turner, M. L. *Macromol. Rapid Comm.* **2009**, *30*, 1889–1892.

[124] Yu, C.-Y.; Horie, M.; Spring, A. M.; Tremel, K.; Turner, M. L. *Macromolecules* **2010**, *43*, 222–232.

[125] Sirringhaus, H.; Brown, P. J.; Friend, R. H.; Nielsen, M. M.; Bechgaard, K.; Langeveld-Voss, B. M. W.; Spiering, A. J. H.; Janssen, R. A. J.; Meijer, E. W.; Herwig, P.; de Leeuw, D. M. *Nature* **1999**, *401*, 685–688.

[126] Li, Y.; Vamvounis, G.; Holdcroft, S. *Macromolecules* **2002**, *35*, 6900–6906.

[127] Ma, W.; Yang, C.; Gong, X.; Lee, K.; Heeger, A. J. *Adv. Funct. Mater.* **2005**, *15*, 1617–1622.

[128] Roncali, J. *Chem. Rev.* **1992**, *92*, 711–738.

[129] Sugimoto, R.; Taketa, S.; Gu, H. B.; Yoshino, K. *Chem. Express* **1986**, *1*, 635–638.

[130] Yamamoto, T.; Sanechika, K.; Yamamoto, A. *J. Polym. Sci., Polym. Lett.* **1980**, *18*, 9–12.

[131] Elsenbaumer, R. L.; Jen, K. Y.; Oboodi, R. *Synth. Met.* **1986**, *15*, 169–174.

[132] Osaka, I.; McCullough, R. D. *Acc. Chem. Res.* **2008**, *41*, 1202–1214.

[133] McCullough, R. D.; Lowe, R. D. *J. Chem. Soc. Chem. Comm.* **1992**, 70–72.

[134] Chen, T.-A.; Rieke, R. D. *J. Am. Chem. Soc.* **1992**, *114*, 10087–10088.

[135] Loewe, R. S.; Khersonsky, S. M.; McCullough, R. D. *Adv. Mater.* **1999**, *11*, 250–253.

[136] Iovu, M. C.; Sheina, E. E.; Gil, R. R.; McCullough, R. D. *Macromolecules* **2005**, *38*, 8649–8656.

[137] Jeffries-El, M.; Sauvé, G.; McCullough, R. D. *Macromolecules* **2005**, *38*, 10346–10352.

[138] Liu, J.; Sheina, E.; Kowalewski, T.; McCullough, R. D. *Angew. Chem. Int. Ed.* **2002**, *41*, 329–332.

[139] Iovu, M. C.; Jeffries-El, M.; Sheina, E. E.; Cooper, J. R.; McCullough, R. D. *Polymer* **2005**, *46*, 8582–8586.

[140] Radano, C. P.; Scherman, O. A.; Stingelin-Stutzmann, N.; Müller, C.; Breiby, D. W.; Smith, P.; Janssen, R. A. J.; Meijer, E. W. *J. Am. Chem. Soc.* **2005**, *127*, 12502–12503.

[141] Boudouris, B. W.; Frisbie, C. D.; Hillmyer, M. A. *Macromolecules* **2008**, *41*, 67–75.

[142] Ge, J.; He, M.; Qiu, F.; Yang, Y. *Macromolecules* **2010**, *43*, 6422–6428.

[143] Gao, D.; Hollinger, J.; Seferos, D. S. *ACS Nano* **2012**, *6*, 7114–7121.

[144] Song, I. Y.; Kim, J.; Im, M. J.; Moon, B. J.; Park, T. *Macromolecules* **2012**, *45*, 5058–5068.

[145] Locke, J. R.; McNeil, A. J. *Macromolecules* **2010**, *43*, 8709–8710.

[146] Iraqi, A.; Barker, G. W. *J. Mater. Chem.* **1998**, *8*, 25–29.

[147] Guillerez, S.; Bidan, G. *Synth. Met.* **1998**, *93*, 123–126.

[148] Kim, Y.; Cook, S.; Tuladhar, S. M.; Choulis, S. A.; Nelson, J.; Durrant, J. R.; Bradley, D. D. C.; Giles, M.; McCulloch, I.; Ha, C.-S.; Ree, M. *Nat. Mater.* **2006**, *5*, 197–203.

[149] Schilinsky, P.; Asawapirom, U.; Scherf, U.; Biele, M.; Brabec, C. J. *Chem. Mater.* **2005**, *17*, 2175–2180.

[150] Stevens, D. M.; Speros, J. C.; Hillmyer, M. A.; Frisbie, C. D. *J. Phys. Chem. C* **2011**, *115*, 20806–20816.

[151] Smith, A. P.; Smith, R. R.; Taylor, B. E.; Durstock, M. F. *Chem. Mater.* **2004**, *16*, 4687–4692.

[152] Nguyen, L. H.; Günes, S.; Neugebauer, H.; Sariciftci, N. S; Banishoeib, F.; Henckens, A.; Cleij, T.; Lutsen, L.; Vanderzande, D. *Sol. Energ. Mater. Sol. C.* **2006**, *90*, 2815–2828.

[153] Huo, L.; Chen, T. L.; Zhou, Y.; Hou, J.; Chen, H.-Y.; Yang, Y.; Li, Y. *Macromolecules* **2009**, *42*, 4377–4380.

[154] Lu, C.; Wu, H. C.; Chiu, Y. C.; Lee, W. Y.; Chen, W. C. *Macromolecules* **2012**, *45*, 3047–3056

[155] Segura, J. L. *Acta Polym.* **1998**, *49*, 319–344.

[156] Huitema, H. E. A.; Gelinck, G. H.; van der Putten, J. B. P. H.; Kuijk, K. E.; Hart, C. M.; Cantatore, E.; Herwig, P. T.; van Breemen, A. J. J. M.; de Leeuw, D. M. *Nature* **2001**, *414*, 599.

[157] Kobayashi, T. *Pure Appl. Chem.* **1995**, *67*, 387–400.

[158] Kossmehl, G.; Härtel, M.; Manecke, G. *Makromolekul. Chem.* **1970**, *131*, 15–54.

[159] Zhang, C.; Sun, J.; Li, R.; Sun, S.-S.; Lafalce, E.; Jiang, X. *Macromolecules* **2011**, *44*, 6389–6396.

[160] Cornelissen, J. J. L. M.; Peeters, E.; Janssen, R. A. J.; Meijer, E. W. *Acta. Polym.* **1998**, *49*, 471–476.

[161] Roncali, J. *Acc. Chem. Res.* **2000**, *33*, 147–156.

[162] Onoda, M.; Morita, S.; Iwasa, T.; Nakayama, H.; Yoshino, K. *J. Chem. Phys.* **1991**, *95*, 8584–8591.

[163] Banishoeib, F.; Henckens, A.; Fourier, S.; Vanhooyland, G.; Breselge, M.; Manca, J.; Cleij, T. J.; Lutsen, L.; Vanderzande, D.; Nguyen, L. H.; Neugebauer, H.; Sariciftci, N. S. *Thin Solid Films* **2008**, *516*, 3978–3988.

[164] Lee, Y.-B.; Shim, H.-K.; Ko, S.-W. *Macromol. Rapid Comm.* **2003**, *24*, 522–526.

[165] Toyoshima, R.; Akagi, K.; Shirakawa, H. *Synth. Met.* **1997**, *84*, 431–432.

[166] Loewe, R. S.; McCullough, R. D. *Chem. Mater.* **2000**, *12*, 3214–3221.

[167] Horie, M.; Shen, I.-W.; Tuladhar, S. M.; Leventis, H.; Haque, S. A.; Nelson, J.; Saunders, B. R.; Turner, M. L. *Polymer* **2010**, *51*, 1541–1547.

[168] Tao, D.; Wagener, K. B. *Macromolecules* **1994**, *27*, 1281–1283.

[169] Miao, Y.-J.; Bazan, G. C. *Macromolecules* **1997**, *30*, 7414–7418.

[170] Nomura, K.; Morimoto, H.; Imanishi, Y.; Ramhani, Z.; Geerts, Y. *J. Polym. Sci., Polym. Chem.* **2001**, *39*, 2463–2470.

[171] Grubbs, R. H. *Tetrahedron* **2004**, *60*, 7117–7140.

[172] Baughman, T. W.; Wagener, K. B. *Adv. Polym. Sci.* **2005**, *176*, 1–42.

[173] Trnka, T. M.; Grubbs, R. H. *Acc. Chem. Res.* **2001**, *34*, 18–29.

[174] Flook, M. M.; Ng, V. W. L.; Schrock, R. R. *J. Am. Chem. Soc.* **2011**, *133*, 1784–1786.

[175] Meek, S. J.; O'Brien, R. V.; Llaveria, J.; Schrock, R. R.; Hoveyda, A. H. *Nature* **2011**, *471*, 461–466.

[176] Keitz, B. K.; Endo, K.; Patel, P. R.; Herbert, M. B.; Grubbs, R. H. *J. Am. Chem. Soc.* **2011**, *134*, 693–699.

[177] Keitz, B. K.; Fedorov, A.; Grubbs, R. H. *J. Am. Chem. Soc.* **2012**, *134*, 2040–2043.

[178] Occhipinti, G.; Hansen, F. R.; Törnroos, K. W.; Jensen, V. R. *J. Am. Chem. Soc.* **2013**, *135*, 3331–3334.

[179] Kobayashi, S.; Pitet, L. M.; Hillmyer, M. A. *J. Am. Chem. Soc.* **2011**, *133*, 5794–5797.

[180] Zhang, J.; Matta, M. E.; Martinez, H.; Hillmyer, M. A. *Macromolecules* **2013**, *46*, 2535–2543.

[181] Fox, H. H.; Schrock, R. R.; O'Dell, R. *Organometallics* **1994**, *13*, 635–639.

[182] Tsuie, B.; Wagener, K. B.; Reynolds, J. R. *Polym. Preprints* **1999**, *40*, 790.

[183] Qin, Y.; Hillmyer, M. A. *Macromolecules* **2009**, *42*, 6429–6432.

[184] Delgado, P. A.; Liu, D. Y.; Kean, Z.; Wagener, K. B. *Macromolecules* **2011**, *44*, 9529–9532.

[185] Speros, J. C.; Paulsen, B. D.; White, S. P.; Wu, Y.; Jackson, E. A.; Slowinski, B. S.; Frisbie, C. D.; Hillmyer, M. A. *Macromolecules* **2012**, *45*, 2190-2199.

[186] Speros, J. C.; Paulsen, B. D.; Slowinski, B. S.; Frisbie, C. D.; Hillmyer, M. A. *ACS Macro Lett.* **2012**, *1*, 986-990.

[187] Bian, L.; Zhu, E.; Tang, J.; Tang, W.; Zhang, F. *Prog. Polym. Sci.* **2012**, *37*, 1292–1331.

[188] Havinga, E. E.; ten Hoeve, W.; Wynberg, H. *Synth. Met.* **1993**, *55*, 299–306.

[189] Carsten, B.; He, F.; Son, H. J.; Xu, T.; Yu, L. *Chem. Rev.* **2011**, *111*, 1493–1528.

[190] Sakamoto, J.; Rehahn, M.; Wegner, G.; Schlüter, A. D. *Macromol. Rapid. Commun.* **2009**, *30*, 653–687.

[191] Mercier, L. G.; Leclerc, M. *Acc. Chem. Res.* **2013**, DOI: 10.1021/ar3003305.

[192] Li, G.; Zhu, R.; Yang, Y. *Nat. Photonics* **2012**, *6*, 153–161.

[193] Park, S. H.; Roy, A.; Beaupré, S.; Cho, S.; Coates, N.; Moon, J. S.; Moses, D.; Leclerc, M.; Lee, K.; Heeger, A. J. *Nat. Photonics* **2009**, *3*, 297–302.

[194] Liang, Y.; Xu, Z.; Xia, J.; Tsai, S.-T. T.; Wu, Y.; Li, G.; Ray, C.; Yu, L. *Adv. Mater.* **2010**, *22*, E135–E138.

Chapter 2

A Systematic Study of Poly(3-hexadecylthienylene vinylene) Molecular Weight*

This chapter describes the design and synthesis of an optimized poly(thienylene vinylene) monomer and its subsequent polymerization by acyclic diene metathesis polymerization. An extensive library of varying molecular weight polymers was prepared. After carefully quantifying molecular weight, polymer bulk morphology was studied. Polymers were ultimately integrated into field-effect transistor and organic photovoltaic devices where the effect of molecular weight on performance was investigated.

* Reproduced in part with permission from Speros, J. C.; Paulsen, B. D.; White, S. J.; Wu, Y.; Jackson, E. A.; Slowinski, B. S.; Frisbie, C. D.; Hillmyer, M. A. *Macromolecules* **2012**, *45*, 2190–2199.

2.1 Introduction

The promise of low-cost, solution-processable solar cells continues to motivate significant academic[1-3] and industrial[4] research in organic photovoltaics (OPVs). Optimization of both photoactive conjugated polymers and OPV architectures has led to efficiency increases from 2.5% in 2001[5] to greater than 7% in the present day.[6-10] Although contemporary devices are approaching practical maximum efficiencies of 11% theoretically predicted by Veldman et al.,[11] fundamental understanding of OPV operation and the connection to molecular parameters of the active layer components is an ongoing challenge. A particularly important parameter for OPV performance is the molecular weight of the conjugated polymer. Prior molecular weight studies have focused on OPVs utilizing poly(alkylthiophene)s (P3ATs)[12-16] and a handful of alternating donor-acceptor (D-A) polymer chain architectures.[17-19] These examples demonstrate an improvement in device efficiency, hole mobility, optical properties, and film morphology with increasing molecular weight. Expanding the scope of materials for which molecular weight influences are observed and understood is desirable.

Acyclic diene metathesis (ADMET) polymerization has been employed to prepare a wide variety of materials ranging from polyethylene derivatives[20] to conjugated polymers.[21-26] Poly(thienylene vinylene)s (PTVs) are a particularly interesting class of low band gap conjugated polymers for OPVs.[27-30] A variety of synthetic methodologies have been exploited to prepare PTVs,[31-38] with maximum OPV efficiencies reaching 2%.[39] Recently, Qin and Hillmyer detailed the synthesis of poly(3-hexylthienylene vinylene) using ADMET polymerization in conjunction with functional group tolerant Grubbs catalysts.[40] Appreciable molecular weights (ca. 10 kg/mol) were reported, but these were only achieved after sequential catalyst additions. Realization of higher molecular weights was likely prevented by poor polymer solubility and catalyst decomposition.

In this chapter the ADMET preparation of seven poly(3-hexadecylthienylene vinylene) (C16-PTV) samples over a range of molecular weights (Scheme 2.1a) is

described. The use of a longer alkyl chain allowed for enhanced solubility at increased chain length. In addition, a more active Grubbs catalyst was utilized to reach high molecular weight at lower catalyst loadings. By addressing deficiencies in the ADMET synthesis of PTVs, we report one of the highest PTV molecular weights to date. The dependence of PTV molecular weight on charge mobility was assessed in a field effect transistor (FET) structure. These materials were then integrated into BHJ OPVs with [6,6]-phenyl-C61-butyric acid methyl ester (PCBM) to elucidate the impact of molecular weight on performance. Finally, a temperature-composition morphology map for C16-PTV:PCBM was constructed using differential scanning calorimetry (DSC), and blend morphology was investigated with atomic force microscopy (AFM).

2.2 Results and Discussion

2.2.1 C16-PTV Synthesis and Characterization

The C16-PTV monomer and corresponding polymer synthesis (Scheme 2.1a) was accomplished following a previous literature report (see Scheme 2.2 in Section 2.4.2).[40] En route to optimizing the Wittig reaction for a high *cis* double bond content, five monomers (M1–M5) having varying distributions of the four potential isomers (Scheme 2.1b) were generated. Isomer distributions were assessed by ^{1}H NMR (Figure 2.1), and the percentages of these isomers and overall *cis*:*trans* (*Z*:*E*) ratios are summarized in Table 2.1. M1–M5 were prepared in three steps with overall yields as high as 67% (see Section 2.4.2) and no detectable impurities as determined by ^{1}H NMR and GC-MS. High yields coupled with synthetic simplicity make this monomer amenable to multi-gram preparation.

Scheme 2.1

Synthesis of C16-PTVs (a) and the four isomers of M (b).

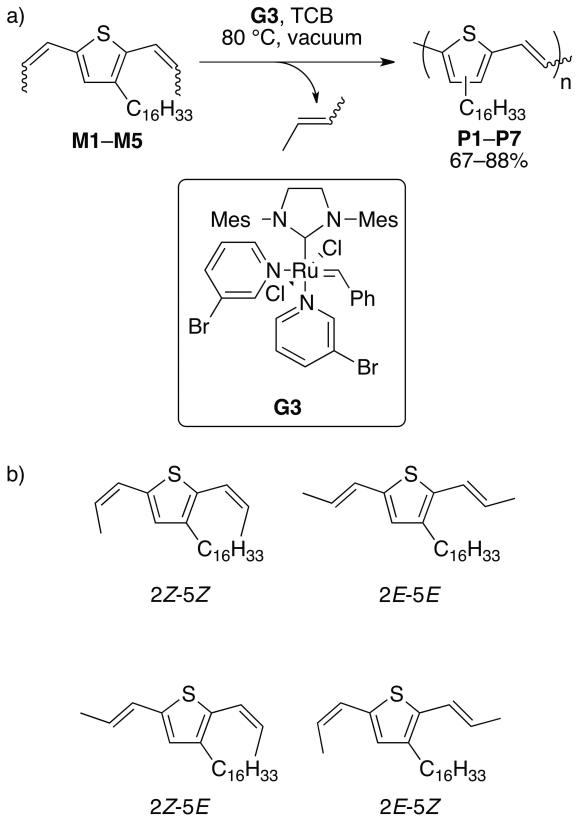

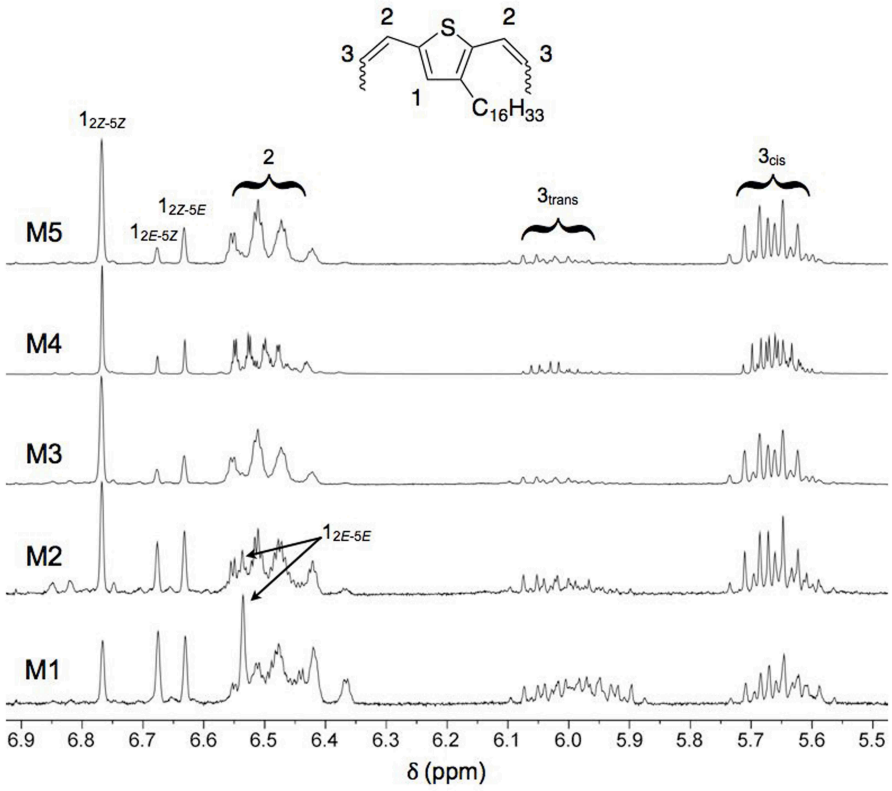

Figure 2.1
^{1}H NMR spectra of M1–M5 illustrating different *Z*:*E* ratios.

To effectively study the impact of molecular weight on device performance a series of C16-PTVs (P1–P7) was prepared by ADMET polymerization using the highly active ruthenium metathesis catalyst having an N-heterocyclic carbene and 3-bromopyridine ligands (G3) developed by Grubbs.[41] P1–P7 were prepared by treating M1–M5 with 1 mol% G3 in 1,2,4-trichlorobenzene (TCB). The equilibrium nature of ADMET was exploited by performing the reaction under reduced pressure to remove the 2-butene byproduct. This technique is necessary to achieve high conversion.[42,43] As stated, a small library of molecular weights was obtained by utilizing monomers having different overall *Z*:*E* ratios and by varying reaction times (Table 2.1). Given the asymmetric nature of the monomer, P1–P7 are obtained as essentially regiorandom polymers. This is supported by

^{1}H NMR analysis where the α-methylene protons on the alkyl chain appear as a broad singlet (ca. 2.5 ppm, Figure 2.2) rather than the triplet observed for regioregular thiophene polymers.[36] Additionally, Zhang et al. demonstrated the transition from four well-resolved to two broad olefinic resonances with decreasing PTV regioregularity.[44] These two broad peaks were observed in our C16-PTV samples (ca. 6.8 ppm, Figure 2.2) further supporting a regiorandom structure and thus the olefin *Z*:*E* ratio could not be accurately determined. PTV regiochemistry has been shown to have little affect on OPV performance.[44]

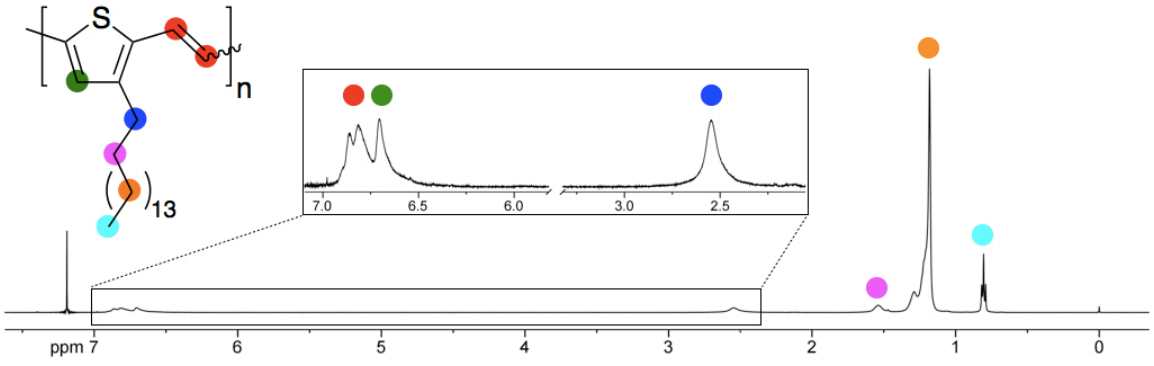

Figure 2.2
Representative ^{1}H NMR spectra of C16-PTV (P7).

The C16-PTV samples were slightly soluble in THF and toluene (ca. 5 mg/mL) and highly soluble in chloroform, *o*-dichlorobenzene, and TCB (>15 mg/mL). Initial molecular weight estimates were determined using size-exclusion chromatography (SEC) in chloroform versus polystyrene standards (Figure 2.3). The polydispersity index (PDI) values trended toward 2 with increasing molecular weight as expected for ADMET polymerization. SEC overestimates molecular weight for rod-like conjugated polymers,[45,46] making alternative molecular weight characterization necessary.

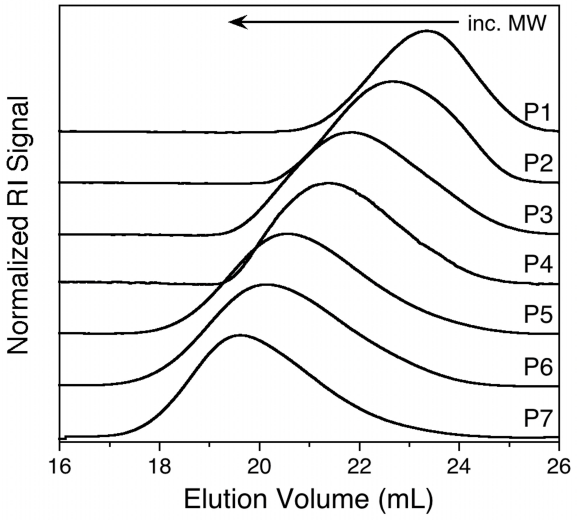

Figure 2.3

SEC chromatograms of P1–P7.

Number-average molecular weight (M_n) values were also determined by ^{1}H NMR analysis (Table 2.1). ADMET represents a step polymerization technique where appreciable molecular weights are only observed at high conversions. Using propenyl and aldehyde[40] end groups it was possible to estimate monomer conversion by comparing to polymer repeat unit resonances. Additionally, treating G3 as a monofunctional impurity that limits polymer molecular weight, the number-average degree of polymerization (X_n) and M_n can be determined (see Figure 2.25 in Section 2.4.3). The molecular weights calculated using ^{1}H NMR are comparable to those from SEC but are almost certainly overestimates. Given the removal of 2-butene, some fraction of polymer chains was likely terminated on one or both ends with ruthenium. However, ruthenium ends were neither observed nor quantified leading to conversion and, ultimately, molecular weight overestimates. Also, polymer purification by Soxhlet extraction removes residual monomer and low molecular weight oligomers leading to artificially high estimates of monomer conversion.

Table 2.1
Monomer isomer ratios and polymer molecular weight values.

Polymer (Monomer)	Z:*E*[a]	A:B:C:D[b]	t (h)	M_n[c] (kg/mol)	$Đ$[c]	X_n[d]	M_n[d] (kg/mol)
P1 (M1)	47:53	21:27:22:30	16	6	1.5	18	6
P2 (M1)	47:53	21:27:22:30	24	8	1.6	24	8
P3 (M2)	67:33	39:20:23:18	20	12	2.0	36	12
P4 (M3)	82:18	68:10:18:4	24	17	1.8	45	15
P5 (M4)	81:19	62:10:19:9	27	24	2.3	72	24
P6 (M5)	83:17	68:10:20:2	48	29	2.4	81	27
P7 (M5)	83:17	68:10:20:2	96[e]	33	2.2	90	30

[a]Overall monomer cis:trans ratio calculated from the relative integration of *Z* and *E* protons in the ^{1}H NMR spectrum. [b]A = 2*Z*-5*Z*, B = 2*Z*-5*E*, C = 2*E*-5*Z*, and D = 2*E*-5*E* as determined from integration of ^{1}H NMR spectrum. [c]Determined by SEC in $CHCl_3$ with a refractive index detector and polystyrene standards. [d]Determined by ^{1}H NMR analysis. [e]Reaction was determined to be complete after 48 h by SEC.

Selected ^{1}H NMR spectral regions of monomer and two representative C16-PTVs are shown in Figure 2.4. The absence of *Z* propenyl end groups in both polymers is indicative of their increased reactivity with G3. Conversely, *E* propenyl end groups persist even after 96 h of polymerization. We previously demonstrated that aldehydes residing on one or both of the polymer chain ends are the result of adventitious oxygen in the reaction solution.[40] Two aldehyde resonances, also highlighted in Figure 2.4b, occur due to monomer asymmetry. In this work, we demonstrate that a simple freeze-pump-thaw (FPT) cycle prior to catalyst loading effectively prevents aldehyde formation (Figure 2.4c). However, this additional manipulation did not lead to increased molecular weight for a given reaction time.

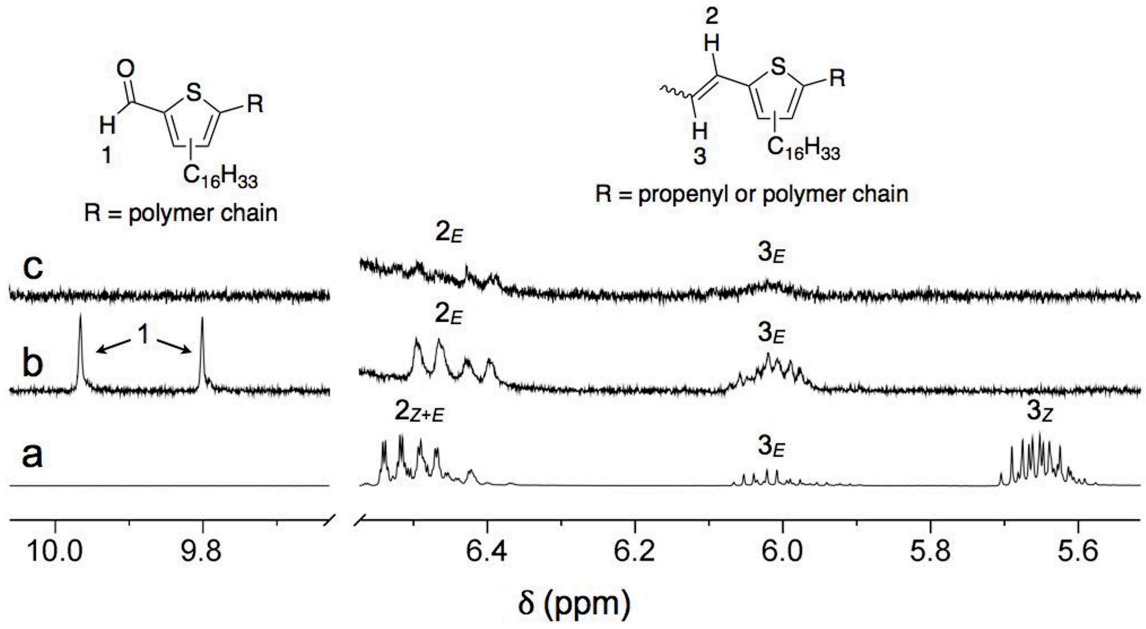

Figure 2.4
^{1}H NMR spectra of (a) monomer, (b) polymer without freeze-pump-thaw (FPT), and (c) polymer with FPT.

In an effort to confirm the increased reactivity of *Z* propenyl end groups and to achieve higher PTV molecular weights an all *Z* propenyl C16 monomer was prepared (Scheme 2.2a). The synthesis of this all *Z* monomer began by dibrominating 3-hexadecylthiophene with N-bromosuccinimide. The dibromo compound was converted to a dialkyne through a palladium-catalyzed Negishi coupling.[47] The dialkyne was then selectively reduced to the all *Z* (97% *Z*) C16 monomer with Lindlar's catalyst (see Section 2.4.2 for complete synthetic details). Although ^{1}H NMR indicated high purity, we were unable to polymerize this monomer using G3. This is presumably due to an undetected impurity left over from hydrogenation. In order to bypass this challenge an all *Z* C6 monomer was prepared (Scheme 2.2b) following the same protocol. The shorter alkyl chain allowed for purification by vacuum distillation following Lindlar hydrogenation. Although this monomer was successfully polymerized with G3, the molecular weight was low (M_n = 4.2 kg/mol, $Đ$ = 1.2). ^{1}H NMR of the C6-PTV showed

no remaining end groups, therefore, the low molecular weight was attributed to the presence of monofunctional monomer or impurities evidenced by ^{1}H NMR (Figure 2.30). In the interest of completeness, an all *E* C16 monomer was prepared as well (Scheme 2.2c). The Schlosser modification to the Wittig reaction was applied to the dialdehyde compound to obtain the all *E* C16 monomer.[48] The bright yellow solid obtained was 97% *E* as determined by ^{1}H NMR. As expected, we were unable to polymerize this monomer, which is believed to be the result of unfavorable steric interactions between catalyst and monomer. This brief study confirms that a high *Z* content is necessary for high molecular weight PTVs, but the Lindlar hydrogenation approach introduces an unknown impurity that prevents high degrees of polymerization. Investigating other routes to all *Z* monomers could potentially lead to significantly increased molecular weights.

Scheme 2.2

Synthesis and polymerization of all *Z* and *E* monomers.

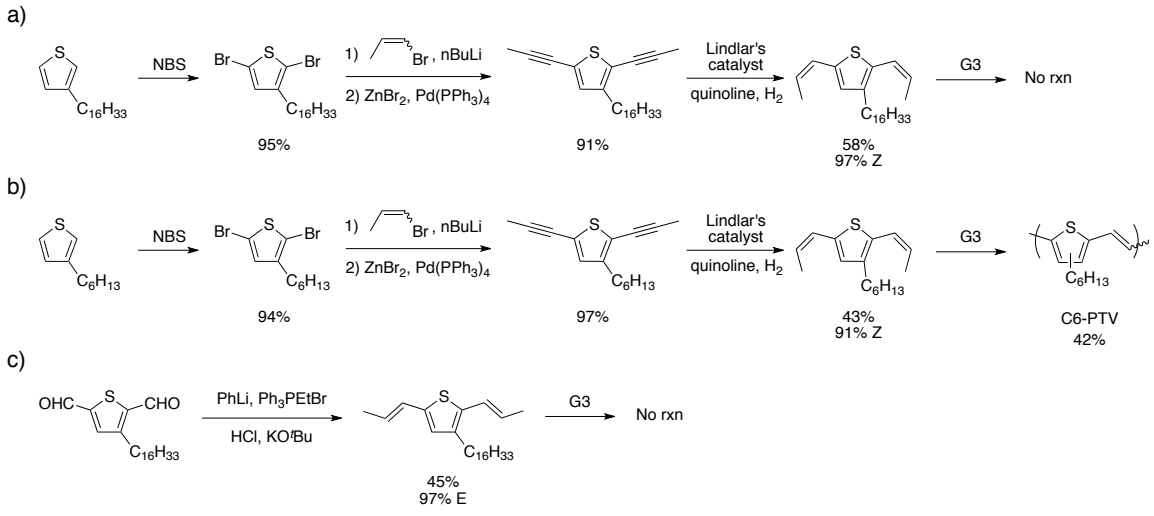

Biagini et al. demonstrated the deliberate end group conversion of ruthenium carbenes to aldehydes during metathesis polymerization.[49] Aldehyde end groups provide a useful synthetic handle for further reaction and functionalization. To demonstrate this, a

C16-PTV partially terminated with aldehydes was treated under McMurry coupling conditions with titanium tetrachloride and zinc in THF. Following workup, the polymer molecular weight was markedly increased (9→12 kg/mol). This is illustrated by the disappearance of aldehyde peaks in the product polymer ^{1}H NMR spectrum and a shift to lower elution volume in the SEC chromatogram (Figure 2.5). Upon further investigation and optimization this method of chain extension could prove suitable for a variety of aldehyde-terminated conjugated polymers and make block polymerization or polymer functionalization strategies synthetically accessible.

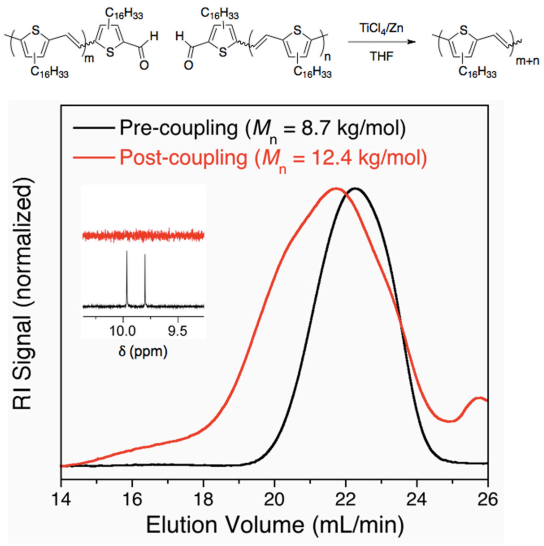

Figure 2.5
McMurry coupling of aldehyde terminated monomer. SEC shows post reaction increase in molecular weight. Inset illustrates disappearance of aldehyde resonances in ^{1}H NMR.

2.2.2 C16-PTV Optical Properties

To understand the role that molecular weight plays on C16-PTV photophysical behavior, P1–P7 were investigated by ultraviolet-visible (UV–vis) absorption spectroscopy in dilute chloroform solutions and as thin films on glass substrates. Figure 2.6a

summarizes the solution data for P1–P7. As molecular weight increased the absorption maximum ($\lambda_{max,1}$) red shifted (Table 2.2) indicative of an increased conjugation length. A second peak ($\lambda_{max,2}$) also appeared with increasing molecular weight. While the first peak is attributed to the π-π* transition, the second is indicative of vibronic structure that results from polymer aggregation. This phenomenon is well documented for conjugated polymers.[16,50] To confirm aggregation-induced absorption, solution spectra of P5 were collected in chlorobenzene at room temperature, at ca. 130 °C, and upon returning to room temperature (Figure 2.6b). Owing to the general thermochromic nature of conjugated polymers,[51,52] there was a blue shift (14 nm) in P5 absorption at elevated temperature. Also, the second absorption peak nearly disappeared (i.e., reduced to shoulder) indicating the breakup of polymer aggregates. Upon cooling the original absorptive features returned suggesting the loss of aggregation induced absorption was not a product of polymer degradation at elevated temperatures.

Indicative of increased ordering in the solid state, a significant red shift (21–51 nm) was observed in going from solution to thin film spectra (Figure 2.6c). Vibronic structure was also apparent for P1–P7, and the associated absorption intensity increased with increasing molecular weight. The optical band gap (E_g^{opt}) of these materials was calculated by converting the onset absorption (λ_{onset}) to energy ($E_g^{opt} = 1240/\lambda_{onset}$) and ranged from 1.65–1.68 eV (Table 2.2). Cyclic voltammetry was also used to calculate the C16-PTV HOMO level (-4.9 eV) from the oxidation onset (Figure 2.7).

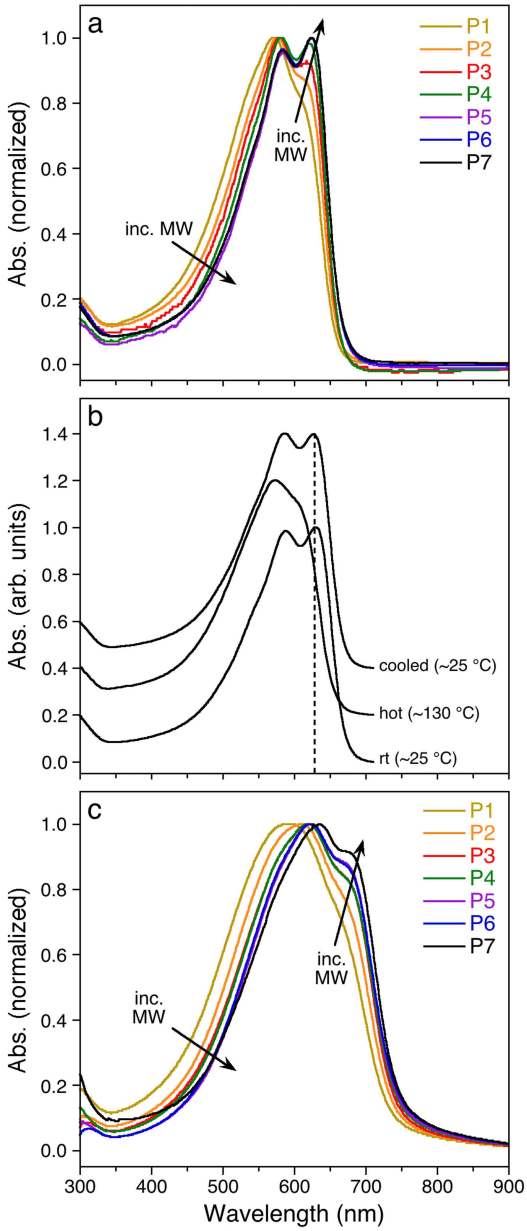

Figure 2.6

UV–vis spectra of (a) P1–P7 in $CHCl_3$ (see Table 2 for concentrations), (b) P5 in chlorobenzene (1×10^{-5} M per repeat unit), and (c) P1–P7 as unannealed thin films on glass. Spectra are offset and a dashed vertical line is added in (b) to make the noted changes more evident.

Table 2.2
UV–vis Data for C16-PTVs.

Entry	UV–vis (Solution)[a]		UV–vis (Film)[b]	
	$\lambda_{max,1}$ (nm)	$\lambda_{max,2}$ (nm)	$\lambda_{max,1}$ (nm)	E_g^{opt} (eV)
P1	571	616[c]	592	1.68
P2	576	617[c]	609	1.66
P3	579	617	619 (675[c])	1.66
P4	581	621	619 (675[c])	1.66
P5	584	624	623 (680[c])	1.66
P6	584	624	623 (680[c])	1.66
P7	584	624	635 (684[c])	1.65

[a]P1 = 2.5×10^{-5} M (repeat unit basis) in $CHCl_3$ and P2–P7 = 1.0×10^{-5} M (repeat unit basis) in $CHCl_3$. [b]Films prepared by spin-coating a 10 mg/mL polymer solution in $CHCl_3$ at 1500 rpm for 40 s. [c]Absorption shoulder.

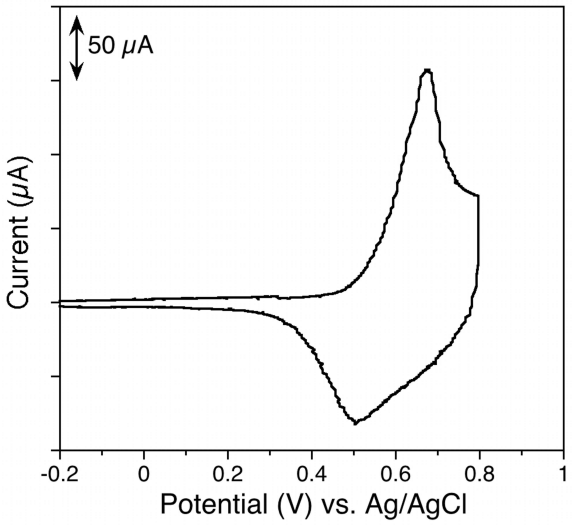

Figure 2.7
Cyclic voltammogram of P7 as a thin film spin coated onto an Au-coated silicon wafer.

2.2.3 C16-PTV Thermal Behavior

Thermogravimetric analysis (TGA) was employed to evaluate polymer thermal stability. Molecular weight was found to have no impact on decomposition temperature (T_d) as all polymers displayed 5% weight loss at 379 °C under a nitrogen atmosphere. P7

was also analyzed in air (Figure 2.8). Although the presence of oxygen reduced the T_d to 324 °C, these C16-PTVs exhibited good thermal stability regardless of molecular weight.

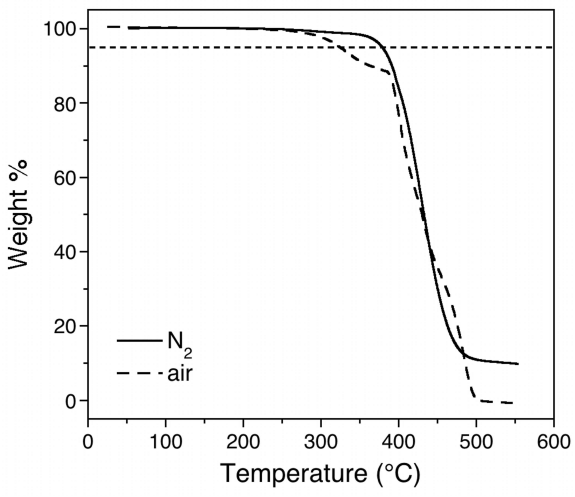

Figure 2.8
Thermogravimetric analysis of P7 in an N_2 and oxidizing (air) atmosphere. Decomposition temperature (T_d) was determined as the temperature where 5% of the polymer weight (dashed line) was lost.

Temperature-dependent wide-angle X-ray scattering (TWAXS) was employed in conjunction with differential scanning calorimetry (DSC) to elucidate the solid state behavior of C16-PTVs as a function of molecular weight (Figure 2.9). Peak assignments in the TWAXS data (Figure 2.9a & b) were made based on WAXS analysis of polymer thin films at 25 °C (see Figure 2.34 in Section 2.4.3). The reflection at 0.58 $Å^{-1}$ was ascribed to the second order lamellar spacing (L2) as a result of alkyl side chain interdigitation. Although the primary lamellar reflection (L1) was outside the measurable q-range for the TWAXS instrument, it was observed by thin film analysis (Figure S11). The position of the L1 reflection gave a spacing of 22.0 Å (Figure 2.9c) that was generally consistent with WAXS of PTVs[30,44] and crystalline hexadecane.[53] The reflections at 0.83 $Å^{-1}$ (7.6 Å) and 1.64 $Å^{-1}$ (3.8 Å) were attributed to the intra- and intermolecular side chain-to-side chain spacings (C), respectively. The somewhat broad

nature of these reflections was expected given the regiorandom nature of the polymer backbone. Finally, the reflection at 1.47 $Å^{-1}$ (4.3 Å) was assigned to the π-stack spacing (π) consistent with PTV literature.[34]

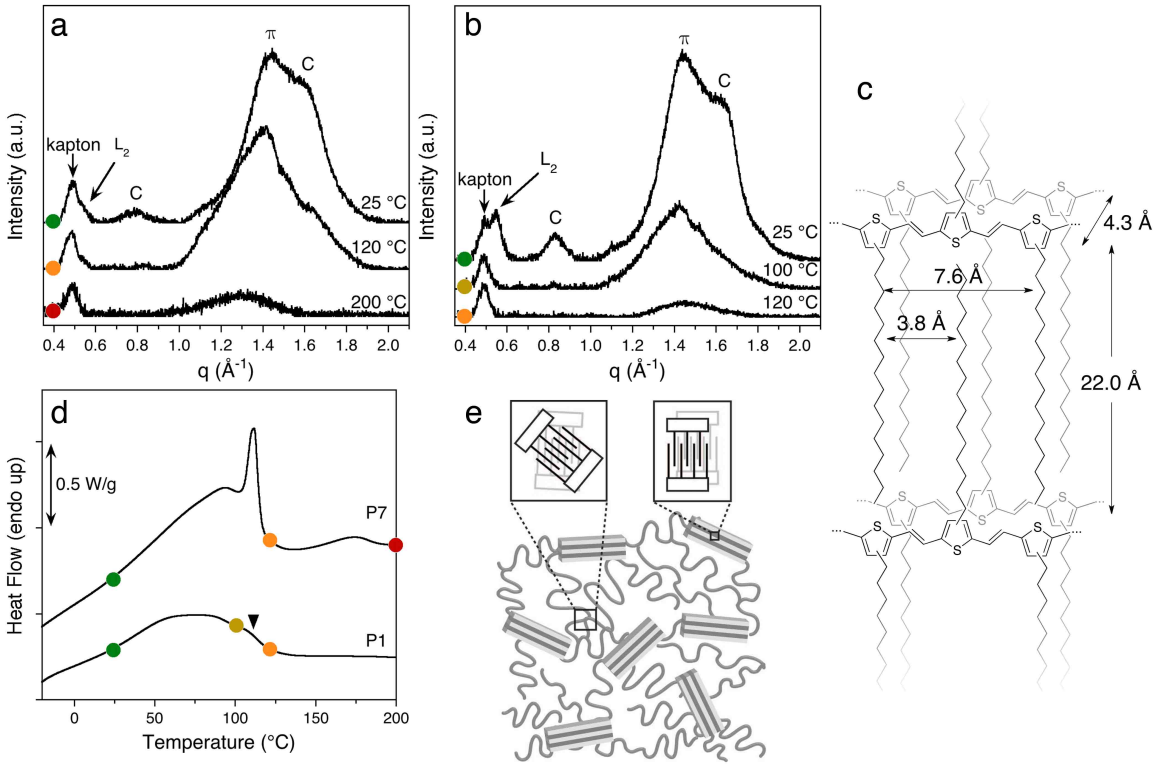

Figure 2.9

TWAXS patterns at various temperatures for (a) P7 and (b) P1. L2 is the second order lamellar reflection, C is both intra- and intermolecular chain-to-chain spacing, and π is the π- spacing. (c) Schematic illustration of C16-PTV crystalline domain with lamellar (22.0 Å), chain-to-chain (7.6, 3.8 Å), and π-stack spacings (4.3 Å) determined from WAXS. (d) DSC thermograms (heating, 10 °C/min) of P1 and P7. The arrowhead on P1 marks the shoulder due to π-stack melting. The colored circles indicate the TWAXS temperatures shown in (a) and (b). (e) Schematic illustration of C16-PTV microstructure with insets highlighting interdigitation in non-π-stacked (left) and π-stacked domains (right).

On heating P7 to 120 °C, the L2 and C reflections were significantly suppressed (Figure 2.9a) and at 200 °C the π-stack reflections were very weak. Three thermal

transitions were evident in the DSC thermogram of P7 (Figure 2.9d). The first, a broad transition centered on ca. 90 °C, was ascribed to the melting of alkyl side chains in non-π-stacked (disordered) polymer regions. The breadth of this transition suggested a large distribution in the degree of chain order (interdigitation).[54] The second sharper transition at 110 °C was ascribed to side chain melting in π-stacked (ordered) polymer regions. The absence of L2 and C reflections at 120 °C supports these DSC assignments. Figure 2.9e shows a schematic representation the two types of side chain environments. The transition at ca. 175 °C was assigned to the melting of polymer π-stacks, and is consistent with the diminished π-stack reflection at 200 °C. Based on literature precedent, we posit that the polymer is in a liquid crystalline state at temperatures above complete side chain melting (> 110 °C) and below melting of the π-stacks (ca. 175 °C).[55]

TWAXS (Figure 2.9b) and DSC (Figure 2.9d) data for the low molecular weight P1 were distinct from the corresponding data acquired for P7. L2 and C reflections for P1 were absent at 100 °C and near complete loss of the π-stack reflections was evident at 120 °C. From the DSC data, the broad transition attributed to side chain melting in more disordered regions of the polymer was centered at about 60 °C as compared to 90 °C for P7. Furthermore, in P1 there was no sharp transition corresponding to side chain melting in well-organized regions as observed at 110 °C for P7. Finally, the π-stack melting was about 65 °C lower than the corresponding melting transition in P7. Taken together, the higher transition temperatures for the higher molecular weight P7 suggest that increased molecular weight enhances the overall thermal stability of polymer crystallites. This enhancement in polymer ordering with molecular weight is consistent with observations from UV–vis spectroscopy (Figure 2.6c).

2.2.4 C16-PTV Hole Transport Properties

Field effect transistor measurements were employed to study the influence of

molecular weight on the hole transport of neat polymer films. P1–P6 exhibited transistor behavior with output curves (Figure 2.10a & b) displaying clear saturation behavior and very low hysteresis, and transfer curves (Figure 2.10c) showing ON/OFF ratios of 10^3 or greater and modest hysteresis. Hole mobility values were extracted from transfer curves of devices operated in the linear regime (i.e., transistor is "on" and gate bias exceeds the drain bias). In this regime the hole mobility may be calculated as follows:

$$\mu = \frac{L}{WC_{OX}V_D}\frac{\partial I_D}{\partial V_G}$$

Where L and W are the respective length and width of the conducting channel, C_{OX} is the capacitance of the gate dielectric, V_D is the applied drain bias, V_G is the swept gate bias, and I_D is the measured drain current.

Figure 2.10d plots FET hole mobilities against molecular weight, clearly showing that higher molecular weight allows for much more efficient hole transport. P1 (M_n = 6.0 kg/mol) exhibited a low FET mobility of only 3.1×10^{-5} cm^2/V·s, while P6 (M_n = 27.0 kg/mol), having a number average molecular weight over four times that of P1, showed well over a two order of magnitude increase in FET mobility (8.0×10^{-3} cm^2/V·s). This improvement in carrier mobility and transistor performance with increasing polymer molecular weight has been previously established.[14,56,57] P2 exhibited a hole mobility of 5.5×10^{-4} cm^2/V·s, consistent with the report of Kim et al. for hexyl substituted PTVs with a similar number of repeat units.[30]

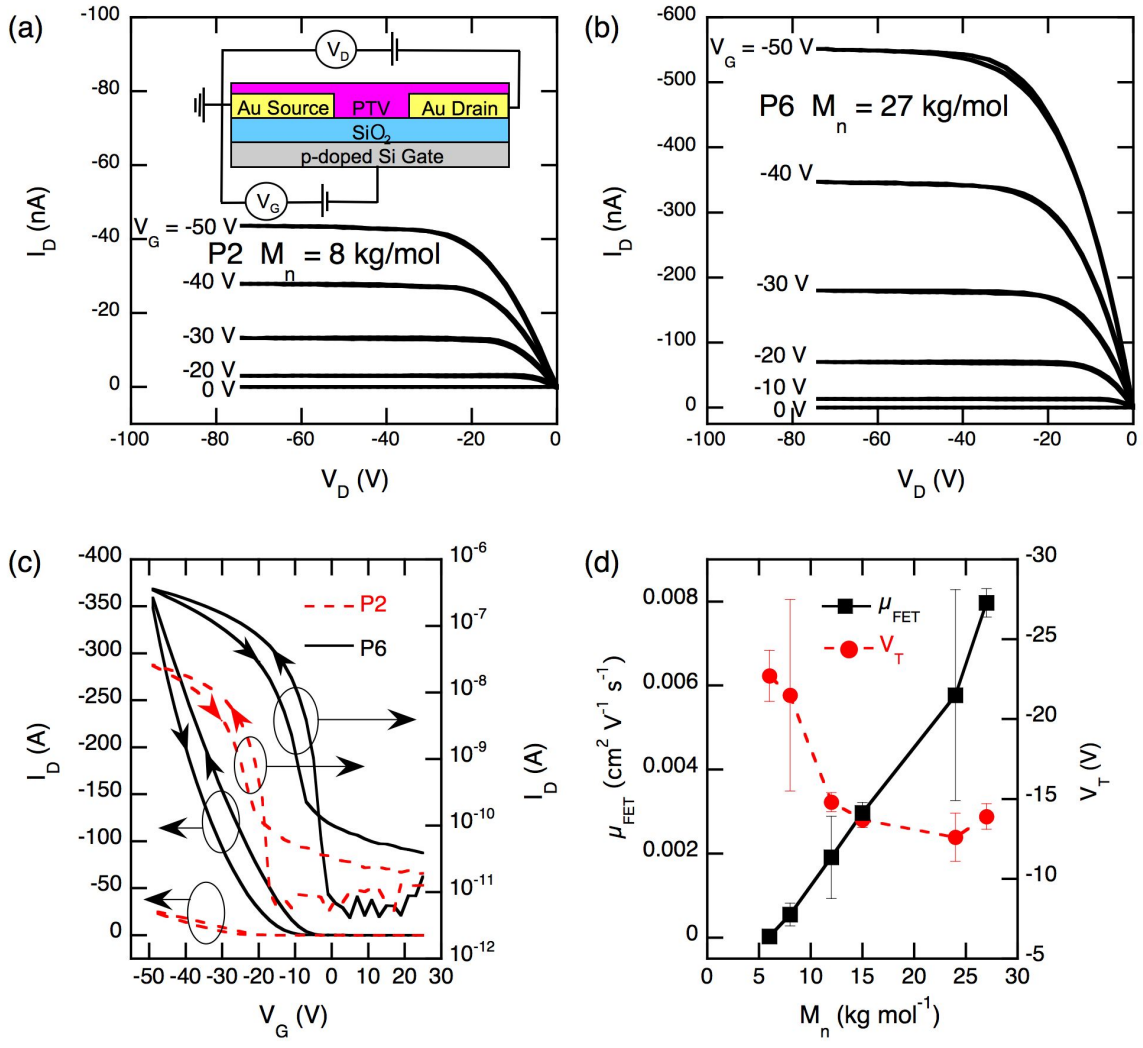

Figure 2.10.
Output curves of (a) P2 and (b) P6 FETs with VG varied from 0 to -50 V. Inset (a): device schematic. (c) Linear and semi-log transfer curves of P2 and P6 FETs with VD held at -10 V. (d) M_n dependence of FET hole mobility and threshold voltage of P1–P6 (error bars one standard deviation).

In addition to hole mobility dependence on molecular weight, FET measurements also revealed a molecular weight dependence on threshold voltage (V_T). Generally, increasing molecular weight leads to a less negative V_T, although this trend appeared to plateau for higher molecular weight (> 10 kg/mol). A large negative V_T is commonly

attributed to an increased trap density, implying that the low molecular weight samples have a higher trap density than the high molecular weight samples, which is also consistent with the mobility trend. Both the hole mobility and threshold voltage dependence on molecular weight are attributed to preferential ordering and increased electronic coupling, which is evident in the aggregation-induced vibronic structure in the solution and film UV–vis spectra (Figure 2.6).

2.2.5 C16-PTV Solar Cell Performance

PX:fullerene BHJ devices were fabricated in a basic ITO/PEDOT:PSS/PX:PCBM/Al structure (inset Figure 2.11a). Employing P7, the devices were optimized for maximum power conversion efficiencies (PCE) by varying thickness and active layer composition. Highest efficiencies were found for a P7:PCBM ratio of 1:4 and an active layer thickness of 100–150 nm. 17 devices incorporating ~150 nm thick 1:4 P7:PCBM blends gave a PCE of 0.80 ± 0.06%, short-circuit current densities (J_{sc}) of 3.32 ± 0.28 mA/cm^2, and open-circuit voltages (V_{oc}) of 0.40 ± 0.05 V under 100 mW/cm^2 simulated AM 1.5 spectrum. A high fill factor (FF) of 0.60 ± 0.03 implies good diode-like behavior. A device schematic and representative *J-V* curve are shown in Figure 2.11a. Likewise, *J-V* measurements carried out in the dark revealed good diode behavior with a rectification ratio of 1600 between +1 and -1 V shown in Figure 2.11b.

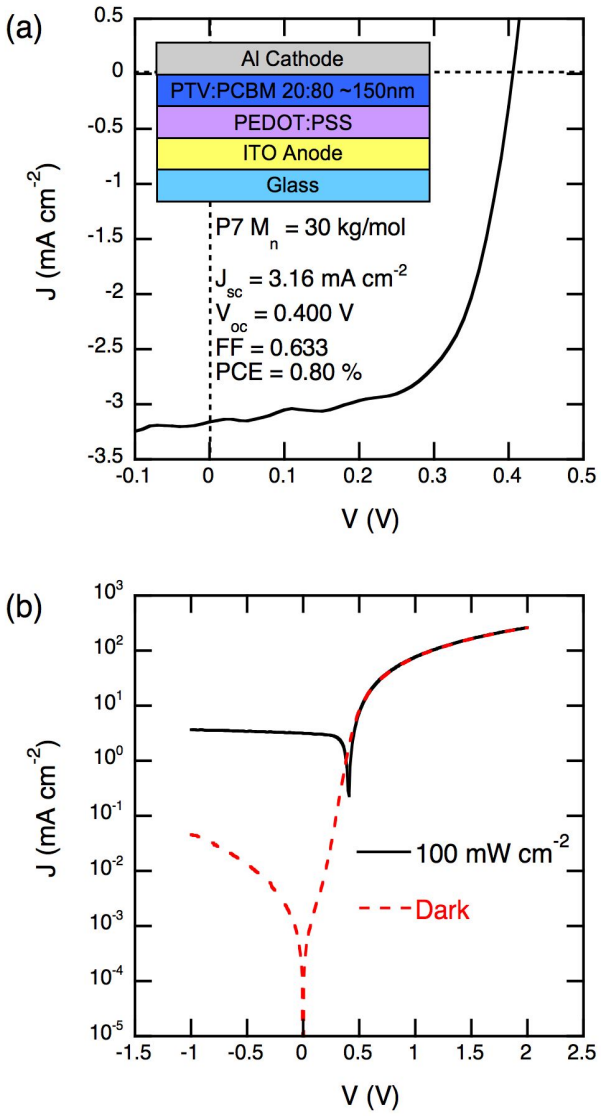

Figure 2.11
Optimized P7 PTV:PCBM 20:80 solar cell *J-V* characteristics under simulated AM 1.5 spectrum plotted on (a) a linear scale and (b) a semi-log scale with corresponding dark diode curve.

To investigate the polymer molecular weight effect on solar cell performance, a series of devices with ca. 100 nm thick 1:4 PX:PCBM active layers were tested. Figure 2.12a shows representative *J-V* curves for each of the polymers investigated, with the clearest

feature being the increase in photocurrent densities when going from P1 to P7. V_{oc} and FF (Figures 2.12b & c) showed weak molecular weight dependence, with V_{oc} decreasing slightly and FF increasing slightly with molecular weight. J_{sc} was strongly dependent on molecular weight (Figure 2.12b), with highest molecular weight devices showing roughly twice the J_{sc} of the lowest molecular weight devices. The strong J_{sc} dependence on molecular weight dominates overall device performance, thus the PCE dependence on molecular weight mirrors the J_{sc} dependence. The shunt and series resistance extracted from the dark diode curves did not display a clear dependence on PTV molecular weight.

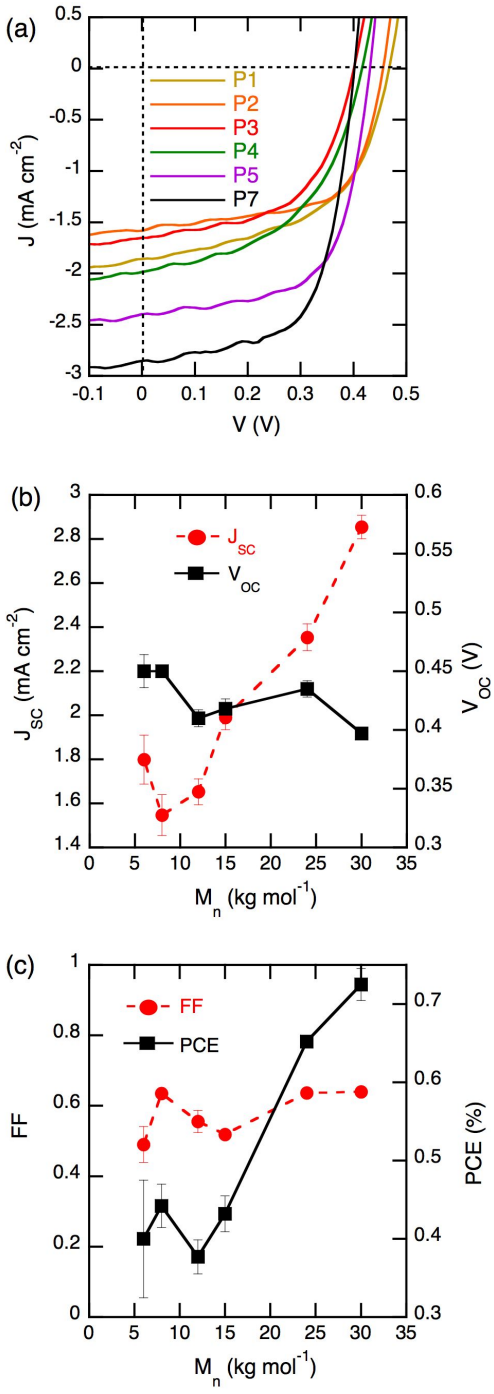

Figure 2.12

M_n dependence of ca. 100 nm thick PTV:PCBM 20:80 solar cells: (a) *J-V* characteristics, (b) J_{sc}, V_{oc}, (c) FF, and PCE of P1–P7 under simulated AM 1.5 spectrum.

The PCE variation with molecular weight correlated well with the hole mobility observations, suggesting that the transport of dissociated holes is a limiting factor in device performance. The PCE and mobility trends with molecular weight are also correlated with the thin film structure as assessed by UV–vis (Figure 2.13). That is, even in composite films containing 80 wt% PCBM there is still systematic evidence of increased aggregation (absorption shoulder ca. 680 nm) at high molecular weight that should favor enhanced hole mobility and thus higher J_{sc}.

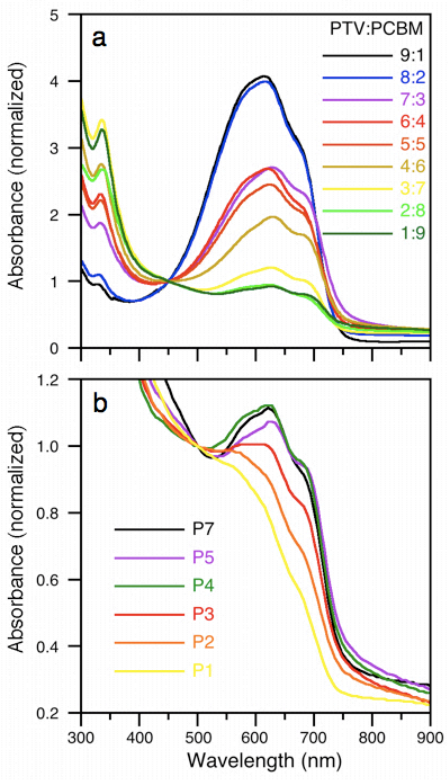

Figure 2.13
Thin film UV–vis spectra of (a) P7:PCBM containing 10–90% PCBM and (b) 1:4 PTV:PCBM using P1–P5 and P7.

One disadvantage of C16-PTV is its relatively weak light absorption, having an absorption coefficient of ca. 3.0×10^4 cm^{-1} at peak absorption (630 nm) (see Figure 2.35 in Section 2.4.3). This value is considerably lower than that of the benchmark polymer

regioregular P3HT,[58] which at peak absorption exceeds 1 × 10^5 cm^{-1}.[59,60] This low absorption of C16-PTV results in most absorption and exciton formation occurring on the PCBM, at optimum device compositions, and undermines the benefits of employing a low band gap material. This is born out in low external quantum efficiency (EQE) at wavelengths of polymer absorption, (Figure 2.14) and illustrates the need for PTV derivatives that absorb more light to achieve higher PCE. For example, PTVs incorporating carboxylate groups have shown photoluminescent behavior resulting in higher PCE ascribed to increased excited state lifetime.[39] Our work would suggest that increasing the molecular weight of such substituted PTVs would lead to significant increases in device performance.

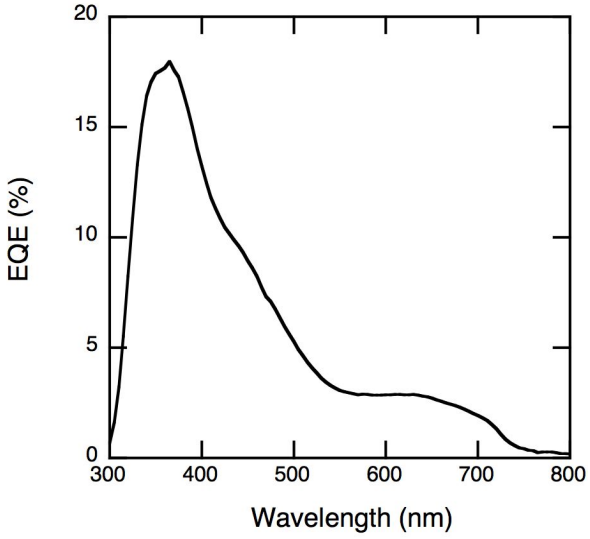

Figure 2.14
External quantum efficiency (EQE) of 1:4 P6:PCBM solar cell.

2.2.6 Phase Behavior & Morphology

In BHJ solar cells, the active layer phase behavior and morphology is of utmost importance, but only recently have polymer:PCBM temperature-composition phase

diagrams been proposed.[61,62] Several groups have since investigated the phase behavior of a variety of polymer:fullerene systems using various thermal, microscopy, and spectroscopy techniques.[63-67] While not strict equilibrium phase diagrams, these studies have provided practical morphology maps pertinent to the device fabrication and testing timescale. To assess the phase behavior of our active layer blends, DSC thermograms were collected for PTV:PCBM blends with varying composition and polymer molecular weight.

The effect of PCBM composition on thermal behavior was investigated using P7. Figure 2.15a shows second heating sweeps (0 to 300 °C) of P7:PCBM blends as a function of composition after initially heating the samples to 300 °C and cooling to 0 °C. At PCBM concentrations ≥ 30 wt% PCBM cold crystallization (150–200 °C) and melting transitions (250–290 °C) were observed. P7:PCBM blends displayed consistent PCBM melting transition temperatures independent of PTV concentration (Figure 2.15). These data indicate the presence of a pure crystalline PCBM phase in blends containing more than 30 wt% PCBM and dissolved PCBM in blends containing less than 30 wt% PCBM. The integrated area of the PCBM crystal melting peaks for each blend, relative to the peak areas of pure PCBM, gave the fraction of crystalline PCBM present. The fraction of a pure crystalline PCBM phase was determined at each composition by applying the lever rule.[61] By this analysis, PCBM was found to have a solubility limit of 27.5 ± 3.8 wt% in P7.

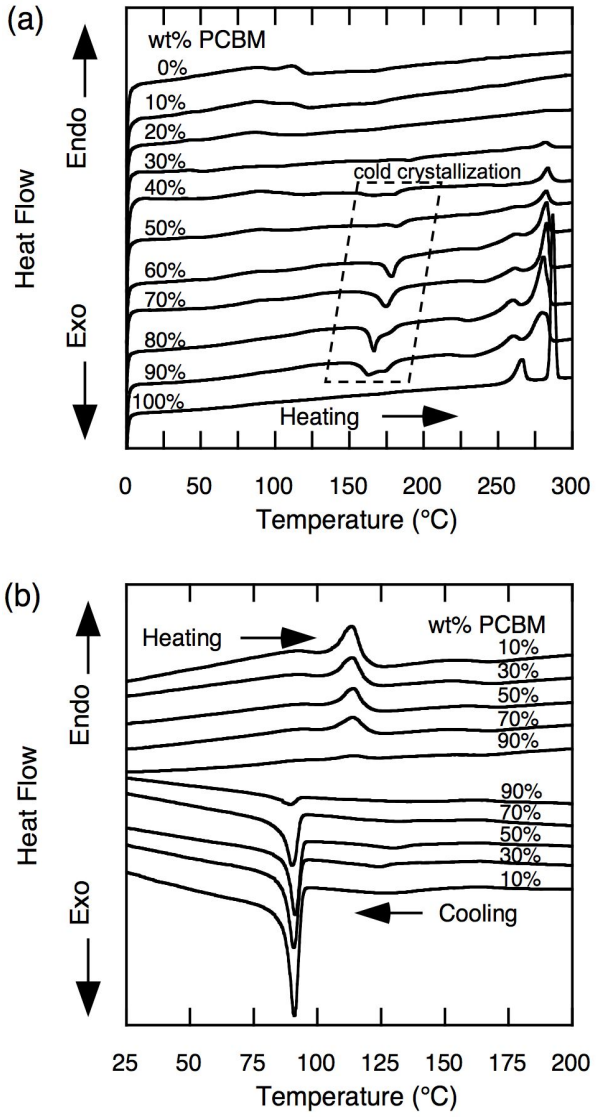

Figure 2.15

DSC thermograms of P7:PCBM at a scan rate of 10 °C/min: (a) second heating of blends up to 300 °C (above PCBM melting transition); (b) first cooling and second heating of blends heated to 225 °C (below PCBM melting transition).

When blends containing more than 30 wt% PCBM were heated to 300 °C no PCBM recrystallization was evident upon cooling at 10 °C/min. This lack of recrystallization was attributed to a quenching of the P7:PCBM blends in a glassy phase

upon cooling. This is further supported by the suppression (in enthalpy) of all (i.e., recrystallization and melting) PTV transitions. Cold crystallization (150–200 °C) of PCBM was observed during the second heating from 0 °C at 10 °C/min. This PCBM cold crystallization has been observed previously.[62-64,66] To substantiate the kinetic trapping of the blends in a glassy state, P7:PCBM blends were first cycled from 0 °C to 300 °C to 0 °C at 10 °C/min. The blends were then heated to 225 °C at 10 °C/min, above the temperature of PCBM cold crystallization. The following cooling to 0 °C and heating to 225 °C (both at 10 °C/min) demonstrated the recovery of PTV transitions.

To assess the polymer thermal behavior in the P7:PCBM blends, DSC thermograms were collected between 0 and 200 °C (Figure 2.15b), well below the PCBM melting transition. As shown, the polymer side chain melting (ca. 90 and 114 °C) and crystallization (90 °C) transitions characteristic of neat P7 were observed even at excessive polymer dilution. Similar behavior was observed at all polymer molecular weights (Figure 2.16). The lack of P7 melting point depression suggests the persistent presence of pure π-stacked domains regardless of PCBM composition, with any dissolved PCBM residing in non-π-stacked PTV domains. Due to the large overlap of the PCBM cold crystallization (ca. 150–200 °C) with the PTV π-stack melting (ca. 175 °C), the temperature of the π-stack transition in the P7:PCBM blends was not strictly assigned.

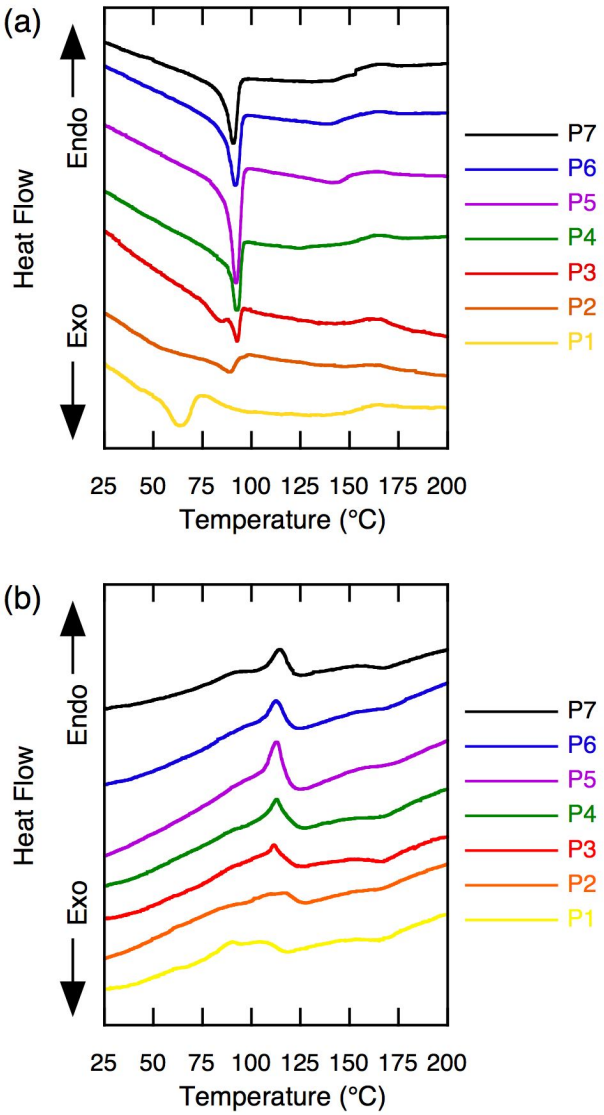

Figure 2.16
DSC thermograms of P1–P7 in 1:4 PTV:PCBM blends at a scan rate of 10 °C/min: (a) first cooling; (b) second heating.

The thermal and crystallographic data revealed the existence of several distinct regions of phase coexistence depending on temperature and composition (Figure 2.17 illustrations). Using the assigned polymer and PCBM melting transitions, in combination with neat PTV TWAXS and PCBM solubility calculations, a temperature-

composition morphology map was generated (Figure 2.17). This morphology map represents the phase behavior that is stable over timescales related to fabrication and characterization of these BHJ devices. Below the polymer side chain melting transitions and the PCBM solubility limit, there exists two-phases: non-π-stacked polymer/PCBM and π-stacked polymer crystallites, denoted as region 1 in Figure 2.17. Above the PCBM solubility limit, excess PCBM crystallizes creating a third phase of crystalline PCBM in addition to non-π-stacked polymer/PCBM and π-stacked polymer crystals, region 2. Above 114 °C and at PCBM compositions exceeding the solubility limit, the polymer side chains are completely melted resulting in liquid crystalline polymer, in equilibrium with a polymer/PCBM melt and crystalline PCBM, region 3. Above 114 °C and below the PCBM solubility limit there exists only liquid crystalline polymer and the polymer/PCBM melt, region 4. As evidenced by TWAXS, above 200 °C polymer π-stacking is disrupted resulting in a single melt for PCBM compositions below the solubility limit (labeled 'melt'). Above the PCBM solubility limit, PCBM crystallites are present in a polymer/PCBM melt, region 5. Finally, above ca. 280 °C, all components form a melt.

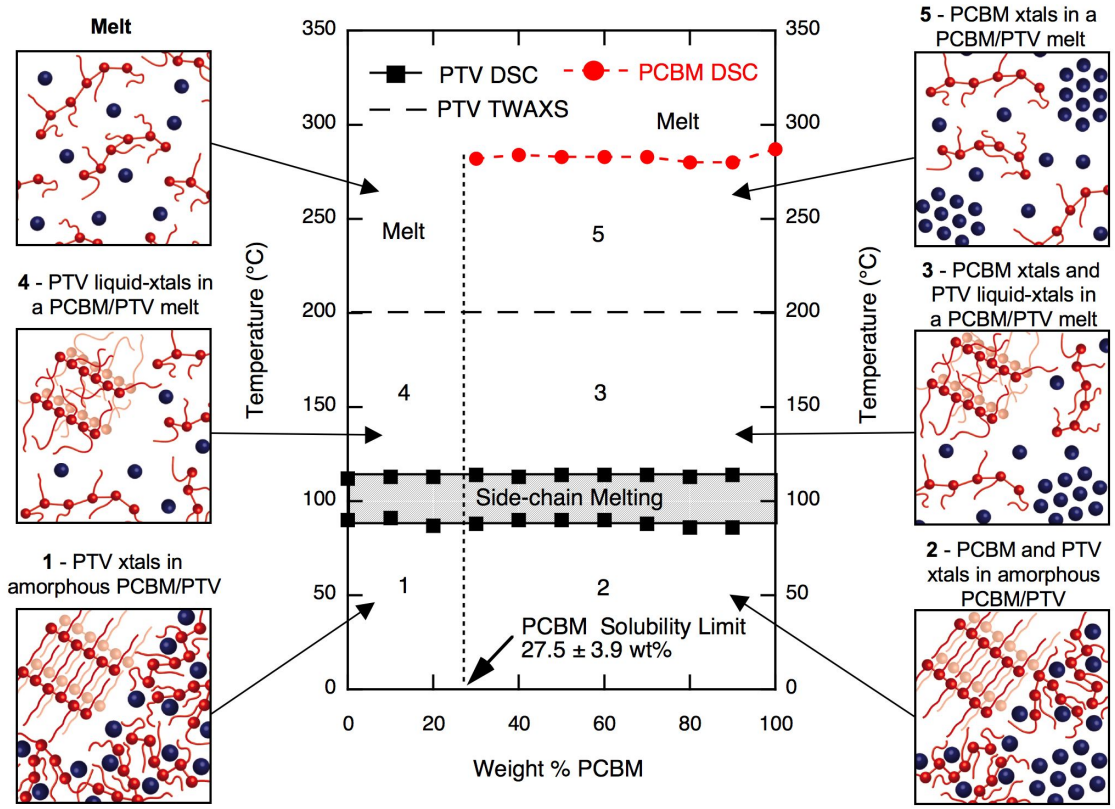

Figure 2.17
Temperature-composition morphology map for the P7:PCBM system with illustrations of the various regions of phase coexistence.

To assess the length scale of the phase separation, the morphology of active layer blends was investigated using AFM. Height and phase images of 20:80, 35:65, and 50:50 P7:PCBM samples prior to Al deposition were collected (Figure 2.18), with the phase images revealing the nanoscale segregation. A fast Fourier transform (FFT) analysis of the phase images was employed to estimate the length scale of the PTV/PCBM phase separation (Figure 2.18).[68,69] The FFT analysis revealed characteristic domain spacings on the order of several tens of nanometers, with the minimum domain spacing of ~50 nm in the 20:80 P7:PCBM sample decreasing to ~40 nm in the 35:65 sample, and further decreasing to ~30 nm in the 50:50 sample. Likewise, images were collected on a similar sample using low molecular weight P1 (20:80) (Figure 2.19). The P1 sample showed

similar PCBM segregation with a minimum domain size of ~35 nm, estimated from FFT. The existence of nanoscale segregation of the donor and acceptor materials is key as exciton diffusion lengths are on the order of 10 nm. The coarsening of the phase segregation with increasing PCBM concentration might be expected to lead to decreased photocurrent density and diminished device performance; however, the opposite is observed to be true. The optimum device active layer composition of 80 wt% PCBM reflects the importance of light absorption and exciton formation, which occurs predominantly on PCBM. Employing a PTV derivative with increased light absorption or photoluminescence would likely shift the optimum PCBM composition closer to the PCBM solubility limit.

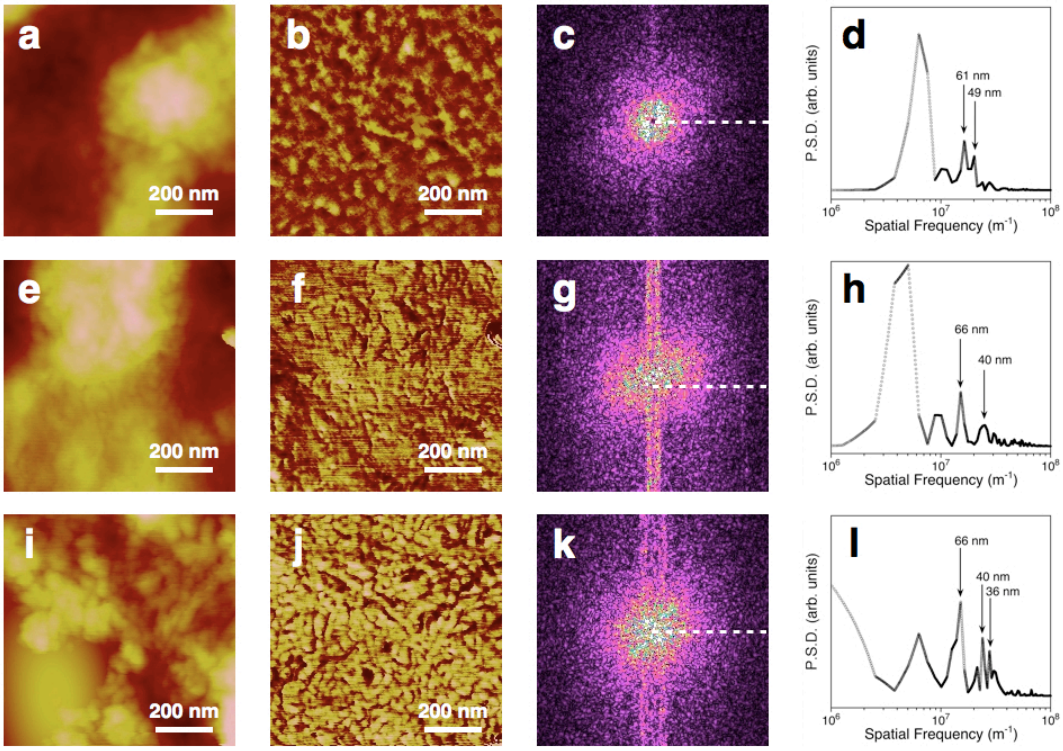

Figure 2.18

AFM (a, e, i) height and (b, f, j) phase images. (c, g, k) Fourier transform of AFM phase images and (d, h, l) P.S.D. plots. First, second, and third rows are P7:PCBM 20:80, 35:65, and 50:50 blends, respectively.

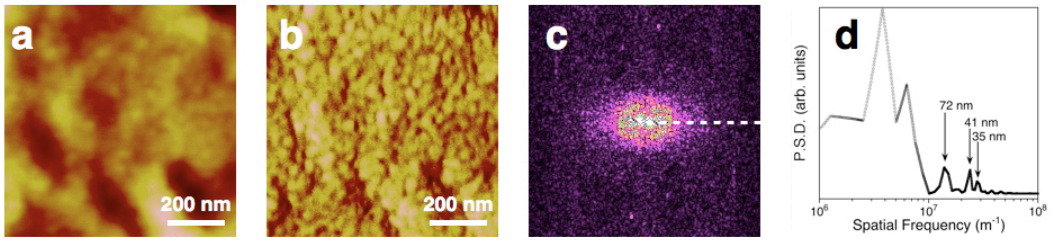

Figure 2.19
AFM (a) height and (b) phase images of 1:4 P1:PCBM. (c) Fourier transform of AFM phase image and (d) P.S.D. plot.

2.3 Conclusions

A series of well-defined C16-PTVs was prepared using ADMET polymerization and integrated in BHJ OPVs for a systematic molecular weight investigation. By varying the monomer *Z*:*E* ratio, using a more active catalyst (G3), and optimizing polymerization conditions a broad range of molecular weights (6–30 kg/mol) was accessed. PCE increased with chain length, reaching a maximum efficiency of 0.80% with P7, which was predominantly the result of an enhanced J_{sc}. This observation was corroborated by FET results, which showed a molecular weight dependent increase in hole mobility brought on by enhanced polymer aggregation. A DSC-based temperature-composition morphology map was also constructed giving a PCBM solubility limit of ca. 28%. We consider this phase behavior to be paramount in assigning the long-term stability of C16-PTV:PCBM films.

ADMET has proven useful in the controlled synthesis of PTVs and has made fundamental molecular weight and phase behavior studies possible. We believe that studies of this nature will contribute to the basic understanding of conjugated polymer behavior and will lead to the development of improved devices and efficiencies. Furthermore, the optimization of polymerization conditions demonstrated herein provides a framework for new CPs prepared by ADMET and opens the door to

additional synthetic studies. Such studies are discussed in subsequent chapters.

2.4 Experimental Details

2.4.1 Materials and Methods

Commercially available solvents and reagents were purchased and used as received from Aldrich and Acros. Degassed THF was purified by passage through an activated alumina column and collected in flame-dried, air-free flasks. All reactions were run under argon or vacuum using standard Schlenk techniques. Poly(3,4-ethylenedioxythiophene):poly(styrenesulfonate) (PEDOT:PSS, Clevios P VP AI 4083) aqueous dispersion and [6,6]-phenyl-C61-butyric acid methyl ester (PCBM) were purchased from Heraeus Materials Technology (West Conshohocken, PA) and American Dye Source (Baie-d'Urfé, Quebec) respectively. A complete description of the characterization techniques employed is available in Appendix A.

2.4.2 Synthetic Details

Scheme 2.3

Synthesis of M1–M5.

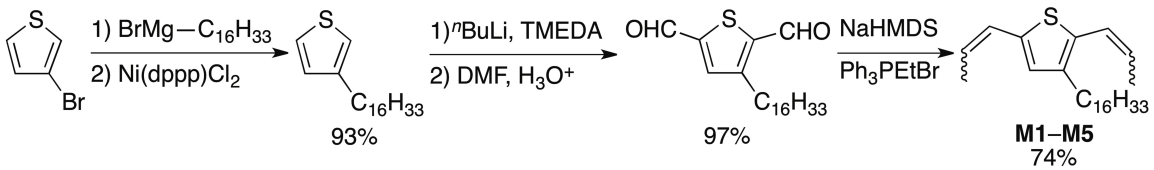

Synthesis of 3-hexadecylthiophene. A 250 mL 3-neck round bottom flask was equipped with a magnetic stir bar, reflux condenser, glass stopcock, liquid addition funnel, and two

rubber septa. Magnesium turnings (3.3 g, 136.5 mmol) were added and the apparatus was flame-dried under vacuum. Anhydrous THF (ca. 125 mL) was transferred via cannula into the flask followed by the addition of 1,2-dibromoethane (ca. 0.5 mL) to activate the magnesium. A solution of 1-bromohexadecane (20.0 mL, 65.5 mmol) in anhydrous THF (ca. 25 mL) was added to the liquid addition funnel via syringe and dripped into the Mg/THF mixture over the course of 20 min. Stirred at room temperature under argon for 2 h. The Grignard solution was transferred via cannula into a second flame-dried flask containing a magnetic stir bar, 3-bromothiophene (5.1 mL, 54.6 mmol), 1,3-bis(diphenylphosphino)propane nickel (II) chloride [Ni(dppp)Cl_2] (0.60 g, 1.1 mmol), and anhydrous THF (ca. 25 mL) held at 0°C. The reaction was stirred under argon for 16 h. Reaction was quenched with 1 M NH_4HCO_3 (ca. 50 mL), H_2O (ca. 75 mL) was added, and extracted with diethyl ether (2 × 75 mL). The combined organics were washed with H_2O, saturated $NaHCO_3$, and brine (ca. 75 mL each) before drying over Na_2SO_4. The solvent was removed under reduced pressure. The remaining residue was dissolved in minimal amount of THF (ca. 15 mL) and precipitated into MeOH (ca. 250 mL, 0 °C). The product was filtered and dried under vacuum overnight to give an off-white solid (15.6 g, 93%). ^{1}H NMR (500 MHz, $CDCl_3$): δ_H (ppm) = 7.23 (dd, 1H, *J* = 4.80, 3.22 Hz, Th-*H*5), 6.93 (d, 1H, *J* = 4.93 Hz, Th-*H*4), 6.91 (d, 1H, *J* = 2.20 Hz, Th-*H*2), 2.61 (t, 2H, *J* = 7.71 Hz, –CH_2–), 1.61 (quintet, 2H, *J* = 7.34, –CH_2–), 1.25 (bs, 26H, –CH_2–), 0.90 (t, 3H, *J* = 6.89 Hz, –CH_3). ^{13}C NMR (125 MHz, $CDCl_3$): δ_C (ppm) = 143.5 (Th-*C*3), 128.5 (Th-*C*4), 125.2 (Th-*C*5), 119.9 (Th-*C*2), 32.6, 30.8, 30.5, 29.9, 29.8, 29.7, 29.6 (2), 22.9 (–*C*$H_2$$CH_3$), 14.4 (–*C*$H_3$). HRGC-MS (EI): $M_{calcd.}$ = 308.2538, M_{found} = 308.2555. Anal. calcd. for $C_{20}H_{36}S$: C 77.85, H 11.76, S 10.39; Found: C 78.64, H 11.96, S 9.23.

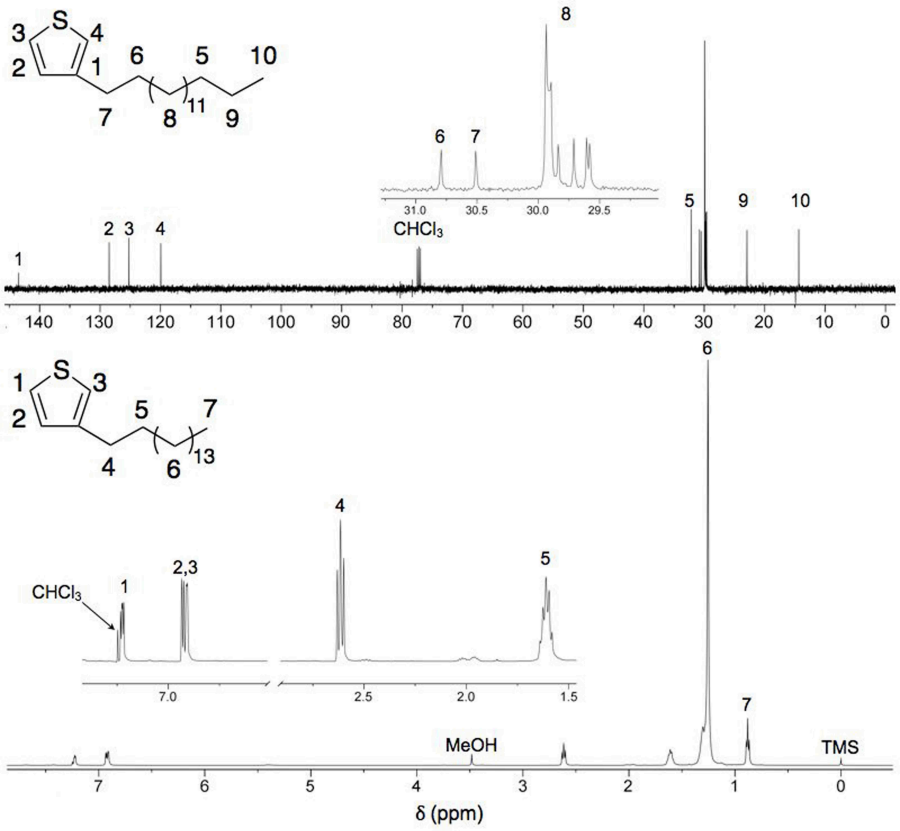

Figure 2.20
^{13}C and ^{1}H NMR spectra of 3-hexadecylthiophene in $CDCl_3$.

Synthesis of 2,5-dicarbaldehyde-3-hexadecylthiophene. A 3-neck 500 mL round bottom flask was equipped with a magnetic stir bar, reflux condenser, glass stopcock, liquid addition funnel, and two rubber septa. The apparatus was flame-dried under vacuum and 3-hexadecylthiophene (10.0 g, 32.4 mmol) was added as a solid under argon purge. Anhydrous hexanes (ca. 200 mL) were transferred via cannula into the flask followed by N,N,N',N'-tetramethylethylenediamine (TMEDA) (12.1 mL, 81.0 mmol) addition via syringe. A 2.5 M solution of *n*-butyllithium in hexanes (32.4 mL, 81.0 mmol) was added to the liquid addition funnel via syringe. The *n*-butyllithium was added to the solution of 3-hexadecylthiophene, TMEDA, and hexanes over the course of 20 min. The solution was refluxed for 1 h following addition. Anhydrous THF (ca. 100 mL) was added to the

flask and cooled to 0 °C on an ice bath, at which point anhydrous N,N'-dimethylformamide (DMF) (10.0 mL, 29.6 mmol) was added via syringe. The reaction was stirred for 1 h before adding 1 M HCl (ca. 150 mL) to quench. The aqueous phase was extracted with diethyl ether (2 × 75 mL), and the combined organics were washed with H_2O (ca. 100 mL) and brine (ca. 100 mL). The solution was dried over Na_2SO_4 and the solvent was removed under reduced pressure to give an orange-brown oil that solidified on standing (11.1 g, 94%). The product was used without further purification. ^{1}H NMR (300 MHz, $CDCl_3$): δ_H (ppm) = 10.14 (s, 1H, Th-5C*H*O), 9.97 (s, 1H, Th-2C*H*O), 7.65 (s, 1H, Th-*H*4), 3.00 (t, 2H, *J* = 7.68 Hz, –CH_2–), 1.70 (quintet, 2H, *J* = 7.46 Hz, –CH_2–), 1.25 (bs, 26H, –CH_2–), 0.88 (t, 3H, *J* = 6.70 Hz, –CH_3). ^{13}C NMR (125 MHz, $CDCl_3$): δ_C (ppm) = 183.7 (–*C*HO), 183.3 (–*C*HO), 152.3 (Th-*C*3), 148.1 (Th-*C*5), 143.6 (Th-*C*2), 137.5 (Th-*C*4), 31.5, 30.0–29.9 (m), 29.8, 29.6 (2), 29.5, 28.8, 23.0 (–*C*$H_2$$CH_3$), 14.4 (–*C*$H_3$). HRGC-MS (EI): $M_{calcd.}$ = 364.2436, M_{found} = 364.2409. Anal. calcd. for $C_{22}H_{36}O_2S$: C 72.48, H 9.95, O 8.78, S 8.79; Found: C 73.47, H 10.10, O 8.00, S 8.22.

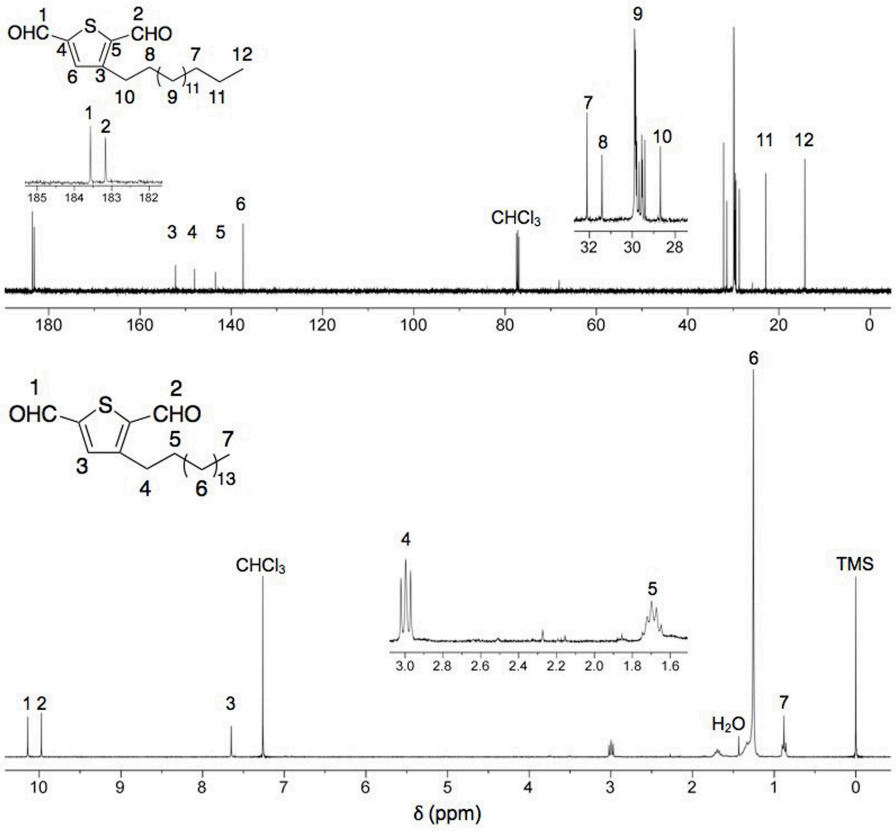

Figure 2.21
^{13}C and ^{1}H NMR spectra of 2,5-dicarbaldehyde-3-hexadecylthiophene in $CDCl_3$.

Synthesis of 2,5-dipropenyl-3-hexadecylthiophene (M1–M5). A 2-neck 500 mL round bottom flask was equipped with a magnetic stir bar, reflux condenser, glass stopcock, and rubber septum. The apparatus was flame dried under vacuum before adding sodium bis(trimethylsilyl)amide (10.5 g, 57.5 mmol) and (ethyl)triphenylphosphonium bromide (21.3 g, 57.5 mmol) under an argon purge. The apparatus was placed under reduced pressure for 30 minutes to dry the solids. Anhydrous hexanes (ca. 300 mL) was transferred into the flask and refluxed for 1 h under argon to form the Wittig reagent (bright orange-red solution). The reaction was cooled to -78 °C on acetone/dry ice bath and the hexanes were removed with a cannula taking care not to remove precipitated Wittig reagent. The cold hexanes wash was repeated with another 300 mL. Residual

hexanes were removed under vacuum and anhydrous THF (ca. 300 mL) was added to dissolve the remaining Wittig reagent. This solution was transferred via cannula into a 500 mL round bottom flask containing anhydrous THF (ca. 100 mL) and 2,5-dicarbaldehyde-3-hexadecylthiophene (10.0 g, 27.4 mmol) held at 0 °C. The reaction was stirred for 30 min. before filtering off $Ph_3P{=}O$. The filtrate was concentrated under reduced pressure to give a dark brown residue, which was dissolved in an ether:hexanes (10:90) solution (ca. 500 mL) and flushed through a silica gel plug to remove residual $Ph_3P{=}O$. The eluent was concentrated and dissolved in hexanes before flushing through a second silica gel plug. The solvent was removed under reduced pressure to give a yellow oil that solidified on standing. The oil was dissolved in THF (ca. 30 mL) and precipitated into MeOH (ca. 300 mL) at -78 °C. The precipitation procedure was repeated and the pale yellow solid was dried under vacuum overnight (8.0 g, 75%). Highest *Z*:*E* from ^{1}H NMR was 83:17. ^{1}H NMR (500 MHz, $CDCl_3$): δ_H (ppm) = 6.76, 6.67, 6.62 (s, 1H, Th-*H*4 isomers), 6.54–6.37 (m, 2H, Th–C*H*=CH–CH_3), 6.07–5.90 (*E*), 5.70–5.58 (*Z*) (m, 2H, Th–CH=C*H*–CH_3), 2.56–2.49 (m, 2H, –CH_2–), 1.98 (*Z*), 1.85 (*E*) (m, 6H, Th–CH=CH–CH_3), 1.54 (m, 2H, –CH_2–), 1.25 (bs, 26H, –CH_2–), 0.88 (t, 3H, *J* = 6.95 Hz, –CH_3). ^{13}C NMR (125 MHz, $CDCl_3$): δ_C (ppm) = 141.3, 141.1, 140.7, 139.1, 138.6, 134.2, 132.0, 130.1, 129.3, 126.4, 125.4, 125.1, 124.8, 124.5 (2), 124.4, 124.1, 123.6, 123.5, 123.1, 121.6 (aromatic and olefinic *C*s), 32.3, 31.1, 30.0 (3), 29.9, 29.8 (2), 29.7 (2), 23.0, 19.0, 18.7, 15.5 (3), 14.5 (aliphatic *C*s). HRGC-MS (EI): $M_{calcd.}$ = 388.3164, M_{found} = 388.3159. Anal. calcd. for $C_{26}H_{44}S$: C 80.34, H 11.41, S 8.25; Found: C 81.35, H 11.39, S 7.45.

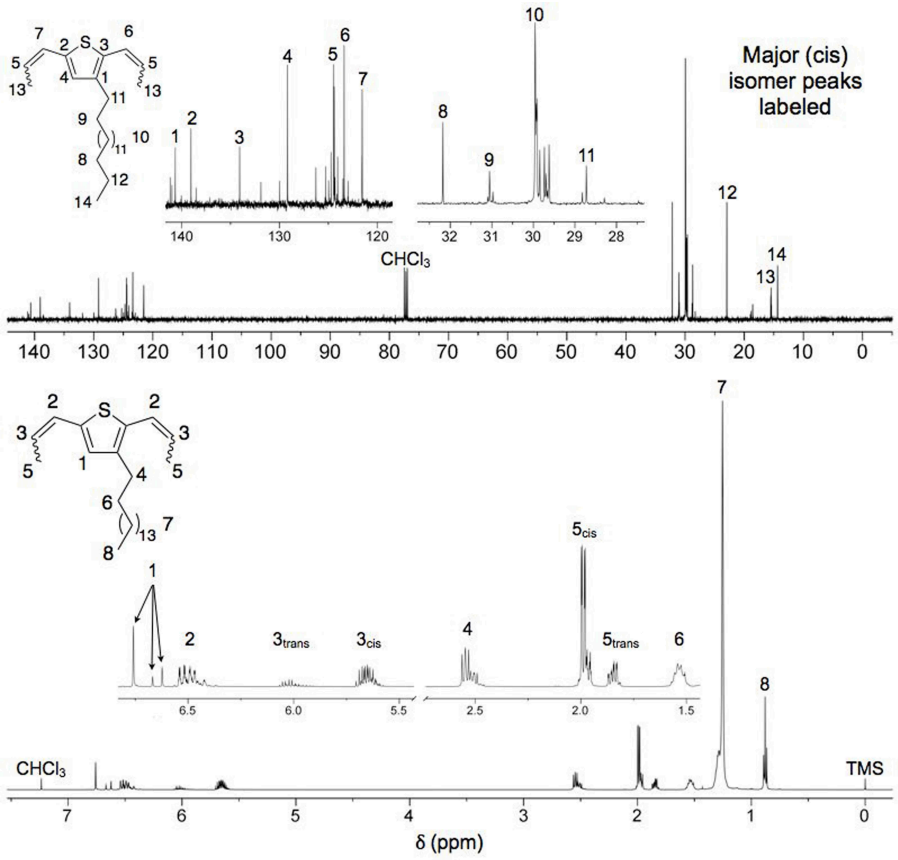

Figure 2.23
^{13}C and ^{1}H NMR spectra of 2,5-dipropenyl-3-hexadecylthiophene.

General synthetic procedure for C16-PTV (P7). An apparatus like that shown in Figure 2.24 was assembled and flame-dried under vacuum. The Schlenk tube was charged with **M5** (1.0 g, 2.57 mmol, *Z*:*E* = 83:17) in a solution of anhydrous 1,2,4-trichlorobenzene (TCB) (15 mL, ca. 0.17 M). The solution was heated to 80 °C and dynamic vacuum was applied for 15 min. to remove oxygen. The flask was placed under an argon atmosphere and G3 (23.0 mg, 0.0257 mmol) was added as a solution in TCB (0.5 mL, ca. 0.05 M). Dynamic vacuum was reapplied. Polymerization progress was observed by color change (yellow→orange→red→purple→dark blue). After 96 h the polymer was precipitated into a 20-fold excess of acetone held at 0 °C and filtered through a Soxhlet thimble. The polymer was purified by Soxhlet extraction with acetone (ca. 100 mL) and chloroform (ca.

100 mL). The chloroform fraction was concentrated to ~10 mL under reduced pressure and precipitated in 20-fold excess of acetone (0 °C). The polymer was filtered and dried under vacuum to obtain the target material as a black solid (0.70 g, 82%). ^{1}H NMR (500 MHz, $CDCl_3$): δ_H (ppm) = 7.00–6.80 (m, 2H, olefinic *H*s), 6.78 (bs, 1H, Th-*H*4), 6.44 (m, *E* end group Th–C*H*=CH–CH_3), 6.01 (m, *E* end group Th–CH=C*H*–CH_3), 2.62 (bs, 2H, –CH_2–), 2.19 (m, *E* end group Th–CH=CH–CH_3), 1.60 (bs, 2H, –CH_2–), 1.25 (bs, 26H, –CH_2–), 0.87 (t, 3H, *J* = 6.80 Hz, –CH_3). SEC ($CHCl_3$, 1 mL/min, RI): M_n = 33.3 kg/mol, M_w = 72.5 kg/mol, PDI = 2.17. Anal. calcd. for $C_{22}H_{36}S$: C 79.45, H 10.91, S 9.64; Found: C 79.67, H 11.07, S 9.46.

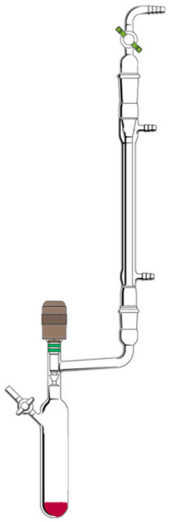

Figure 2.24
ADMET polymerization apparatus.

C16-PTV (P1). M1 (0.50 g, 1.3 mmol, *Z:E* = 47:53) in TCB (6 mL). Added G3 (11.5 mg, 0.013 mmol) in TCB (1 mL) and polymerized for 16 h before workup (0.29 g, 67%).

C16-PTV (P2). M1 (0.30 g, 0.77 mmol, *Z*:*E* = 47:53) in TCB (4 mL). Added G3 (7.0 mg, 0.0077 mmol) in TCB (1 mL) and polymerized for 24 h before workup (0.19 g, 73%).

C16-PTV (P3). M2 (0.30 g, 0.77 mmol, *Z*:*E* = 67:33) in TCB (5 mL). Added G3 (7.0 mg, 0.0077 mmol) in TCB (1 mL) and polymerized for 20 h before workup (0.22 g, 85%).

C16-PTV (P4). M3 (0.30 g, 0.77 mmol, *Z*:*E* = 82:18) in TCB (5 mL). Added G3 (7.0 mg, 0.0077 mmol) in TCB (1 mL) and polymerized for 24 h before workup (0.25 g, 96%).

C16-PTV (P5). M4 (0.30 g, 0.77 mmol, *Z*:*E* = 81:19) in TCB (5 mL). Added G3 (7.0 mg, 0.0077 mmol) in TCB (1 mL) and polymerized for 27 h before workup (0.23 g, 88%).

C16-PTV (P6). M5 (0.50 g, 1.29 mmol, *Z*:*E* = 83:17) in TCB (6 mL). Degassed with three freeze-pump-thaw cycles before adding G3 (11.0 mg, 0.0129 mmol) in TCB (0.5 mL). Polymerized for 48 h before workup (0.40 g, 93%).

2,5-dibromo-3-hexadecylthiophene. A 200 mL round bottom flask was flame dried and equipped with a magnetic stirring bar. 3-hexadecylthiophene (5.0 g, 16.2 mmol) and 100 mL THF were added. The flask was sealed with a rubber septum and purged with argon. The solution was cooled to 0 °C and N-bromosuccinimide (recrystallized, 5.91 g, 33.2 mmol) was added. The flask was covered with aluminum foil, allowed to warm to room temperature, and stirred under argon for 48 h. Residual bromine was quenched by the addition of 50 mL saturated $NaHSO_3$. The phases were separated and the aqueous phase

was extracted with 100 mL diethyl ether. The combined organics were dried over Na_2SO_4 and the solvent was removed by rotary evaporation. The residue was dissolved in 10 mL THF and precipitated in 100 mL methanol. The pale yellow solid was isolated by filtration and dried under vacuum (7.15 g, 95%). ^{1}H NMR (500 MHz, $CDCl_3$): δ_H = 6.77 (s, 1H), 2.50 (t, *J* = 7.7 Hz, 2H), 1.52 (quintet, *J* = 7.5 Hz, 2H), 1.26 (s, 26H), 0.88 (t, *J* = 7.0 Hz, 3H). ^{13}C NMR (125 MHz, $CDCl_3$): δ_C = 143.3, 131.3, 110.6, 108.2, 32.3, 29.99, 29.92, 29.88, 29.82, 29.72, 29.5, 23.1, 14.5.

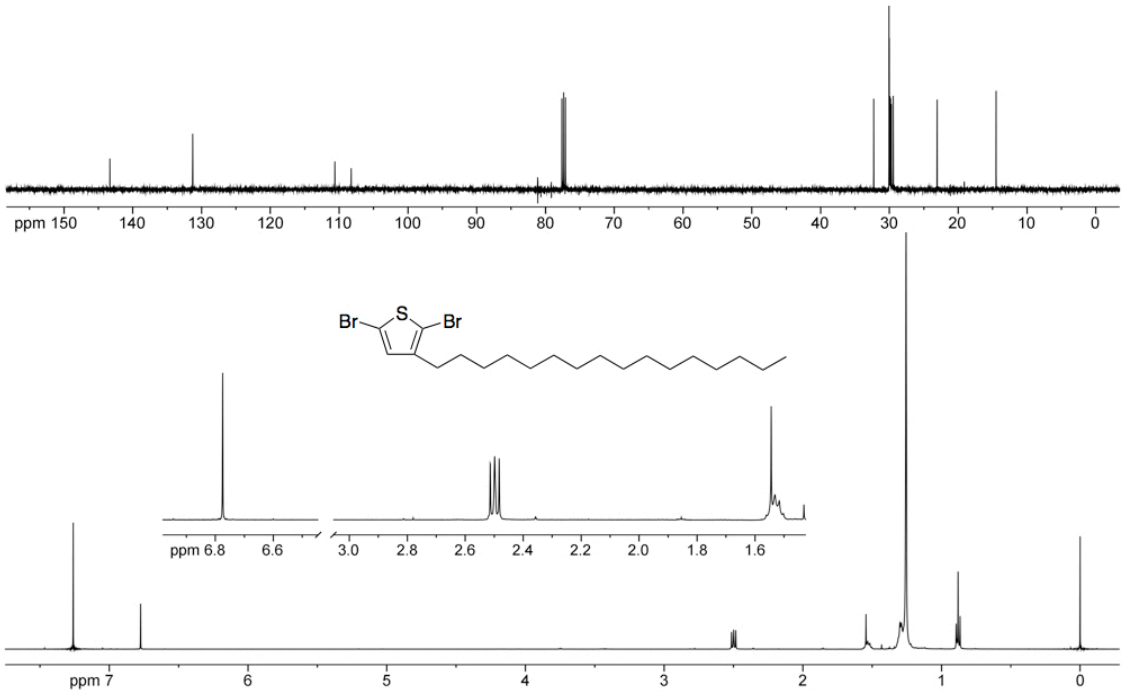

Figure 2.25
^{1}H and ^{13}C NMR spectra of 2,5-dibromo-3-hexadecylthiophene.

3-hexadecyl-2,5-di(prop-1-yn-1-yl)thiophene. A 100 mL reaction flask was equipped with a magnetic stirring bar and sealed with a rubber septum. The flask was flame dried and placed under argon before adding 1-bromo-1-propene (2.4 mL, 27.5 mmol) and 20 mL anhydrous THF via syringe. The solution was cooled to -78 °C on an acetone/dry ice bath before carefully adding *n*-butyllithium (2.5 M hexanes, 22.8 mL, 56.8 mmol) via

syringe. The reaction became cloudy and was stirred for 2 h. A second 100 mL 2-neck round bottom flask was equipped with a magnetic stirring bar, rubber septum, reflux condenser, and stopcock. Added $ZnBr_2$ (5.8 g, 25.8 mmol) and flame dried. Anhydrous THF (20 mL) was added to dissolve $ZnBr_2$ followed by the solution from the first flask. Heat evolved and the reaction was stirred for an additional 20 min before adding 2,5-dibromo-3-hexadecylthiophene (4.0 g, 8.6 mmol) in 20 mL anhydrous THF. Tetrakis(triphenylphosphine)palladium(0) (1.0 g, 0.86 mmol) was added as a solid under positive argon pressure. The solution turned yellow and the reaction was stirred for 20 h at 60 °C under argon. The brown-green solution was cooled to room temperature before pouring into 250 mL of 1 M HCl. The organics were separated and the aqueous phase was extracted with diethyl ether (3 × 100 mL). The combined organics were dried over Na_2SO_4 and the solvent was removed by rotary evaporation. Column chromatography with hexanes afforded pure product as a light yellow solid (3.2 g, 97%). ^{1}H NMR (500 MHz, $CDCl_3$): δ_H = 6.82 (s, 1H), 2.57 (t, J = 7.6 Hz, 1H), 2.09 (s, 3H), 2.05 (s, 3H), 1.55 (quintet, J = 7.5 Hz, 2H), 1.25 (s, 26H), 0.88 (t, J = 7.0 Hz, 3H).

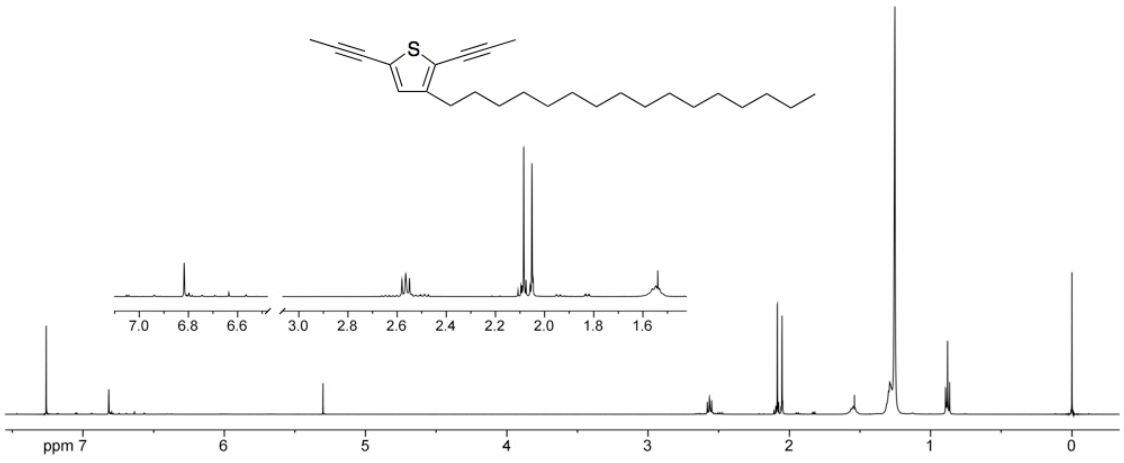

Figure 2.26
^{1}H NMR spectrum of 3-hexadecyl-2,5-di(prop-1-yn-1-yl)thiophene.

3-hexadecyl-2,5-di((*Z*)-prop-1-en-1-yl)thiophene. A 2-neck 100 mL round bottom flask was equipped with a magnetic stirring bar and two rubber septa. The flask was flame dried with a nitrogen purge before adding Lindlar's catalyst (5% Pd on $CaCO_3$, 275 mg, 0.13 mmol), quinolone (185 μL, 1.6 mmol), 3-hexadecyl-2,5-di(prop-1-yn-1-yl)thiophene (1.0 g, 2.6 mmol), and 40 mL hexanes. The suspension was degassed with argon for 10 minutes before bubbling hydrogen (using balloon) for 30 minutes. The reaction was stirred at room temperature under a hydrogen atmosphere for 24 h at which point ^{1}H NMR confirmed complete conversion. The solution was filtered through a plug of silica gel with hexanes. The solvent was removed by rotary evaporation. The resultant yellow oil was dissolved in 5 mL THF and precipitated in 200 mL MeOH at 0 °C. Filtered and dried under vacuum to give an off-white solid (0.58 g, 58%). ^{1}H NMR (300 MHz, $CDCl_3$): δ_H = 6.77 (s, 1H), 6.51 (ddd, *J* = 13.3, 11.6, 1.7 Hz, 2H), 5.67 (dt, *J* = 11.5, 7.4 Hz, 2H), 2.55 (t, *J* = 7.7 Hz, 2H), 2.01 (d, *J* = 1.7 Hz, 3H), 1.98 (d, *J* = 1.7 Hz, 3H), 1.52 (quintet, *J* = 5.5 Hz, 2H), 1.25 (s, 26H), 0.88 (t, *J* = 6.7 Hz, 3H). ^{13}C NMR (125 MHz, $CDCl_3$): δ_C = 152.6, 144.4, 139.0, 129.0, 126.0, 125.5, 121.5, 32.0, 30.69, 30.54, 29.74, 29.66, 29.53, 29.41, 22.7, 14.2.

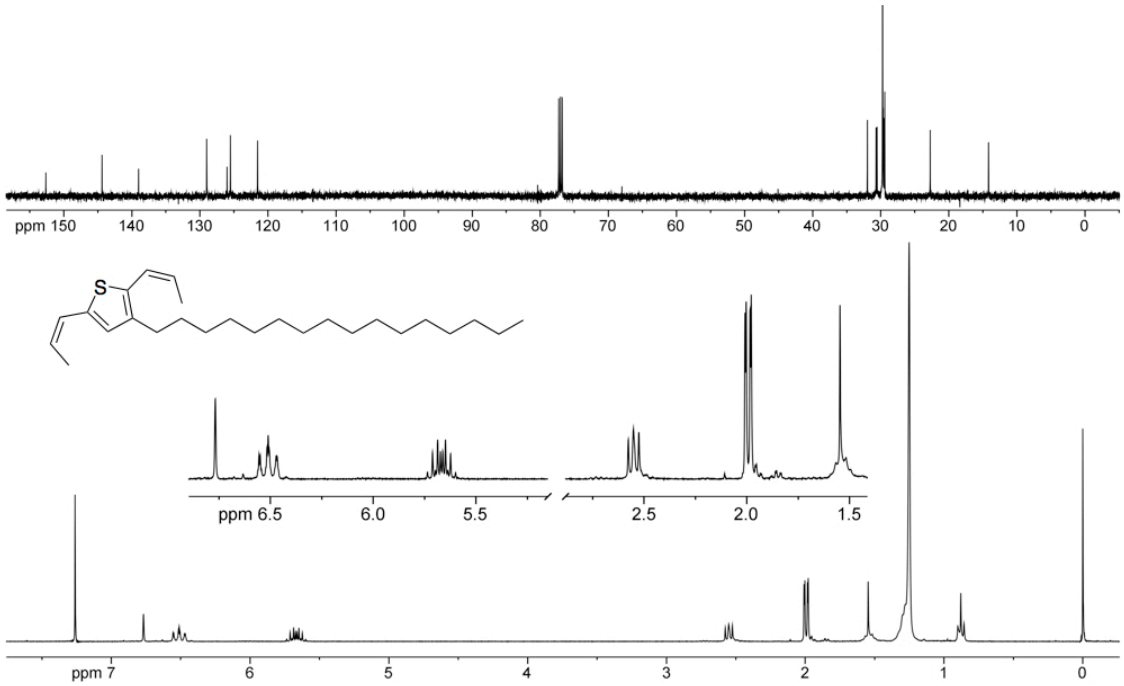

Figure 2.27
^{1}H and ^{13}C NMR spectra of 3-hexadecyl-2,5-di((*Z*)-prop-1-en-1-yl)thiophene.

Polymerization of 3-hexadecyl-2,5-di((*Z*)-prop-1-en-1-yl)thiophene. The same polymerization procedure outlined above was used. Solution turned brown-yellow immediately after catalyst addition and no reaction (polymerization) was observed.

2,5-dibromo-3-hexylthiophene. A 500 mL round bottom flask was equipped with a magnetic stirring bar. 3-hexylthiophene (16.5 mL, 91.5 mmol) and 250 mL THF were added. The flask was sealed with a rubber septum and purged with argon while cooling to 0 °C. N-bromosuccinimide (34.2 g, 192.2 mmol) was added in one portion. The flask was covered with aluminum foil, allowed to warm to room temperature, and stirred under argon for 48 h. Residual bromine was quenched with 50 mL saturated $NaHSO_3$. The organic phase was separated and washed with 100 mL 1 M HCl. The combined aqueous phases were extracted with 200 mL diethyl ether. The combined organics were washed

with water and brine and dried over Na_2SO_4. The solvents were removed by rotary evaporation and the residue was dissolved in hexanes and flushed through a plug of silica gel to remove succinimide. The solvent was removed by rotary evaporation and the remaining liquid was vacuum distilled (85 °C, 50 mtorr) twice to afford pure product as a pale yellow liquid (27.9 g, 94%). ^{1}H NMR (300 MHz, $CDCl_3$): δ_H = 6.78 (s, 1H), 2.50 (t, *J* = 7.6 Hz, 2H), 1.51 (quintet, *J* = 7.4 Hz, 2H), 1.29 (s, 6H), 0.89 (t, *J* = 6.6 Hz, 3H).

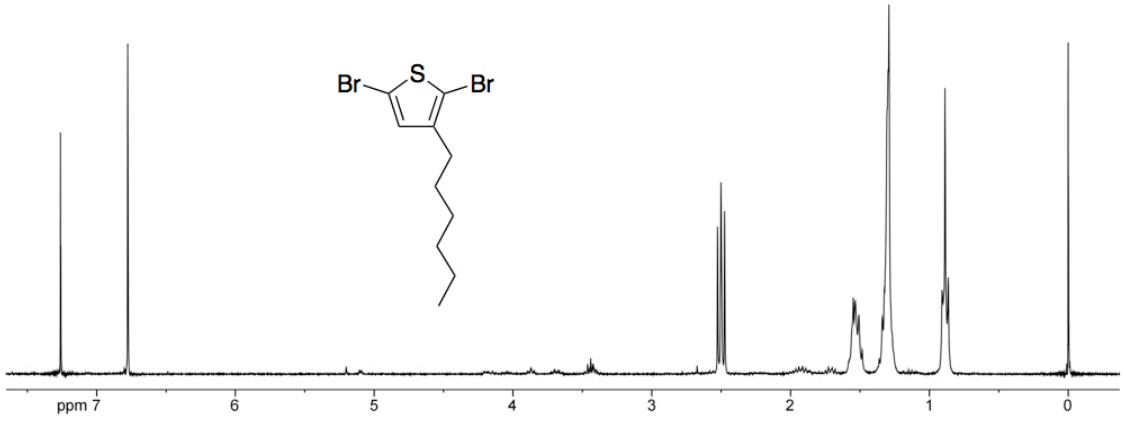

Figure 2.28
^{1}H NMR spectrum of 2,5-dibromo-3-hexylthiophene.

3-hexyl-2,5-di(prop-1-yn-1-yl)thiophene. The same procedure used for 3-hexadecyl-2,5-di(prop-1-yn-1-yl)thiophene was followed. The product was isolated as a clear oil (0.73 g, 97%). ^{1}H NMR (300 MHz, $CDCl_3$): δ_H = 6.82 (s, 1H), 2.57 (t, *J* = 7.6 Hz, 2H), 2.09 (s, 2H), 2.05 (s, 2H), 1.54 (quintet, *J* = 7.0 Hz, 2H), 1.29 (s, 6H), 0.88 (t, *J* = 6.6 Hz, 3H).

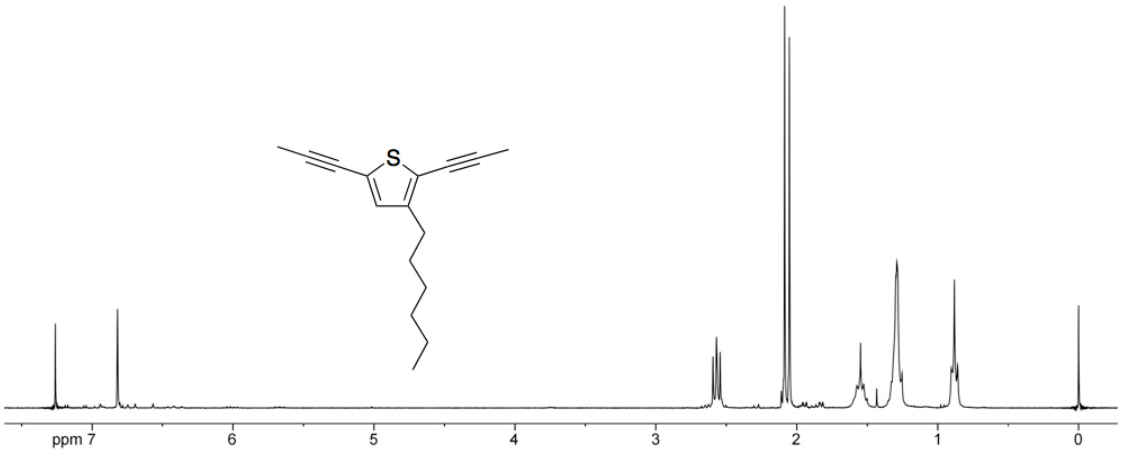

Figure 2.29
^{1}H NMR spectrum of 3-hexyl-2,5-di(prop-1-yn-1-yl)thiophene.

3-hexyl-2,5-di((*Z*)-prop-1-en-1-yl)thiophene. The same procedure used for 3-hexadecyl-2,5-di((*Z*)-prop-1-en-1-yl)thiophene was followed. The reaction was allowed to proceed for 120 h. The product was isolated as a clear oil by Kugelrohr distillation (0.32 g, 43%). ^{1}H NMR (500 MHz, $CDCl_3$): δ_H = 6.77 (s, 1H), 6.55-6.47 (m, 2H), 5.71-5.62 (m, 2H), 2.55 (t, *J* = 7.7 Hz, 2H), 2.00 (d, *J* = 1.7 Hz, 3H), 1.99 (d, *J* = 1.7 Hz, 3H), 1.57-1.51 (m, 2H), 1.29 (s, 6H), 0.88 (t, *J* = 6.9 Hz, 3H).

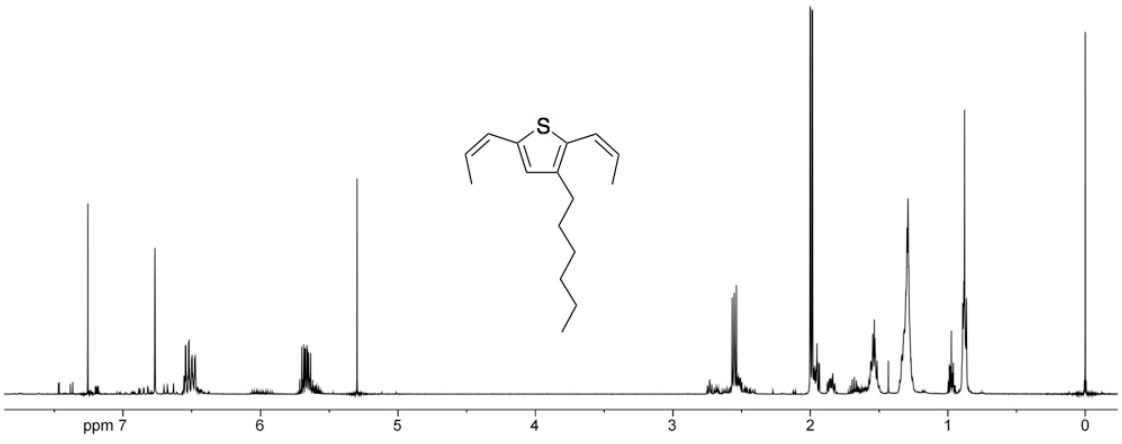

Figure 2.30
^{1}H NMR spectrum of 3-hexyl-2,5-di((*Z*)-prop-1-en-1-yl)thiophene.

Polymerization of 3-hexyl-2,5-di((*Z*)-prop-1-en-1-yl)thiophene. The same polymerization procedure outlined above was used. The reaction was quenched with 0.5 mL ethyl vinyl ether after 42 h. The polymer was precipitated from 150 mL acetone (0 °C) and transferred to a soxhlet thimble. The polymer was extracted with acetone overnight and into $CHCl_3$. The $CHCl_3$ fraction was concentrated under reduced pressure. The residual polymer was stirred in boiling acetone for 1 h before filtering (32 mg, 42%). ^{1}H NMR (500 MHz, $CDCl_3$): δ_H = 6.92 (m, 2H), 6.78 (s, 1H), 2.62 (s, 2H), 1.61 (s, 2H), 1.35 (s, 6H), 0.92 (s, 3H). SEC ($CHCl_3$, 1 mL/min) M_n = 4.2 kg/mol, M_w = 5.1 kg/mol, $Đ$ = 1.2.

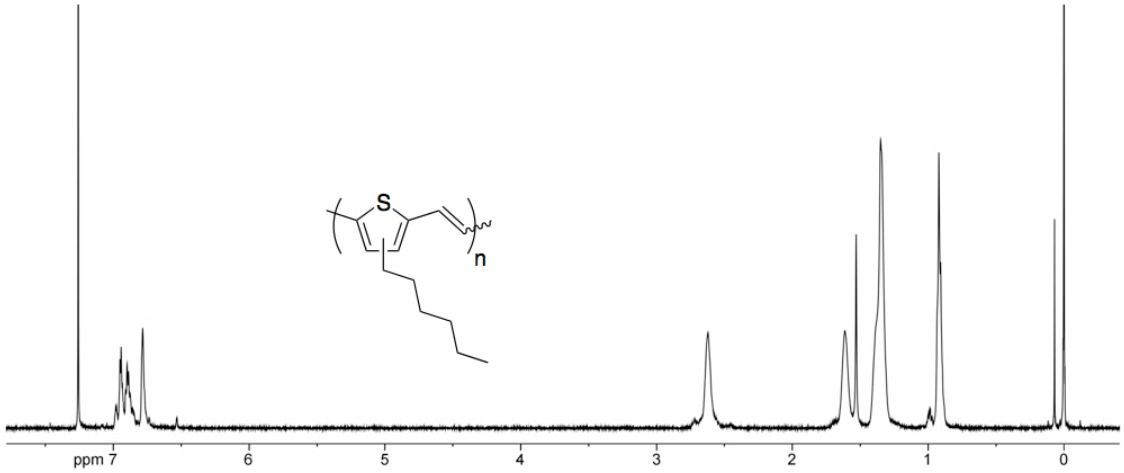

Figure 2.31

^{1}H NMR spectrum of C6-PTV.

3-hexadecyl-2,5-di((*E*)-prop-1-en-1-yl)thiophene. A 50 mL reaction flask was equipped with a magnetic stirring bar and septum before flame drying. Ethyltriphenylphosphonium bromide (2.03 g, 5.5 mmol) was added under positive argon pressure and was dried under high vacuum for 10 min. Anhydrous THF (5 mL) was added via syringe followed by the slow addition of phenyllithium (1.8 M in butyl ether, 3.05 mL, 5.5 mmol). The reaction turned red-brown. The reaction was stirred for 20 min and cooled to -78 °C using a dry ice/acetone bath. 3-hexadecylthiophene-2,5-

dicarbaldehyde (1.0 g, 2.7 mmol) was slowly added as a solution in 5 mL anhydrous diethyl ether. The reaction was allowed to warm to -40 °C and stirred for 20 min. Phenyllithium (3.05 mL, 5.5 mmol) was again added and the red-brown color returned. The reaction was allowed to warm to -30 °C and stirred for 20 min. 1 M HCl in ether (5.5 mL, 5.5 mmol) was slowly added to the reaction followed by the addition of potassium *tert*-butoxide (0.83 g, 7.4 mmol). The reaction was warmed to room temperature and stirred for 90 min at which point it was dark purple-red in color. The reaction was quenched by pouring into 30 mL H_2O. The aqueous phase was extracted with CH_2Cl_2 (3 × 30 mL). The combined organics were washed with brine and dried over Na_2SO_4. The solvent was removed by rotary evaporation. The residue was flushed through a plug of silica gel using hexanes. The hexanes were removed by rotary evaporation and the residue was purified further by dissolving in THF (5 mL) and precipitating in 150 mL methanol (0 °C). The bright yellow product was filtered and dried under vacuum (0.48 g, 45%). ^{1}H NMR (500 MHz, $CDCl_3$): δ_C = 6.54 (s, 1H), 6.43 (ddd, *J* = 37.3, 15.5, 1.7 Hz, 2H), 5.95 (ddq, *J* = 17.2, 15.5, 6.7 Hz, 2H), 2.48 (t, *J* = 7.7 Hz, 2H), 1.84 (ddd, *J* = 11.6, 6.7, 1.6 Hz, 6H), 1.50 (quintet, *J* = 7.4 Hz, 2H), 1.25 (s, 26H), 0.88 (t, *J* = 7.0 Hz, 3H).

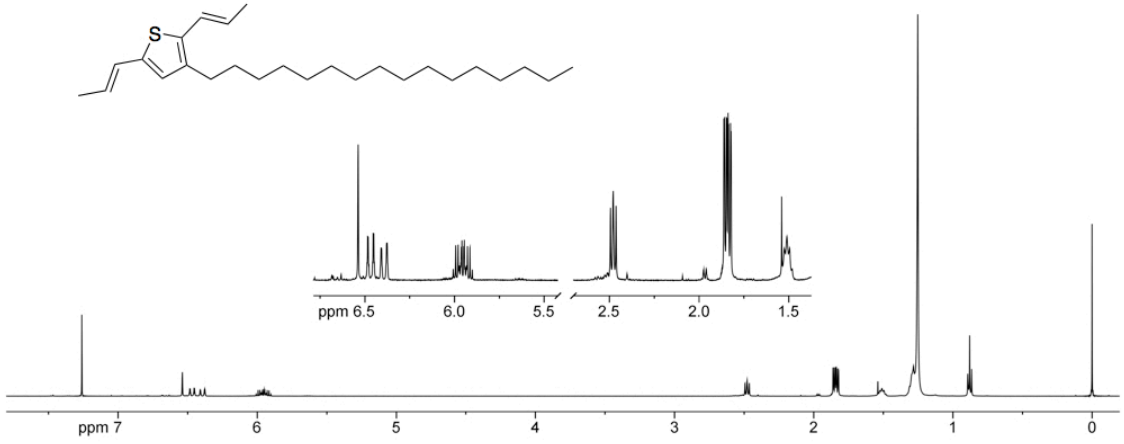

Figure 2.32
^{1}H NMR spectrum of 3-hexadecyl-2,5-di((*E*)-prop-1-en-1-yl)thiophene.

Polymerization of 3-hexadecyl-2,5-di((*E*)-prop-1-en-1-yl)thiophene. The same polymerization procedure **outlined** above was used. Solution turned brown-yellow immediately after catalyst addition and no reaction (polymerization) was observed.

2.4.3 Additional Data and Details

^{1}H NMR Molecular Weight Analysis

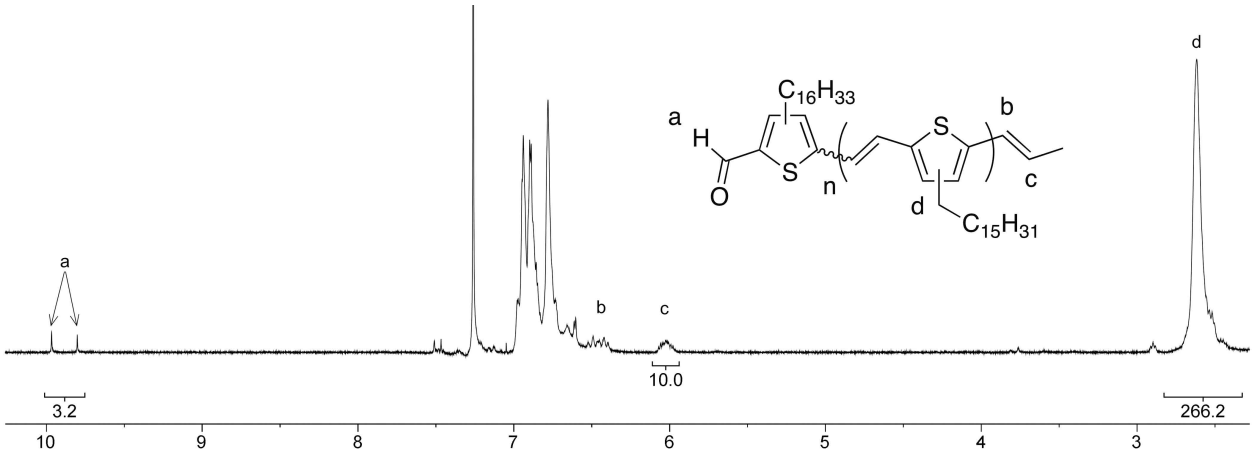

Figure 2.33.
^{1}H NMR spectrum of P1 highlighting end group and repeat unit integrals. Integral values are arbitrary.

Propenyl (c) and aldehyde (a) end groups, when compared to main chain resonances, can be used to quantify polymer conversion. The aldehyde resonances were propenyl groups before reaction with oxygen, and though unreactive, are still counted as chain ends. At 0% conversion the propenyl and α-methylene integrals are 1:1, and at 50% conversion they are 1:2. Following this trend and assuming no converted monomer is lost during workup, conversion (p) can be determined by dividing the end group integrals by repeat unit integrals (d).

$$p = 1 - \frac{a+c}{d} = 1 - \frac{13.2}{266.2} = 0.95$$

ADMET is a step polymerization, and as such, molecular weight estimation is made possible by the Carothers equation (Odian, G. *Principles of Polymerization*; John Wiley & Sons, Inc.: Hoboken, NJ, 2004; pp 50–79.) In this case it is assumed that **G3** acts as a monofunctional contaminant that limits molecular weight. From this the stoichiometric imbalance (r) can be calculated using the monomer:catalyst mole ratio (100:1) where N_A refers to the total number of reactive groups (2 per monomer) and N_B refers the monofunctional impurity (**G3**). The coefficient of 2 in front of N_B is necessary because one catalyst molecule has the same quantitative effect as one monomer molecule.

$$r = \frac{N_A}{N_A + 2N_B} = \frac{200}{200 + 2} = 0.99$$

Combining p and r into the Carothers equation for stoichiometric imbalance gives the predicted number-average degree of polymerization (X_n).

$$X_n = \frac{1+r}{1+r-2rp} = \frac{1.99}{1.99 - 2(0.99)(0.95)} = 18$$

Multiplying X_n by the repeat unit molecular weight (M_0), and neglecting end groups, gives the number-average molecular weight (M_n).

$$M_n = X_n \times M_0 = 18 \times 332.59\ g \cdot mol^{-1} = 6.0\ kg \cdot mol^{-1}$$

WAXS Analysis of C16-PTVs

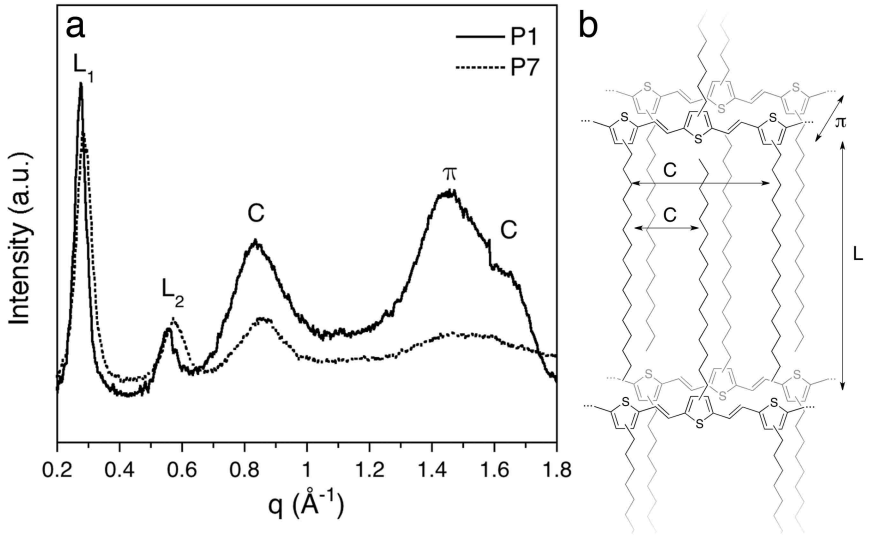

Figure 2.34

(a) WAXS of **P1** and **P7** as thin films on quartz substrates. (b) Schematic illustration of crystalline C16-PTV domain. L refers to lamellar spacing, C to chain-to-chain, and π to π-stack.

Determination of C16-PTV Absorption Coefficient

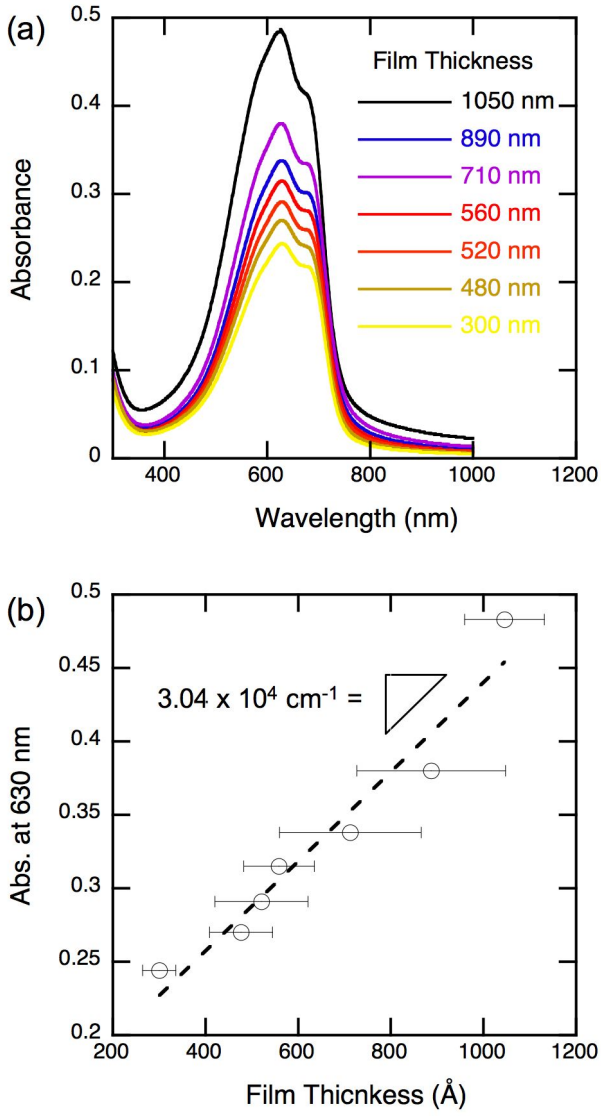

Figure 2.35

(a) UV-Vis spectra of **P6** films with various thickness and (b) plot of absorbance vs. film thickness as λ = 630 nm from which absorption coefficient was extracted.

2.5 References

[1] Günes, S.; Neugebauer, H.; Sariciftci, N. S. *Chem. Rev.* **2007**, *107*, 1324–1338.

[2] Thompson, B. C.; Fréchet, J. M. J. *Angew. Chem. Int. Ed.* **2008**, *47*, 58–77.

[3] Heeger, A. J. *Chem. Soc. Rev.* **2010**, *39*, 2354–2371.

[4] Service, R. F. *Science* **2011**, *332*, 293.

[5] Shaheen, S.; Brabec, C.; Sariciftci, N. S.; Padinger, F.; Fromherz, T.; Hummelen, J. C. *Appl. Phys. Lett.* **2001**, *78*, 841–843.

[6] Chen, H.-Y.; Hou, J.; Zhang, S.; Liang, Y.; Yang, G.; Yang, Y.; Yu, L.; Wu, Y.; Li, G. *Nat. Photonics* **2009**, *3*, 649–653.

[7] Liang, Y.; Xu, Z.; Xia, J.; Tsai, S.-T.; Wu, Y.; Li, G.; Ray, C.; Yu, L. *Adv. Mater.* **2010**, *22*, E135-E138.

[8] Price, S. C.; Stuart, A. C.; Yang, L.; Zhou, H.; You, W. *J. Am. Chem. Soc.* **2011**, *133*, 4625–4631.

[9] Zhou, H.; Yang, L.; Stuart, A. C.; Price, S. C.; Liu, S.; You, W. *Angew. Chem. Int. Ed.* **2011**, *50*, 2995–2998.

[10] Chu, T.-Y.; Lu, J.; Beaupré, S.; Zhang, Y.; Pouliot, J.-R.; Wakim, S.; Zhou, J.; Leclerc, M.; Li, Z.; Ding, J.; Tao, Y. *J. Am. Chem. Soc.* **2011**, *133*, 4250–4253.

[11] Veldman, D.; Meskers, S. C. J.; Janssen, R. A. J. *Adv. Funct. Mater.* **2009**, *19*, 1939–1948.

[12] Zen, A.; Pflaum, J.; Hirschmann, S.; Zhuang, W.; Jaiser, F.; Asawapirom, U.; Rabe, J. P.; Scherf, U.; Neher, D. *Adv. Funct. Mater.* **2004**, *14*, 757–764.

[13] Schilinsky, P.; Asawapirom, U.; Scherf, U.; Biele, M.; Brabec, C. J. *Chem. Mater.* **2005**, *17*, 2175–2180.

[14] Kline, R. J.; McGehee, M. D.; Kadnikova, E. N.; Liu, J.; Fréchet, J. M. J.; Toney, M. F. *Macromolecules* **2005**, *38*, 3312–3319.

[15] Hiorns, R. C.; de Bettignies, R.; Leroy, J.; Bailly, S.; Firon, M.; Sentein, C.; Khoukh, A.; Preud'homme, H.; Dagron-Lartigau, C. *Adv. Funct. Mater.* **2006**, *16*, 2263–2273.

[16] Chang, J.-F.; Clark, J.; Zhao, N.; Sirringhaus, H.; Breiby, D. W.; Andreasen, J. W.; Nielsen, M. M.; Giles, M.; Heeney, M.; McCulloch, I. *Phys. Rev. B* **2006**, *74*, 115318.

[17] Müller, C.; Wang, E.; Andersson, L. M.; Tvingstedt, K.; Zhou, Y.; Andersson, M. R.; Inganäs, O. *Adv. Funct. Mater.* **2010**, *20*, 2124–2131.

[18] Coffin, R. C.; Peet, J.; Rogers, J.; Bazan, G. C. *Nature Chem.* **2009**, *1*, 657–661.

[19] Huang, J.-H.; Chen, F.-C.; Chen, C.-L.; Huang, A. T.; Hsiao, Y.-S.; Teng, C.-M.; Yen, F.-W.; Chen, P.; Chu, C.-W. *Org. Electron.* **2011**, *12*, 1755–1762.

[20] Baughman, T. W.; Wagener, K. B. *Adv. Polym. Sci.* **2005**, *176*, 1–42.

[21] Tao, D.; Wagener, K. B. *Macromolecules* **1994**, *27*, 1281–1283.

[22] Fox, H. H.; Schrock, R. R.; O'Dell, R. *Organometallics* **1994**, *13*, 635–639.

[23] Miao, Y.-J.; Bazan, G. C. *Macromolecules* **1997**, *30*, 7414–7418.

[24] Tsuie, B.; Wagener, K. B.; *Polym. Prepr.* **1999**, *40*, 709.

[25] Nomura, K.; Morimoto, H.; Imanishi, Y.; Ramhani, Z.; Geerts, Y. *Polym. Sci., Polym. Chem.* **2001**, *39*, 2463–2470.

[26] Delgado, P. A.; Liu, D. Y.; Kean, Z.; Wagener, K. B. *Macromolecules* **2011**, *44*, 9529–9532.

[27] Smith, A. P.; Smith, R. R.; Taylor, B. E.; Durstock, M. F. *Chem. Mater.* **2004**, *16*, 4687–4692.

[28] Huong Nguyen, L.; Günes, S.; Neugebauer, H.; Serdar Sariciftci, N.; Banishoeib, F.; Henckens, A.; Cleij, T.; Lutsen, L.; Vanderzande, D. *Sol. Energy Mater. Sol. Cells* **2006**, *90*, 2815–2828.

[29] Girotto, C.; Cheyns, D.; Aernouts, T.; Banishoeib, F.; Lutsen, L.; Cleij, T. J.; Vanderzande, D.; Genoe, J.; Poortmans, J.; Heremans, P. *Org. Electron.* **2008**, *9*, 740–746.

[30] Kim, J. Y.; Qin, Y.; Stevens, D. M.; Ugurlu, O.; Kalihari, V.; Hillmyer, M. A.; Frisbie, C. D. *J. Phys. Chem. C* **2009**, *113*, 10790–10797.

[31] Kossmehl, V. G.; Härtel, M.; Manecke, G. *Makromol. Chem. Commun.* **1987**, *131*, 15–54.

[32] Yamada, S.; Tokito, S.; Tsutsui, T.; Saito, S. *J. Chem. Soc., Chem. Commun.* **1987**, 1448–1449.

[33] Jen, K.-Y.; Maxfield, M.; Shacklette, L. W.; Elsenbaumer, R. L. *J. Chem. Soc., Chem. Commun.* **1987**, 309-311.

[34] Banishoeib, F.; Henckens, A.; Fourier, S.; Vanhooyland, G.; Breselge, M.; Manca, J.; Cleij, T. J.; Lutsen, L.; Vanderzande, D.; Nguyen, L. H.; Neugebauer, H.; Sariciftci, N. S. *Thin Solid Films* **2008**, *516*, 3978–3988.

[35] Cornelissen, J. J. L. M.; Peeters, E.; Janssen, R. A. J.; Meijer, E. W. *Acta Polym.* **1998**, *49*, 471–476.

[36] Lim, J.-C.; Suzuki, M.; Saegusa, T. *Polym. Bull.* **1993**, *31*, 651–658.

[37] Loewe, R. S.; McCullough, R. D. *Chem. Mater.* **2000**, *12*, 3214–3221.

[38] Zhou, E.; Tan, Z.; Yang, Y.; Huo, L.; Zou, Y.; Yang, C.; Li, Y. *Macromolecules* **2007**, *40*, 1831–1837.

[39] Huo, L.; Chen, T. L.; Zhou, Y.; Hou, J.; Chen, H.-Y.; Yang, Y.; Li, Y. *Macromolecules* **2009**, *42*, 4377–4380.

[40] Qin, Y.; Hillmyer, M. A. *Macromolecules* **2009**, *42*, 6429–6432.

[41] Love, J. A.; Morgan, J. P.; Trnka, T. M.; Grubbs, R. H. *Angew. Chem. Int. Ed.* **2002**, *41*, 4035–4037.

[42] Wagener, K. B.; Boncella, J. M.; Nel, J. G. *Macromolecules* **1991**, *24*, 2649–2657.

[43] Lehman, S. E.; Wagener, K. B. *Macromolecules* **2002**, *35*, 48–53.

[44] Zhang, C.; Sun, J.; Li, R.; Sun, S.-S.; Lafalce, E.; Jiang, X. *Macromolecules* **2011**, *44*, 6389–6396.

[45] Liu, J.; Loewe, R. S.; McCullough, R. D. *Macromolecules* **1999**, *32*, 5777–5785.

[46] Holdcroft, S. *J. Polym. Sci., Polym. Phys.* **1991**, *29*, 1585–1588.

[47] Zhang, W.; Kraft, S.; Moore, J. S. *J. Am. Chem. Soc.* **2004**, *126*, 329–335.

[48] Duffield, J. J.; Pettit, G. R. *J. Nat. Prod.* **2001**, *64*, 472–479.

[49] Biagini, S. C. G.; Gareth Davies, R.; Gibson, V. C.; Giles, M. R.; Marshall, E. L.; North, M. *Polymer* **2001**, *42*, 6669–6671.

[50] Clark, J.; Silva, C.; Friend, R. H.; Spano, F. C. *Phys. Rev. Lett.* **2007**, *98*, 206406.

[51] Salaneck, W. R.; Inganäs, O.; Themans, B.; Nilsson, J. O.; Sjögren, B.; H Österholm, J. E.; Brédas, J. L.; Svensson, S. *J. Chem. Phys.* **1988**, *89*, 4613–4619.

[52] Inganäs, O.; Salaneck, W. R.; Österholm, J. E.; Laakso, J. *Synth. Met.* **1988**, *22*, 395–406.

[53] Métivaud, V.; Lefèvre, A.; Ventolà, L.; Négrier, P.; Moreno, E.; Calvet, T.; Mondieig, D.; Cuevas-Diarte, M. A. *Chem. Mater.* **2005**, *17*, 3302–3310.

[54] Park, K.; Levon, K. *Macromolecules* **1997**, *30*, 3175–3183.

[55] Hamilton, R.; Bailey, C.; Duffy, W.; Heeney, M.; Shkunov, M.; Sparrowe, D.; Tierney, S.; McCulloch, I.; Kline, R. J.; DeLongchamp, D. M.; Chabinyc, M. *Proc. SPIE* **2006**, *6336*, 633611.

[56] Kline, R. J.; McGehee, M. D.; Kadnikova, E. N.; Liu, J.; Fréchet, J. M. J. *Adv. Mater.* **2003**, *15*, 1519–1522.

[57] Goh, C.; Kline, R. J.; McGehee, M. D.; Kadnikova, E. N.; Fréchet, J. M. J. *Appl. Phys. Lett.* **2005**, *86*, 122110.

[58] Diliën, H.; Palmaerts, A.; Lenes, M.; de Boer, B.; Blom, P.; Cleij, T. J.; Lutsen, L.; Vanderzande, D. *Macromolecules* **2010**, *43*, 10231–10240.

[59] Kim, Y.; Cook, S.; Choulis, S. A.; Nelson, J.; Durrant, J. R.; Bradley, D. D. C. *Chem. Mater.* **2004**, *16*, 4812–4818.

[60] Kim, Y.; Cook, S.; Tuladhar, S. M.; Choulis, S. A.; Nelson, J.; Durrant, J. R.; Bradley, D. D. C.; Giles, M.; Mcculloch, I.; Ha, C. S.; Ree, M. *Nat. Mater.* **2006**, *5*, 197–203.

[61] Kim, J. Y.; Frisbie, C. D. *J. Phys. Chem. C* **2008**, *112*, 17726–17736.

[62] Müller, C.; Ferenczi, T. A. M.; Campoy-Quiles, M.; Frost, J. M.; Bradley, D. D. C.; Smith, P.; Stingelin-Stutzmann, N.; Nelson, J. *Adv. Mater.* **2008**, *20*, 3510–3515.

[63] Zhao, J.; Swinnen, A.; Van Assche, G.; Manca, J.; Vanderzande, D.; Mele, B. V. *J. Phys. Chem. B* **2009**, *113*, 1587–1591.

[64] Hopkinson, P. E.; Staniec, P. A.; Pearson, A. J.; Dunbar, A. D. F.; Wang, T.; Ryan, A. J.; Jones, R. A. L.; Lidzey, D. G.; Donald, A. M. *Macromolecules* **2011**, *44*, 2908–2917.

[65] Miller, N. C.; Gysel, R.; Miller, C. E.; Verploegen, E.; Beiley, Z.; Heeney, M.; McCulloch, I.; Bao, Z. N.; Toney, M. F.; McGehee, M. D. *J. Polym. Sci., Polym. Phys.* **2011**, *49*, 499–503.

[66] Müller, C.; Bergqvist, J.; Vandewal, K.; Tvingstedt, K. Anselmo, A. S.; Magnusson, R.; Alonso, M. I.; Moons, E.; Arwin, H.; Campoy-Quiles, M.; Inganäs, O. *J. Mater. Chem.* **2011**, *21*, 10676–10684.

[67] Zhao, J.; Bertho, S.; Vandenbergh, J.; Van Assche, G.; Manca, J.; Vanderzande, D.; Yin, X.; Shi, J.; Cleij, T.; Lutsen, L.; Van Mele, B. *Phys. Chem. Chem. Phys.* **2011**, *13*, 12285–12292.

[68] Kim, J. Y.; Qin, Y.; Stevens, D. M.; Kalihari, V.; Hillmyer, M. A.; Frisbie, C. D. *J. Phys. Chem. C* **2009**, *113*, 21928–21936.

[69] Ma, W.; Yang, C.; Heeger, A. J. *Adv. Mater.* **2007**, *19*, 1387–1390.

Chapter 3

Poly(thienylene vinylene) Energy Level Control Through ADMET Copolymerization[†]

This chapter describes the design and synthesis of three dipropenyl monomers for metathesis polymerization. Homopolymerization afforded three poly(thienylene vinylene)s with distinct optoelectronic properties. Binary monomer combinations over a range of compositions gave three copolymer series with tunable energy levels. These levels could be tuned simply by varying monomer feed ratio during polymerization. The utility of this method was further demonstrated by the preparation of a stoichiometric terpolymer. Conclusions based on these copolymers were drawn from studying both optical and electronic behavior.

[†] Reproduced in part with permission from Speros, J. C.; Paulsen, B. D.; Slowinski, B. S.; Frisbie, C. D.; Hillmyer, M. A. *ACS Macro Lett.* **2012**, *1*, 986–990. Copyright 2012 American Chemical Society.

3.1 Introduction

The ability to tune the properties of conjugated polymers (CPs) through chemical modification has allowed for their integration in sensors,[1] organic light-emitting diodes,[2] field-effect transistors,[3] and organic photovoltaics (OPVs).[4] OPVs are of particular interest because cost-effective solution processing techniques can be used for their preparation. State-of-the-art OPV power conversion efficiencies now lie in the 7–10% range[5-8] as a result of both device optimization and the development of low band gap CPs typically having a perfectly alternating sequence of donor and acceptor (D-A) monomeric units.[9] Low band gap CPs are desirable because they often afford efficient and broad absorption of the solar spectrum. Systematic tuning of the band gap in a homologous set of CP materials can be ideally used to optimize OPV performance. However, such tunability can be synthetically difficult to achieve in conventional D-A polymers. Here we describe an approach to tunable energy levels based on copolymerization of structurally and electronically distinct monomers.

Few researchers have explored statistical copolymerization methods for the preparation of CPs. Unlike the alternating D-A approach,[10] a primary advantage of this strategy is the ability to probe non-stoichiometric monomer combinations instead of the 1:1 composition imposed by an alternating architecture. Some of the earliest examples of random CPs were aimed at tuning photoluminescence properties and were prepared by Yamamoto coupling of various dibromo monomers.[11,12] However, a broad composition range was not studied. More recent examples of random CPs make use of palladium-catalyzed Suzuki and Stille coupling strategies.[13,14] These routes require lengthy syntheses of, for example, one diboronic ester/ditin monomer and two dibromo monomers. Additionally, given the alternating nature of these polymerizations only half of the composition window is accessible. Recently, Thompson and coworkers built on the utility of this approach by demonstrating "semi-random" CPs using 2-bromo-5-trimethyltin-3-hexylthiophene, 2,5-bis(trimethyltin)-thiophene, and 4,7-dibromo-2,1,3-

benzothiadiazole or dibromo-bisthiophene-diketopyrrolopyrrole monomers and Stille coupling conditions.[15,16] They demonstrated that a small percentage of acceptor moiety in the copolymer backbone had a significant impact on the optoelectronic properties. More recently, this group expanded their Stille coupling approach to "semi-random" CPs by demonstrating control of open-circuit voltage[17] and optimization of OPV efficiency.[18] Inspired by this approach, we sought a methodology that would tolerate a wide variety of functionality, only require two monomers, and avoid the use of tin-containing monomers.

Acyclic diene metathesis (ADMET) polymerization is a step-growth polymerization that typically links α,ω-dienes to generate linear polymers with unsaturated repeat units.[19] ADMET polymerization has been used to prepare polymers for diverse applications.[20] In the CP arena, poly(acetylenes),[21] poly(phenylene vinylenes),[22] poly(fluorene vinylenes),[23] poly(carbazole vinylenes),[24] and poly(thienylene vinylenes)[25,26] (PTVs) have all been prepared by ADMET polymerization. This polymerization technique has also been used to prepare statistical non-conjugated copolymers.[27,28] However, the preparation of statistical CPs by ADMET has yet to be investigated.

This chapter describes the first example of statistical CPs prepared by ADMET polymerization. The Venn diagram in Figure 3.1 illustrates the ability of this approach to tune the chemistry and therefore the properties of CPs. By taking advantage of compositional differences a wide range of properties can be probed with high precision and minimal synthetic effort.

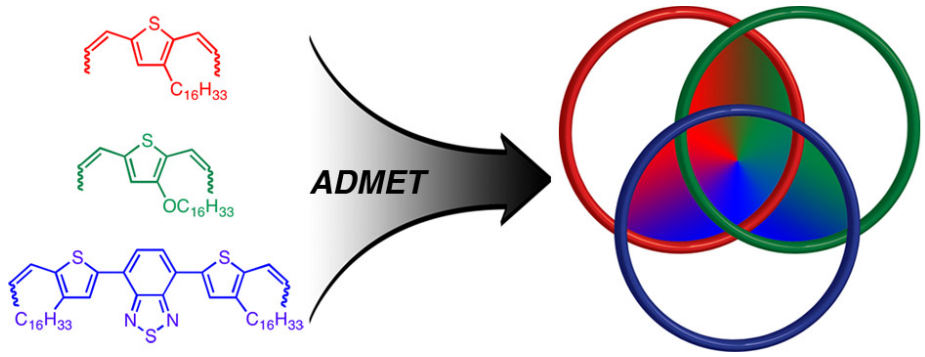

Figure 3.1
Venn diagram illustrating the three dipropenyl monomers and the concept of tunability (overlap) through copolymerization.

3.2 Results and Discussion

3.2.1 Monomer Synthesis

We synthesized three monomers all sharing the same reactive dipropenyl functionality (Figure 3.1 & Scheme 3.1a). For consistency the same hexadecyl solubilizing side chain was installed in all three monomers. Monomers were also designed to be electron rich (OC16) or electron poor (TBT) as compared to the "neutral" variant (C16). The C16 monomer was prepared following a previous literature report[26] in 68% overall yield with a *Z*:*E* ratio of 83:17. The synthesis of OC16 began by treating 3-bromothiophene with the sodium alkoxide of 1-hexadecanol in the presence of copper iodide. Lithiation of the 3-hexadecyloxythiophene product with *n*-butyllithium followed by treatment with N,N-dimethylformamide (DMF) and acidic workup afforded the dialdehyde. A salt-free Wittig reaction provided OC16 in 52% overall yield with a *Z*:*E* ratio of 65:35. Synthesis of the TBT monomer began with the Stille coupling of 4,7-dibromo-2,1,3-benzothiadiazole and 2-tributylstannyl-4-hexadecylthiophene catalyzed by bis(triphenylphosphine) palladium (II) chloride. The product was treated with DMF and phosphorus oxychloride under Vilsmeier-Haack conditions to afford the

dialdehyde.[29] The conversion of dialdehyde to TBT under salt-free Wittig conditions gave an overall yield of 16% and a *Z*:*E* ratio of 62:38 (see Section 3.4.2 for complete synthetic details).

Scheme 3.1

Homopolymer synthesis by ADMET (a) and copolymer structures (b).

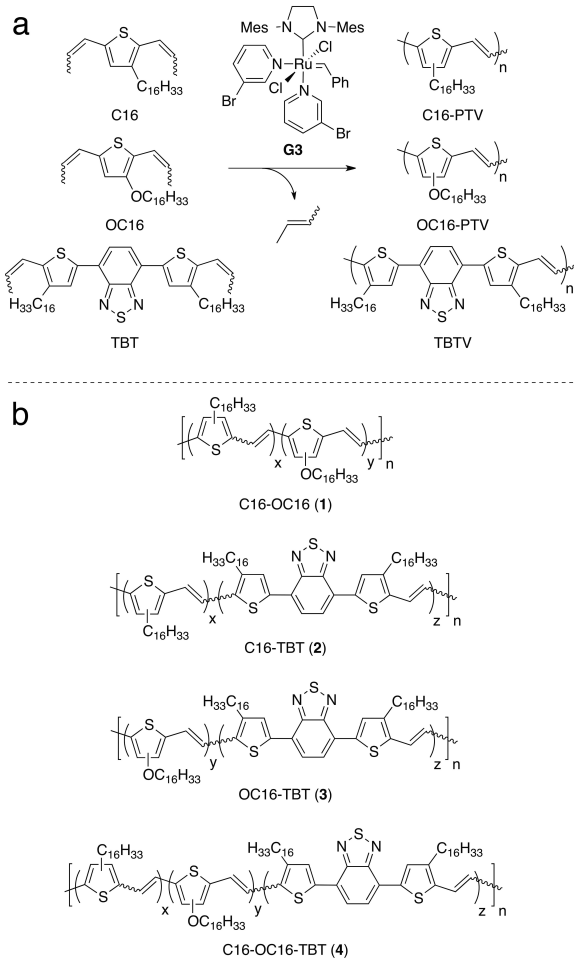

3.2.2 Polymer Synthesis and Characterization

The respective low band gap homopolymers (Scheme 3.1a) and a broad range of copolymers (Scheme 3.1b) were synthesized by ADMET polymerization. All polymers were prepared using a highly active 3-bromopyridine functionalized ruthenium metathesis catalyst (G3).[30] Homo- and copolymerization of C16, OC16, and TBT monomers was conducted under reduced pressure (20–50 mtorr) in anhydrous 1,2,4-trichlorobenzene with G3 (1 mol%). Polymerizations were allowed to proceed for 16–48 h before precipitation in a non-solvent (methanol or acetone) and purification by Soxhlet extraction with the same non-solvent (see Section 3.4.2 for complete synthetic details). Relative number-average molecular weights were determined by size-exclusion chromatography (SEC) in chloroform versus polystyrene standards. ^{1}H NMR spectroscopy was employed to characterize all polymers and to determine the average monomer composition in the copolymer structures. However, the NMR data was not useful with respect to sequence distribution determination. Optical behavior was analyzed in dilute chloroform solutions (10^{-5} M in monomer repeat units) by ultraviolet-visible spectroscopy (UV–vis). Absorption maxima (λ_{max}) for C16-PTV, OC16-PTV, and TBTV homopolymers were 582, 634, and 662 nm, respectively (Figure 3.2a). As observed previously, C16-PTV displayed a second λ_{max} (623 nm) suggesting aggregation-induced vibronic fine structure. TBTV also showed a second peak at 422 nm likely due to the π-π^* transition; we attribute the peak at 662 nm to intramolecular charge transfer.[31] Thin film UV–vis spectra demonstrated predictable red shifts in absorption maxima as

compared to homopolymer solution spectra (Figure 3.2b). Values of the optical band gaps (E_g^{opt}) were determined from the onset of absorption in the polymer thin film (E_g^{opt} = 1240 / λ_{onset}). C16-PTV was found to have an E_g^{opt} of 1.66 eV, while both OC16-PTV and TBTV gave a value of 1.49 eV. All spectroscopic and chromatographic data are summarized in Table 3.1.

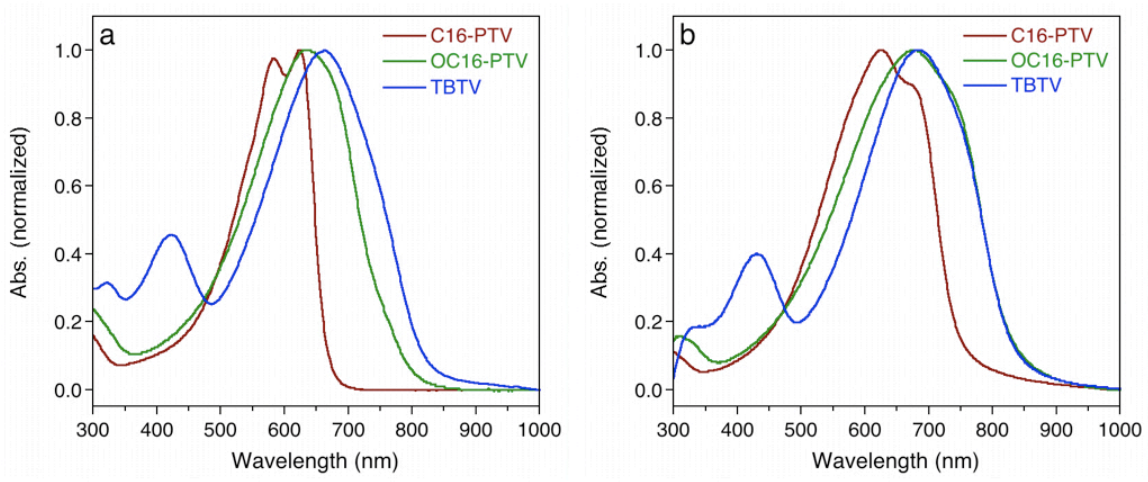

Figure 3.2
UV–vis (a) solution and (b) film spectra of C16-PTV, OC16-PTV, and TBTV.

Table 3.1
NMR, SEC, and UV–vis data for homo- and copolymers.

sample ID[a]	observed ratio[b]	M_n (kg/mol)[c]	$Đ_M$[c]	$\lambda_{max,soln}$ (nm)[d]	$\lambda_{max,film}$ (nm)[e]	E_g^{opt} (eV)[f]
C16-PTV	–	33	2.2	582 (623)	625 (677)	1.66
OC16-PTV	–	4	1.6	634	676	1.49
TBTV	–	7	1.9	662 (422)	683 (429)	1.49
C16-OC16	C16:OC16					
1a (90:10)	89:11	34	2.8	591 (626)	632 (682)	1.64
1b (80:20)	80:20	14	1.9	593 (629)	630	1.62
1c (70:30)	68:32	9	1.7	595	630	1.59
1d (60:40)	56:44	7	3.3	587	627	1.58
1e (50:50)	47:53	8	1.5	602	639	1.56
1f (40:60)	37:63	7	2.2	621	656	1.55
1g (30:70)	27:73	3	1.4	601	644	1.55
1h (20:80)	19:81	8	1.5	619	659	1.53
1i (10:90)	8:92	5	1.3	600	635	1.53
C16-TBT	C16:TBT					
2a (95:5)	95:5	10	1.7	580 (611)	620	1.59
2b (80:20)	79:21	6	1.2	622	660	1.50
2c (60:40)	63:37	6	1.4	641 (435)	678 (460)	1.49
2d (40:60)	41:59	5	1.4	649 (433)	680 (446)	1.49
2e (20:80)	22:78	6	1.5	662 (430)	686 (439)	1.49
OC16-TBT	OC16:TBT					
3a (75:25)	78:22	3	1.1	638	686	1.46
3b (50:50)	55:45	4	1.2	640 (433)	685 (452)	1.46
3c (25:75)	23:77	4	1.2	645 (423)	681 (437)	1.48
C16-OC16-TBT	C16:OC16:TBT					
4 (1:1:1)	0.36:0.34:0.30	4	1.2	624 (434)	670 (440)	1.49

[a]Values in parentheses are monomer feed ratios. [b]Determined by integration of appropriate resonances in ^{1}H NMR spectra. [c]Determined by SEC in $CHCl_3$ versus polystyrene standards. [d]ca. 10^{-5} M in repeat unit in $CHCl_3$; values in parentheses are secondary peaks/shoulders [e]Polymer film spin coated from $CHCl_3$ onto glass substrates; values in parentheses are secondary peaks/shoulders [f]Determined from onset absorption of thin film (E_g^{opt} = 1240 (nm eV)/λ_{onset} (nm)).

3.2.3 C16-OC16 Copolymers

The C16:OC16 ratios in isolated copolymers (**1a–i**) were quantified using ^{1}H NMR spectroscopy (Figure 3.3) and were within a few percent of the feed ratios in all cases (Table 3.1). Additionally, λ_{onset} of C16-OC16 thin films shifted to longer wavelengths (lower E_g^{opt}) as more OC16 was incorporated into the copolymer (Figure 3.9a). Although the molar mass range in this polymer series was large (3–34 kg/mol), this likely had minimal impact on E_g^{opt}, which in PTVs has been shown to saturate around ten repeat units.[32] Therefore, we posit that the observed differences in E_g^{opt} are largely the result of copolymer composition. Figure 3.4 demonstrates the agreement between the predicted and actual E_g^{opt} based on the sum of the mole fraction weighted values of the homopolymer bandgaps.

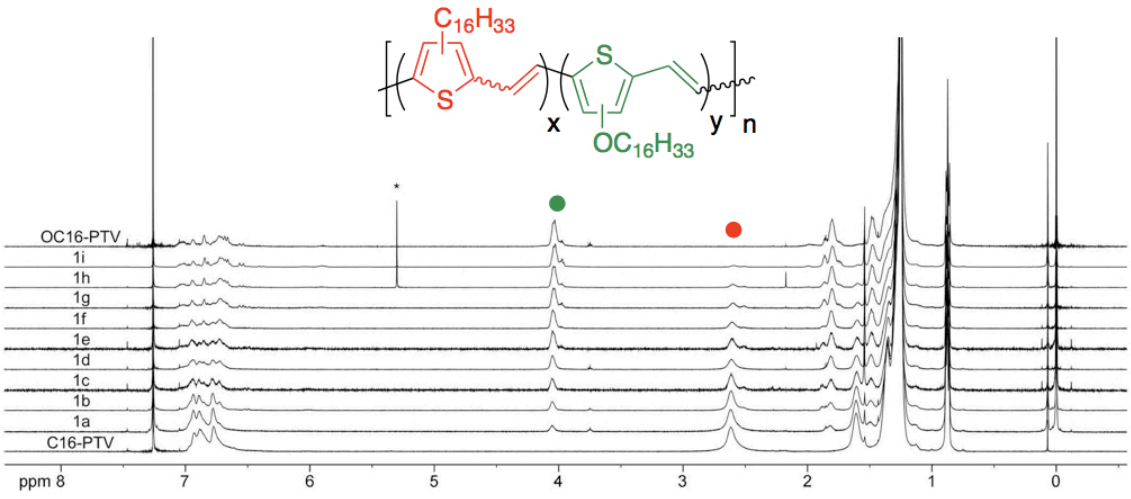

Figure 3.3
^{1}H NMR spectra of series **1**. Colored circles correspond to resonances used to quantify copolymer composition.

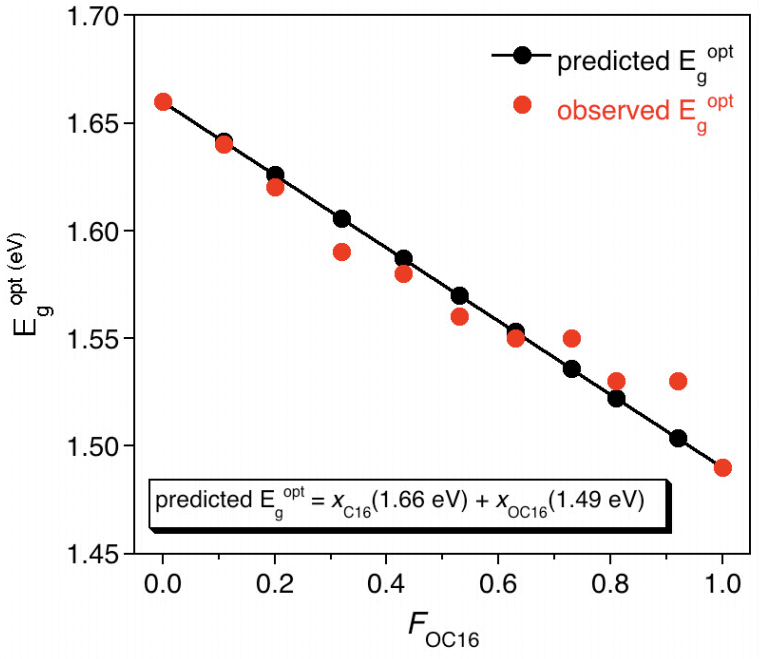

Figure 3.4
Predicted (see mixing equation) and measured (UV–vis) E_g^{opt} of series **1** versus mole fraction (*F*) of OC16 in the copolymer.

3.2.4 C16-TBT Copolymers

The second copolymer series employed the C16 and TBT monomers (**2a–e**), and again the feed ratios closely matched the average copolymer compositions as determined by ^{1}H NMR spectroscopy (Figure 3.5). All isolated polymers were of roughly the same apparent molar mass (M_n ca. 6 kg/mol) and molar-mass dispersity allowing for direct comparison of optical behavior. Copolymers in this series could be monitored qualitatively by color change (Figure 3.6). Unlike series **1**, which showed a progressive shift in E_g^{opt}, the E_g^{opt} of this series saturated upon addition of 20% TBT monomer. As suggested by Thompson and coworkers,[15,16,18] applying this "trace acceptor" concept to other CP systems may allow for significantly altered absorptive properties with minimal changes to the overall polymer composition.

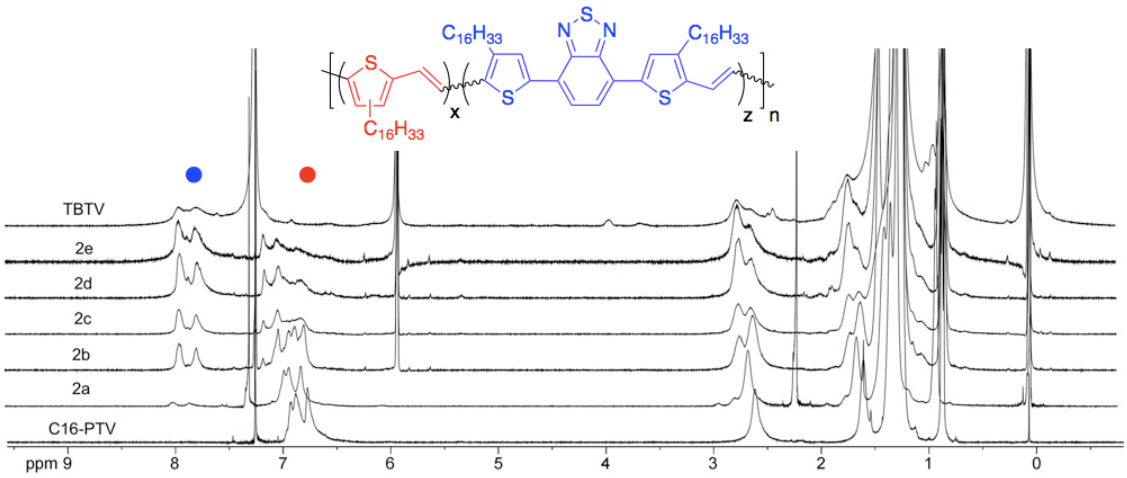

Figure 3.5

^{1}H NMR spectra of series **2**. Colored circles correspond to resonances used to quantify copolymer composition.

Figure 3.6

Series **2** polymer solutions in $CHCl_3$.

3.2.5 OC16-TBT Copolymers

The OC16 and TBT monomers were used in preparation of the third copolymer series (**3a–c**), and average copolymer composition calculated using ^{1}H NMR spectroscopy was very close to the feed ratios (Figure 3.7). The π-π* transition from TBT proved a useful means of confirming the increase in TBT content (Figures 3.9c and 3.28c). Interestingly, the E_g^{opt} of all three copolymers was slightly lower than that of the parent homopolymers. This is possibly the result of intramolecular charge transfer; the same phenomenon attributed to reduced band gap in D-A materials.[33]

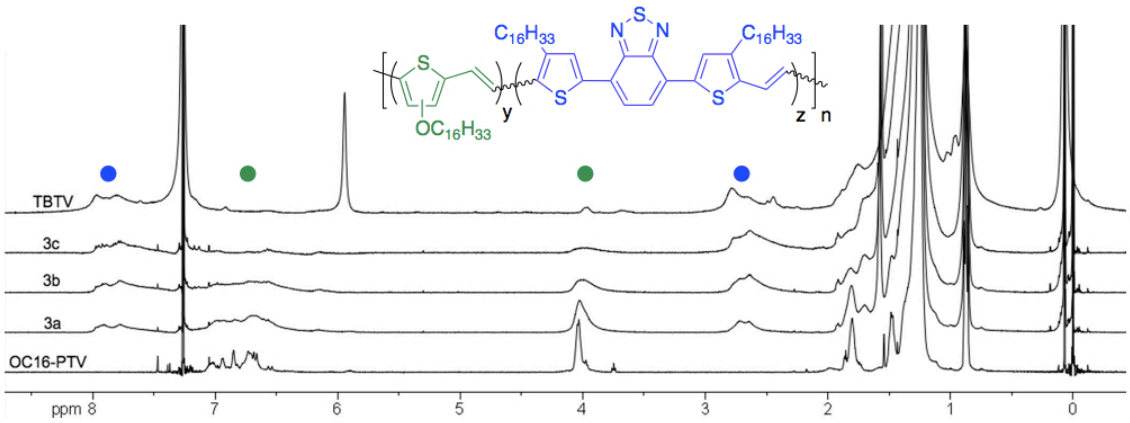

Figure 3.7
^{1}H NMR spectra of series **3**. Colored circles correspond to resonances used to quantify copolymer composition.

3.2.6 C16-OC16-TBT Terpolymer

To demonstrate the synthetic versatility of this copolymerization approach a terpolymer (**4**) was prepared by combining equimolar amounts of the three monomers. The terpolymer composition from ^{1}H NMR spectroscopy (Figure 3.8) was close to the feed ratio. In addition, **4** exhibited a much broader absorption than the respective

homopolymers in solution (Figure 3.9d) and as a thin film (Figure 3.28d) by UV–vis spectroscopy.

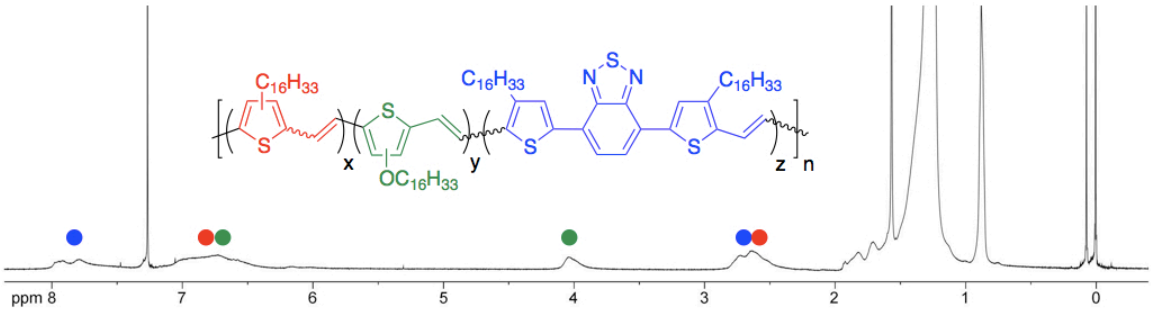

Figure 3.8

^{1}H NMR spectra of **4**. Colored circles correspond to resonances used to quantify copolymer composition.

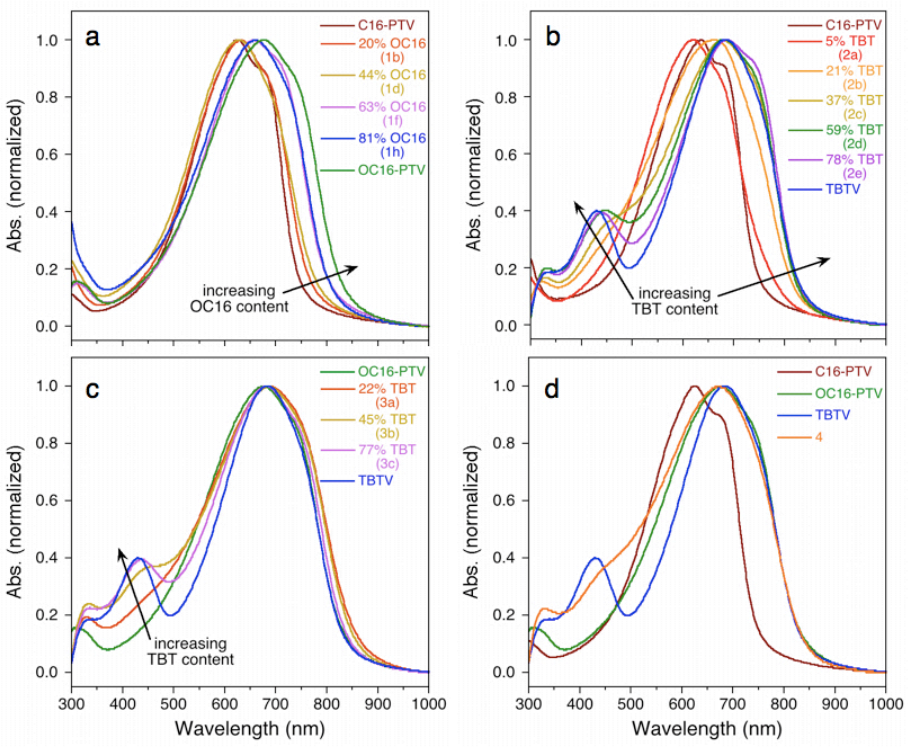

Figure 3.9
UV–vis spectra of (a) C16-OC16 (**1**), (b) C16-TBT (**2**), (c) OC16-TBT (**3**), and (d) C16-OC16-TBT (**4**) as thin films on glass substrates. Corresponding homopolymers are shown in each series to highlight trends.

3.2.7 Electronic Behavior

The homo- and copolymers were characterized by cyclic voltammetry (CV) to quantify the impact of copolymerization on the position of the highest occupied molecular orbital (HOMO). The room temperature ionic liquid 1-butyl-1-methylpyrrolidinium bis(trifluoromethylsulfonyl)imide ([P14][TFSA]) was employed as the electrolyte system as its broad window of electrochemical stability provided high sweep-to-sweep stability and sample-to-sample reproducibility.[34] The HOMO level of

each polymer was calculated from the onset of electrochemical oxidation (Figures 3.10 and 3.29). The measured reference potentials for each sample were internally calibrated using the standard redox couple cobaltocenium hexafluorophosphate ($CcPF_6$) known to undergo a reversible reduction at -1350 mV vs the ferrocene redox couple in ionic liquids.[35,36] Taking the ferrocene oxidation potential to lie 5.1 eV below vacuum level,[37] the HOMO levels were calculated as $E_{HOMO} = -(E_{(onset,ox\ vs\ Cc+/o)} + 3.75)$ eV. The HOMO level positions of C16-PTV, OC16-PTV, and TBTV were -5.12, -4.81, and -5.23 eV, respectively. For reference, regioregular poly(3-hexylthiophene) measured in the same electrolyte system gave a HOMO level position of -5.06 eV. The data collected from CV is summarized in Table 3.2.

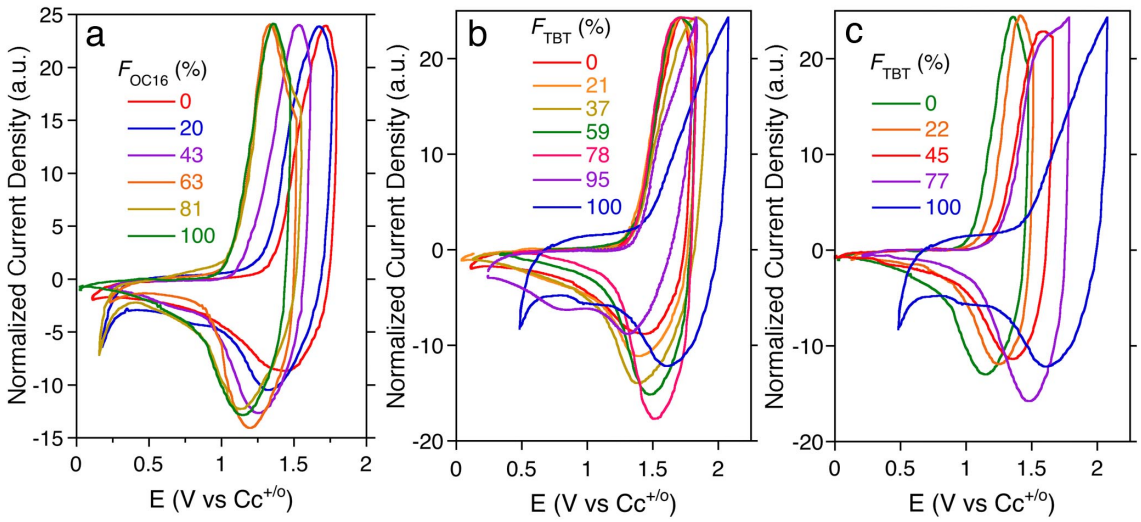

Figure 3.10

CV of series (a) **1**, (b) **2**, and (c) **3**.

Table 3.2
CV and UV–vis data.

sample ID	HOMO (eV)[a]	LUMO (eV)[b]	E_g^{opt} (eV)[c]
C16-PTV	-5.12	-3.46	1.66
OC16-PTV	-4.81	-3.32	1.49
TBTV	-5.23	-3.74	1.49
C16-OC16			
1b	-5.05	-3.43	1.62
1d	-4.97	-3.39	1.58
1f	-4.87	-3.32	1.55
1h	-4.85	-3.32	1.53
C16-TBT			
2a	-5.12	-3.53	1.59
2b	-5.10	-3.60	1.50
2c	-5.10	-3.61	1.49
2d	-5.12	-3.63	1.49
2e	-5.11	-3.62	1.49
OC16-TBT			
3a	-4.90	-3.44	1.46
3b	-4.99	-3.53	1.46
3c	-5.06	-3.58	1.48
C16-OC16-TBT			
4	-5.09	-3.60	1.49

[a] $E_{HOMO} = -(E_{(onset,ox\ vs\ Cc+/o)} + 3.75)$ eV [b] Estimated: E_{LUMO} eV = E_{HOMO} eV + E_g^{opt} eV [c] Determined from onset absorption of thin film (E_g^{opt} = 1240 (nm eV)/λ_{onset} (nm)).

Copolymers of C16-TBT demonstrated saturation behavior in both HOMO level and E_g^{opt} (Figure 3.11a). Upon incorporation of 22% C16 into the TBTV polymer chain the HOMO level position was immediately pinned to that of the C16-PTV homopolymer (≈ -5.1 eV). On the other hand, the E_g^{opt} saturated at the TBTV homopolymer value of ~1.5 eV at 21% TBT monomer incorporation. This behavior is consistent with the generally accepted concept that the acceptor monomer (TBT) sets the

LUMO level, and the donor monomer (C16) sets the HOMO level[9] even at low levels of incorporation.[15]

Interestingly, the C16-OC16 and OC16-TBT copolymers did not follow the saturation behavior observed for C16-TBT. Instead, the HOMO level increased (310 meV range) and the E_g^{opt} decreased (170 meV range) monotonically with increasing OC16 content in the C16-OC16 copolymers (Figure 3.11b). Likewise, the HOMO levels of OC16-TBT copolymers could be tuned over a 420 meV range (Figure 3.11c). However, despite the increase in HOMO level in the OC16-TBT copolymers, the E_g^{opt} varied little as the respective homopolymers had identical band gaps.

Finally, the HOMO level position of the terpolymer (**4**) (36% C16, 34% OC16, and 30 % TBT) was determined by CV (-5.09 eV, Figure 3.29) and was consistent with that of the copolymers containing approximately 36% OC16. The E_g^{opt} (1.49 eV) was consistent with that of the copolymers containing approximately 30% TBT according to the relationships shown in Figure 3.11.

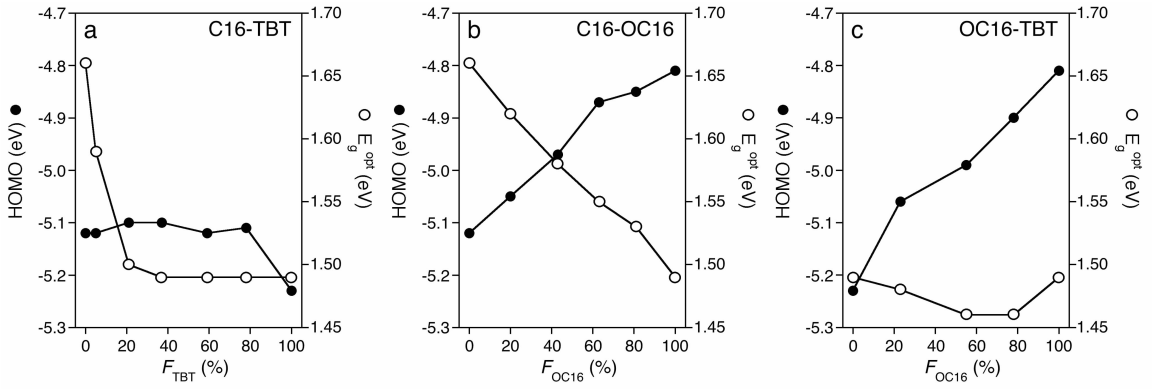

Figure 3.11
HOMO level position from CV (filled circles) and E_g^{opt} from UV–vis (open circles) versus polymer composition (*F*) of (a) C16-TBT, (b) C16-OC16, and (c) OC16-TBT thin films.

3.3 Conclusions

The nonlinear behavior observed in C16-TBT copolymers (Figure 3.11a) is consistent with related phenomena in other D-A polymers. However, this explanation does not adequately describe the monotonic behavior observed for the HOMO levels in the C16-OC16 and OC16-TBT copolymers. This is perhaps due to the relatively large differences between HOMO levels of the corresponding homopolymers. As illustrated by Figure 3.12, we have shown that ADMET polymerization is an ideal means of generating CPs with precisely controlled optoelectronic properties and allows for systematic combination and optimization of various CP properties (e.g., HOMO/LUMO levels, band gap, photoluminescence, absorption strength, charge transport, etc.) with minimal synthetic effort. The application of this approach to CP systems with broader optoelectronic properties and integration of those polymers into OPV devices is described in the following chapter.

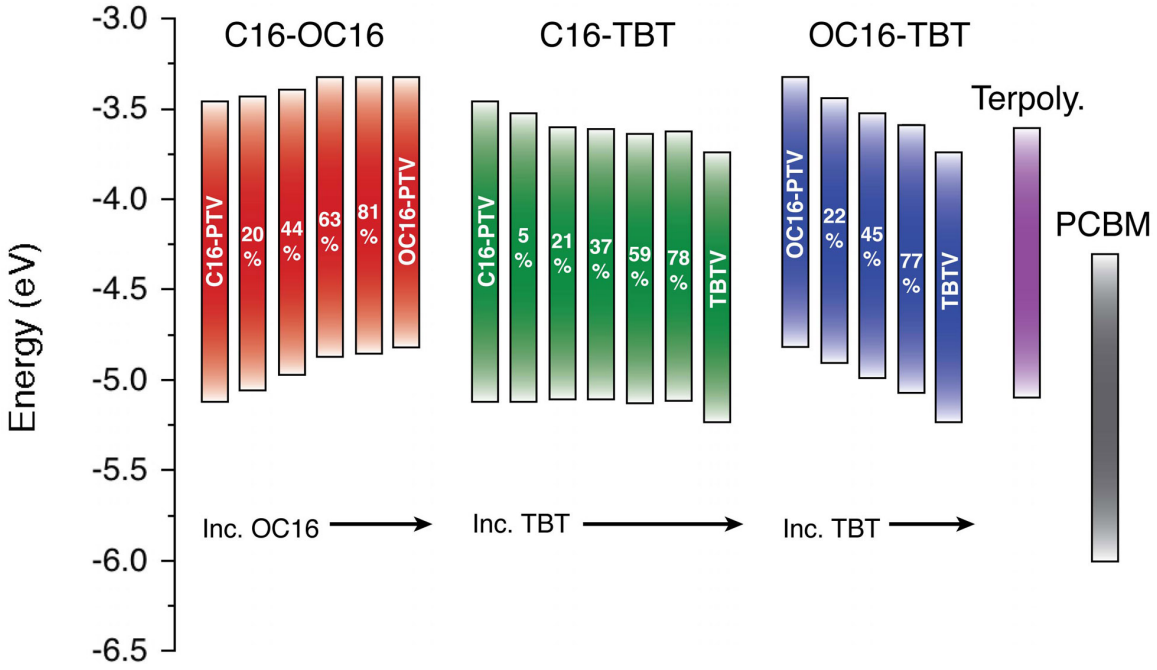

Figure 3.12
Band diagram of C16-OC16 (red), C16-TBT (green), and OC16-TBT (blue) series. The terpolymer (purple) and PCBM (gray) are shown for completeness. LUMO levels were estimated from HOMO levels and E_g^{opt} (LUMO = HOMO + E_g^{opt}).

3.4 Experimental Details

3.4.1 Materials and Methods

C16 and C16-PTV were prepared according to previous work.[26] Commercially available solvents and reagents were purchased and used as received from Aldrich and Acros. Degassed THF was purified by passage through an activated alumina column and collected in flame-dried, air-free flasks. N,N,N',N'-tetramethylethylenediamine (TMEDA) was dried over molecular sieves and distilled under vacuum from *n*-butyllithium. All reactions were run under argon or vacuum using standard Schlenk techniques. The ionic liquid, 1-butyl-1-methylpyrrolidinium

bis(trifluoromethylsulfonyl)imide ([P14][TFSI]), was purchased from EMD Chemicals (Gibbstown, NJ). Cobaltocenium hexafluorophosphate ($CcPF_6$) was purchased from Sigma-Aldrich (St. Louis, MO). A complete description of the characterization techniques employed is available in Appendix A.

3.4.2 Synthetic Details

Scheme 3.2

Synthesis of OC16.

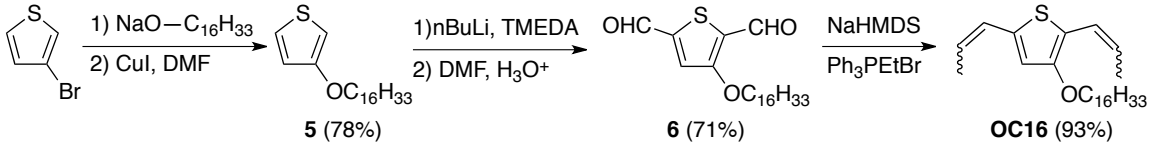

Synthesis of 3-hexadecyloxythiophene (5). A 100 mL round bottom flask was equipped with a magnetic stir bar and flame dried. 1-hexadecanol (82 g, 338 mmol) was added and heated to 110 ˚C to facilitate melting. Added sodium chunks (2.0 g, 86 mmol) and stirred 40 h under argon. Distilled residual 1-hexadecanol before adding anhydrous DMF (ca. 50 mL) and 3-bromothiophene (10 g, 61 mmol) via syringe. Copper (I) iodide (2.3 g, 12 mmol) was added as a solid and the reaction was stirred for 20 h under argon at 110 ˚C. Observed copper mirror on walls of flask. Poured reaction into 1 M NH_4Cl (ca. 250 mL) and extracted with hexanes (2 × 150 mL). Residual solvent was removed under reduced pressure. Distilled off remaining 1-hexadecanol and remaining residue was purified by column chromatography (CH_2Cl_2). Removal of solvent gave product as an off-white solid (15.5 g, 78%). ^{1}H-NMR (300 MHz, $CDCl_3$): δ_H (ppm) = 7.17 (dd, 1H, *J* = 5.25, 3.12 Hz, Th-*H*5), 6.75 (dd, 1H, *J* = 5.24, 1.55 Hz, Th-*H*4), 6.22 (dd, 1H, *J* = 3.12, 1.54 Hz, Th-*H*2), 3.93 (t, 2H, *J* = 6.54 Hz, –OCH_2–), 1.77 (quintet, 2H, *J* = 14.35, 5.99 Hz, –OCH$_2$CH_2–), 1.44 (m, 2H, –O(CH$_2$)$_2$CH_2–), 1.26 (bs, 24 H, –CH_2–), 0.88 (t, 3H, *J* = 6.66 Hz, –CH_3). ^{13}C NMR (125 MHz, $CDCl_3$): δ_C (ppm) = 158.3 (Th-*C*3),

124.7 (Th-*C*5), 119.8 (Th-*C*4), 97.1 (Th-*C*2), 70.5 (–O*C*H_2–), 32.2 (–*C*$H_2$$CH_2$$CH_3$), 29.9 (2), 29.8 (2), 29.6 (2), 29.5 (–*C*H_2–), 26.3 (–O(CH_2)$_2$*C*H_2–), 22.9 (–*C*$H_2$$CH_3$), 14.4 (–*C*$H_3$). HRGC-MS (EI): $M_{calcd.}$ = 324.2487, M_{found} = 324.2487. Anal. calcd. for C20H36OS: C 74.01, H 11.18, O 4.93, S 9.88; Found: C 74.87, H 11.33, O 4.68, S 9.05.

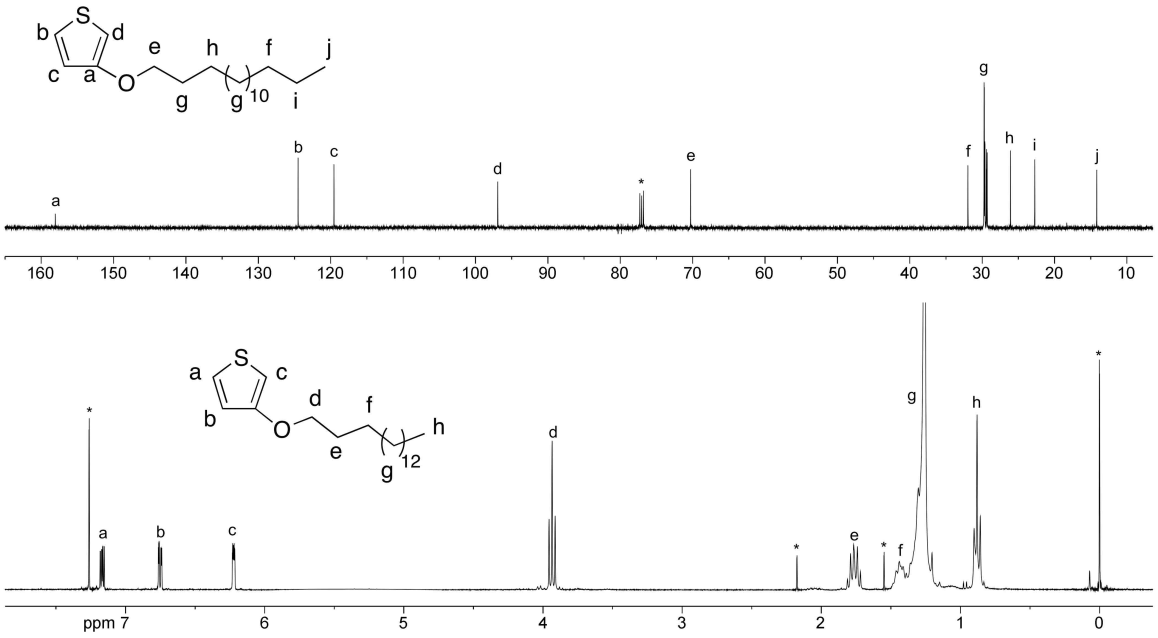

Figure 3.13

^{1}H and ^{13}C NMR spectra of **5**.

Synthesis of 2,5-dicarbaldehyde-3-hexadecyloxythiophene (6). A 3-neck 250 mL round bottom flask was equipped with a magnetic stir bar, reflux condenser, glass stopcock, liquid addition funnel, and two rubber septa. The apparatus was flame-dried under vacuum before adding **2** (14.0 g, 43 mmol) as a solid under argon purge. Anhydrous hexanes (ca. 100 mL) were cannulated into the flask followed by TMEDA (16.2 mL, 108 mmol) via syringe. A 2.5 M solution of *n*-butyllithium in hexanes (43.1 mL, 108

mmol) was added to the addition funnel via syringe. The *n*-butyllithium was added dropwise to the solution of **5**, TMEDA, and hexanes over the course of 30 min. Refluxed for 1 h following addition. Cannulated anhydrous THF (ca. 120 mL) into flask and cooled to 0 °C, at which point anhydrous N,N'-dimethylformamide (DMF) (13.3 mL, 172 mmol) was added via syringe. Stirred for 1 h before pouring into 3 M HCl (ca. 150 mL). Neutralized with saturated $NaHCO_3$ and added additional 500 mL H_2O. Extracted with diethyl ether (3 × 200 mL). The combined organics were dried over Na_2SO_4 and solvent was removed under reduced pressure to give brown oil. Dissolved in THF (ca. 20 mL) and precipitated into MeOH (ca. 200 mL) at 0 °C. Filtered and dried under vacuum to give brown solid (11.6 g, 71%). ^{1}H NMR (300 MHz, $CDCl_3$): δ_H (ppm) = 10.14 (s, 1H, Th-5C*H*O), 9.89 (s, 1H, Th-2C*H*O), 7.49 (s, 1H, Th-*H*4), 4.20 (t, 2H, *J* = 6.52 Hz, –OC*H*$_2$–), 1. 85 (quintet, 2H, *J* = 14.34, 6.99 Hz, –OCH$_2$C*H*$_2$–), 1.47 (m, 2H, –O(CH$_2$)$_2$C*H*2–), 1.26 (bs, 24H, –CH$_2$–), 0.88 (t, 3H, *J* = 6.69 Hz, –C*H*$_3$). ^{13}C NMR (125 MHz, $CDCl_3$): δ_C (ppm) = 183.1 (–*C*HO), 182.5 (–*C*HO), 163.4 (Th-*C*3), 146.7 (Th-*C*5), 127.8 (Th-*C*2), 121.6 (Th-*C*4), 72.6 (–O*C*H$_2$–), 32.1 (–*C*H$_2$CH$_2$CH$_3$), 29.9 (3), 29.8, 29.7, 29.6, 29.5, 29.3 (–*C*H$_2$–), 26.0 (–O(CH$_2$)$_2$*C*H$_2$–), 22.9 (–*C*H$_2$CH$_3$), 14.3 (–*C*H$_3$). HRGC-MS (EI): $M_{calcd.}$ = 380.2385, M_{found} = 380.2386. Anal. calcd. for $C_{22}H_{36}O_3S$: C 69.43, H 9.53, O 12.61, S 8.43; Found: C 69.94, H 9.58, O 11.91, S 7.81.

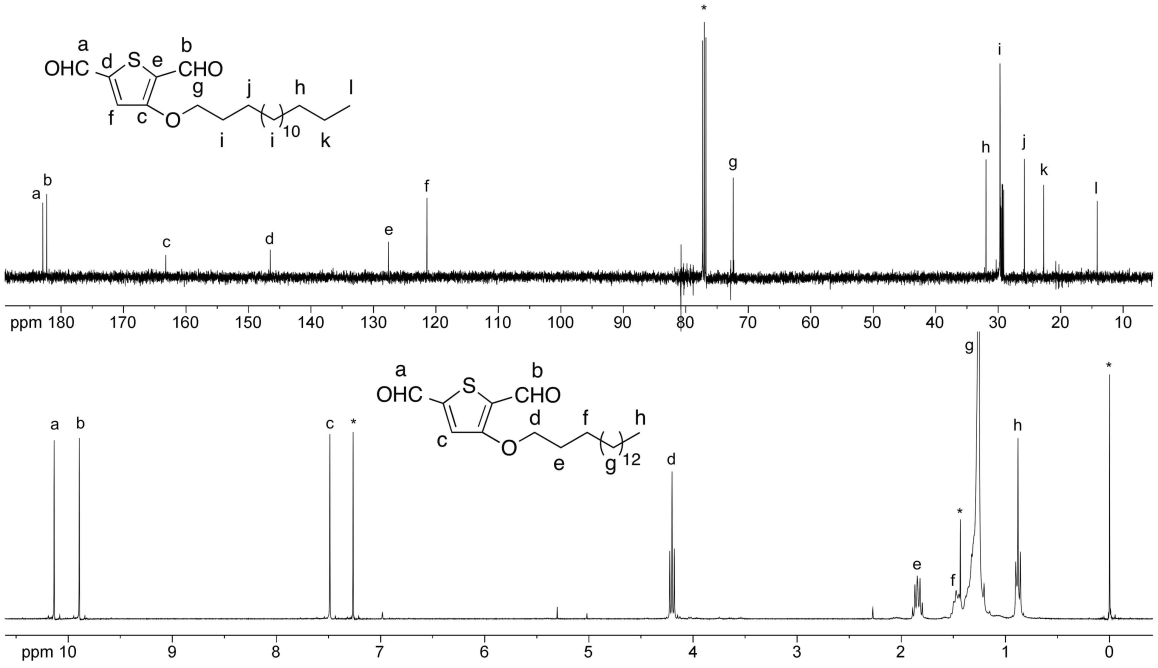

Figure 3.14

^{1}H and ^{13}C NMR spectra of **6**.

Synthesis of 2,5-dipropenyl-3-hexadecyloxythiophene (OC16). A 2-neck 500 mL round bottom flask was equipped with a magnetic stir bar, reflux condenser, glass stopcock, and rubber septum. Flame dried apparatus under vacuum before adding sodium bis(trimethylsilyl)amide (10.1 g, 55.2 mmol) and (ethyl)triphenylphosphonium bromide (20.5 g, 55.2 mmol) under argon purge. Pulled vacuum and backfilled with argon (5x) to dry solids. Cannulated anhydrous hexanes (ca. 300 mL) into flask and refluxed for 1 h under argon to form Wittig reagent (bright orange-red solution). Cooled to -78 °C on acetone/dry ice bath and removed hexanes with a cannula taking care not to remove precipitated Wittig reagent. Repeated cold hexane wash with another 300 mL. Removed residual hexanes under high vacuum and added anhydrous THF (ca. 300 mL) to dissolve remaining Wittig reagent. This solution was cannulated into a 500 mL round bottom flask containing anhydrous THF (ca. 100 mL) and **6** (10.0 g, 26.3 mmol) held at 0 °C. Allowed to warm to room temperature and stirred for 45 min. before filtering off

$Ph_3P{=}O$. Concentrated filtrate under reduced pressure to give a dark brown residue. Dissolved residue in an ether:hexanes (10:90) solution (ca. 500 mL) and flushed through silica gel column to remove residual $Ph_3P{=}O$. Eluent was concentrated and dissolved in hexanes before flushing through a second silica gel plug. The solvent was removed under reduced pressure to give light yellow oil that solidified on standing. Dissolved oil in CH_2Cl_2 (ca. 15 mL) and precipitated into MeOH (ca. 150 mL) at 0 °C. Filtered and dried under vacuum to give off-white solid (9.8 g, 93%). *Z*:*E* from ^{1}H NMR was 67:33. ^{1}H NMR (500 MHz, $CDCl_3$): δ_H (ppm) = 6.71, 6.60, 6.53 (s, 1H, Th-*H*4 isomers), 6.65–6.32 (m, 2H, Th–C*H*=CH–CH_3), 6.10–5.80 (*E*) & 5.72–5.47 (*Z*) (m, 2H, Th–CH=C*H*–CH_3), 3.96 (m, 2H, –OCH_2–), 1.97 (*Z*) & 1.84 (*E*) (m, 6H, Th–CH=CH–CH_3), 1.73 (m, 2H, –OCH_2CH2–), 1.42 (m, 2H, –$O(CH_2)_2CH_2$–), 1.25 (bs, 26H, –CH_2–), 0.88 (t, 3H, *J* = 6.95 Hz, –CH_3). ^{13}C NMR (125 MHz, $CDCl_3$): δ_C (ppm) = 152.4 (Th-*C*3), 137.6 (Th-*C*5), 125.1 & 124.9 (Th–CH=*C*H–CH_3), 122.6 & 121.3 (Th–*C*H=CH–CH_3), 118.9 (Th-*C*2), 114.8 (Th-*C*4), 71.8 (–O*C*H_2–), 32.2 & 30.5 (–*C*$H_2CH_2CH_3$), 29.9 (2), 29.8, 29.6 (–*C*H_2–), 26.2 (–$O(CH_2)_2$*C*H_2–), 22.9 (–*C*H_2CH_3), 18.8 & 18.4 (Th–CH=CH–*C*H_3), 14.3 (–*C*H_3). HRGC-MS (EI): $M_{calcd.}$ = 404.3113, M_{found} = 404.3086. Anal. calcd. for $C_{26}H_{44}OS$: C 77.16, H 10.96, O 3.95, S 7.92; Found: C 77.42, H 10.89, O 4.07, S 7.95.

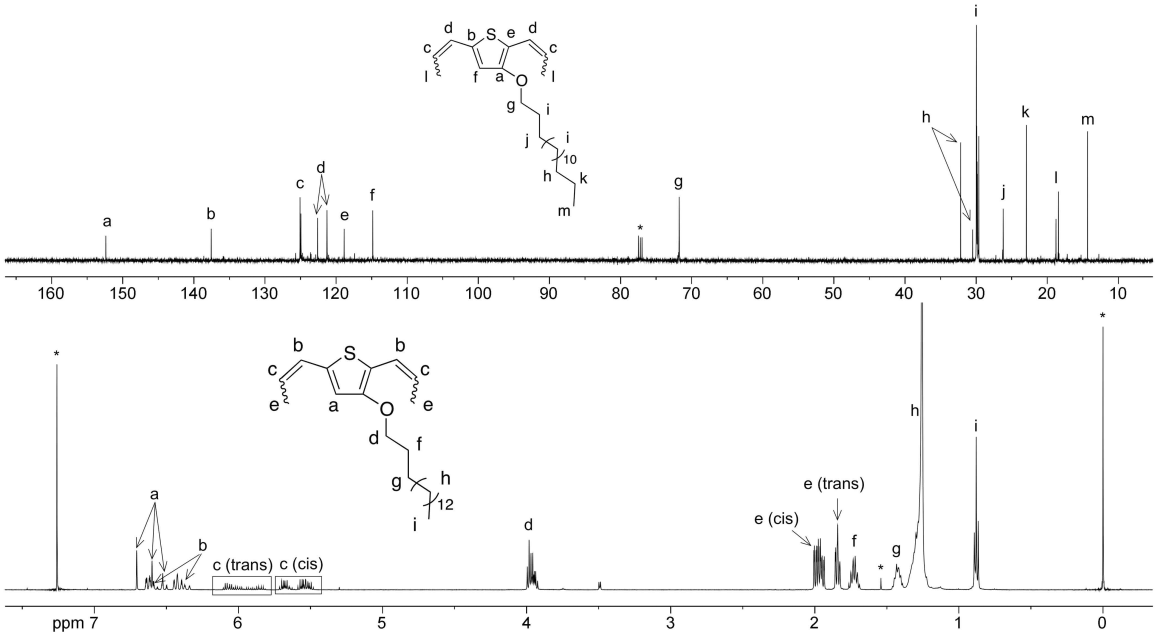

Figure 3.15

^{1}H and ^{13}C NMR spectra of OC16.

Scheme 3.3

Synthesis of TBT. Conditions: (a) i) Mg, $BrC_{16}H_{33}$ ii) $Ni(dppp)Cl_2$ (b) i) $^{n}BuLi$, TMEDA ii) Bu_3SnCl (c) TEA, $SOCl_2$ (d) HBr, Br_2 (e) $PdCl_2(PPh_3)_2$ (f) DMF, $POCl_3$ (g) NaHMDS, Ph_3PEtBr

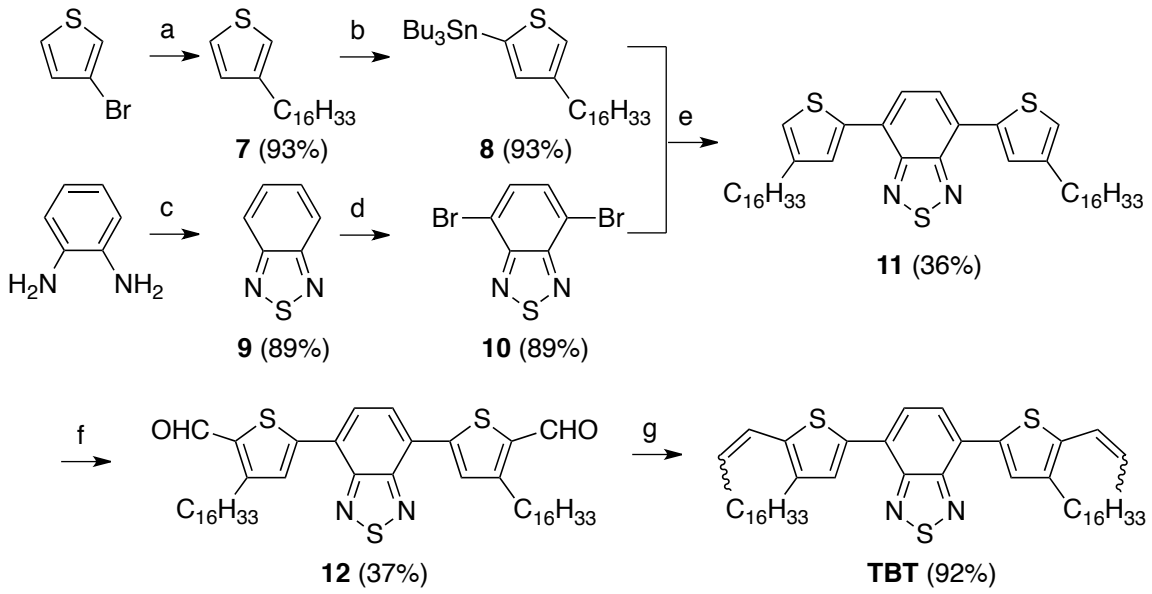

Synthesis of 3-hexadecylthiophene (7). A 250 mL 3-neck round bottom flask was equipped with a magnetic stir bar, reflux condenser, glass stopcock, liquid addition funnel, and two rubber septa. Magnesium turnings (3.3 g, 136.5 mmol) were added and the apparatus was flame-dried under vacuum. Anhydrous THF (ca. 125 mL) was cannulated into the flask followed by the addition of 1,2-dibromoethane (ca. 0.5 mL) to activate the magnesium. A solution of 1-bromohexadecane (20.0 mL, 65.5 mmol) in anhydrous THF (ca. 25 mL) was added to the liquid addition funnel via syringe and dripped into the Mg/THF mixture over the course of 20 min. Stirred at room temperature under argon for 2 h. The Grignard solution was cannulated into a second flame-dried flask containing a magnetic stir bar, 3-bromothiophene (5.1 mL, 54.6 mmol), 1,3-bis(diphenylphosphino)propane nickel (II) chloride [$Ni(dppp)Cl_2$] (0.60 g, 1.1 mmol), and anhydrous THF (ca. 25 mL) held at 0°C. Stirred under argon for 16 h. Reaction was

quenched with 1 M NH_4HCO_3 (ca. 50 mL), H_2O (ca. 75 mL) was added, and extracted with diethyl ether (2 × 75 mL). The combined organics were washed with H_2O, saturated $NaHCO_3$, and brine (ca. 75 mL each). Dried over Na_2SO_4 and removed solvent under reduced pressure. The remaining residue was dissolved in minimal amount of THF (ca. 15 mL) and precipitated into MeOH (ca. 250 mL, 0 °C). Filtered and dried under vacuum overnight to give an off-white solid (15.6 g, 93%). ^{1}H NMR (500 MHz, $CDCl_3$): δ_H (ppm) = 7.23 (dd, 1H, *J* = 4.80, 3.22 Hz, Th-*H*5), 6.93 (d, 1H, *J* = 4.93 Hz, Th-*H*4), 6.91 (d, 1H, *J* = 2.20 Hz, Th-*H*2), 2.61 (t, 2H, *J* = 7.71 Hz, –CH_2–), 1.61 (quintet, 2H, *J* = 7.34, –CH_2–), 1.25 (bs, 26H, –CH_2–), 0.90 (t, 3H, *J* = 6.89 Hz, –CH_3). ^{13}C NMR (125 MHz, $CDCl_3$): δ_C (ppm) = 143.5 (Th-*C*3), 128.5 (Th-*C*4), 125.2 (Th-*C*5), 119.9 (Th-*C*2), 32.6 (–*C*$H_2$$CH_2CH_3$), 30.8, 30.5, 29.9, 29.8, 29.7, 29.6 (2) (–*C*H_2–), 22.9 (–*C*$H_2$$CH_3$), 14.4 (–*C*$H_3$). HRGC-MS (EI): $M_{calcd.}$ = 308.2538, M_{found} = 308.2555. Anal. calcd. for $C_{20}H_{36}S$: C 77.85, H 11.76, S 10.39; Found: C 78.64, H 11.96, S 9.23.

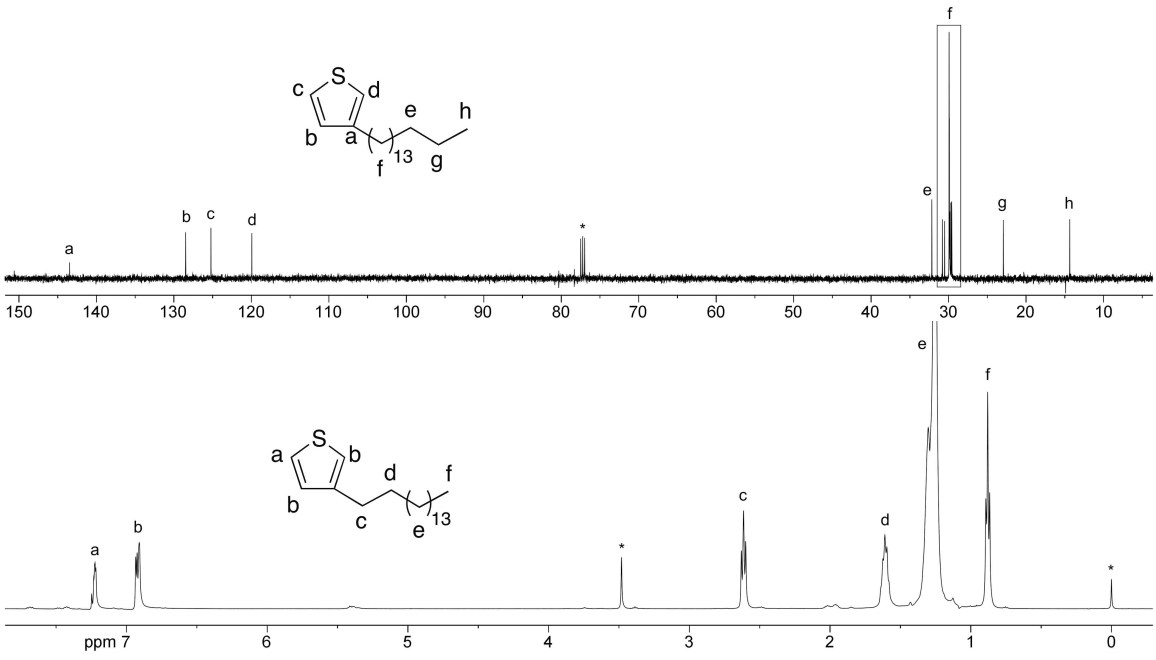

Figure 3.16

^{1}H and ^{13}C NMR spectra of **7**.

Synthesis of 2-tributylstannyl-4-hexadecylthiophene (8). A 2-neck 500 mL round bottom flask was equipped with a magnetic stir bar, liquid addition funnel, and two rubber septa. Flame dried under argon purge. Added **7** (10.0 g, 32.4 mmol) as solid, anhydrous THF (ca. 300 mL) via cannula, and TMEDA (7.3 mL, 48.6 mmol) via syringe. Cooled to -78 °C and added *n*-butyllithium (19.7 mL, 2.5 M hexanes, 49.2 mmol) dropwise over course of 45 min. Allowed to stir under argon while warming to room temperature (ca. 1.5 h). Returned dark brown solution to -78 °C before adding tributyltin chloride (13.1 mL, 48.6 mmol) dropwise over course of 15 min. Returned to room temperature and stirred for 2 h before pouring into H_2O (ca. 300 mL). Extracted with hexanes (3 × 200 mL) and dried over Na_2SO_4. A cloudy liquid was obtained upon solvent removal. Flushed through plug of neutral alumina with hexanes and removed solvent to obtain product as a clear liquid (18.0 g, 93%). Used product without further purification. ^{1}H NMR (300 MHz, $CDCl_3$): δ_H (ppm) = 7.19 (s, 1H, Th-*H*5), 6.97 (s, 1H, Th-*H*3), 2.65 (t, 2H, *J* = 7.74 Hz, Th–C*H*$_2$–), 1.64–1.51 (m, 8H, –C*H*$_2$–), 1.37–1.25 (m, 32H, –C*H*$_2$–), 1.09 (m, 6H, –C*H*$_2$–), 0.90 (m, 12 H, –C*H*$_3$). ^{13}C NMR (125 MHz, $CDCl_3$): δ_C (ppm) = 144.6 (Th-*C*4), 137.0 (Th-*C*3), 136.4 (Th-*C*2), 125.6 (Th-*C*5), 32.1, 30.9, 30.2, 29.9 (2), 29.8, 29.7 (2), 29.6, 29.1 (–*C*H$_2$–), 27.4 (Sn–CH$_2$*C*H$_2$–), 22.9 (Sn–(CH$_2$)$_2$*C*H$_2$–), 14.3 (–*C*H$_3$), 13.9 (Sn–*C*H$_2$–), 10.9 (Sn–(CH$_2$)$_3$*C*H$_3$). HRGC-MS (EI): $M_{calcd.}$ = 598.3594, M_{found} = 597.3567. Anal. calcd. for $C_{32}H_{62}SSn$ C 64.31, H 10.46; Found: C 66.24, H 10.90.

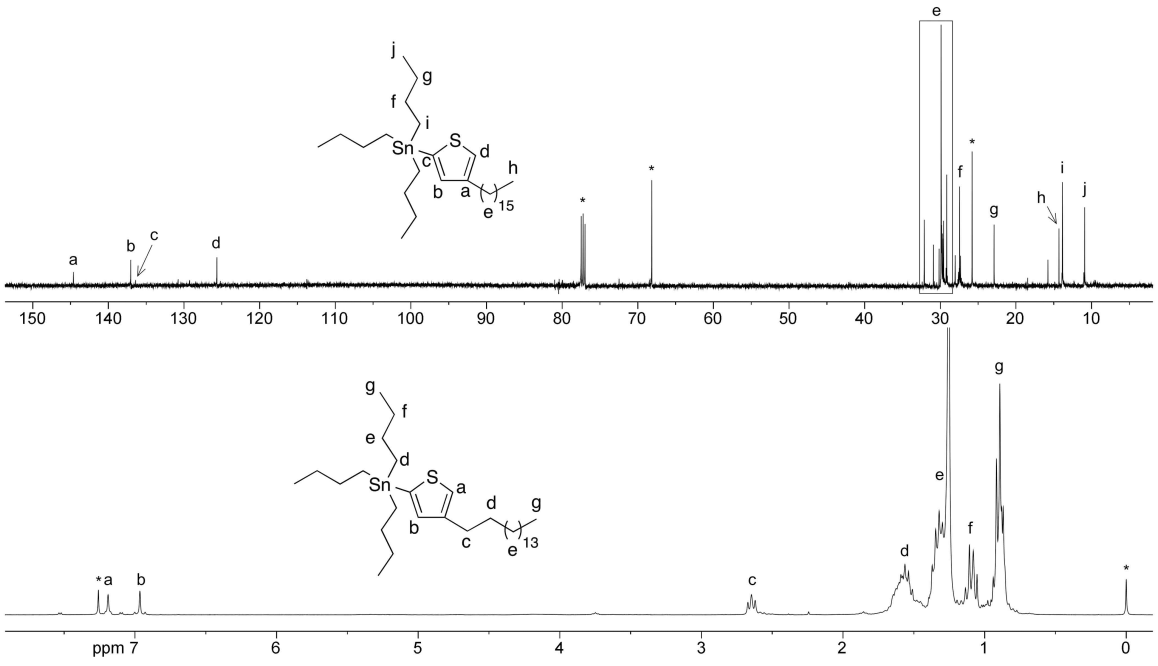

Figure 3.17

^{1}H and ^{13}C NMR spectra of **8**.

Synthesis of 2,1,3-benzothiadiazole (9). A 1 L round bottom flask was equipped with a stir bar and flame dried. Added *o*-phenylenediamine (30.0 g, 277 mmol), triethylamine (TEA) (154 mL, 1.11 mol), and CH_2Cl_2 (ca. 600 mL). Stirred under argon overnight to dissolve. Using a liquid addition funnel thionyl chloride (40.4 mL, 554 mmol) was *slowly* added over the course of 3 h. Solution turned orange-brown and triethylamine hydrochloride salt precipitated. Reaction was refluxed for 4 h before cooling to room temperature. Solvent was removed under reduced pressure. Residue was extracted into CH_2Cl_2 (4 × 200 mL) from H_2O (ca. 1 L). Combined organics were dried over Na_2SO_4 and the solvent was again removed under reduced pressure. Sublimed (50 °C, 20 mtorr) to isolate product as yellow crystals (33.4 g, 89%). ^{1}H NMR (500 MHz, $CDCl_3$): δ_H (ppm) = 8.01 (m, 2H, Bz-*H*2), 7.59 (m, 2H, Bz-*H*3). ^{13}C NMR (125 MHz, $CDCl_3$): δ_C (ppm) = 155.0 (Bz-*C*1), 129.5 (Bz-*C*3), 121.7 (Bz-*C*2). HRGC-MS (EI): $M_{calcd.}$ =

136.0095, M_{found} = 136.0089. Anal. calcd. for $C_6H_4N_2S$: C 52.92, H 2.96, N 20.57, S 23.55; Found: C 52.62, H 2.84, N 20.31, S 23.66.

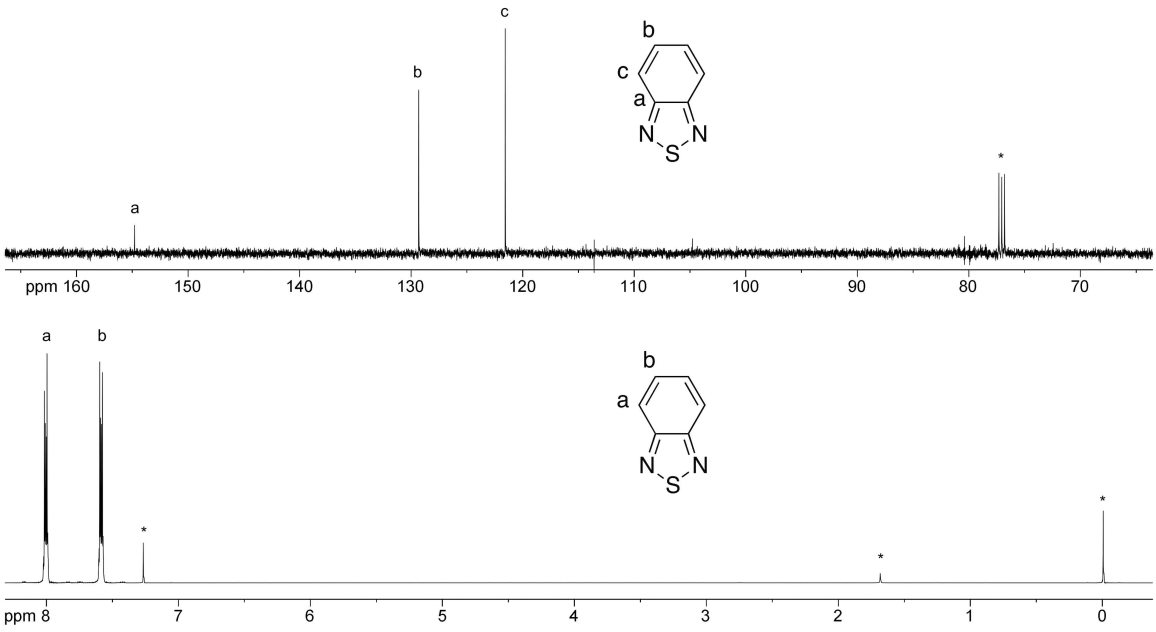

Figure 3.18

^1H and ^{13}C NMR spectra of **9**.

Synthesis of 4,7-dibromo-2,1,3-benzothiadiazole (10). A 1 L round bottom flask was equipped with a magnetic stir bar before adding **9** (20.0 g, 147 mmol) and concentrated HBr (48 wt. %, ca. 300 mL). The flask was fitted with an addition funnel to which Br_2 (22.6 mL, 441 mmol) and HBr (ca. 150 mL) were added. Br_2 solution was *slowly* added over course of 2.5 h during which time an orange precipitate formed. Refluxed for 4 h before quenching excess Br_2 with a saturated $NaHSO_3$ solution. Filtered rinsing with copious amounts of H_2O and cold diethyl ether (ca. 300 mL). Product was isolated as yellow needles (38.4 g, 89%). ^1H NMR (500 MHz, d_6-DMSO): δ_H (ppm) = 7.97 (s, 2H, Bz-*H*). ^{13}C NMR (125 MHz, d_8-THF): δ_C (ppm) = 154.1 (Bz-*C*1), 133.5 (Bz-*C*3), 114.7 (Bz-*C*2). HRGC-MS (EI): $M_{calcd.}$ = 291.8305, M_{found} = 291.8287. Anal. calcd. for

$C_6H_2Br_2N_2S$: C 24.51, H 0.69, Br 54.21, N 9.53, S 10.91; Found: C 24.75, H 0.61, Br 54.21, N 9.53, S 10.94.

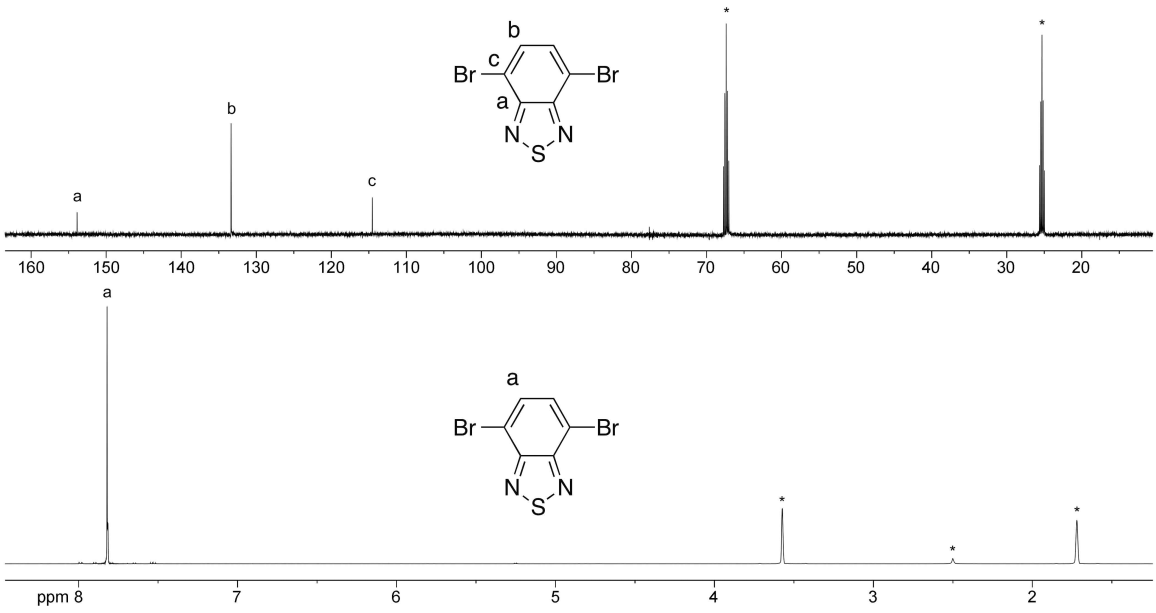

Figure 3.19

^1H and ^{13}C NMR spectra of **10**.

Synthesis of 4,7-Bis(4-hexadecyl-2-thienyl)-2,1,3-benzothiadiazole (11). A 2-neck 250 mL round bottom flask was equipped with a magnetic stir bar, rubber septum, reflux condenser, and stopcock. The apparatus was flame dried before adding **10** (3.56 g, 12.1 mmol) under an argon purge. Cannulated anhydrous THF (ca. 100 mL) in and added **8** (17.35 g, 29.0 mmol) via syringe. Bis(triphenylphosphine)palladium (II) dichloride (168 mg, 0.24 mmol) was added as a solid. The reaction was refluxed under argon for 20 h during which time a dark orange color was observed. The solvent was removed under reduced pressure and the resulting dark orange residue was purified by column chromatography (SiO_2, CH_2Cl_2:hexanes 1:9) to give a bright orange solid (3.25 g, 36%). ^1H NMR (300 MHz, $CDCl_3$): δ_H (ppm) = 7.98 (s, 2H, Th-*H*5), 7.83 (s, 2H, Bz-*H*3),

7.04 (s, 2H, Th-*H*3), 2.69 (t, 4H, *J* = 7.65 Hz, Th–CH_2–), 1.70 (quintet, 4H, *J* = 7.33, Th–CH_2C*H_2*–), 1.25 (bs, 52H, –CH_2–), 0.88 (t, 6H, *J* = 6.57 Hz, –CH_3). ^{13}C NMR (125 MHz, $CDCl_3$): δ_C (ppm) = 152.8 (Bz-*C*1), 144.6 (Th-*C*2), 139.2 (Th-*C*4), 129.2 (Th-*C*3), 126.2 (Bz-*C*2), 125.7 (Bz-*C*3), 121.7 (Th-*C*5), 32.2 (–*C*$H_2CH_2CH_3$), 30.9 (Th–CH_2C*H_2*–), 30.7 (Th–*C*H_2–), 29.9 (2), 29.7, 29.6 (–*C*H_2–), 22.9 (–*C*H_2CH_3), 14.4 (–*C*H_3). HRGC-MS (EI): $M_{calcd.}$ = 748.4858, M_{found} = 748.4850. Anal. calcd. for $C_{46}H_{72}N_2S_3$: C 73.74, H 9.69, N 3.74, S 12.84; Found: C 73.71, H 9.80, N 3.71, S 12.66.

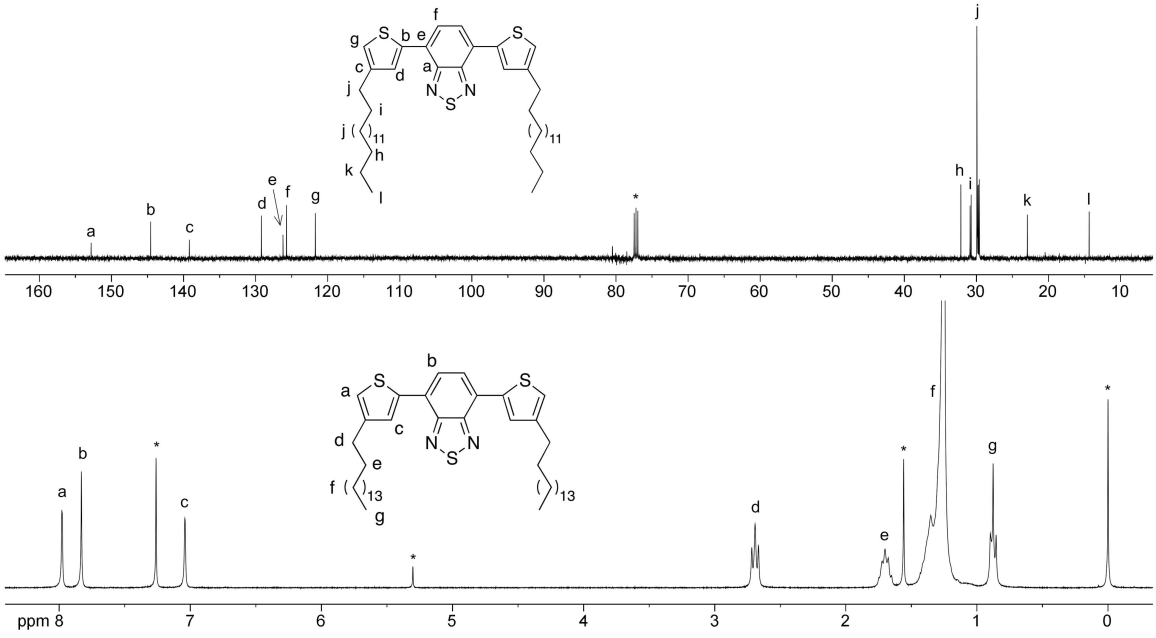

Figure 3.20

^{1}H and ^{13}C NMR spectra of **11**.

Synthesis of 4,7-Bis(5-carbaldehyde-4-hexadecyl-2-thienyl)-2,1,3-benzothiadiazole (12). A 3-neck 500 mL round bottom flask was equipped with a magnetic stir bar, liquid addition funnel, reflux condenser, glass stopcock, and two rubber septa. Flame dried the apparatus before adding anhydrous DMF (1.85 mL, 24.0 mmol) via syringe. Cooled to 0 °C before *slowly* adding phosphorus oxychloride ($POCl_3$, 2.0 mL, 21.6 mmol). Stirred

at room temperature under argon for 1 h. Dissolved **11** (3.0 g, 4.0 mmol) in 1,2-dichloroethane (ca. 150 mL) and transferred to addition funnel. Added dropwise to Vilsmeier reagent over course of 20 min and refluxed 20 h. Poured dark red solution into 2 M NaOAc (ca. 300 mL) and stirred for 2 h. Extracted mixture with CH_2Cl_2 (3 × 300 mL) and dried over Na_2SO_4. Solvent was removed under reduced pressure and the resultant residue was purified by careful column chromatograpy with CH_2Cl_2:hexanes (1:1) then CH_2Cl_2 then $CHCl_3$. Product was isolated as a dark orange-red solid (1.18 g, 37%). ^{1}H NMR (500 MHz, $CDCl_3$): δ_H (ppm) = 10.11 (s, 2H, –C*H*O), 8.10 (s, 2H, Th-*H*3), 8.01 (s, 2H, Bz-*H*3), 3.04 (t, 4H, *J* = 7.68, Th–CH_2–), 1.77 (quintet, 4H, *J* = 7.52 Hz, Th–CH_2CH_2–), 1.43 (quintet, 4H, *J* = 7.14, Th–$(CH_2)_2$CH_2–), 1.25 (bs, 48H, –CH_2–), 0.87 (t, 6H, *J* = 6.74 Hz, –CH_3). ^{13}C NMR (75 MHz, 1,1,2,2-tetrachloroethane-d_2): δ_C (ppm) = 181.8 (–*C*HO), 152.9 (Th-*C*4), 152.3 (Bz-*C*1), 146.4 (Th-*C*2), 138.3 (Th-*C*5), 131.0 (Th-*C*3), 126.6 (Bz-*C*3), 125.2 (Bz-*C*2), 31.7 (–*C*$H_2$$CH_2$$CH_3$), 31.1 (Th–$CH_2$*C*$H_2$–), 30.3 (Th–*C*$H_2$–), 29.4, 29.3, 29.2, 29.1, 28.6 (–*C*H_2–), 22.4 (–*C*$H_2$$CH_3$), 13.8 (–*C*$H_3$). HRGC-MS (EI): $M_{calcd.}$ = 804.4756, M_{found} = 804.4754. Anal. calcd. for $C_{48}H_{72}N_2O_2S_3$: C 71.59, H 9.01, N 3.48, O 3.97, S 11.95; Found: C 70.86, H 8.85, N 3.43, O 3.77, S 11.55.

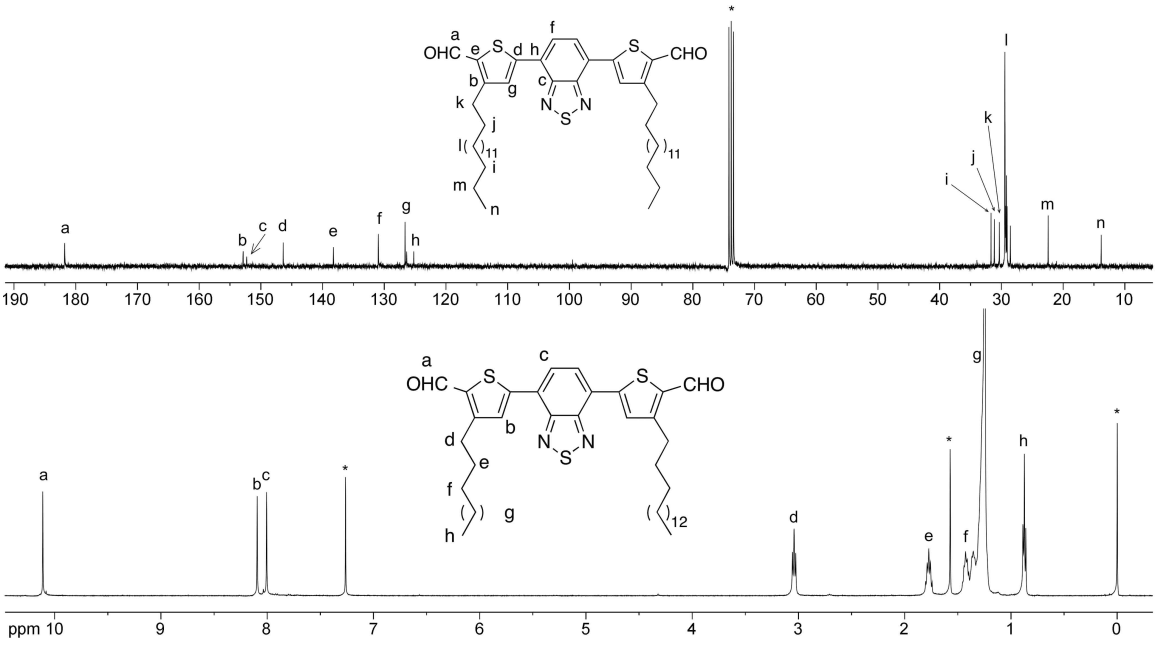

Figure 3.21

^{1}H and ^{13}C NMR spectra of **12**.

Synthesis of 4,7-Bis(5-propenyl-4-hexadecyl-2-thienyl)-2,1,3-benzothiadiazole (TBT). A 2-neck 100 mL round bottom flask was equipped with a magnetic stir bar, reflux condenser, glass stopcock, and rubber septum. Flame dried apparatus before adding sodium bis(trimethylsilyl) amide (0.92 g, 5.0 mmol) and ethyltriphenylphosphonium bromide (1.86 g, 5.0 mmol) under argon purge. The apparatus was pumped and backfilled with argon (5x) to remove residual air and moisture. Cannulated anhydrous hexanes (ca. 50 mL) into flask and refluxed for 1 h during which time the dark orange-red Wittig reagent formed. Cooled to -78 °C and removes hexanes via syringe taking care not to remove precipitated Wittig reagent. Repeated cold hexanes wash with another 50 mL. Residual hexanes were removed under vacuum. Anhydrous THF (ca. 60 mL) was added to dissolve ylide. This solution was *carefully* (taking care not to transfer salts) cannulated into a separate 200 mL round bottom flask containing anhydrous THF (ca. 40 mL) and **12** (1.00 g, 1.24 mmol) held at 0 °C. Stirred for 1 h while warming to room

temperature. Removed solvent under reduced pressure and flushed through plug of silica gel with hexanes to remove $Ph_3P{=}O$. Eluent was concentrated, dissolved in minimal $CHCl_3$, and precipitated in MeOH (ca. 200 mL) at 0 °C. Product was isolated by filtration and dried under vacuum to give a dark red-purple solid (0.95 g, 92%). *Z*:*E* from ^{1}H NMR was 62:38. ^{1}H NMR (500 MHz, $CDCl_3$): δ_H (ppm) = 7.98, 7.89 (isomers, d, 2H, *J* = 3.63 Hz, Th-*H*3), 7.79–7.63 (m, 2H, Bz-*H*3), 6.63–6.56 (m, 2H, Th–C*H*=CHCH$_3$), 6.20–6.11 (m, 2H, *E* Th–CH=C*H*CH$_3$), 5.83–5.75 (m, 2H, *Z* Th–CH=C*H*CH$_3$), 2.66 (m, 4H, Th–CH_2–), 2.09 (dt, 3H, *J* = 7.32, 1.69 Hz, *Z* Th–CH=CHCH_3), 1.92 (dd, 3H, *J* = 6.70, 1.51 Hz, *E* Th–CH=CHCH_3), 1.66 (m, 4H, Th–CH$_2$CH_2–), 1.25 (bs, 52H, –CH_2–), 0.87 (t, 6H, *J* = 6.97 Hz, –CH_3). ^{13}C NMR (125 MHz, $CDCl_3$): δ_C (ppm) = 152.9 (Bz-*C*1), 142.4 (Th-*C*2), 140.2 & 138.1 (Th-*C*4), 137.4 & 135.6 (Th-*C*5), 130.5 & 129.8 (Th-*C*3), 126.4 (Bz-*C*2), 125.7 (2) (Th–CH=*C*HCH$_3$), 125.4 (Bz-*C*3), 122.9, 121.5 (Th-*C*H=CHCH$_3$), 32.2 (–*C*H$_2$CH$_2$CH$_3$), 31.2, 31.6 (Th–CH$_2$*C*H$_2$–), 29.9 (2), 29.7 (2), 29.6, (–*C*H$_2$–), 29.1, 28.6 (Th–*C*H$_2$–), 22.9 (–*C*H$_2$CH$_3$), 19.0, 15.8 (Th–CH=CH*C*H$_3$), 14.4 (–*C*H$_3$). HRGC-MS (EI): $M_{calcd.}$ = 828.5484, M_{found} = 748.4850. Anal. calcd. for $C_{52}H_{80}N_2S_3$: C 75.30, H 9.72, N 3.38, S 11.60; Found: C 75.54, H 9.92, N 3.34, S 11.33.

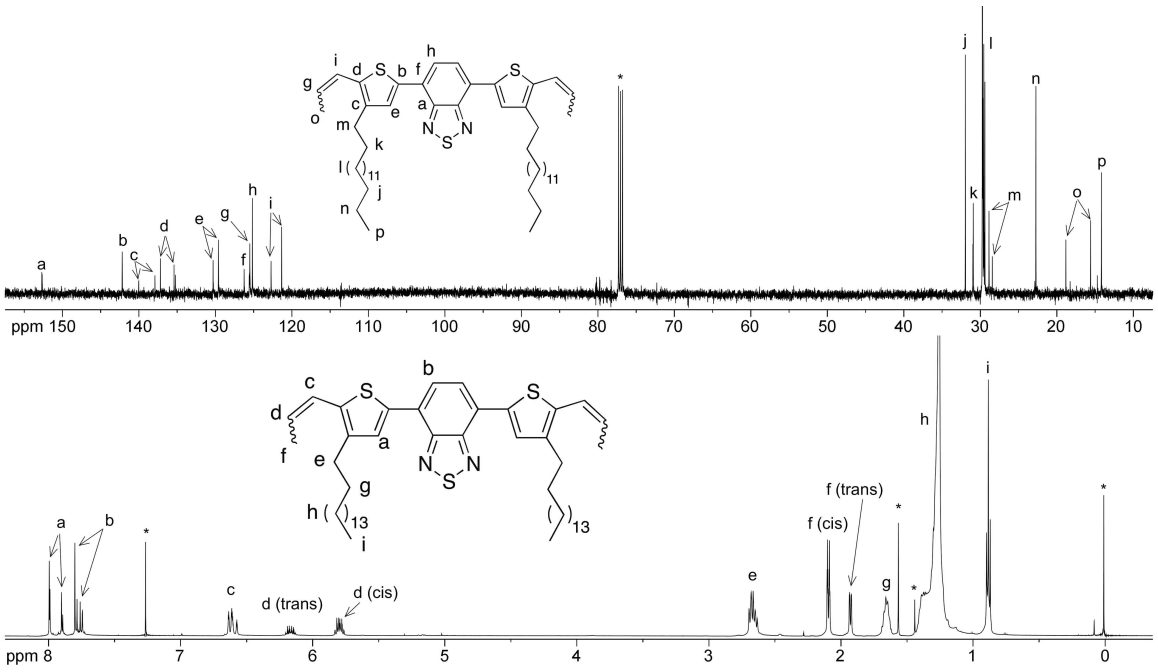

Figure 3.22

^{1}H and ^{13}C NMR spectra of TBT.

General polymerization procedure. An apparatus like that described in Figure 2.24 was assembled and flame-dried under vacuum before placing under argon. The Schlenk tube was charged with monomer(s) in a solution of anhydrous 1,2,4-trichlorobenzene (TCB) (ca. 0.15 M). The solution was degassed by freeze-pump-thaw and heated to 80 °C. G3 (1 mol%) was added as a solution in TCB (ca. 0.05 M). Dynamic vacuum was applied and the polymerization was run for 16–48 h. The polymer was precipitated into a 20-fold excess of non-solvent (acetone or methanol) held at 0 °C. Filtered through a Soxhlet thimble and purified by Soxhlet extraction with non-solvent (ca. 100 mL). Extracted into chloroform (ca. 100 mL) and concentrated under reduced pressure before reprecipitating in non-solvent (0 °C). Filtered and dried under vacuum to obtain the target material as a black solid.

C16-PTV. C16 (1.0 g, 2.57 mmol) was dissolved in TCB (15 mL). Added G3 (23 mg, 0.026 mmol) in TCB (0.5 mL) and allowed polymerization to proceed for 48 h before workup (0.70 g, 82%). ^{1}H NMR (500 MHz, $CDCl_3$): δ_H (ppm) = 7.00–6.80 (m, 2H, olefinic *H*s), 6.78 (bs, 1H, Th-*H*4), 2.61 (bs, 2H, –C*H*$_2$–), 1.60 (bs, 2H, –C*H*$_2$–), 1.25 (bs, 26H, –C*H*$_2$–), 0.87 (t, 3H, *J* = 6.62 Hz, –C*H*$_3$). Anal. calcd. for $C_{22}H_{36}S$: C 79.45, H 10.91, S 9.64; Found: C 79.67, H 11.07, S 9.46.

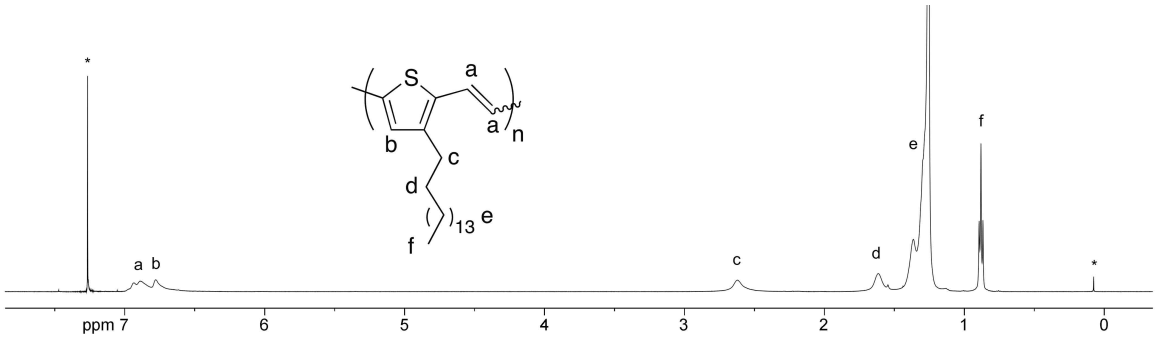

Figure 3.23

^{1}H NMR spectra of C16-PTV.

OC16-PTV. OC16 (0.5 g, 1.24 mmol) was dissolved in TCB (7 mL). Added G3 (11 mg, 0.012 mmol) in TCB (0.5 mL) and allowed polymerization to proceed for 48 h before workup (0.38 g, 88%). ^{1}H NMR (500 MHz, $CDCl_3$): δ_H (ppm) = 7.1–6.6 (m, 3H, aromatic and olefinic *H*s), 4.04 (bs, 2H, Th–OC*H*$_2$–), 1.80 (bs, 2H, Th–OCH$_2$–C*H*$_2$–), 1.48 (bs, 2H, Th–O–(CH$_2$)$_2$–C*H*$_2$–), 1.25 (bs, 24H, –C*H*$_2$–), 0.87 (t, 3H, *J* = 6.85 Hz, –C*H*$_3$). Anal. calcd. for $C_{22}H_{36}OS$: C 75.80, H 10.41, O 4.59, S 9.20; Found: C 74.79, H 10.27, O 4.70, S 8.98.

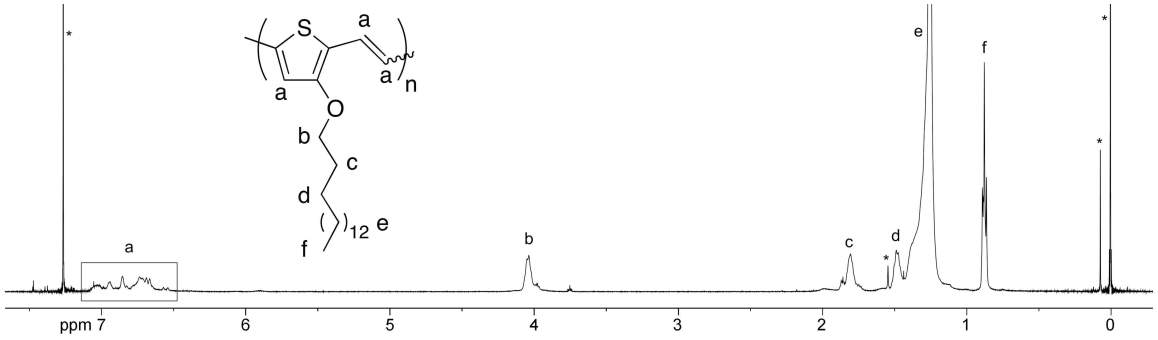

Figure 3.24

^{1}H NMR spectra of OC16-PTV.

TBTV. TBT (100 mg, 0.12 mmol) was dissolved in TCB (4 mL). Added G3 (1 mg, 0.0012 mmol) in TCB (0.3 mL) and allowed polymerization to proceed for 16 h before workup (92 mg, 99%). ^{1}H NMR (500 MHz, $Cl_2CDCDCl_2$): δ_H (ppm) = 8.3–7.5 (m, 6H, aromatic and olefinic *H*s), 3.0–2.4 (m, 4H, Th–C*H*$_2$–), 2.0–0.8 (m, 62H, alkyl *H*s). Anal. calcd. for $C_{48}H_{72}N_2S_3$: C 74.55, H 9.38, N 3.62, S 12.44; Found: C 74.46, H 9.18, N 3.43, S 12.18.

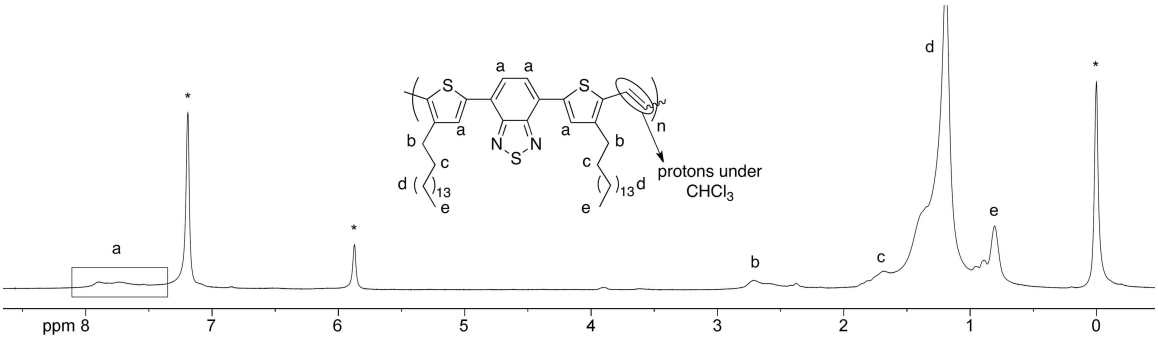

Figure 3.25

^{1}H NMR spectra of TBTV.

3.4.3 Additional Data and Details

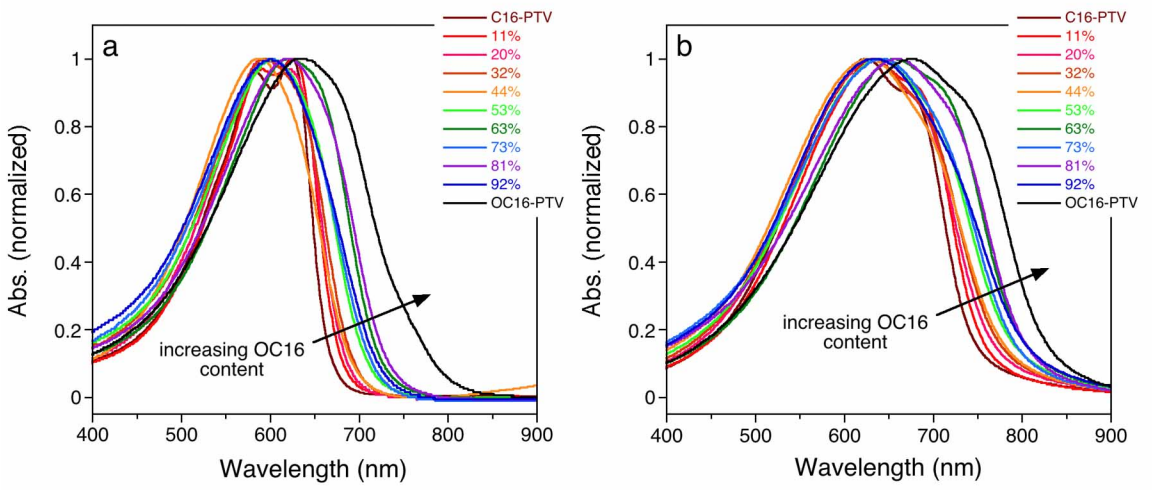

Figure 3.26
Complete UV–vis (a) solution and (b) film spectra of series **1**. Copolymers are labeled with observed OC16 content.

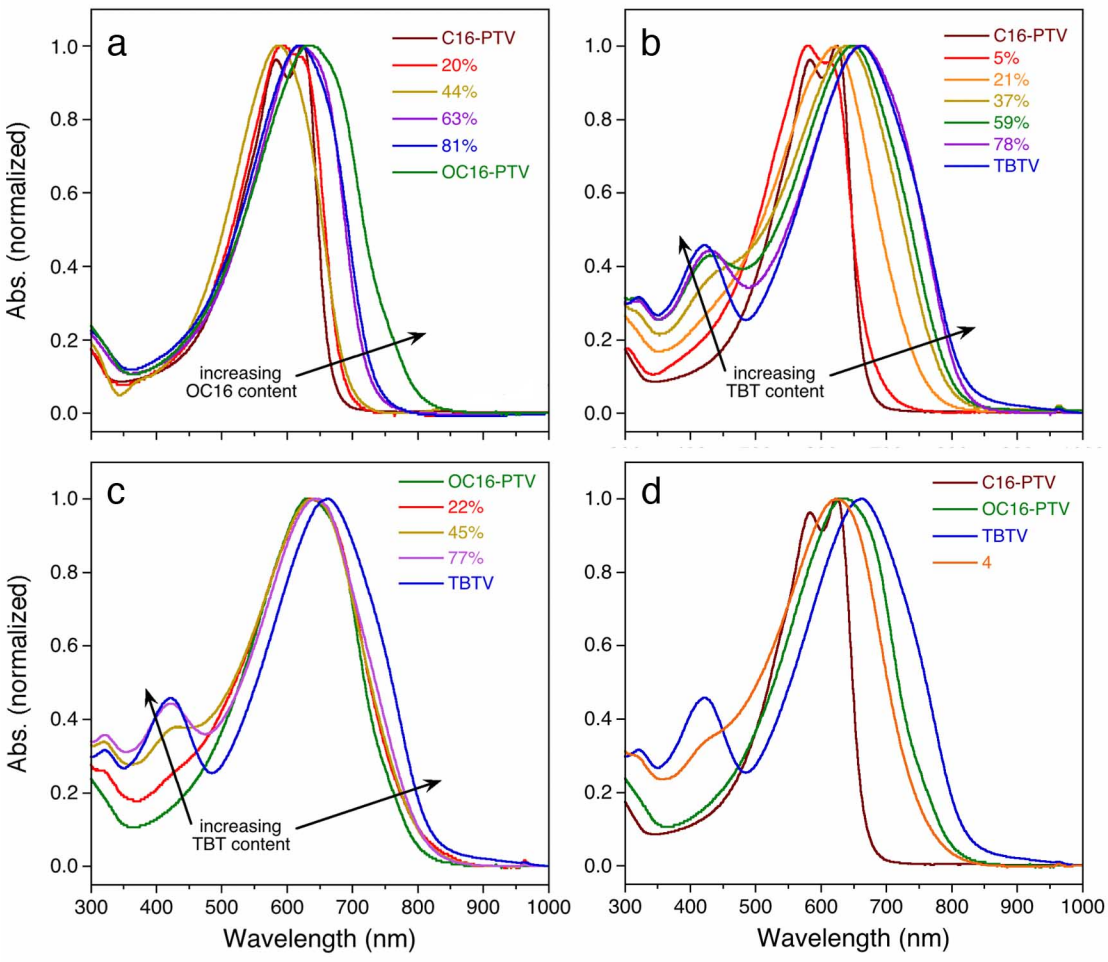

Figure 3.28

UV–vis spectra of series (a) **1**, (b) **2**, (c) **3** and (d) **4** as dilute (ca. 10^{-5} M, repeat unit basis) solutions in $CHCl_3$. Hompolymers are shown for each series to highlight trends. Copolymers are labeled with observed OC16 (a) and TBT (b & c) content.

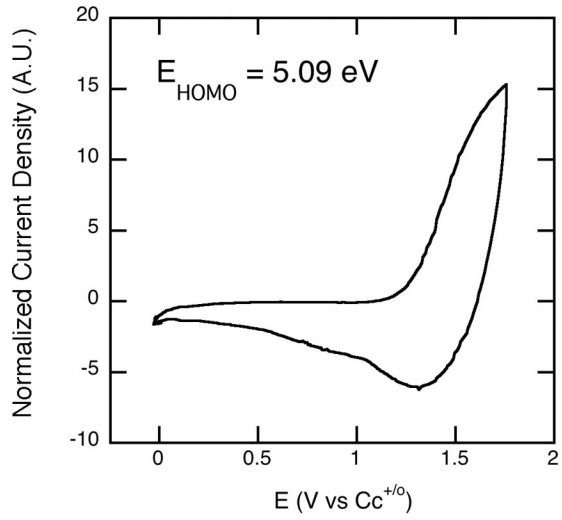

Figure 3.29

CV of **4**.

3.5 References

[1] McQuade, D. T.; Pullen, A. E.; Swager, T. M. *Chem. Rev.* **2000**, *100*, 2537–2574.

[2] Friend, R. H.; Gymer, R. W.; Holmes, A. B.; Burroughes, J. H.; Marks, R. N.; Taliani, C.; Bradley, D. D. C.; Dos Santos, D. A.; Brédas, J. L.; Lögdlund, M.; Salaneck, W. R. *Nature* **1999**, *397*, 121–128.

[3] Katz, H. E.; Bao, Z.; Gilat, S. L. *Acc. Chem. Res.* **2001**, *34*, 359–369.

[4] Günes, S.; Neugebauer, H.; Sariciftci, N. S. *Chem. Rev.* **2007**, *107*, 1324–1338.

[5] Zhou, H.; Yang, L.; Stuart, A. C.; Price, S. C.; Liu, S.; You, W. *Angew. Chem. Int. Ed.* **2011**, *50*, 2995–2998.

[6] Chu, T.-Y.; Lu, J.; Beaupré, S.; Zhang, Y.; Pouliot, J.-R.; Wakim, S.; Zhou, J.; Leclerc, M.; Li, Z.; Ding, J.; Tao, Y. *J. Am. Chem. Soc.* **2011**, *133*, 4250–4253.

[7] He, Z.; Zhong, C.; Huang, X.; Wong, W.-Y.; Wu, H.; Chen, L.; Su, S.; Cao, Y. *Adv. Mater.* **2011**, *23*, 4636–4643.

[8] Service, R. F. *Science* **2011**, *332*, 293.

[9] Chen, J.; Cao, Y. *Acc. Chem. Res.* **2009**, *42*, 1709–1718.

[10] Cheng, Y.-J.; Yang, S.-H.; Hsu, C.-S. *Chem. Rev.* **2009**, *109*, 5868–5923.

[11] Kreyenschmidt, M.; Klaerner, G.; Fuhrer, T.; Ashenhurst, J.; Karg, S.; Chen, W. D.; Lee, V. Y.; Scott, J. C.; Miller, R. D. *Macromolecules* **1998**, *31*, 1099–1103.

[12] Lee, J.-I.; Klaerner, G.; Davey, M. H.; Miller, R. D. *Synth. Met.* **1999**, *102*, 1087–1088.

[13] Chen, X.; Schulz, G. L.; Han, X.; Zhou, Z.; Holdcroft, S. *J. Phys. Chem. C.* **2009**, *113*, 8505–8512.

[14] Chen, C.-H.; Hsieh, C.-H.; Dubosc, M.; Cheng, Y.-J.; Hsu, C.-S. *Macromolecules* **2010**, *43*, 697–708.

[15] Burkhart, B.; Khlyabich, P. P.; Canak, T. C.; LaJoie, T. W.; Thompson, B. C. *Macromolecules* **2011**, *44*, 1242–1246.

[16] Khlyabich, P. P.; Burkhart, B.; Ng, C. F.; Thompson, B. C. *Macromolecules* **2011**, *44*, 5079–5084.

[17] Burkhart, B.; Khlyabich, P. P.; Thompson, B. C. *Macromolecules* **2012**, *45*, 3740–3748.

[18] Burkhart, B.; Khlyabich, P. P.; Thompson, B. C. *ACS Macro Lett.* **2012**, *1*, 660-666.

[19] Lehman Jr., S. E.; Wagener, K. B. In *Handbook of Metathesis*; Grubbs, R. H., Ed., Wiley-VCH Verlag GmbH & Co.: Weinheim, 2003; Vol. 3.

[20] Baughman, T. W.; Wagener, K. B. *Adv. Polym. Sci.* **2005**, *176*, 1–42.

[21] Tao, D.; Wagener, K. B. *Macromolecules* **1994**, *27*, 1281–1283.

[22] Nomura, K.; Miyamoto, Y.; Morimoto, H.; Geerts, Y. *J. Polym. Sci., Polym. Chem.* **2005**, *43*, 6166–6177.

[23] Nomura, K.; Morimoto, H.; Imanishi, Y.; Ramhani, Z.; Geerts, Y. *J. Polym. Sci., Polym. Chem.* **2001**, *39*, 2463–2470.

[24] Yamamoto, N.; Ito, R.; Geerts, Y.; Nomura, K. *Macromolecules* **2009**, *42*, 5104–5111.

[25] Qin, Y.; Hillmyer, M. A. *Macromolecules* **2009**, *42*, 6429–6432.

[26] Speros, J. C.; Paulsen, B. D.; White, S. P.; Wu, Y.; Jackson, E. A.; Slowinski, B. S.; Frisbie, C. D.; Hillmyer, M. A. *Macromolecules* **2012**, *45*, 2190–2199.

[27] Wagener, K.; Brzezinska, K.; Anderson, J. D.; Dilocker, S. *J. Polym. Sci., Polym. Chem.* **1997**, *35*, 3441–3449.

[28] Sworen, J. C.; Smith, J. A.; Wagener, K. B.; Baugh, L. S.; Rucker, S. P. *J. Am. Chem. Soc.* **2003**, *125*, 2228–2240.

[29] Wen, S.; Pei, J.; Li, P.; Zhou, Y.; Cheng, W.; Dong, Q.; Li, Z.; Tian, W. *J. Polym. Sci., Polym. Chem.* **2011**, *49*, 2715–2724.

[30] Love, J. A.; Morgan, J. P.; Trnka, T. M.; Grubbs, R. H. *Angew. Chem. Int. Ed.* **2002**, *41*, 4035–4037.

[31] He, Y.; Zhao, G.; Min, J.; Zhang, M.; Li, Y. *Polymer* **2009**, *50*, 5055-5058.

[32] Jestin, I.; Frere, P.; Mercier, N.; Levillain, E.; Stievenard, D.; Roncali, J. *Journal of the American Chemical Society* **1998**, *120*, 8150–8158.

[33] Jenekhe, S. A.; Lu, L.; Alam, M. M. *Macromolecules* **2001**, *34*, 7315–7324.

[34] Paulsen, B. D.; Frisbie, C. D. *J. Phys. Chem. C* **2012**, *116*, 3132–3141.

[35] Hultgren, V. M.; Mariotti, A. W. A.; Bond, A. M.; Wedd, A. G. *Anal. Chem.* **2002**, *74*, 3151–3156.

[36] Shiddiky, M. J. A.; Torriero, A. A. J.; Zhao, C.; Burgar, I.; Kennedy, G.; Bond, A. M. *J. Am. Chem. Soc.* **2009**, *131*, 7976–7989.

[37] Cardona, C. M.; Li, W.; Kaifer, A. E.; Stockdale, D.; Bazan, G. C. *Adv. Mater.* **2011**, *23*, 2367–2371.

Chapter 4

Donor–Acceptor Copolymers Prepared by ADMET Polymerization

This chapter, a continuation of the concepts outlined in the previous chapter, describes the design and synthesis of two electron-rich divinyl monomers and their copolymerization with an electron-poor dipropenyl monomer. Binary monomer combinations over a range of compositions gave two donor–acceptor copolymer series with tunable optoelectronic behavior. Copolymer performance in organic solar cells was also evaluated.

4.1 Introduction

Conjugated polymers (CPs) are promising materials for use in a wide variety of electronic devices[1] including organic solar cells (OSCs).[2] Their ready solubility allows for room temperature solution processing into thin, lightweight, and mechanically flexible devices, which can ultimately result in rapid cost effective production.[3] Increasing concerns over global energy supply have pushed OSCs to the forefront of emerging energy technologies. Consequently, the past decade has seen efficiency improvements from 3.5%[4] to approximately 9%.[5] Most high efficiency OSCs make use of alternating donor-acceptor (D-A) copolymers where the two monomers are present in stoichiometric (1:1) amounts. However, little research has focused on non-stoichimetric D-A polymers. These statistical copolymers warrant investigation as they may lead to enhanced OSC performance and/or finely tuned electronic properties.

Although earlier examples of statistical CPs exist (see Section 3.1), Thompson and coworkers were among the first to demonstrate the value of this approach. Using metal-catalyzed coupling chemistry they prepared "semi-random" CPs[6-8] and demonstrated efficiencies near 5%.[9,10] Other research groups have employed similar copolymerization concepts to achieve efficiencies in the 3–5% range.[11-13] However, all of these copolymerization techniques fail to explore the entire composition window. This deficiency was noted in Chapter 3 and was part of the reason acyclic diene metathesis (ADMET) polymerization was employed to generate random conjugated polymers.[14] Although we were able to demonstrate tuned compositions and optoelectronic properties, the polymers were found unfit for integration into OSCs. First, most of the isolated copolymers were of low molar mass, which is known to reduce OSC performance.[15-19] Second, the copolymer HOMO levels were not sufficiently deep, and, given the correlation between HOMO level and open-circuit voltage (V_{oc}),[20] would have resulted in low OSC efficiencies. Therefore, this chapter focuses on the synthesis of two new

electron-rich (donor) monomers that will address the shortcomings of the previous system.

The electron-poor (acceptor) dipropenyl TBT monomer discussed in Chapter 3 was employed again in this study as it is a common component in high performance CPs.[21,22] However, two new divinyl donor monomers based on fluorene (F) and carbazole (C) were chosen for copolymerization with TBT (Figure 4.1). Both of these monomers address the previously described limitations of the Chapter 3 system. First, these monomers are known to achieve high molar mass during ADMET homopolymerization,[23] and we expected that this would carry over to copolymerization. Second, homopolymers of fluorene and carbazole have deep HOMO levels,[24,25] which could serve to improve OSC efficiency by increasing V_{oc}. Additionally, the TBT-F and TBT-C copolymers are vinyl-containing analogs of high performance CPs.[21,26] We would therefore anticipate improved OSC performance compared to other vinyl containing CPs we have previously prepared.

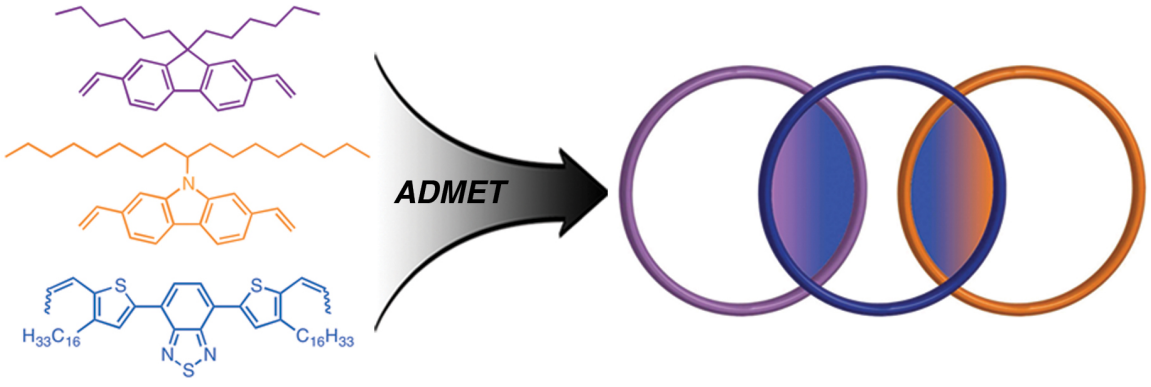

Figure 4.1
Venn diagram illustrating the three monomers and the concept of tunability (overlap) through copolymerization.

In this study, we (i) describe the careful preparation and thorough characterization of two new CP series; (ii) demonstrate the tunability of copolymer optical properties and

energy levels; and (iii) integrate copolymers into OSCs to achieve our highest efficiencies to date.

4.2 Results and Discussion

4.2.1 Monomer Synthesis

For this study two electron-rich divinyl monomers (Scheme 4.1) and an electron-poor dipropenyl monomer were synthesized. The 2,7-divinyl-9,9'-di-n-hexylfluorene (F) monomer was prepared by treating commercially available 2,7-dibromo-9,9'-dihexylfluorene (**1**) with n-butyllithium at -78 ˚C to form the dilithiated species. This species was reacted with N,N-dimethylformamide to yield the dialdehyde (**2**) which was isolated after acidic workup. Standard Wittig chemistry saw the conversion of the dialdehyde intermediate to F, a low melting white solid, with 65% overall yield. Preparation of 2,7-divinyl-N-9'-heptadecanylcarbazole (C) was more involved and followed a convergent synthesis of the carbazole and alkyl functionalities. First, a Grignard reaction employing ethyl formate (**3**) and three equivalents of octyl magnesium bromide afforded a secondary alcohol (**4**), which was tosylated (**5**) with p-toluenesulfonyl chloride. Second, 4,4'-dibromobiphenyl (**6**) was converted to the 2-nitro compound (**7**) using fuming nitric acid. The Cadogan ring-closing reaction successfully converted the nitro compound to the dibromocarbazole (**8**). Nucleophilic attack of the carbazole on the tosylated alkane in the presence of potassium hydroxide afforded the alkyl-substituted dibromocarbazole (**9**). The same chemistry employed in the preparation of F was used to complete the synthesis of C, a white solid, in 26% overall yield. The dipropenyl electron acceptor, 4,7-bis(4-hexadecyl-5-propenyl-2-thienyl)-2,1,3-benzothiadiazole (TBT), was prepared according to previous report[14] (see Section 4.4.2 for complete synthetic details).

Scheme 4.1

Synthesis of F (a) and C (b).

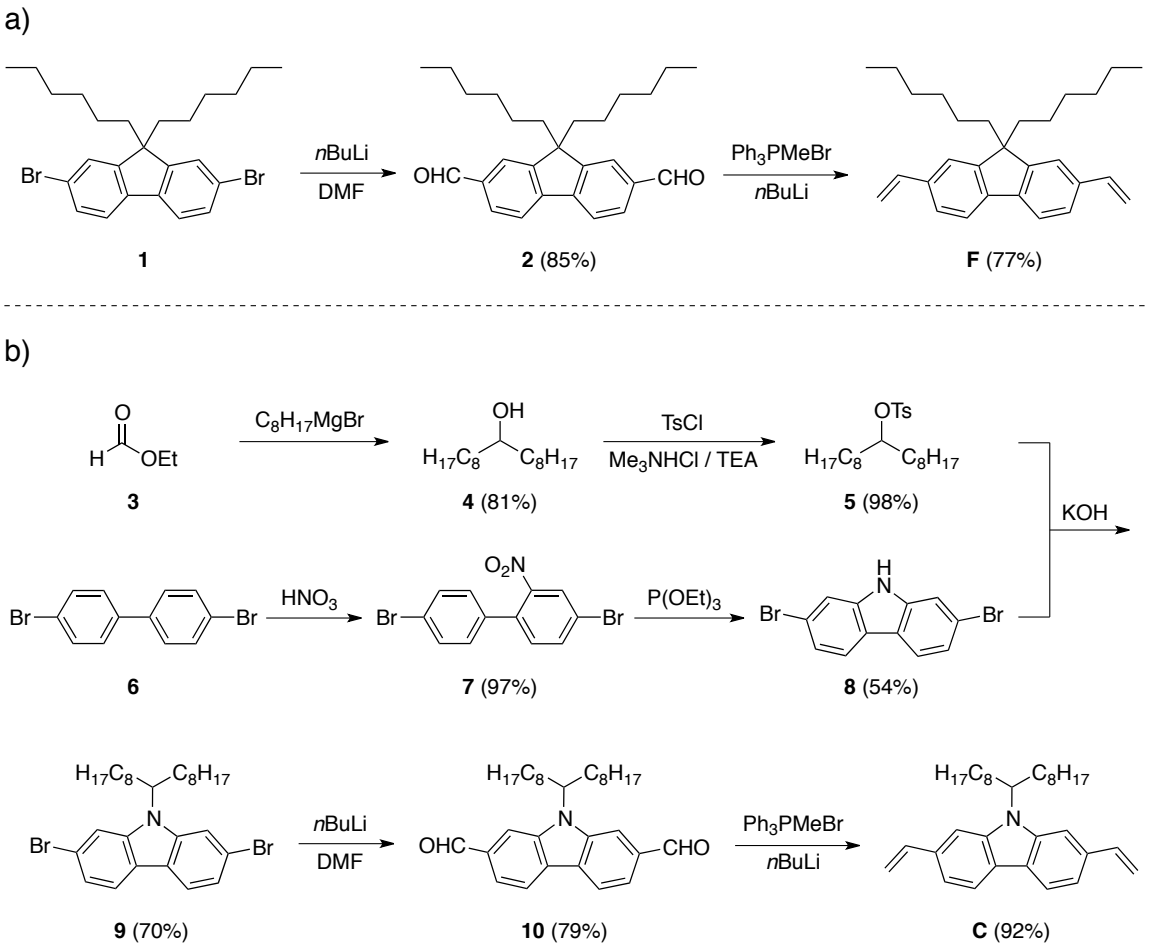

4.2.2 Polymer Synthesis and Characterization

All homopolymers (Scheme 4.2a) and copolymers (Scheme 4.2b) were prepared by ADMET polymerization using the N-heterocyclic carbene functionalized ruthenium metathesis catalyst (G2).[27,28] It should be noted that Chapters 2, 3, and 5 demonstrate the polymerization of dipropenyl monomers. These moieties were chosen because they are

less susceptible to decomposition, thus increasing monomer stability.[29] Additionally, longer catalyst lifetimes are expected during ADMET polymerization because the ethylidene-ruthenium intermediates (dipropenyl) are more stable than their methylidene-ruthenium (divinyl) counterparts.[30] However, existing literature demonstrates the successful ADMET polymerization of F and C (divinyl) without observation of side reactions or monomer decomposition.[23,31] This same literature demonstrates greater polymer molecular weights when G2 is used. This is contrary to the use of the more active G3 employed in Chapters 2, 3, and 5. Although the exact reason for this difference is not understood, it hypothesized that a pyridine-coordinated dormant species is formed when using G3.[23] Considering the increased reactivity (i.e., reduced steric hindrance) of the divinyl monomers, the use of a highly active catalyst (i.e., G3) is unnecessary for polymerization and a more robust catalyst (i.e., G2) can be employed.

Scheme 4.2

Homopolymer (a) and copolymer (b) synthesis.

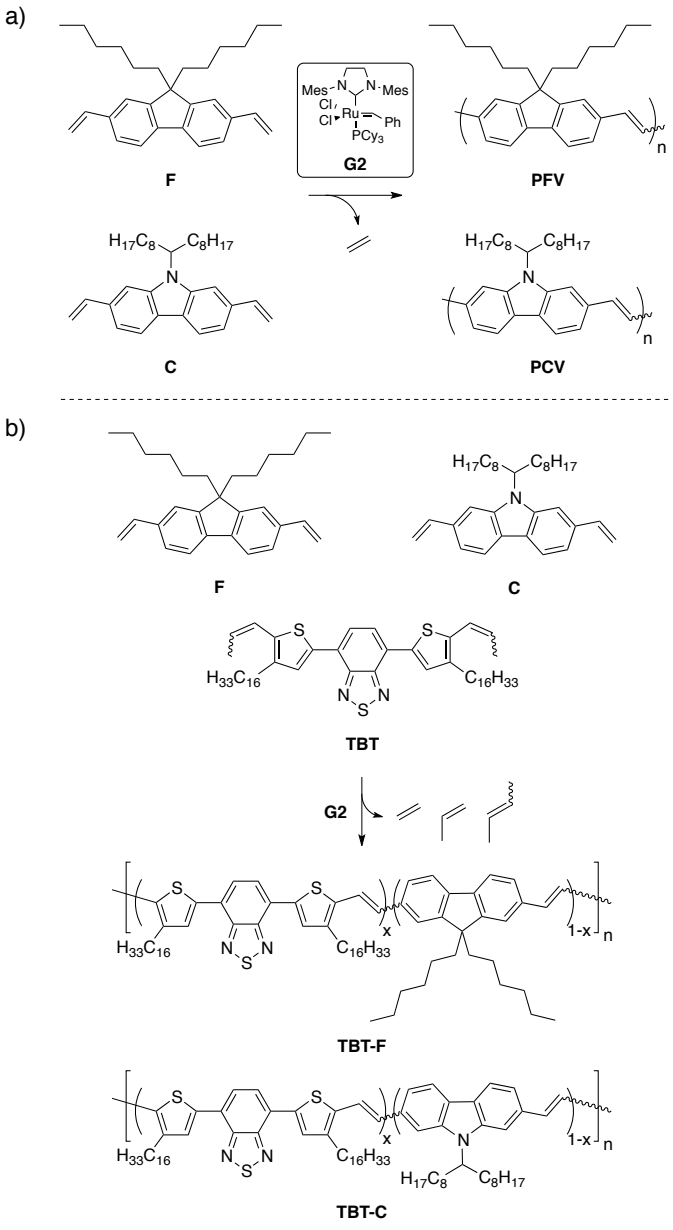

All polymerizations of F, C, and TBT were conducted under reduced pressure (20–50 mtorr) in anhydrous 1,2,4-trichlorobenzene with G2 (1-2 mol%). After polymerization for 15–48 h reactions were quenched by the addition of ethyl vinyl ether and precipitated into a non-solvent (methanol or acetone). Polymers were purified by Soxhlet extraction with the same non-solvent used for precipitation (see Section 4.4.2 for complete synthetic details). Relative polymer molecular weights were determined by size-exclusion chromatography (SEC) in chloroform versus polystyrene standards. ^{1}H NMR spectroscopy was employed to characterize polymers and to quantify the monomer composition in copolymer samples. NMR data was not useful with respect to copolymer sequence distribution. Optical behavior was studied in dilute chloroform solutions (10^{-5} M in monomer repeat units) and as thin films on glass substrates by ultraviolet–visible (UV–vis) spectroscopy. Absorption maxima (λ_{max}) for PFV, PCV, and TBTV homopolymers were 424, 456, and 662 nm, respectively (Figure 4.2a). Secondary absorption features were evidenced in all polymers. The shoulder in PFV and the smaller λ_{max} in PCV were both indicative of aggregation-induced vibronic fine structure. The peak at 442 nm in TBTV was attributed to the π-π* transition, while the principal absorption was a product of intramolecular charge transfer.[32] Thin film UV–vis spectra of PFV and PCV did not demonstrate the significant red shifts typical of CPs (Figure 4.2b). Although vibronic features were still present, the wavelength values themselves were virtually unchanged. The absence of red shift, a product of backbone π-stacking, in both PFV and PCV is likely due to the branched alkyl chains, which prevent polymer ordering beyond the level observed in solution. This effect was ultimately deemed beneficial when preparing copolymers with the highly insoluble TBTV. A red shift of approximately 20 nm in the primary absorption of TBTV was observed in the thin film. This shift would likely be larger if it were not for the limited solubility of TBTV in solution, which results in an artificially high λ_{max}. Optical band gap (E_g^{opt}) values were determined from the onset of absorption in the polymer thin film ($E_g^{opt} = 1240/\lambda_{onset}$). The large difference between

the E_g^{opt} of the electron-rich polymers (ca. 2.6 eV) and that of TBTV (1.49 eV) allows for significant tuning of the absorption profile through copolymerization. All spectroscopic and chromatographic data are summarized in Table 4.1.

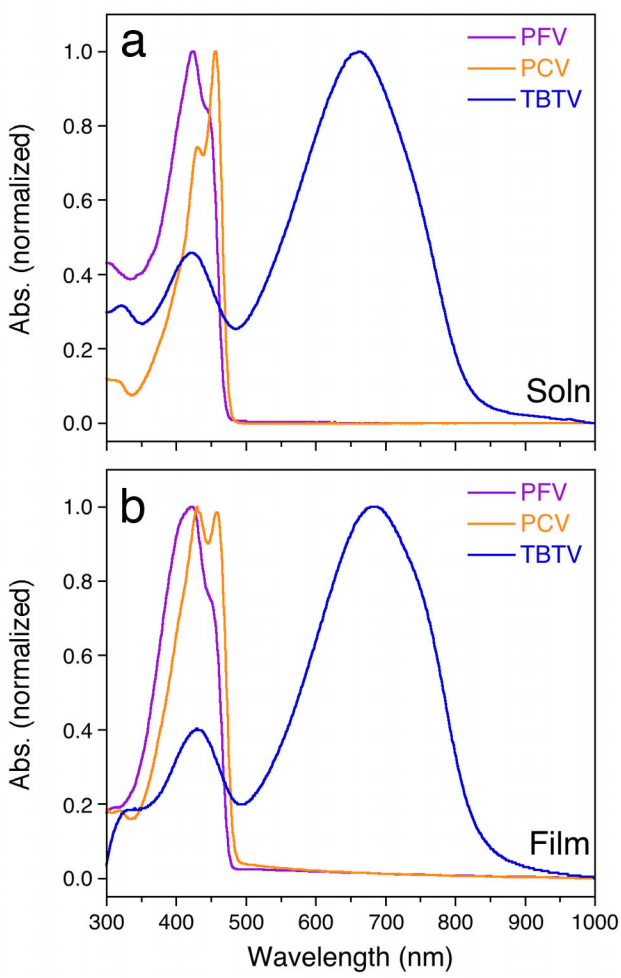

Figure 4.2
UV–vis (a) solution and (b) film spectra of PFV, PCV, and TBTV.

Table 4.1
NMR, SEC, and UV–vis data for homo- and copolymers.

sample ID[a]	observed ratio[b]	M_n (kg/mol)[c]	$Đ_M$[c]	$\lambda_{max,soln}$ (nm)[d]	$\lambda_{max,film}$ (nm)[e]	E_g^{opt} (eV)[f]
PFV	–	6	2.8	424, 447[g]	422, 453[g]	2.57
PCV	–	17	1.3	430, 456	430, 458	2.55
TBTV[b]	–	7	1.9	422, 662	429, 683	1.49
TBT-F	TBT:F					
1a (80:20)	77:23	8	1.7	426, 597	431, 652	1.51
1b (60:40)	58:42	13	1.8	428, 576	430, 608	1.57
1c (50:50)	48:52	22	2.3	428, 566	432, 614	1.58
1d (40:60)	39:61	31	2.3	428, 562	429, 585	1.65
1e (20:80)	23:77	39	2.5	429, 451, 552	429, 452, 575	1.77
TBT-C	TBT:C					
2a (80:20)	79:21	6	2.0	420, 587	429, 635	1.56
2b (60:40)	64:36	11	2.4	426, 578	433, 627	1.57
2c (50:50)	51:49	17	2.0	428, 571	433, 612	1.62
2d (40:60)	43:57	25	1.9	433, 569	435, 607	1.66
2e (20:80)	21:79	49	1.8	429, 450, 554	430, 454, 584	1.77

[a]Values in parentheses are monomer feed ratios. [b]Determined by integration of appropriate resonances in ^{1}H NMR spectra. [c]Determined by SEC in $CHCl_3$ versus polystyrene standards. [d]ca. 10^{-5} M in repeat unit in $CHCl_3$; values indicate peaks in absorbance. [e]Polymer film spin coated from $CHCl_3$ onto glass substrates; values indicate peaks in absorbance. [f]Determined from onset absorption of thin film (E_g^{opt} = 1240 (nm eV)/λ_{onset} (nm)). [g]Absorption shoulder. [b]Values taken from Table 3.1.

4.2.3 TBT-F Copolymers

The TBT:F ratios in isolated copolymers (**1a–e**) were quantified using ^{1}H NMR spectroscopy (Figure 4.3) and were near the feed ratios in all cases (Table 4.1). Copolymer molar mass was observed to increase with increasing F content. This was expected as the less sterically hindered divinyl monomer (F) is thought to polymerize more readily than the dipropenyl (TBT). Although this could not be confirmed spectroscopically (i.e., NMR), it is reasonable to assume that because of this inherent

difference in polymerizability the copolymer sequence distribution could be gradient-like initially. However, the long polymerization times employed allow ample time for cross metathesis and sequence randomization. The λ_{onset} of TBT-F solutions and thin films shifted to longer wavelengths (lower E_g^{opt}) as more TBT was incorporated into the copolymer (Figure 4.4). It is worth noting that although E_g^{opt} did not scale linearly with copolymer composition, a band gap range in excess of 1 eV was probed through this copolymerization technique. Finally, copolymers in this series could be monitored qualitatively by color change (Figure 4.6), which suggests possible colorimetric applications.[33]

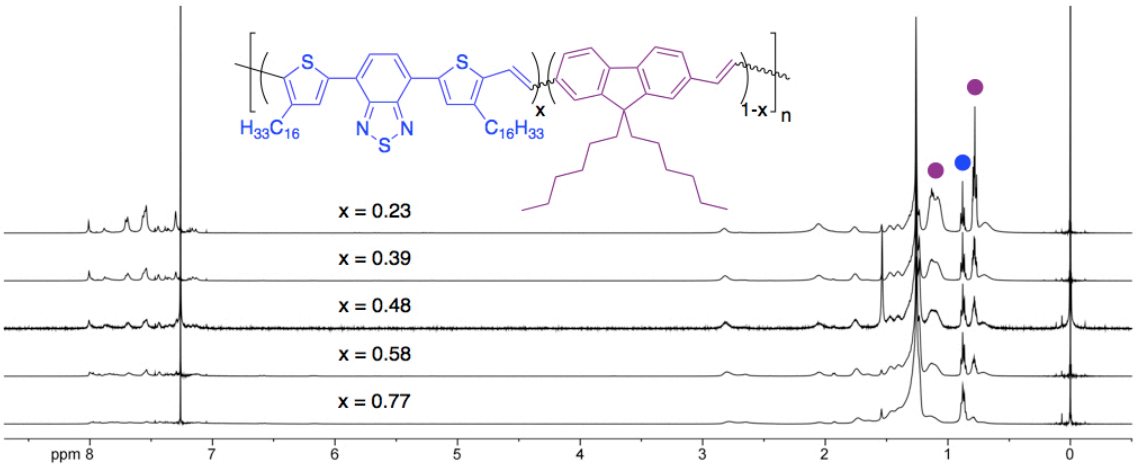

Figure 4.3

^{1}H NMR spectra of series **1**. Colored circles correspond to resonances used to quantify copolymer composition.

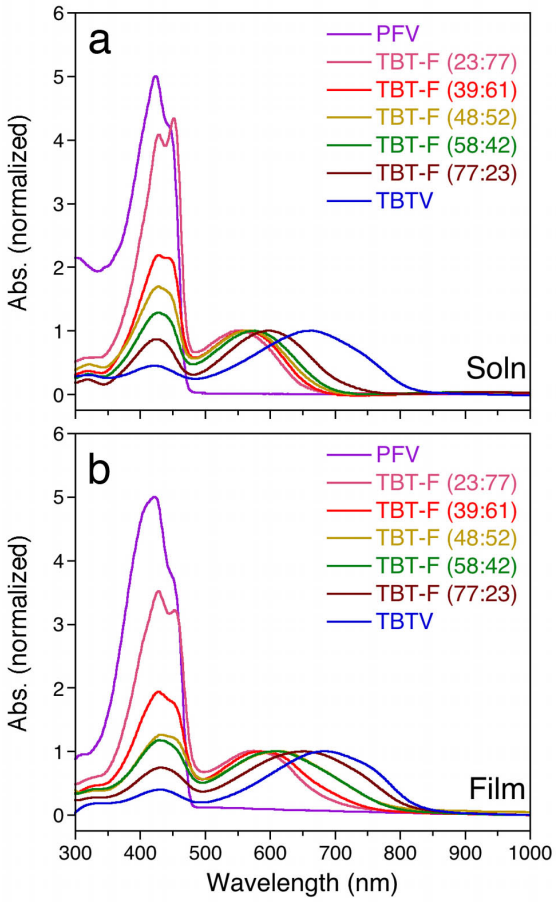

Figure 4.4

UV–vis (a) solution and (b) film spectra of the TBT-F series. All spectra except PFV normalized to the second (TBT) absorption peak. Corresponding homopolymers are shown to highlight trends.

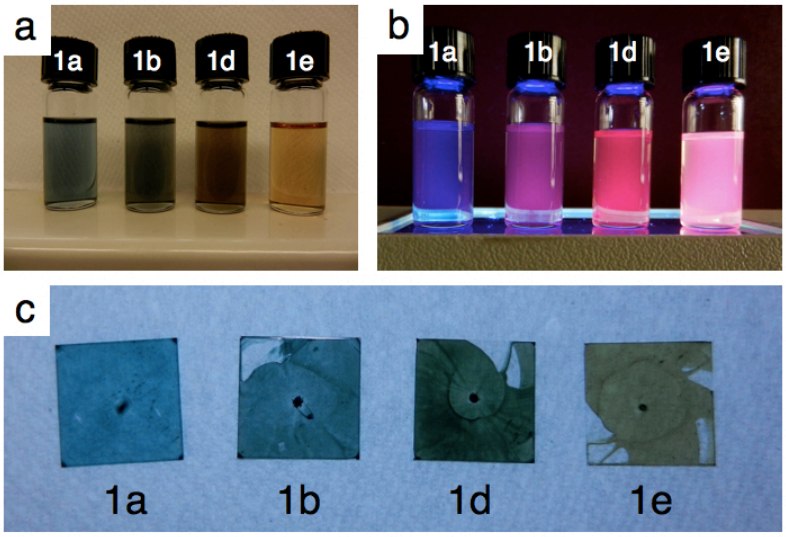

Figure 4.5
Images of TBT-F series (copolymer **1c** omitted) (a) in solution under ambient light, (b) in solution under UV light, and (c) as thin films under ambient light.

4.2.4 TBT-C Copolymers

Carbazole differs from fluorene by one atom (nitrogen bridgehead rather than carbon). Consequently, the molar mass (Table 4.1) and spectroscopic (Figures 4.6-4.8) behavior of the TBT-C series was expectedly similar to that described for TBT-F (Section 4.2.3).

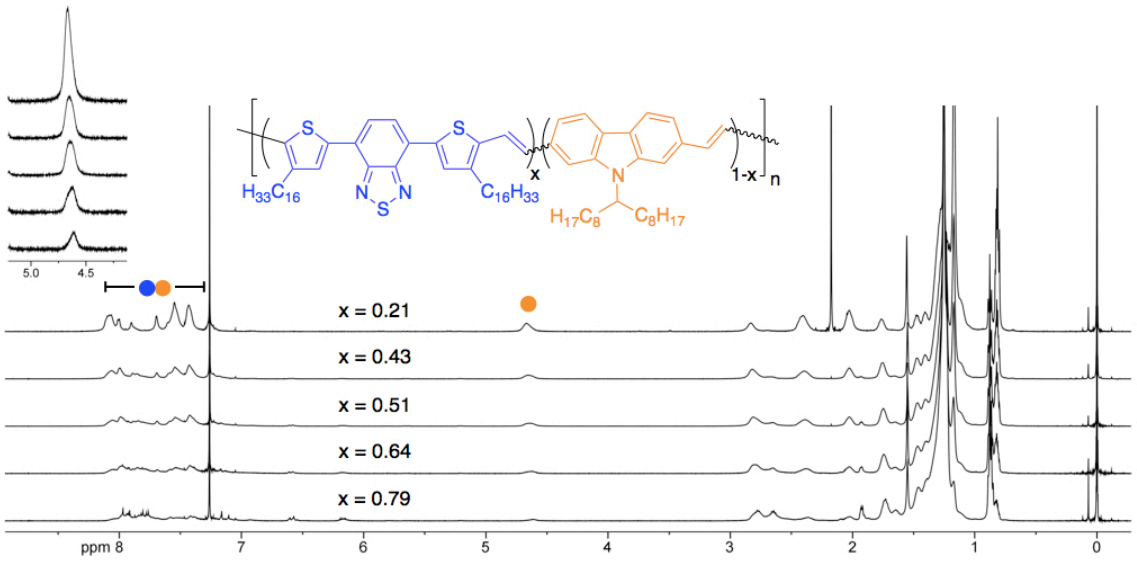

Figure 4.6

^{1}H NMR spectra of series **2**. Colored circles correspond to resonances used to quantify copolymer composition.

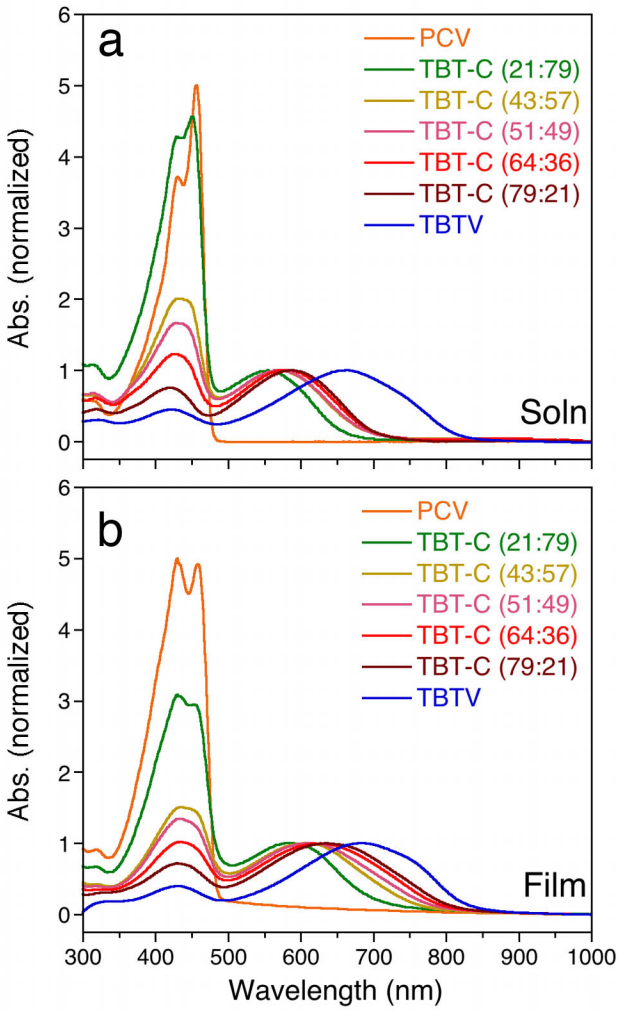

Figure 4.7

UV–vis (a) solution and (b) film spectra of the TBT-C series. All spectra except PCV normalized to the second (TBT) absorption peak. Corresponding homopolymers are shown to highlight trends.

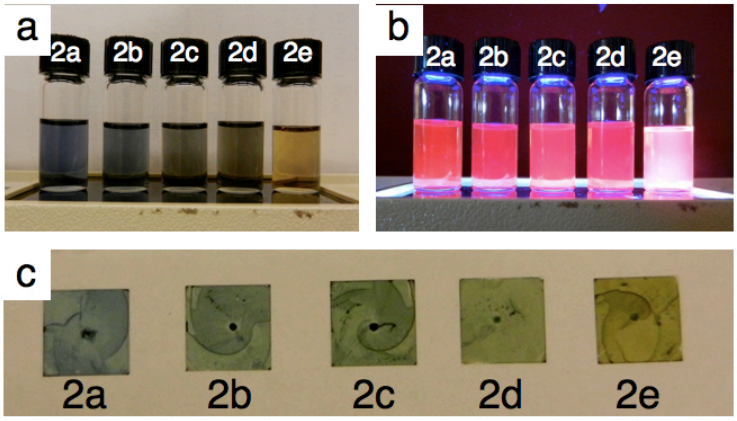

Figure 4.8
Images of TBT-C series (a) in solution under ambient light, (b) in solution under UV light, and (c) as thin films under ambient light.

4.2.5 Electronic Behavior

All polymers were characterized by cyclic voltammetry (CV) to quantify the impact of copolymerization on the position of the highest occupied molecular orbital (HOMO). The same CV procedure outlined in Section 3.2.7 was employed here, and HOMO levels were calculated from the onset of electrochemical oxidation (Figure 4.9). The HOMO level positions of PFV, PCV, and TBTV were -5.85, -5.57, and -5.28 eV, respectively. The data collected from CV is summarized in Table 4.2.

Table 4.2
CV and UV–vis data.

sample ID	HOMO (eV)[a]	LUMO (eV)[b]	E_g^{opt} (eV)[c]
PFV	-5.85	-3.28	2.57
PCV	-5.57	-3.02	2.55
TBTV	-5.28	-3.79	1.49
TBT-F			
1a	-5.42	-3.91	1.51
1b	-5.51	-3.94	1.57
1c	-5.60	-4.02	1.58
1d	-5.62	-3.97	1.65
1e	-5.81	-4.04	1.77
TBT-C			
2a	-5.30	-3.74	1.56
2b	-5.20	-3.63	1.57
2c	-5.40	-3.78	1.62
2d	-5.50	-3.84	1.66
2e	-5.57	-3.80	1.77

[a] $E_{HOMO} = -(E_{(onset,ox\ vs\ Cc+/o)} + 3.75)$ eV [b] Estimated: E_{LUMO} (eV) = E_{HOMO} (eV) + E_g^{opt} (eV) [c] Determined from onset absorption of thin film (E_g^{opt} = 1240 (nm eV)/λ_{onset} (nm)).

Both copolymer series showed similar behavior in HOMO level as a function of copolymer composition. Increasing electron-rich monomer content resulted in a relatively monotonic (with the exception of copolymer **2b**) decrease in HOMO level. This behavior was anticipated because the HOMO levels of PFV and PCV are both similar and significantly lower than that of TBTV. These levels were tuned over a significant range: 570 meV for the TBT-F series and 290 meV for the TBT-C series. Recall, V_{oc} scales directly with the difference between the HOMO level of the electron-donating CP and the LUMO level of the electron-accepting fullerene.[20] Increasing this difference (i.e., deeper HOMO) should result in increased OSC performance.

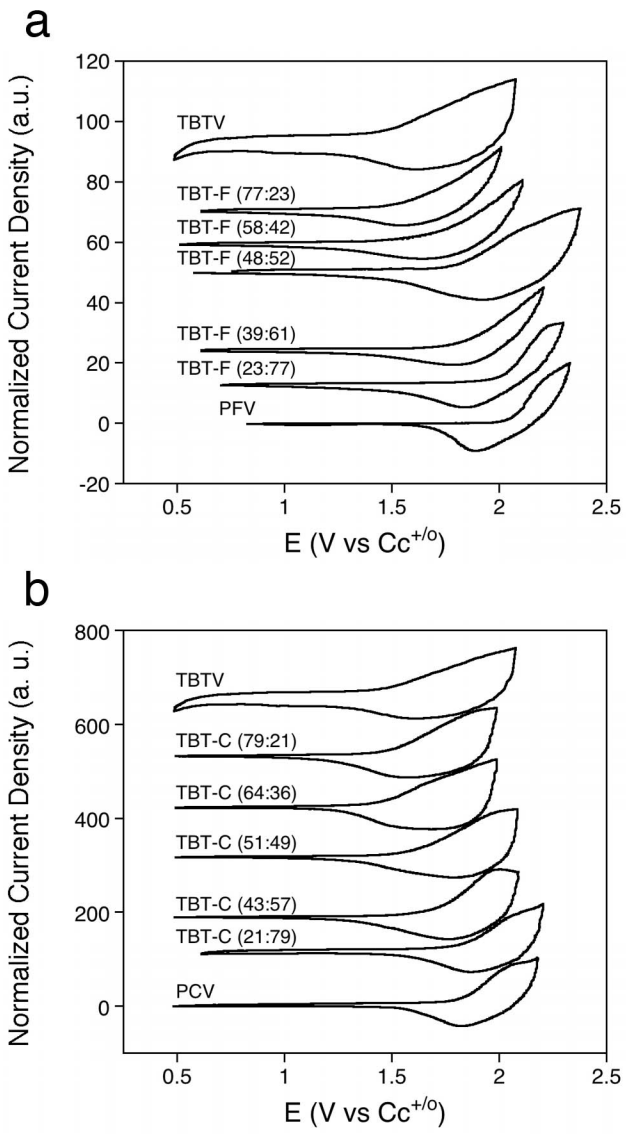

Figure 4.9

CV of (a) TBT-F and (b) TBT-C series.

Considering the optical similarities between PFV and PCV discussed earlier, is comes as no surprise that the trend in E_g^{opt} is similar for each series. In both cases, there is an immediate decrease in E_g^{opt} upon ca. 20% incorporation of TBT (Figure 4.10). After that, E_g^{opt} decreases somewhat linearly with increasing TBT content, but the decrease is minimal by comparison. This "trace acceptor" behavior is akin to that discussed in

Section 3.2.4 and suggests that CP properties can be altered significantly with minimal changes to the overall polymer composition.

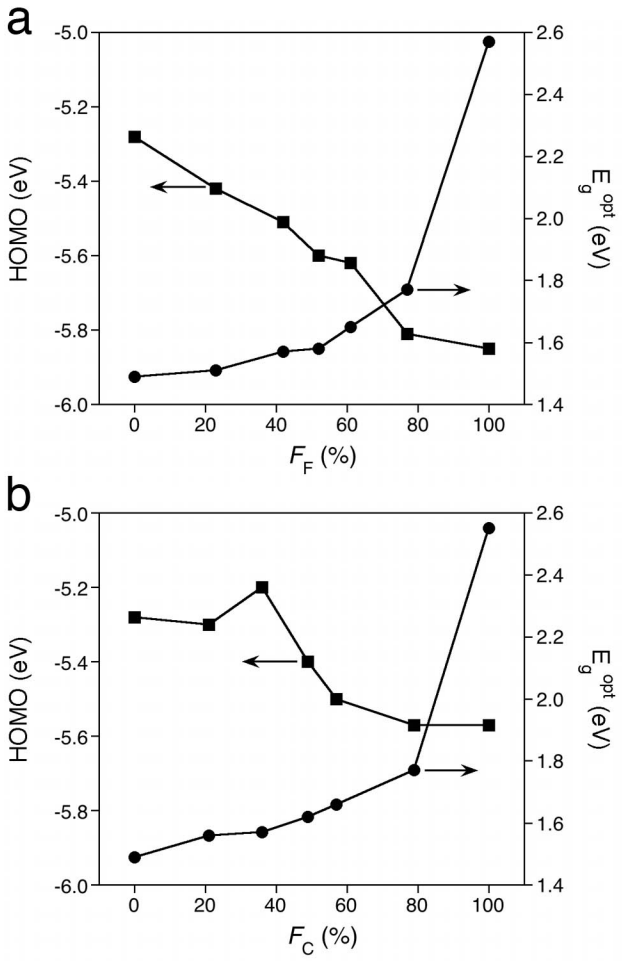

Figure 4.10
HOMO level position from CV (squares) and E_g^{opt} from UV–vis (circles) versus copolymer composition (*F*) of (a) TBT-F and (b) TBT-C thin films.

4.2.6 Solar Cell Performance

Bulk-heterojunction (BHJ) solar cells were fabricated and characterized using 1:1 TBT-F (**1c**) and TBT-C (**2c**) copolymers as the electron donors and $PC_{70}BM$ as the electron acceptor (polymer:$PC_{70}BM$ = 1:4) (Figure 4.11). The device geometry,

ITO/PEDOT:PSS/polymer:$PC_{70}BM$/TiO_2/$PC_{70}BM$, and its fabrication are described in Section 4.4.1. As anticipated, the deep HOMO levels induced by fluorene and carbazole resulted in correspondingly large V_{oc} values (Table 4.3). These values were significantly greater than the V_{oc} obtained from solar cells prepared with C16-PTV (Chapter 2). In addition, the TBT-F solar cells demonstrated a short-circuit current density (J_{sc}) approximately two times greater those prepared from TBT-C and C16-PTV. Consequently, TBT-F solar cells achieved the highest power conversion efficiency (PCE) in both this study and this thesis. It is worth noting that the fill factor (FF), a measure of device quality, is relatively low for both TBT-F and TBT-C solar cells. This suggests that there is room for additional device optimization (i.e., increased efficiency).

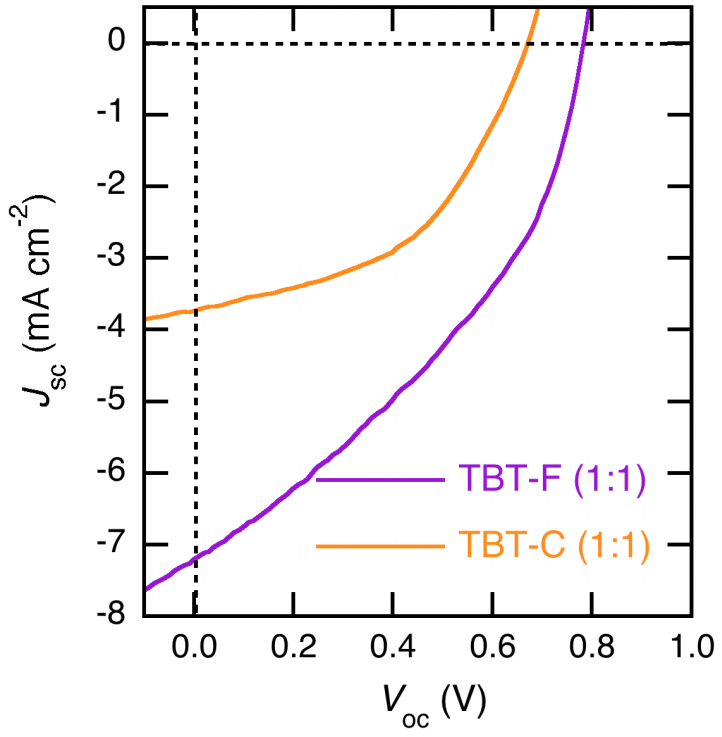

Figure 4.11

J-V characteristics of OSCs prepared from 1:1 TBT-F or TBT-C with $PC_{70}BM$ (polymer:$PC_{70}BM$ = 1:4).

Table 4.3
OSC data.

Polymer	V_{oc} (V)	J_{sc} (mA cm^{-2})	FF	PCE (%)
TBT-F (**1c**)	0.78	7.2	0.38	2.13
TBT-C (**2c**)	0.67	3.7	0.48	1.19
C16-PTV[a]	0.40	3.2	0.63	0.80

[a]C16-PTV OSC data from Chapter 2 included for comparison.

4.3 Conclusions

The ADMET copolymerization approach introduced in Chapter 3 was successfully applied to generate two new copolymer series. The polymers in these series were of significantly higher molar mass than those described in Chapter 3. Additionally, the deep HOMO levels of both fluorene and carbazole allowed for energy level tuning over a wide range of values (Figure 4.12). Finally, OSCs prepared from this polymer demonstrated high V_{oc} values, which resulted in our highest efficiency thus far.

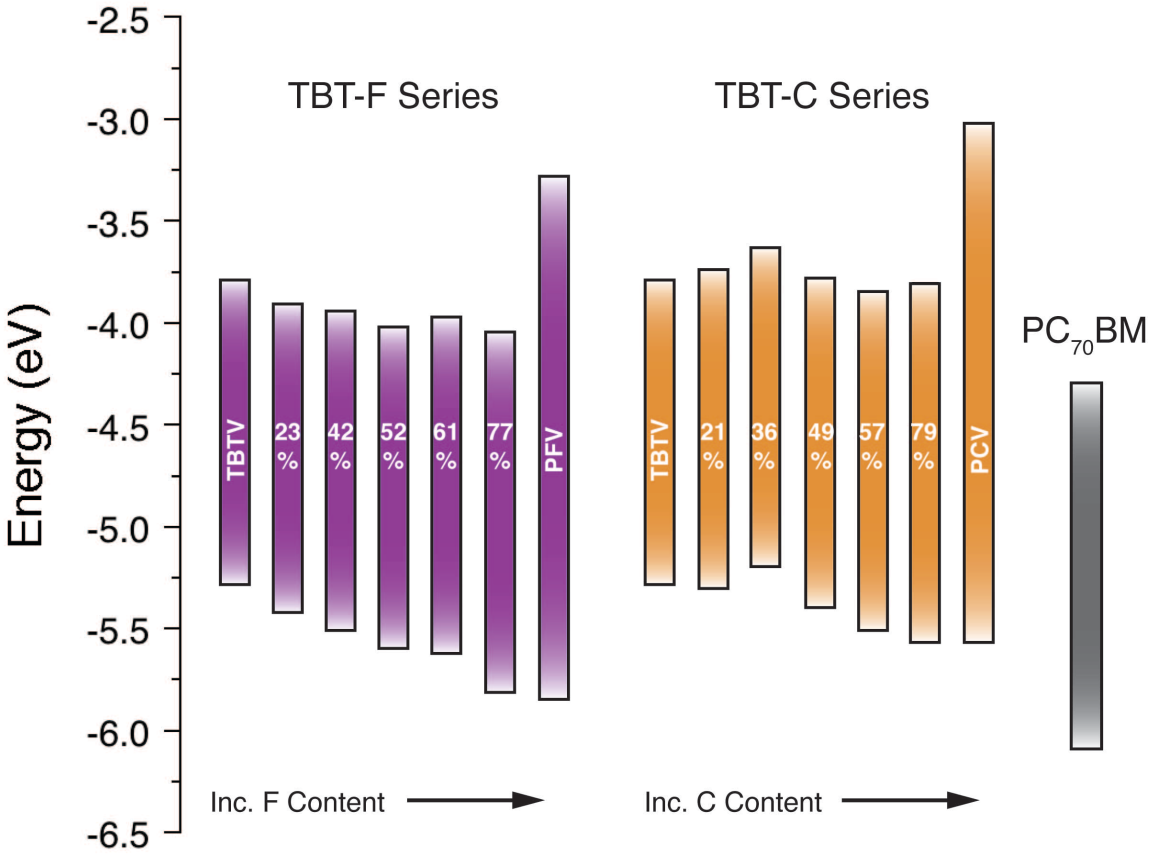

Figure 4.12
Band diagram of TBT-F (purple) and TBT-C (orange) series. $PC_{70}BM$ (gray) is shown for completeness. LUMO levels were estimated from HOMO levels and E_g^{opt} (LUMO = HOMO + E_g^{opt}).

4.4 Experimental Details

4.4.1 Materials and Methods

2,7-Divinyl-9,9'-di-*n*-hexylfluorene (F),[23,34] 2,7-divinyl-*N*-9'-heptadecanylcarbazole (C),[23,35,36] and 4,7-bis(4-hexadecyl-5-propenyl-2-thienyl)-2,1,3-benzothiadiazole (TBT)[14] were prepared according to previous work. The commercially available solvents and reagents for these syntheses were purchased and used as received from Aldrich and Acros.

Degassed THF was purified by passage through an activated alumina column and collected in flame-dried, air-free flasks. 1,2,4-trichlorobenzene (TCB) was degassed with argon and distilled under vacuum. All reactions were run under argon or vacuum using standard Schlenk techniques. A complete description of the characterization techniques employed is available in Appendix A.

OSC fabrication began with patterned ITO substrates, which were successively sonicated for ten minutes each in acetone, MeOH, and IPA. The substrates were blown dry with N_2 between each sonication. This was followed by a 10 minute UV-Ozone exposure, directly followed by PEDOT:PSS spin coating from an aqueous suspension diluted 1:1 (v/v) with MeOH. PEDOT:PSS coated substrates were then transferred to a glove box and dried on a hot plate at 130 °C for 20–30 minutes. Active layers were deposited by spin coating a 1:4 polymer:fullerene solution with a total concentration of 40 mg mL^{-1} in dichlorobenzene. In the case of TBT-C, 3 vol% diiodooctane was added to the solution prior to spin coating. Spin coating was carried out in a glove box at 1000 rpm for 60 seconds. Active layer films were dried slowly in covered petri dishes at ambient temperature. An additional hole-blocking layer was formed by spin coating a 5 mg mL^{-1} (EtOH) TiO_2 nanoparticle suspension at 4000 rpm for 60 seconds. Finally, devices were capped with 100 nm thick Al cathode grown via thermal evaporation.

4.4.2 Synthetic Details

2,7-Diformyl-9,9'-di-*n*-hexylfluorene (2). A 250 mL reaction flask was equipped with a magnetic stirring bar and flame dried. Commercially available 2,7-dibromo-9,9'-dihexylfluorene (5.00 g, 10.2 mmol) was added and the flask was evacuated and refilled with argon. Anhydrous THF (70 mL) was cannulated into the flask and the solution was cooled to -78 °C. Using a syringe, *n*-butyllithium (2.5 M hexanes, 8.60 mL, 21.4 mmol)

was slowly added. The reaction became cloudy and was stirred at -78 °C for 1 h. Anhydrous DMF (2.40 mL, 31.6 mmol) in a solution of anhydrous THF (20 mL) was added via syringe. The reaction was allowed to warm to room temperature and stirred for 20 h. The reaction was quenched with 50 mL 1 M HCl and extracted with diethyl ether (2 × 100 mL). The combined organics were washed with 100 mL water and dried over Na_2SO_4. The solvent was removed by rotary evaporation, and the crude product was purified by column chromatography with 8:1 hexanes/ethyl acetate to afford a light yellow solid (3.4 g, 85%). ^{1}H NMR (300 MHz, $CDCl_3$): δ_H = 10.11 (s, 2H), 7.96-7.90 (m, 6H), 2.10-2.04 (m, 4H), 1.12-0.95 (m, 12H), 0.74 (t, *J* = 6.9 Hz, 6H), 0.57-0.52 (m, 4H).

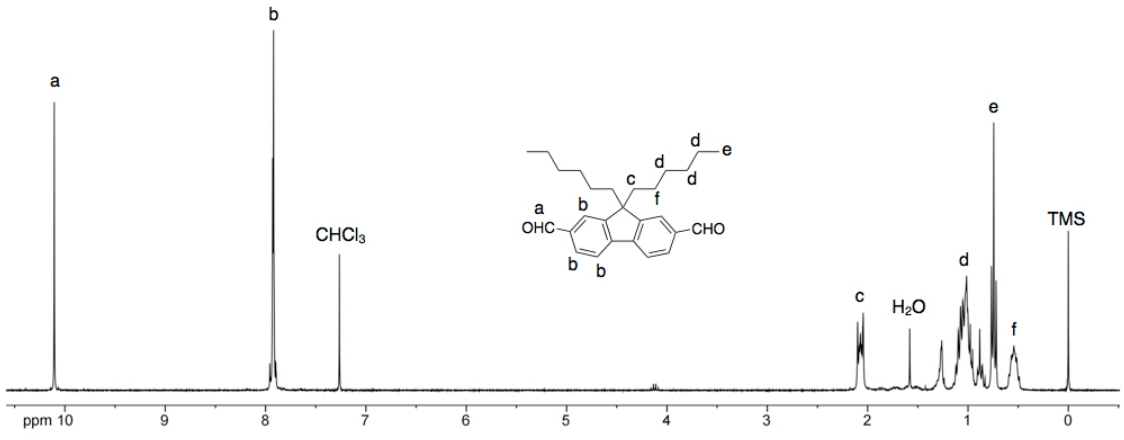

Figure 4.13

^{1}H NMR of **2**.

2,7-Divinyl-9,9'-di-*n*-hexylfluorene (F). A 250 mL reaction flask was equipped with a magnetic stirring bar and flame dried. Methyltriphenylphosphonium bromide (8.25 g, 23.1 mmol) was added and the flask was placed under vacuum for 30 min. Anhydrous THF (100 mL) was cannulated into the flask and the suspension was cooled to 0 °C. Using a syringe, *n*-butyllithium (2.5 M hexanes, 9.40 mL, 23.5 mmol) was slowly added.

The reaction was stirred for 30 min at 0 °C to form the Wittig reagent. **2** (3.0 g, 7.7 mmol) was added in a solution of anhydrous THF (25 mL) via cannula. The reaction was allowed to warm to room temperature and stirred for 4 h. The solvent was removed by rotary evaporation. The brown residue was dissolved in MeOH (30 mL) and extracted with hexanes (3 × 100 mL). The hexanes were removed by rotary evaporation, and the resultant residue was purified by column chromatography with hexanes to afford product as a low melting white solid (2.3 g, 77%). ^{1}H NMR (300 MHz, $CDCl_3$): δ_H = 7.62 (d, *J* = 7.8 Hz, 2H), 7.39 (dd, *J* = 7.8, 1.5 Hz, 2H), 7.35 (s, 2H), 6.80 (dd, *J* = 17.6, 10.9 Hz, 2H), 5.80 (dd, *J* = 17.6, 0.8 Hz, 2H), 5.26 (dd, *J* = 10.9, 0.7 Hz, 2H), 1.98-1.93 (m, 4H), 1.14-1.00 (m, 12H), 0.75 (t, *J* = 6.9 Hz, 6H), 0.67-0.57 (m, 4H).

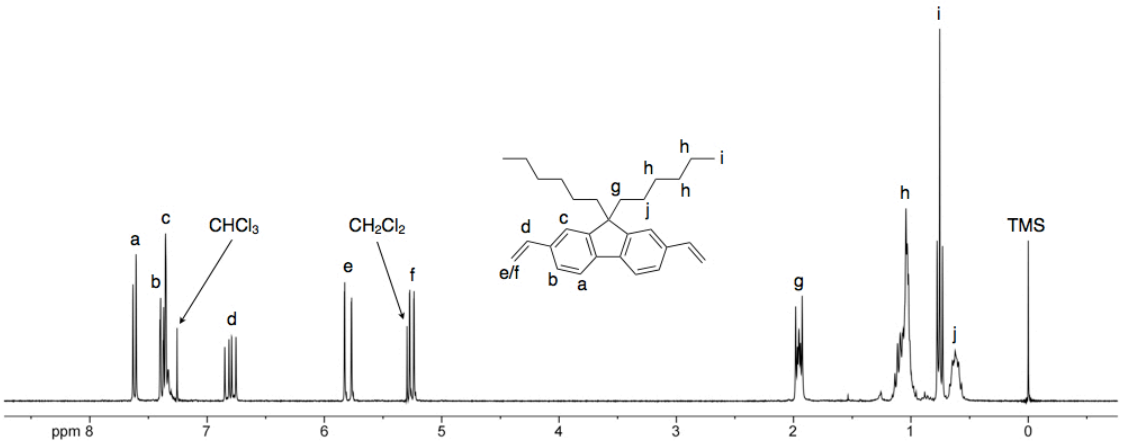

Figure 4.14

^{1}H NMR of **F**.

Heptadecan-9-ol (4). A 2-neck 250 mL round bottom flask was equipped with a magnetic stirring bar, an addition funnel, and two rubber septa. Magnesium (14.6 g, 600 mmol) turnings were added to the flask and the apparatus was flame dried. Anhydrous THF (250 mL) was added under argon via cannula. 1,2-dibromoethane (1 mL) was added to the suspension via syringe to activate the magnesium. After stirring at room

temperature for 20 min a solution of 1-bromooctane (52.2 mL, 300 mmol) in anhydrous THF (50 mL) was added dropwise via addition funnel. Following addition the reaction was stirred for 90 min before transferring (Note: take care not to clog cannula) to a second 500 mL round bottom containing ethyl formate (8.04 mL, 100 mmol) and 50 mL anhydrous THF held at -78 °C. The reaction was allowed to reach room temperature and stirred for 18 h. The reaction was carefully quenched with MeOH (10 mL) followed by the addition of saturated NH_4Cl (200 mL). The mixture was extracted with diethyl ether (2 × 350 mL), and the combined organics were washed with 750 mL of brine before drying over $MgSO_4$. The solvent was removed by rotary evaporation, and the residue was purified by recrystallization (hexanes, 0 °C, 2x) (20.8 g, 81%). ^{1}H NMR (300 MHz, $CDCl_3$): δ_H = 3.57 (s, 1H), 1.42-1.25 (m, 28H), 0.87 (t, J = 6.7 Hz, 6H).

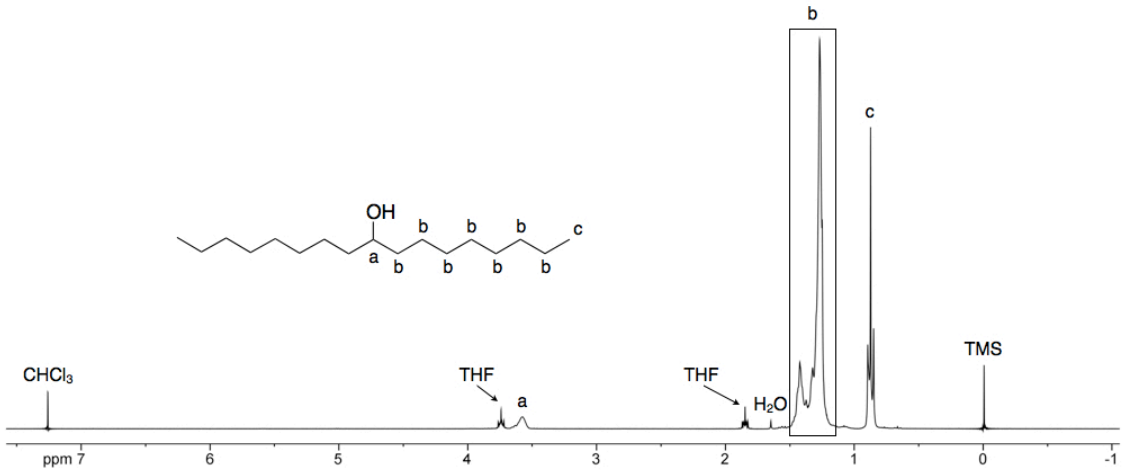

Figure 4.15

^{1}H NMR of **4**.

9-Heptadecane-p-toluenesulfonate (5). A 2-neck 500 mL round bottom flask was flame dried before adding a magnetic stirring bar, **4** (20.0 g, 78.0 mmol), triethylamine (27.0 mL, 195 mmol), and trimethylamine hydrochloride (7.45 g, 78.0 mmol). CH_2Cl_2 (70 mL) was added and the reaction was cooled to 0 °C while stirring under argon. *P*-

toluenesulfonyl chloride (18.6 g, 97.5 mmol) in CH_2Cl_2 was added to the cooled solution and the reaction was allowed to proceed for 90 min. Water (200 mL) was added and the mixture was extracted with CH_2Cl_2 (3 × 150 mL). The combined organics were washed with water and brine before drying over Na_2SO_4. The solvent was removed by rotary evaporation, and the residue was purified by column chromatography with 9:1 hexanes/ethyl acetate to give pure product as a clear oil that crystallized on standing (31.5 g, 98%). ^{1}H NMR (300 MHz, $CDCl_3$): δ_H = 7.79 (d, *J* = 8.3 Hz, 2H), 7.32 (d, *J* = 8.1 Hz, 2H), 4.53 (quintet, *J* = 6.0 Hz, 1H), 2.44 (s, 3H), 1.56 (m, 4H), 1.27-1.17 (m, 24H), 0.88 (t, *J* = 6.9 Hz, 6H).

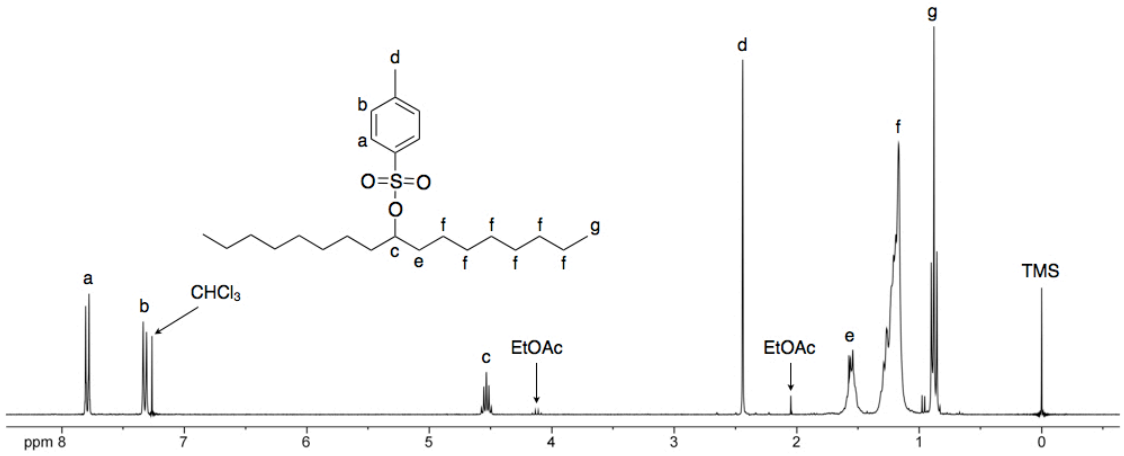

Figure 4.16

^{1}H NMR of **5**.

4,4'-Dibromo-2-nitrobiphenyl (7). A 1 L round bottom flask was equipped with a magnetic stirring bar before adding 4,4'-dibromobiphenyl (40.0 g, 128 mmol) and 600 mL glacial acetic acid. The mixture was heated to 100 °C and 175 mL of fuming (*caution*) nitric acid was added over the course of 30 min via addition funnel. The reaction was stirred at 100 °C for an additional 4 h. The reaction was poured into 2.5 L of ice water to precipitate the product, which was collected by filtration and washed with 300

mL ethanol (45.7 g, 97%). ^{1}H NMR (300 MHz, $CDCl_3$): δ_H = 8.03 (d, *J* = 2.0 Hz, 1H), 7.76 (dd, *J* = 8.3, 2.0 Hz, 1H), 7.56 (d, *J* = 8.4 Hz, 2H), 7.29 (d, *J* = 8.2 Hz, 1H), 7.16 (d, *J* = 8.4 Hz, 2H).

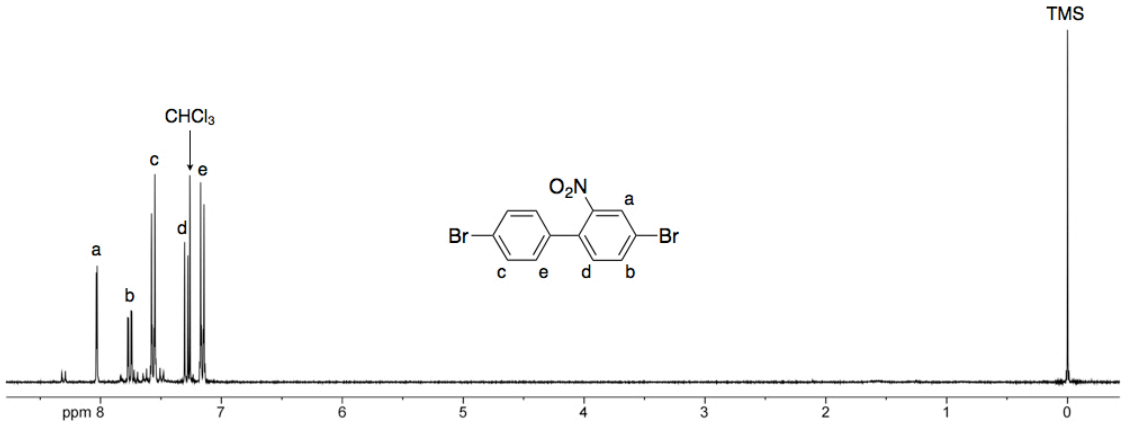

Figure 4.17

^{1}H NMR of **7**.

2,7-Dibromocarbazole (8). A 2-neck 250 mL round bottom flask was equipped with a magnetic stirring bar, reflux condenser, and two rubber septa. The apparatus was flamed dried before adding **7** (30.0 g, 84.0 mmol) and triethyl phosphite (115 mL). The reaction was refluxed (160 °C) under argon for 24 h. The excess triethyl phosphite was removed by vacuum distillation. The remaining brown solution was poured into 500 mL of ice water and extracted with diethyl ether (2 × 250 mL). The combined organics were washed with brine and dried over Na_2SO_4. The solvent was removed by rotary evaporation, and the residue was purified by gradient column chromatography with 9:1 hexanes/CH_2Cl_2 → CH_2Cl_2 to afford product as a pale yellow crystalline solid (14.8 g, 54%). ^{1}H NMR (300 MHz, $CDCl_3$): δ_H = 8.07 (bs, 1H), 7.88 (d, *J* = 8.3 Hz, 2H), 7.57 (d, *J* = 1.7 Hz, 2H), 7.36 (dd, *J* = 8.3, 1.7 Hz, 2H).

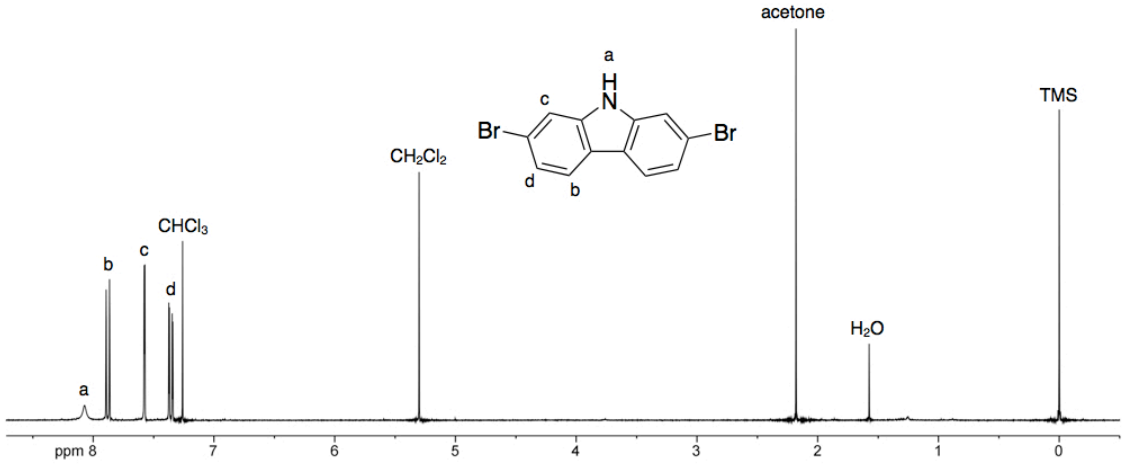

Figure 4.18

^{1}H NMR of **8**.

***N*-9'-Heptadecanyl-2,7-dibromocarbazole (9).** A 2-neck 250 mL round bottom flask was equipped with a magnetic stirring bar, addition funnel, and two rubber septa. The apparatus was flame dried before adding **8** (10.0 g, 30.8 mmol), freshly powdered KOH (8.60 g, 154 mmol), and 75 mL DMSO. After **8** dissolved, **5** (19.0 g, 46.2 mmol) was added dropwise via addition funnel as a solution in DMSO (50 mL). The reaction was stirred at room temperature under argon for 20 h. The reaction was poured into 500 mL water and extracted with hexanes (3 × 250 mL). The combined organics were washed with brine and dried over Na_2SO_4. The solvent was removed by rotary evaporation, and the residue was purified by column chromatography with hexanes to afford pure product as a white solid (12.2 g, 70%). ^{1}H NMR (300 MHz, $CDCl_3$): δ_H = 7.90 (t, J = 8.6 Hz, 2H), 7.69 (s, 1H), 7.53 (s, 1H), 7.34-7.31 (m, 2H), 4.41 (tt, J = 10.1, 5.1 Hz, 1H), 2.26-2.13 (m, 2H), 2.02-1.84 (m, 2H), 1.26-1.14 (m, 22H), 0.97 (m, 2H), 0.83 (t, J = 6.9 Hz, 6H). Multiple and broad peaks in NMR are due to atropisomerism.[37]

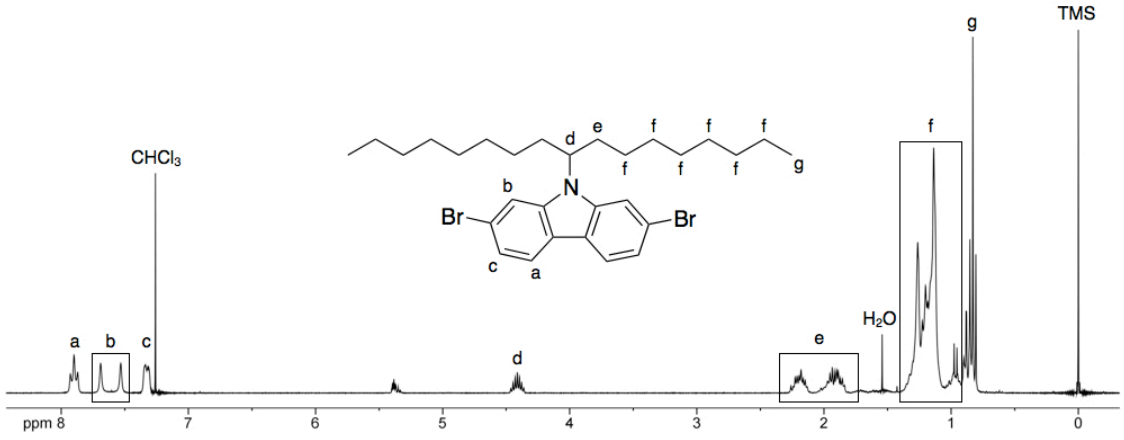

Figure 4.19

^{1}H NMR of **9**.

***N*-9'-Heptadecanyl-2,7-bis(formyl)carbazole (10).** A 100 mL reaction flask was equipped with a magnetic stirring bar and flame dried. **9** (5.0 g, 8.9 mmol) was added, and the flask was put under vacuum for 30 min. Anhydrous THF (60 mL) was added via cannula, and the solution was cooled to -78 °C. Using a syringe, *n*-butyllithium (2.5 M hexanes, 7.85 mL, 19.6 mmol) was carefully added dropwise. The reaction was stirred for 1 h at -78 °C before adding anhydrous DMF (2.40 mL, 31.2 mmol) via syringe. The reaction was stirred at room temperature for 18 h under argon, poured into 20 mL of 1 M HCl, and extracted with diethyl ether (2 × 100 mL). The combined organics were washed with brine and dried over Na_2SO_4. The solvent was removed by rotary evaporation, and the resultant residue was purified by column chromatography with 5-7% ethyl acetate/hexanes to afford product as a yellow crystalline solid (3.25 g, 79%). ^{1}H NMR (500 MHz, $CDCl_3$): δ_H = 10.18 (s, 2H), 8.30 (bs, 2H), 8.14 (bs, 1H), 8.01 (bs, 1H), 7.79 (bs, 2H), 4.70 (tt, *J* = 10.1, 5.1 Hz, 1H), 2.36-2.28 (m, 2H), 2.06-1.99 (m, 2H), 1.26-1.10 (m, 22H), 1.00-0.94 (m, 2H), 0.80 (t, *J* = 7.2 Hz, 6H). Multiple and broad peaks in NMR are due to atropisomerism.[37]

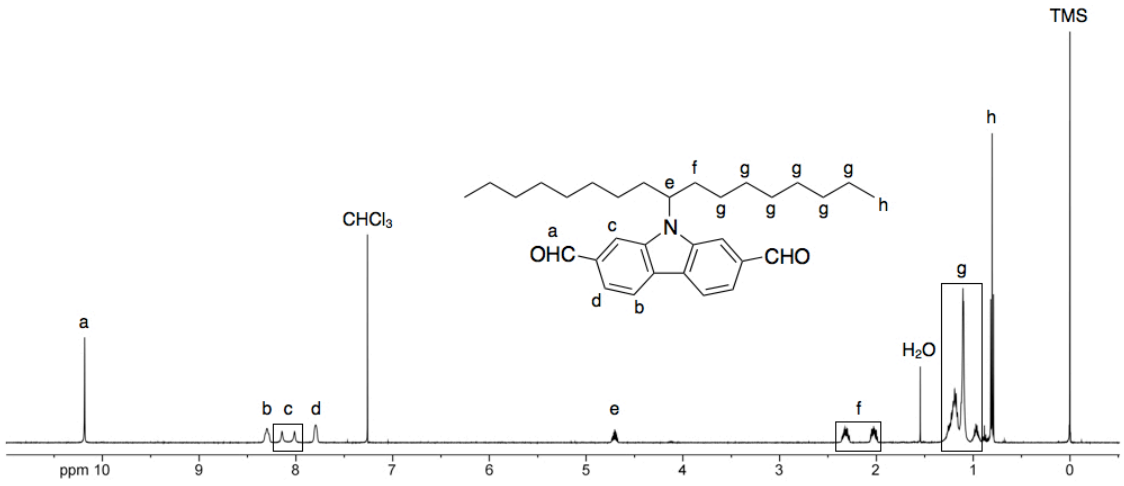

Figure 4.20

^{1}H NMR of **10**.

2,7-Divinyl-*N*-9'-heptadecanylcarbazole (C). A 250 mL reaction flask was equipped with a magnetic stirring bar and flame dried. Methyltriphenylphosphonium bromide (6.97 g, 19.5 mmol) was added and the flask was placed under vacuum for 30 min. Anhydrous THF (100 mL) was cannulated into the flask and the suspension was cooled to 0 °C. Using a syringe, *n*-butyllithium (2.5 M hexanes, 7.90 mL, 19.8 mmol) was slowly added. The reaction was stirred for 30 min at 0 °C to form the Wittig reagent. **10** (3.0 g, 6.5 mmol) was added in a solution of anhydrous THF (25 mL) via cannula. The reaction was allowed to warm to room temperature and stirred for 4 h. The reaction was then poured into 300 mL of water and extracted with diethyl ether (2 × 100 mL). The combined organics were washed with water and brine. The solvent was removed by rotary evaporation, and the resultant residue was purified by column chromatography with 0–2% ethyl acetate/hexanes to afford product as a clear oil that solidified on standing (2.7 g, 92%). ^{1}H NMR (300 MHz, $CDCl_3$): δ_H = 8.00 (t, *J* = 8.3 Hz, 2H), 7.52 (bs, 1H), 7.36-7.31 (m, 3H), 6.90 (dd, *J* = 17.5, 10.9 Hz, 2H), 5.84 (d, *J* = 17.6 Hz, 2H), 5.29 (d, *J* = 10.9 Hz, 2H), 4.55 (tt, *J* = 10.1, 5.0 Hz, 1H), 2.35-2.22 (m, 2H), 1.96-1.88 (m, 2H),

1.27-1.12 (m, 22H), 1.04-0.99 (m, 2H), 0.82 (t, J = 6.9 Hz, 6H). Multiple and broad peaks in NMR are due to atropisomerism.[37]

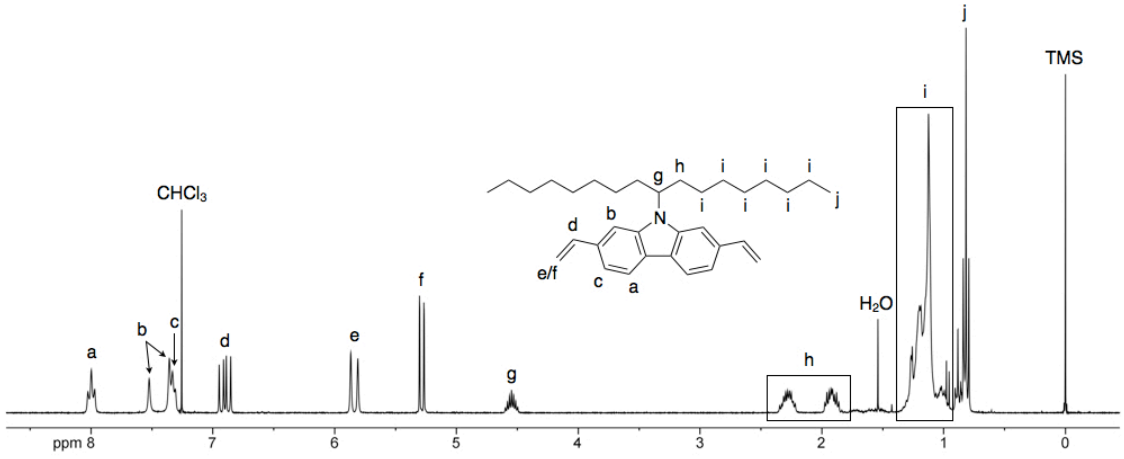

Figure 4.21

^{1}H NMR of **C**.

Poly(9,9-di-*n*-hexylfluorene-2,7-vinylene) (PFV). An apparatus like that shown in Figure 2.24 was assembled and flame dried under vacuum. The 50 mL Schlenk tube was charged with **F** (200 mg, 0.52 mmol) in a solution of anhydrous TCB (4 mL). The solution was heated to 80 °C and dynamic vacuum was applied for 30 min. to remove oxygen. The flask was placed under an argon atmosphere and G2 (14 mg, 0.016 mmol) was added as a solution in TCB (0.25 mL). Dynamic vacuum was reapplied. After 15 h the reaction was quenched by the addition of ethyl vinyl ether (3 drops). The polymer was precipitated in MeOH (150 mL, 0 °C) and filtered through a Soxhlet thimble. The polymer was purified by Soxhlet extraction with methanol (ca. 100 mL) and chloroform (ca. 100 mL). The chloroform fraction was concentrated to ca. 10 mL under reduced pressure and precipitated in MeOH (100 mL, 0 °C). The polymer was filtered and dried under vacuum to obtain the target material as a bright yellow solid (149 mg, 80%). ^{1}H NMR (500 MHz, $CDCl_3$): δ_H = 7.70-7.28 (m, 8H), 2.06-1.99 (m, 4H), 1.14-1.05 (m,

12H), 0.79-0.75 (m, 6H), 0.67 (s, 4H), vinyl end groups: 6.82 (dd, *J* = 17.5, 10.9 Hz), 5.82 (d, *J* = 17.6 Hz), 5.27 (d, *J* = 10.9 Hz).

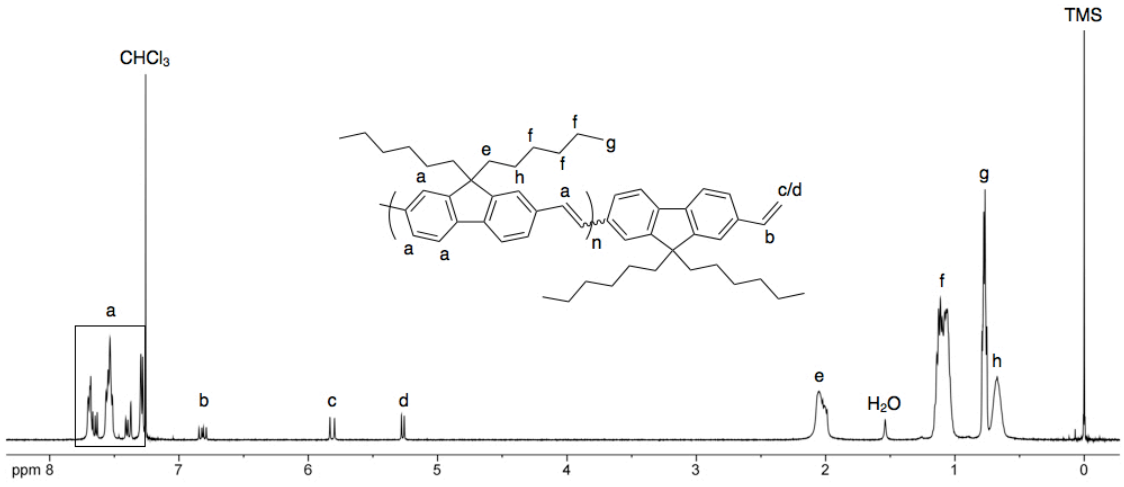

Figure 4.22

^{1}H NMR of **PFV**.

Poly(*N*-9'-heptadecanylcarbazole-2,7-vinylene) (PCV). An apparatus like that shown in Figure 2.24 was assembled and flame dried under vacuum. The 50 mL Schlenk tube was charged with **C** (250 mg, 0.55 mmol) in a solution of anhydrous TCB (4.5 mL). The solution was heated to 80 °C and dynamic vacuum was applied for 30 min. to remove oxygen. The flask was placed under an argon atmosphere and G2 (9.3 mg, 0.011 mmol) was added as a solution in TCB (0.5 mL). Dynamic vacuum was reapplied. After 24 h the reaction was quenched by the addition of ethyl vinyl ether (3 drops). The polymer was precipitated in acetone (150 mL, 0 °C) and filtered through a Soxhlet thimble. The polymer was purified by Soxhlet extraction with acetone (ca. 100 mL) and chloroform (ca. 100 mL). The chloroform fraction was concentrated to ca. 10 mL under reduced pressure and precipitated in acetone (150 mL, 0 °C). The polymer was filtered and dried under vacuum to obtain the target material as a bright yellow solid (182 mg, 77%). ^{1}H NMR (500 MHz, $CDCl_3$): δ_H = 8.09-8.06 (m, 2H), 7.70 (s, 1H), 7.55 (s, 3H), 7.43 (s, 2H),

4.67 (s, 1H), 2.42 (s, 2H), 2.03 (s, 2H), 1.20 (bs, 24H), 0.81 (t, J = 7.0 Hz, 6H), vinyl end groups: 6.92 (dd, J = 17.3, 10.7 Hz), 5.85 (d, J = 18.4 Hz), 5.30 (d, J = 10.8 Hz).

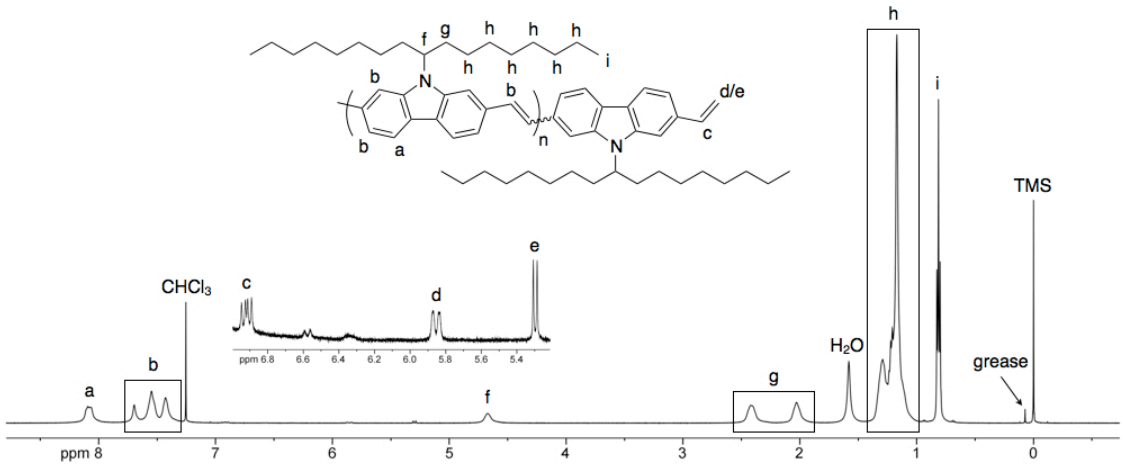

Figure 4.23

^{1}H NMR of **PCV**.

General Copolymerization Procedure. An apparatus like that shown in Figure 2.24 was assembled and flame-dried under vacuum before placing under argon. The Schlenk tube was charged with monomers in a solution of anhydrous TCB (ca. 0.15 M). The solution was heated to 80 °C and dynamic vacuum was applied for 30 min. to remove oxygen. The flask was placed under an argon atmosphere and G2 (1 mol%) was added as a solution in TCB (0.5 mL). Dynamic vacuum was reapplied and the polymerization was run for 15–48 h. The reaction was quenched by the addition of ethyl vinyl ether (3 drops), and the polymer was precipitated into a 20-fold excess of non-solvent (methanol or acetone) held at 0 °C. The precipitate was filtered through a Soxhlet thimble and purified by Soxhlet extraction with non-solvent (ca. 100 mL). The polymer was extracted into chloroform (ca. 100 mL) and concentrated under reduced pressure before precipitating into non-solvent (0 °C). The polymer was collected via filtration and dried under vacuum to obtain the

target material as a dark solid. Copolymer composition was determined by ^{1}H NMR analysis.

4.5 References

[1] Forrest, S. R. *Nature* **2004**, *428*, 911–918.

[2] Li, G.; Zhu, R.; Yang, Y. *Nat. Photonics* **2012**, *6*, 153–161.

[3] Sommer-Larsen, P.; Jørgensen, M.; Søndergaard, R. R.; Hösel, M.; Krebs, F. C. *Energy Technol.* **2013**, *1*, 15–19.

[4] Padinger, F.; Rittberger, R. S.; Sariciftci, N. S. *Adv. Funct. Mater.* **2003**, *13*, 85–88.

[5] He, Z.; Zhong, C.; Su, S.; Xu, M.; Wu, H.; Cao, Y. *Nat. Photonics* **2012**, *6*, 591–595.

[6] Burkhart, B.; Khlyabich, P. P.; Canak, T. C.; LaJoie, T. W.; Thompson, B. C. *Macromolecules* **2011**, *44*, 1242–1246.

[7] Burkhart, B.; Khlyabich, P. P.; Thompson, B. C. *Macromolecules* **2012**, *45*, 3740–3748.

[8] Rudenko, A. E.; Wiley, C. A.; Stone, S. M.; Tannaci, J. F.; Thompson, B. C. *J. Polym. Sci., Polym. Chem.* **2012**, *50*, 3691–3697.

[9] Khlyabich, P. P.; Burkhart, B.; Ng, C. F.; Thompson, B. C. *Macromolecules* **2011**, *44*, 5079–5084.

[10] Burkhart, B.; Khlyabich, P. P.; Thompson, B. C. *ACS Macro Lett.* **2012**, *1*, 660–666.

[11] Nielsen, C. B.; Ashraf, R. S.; Schroeder, B. C.; D'Angelo, P.; Watkins, S. E.; Song, K.; Anthopoulos, T. D.; McCulloch, I. *Chem. Commun.* **2012**, *48*, 5832–5834.

[12] Song, C. E.; Kang, I.-N.; Kim, J.-H.; Hwang, D.-H.; Lee, J.-C.; Ahn, T.; Shin, W. S.; Moon, S.-J.; Lee, S. K. *J. Polym. Sci., Polym. Chem.* **2013**, *15*, 1512–1519.

[13] Li, J.; Ong, K.-H.; Sonar, P.; Lim, S.-L.; Ng, G.-M.; Wong, H.-K.; Tan, H.-S.; Chen, Z.-K. *Polym. Chem.* **2013**, *4*, 804–811.

[14] Speros, J. C.; Paulsen, B. D.; Slowinski, B. S.; Frisbie, C. D.; Hillmyer, M. A. *ACS Macro Lett.* **2012**, *1*, 986–990.

[15] Ma, W.; Kim, J. Y.; Lee, K.; Heeger, A. J. *Macromol. Rapid Commun.* **2007**, *28*, 1776–1780.

[16] Ballantyne, A. M.; Chen, L.; Dane, J.; Hammant, T.; Braun, F. M.; Heeney, M.; Duffy, W.; McCulloch, I.; Bradley, D. D. C.; Nelson, J. *Adv. Funct. Mater.* **2008**, *18*, 2373–2380.

[17] Moet, D. J. D.; Lenes, M.; Kotlarski, J. D.; Veenstra, S. C.; Sweelssen, J.; Koetse, M. M.; de Boer, B.; Blom, P. W. M. *Org. Electron.* **2009**, *10*, 1275–1281.

[18] Tong, M.; Cho, S.; Rogers, J. T.; Schmidt, K.; Hsu, B. B. Y.; Moses, D.; Coffin, R. C.; Kramer, E. J.; Bazan, G. C.; Heeger, A. J. *Adv. Funct. Mater.* **2010**, *20*, 3959–3965.

[19] Speros, J. C.; Paulsen, B. D.; White, S. P.; Wu, Y.; Jackson, E. A.; Slowinski, B. S.; Frisbie, C. D.; Hillmyer, M. A. *Macromolecules* **2012**, *45*, 2190–2199.

[20] Brabec, C. J.; Cravino, A.; Meissner, D.; Sariciftci, N. S.; Fromherz, T.; Rispens, M. T.; Sanchez, L.; Hummelen, J. C. *Adv. Funct. Mater.* **2001**, *11*, 374–380.

[21] Park, S. H.; Roy, A.; Beaupré, S.; Cho, S.; Coates, N.; Moon, J. S.; Moses, D.; Leclerc, M.; Lee, K.; Heeger, A. J. *Nat. Photonics* **2009**, *3*, 297–302.

[22] Stuart, A. C.; Tumbleston, J. R.; Zhou, H. X.; Li, W. T.; Liu, S. B.; Ade, H.; You, W. *J. Am. Chem. Soc.* **2013**, *135*, 1806–1815.

[23] Yamamoto, N.; Ito, R.; Geerts, Y.; Nomura, K. *Macromolecules* **2009**, *42*, 5104–5111.

[24] Janietz, S.; Bradley, D. D. C.; Grell, M.; Giebeler, C.; Inbasekaran, M.; Woo, E. P. *Appl. Phys. Lett.* **1998**, *73*, 2453–2455.

[25] Li, J. L.; Dierschke, F.; Wu, J. S.; Grimsdale, A. C.; Müllen, K. *J. Mater. Chem.* **2006**, *16*, 96–100.

[26] Veldman, D.; İpek, Ö.; Meskers, S. C. J.; Sweelssen, J.; Koetse, M. M.; Veenstra, S. C.; Kroon, J. M.; van Bavel, S. S.; Loos, J.; Janssen, R. A. J. *J. Am. Chem. Soc.* **2008**, *130*, 7721–7735.

[27] Scholl, M.; Ding, S.; Lee, C. W.; Grubbs, R. H. *Org. Lett.* **1999**, *1*, 953–956.

[28] Bielawski, C. W.; Grubbs, R. H. *Angew. Chem., Int. Ed.* **2000**, *39*, 2903–2906.

[29] Qin, Y.; Hillmyer, M. A. *Macromolecules* **2009**, *42*, 6429–6432.

[30] Patel, J.; Mujcinovic, S.; Jackson, W. R.; Robinson, A. J.; Serelis, A. K.; Such, C. *Green Chem.* **2006**, *8*, 450–454.

[31] Nomura, K.; Morimoto, H.; Imanishi, Y.; Ramhani, Z.; Geerts, Y. *J. Polym. Sci., Polym. Chem.* **2001**, *39*, 2463–2470.

[32] He, Y.; Zhao, G.; Min, J.; Zhang, M.; Li, Y. *Polymer* **2009**, *50*, 5055–5058.

[33] Dyer, A. L.; Thompson, E. J.; Reynolds, J. R. *ACS Appl. Mater. Interfaces* **2011**, *3*, 1787–1785.

[34] Wang, W.; Xu, J.; Lai, Y.-H.; Wang, F. *Macromolecules* **2004**, *37*, 3546–3553.

[35] Dierschke, F.; Grimsdale, A. C.; Müllen, K. *Synthesis* **2003**, 2470–2472.

[36] Blouin, N.; Michaud, A.; Leclerc, M. *Adv. Mater.* **2007**, *19*, 2295-2300.

[37] Clayden, J. *Tetrahedron* **2004**, *60*, 4335–4335.

Chapter 5

Effects of Olefin Content and Alkyl Chain Placement on PTV Optoelectronic and Morphological Properties[‡]

This chapter introduces the concept of olefin dilution in an effort to improve the performance of organic solar cells prepared from PTV-like polymers. Additionally, systematic changes to alkyl substitution patterns manifested as significant differences in optical, thermal, and microstructural properties. Thorough density functional theory (DFT) analysis provided support for the observed differences among all polymers.

[‡] Reproduced in part with permission from Speros, J. C.; Martinez, H.; Paulsen, B. D.; White, S. P.; Bonifas, A. D.; Goff, P. C.; Frisbie, C. D.; Hillmyer, M. A. *Macromolecules* **2013**, *Submitted*.

5.1 Introduction

The synthetic versatility of semiconducting conjugated polymers (CPs) has made them ideal candidates for use in solution-processed organic solar cells (OSCs),[1,2] light emitting devices,[3] and transistors.[4] Owing to a low band gap (E_g^{opt}), poly(thienylene vinylenes) (PTVs) represent a promising CP scaffold for use in OSCs. However, despite their first reported synthesis over forty years ago,[5] PTVs have yet to demonstrate appreciable efficiencies in OSCs compared to other CPs. This is due largely to exceedingly weak photoluminescence (PL),[6] which suggests short-lived and difficult to separate excitons. Olejnik and coworkers further supported this PL-performance correlation by demonstrating the rapid internal conversion of the primary PTV exciton to a low energy non-PL state.[7] By comparison, poly(3-hexylthiophene) (P3HT) is much more photoluminescent with demonstrated solution quantum yields ranging from 9–40%.[8-10] Additionally, P3HT performs better in OSCs with overall energy conversion efficiencies around 5%.[11,12] The first PTV to achieve moderate efficiency (2.01%) in an OSC was prepared when researchers functionalized the PTV backbone with a carboxylate moiety and inadvertently increased PL.[13]

Recently, researchers reported the synthesis of a biaxially extended PTV-like polymer, poly[(E)-5,5‴-bis(2-ethylhexyl)-2′-methyl-5″-(prop-1-en-1-yl)-2,3′:5′,2″:4″,2‴-quaterthiophene] (P4TV, Figure 5.1), that gave an efficiency in OSCs of 4.04%.[14] The authors attributed the enhanced efficiency to broadened absorption and a high level of structural organization leading to increased hole mobilities. Although this likely contributed to an improved OSC efficiency, the authors did not address the possibility that by increasing the thiophene to olefin ratio (i.e., olefin dilution) in the polymer repeat unit they may have also enhanced PL. In other words, it is possible that the authors prepared a polymer that struck an ideal balance between low band gap PTVs and high mobility, photoluminescent poly(thiophenes).

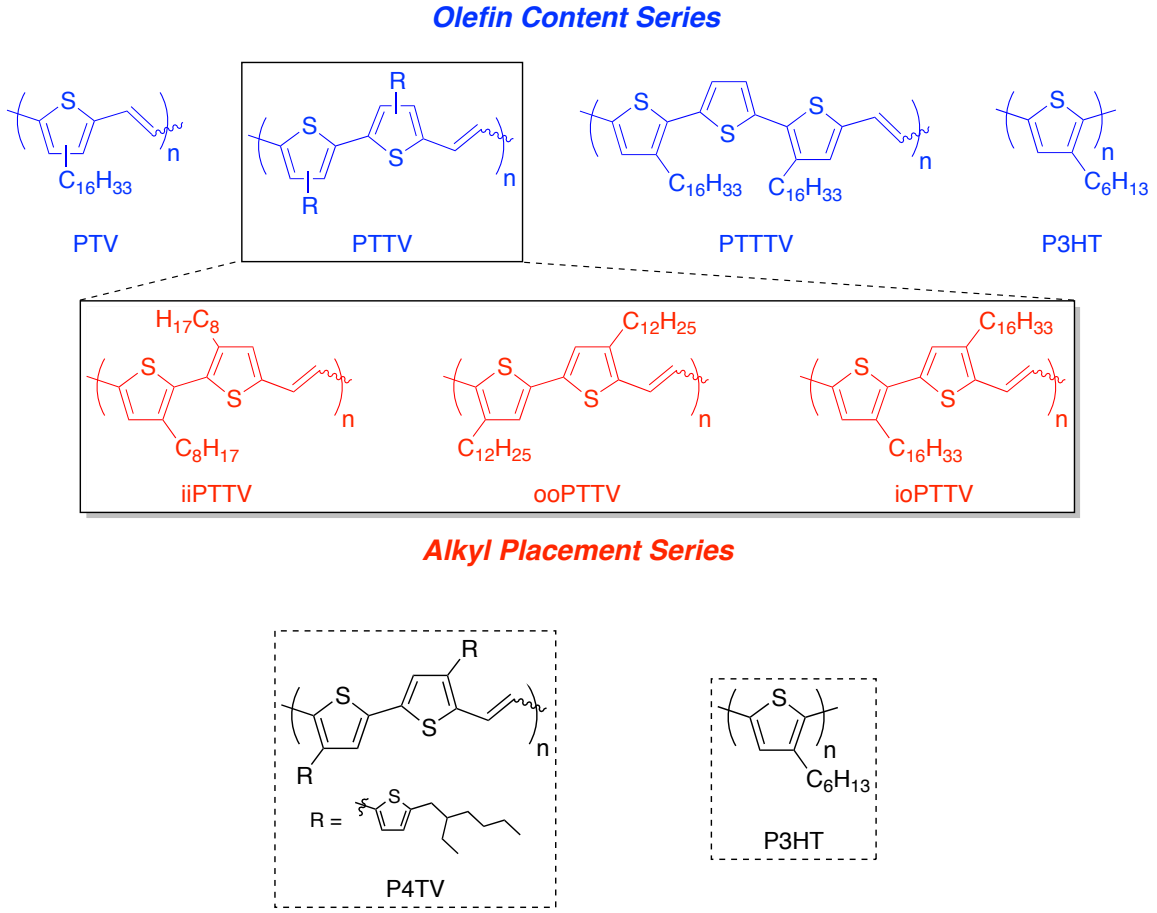

Figure 5.1
Olefin content and alkyl placement series.

We have previously demonstrated the use of acyclic diene metathesis (ADMET) polymerization for the preparation of various PTVs.[15-17] Herein, we use ADMET to prepare poly[3,4'-dihexadecyl-5-methyl-5'-(prop-1-en-1-yl)-2,2'-bithiophene] (ioPTTV) and poly[3,3"-dihexadecyl-5-methyl-5"-(prop-1-en-1-yl)-2,2':5',2"-terthiophene] (PTTTV) to systematically study the impact of olefin dilution on optical, morphological, and electronic properties (Figure 5.1). Two additional PTTVs (Figure 5.1) were prepared: Poly[3,3'-dioctyl-5-methyl-5'-(prop-1-en-1-yl)-2,2'-bithiophene] (iiPTTV) and poly[4,4'didodecyl-5-methyl-5'-(prop-1-en-1-yl)-2,2'-bithiophene]

(ooPTTV). These two structures differ in terms of alkyl substitution, which allowed us to investigate the importance of alkyl chain position as this has been found to significantly impact CP performance.[18-26] These structural variations have not been investigated systematically for PTV-based materials. Finally, it should be noted that the alkyl chain length of iiPTTV and ooPTTV differs from that of other polymers in this report. Although C16 was desired for ideal comparison, challenges encountered during monomer synthesis necessitated these differences.

In this study, we (i) describe the preparation and thorough characterization of four PTV-like polymers; (ii) take advantage of the high solubility of iiPTTV and PTTTV to answer long-standing questions related to PTV molar mass and stereochemistry; (iii) demonstrate PL, a phenomenon rarely observed in PTVs; (iv) perform in-depth computational analyses to support observations in polymer optoelectronic and solid state behavior; and (v) prepare OSCs to achieve efficiencies over 1%.

5.2 Results and Discussion

5.2.1 Synthesis and Characterization

For this study four new monomers (**4**, **8**, **13**, **16**) were prepared in good yields for ADMET polymerization (Scheme 5.1). Compounds **2**,[27] **6**,[28] **11**,[29] and **14**[30] were synthesized according to previous literature reports. The dialdehydes (**3**, **7**, **12**, **15**) were formed by treating the parent bithiophenes (**2**, **6**, **11**) or terthiophene (**14**) with n-butyllithium in the presence of N,N,N',N'-tetramethylethylenediamine (TMEDA) to form a dilithiated intermediate. Treatment with N,N-dimethylformamide (DMF) followed by acidic workup afforded the dialdehyde product, which was subsequently converted to the dipropenyl monomer under salt-free Wittig conditions (see Section 5.4.2 for complete synthetic details). Dipropenyl monomers were chosen over the more reactive divinyl monomers because they are far less susceptible to free-radical

polymerization and/or side reactions, and longer catalyst lifetimes are expected during ADMET because the ethylidene-ruthenium intermediates (dipropenyl monomer) that form are more stable than the methylidene-ruthenium (divinyl monomer) versions.[31]

Scheme 5.1

Monomer synthesis.

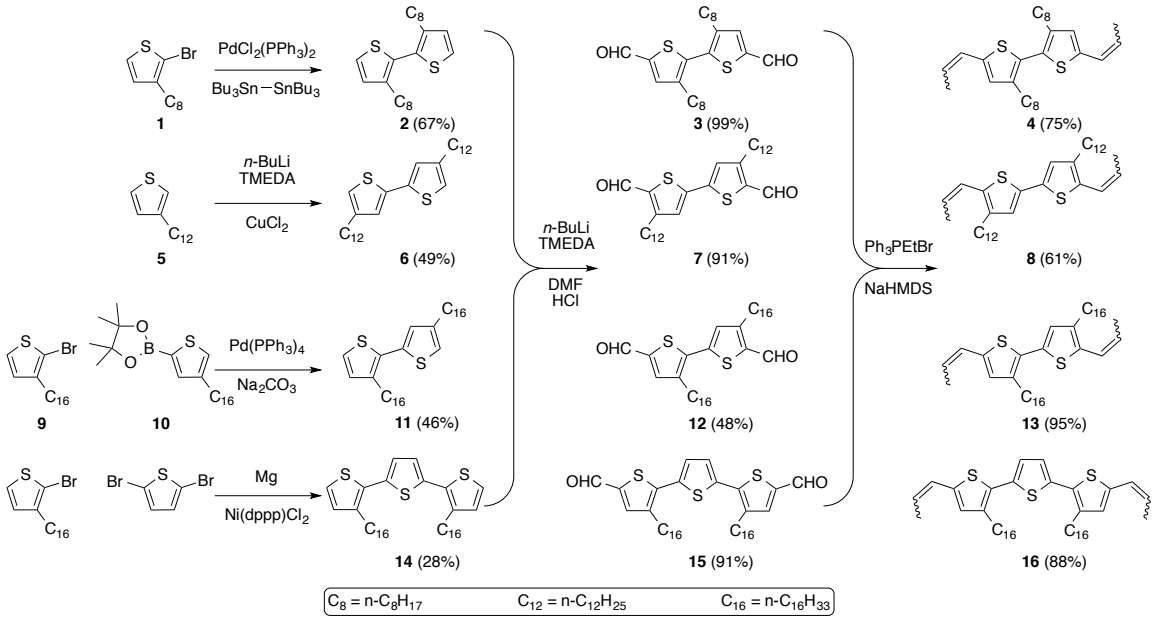

Monomers **4**, **8**, **13**, and **16** were converted to polymers (iiPTTV, ooPTTV, ioPTTV, PTTTV, respectively) using a pyridine-based ruthenium metathesis catalyst (G3)[32] and the same ADMET procedure detailed in a previous report (Scheme 5.2).[16] The three bithiophene polymers (PTTVs) are identified by the position of the linear alkyl chains (i.e., ii = in/in, oo = out/out, io = in/out) with respect to the thiophene–thiophene bond. PTTVs similar to iiPTTV and ooPTTV have been prepared before using oxidative polymerization or organometallic polycondensation techniques.[18,33-36] iiPTTV, ooPTTV, and PTTTV were obtained as regioregular polymers given the symmetry of their respective monomers (**4**, **8**, and **16**). Conversely, monomer **13** is asymmetric, and

ioPTTV was obtained as a regiorandom polymer. iiPTTV, ioPTTV, and PTTTV were obtained in high molar mass (≥35 kg mol^{-1}) as determined by size-exclusion chromatography (SEC) compared to polystyrene standards (Table 5.1). However, ooPTTV was sparingly soluble in the polymerization (1,2,4-trichlorobenzene) and SEC (chloroform) solvents leading to low molar mass values. All monomers and polymers were characterized with ^{1}H NMR spectroscopy (Figures 5.21–5.41) and molar mass was also determined by end-group analysis (Table 5.1).

Scheme 5.2

Polymer synthesis.

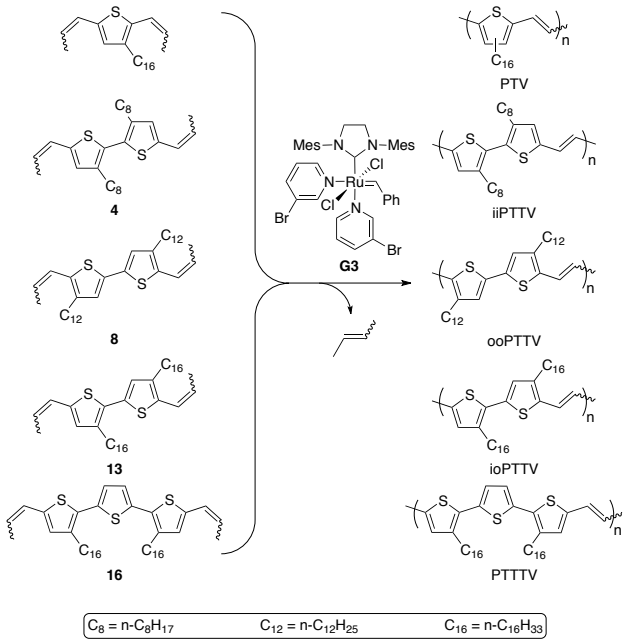

Table 5.1
Polymer molar mass and thermal data.

Polymer	M_n[a] (kg mol^{-1})	M_w[a] (kg mol^{-1})	$Đ$[a]	M_n[b] (kg mol^{-1})	T_d[c] (°C)
PTV	33	73	2.2	30	379
iiPTTV	36	79	2.2	17	402
ooPTTV	4	5	1.3	1	374
ioPTTV	35	88	2.5	13	400
PTTTV	40	112	2.8	20	386

[a]Determined by SEC in $CHCl_3$ with a refractive index detector and polystyrene standards. [b]Determined by ^{1}H NMR analysis. [c]T_d determined at 5% weight loss.

The high solubility in THF of iiPTTV allowed for absolute molar mass characterization by SEC with coupled light-scattering and refractive index detectors. The molar mass values determined from this analysis (M_n = 19 kg mol^{-1}, $M_{w,abs}$ = 35 kg mol^{-1}) are in agreement with the value determined by NMR spectroscopy (M_n = 17 kg mol^{-1}). This result is corroborated by literature where SEC analysis using polystyrene standards has been shown to significantly overestimate the molar mass of rod-like CPs.[37-39] The thermal stability of the polymers was quantified using thermogravimetric analysis (TGA, 10 °C min^{-1}) in a nitrogen atmosphere (Table 5.1, Figure 5.2). Although polymer architecture had a slight impact on decomposition temperature (T_d), all polymers displayed a 5% weight loss above 374 °C.

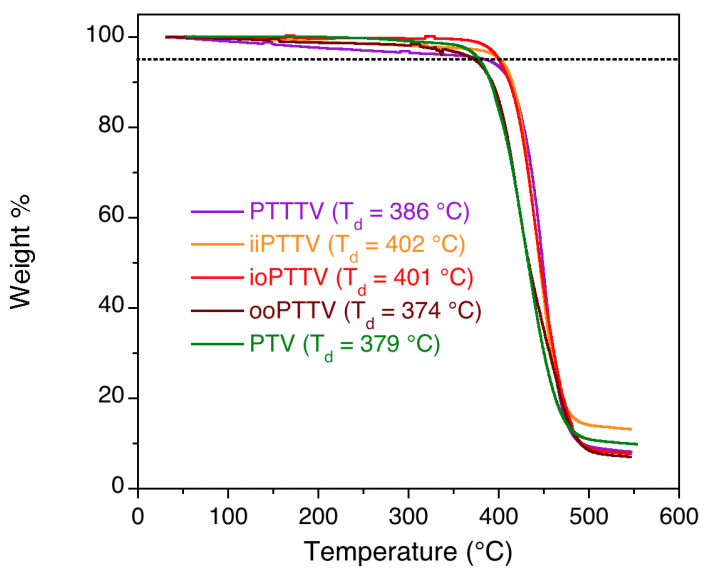

Figure 5.2
Thermogravimetric analysis of polymers in a nitrogen atmosphere. Decomposition temperature (T_d) was determined as the temperature where 5% of the polymer weight (dashed line) was lost.

5.2.2 Polymer Stereochemistry

It is known that ADMET polymerization favors olefins with *trans* stereochemistry (*cis*:*trans* ~ 1:4),[40,41] and we have long sought to confirm this observation in our PTVs. We suspect that long polymerization times coupled with the unfavorable steric interactions of the *cis* configuration would provide a predominantly *trans* PTV backbone. However, strong evidence in support of this hypothesis has been difficult to obtain. PTVs lack the necessary solubility in common NMR spectroscopy solvents (e.g., $CDCl_3$) to obtain high quality ^{13}C NMR spectra. However, two of the polymers prepared in this study (iiPTTV and PTTTV) demonstrated excellent solubility in $CDCl_3$. In addition, these polymers are regioregular owing to their preparation from symmetric monomers (Scheme 5.2). These two characteristics allowed for the facile collection and interpretation of ^{13}C NMR spectra (Figure 5.3a). On investigation, iiPTTV demonstrated the predicted five

resonances in the downfield region. This would not be the case if both olefin (*cis* and *trans*) stereoisomers were present. This result provides additional support to the majority *trans* hypothesis. PTTTV also demonstrated five peaks, which is two less than the predicted seven. However, this could be a product of overlap (see resonance at ca. 130 ppm) and still suggests a single polymer stereochemistry. Both polymers exhibited a resonance around 121.5 ppm, which was tentatively assigned to the *trans* alkene based on a *trans* model compound (Figure 5.4b). Although ^{13}C NMR spectroscopy does not provide the same quantitative information as ^{1}H NMR, no peaks were observed that could be assigned to the *cis* olefin.

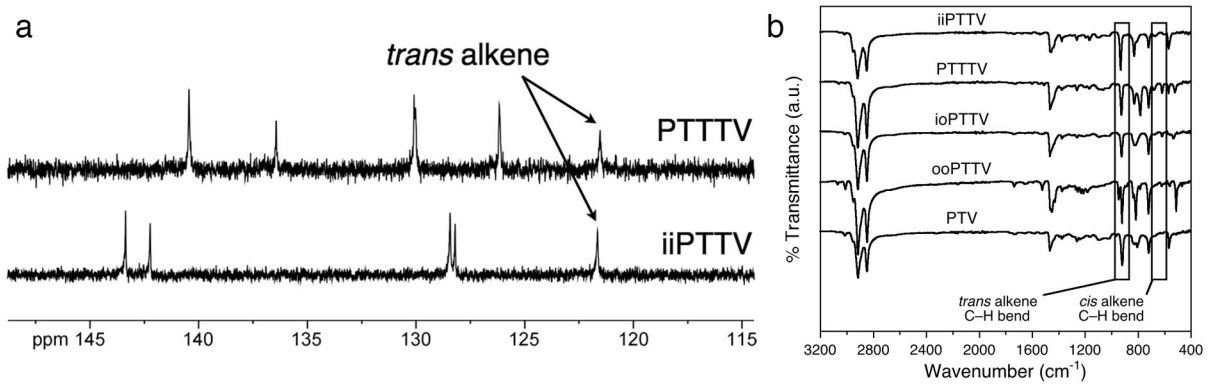

Figure 5.3
(a) Aromatic region of iiPTTV and PTTTV ^{13}C NMR spectra with *trans* alkene resonances labeled. (b) ATR-IR spectra of all polymers with *trans* and *cis* alkene bend regions highlighted.

In order to provide additional support for a predominantly *trans* backbone, attenuated total reflectance infrared (ATR-IR) spectra were collected for all PTVs in the solid state (Figure 3b). Out-of-plane alkene C–H bending is known to give strong IR peaks for both *cis* (600–700 cm^{-1}) and *trans* (900–1000 cm^{-1}) stereoisomers.[42,43] In support of a *trans* backbone, all PTVs showed a strong peak at ca. 925 cm^{-1}, while no obvious peaks were observed in the *cis* region. This observation and the IR spectra in general are in good agreement with literature examples of PTTVs.[18,33] The ATR-IR spectra of the *trans*

model compound provided further support for a predominantly *trans* stereochemistry (Figure 5.4c).

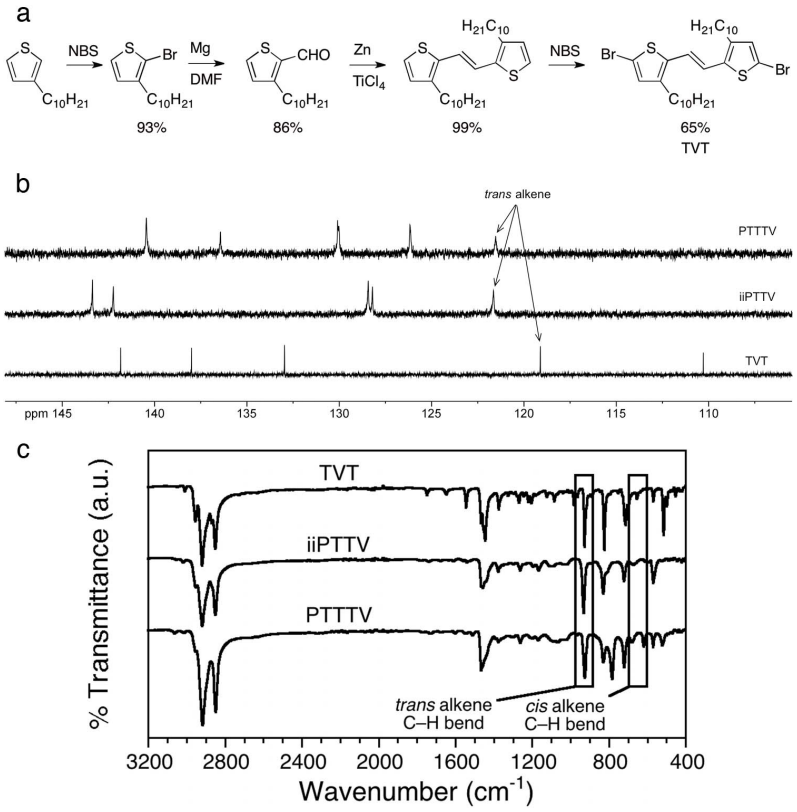

Figure 5.4

(a) Synthesis of *trans* model compound (TVT). Prepared in 51% overall yield by following previous literature reports.[35,44,45] (b) ^{13}C NMR spectra with peaks corresponding to the *trans* alkene labeled. (c) ATR-IR spectra highlighting the presence of a *trans* alkene bend and the absence of a *cis* alkene bend.

5.2.3 Optical Behavior

To understand the role that olefin dilution plays in photophysical behavior ioPTTV and PTTTV were investigated by ultraviolet–visible absorption spectroscopy (UV–vis) in dilute chloroform solutions and as thin films on glass substrates (Table 5.2). Spectra of poly(3-hexylthiophene) (P3HT) and poly(3-hexadecylthienylene vinylene) (PTV) were recorded for comparison. The solution spectra of ioPTTV and PTTTV confirm the

ability to optically tune absorptive behavior through olefin dilution (Figure 5.5a); as the ratio of olefin to thiophene decreases (PTV[1:1] → ioPTTV[1:2] → PTTTV[1:3] → P3HT[0:1]) both the absorption maximum (λ_{max}) and absorption onset blue shift.

Table 5.2
Polymer optical data.

Polymer[a]	$\lambda_{max,soln}$[b] (nm)	$\lambda_{max,film}$[c] (nm)	Δ[d] (nm)	E_g^{opt}[e] (eV)	α[f] ($\times 10^4$ cm^{-1})	PL[g] (nm)	Φ[h] (%)
PTV	582	625	43	1.67	3.0[i]	–	0.0
ioPTTV	535	589	54	1.76	5.2	625	1.3
PTTTV	503	560	57	1.86	5.7	591	2.0
P3HT	454	558	104	1.92	–	–	–
iiPTTV	436	437	1	2.34	5.9	568	3.8
ooPTTV	536	575	39	1.69	–	–	0.0

[a]First four polymers are in order of decreasing olefin content. [b]1×10^{-5} M (repeat unit basis) in $CHCl_3$. [c]Films prepared by spin coating a 10 mg/mL polymer solution in $CHCl_3$ at 2000 rpm for 40 s. [d]$\Delta = \lambda_{max,film} - \lambda_{max,soln}$ [e]Determined from absorption onset of film ($E_g^{opt} = 1240/\lambda_{onset}$). [f]Absorption coefficient determined from UV–vis of thin films with varying thickness. [g]Maximum PL wavelength measured in $CHCl_3$ solution. [h]Quantum yield from PL measurements. [i]Value determined from previous work.[16]

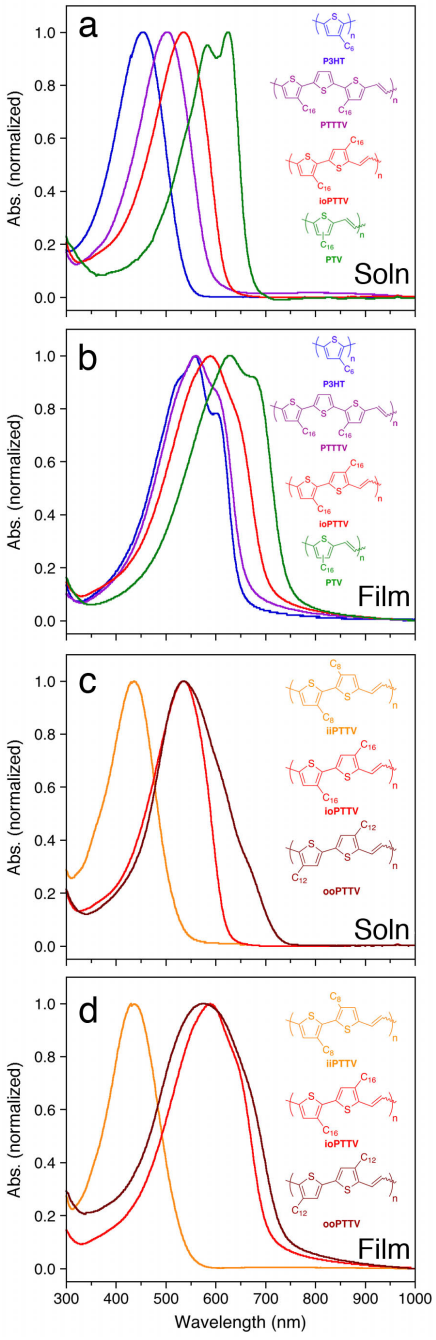

Figure 5.5

UV–vis spectra of olefin dilution (a, b) and alkyl chain position (c, d) series. Solution spectra (a, c) were collected in $CHCl_3$ and film spectra (b, d) were obtained by spin

coating from $CHCl_3$ solutions on glass substrates. C6 = n-hexyl, C8 = n-octyl, C12 = n-dodecyl, and C16 = n-hexadecyl.

The thin film λ_{max} values of ioPTTV and PTTTV demonstrate significant red shifts (57 and 54 nm, respectively) when compared to solution spectra (Figure 5.5b). In addition, the polymers follow the same trend observed in solution. As the olefin is diluted the λ_{max} decreases and the E_g^{opt} (E_g^{opt} = 1240/λ_{onset}) increases (1.76 eV for ioPTTV and 1.86 eV for PTTTV). All polymers in Figure 5.5b show a vibronic absorption shoulder, which suggests a high degree of chain ordering in the solid state.[16]

When comparing UV–vis of the three PTTV polymers with varying side chain substitution patterns (Figure 5.5c, d), it becomes clear that alkyl chain position significantly impacts optical properties. Despite containing an olefin in the backbone the absorption of iiPTTV in solution is blue shifted with regard to P3HT. We hypothesize that this is due to a steric interaction between the octyl chains, which causes severe backbone twisting and disrupts conjugation. Further support for this hypothesis is provided by the iiPTTV film spectrum, which demonstrates virtually no red shift in λ_{max}. In addition, there is no observable vibronic absorption, which suggests iiPTTV is largely amorphous in the solid state. Opposite behavior is observed for ooPTTV where the steric interaction is minimized allowing for enhanced conjugation and absorption with a significantly larger red shift in the solid state. Lowe et al. demonstrated similar absorption behavior for PTTVs of comparable architecture.[18] When comparing iiPTTV to ooPTTV it becomes clear that ioPTTV strikes a balance between absorption and solubility behavior. However, indicative of enhanced ordering, ooPTTV displays a vibronic shoulder and a E_g^{opt} lower than that of ioPTTV.

In addition to PTTV homopolymers we attempted to achieve the same balance of solubility and optical performance observed in ioPTTV by copolymerizing the iiPTTV and ooPTTV monomers.[17] The copolymers were prepared with **4:8** (ii-monomer:oo-monomer) feed ratios of 1:1 and 1:3. As indicated by Figure 5.6 and Table 5.3, we were

able to tune optical properties between that of iiPTTV and ooPTTV. In fact, the optical behavior of the 1:3 copolymer was quite similar to that of ioPTTV. However, this copolymer demonstrated poor solubility and a low molar mass (M_n = 6 kg mol^{-1}) suggesting that the incorporation of the highly soluble iiPTTV moiety cannot overcome the insolubility of the ooPTTV.

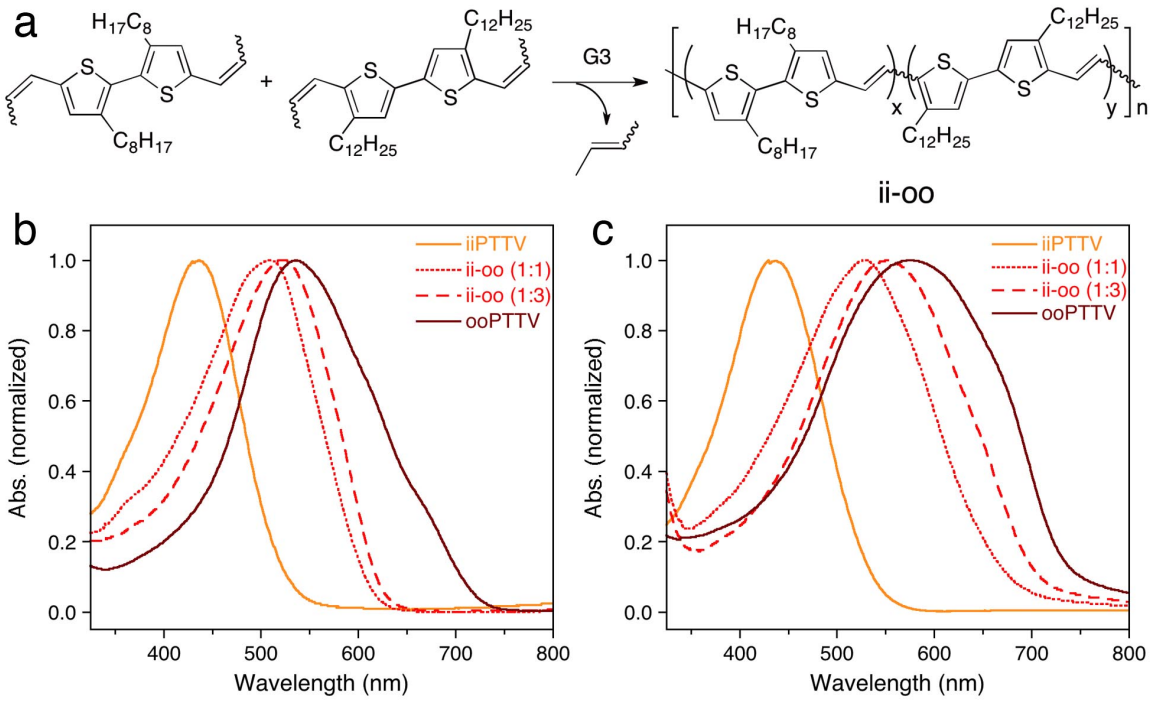

Figure 5.6
(a) ii-oo polymer synthesis. Solution (b) and film (c) UV–vis spectra of iiPTTV, ii-oo copolymers, and ooPTTV.

Table 5.3
Copolymer data.

Feed Ratio (ii:oo)	Actual Ratio (ii:oo)[a]	M_n[a] (kg/mol)	M_n[b] (kg/mol)	$Đ$[b]	$\lambda_{max,soln}$[c] (nm)	$\lambda_{max,film}$[d] (nm)	$\Delta\lambda_{max}$ (nm)	E_g^{opt}[d] (eV)
1:1	50:50	15	27	2.7	509	529	20	1.85
1:3	36:64	3	6	1.8	522	552	30	1.75

[a]Determined by ^{1}H NMR analysis in $CDCl_3$. [b]Determined by SEC in $CHCl_3$ with a refractive index detector and polystyrene standards. [c]1×10^{-5} M (repeat unit basis) in $CHCl_3$. [d]Films prepared by spin coating a 10 mg mL^{-1} polymer solution in $CHCl_3$ at 2000 rpm for 40 s.

The strength of optical absorption of each polymer (excluding ooPTTV, whose low solubility inhibited uniform film formation and thus reliable thickness measurement) was evaluated by extracting the absorption coeffecient (α) from thickness dependence of peak absorption (Figure 5.7). PTTTV, ioPTTV, and iiPTTV all display values of α between 5×10^4 and 6×10^4 cm^{-1}. While this is a significant improvement over PTV (3.0×10^4 cm^{-1}), it falls short of P3HT, which exceeds 1.0×10^5 cm^{-1}.

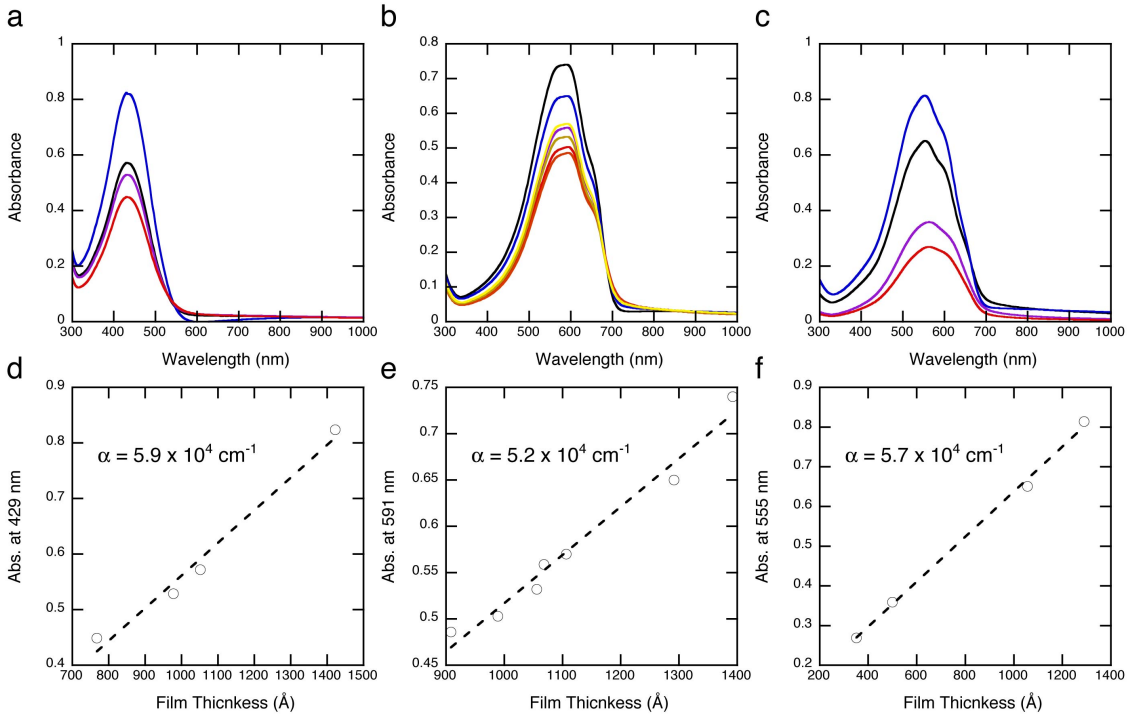

Figure 5.7
UV–vis spectra of (a) iiPTTV, (b) ioPTTV, and (c) PTTTV films of various thickness. Plot of absorbance (at λ_{max}) versus film thickness for (d) iiPTTV, (e) ioPTTV, and (f) PTTTV from which the absorption coefficient was determined.

By preparing PTTVs and PTTTV we hypothesized that the increased thiophene content would serve to increase PL, which would indicate longer-lived excitons and should result in improved OSC performance. Consequently, PL was measured for all polymers in $CHCl_3$ (Figure 5.8). All data was scaled to account for instrument fluctuations and differences in polymer absorption strengths. iiPTTV gave the most intense PL, with a peak at 568 nm that agreed with literature. PTTTV and ioPTTV followed in intensity with peaks at 591 and 625 nm, respectively. ooPTTV and PTV demonstrated no observable PL. Figure 5.8a details the olefin dilution series and supports the hypothesis that an increase in thiophene content leads to an increase in PL intensity. The increase in intensity is also matched by an increase in quantum yield (Φ, Table 5.2)

when going from PTV (Φ = 0%) to P3HT (Φ = 40%). The alkyl chain position (Figure 5.8b) on PTTVs was also observed to directly impact PL. We suspect that the least soluble polymer (ooPTTV) had no observable PL because the formation of polymer aggregates in solution provides other nonradiative relaxation pathways for an excited state.[46] For the opposite reasons iiPTTV gave the most intense PL.

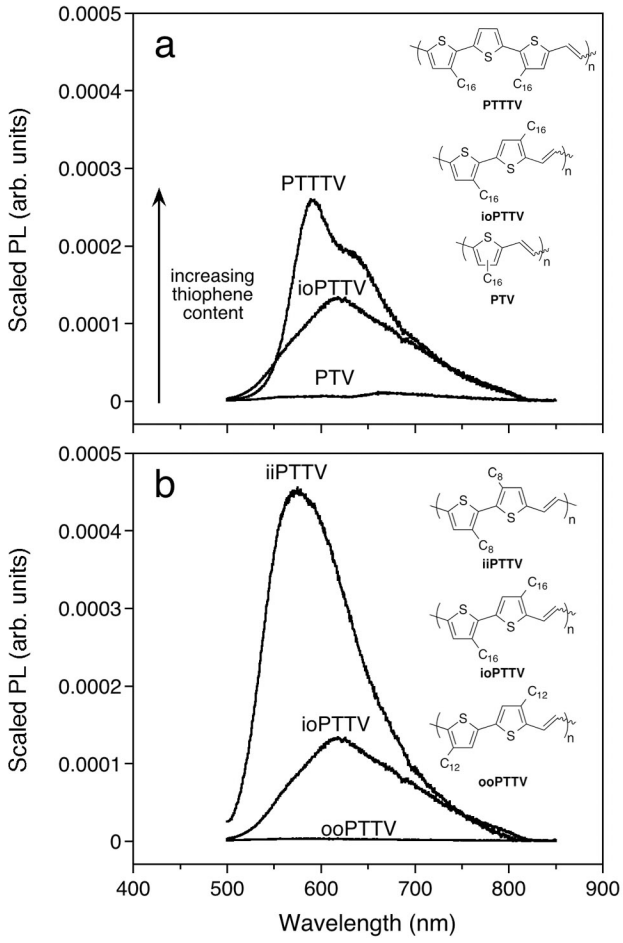

Figure 5.8
PL spectra of olefin dilution (a) and alkyl chain position (b) series collected in $CHCl_3$. C8 = n-octyl, C12 = n-dodecyl, and C16 = n-hexadecyl.

5.2.4 Solid State Behavior

Differential scanning calorimetry (DSC) was employed to study polymer thermal properties and, by association, morphology. Every polymer was initially heated to 230 °C (10 °C min^{-1}) to remove thermal history. Polymers were then cooled to -30 °C (10 °C min^{-1}) before heating again to 230 °C (10 °C min^{-1}). The data from the second heating is shown in Figure 5.9. Two melting transitions (T_m) at 111 °C and 128 °C were observed for ioPTTV. The first and larger melt is attributed to the melting of interdigitated polymer side chains while the second is likely due to π-stack dissociation. The thermogram of ooPTTV showed two strong melts at 180 and 198 °C, which were too high to attribute to the melting of side chains. Instead, the low molar mass (4 kg mol^{-1}) and insolubility of ooPTTV suggest that these transitions result from strong π-stacking in the polymer bulk. A distribution of crystallites is a potential explanation for the multiple melting peaks. Three melting peaks are observed for PTTTV (44, 94, and 108 °C). Based on previous PTV analysis[16] the first peak was assigned to melting of interdigitated side chains in amorphous polymer domains, the second was due to side chain melting in crystalline polymer domains, and the third peak is indicative of π-stack melting. DSC analysis of iiPTTV showed no melting transistions, but a glass transition (T_g) was observed at 8 °C. This behavior provides substantial support for UV–vis observations which predicted an amorphous iiPTTV bulk.

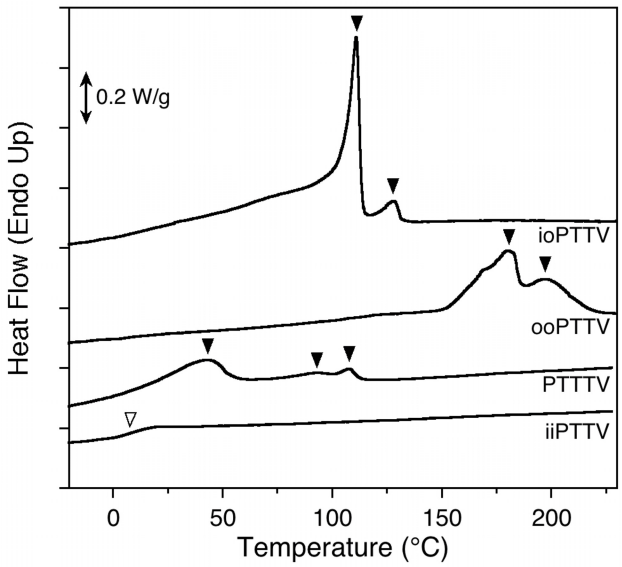

Figure 5.9
DSC thermograms (second heating, 10 °C min^{-1}) of ioPTTV, ooPTTV, PTTTV, and iiPTTV (black triangles = T_m and white triangle = T_g).

Wide-angle X-ray scattering (WAXS) was performed on PTTV and PTTTV thin films drop cast on glass slides from chloroform (ca. 10–20 mg mL^{-1}). Once dry, the films were removed from the glass and mounted on a quartz substrate before recording out-of-plane diffraction patterns (Figure 5.10). With the exception of ooPTTV, all polymers formed flexible, free-standing films (Figure 5.11). ioPTTV (Figure 5.10a, b) gave a lamellar (i.e., alkyl chain interdigitation) spacing (L_1, 2θ = 3.8°) of 23.0 Å, an alkyl chain-to-alkyl chain spacing (C_1, 2θ = 11.8°) of 7.5 Å, and a π-stack value (π, 2θ = 20.3°) of 4.4 Å. This diffraction pattern and the values obtained from it are similar to values reported earlier for PTV.[16] ooPTTV (Figure 5.10c, d) demonstrated a high degree of crystalline order as a fourth order lamellar peak (L_4) was evidenced. A shorter alkyl chain (dodecyl v. hexadecyl) resulted in a slightly smaller lamellar spacing (2θ = 4.4°, 20.1 Å), while a reduced π-stack spacing (2θ = 21.5°, 4.1 Å) suggested greater backbone planarity. The principal chain-to-chain spacing peak (C1) was obscured by strong L2 and L3 peaks, but the second order peak (C2) was evident. The pattern observed for ooPTTV agreed well

with previously reported WAXS data for similar polymers.[36] PTTTV gave evidence of side chain interdigitation (2θ = 4.2°, 21.0 Å), but did not have strong chain-to-chain or π-stack interactions (Figure 5.10e, f). Finally, in keeping with DSC observations iiPTTV showed no evidence of long-range order (Figure 5.10g, h). The three broad amorphous halos observed were not clear enough to assign with a high level of confidence.

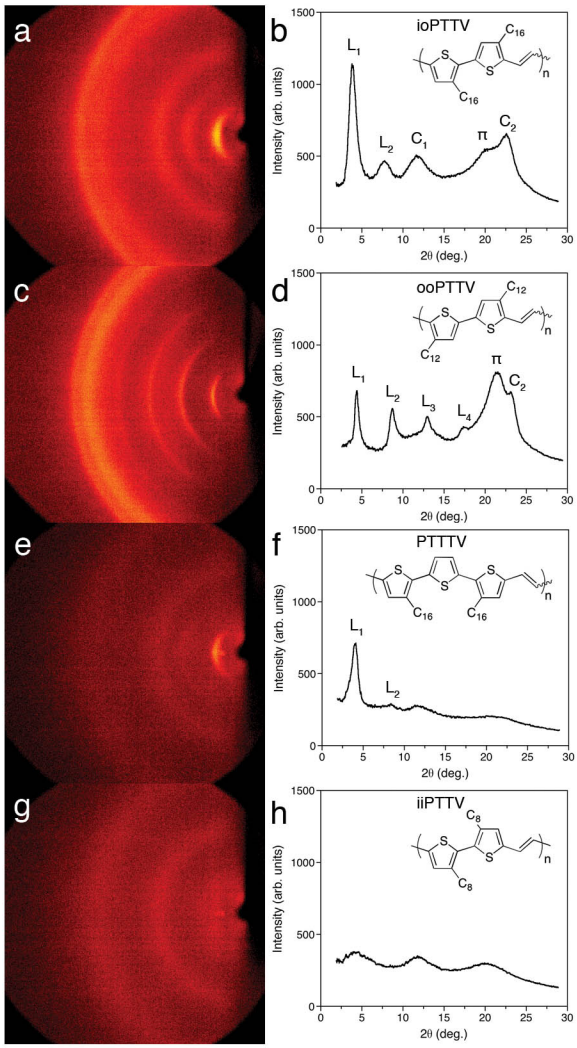

Figure 5.10

WAXS 2D diffraction patterns (a, c, e, g) and corresponding 1D integrations (b, d, f, h) of ioPTTV, ooPTTV, PTTTV, and iiPTTV. L refers to lamellar, C to chain-to-chain, and π to π-stack spacings.

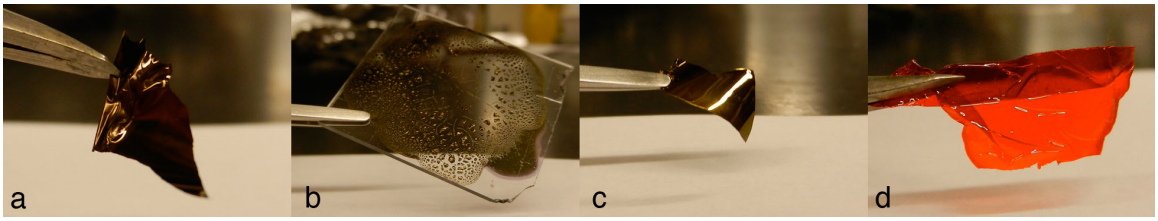

Figure 5.11
Films of ioPTTV (a), ooPTTV (b), PTTTV (c), and iiPTTV (d) used for WAXS analysis. Note the ideal optical and film qualities of ioPTTV and PTTTV. ooPTTV forms a poor film, but has good optical behavior. iiPTTV forms a good film, but has poor optical qualities.

5.2.5 Computational Analysis

The combined observations from UV–vis, DSC, and WAXS all support the semicrystalline nature of ioPTTV, ooPTTV, and PTTTV and the amorphous character of iiPTTV. We hypothesize that this difference in behavior is largely the result of steric interactions. For example, the low band gap in PTVs is caused by a reduction in thiophene-thiophene steric interactions. This leads to enhanced coplanarity and greater orbital overlap, which ultimately manifests as a reduced band gap.[47] This also suggests that PTVs would have a relatively high degree of crystallinity. In order to better understand PTTV and PTTTV solid-state behavior, density functional theory (DFT) calculations were performed on simplified polymer repeat units. Using Gaussian 09,[48] gas-phase geometries of pentamers were optimized using the M06-2X functional[49] with the 6-311+G(d,p) basis set,[50] and structural data was taken from the center monomeric unit. Less complex geometries were also optimized and found to trend well with the pentamer results (Figure 5.12).

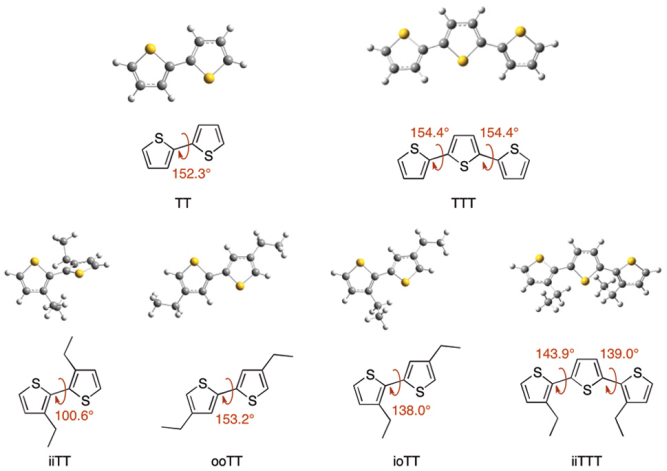

Figure 5.12
Optimized geometries of TT and TTT with and without alkyl substituents. Simplified structures are drawn below each molecule with θ_{tt} shown in red.

First, a baseline was established by optimizing the geometry of unsubstituted thiophene and thienylene vinylene pentamers (Figure 5.13a). From this the thiophene-thiophene and thiophene-olefin dihedral angles (θ_{tt} and θ_{to}, respectively) were found to be approximately 20.9 and 0.0°, where 0° implies a completely planar structure. Pentamers of PTTV and PTTTV were calculated and found to have reduced θ_{tt} (11.1 and 16.1°, respectively) with little change to θ_{to} (ca. 1°). It should be noted that θ_{tt} increased with increasing thiophene content. Although this was expected, it provides further explanation for the optical behavior observed in the olefin content series (Figure 5.5a, b).

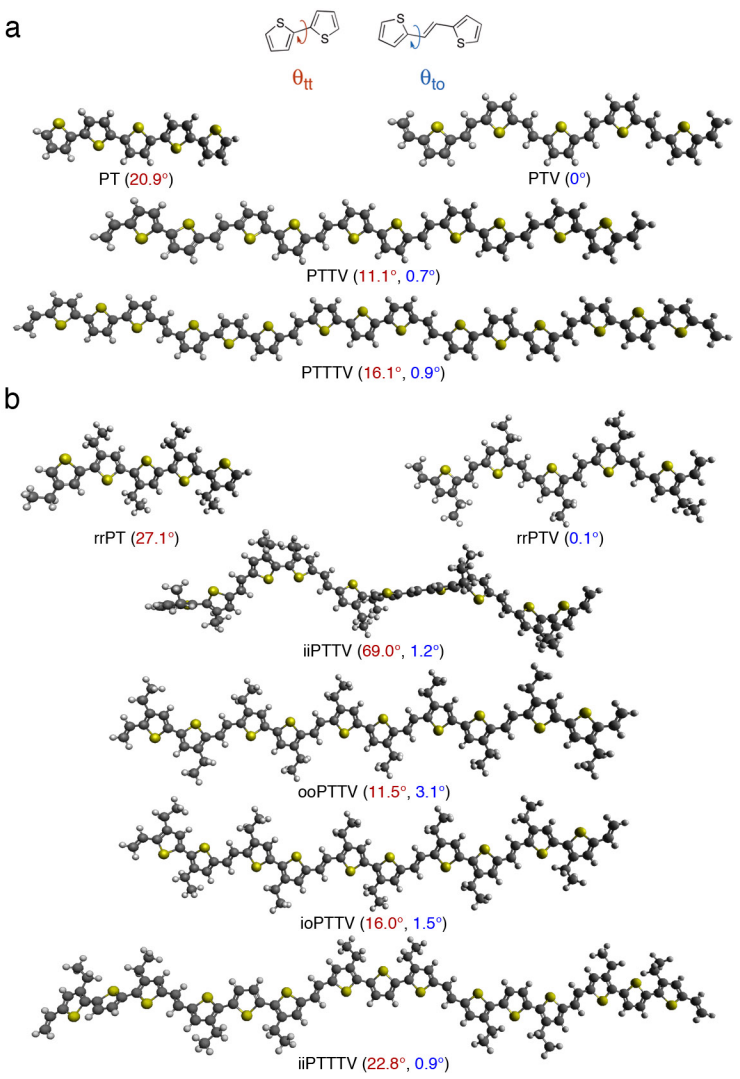

Figure 5.13
Optimized geometries from DFT analysis for substituted (a) and unsubstituted (b) pentamers with θ_{tt} (red) and θ_{to} (blue) values.

Following optimization of unsubstituted pentamers, the impact of alkyl chain position was investigated (Figure 5.13b). Long linear alkyl chains were replaced with ethyl chains. This reduced calculation time without seriously affecting geometric accuracy. It is also important to mention that only regioregular models were taken into account for asymmetric monomers. Similar to unsubstituted PTV, the substituted θ_{to} value for PTV

(rrPTV), iiPTTV, ioPTTV and PTTTV (iiPTTTV) was always near 0°. A different trend was observed for θ_{tt}. In regioregular 3-ethyl polythiophene (rrPT) θ_{tt} increased to 27.1°. For iiPTTV a large θ_{tt} (69.0°) was observed. This is a result of having both alkyl chains proximal to one another, which severely disrupts conjugation leading to reduced ordering in the polymer. This supports the observed UV–vis, DSC, and WAXS behavior that suggest iiPTTV is largely amorphous and is similar to the behavior observed in regiorandom 3-substituted polythiophenes.[51] In contrast, having both alkyl chains distal to one another (ooPTTV) should result in a minimized steric interaction. The θ_{tt} of approximately 11.5° confirms this. In fact, this is approximately the same angle observed with no alkyl substitution and suggests a high degree of coplanarity, conjugation, and crystallinity (i.e., poor solubility). In this particular model, with both alkyl chains in proximity to the olefin, a small disruption was seen in θ_{to}, which increased to 3.1°. In accordance with previous observations, the ioPTTV θ_{tt} value (16.0°) fell between that of iiPTTV and ooPTTV, but was far closer to ooPTTV. The θ_{tt} calculated for iiPTTTV (22.8°) is between that of PT and rrPT and suggests that the alkyl chains are in the optimal position.

From this computational study a number of conclusions can be drawn. First, the presence of olefin spacers serves to planarize the conjugated polymer backbone regardless of thiophene content or alkyl chain substitution. This is perhaps most evident in the iiPTTV pentamer where the twisting only occurs between thiophene rings. Second, whether substituted or unsubstituted, the olefin content series demonstrates dihedral angles that scale directly with thiophene content. Finally, the position of alkyl side chains is as important to polymer microstructure as backbone composition.

5.2.6 Energy Level Determination

The position of the highest occupied molecular orbital (HOMO) of each polymer was determined from thin film cyclic voltammograms (Table 5.4) collected in the room temperature molten salt 1-butyl-1-methylpyrrolidinium bis(trifluoromethylsulfonyl)imide (P14-TFSA) (Figure 5.14). Due to the broad electrochemical stability window of P14-TFSA, all polymers displayed stable quasi-reversible oxidation with high sweep-to-sweep reproducibility. Using an internal calibrant, cobaltocenium hexafluorophosphate ($CcPF_6$), the voltage onset of electrochemical oxidation was converted to the vacuum scale, E (eV) = E (V vs $Cc^{+/o}$) + 3.75,[17] which is equivalent to the ferrocene redox couple ($Fc^{+/o}$) residing at a depth of 5.1 eV.[52] For reference, in this system the benchmark polymer regioregular P3HT displays a HOMO position of 5.06 eV below vacuum level.

Table 5.4
CV, FET, and OSC data.

Polymer	HOMO[a] (eV)	μ_h[b] ($cm^2\ V^{-1}\ s^{-1}$)	V_{oc} (V)	J_{sc} ($mA\ cm^{-2}$)	FF	*PCE* (%)
PTV	-5.10	8.0×10^{-3}	0.41	4.4 ± 0.3	0.54 ± 0.01	0.98 ± 0.07
iiPTTV	-5.45	–	–	–	–	–
ooPTTV	-5.31	~ 3×10^{-5}	–	–	–	–
ioPTTV	-5.23	4.1×10^{-3}	0.49	4.3 ± 0.1	0.52 ± 0.01	1.10 ± 0.03
PTTTV	-5.15	1.1×10^{-3}	0.46	3.7 ± 0.1	0.58 ± 0.01	0.98 ± 0.03

[a]Determined in P14-TFSA with a $CcPF_6$ reference electrode calibrant.
[b]Extracted from transfer curves collected in the linear regime.

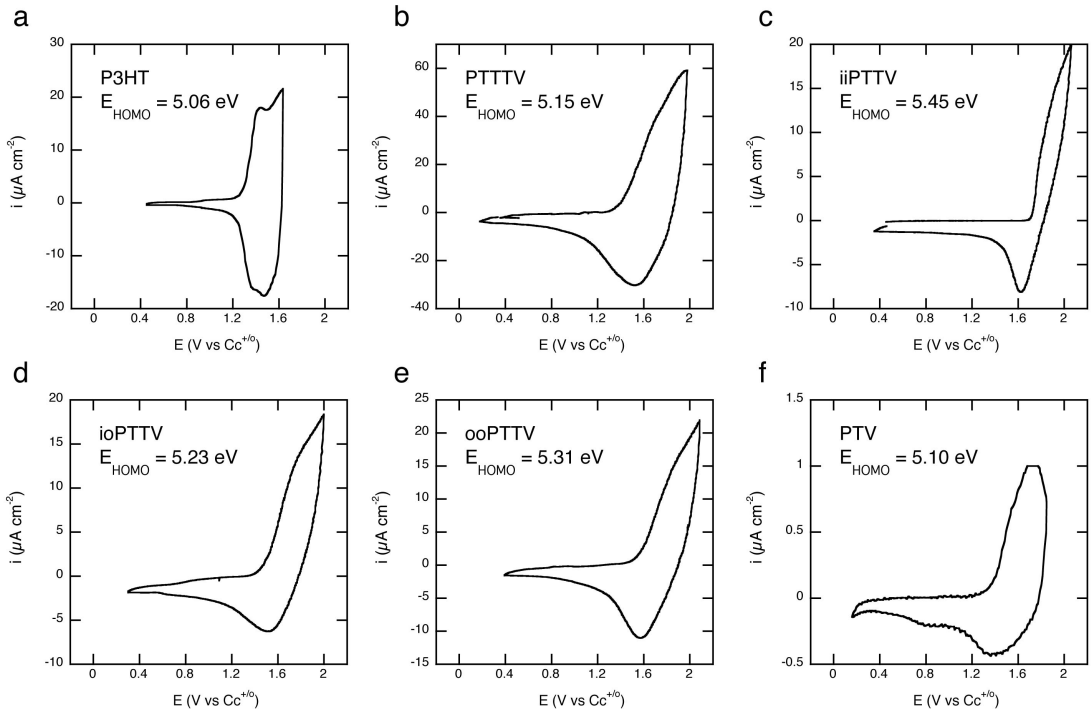

Figure 5.14
CV of (a) P3HT, (b) PTTTV, (c) iiPTTV, (d) ioPTTV, (e) ooPTTV, and (f) PTV.

The bithiophene polymers displayed the deepest HOMO levels: -5.45, -5.31, -5.23 eV, for iiPTTV, ooPTTV, and ioPTTV, respectively. PTTTV and PTV displayed HOMO levels of -5.15 and -5.10 eV, respectively. The LUMO positions were estimated by the addition of the optical band gap to the HOMO level. In order to compare polymer energy levels, Figure 5.15 illustrates a band diagram constructed from UV–vis and CV data.

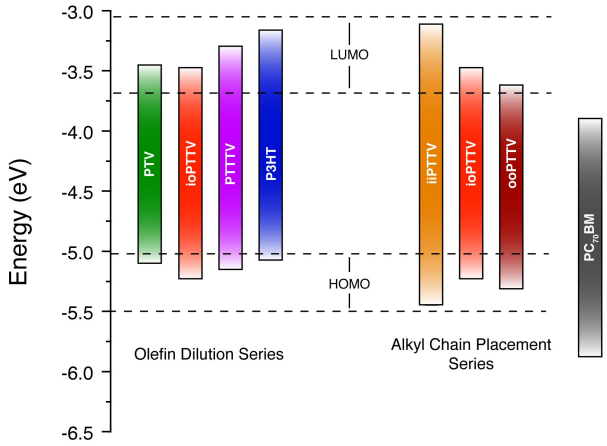

Figure 5.15

Band diagram of both polymer series. HOMO level was determined from CV and LUMO level was estimated using HOMO level and optical band gap data (LUMO = HOMO + E_g^{opt}). $PC_{70}BM$ is included for comparison.

The increased depth of the iiPTTV HOMO is expected due to the increased E_g^{opt}, which requires a shallower LUMO and deeper HOMO. In fact, the relationship of E_g^{opt} and HOMO depth between iiPTTV and ioPTTV is analogous to that of regiorandom and regioregular P3HT, which is ascribed to the presence or absence of crystallinity.[53] The relationship between HOMO depth and polymer structure is less clear for the case of ooPTTV and ioPTTV. As expected, the highly planar ooPTTV shows a lower E_g^{opt} than that of the ioPTTV,[54] but the decrease is minimal. Therefore, due to their comparable band gaps, ioPTTV and ooPTTV provide an uncommon view of the effect on planarity on HOMO depth. It is reasonable to expect the HOMO level of ooPTTV to be shallower than that of ioPTTV due to the shorter alkyl chains[55] and the more planar backbone, however the opposite is observed, with the ooPTTV HOMO being nearly 0.1 eV deeper. Additionally, across the entire series of polymers, it is not immediately clear why the bithiophene polymers would display a deeper HOMO level then either mono or terthiopene polymers, yet the variation is significant, and is born out in the photovoltaic performance discussed below.

5.2.7 Transistor and Solar Cell Performance

The charge transport properties were investigated using thin film transistor test beds (Table 5.4). The hole mobility, μ_h, of iiPTTV was too low such that no transistor behavior was observed. ooPTTV gave non-ideal transistor behavior, with weak device turn on and an ambiguous threshold voltage (Figure 5.16), regardless of coating solvent choice or dielectric surface treatment. ooPTTV mobility was estimated to be ca. 3×10^{-5} $cm^2\ V^{-1}\ s^{-1}$, but this is likely suppressed due to poor film quality (poor solubility). PTTTV and ioPTTV both displayed idealized transistor behavior, with clear saturation (Figure 5.17a, b), when spin-coated from chloroform on n-octadecyltrichlorosilane (OTS) treated substrates, with μ_h values of 1.1×10^{-3} and 4.1×10^{-3} $cm^2\ V^{-1}\ s^{-1}$, respectively. These are similar to the previously reported value of PTV hole mobility (8.0×10^{-3} $cm^2\ V^{-1}\ s^{-1}$).[16] Excluding ooPTTV, whose low mobility is ascribed to poor film quality, the μ_h values of PTV, ioPTTV, and PTTTV where inversely correlated to HOMO level depth. Additionally, the mobility increased with increasing chain planarity, further exemplifying the effect of improved charge transport with improved molecular ordering in thienylene vinylene systems.

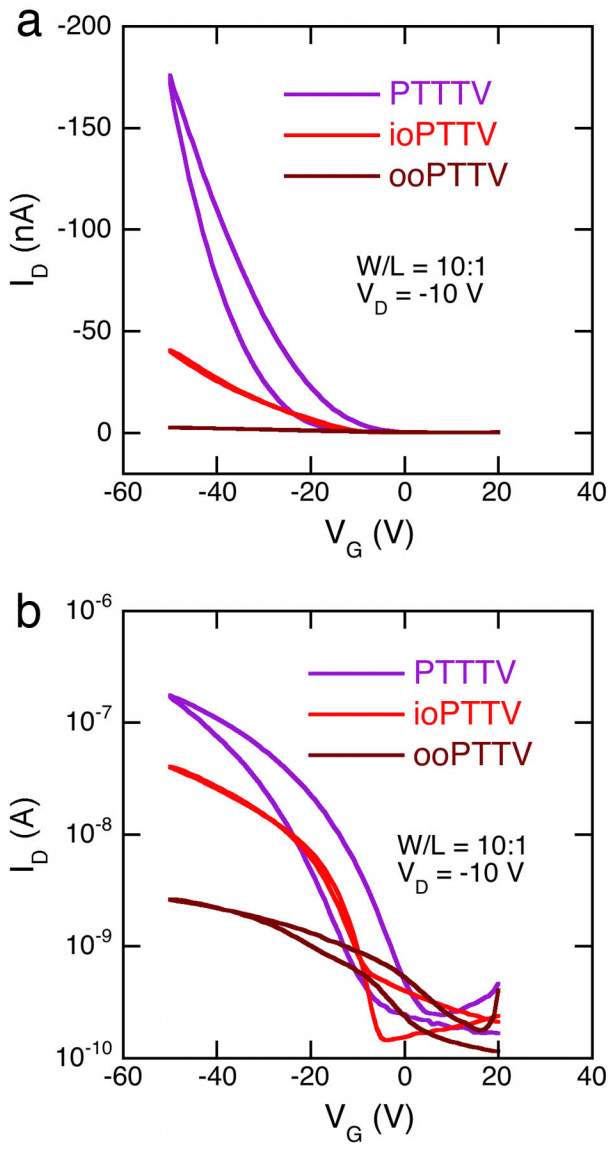

Figure 5.16

Linear (a) and semi-log (b) transfer curves of field effect transistors employing PTTV, ioPTTV, and ooPTTV as the semiconducting channel. W/L is the width to length ratio of the semiconductor channel. V_D is the drain voltage.

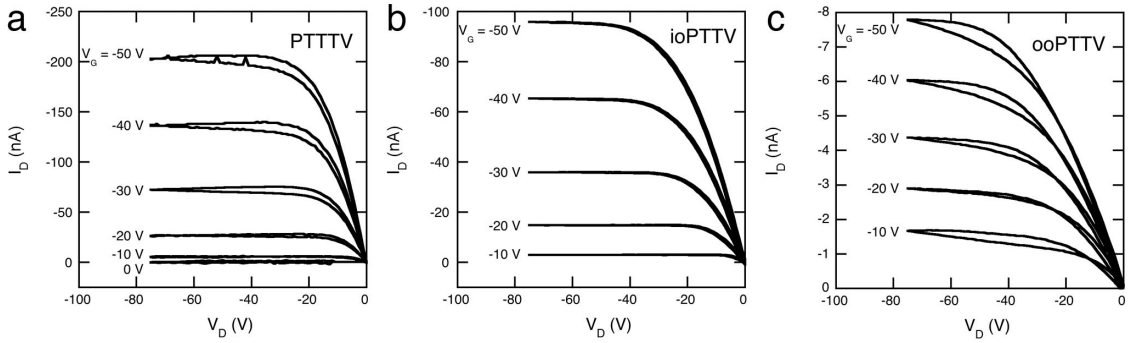

Figure 5.17
Output curves of field effect transistors employing (a) PTTTV, (b) ioPTTV, and (c) ooPTTV as the seminconducting channel.

Finally, PTV, ioPTTV, and PTTTV were incorporated as the donor in polymer-fullerene bulk heterojunction OSCs with the fullerene acceptor $PC_{70}BM$ in a 1:2 ratio (Figure 5.18). The V_{oc} of each polymer scaled directly with the variation in HOMO level, evidencing the effect of HOMO level depth on device performance. The short circuit current densities ranged from 3.7 to 4.4 mA cm^{-2}, and the fill factors all exceeded 0.5. This resulted in device power conversion efficiencies of ca. 1% (Table 5.4).

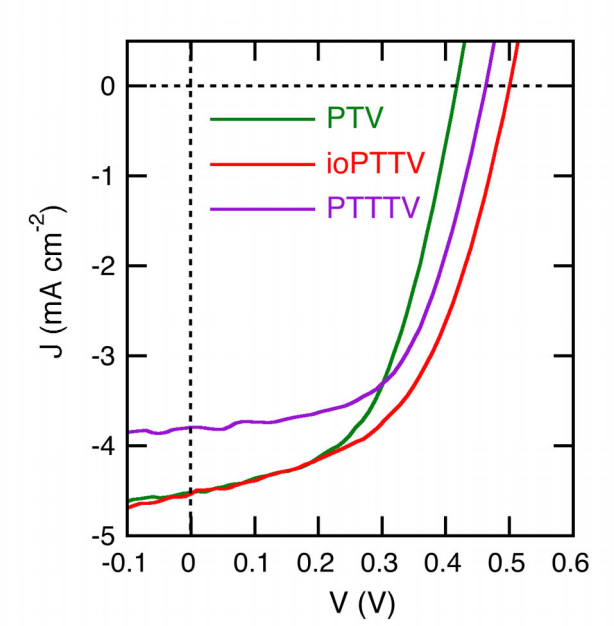

Figure 5.18
J-V characteristics of PTV, ioPTTV, and PTTTV based solar cells, with a 1:2 polymer:$PC_{70}BM$ blend ratio, under simulated AM1.5 spectrum.

Variable light intensity *J-V* curves were also collected (Figure 5.19). All three polymers showed increased V_{oc} with increased light intensity (Figure 5.20a). Conversely, fill factor decreased with increased light intensity (Figure 5.20b), resulting in maximum power conversion efficiency occurring at about one sun intensity (100 mW cm^{-2}) (Figure 5.20c). The low ioPTTV and PTTTV absorption coefficients coupled with peak OSC performance at high fullerene loading (80 wt%) suggests a reliance on fullerene absorption that we have previously documented.[16] This is a significant, and apparently common, limitation to PTV based device performance. For future PTV polymers to achieve high OSC efficiencies they must demonstrate increased absorption coefficients to produce higher photocurrent densities.

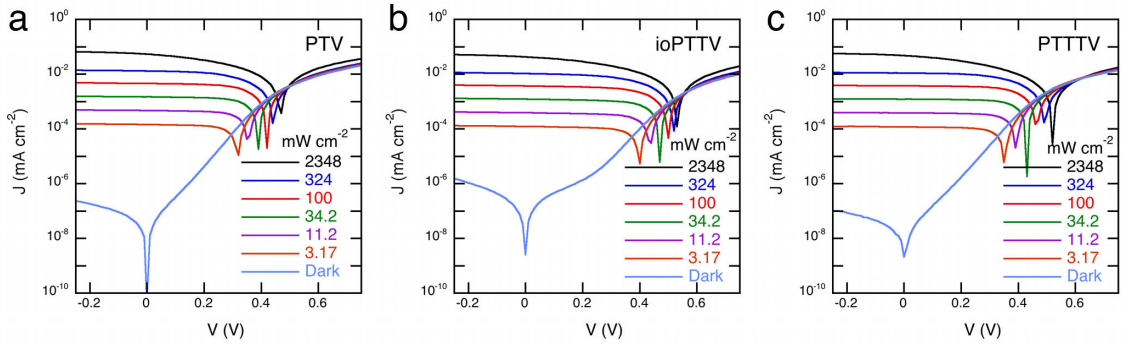

Figure 5.19

Dark and variable light intensity semi-log *J-V* characteristics of (a) PTV, (b) ioPTTV, and (c) PTTTV based solar cells, with a 1:2 polymer:$PC_{70}BM$ blend ratio.

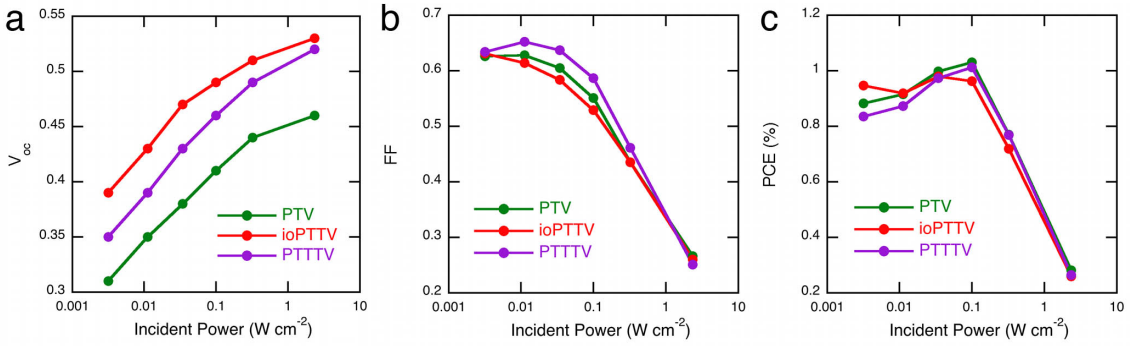

Figure 5.20

Light intensity dependent (a) V_{oc}, (b) fill factor, and (c) power conversion efficiency of PTV, ioPTTV, and PTTTV based solar cells, with a 1:2 polymer:$PC_{70}BM$ blend ratio.

5.3 Conclusions

Four well-defined PTV-based polymers were prepared using ADMET polymerization. These polymers fit nicely into two series, which sought to probe the impact of olefin content and alkyl chain placement. Using the concept of olefin dilution we were able to tune the optical absorption behavior between that of PTV and P3HT. In addition, increasing the thiophene content allowed for the observation of PL, a phenomenon rare to PTVs. Within the olefin dilution series the solar cell V_{oc} was found

to scale directly with HOMO level, and efficiencies of approximately 1% were achieved. The impact of PTTV alkyl substitution pattern on optical behavior, thermal properties, and polymer microstructure was examined. The conclusions drawn from these analyses were supported by thorough density functional calculations. In addition, ^{13}C NMR and IR analysis of iiPTTV and PTTTV supported a long-standing hypothesis of an all *trans* PTV backbone. These systematic studies of PTVs highlight the tremendous impact that seemingly small chemical modifications can have on CP behavior. It is our belief that investigating minute adjustments to CP scaffolds is the best way to identify the most promising candidates for OSCs.

Despite significantly increasing PL, solar cell efficiencies obtained in this work were not high by contemporary OSC standards. This suggests that improving PL is not as important as increasing charge transport or absorption coefficient. Therefore, we believe that the ooPTTV scaffold merits continued investigation. Its highly planar architecture suggests that high charge mobilities could be achieved if steps were taken to improve solubility (e.g., branched alkyl chains). Also, increasing the absorption coefficient of ooPTTV through additional chemical modification would likely lead to improved OSC performance. ADMET is a powerful tool for the assembly of high molar mass conjugated polymers, and we believe it could find utility in the assembly of a multitude of conjugated systems beyond PTVs.

5.4 Experimental Details

5.4.1 Materials and Methods

PTV was prepared according to previous work.[16] Commercially available solvents and reagents were purchased and used as received from Aldrich and Acros. Degassed THF was purified by passage through an activated alumina column and collected in flame-

dried, air-free flasks. N,N,N',N'-tetramethylethylenediamine (TMEDA) was dried over molecular sieves and distilled under vacuum from n-butyllithium. All reactions were run under argon or vacuum using standard Schlenk techniques. A complete description of the characterization techniques employed is available in Appendix A.

Absorption spectra (for photoluminescence) of the polymers dissolved in chloroform were collected on an Olis Cary 14 spectrophotometer. Samples were prepared at a concentration that resulted in an absorbance maximum of approximately 0.3 in a 1 cm quartz cuvette. Photoluminescence spectra were collected using a SPEX Fluorolog 1680 0.2 m double spectrometer at an excitation wavelength of 475 nm. Quantum yields (Φ_i) of the polymers were calculated according to the following equation

$$\Phi_i = \Phi_R \frac{\int PL_i}{\int PL_R} \frac{A_{R,\lambda}}{A_{i,\lambda}} \frac{n_i^2}{n_R^2}$$

where Φ_R is the quantum yield of a reference dye, $\int PL_i$ and $\int PL_R$ are the integrated photoluminescence intensity of the sample and reference, respectively, $A_{i,\lambda}$ and $A_{R,\lambda}$ are the respective value of absorption for the sample and reference at the excitation wavelength, and n_i and n_r are the refractive indices of the sample and reference solvents, respectively. The reference dye employed was 4-(dicyanomethylene)-2-methyl-6-(p-dimethylaminostyryl)-4H-pyran (DCM) in methanol with a Φ_R of 0.43.[56] PL was scaled according to the following equation

$$PL_{scaled} = PL_{sample} \times \frac{A_{R,475\,nm}}{\int PL_R} \times \frac{1}{A_{sample,475\,nm}}$$

to account for instrument fluctuations during measurements and the differences in polymer absorption strengths.

Gas-phase geometries were fully optimized at the density functional level of theory making use of the M06-2X functional and the 6-311+G(d,p) basis set. All structures were characterized as local minima from computation of analytic vibrational frequencies. The M06-2X functional was chosen for these molecules since some dispersion interactions may play a key role in the most stable geometries.[57,58] All calculations were accomplished with the Gaussian 09 electronic structure program suite.

5.4.2 Synthetic Details

3-Octylthiophene. A 250 mL 3-neck round bottom flask was equipped with a magnetic stir bar, reflux condenser, glass stopcock, liquid addition funnel, and two rubber septa. Magnesium turnings (3.8 g, 156.4 mmol) were added and the apparatus was flame-dried under vacuum. Anhydrous THF (120 mL) was transferred via cannula into the flask followed by the addition of 1,2-dibromoethane (0.5 mL) to activate the magnesium. A solution of 1-bromooctane (13.5 mL, 78.2 mmol) in anhydrous THF (25 mL) was added to the liquid addition funnel via syringe and dripped into the Mg/THF mixture over the course of 20 min. After addition the solution was stirred at 40 °C under argon for 1.5 h. The solution was then allowed to cool to room temperature. The Grignard solution was transferred via cannula into a second flame-dried flask containing a magnetic stir bar, 3-bromothiophene (4.9 mL, 54.13 mmol), [1,3-bis(diphenylphosphino)propane]dichloronickel(II) (0.57 g, 1.0 mmol), and anhydrous THF (25 mL) held at 0 °C. The reaction was stirred under argon for 16 h. The reaction was quenched with 1 M NH_4HCO_3 (50 mL), H_2O (75 mL) was added, and extracted with diethyl ether (2 × 75 mL). The combined organics were dried over $MgSO_4$. The solvent was removed under reduced pressure. The remaining residue was distilled at 66 °C (0.3 mmHg) to give a colorless liquid (9.1 g, 89%). The NMR data is in agreement

with previous literature reports.[59] ^{1}H NMR (500 MHz, $CDCl_3$): δ_H (ppm) = 7.25 (dd, J = 4.80 Hz, J = 2.90 Hz, 1H), 6.96 (d, J = 4.90 Hz, 1H), 6.93 (m, 1H), 2.64 (t, J = 7.60 Hz, 2H), 1.66 (quintet, J =7.20 Hz, 2H), 1.30 (bs, 10H), 0.90 (t, J = 6.90 Hz, 3H). ^{13}C NMR (125 MHz, $CDCl_3$): δ_C (ppm) = 143.4, 128.4, 125.2, 119.9, 32.0, 30.7, 30.4, 29.6, 29.5, 29.4, 22.8, 14.3. HRGC-MS (EI): $M_{calcd.}$ = 196.1286, M_{found} = 196.1293.

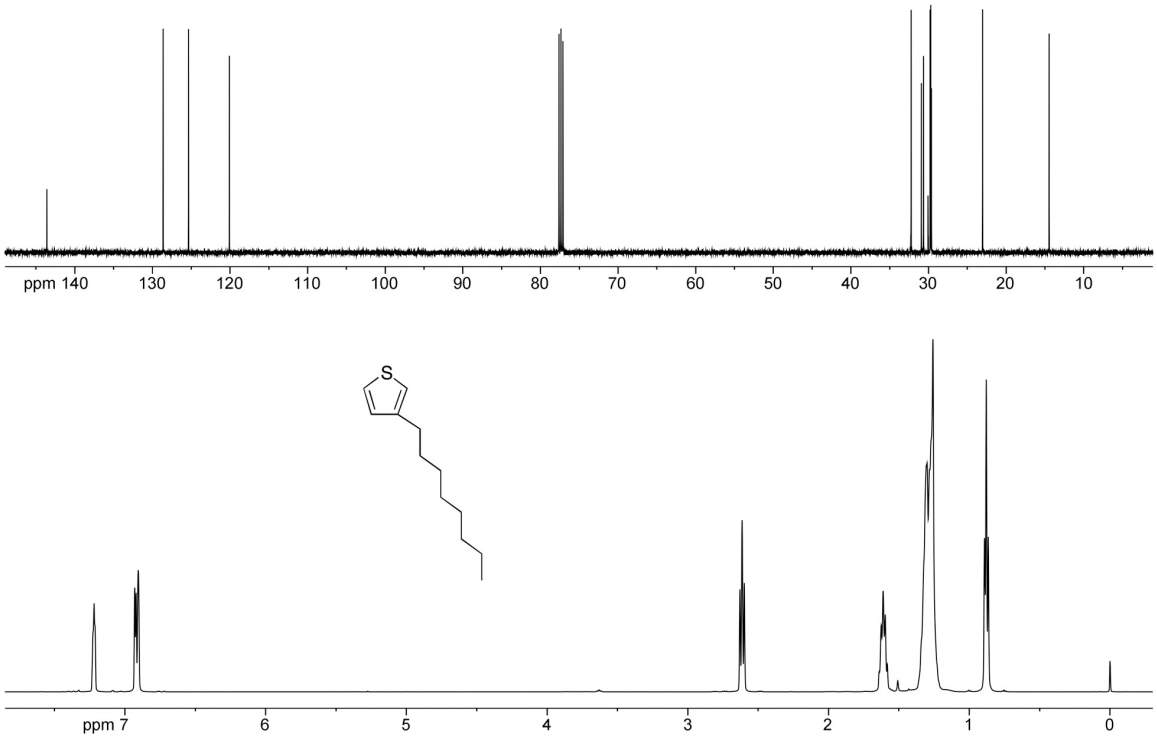

Figure 5.21
^{13}C and ^{1}H NMR spectra of 3-octylthiophene.

2-Bromo-3-octylthiophene (1). A 250 mL round bottom flask was equipped with a magnetic stir bar and anhydrous THF (120 ml) and 3-octylthiophene (9.0 g, 45.84 mmol) were added. The reaction mixture was cooled to 0 °C and N-bromosuccinimide (7.75 g, 43.54 mmol) was added in one portion. The flask was covered with aluminum foil and the reaction mixture was stirred at room temperature for 16 h. Water (100 mL) and NaCl (12 g) were added to the reaction and stirred for 15 min. The organic layer was

separated and dried over $MgSO_4$. The solvent was removed under reduced pressure. The remaining residue was distilled at 77 °C (0.3 mmHg) to give a colorless liquid (12.0 g, 95%). The NMR data is in agreement with previous literature reports.[59] ^{1}H NMR (500 MHz, $CDCl_3$): δ_H (ppm) = 7.18 (d, J = 5.6 Hz, 1H), 6.80 (d, J = 5.6 Hz, 1H), 2.57 (t, J = 7.7 Hz, 2H), 1.58 (quintet, J = 7.4 Hz, 2H), 1.33–1.27 (bs, 12H), 0.90 (t, J = 7.0 Hz, 3H). ^{13}C NMR (125 MHz, $CDCl_3$): δ_C (ppm) = 142.1, 128.4, 125.2, 108.9, 32.0, 29.9, 29.9, 29.5, 29.4, 29.4, 22.8, 14.3. HRGC-MS (EI): $M_{calcd.}$ = 274.0391, M_{found} = 274.0373.

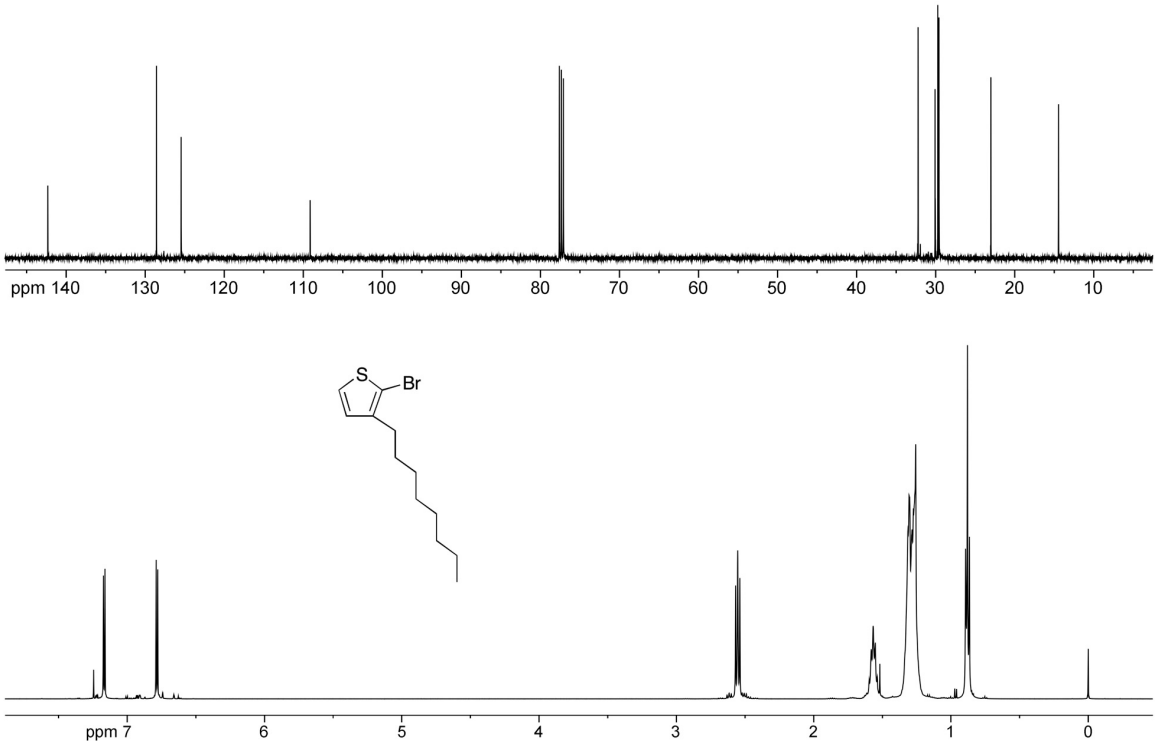

Figure 5.22

^{13}C and ^{1}H NMR spectra of **1**.

3,3'-Dioctyl-2,2'-bithiophene (2). To a 2-neck 50 mL round bottom flask with a magnetic stir bar was added 2-bromo-3-octylthiophene (1.83 mL, 8.0 mmol), bis(tributyltin) (2.0 mL, 4.0 mmol), and 10 mL anhydrous N,N-dimethylformamide. The flask was sealed with two rubber septa and the solution was degassed for 20 min with

argon. Bis(triphenylphosphine)palladium(II) chloride (56 mg, 0.080 mmol) was added as a solid and the reaction was stirred at 85 °C under argon for 24 h. The DMF was removed under high vacuum and the remaining residue was passed through a silica gel plug with hexanes. The solvent was removed under reduced pressure and the remaining liquid was purified by bulb-to-bulb (Kugelrohr) distillation. Unreacted 2-bromo-3-octylthiophene and $SnBu_3Br$ were removed first (100 °C, 0.02 mmHg) followed by the product (clear oil, 185 °C, 0.02 mmHg, 1.04 g, 67%). The NMR data is in agreement with previous literature reports.[60,61] ^{1}H NMR (500 MHz, $CDCl_3$): δ_H (ppm) = 7.29 (d, *J* = 5.3 Hz, 2H), 6.81 (d, *J* = 5.3 Hz, 2H), 2.53 (t, *J* = 7.9 Hz, 4H), 1.57 (quintet, *J* =7.7 Hz, 4H), 1.26 (bs, 20H), 0.90 (t, *J* = 6.9 Hz, 6H). ^{13}C NMR (125 MHz, $CDCl_3$): δ_C (ppm) = 142.4, 128.8, 128.8, 125.3, 32.0, 30.9, 29.6, 29.6, 29.4, 28.9, 22.8, 14.3. HRGC-MS (EI): $M_{calcd.}$ = 390.2415, M_{found} = 390.2387. Anal. calcd. for $C_{24}H_{38}S_2$: C 73.78, H 9.80; Found: C 73.72, H 9.81.

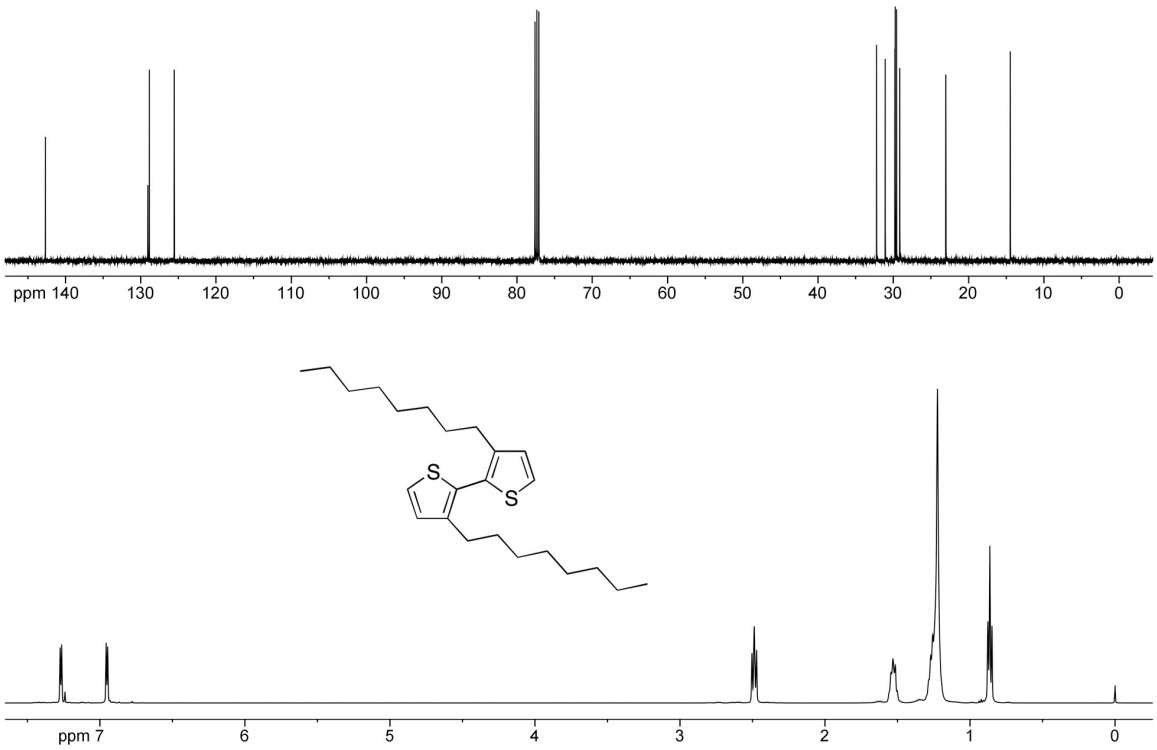

Figure 5.23

^{13}C and ^{1}H NMR spectra of **2**.

3,3'-Dioctyl-[2,2'-bithiophene]-5,5'-dicarbaldehyde (3). A 2-neck 100 mL round bottom flask was equipped with a magnetic stir bar, reflux condenser, and a rubber septum. The apparatus was flame-dried under vacuum and **2** (810 mg, 2.1 mmol) was added. Anhydrous hexanes (27 mL) were transferred via cannula into the flask followed by TMEDA (0.79 mL, 5.3 mmol) addition via syringe. N-butyllithium in (2.5 M in hexanes, 2.12 mL, 5.3 mmol) was added dropwise via syringe to the solution of **2**, TMEDA, and hexanes over the course of 5 min. The solution was refluxed for 1 h following addition. Anhydrous THF (13 mL) was added to the flask and cooled to 0 °C, at which point anhydrous DMF (0.65 mL, 8.48 mmol) was added via syringe. The reaction was stirred for 30 min at 0 °C and 30 min at room temperature before adding 1 M HCl (25 mL) to quench. The aqueous phase was extracted with diethyl ether (2 × 25 mL) and the combined organics were washed with brine (50 mL). The solution was dried over Na_2SO_4 and the solvent was removed under reduced pressure to give an orange-brown oil. The product was purified by column chromatography (hexanes:ethyl acetate 9:1) as an eluent to give light yellow liquid (830 mg, 90%). ~2% of regio isomer (ioTT) is present. ^{1}H NMR (500 MHz, $CDCl_3$): δ_H (ppm) = 9.89 (s, 2H), 7.66 (s, 2H), 2.56 (t, J = 7.7 Hz, 4H), 1.57 (quintet, J =7.6 Hz, 4H), 1.22 (bs, 20H), 0.86 (t, J = 7.0 Hz, 6H). ^{13}C NMR (125 MHz, $CDCl_3$): δ_C (ppm) = 182.9, 144.6, 143.6, 137.6, 137.6, 32.0, 30.6, 29.4, 29.4, 29.3, 29.0, 22.8, 14.2. HRGC-MS (EI): $M_{calcd.}$ = 446.2313, M_{found} = 446.2286. Anal. calcd. for $C_{26}H_{38}O_2S_2$: C 69.91, H 8.57, S 14.36; Found: C 68.48, H 8.44, S 13.75.

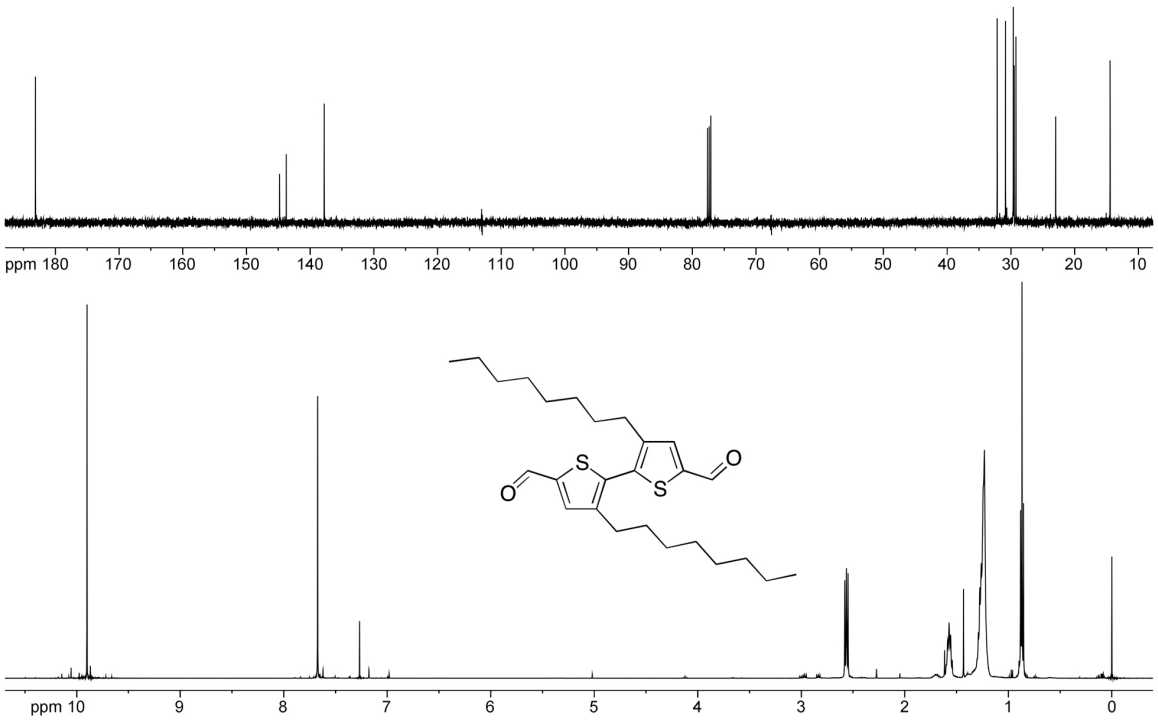

Figure 5.24

^{13}C and ^{1}H NMR spectra of **3**.

3,3'-Dioctyl-5,5'-dipropenyl-2,2'-bithiophene (4). A 2-neck 100 mL round bottom flask was equipped with a magnetic stir bar, reflux condenser, glass stopcock, and rubber septum. The apparatus was flame dried under vacuum before adding sodium bis(trimethylsilyl)amide (1.0 g, 5.44 mmol) and (ethyl)triphenylphosphonium bromide (2.0 g, 5.44 mmol) under an argon purge. The apparatus was placed under reduced pressure for 30 minutes to dry the solids. Anhydrous hexanes (40 mL) were transferred into the flask and refluxed for 1 h under argon to form the Wittig reagent (bright orange-red solution). The reaction was cooled to -78 °C the hexanes were removed with a cannula taking care not to remove precipitated Wittig reagent. The cold hexanes wash was repeated with another 40 mL. Residual hexanes were removed under vacuum and anhydrous THF (40 mL) was added to dissolve the remaining Wittig reagent. This

solution was transferred via cannula into a 100 mL round bottom flask containing anhydrous THF (10 mL) and 3,3'-dioctyl-2,2'-bithiophene-5,5'-dicarbaldehyde (810 mg, 1.8 mmol) held at 0 ˚C. The reaction was stirred for 30 min at 0 ˚C and 30 min at room temperature. The solution was concentrated under reduced pressure to give a dark brown solid. To this solid hexanes (~25 mL) were added and the solution was filtered to remove $Ph_3P=O$. The filtrate was concentrated under reduced pressure and the residual liquid was purified by column chromatography using hexanes as an eluent to remove residual $Ph_3P=O$. The solvent was removed under reduced pressure to give a yellow oil (640 mg, 75%). *Z*:*E* from ^{1}H NMR was 83:17. ~2% of regio isomer (ioTT) is present. ^{1}H NMR (500 MHz, $CDCl_3$): δ_H (ppm) = 6.85, 6.83, 6.71 (s, 2H, *Z* and *E* isomers), 6.50 (*Z*), 6.45 (*E*) (m, 2H), 6.03 (*E*), 5.69 (*Z*) (m, 2H), 2.50-2.43 (m, 4H), 1.98 (*Z*), 1.85 (*E*) (m, 6H), 1.54 (m, 4H), 1.23 (bs, 20H), 0.87 (t, *J* = 6.9 Hz, 6H). δ_C (ppm) = 142.8, 142.2, 142.2, 140.8, 129.2, 129.0, 126.2, 126.0, 125.1, 124.7, 123.5, 32.2, 31.0, 29.8, 29.6, 29.1, 23.0, 18.7, 15.5, 14.5. HRGC-MS (EI): $M_{calcd.}$ = 470.3041, M_{found} = 470.3019. Anal. calcd. for $C_{30}H_{46}S_2$: C 75.30, H 9.24, S 15.46; Found: C 75.42, H 9.27, S 15.17.

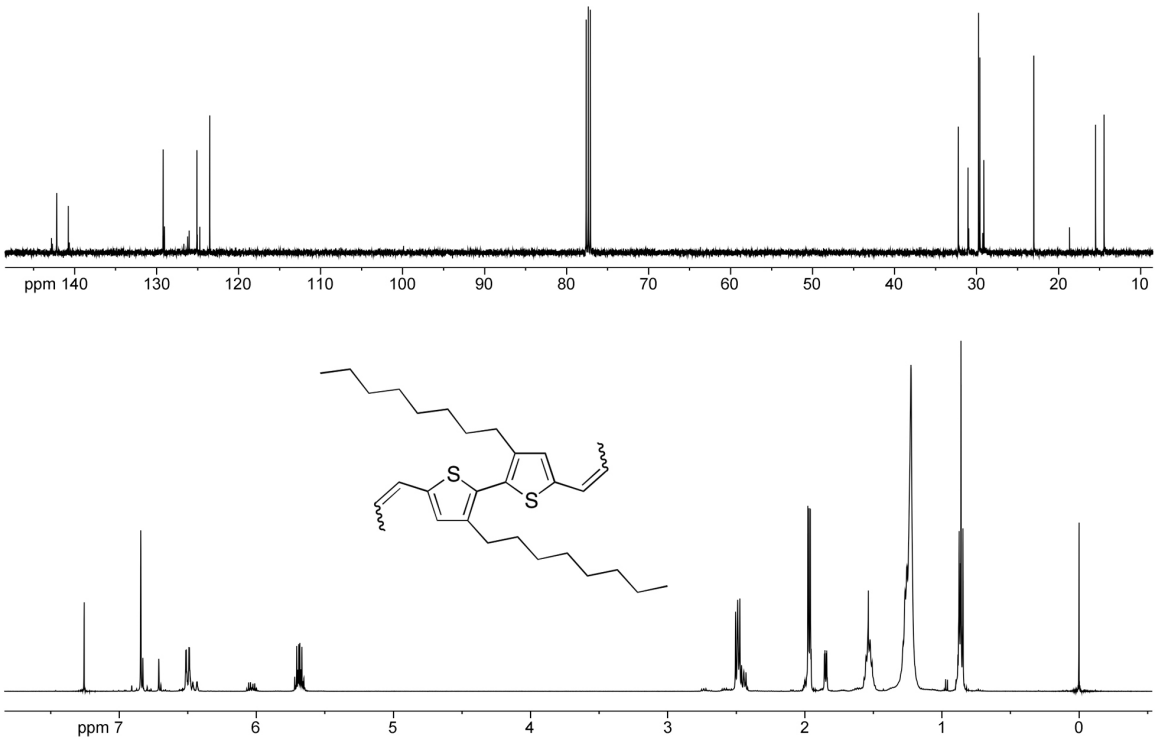

Figure 5.25

^{13}C and ^{1}H NMR spectra of **4**.

3-Dodecylthiophene (5). A 2-neck 250 mL round bottom flask was equipped with a magnetic stir bar, reflux condenser, stopcock, and rubber septum. Magnesium turnings (1.92 g, 79.7 mmol) were added and the apparatus was flame-dried under vacuum. Anhydrous THF (100 mL) was added via cannula and dibromoethane (0.25 mL) via syringe. The suspension was stirred vigorously for 10 min before slowly adding 1-bromodecane (17.7 mL, 73.6 mmol) via syringe. Refluxed for 90 min before cooling to 0 °C. 3-bromothiophene (5.75 mL, 61.3 mmol) and [bis(diphenylphosphino)propane]dichloronickel (II) (0.67 g, 1.23 mmol) were added via cannula as a suspension in THF (50 mL). The reaction was stirred at room temperature overnight. The reaction mixture was poured into 200 mL of 1M NH_4Cl and extracted with diethyl ether (2 × 50 mL). The combined organics were washed with brine (50 mL)

and dried over Na_2SO_4. The solvent was removed under reduced pressure and the residue was dissolved in minimal THF (10 mL) and precipitated into MeOH (800 mL, -78 °C). The solid was quickly filtered, dissolved in hexanes, dried over Na_2SO_4, and concentrated under reduced pressure to give product as a yellow liquid (14.84 g, 96%). ^{1}H NMR (500 MHz; $CDCl_3$): δ_H (ppm) = 7.22 (dd, *J* = 4.6, 3.1 Hz, 1H), 6.93 (d, *J* = 4.9 Hz, 1H), 6.91 (d, *J* = 1.8 Hz, 1H), 2.61 (t, *J* = 7.7 Hz, 2H), 1.61 (quintet, *J* = 7.2 Hz, 2H), 1.26 (bs, 18H), 0.88 (t, *J* = 6.8 Hz, 3H). ^{13}C NMR (125 MHz, $CDCl_3$): δ_C (ppm) = 143.6, 128.6, 125.3, 120.1, 32.3, 32.0, 30.9, 30.7, 30.1 (2), 30.0 (2), 29.9, 29.7, 23.1, 14.5. HRGC-MS (EI): $M_{calcd.}$ = 252.1912, M_{found} = 252.1893. Anal. calcd. for $C_{16}H_{28}S$: C 76.12, H 11.18, S 12.70; Found: C 77.50, H 11.33, S 11.28.

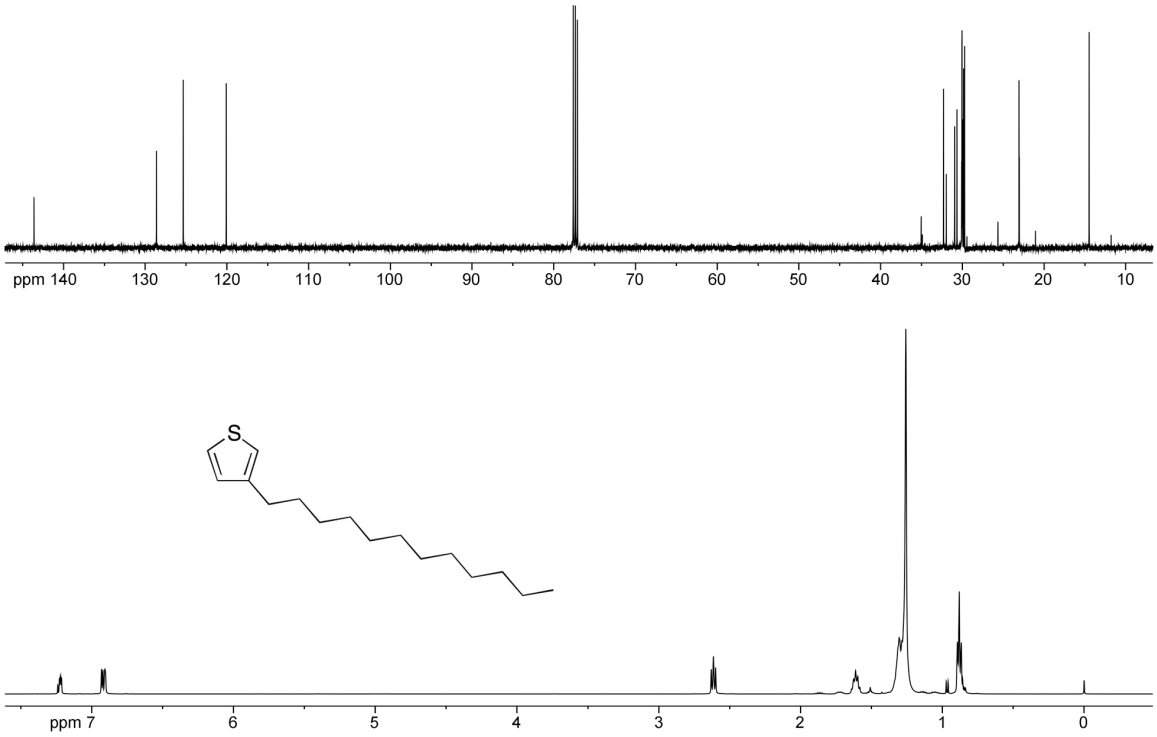

Figure 5.26

^{13}C and ^{1}H NMR spectra of **5**.

4,4'-Didodecyl-2,2'-bithiophene (6). A 100 mL conical flask was equipped with a magnetic stir bar and rubber septum. The flask was flame-dried under nitrogen before anhydrous THF (40 mL) and n-butyllithium (2.5 M in hexanes, 8.7 mL, 21.8 mmol) were added. The mixture was cooled to -78 °C before adding TMEDA (3.3 mL, 21.8 mmol) via syringe. Stirred for 30 min before transferring (syringe) to a flame-dried liquid addition funnel attached to a 250 mL round bottom flask containing THF (75 mL) and **5** (5.5 mL, 19.8 mmol). After dropwise addition the reaction was stirred at 40 °C for 1 h before cooling to -78 °C and adding copper(II) chloride (3.33 g, 24.8 mmol). The reaction was warmed to room temperature and stirred for 90 min. Water (200 mL) was added and the reaction was acidified with concentrated HCl (ca. 10 mL). The mixture was extracted with CH_2Cl_2 (3 × 200 mL). The combined organics were washed with brine (200 mL) and dried over $MgSO_4$. The solvent was removed under reduced pressure and the residue was dissolved in hexanes and flushed through a plug of silica gel. The silica gel procedure was repeated, and the remaining product was purified by recrystallization from hexanes at -78 °C to give a light yellow solid (2.46 g, 49%). ^{1}H NMR (500 MHz; $CDCl_3$): δ_H (ppm) = 6.97 (d, J = 1.3 Hz, 2H), 6.76 (d, J = 0.9 Hz, 2H), 2.56 (t, J = 7.7 Hz, 4H), 1.61 (quintet, J = 7.3 Hz, 4H), 1.26 (bs, 36H), 0.88 (t, J = 7.0 Hz, 6H). ^{13}C NMR (125 MHz; $CDCl_3$): δ_C (ppm) = 144.3, 137.7, 125.2, 119.0, 32.3, 30.9, 30.8, 30.1, 30.0, 30.0, 29.9, 29.8, 29.7, 29.7, 23.1, 14.5. HRGC-MS (EI): $M_{calcd.}$ = 502.3667, M_{found} = 502.3655. Anal. calcd. for $C_{32}H_{54}S_2$: C 76.43, H 10.82, S 12.75; Found: C 77.25, H 10.96, S 11.80.

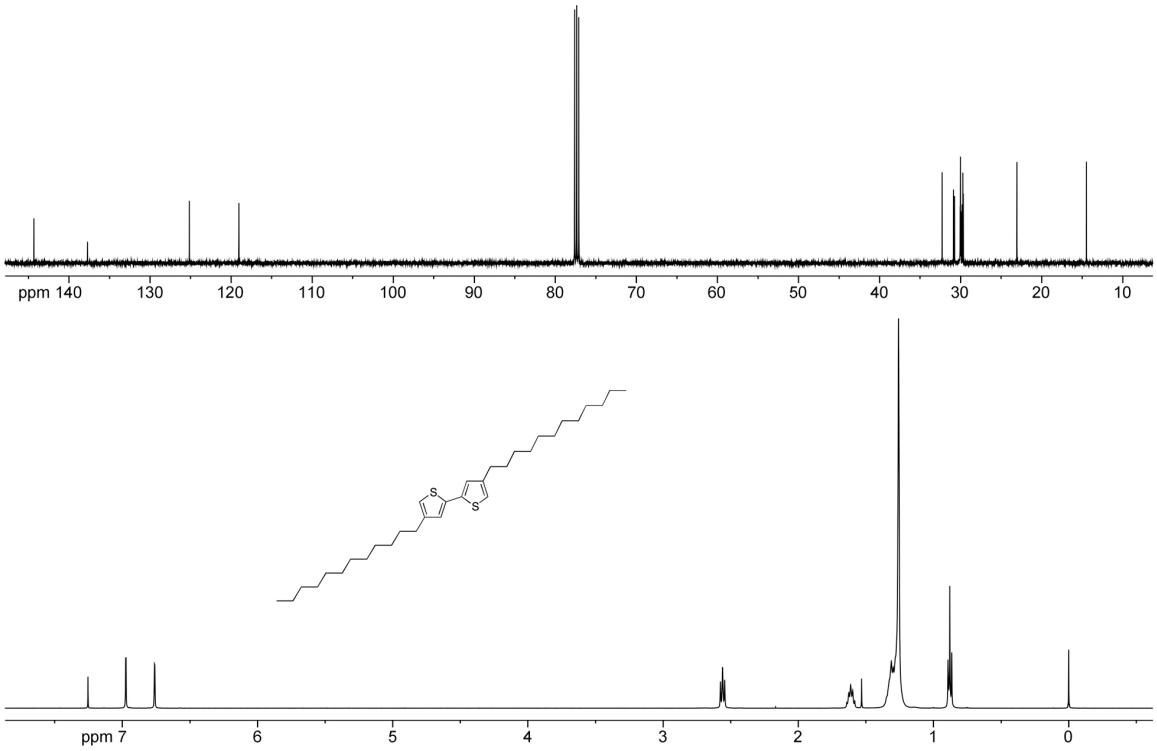

Figure 5.27

^{13}C and ^{1}H NMR spectra of **6**.

4,4'-Didodecyl-[2,2'-bithiophene]-5,5'-dicarbaldehyde (7). A 2-neck 100 mL round bottom flask was equipped with a magnetic stir bar, reflux condenser, and two rubber septa. The flask was flame-dried under nitrogen before adding **6** (2.00 g, 3.98 mmol), anhydrous hexanes (60 mL), and TMEDA (1.5 mL, 9.95 mmol). N-butyllithium (2.5 M in hexanes, 4.0 mL, 9.95 mmol) was slowly added via syringe and the solution was refluxed for 45 min. The reaction was cooled to 0 °C and added anhydrous THF (30 mL) via syringe. Anhydrous DMF (1.25 mL, 15.92 mmol) was added via syringe and the reaction was stirred at room temperature for 45 min. The reaction was poured into 1 M HCl (50 mL) and extracted with diethyl ether (3 × 100 mL). The combined organics were washed with brine (100 mL) and dried over Na_2SO_4. The solvent was removed under reduced pressure and the residue was dissolved in THF (25 mL) before

precipitating into MeOH (150 mL, 0 °C). The product was isolated by filtration as a yellow solid (2.00 g, 91%). ^{1}H NMR (500 MHz; $CDCl_3$): δ_H (ppm) = 10.02 (s, 2H), 7.19 (s, 2H), 2.94 (t, *J* = 7.7 Hz, 4H), 1.69 (quintet, *J* = 7.5 Hz, 4H), 1.26 (bs, 36H), 0.88 (t, *J* = 7.0 Hz, 6H). ^{13}C NMR (125 MHz; $CDCl_3$): δ_C (ppm) = 182.1, 154.0, 144.4, 138.1, 128.9, 32.3, 31.7, 30.1, 30.0 (3), 29.8, 29.7, 29.6, 28.9, 23.0, 14.5. HRGC-MS (EI): $M_{calcd.}$ = 558.3565, M_{found} = 558.3562. Anal. calcd. for $C_{34}H_{54}O_2S_2$: C 73.06, H 9.74, S 11.47; Found: C 73.92, H 9.87, S 10.89.

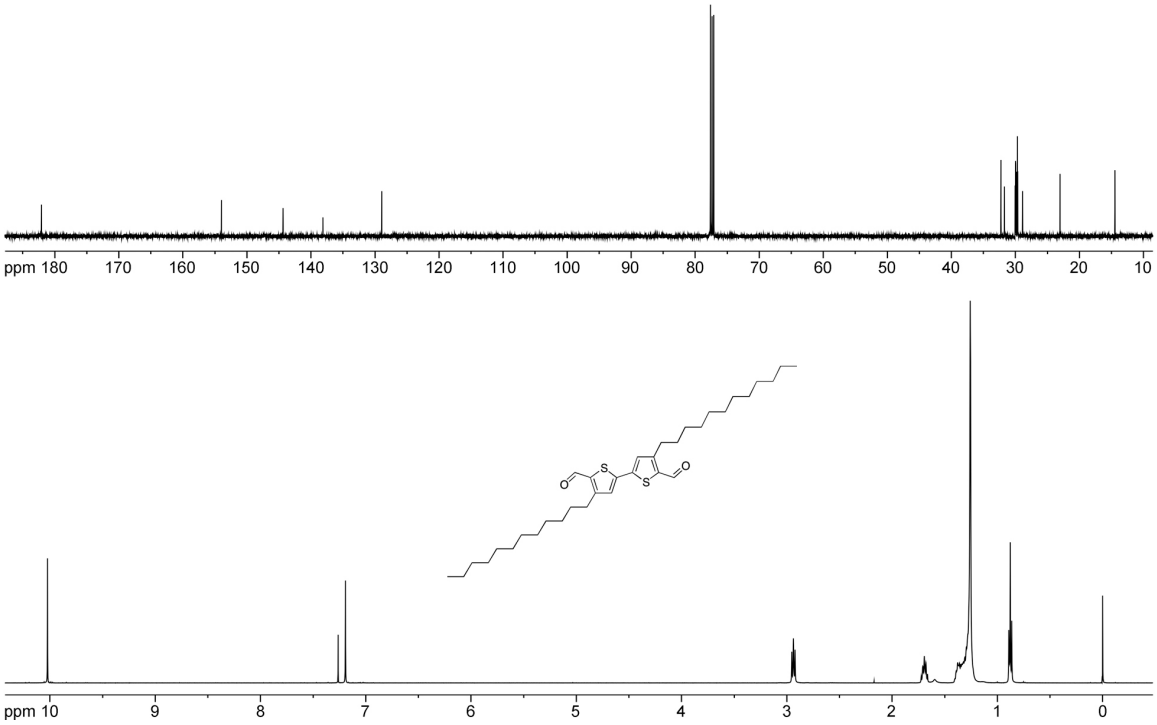

Figure 5.28

^{13}C and ^{1}H NMR spectra of **7**.

4,4'-Didodecyl-5,5'-dipropenyl-2,2'-bithiophene (8). A 2-neck 100 mL round bottom flask was equipped with a magnetic stir bar, reflux condenser, stopcock, and rubber septum. The flask was flame-dried under vacuum before adding ethyltriphenylphosphonium bromide (3.00 g, 8.10 mmol) and sodium

bis(trimethylsilyl)amide (1.50 g, 8.10 mmol) as solids. The apparatus was placed under vacuum for 30 min before adding anhydrous hexanes (50 mL) via cannula. The suspension was refluxed for 1 h to generate the bright orange-red Wittig reagent. The reaction was cooled to -78 °C and the precipitated solids were allowed to settle. The residual solvent was removed via syringe. The washing procedure was repeated by adding anhydrous hexanes (50 mL), stirring, and removing from the solid. The orange solid was dried under vacuum and dissolved in anhydrous THF (25 mL). The Wittig solution was transferred to a flame-dried 100 mL round bottom flask containing **7** (1.50 g, 2.7 mmol) and anhydrous THF (25 mL) held at 0 °C. The reaction was stirred at room temperature for 30 min before removing the solvent under reduced pressure. The residue was dissolved in hexanes and flushed through a plug of silica gel. The solvent was removed under reduced pressure and the residue was dissolved in THF (10 mL) before precipitating into MeOH (150 mL, 0 °C). The product was isolated by filtration as a bright yellow solid (0.96 g, 61%) Mixture of isomers (*ZZ* = 71%, *ZE* = 26%, *EE* = 3%, overall *Z*:*E* = 83:17). ^{1}H NMR (500 MHz; $CDCl_3$): δ_H (ppm) = 6.95 (*ZZ*), 6.90 (*ZE*), 6.86 (*ZE*), 6.81 (*EE*) (4 singlets, 2H), 6.55-6.51 (m, 2H), 5.96 (*E*), 5.68 (*Z*) (m, 2H), 2.55 (m, 4H), 2.00 (*Z*), 1.87 (*Z*) (m, 6H), 1.57 (quintet, *J* = 7.2 Hz, 4H), 1.25 (bs, 38H), 0.88 (t, *J* = 7.0 Hz, 6H). ^{13}C NMR (125 MHz; $CDCl_3$): δ_C (ppm) = 142.0, 142.0, 140.0, 135.7, 135.6, 133.1, 125.8, 125.4, 125.2, 125.1, 124.6, 123.0, 121.5, 32.3, 31.1, 30.1, 30.0 (3), 29.8, 29.8, 29.8, 29.7, 29.1, 23.1, 19.0, 15.7, 14.5. HRGC-MS (EI): $M_{calcd.}$ = 582.4293, M_{found} = 582.4291. Anal. calcd. for $C_{38}H_{62}S_2$: C 78.28, H 10.72, S 11.00; Found: C 79.31, H 11.03, S 9.84.

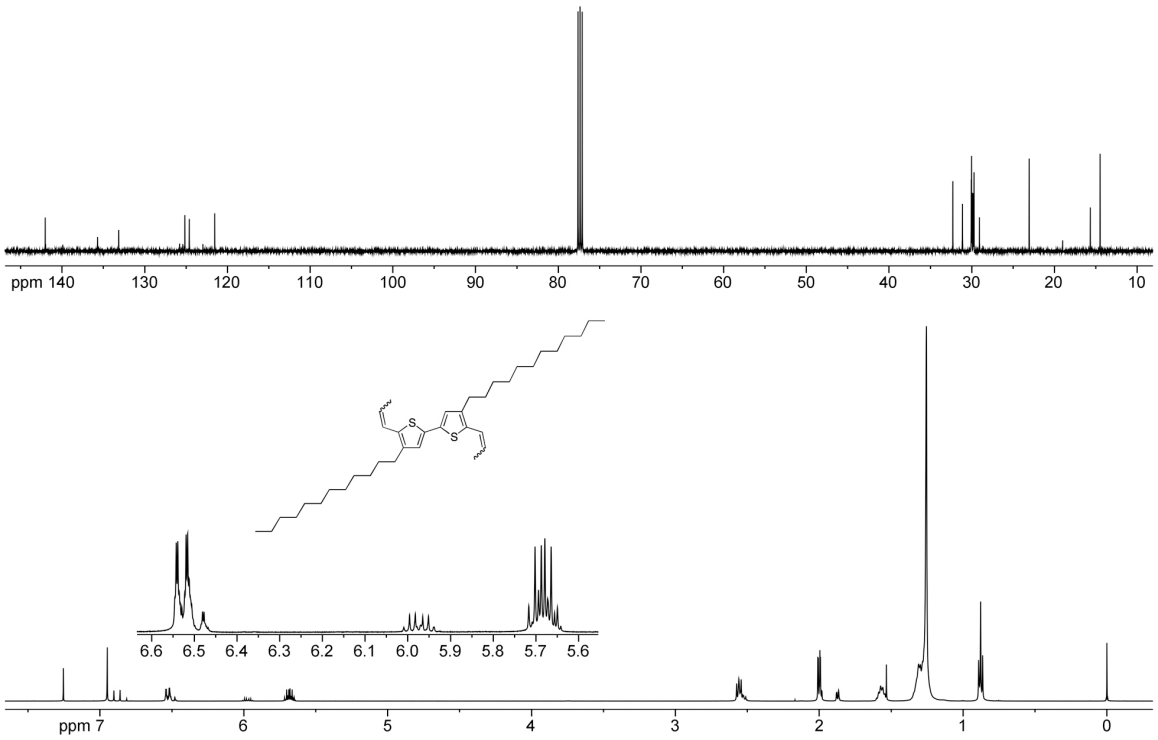

Figure 5.29

^{13}C and ^{1}H NMR spectra of **8**.

2-Bromo-3-hexadecylthiophene (9). A 250 mL round bottom flask was equipped with a magnetic stir bar and 3-hexadecylthiophene (10.00 g, 32.4 mmol) in THF (200 mL) was added. The solution was cooled to 0 °C before adding N-bromosuccinimide (5.77 g, 32.4 mmol) in one portion. The flask was sealed with a rubber septum and the reaction was stirred under argon in the dark for 20 h. The solvent was removed under reduced pressure and the residue was flushed through a plug of silica gel with hexanes. The solvent was removed under reduced pressure and the residue was dissolved in THF (20 mL) before precipitating into MeOH (300 mL, 0 °C). The product was isolated by filtration and dried under vacuum to give a white solid (10.86 g, 87%). ^{1}H NMR (500 MHz; $CDCl_3$): δ_H (ppm) = 7.18 (d, J = 5.6 Hz, 1H), 6.79 (d, J = 5.6 Hz, 1H), 2.55 (t, J = 7.7 Hz, 2H), 1.57 (quintet, J = 7.0 Hz, 2H), 1.25 (bs, 36H), 0.88 (t, J = 6.9 Hz, 3H). ^{13}C NMR (125

MHz; $CDCl_3$): δ_C (ppm) = 142.3, 128.6, 125.5, 109.1, 32.3, 30.1 (2), 30.0 (2), 29.9, 29.8, 29.7, 29.6, 23.1, 14.5. HRGC-MS (EI): $M_{calcd.}$ = 386.1643, M_{found} = 386.1643. Anal. calcd. for $C_{20}H_{35}BrS$: C 62.00, H 9.10, Br 20.62, S 8.28; Found: C 62.13, H 9.03, Br 20.38, S 8.03.

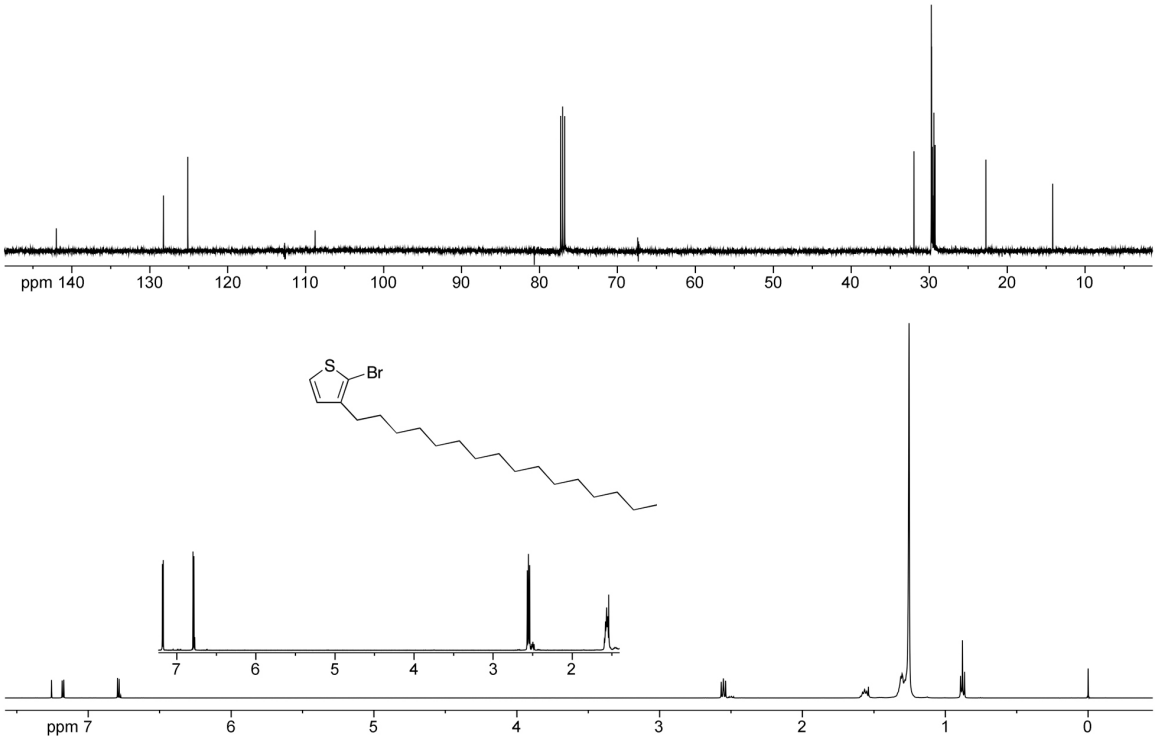

Figure 5.30

^{13}C and ^{1}H NMR spectra of **9**.

2-(4-Hexadecylthiophen-2-yl)-4,4,5,5-tetramethyl-1,3,2-dioxaborolane (10). A 2-neck 50 mL round bottom flask was equipped with a magnetic stir bar, reflux condenser, and two rubber septa. The apparatus was flame-dried under nitrogen before adding 3-hexadecylthiophene (2.00 g, 6.50 mmol) and anhydrous THF (20 mL). The solution was cooled to -10 °C before adding TMEDA (1.10 mmol, 7.15 mmol) and t-butyllithium (1.7 M in pentane, 4.9 mL, 8.33 mmol). The reaction was warmed to 60 °C and stirred for 15 min before cooling to -10 °C and adding 2-isopropoxy-4,4,5,5-tetramethyl-1,3,2-

dioxaborolane (1.50 mL, 7.15 mmol). The reaction was stirred at room temperature under argon overnight before pouring into 0.1 M HCl (50 mL) and extracting with diethyl ether (2 × 50 mL). The combined organics were washed with brine (50 mL) and dried over Na_2SO_4. The solvent was removed under reduced pressure and the residue purified by silica gel column chromatography (hexanes:ethyl acetate 9:1). The product was isolated as an off-white low-melting solid (1.70 g, 61%). ^{1}H NMR (500 MHz; $CDCl_3$): δ_H (ppm) = 7.47 (s, 1H), 7.20 (s, 1H), 2.62 (t, *J* = 7.7 Hz, 2H), 1.61 (quintet, *J* = 7.5 Hz, 2H), 1.34 (bs, 12H), 1.25 (s, 26H), 0.88 (t, *J* = 6.8 Hz, 3H). ^{13}C NMR (125 MHz; $CDCl_3$): δ_C (ppm) = 144.7, 138.5, 127.6, 84.0, 32.0, 30.7, 30.0, 29.7 (2), 29.6, 29.5, 29.4, 29.3, 24.8, 22.7, 14.2. HRGC-MS (EI): $M_{calcd.}$ = 434.3390, M_{found} = 434.3392. Anal. calcd. for $C_{26}H_{47}BO_2S$: C 71.87, H 10.90, S 7.38; Found: C 72.02, H 10.80, S 7.48.

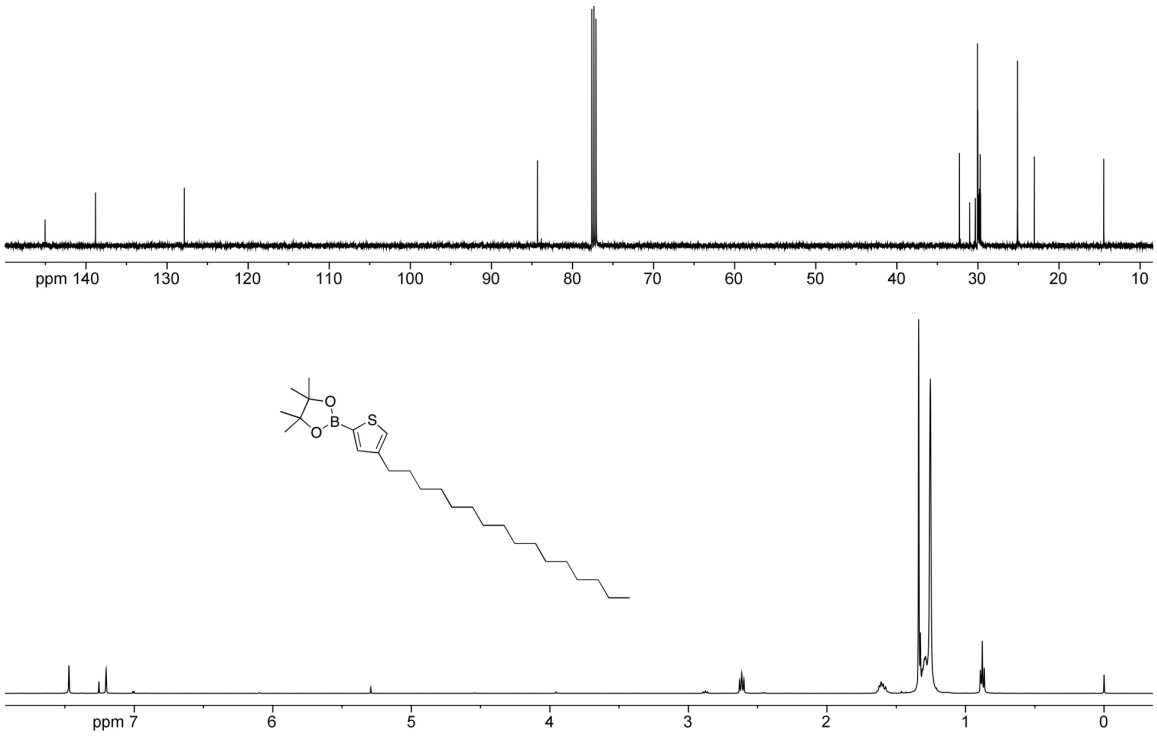

Figure 5.31

^{13}C and ^{1}H NMR spectra of **10**.

3,4'-Dihexadecyl-2,2'-bithiophene (11). A 2-neck 100 mL round bottom flask was equipped with a magnetic stir bar, reflux condenser, and two rubber septa. The apparatus was flame-dried under argon before adding **9** (1.34 g, 3.45 mmol), **10** (1.50 g, 3.45 mmol), toluene (25 mL), and 2 M Na_2CO_3 (25 mL). The solution was degassed with argon for 45 min before adding tetrakis(triphenylphosphine)palladium(0) (0.24 g, 0.21 mmol) as a solid. The reaction was heated to 90 ˚C and stirred under argon overnight. The reaction was poured into water (100 mL) and extracted with diethyl ether (2 × 75 mL). The combined organics were washed with brine (50 mL) and dried over Na_2SO_4. The solvent was removed under reduced pressure and the residue was flushed through plug of silica gel with hexanes. The hexanes were concentrated to 100 mL and slowly cooled to -35 ˚C at which point the product precipitated as a yellow solid. The product was filtered and dried under vacuum. (0.96 g, 46%). ^{1}H NMR (500 MHz; $CDCl_3$): δ_H (ppm) = 7.13 (d, *J* = 5.2 Hz, 1H), 6.93 (s, 1H), 6.91 (d, *J* = 5.2 Hz, 1H), 6.87 (s, 1H), 2.73 (t, *J* = 7.8 Hz, 2H), 2.59 (t, *J* = 7.7 Hz, 2H), 1.62 (dq, *J* = 14.8, 7.4 Hz, 4H), 1.26 (bs, 52H), 0.88 (t, *J* = 6.8 Hz, 6H). ^{13}C NMR (125 MHz; $CDCl_3$): δ_C (ppm) = 143.9, 139.7, 136.2, 131.3, 130.2, 127.7, 123.7, 120.2, 32.3, 31.1, 30.9, 30.8, 30.1, 30.0 (2), 29.9 (2), 29.8, 29.7 (2), 29.5, 23.1, 14.5. HRGC-MS (EI): $M_{calcd.}$ = 614.4919, M_{found} = 614.4884. Anal. calcd. for $C_{40}H_{70}S_2$: C 78.10, H 11.47, S 10.43; Found: C 78.36, H 11.35, S 10.16.

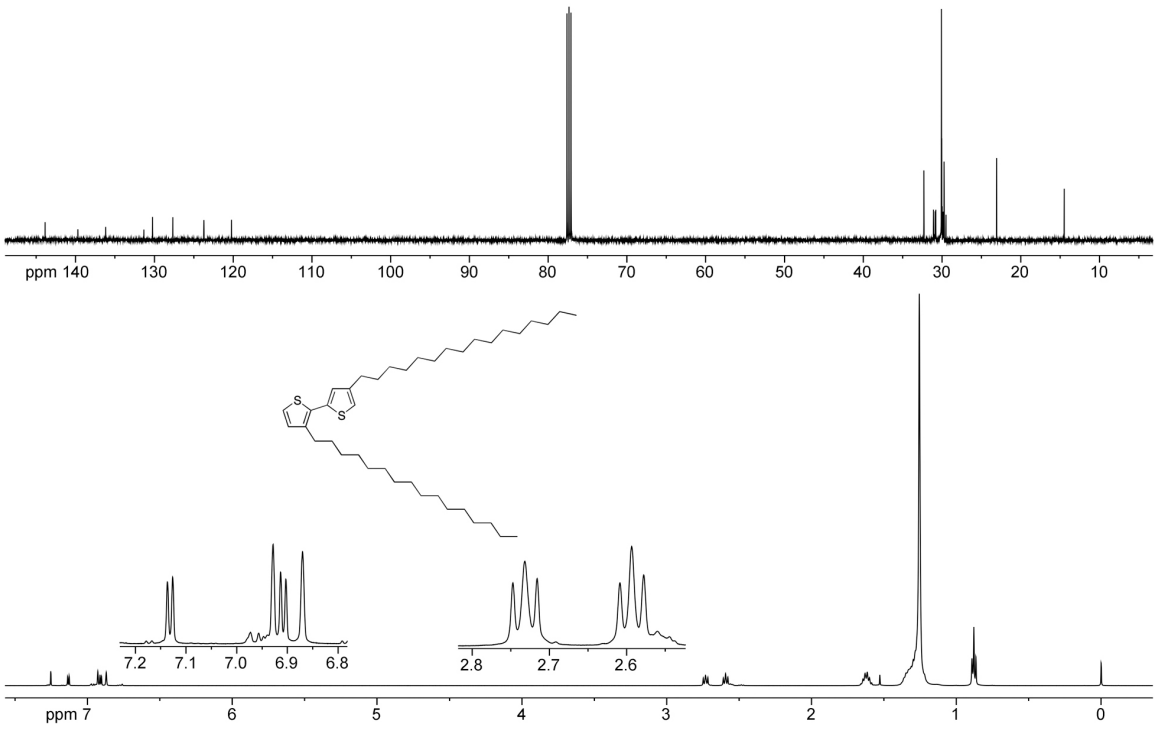

Figure 5.32

^{13}C and ^{1}H NMR spectra of **11**.

3,4'-Dihexadecyl-[2,2'-bithiophene]-5,5'-dicarbaldehyde (12). A 2-neck 100 mL round bottom flask was equipped with a magnetic stir bar, reflux condenser, and two rubber septa. The flask was flame-dried under nitrogen before adding **11** (0.80 g, 1.30 mmol), anhydrous hexanes (40 mL), and TMEDA (0.49 mL, 3.25 mmol). N-butyllithium (2.5 M in hexanes, 1.3 mL, 3.25 mmol) was slowly added via syringe and the solution was refluxed for 1 h. The reaction was cooled to 0 °C and added anhydrous THF (20 mL) via syringe. Anhydrous DMF (0.40 mL, 5.20 mmol) was added via syringe and the reaction was stirred at room temperature for 30 min. The reaction was poured into 1 M HCl (50 mL) and extracted with diethyl ether (2 × 75 mL). The combined organics were washed with brine (50 mL) and dried over Na_2SO_4. The solvent was removed under reduced pressure and the residue was dissolved in THF (10 mL) before precipitating into MeOH

(150 mL, 0 °C). The product was purified by silica gel column chromatography (hexanes:CH_2Cl_2 3:1→2:3) and isolated as a yellow-green solid (0.42 g, 48%). ^{1}H NMR (500 MHz; $CDCl_3$): δ_H (ppm) = 10.05 (s, 1H), 9.86 (s, 1H), 7.61 (s, 1H), 7.17 (s, 1H), 2.96 (t, *J* = 7.7 Hz, 2H), 2.83 (t, *J* = 7.8 Hz, 2H), 1.73-1.65 (m, 4H), 1.25 (bs, 52H), 0.88 (t, *J* = 6.8 Hz, 6H). ^{13}C NMR (125 MHz; $CDCl_3$): δ_C (ppm) = 183.0, 182.2, 153.4, 143.5, 142.9, 142.0, 139.7, 139.1, 138.6, 130.7, 32.3, 31.8, 30.6, 30.1, 30.0 (2), 29.9 (3), 29.8, 29.7, 29.7, 28.8, 23.0, 14.5. HRGC-MS (EI): $M_{calcd.}$ = 670.4817, M_{found} = 670.4823. Anal. calcd. for $C_{42}H_{70}O_2S_2$: C 75.16, H 10.51, S 9.56; Found: C 75.26, H 10.37, S 9.49.

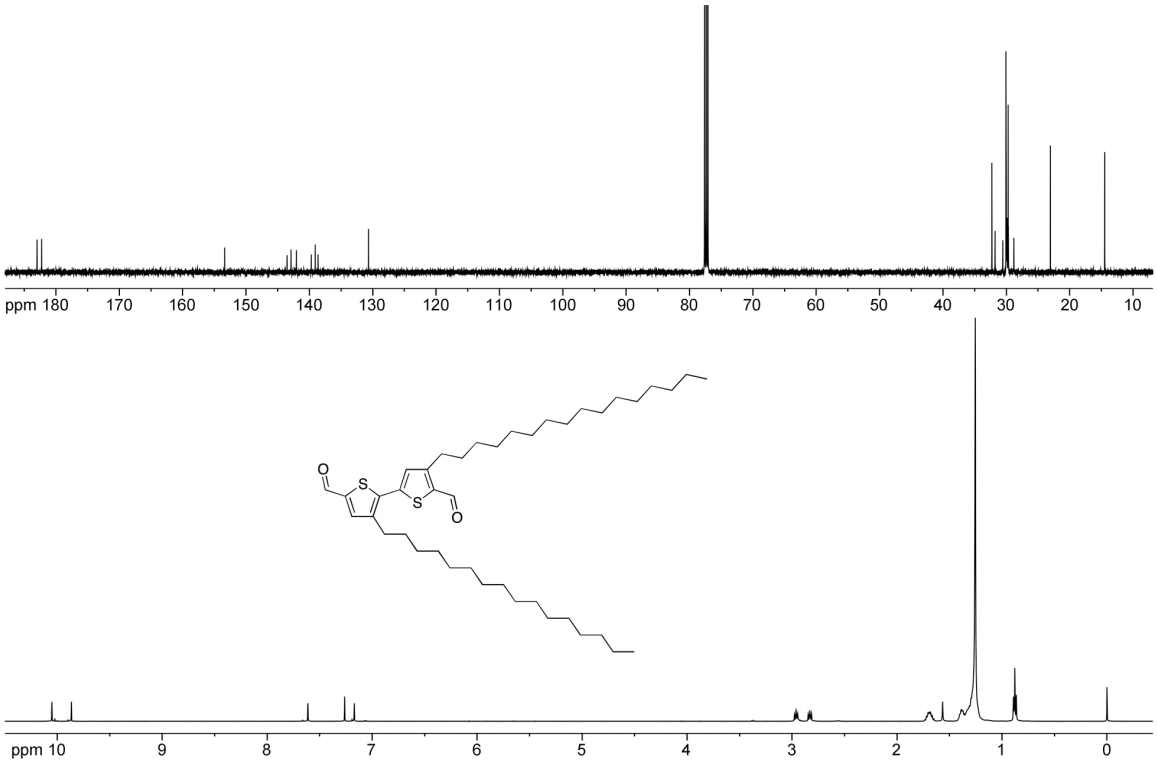

Figure 5.33

^{13}C and ^{1}H NMR spectra of **12**.

3,4'-Dihexadecyl-5,5'-dipropenyl-2,2'-bithiophene (13). A 2-neck 50 mL round bottom flask was equipped with a magnetic stir bar, reflux condenser, stopcock, and rubber septa. The flask was flame-dried under vacuum before adding ethyltriphenylphosphonium

bromide (0.67 g, 1.80 mmol) and sodium bis(trimethylsilyl)amide (0.33 g, 1.80 mmol) as solids. The apparatus was placed under vacuum for 30 min before adding anhydrous hexanes (20 mL) via syringe. The suspension was refluxed for 1 h to generate the bright orange-red Wittig reagent. The reaction was cooled to -78 °C and the precipitated solids were allowed to settle. The residual solvent was removed via syringe. The washing procedure was repeated by adding anhydrous hexanes (20 mL), stirring, and removing from the solid. The orange solid was dried under vacuum and dissolved in anhydrous THF (10 mL). The Wittig solution was transferred to a flame-dried 50 mL round bottom flask containing **12** (0.40 g, 0.60 mmol) and anhydrous THF (10 mL) held at 0 °C. The reaction was stirred at room temperature for 30 min before removing the solvent under reduced pressure. The residue was dissolved in hexanes and flushed through a plug of silica gel. The solvent was removed under reduced pressure and the residue was dissolved in THF (5 mL) before precipitating into MeOH (100 mL, 0 °C). The product was isolated by filtration as a bright yellow solid (0.40 g, 95%) Mixture of isomers (*Z*:*E* = 82:18). ^{1}H NMR (500 MHz; $CDCl_3$): δ_H (ppm) = 6.90, 6.87, 6.82, 6.79, 6.77, 6.66 (multiple singlets, 2H), 6.56-6.45 (m, 2H), 6.01 (*E*), 5.68 (*Z*) (m, 2H), 2.75-2.68 (m, 2H), 2.60-2.54 (m, 2H), 1.99 (*Z*), 1.86 (*E*) (m, 6H), 1.65-1.56 (m, 4H), 1.25 (s, 52H), 0.88 (t, *J* = 6.9 Hz, 6H). ^{13}C NMR (125 MHz; $CDCl_3$): δ_C (ppm) = 141.5 (2), 140.8, 139.6, 139.4, 139.1, 139.0, 138.8, 138.6, 136.5, 134.8, 134.6, 134.1, 133.9, 132.6, 131.2, 130.8 (2), 128.1, 127.8, 127.4, 127.3, 126.1, 125.4, 125.1, 125.0, 124.7 (2), 124.6 (2), 123.4, 122.9, 121.5, 31.2, 31.2, 31.1, 31.0, 30.9 (2), 30.0 (3), 29.9 (3), 29.8 (3), 29.6, 29.0, 19.0, 18.7, 15.7 (2), 15.5 (2), 14.5. HRGC-MS (EI): $M_{calcd.}$ = 694.5545, M_{found} = 694.5581. Anal. calcd. for $C_{46}H_{78}S_2$: C 79.47, H 11.31, S 9.22; Found: C 79.48, H 11.24, S 9.31.

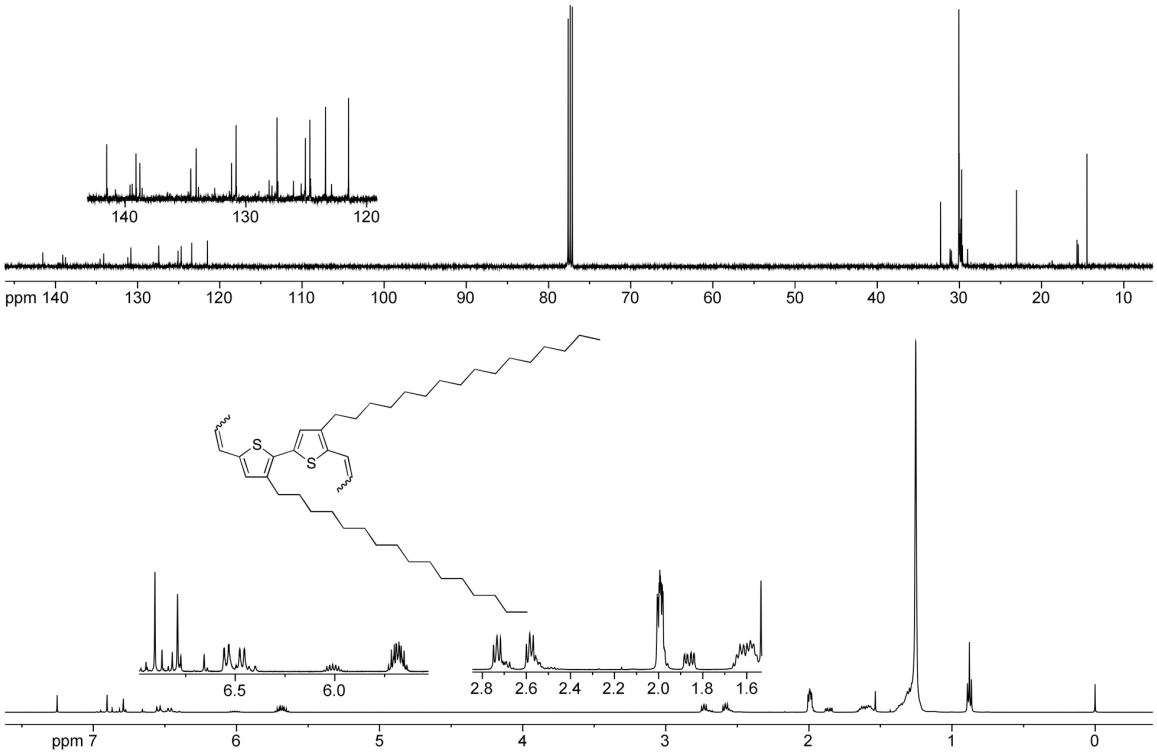

Figure 5.34

^{13}C and ^{1}H NMR spectra of **13**.

3,3"-Dihexadecyl-2,2':5',2"-terthiophene (14). A 250 mL 2-neck round bottom flask was equipped with a magnetic stir bar and liquid addition funnel before adding magnesium turnings (3.90 g, 161.3 mmol), sealing with two rubber septa, and flame drying under nitrogen. Anhydrous THF (150 mL) was added via cannula followed by 1,2-dibromoethane (0.5 mL) via syringe. The suspension was stirred vigorously for 10 min. Meanwhile, **9** (10.0 g, 25.8 mmol) and anhydrous THF (50 mL) were added to the addition funnel. The solution was added dropwise over the course of 45 min. The reaction was warmed to 60 °C for 2 h and cooled to room temperature before transferring to a 500 mL 2-neck round bottom flask containing 2,5-dibromothiophene (1.16 mL, 10.3 mmol), [bis(diphenylphosphino)propane]dichloronickel(II) (115 mg, 0.21 mmol), and anhydrous THF (50 mL). The reaction was warmed to 65 °C and stirred overnight.

The reaction solution was poured into 1 M NH_4Cl (250 mL) and extracted with diethyl ether (2 × 150 mL). The combined organics were dried over Na_2SO_4 and the solvent was removed under reduced pressure. The residue was flushed through a plug of silica gel with pentane to remove catalyst residues and $MgBr_2$. The solution was concentrated to 200 mL and cooled to -78 °C to precipitate a yellow solid. The solid was isolated by filtration and reprecipitated from pentane at -78 °C twice more. The remaining solid was purified by column chromatography with pentane to give pure product (2.00 g, 28%). ^{1}H NMR (500 MHz; $CDCl_3$): δ_H (ppm) = 7.16 (d, *J* = 5.2 Hz, 2H), 7.05 (s, 2H), 6.93 (d, *J* = 5.2 Hz, 2H), 2.77 (t, *J* = 7.8 Hz, 4H), 1.64 (dt, *J* = 15.1, 7.6 Hz, 4H), 1.25 (bs, 52H), 0.88 (t, *J* = 6.9 Hz, 6H). ^{13}C NMR (125 MHz; $CDCl_3$): δ_C (ppm) = 140.0, 136.4, 130.7, 130.4, 126.4, 124.1, 32.3, 31.1, 30.1, 30.0 (2), 29.9 (2), 29.7, 29.6, 23.1, 14.5. HRGC-MS (EI): $M_{calcd.}$ = 696.4796, M_{found} = 696.4755. Anal. calcd. for $C_{44}H_{72}S_3$: C 75.79, H 10.41, S 13.80; Found: C 75.51, H 10.18, S 13.53.

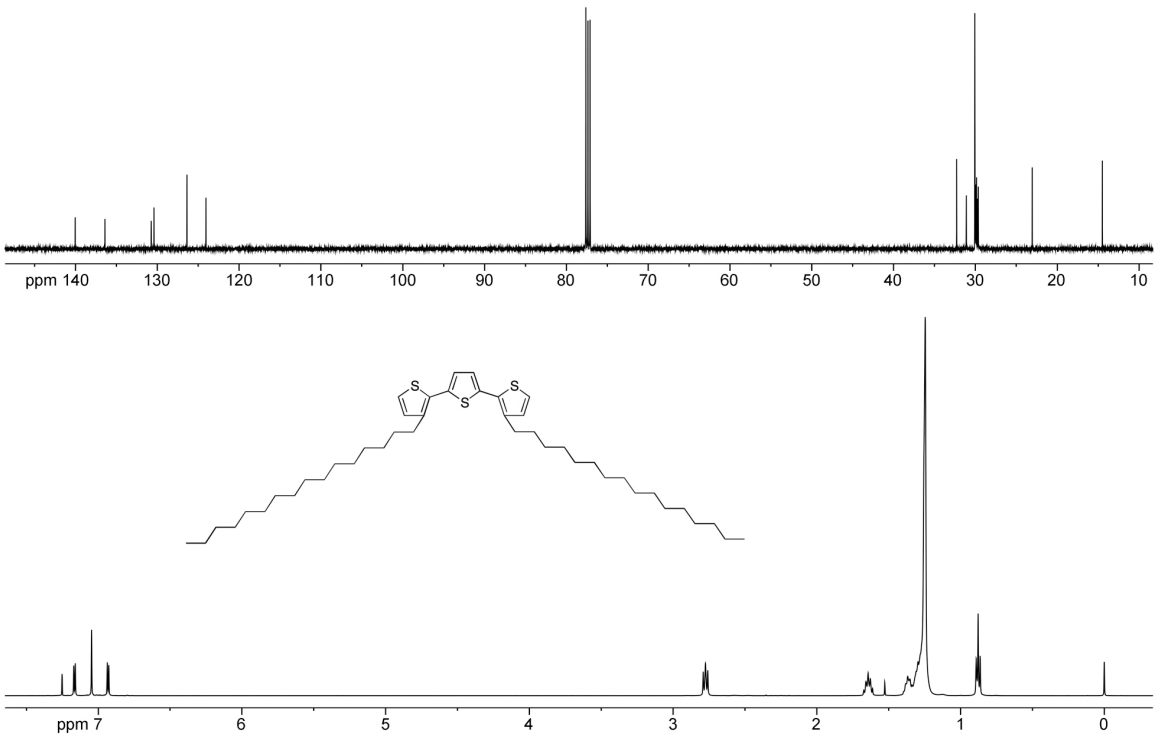

Figure 5.35

^{13}C and ^{1}H NMR spectra of **14**.

3,3''-Dihexadecyl-[2,2':5',2''-terthiophene]-5,5''-dicarbaldehyde (15). A 2-neck 100 mL round bottom flask was equipped with a magnetic stir bar, reflux condenser, and two rubber septa. The flask was flame-dried under nitrogen before adding **14** (1.80 g, 2.60 mmol), anhydrous hexanes (50 mL), and TMEDA (0.97 mL, 6.50 mmol). N-butyllithium (2.5 M in hexanes, 2.6 mL, 6.50 mmol) was slowly added via syringe and the solution was refluxed for 10 min. The reaction was cooled to 0 °C and added anhydrous THF (25 mL) via syringe. Anhydrous DMF (0.80 mL, 10.40 mmol) was added via syringe and the reaction was stirred at room temperature for 30 min. The reaction was poured into 1 M HCl (50 mL) and extracted with diethyl ether (2 × 100 mL). The combined organics were washed with brine (100 mL) and dried over Na_2SO_4. The solvent was removed under reduced pressure and the residue was dissolved in THF (5 mL) before precipitating into MeOH (150 mL, 0 °C). The product was isolated by filtration as a brown solid (1.79 g, 91%). ^{1}H NMR (500 MHz; $CDCl_3$): δ_H (ppm) = 9.85 (s, 2H), 7.61 (s, 2H), 7.28 (s, 2H), 2.83 (t, J = 7.8 Hz, 4H), 1.69 (quintet, J = 7.6 Hz, 4H), 1.40 (quintet, J = 7.1 Hz, 4H), 1.25 (bs, 48H), 0.88 (t, J = 6.8 Hz, 6H). ^{13}C NMR (125 MHz; $CDCl_3$): δ_C (ppm) = 182.9, 141.3, 141.2, 140.5, 139.2, 137.0, 128.3, 32.3, 30.7, 30.1, 30.0, 29.9 (2), 29.8, 29.7, 23.0, 14.5. HRGC-MS (EI): $M_{calcd.}$ = 752.4694, M_{found} = 752.4653. Anal. calcd. for $C_{46}H_{72}O_2S_3$: C 73.35, H 9.63, S 12.77; Found: C 73.08, H 9.35, S 12.51.

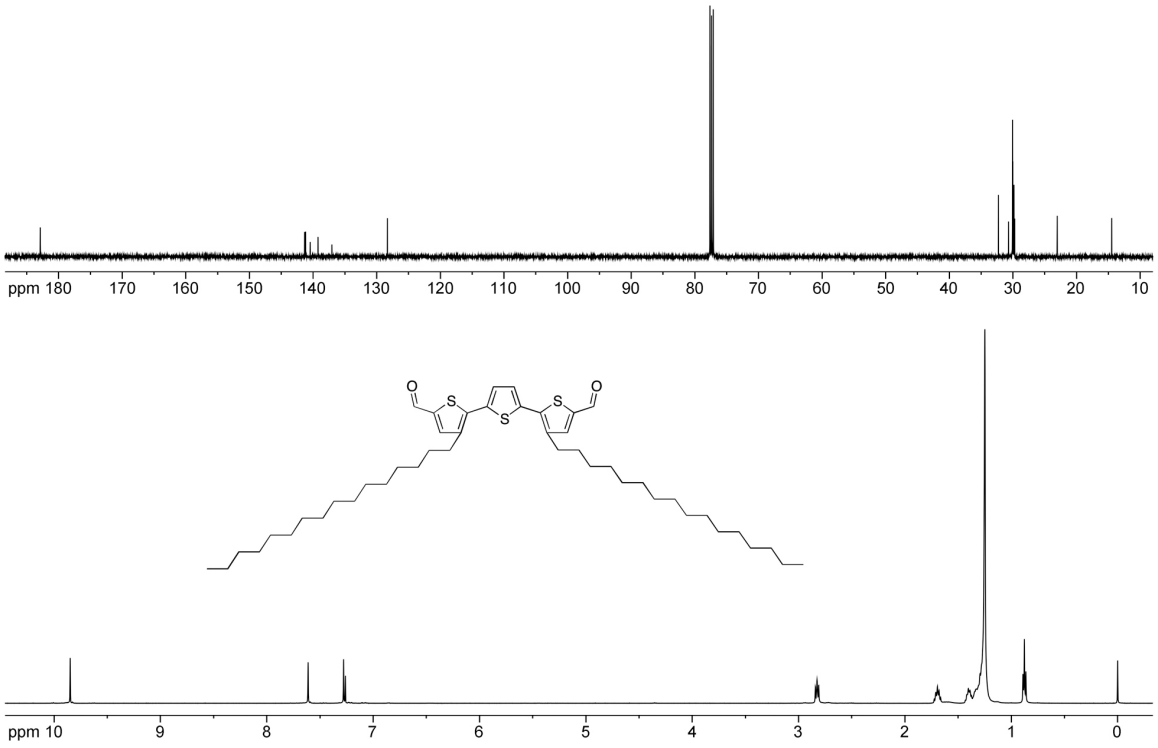

Figure 5.36

^{13}C and ^{1}H NMR spectra of **15**.

3,3''-Dihexadecyl-5,5'-dipropenyl-2,2':5',2''-terthiophene (16). A 2-neck 100 mL round bottom flask was equipped with a magnetic stir bar, reflux condenser, stopcock, and rubber septum. The flask was flame-dried under vacuum before adding ethyltriphenylphosphonium bromide (2.20 g, 6.00 mmol) and sodium bis(trimethylsilyl)amide (1.10 g, 6.00 mmol) as solids. The apparatus was placed under vacuum for 30 min before adding anhydrous hexanes (50 mL) via syringe. The suspension was refluxed for 1 h to generate the bright orange-red Wittig reagent. The reaction was cooled to -78 °C, and the precipitated solids were allowed to settle. The residual solvent was removed via syringe. The washing procedure was repeated by adding anhydrous hexanes (50 mL), stirring, and removing from the solid. The orange solid was dried under vacuum and dissolved in anhydrous THF (25 mL). The Wittig solution was

transferred to a flame-dried 100 mL round bottom flask containing **15** (1.50 g, 2.00 mmol) and anhydrous THF (25 mL) held at 0 °C. The reaction was stirred at room temperature for 30 min before removing the solvent under reduced pressure. The residue was dissolved in hexanes and flushed through a plug of silica gel. The solvent was removed under reduced pressure and the residue was dissolved in THF (10 mL) before precipitating into MeOH (175 mL, 0 °C). The product was isolated by filtration as a bright yellow-orange solid (1.36 g, 88%) Mixture of isomers (*ZZ* = 60%, *EE* = 40%, *Z*:*E* = 80:20). ^{1}H NMR (500 MHz; $CDCl_3$): δ_H (ppm) = 7.06-7.02 (m, 2H), 6.81 (*ZZ*), 6.68 (*ZE*) (2 singlets, 2H) 6.49-6.41 (2 doublets, 2H), 6.04 (*E*), 5.69 (*Z*) (m, 2H), 2.73 (m, 4H), 1.99 (*Z*), 1.85 (*E*) (2 doublets, *J* = 6.9 Hz, 6H), 1.64 (quintet, *J* = 7.6 Hz, 4H), 1.38 (quintet, *J* = 7.0 Hz, 4H), 1.25 (bs, 48H), 0.88 (t, *J* = 6.9 Hz, 6H). ^{13}C NMR (125 MHz; $CDCl_3$): δ_C (ppm) = 141.2, 140.0, 139.5, 139.1 (2), 136.3, 136.1, 130.8, 130.6, 127.8, 126.4, 126.0 (2), 125.9, 125.4, 124.6, 123.3, 32.3, 31.0, 30.9, 30.0 (3), 29.9, 29.8, 29.7, 29.6, 23.1, 18.7, 15.6, 14.5. HRGC-MS (EI): $M_{calcd.}$ = 776.5422, M_{found} = 776.5360. Anal. calcd. for $C_{50}H_{80}S_3$: C 77.25, H 10.37, S 12.37; Found: C 77.45, H 10.17, S 12.10.

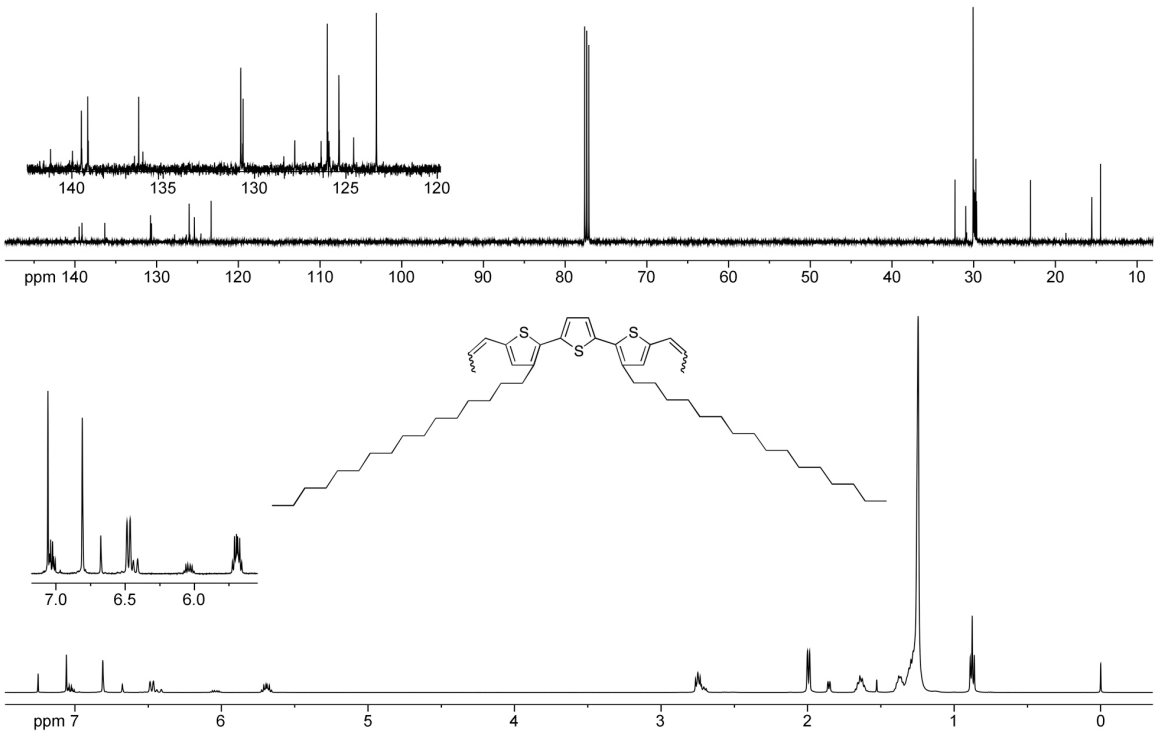

Figure 5.37

^{13}C and ^{1}H NMR spectra of **16**.

General polymerization procedure. An apparatus like that described previously was assembled and flame-dried under vacuum before placing under argon. The Schlenk tube was charged with monomer in a solution of anhydrous 1,2,4-trichlorobenzene (TCB) (ca. 0.15 M). The solution was degassed by applying vacuum at 80 °C for 20 min. G3 (ca. 1 mol%) was added as a solution in TCB (ca. 0.05 M). Dynamic vacuum was applied and the polymerization was run for 2–50 h before quenching with 0.5 mL of ethyl vinyl ether. The polymer was precipitated into a 20-fold excess of non-solvent (acetone or methanol) held at 0 °C. The solution was filtered through a Soxhlet thimble and purified by Soxhlet extraction with non-solvent (ca. 100 mL). The polymer was extracted into chloroform (ca. 100 mL) and concentrated under reduced pressure before reprecipitating in non-solvent (0 °C). Filtered and dried under vacuum to obtain the target material.

iiPTTV. 4 (268 mg, 0.57 mmol, *Z*:*E* = 83:17) was dissolved in TCB (5 mL). G3 (6.0 mg, 0.0068 mmol) in TCB (1 mL) was added and polymerized for 40 h before workup. Isolated product as an orange-red solid (196 mg, 83%). ^{1}H NMR (500 MHz, $CDCl_3$): δ_H (ppm) = 6.94 (bs, 2H), 6.92 (bs, 2H), 2.51 (bs, 4H), 1.56 (bs, 4H), 1.25 (bs, 20H), 0.87 (t, *J* = 6.3 Hz, 6H). ^{13}C NMR (125 MHz, $CDCl_3$): δ_C (ppm) = 143.4, 142.2, 128.4, 128.2, 121.7, 32.3, 30.9, 29.77, 29.60, 29.3, 23.1, 14.5. IR (solid) $\bar{\nu}_{max}$ (cm^{-1}): 2919, 2850, 1456, 931, 829, 721. Anal. calcd. for $C_{26}H_{38}S_2$: C 75.30, H 9.24, S 15.26; Found: C 75.42, H 9.27, S 15.17.

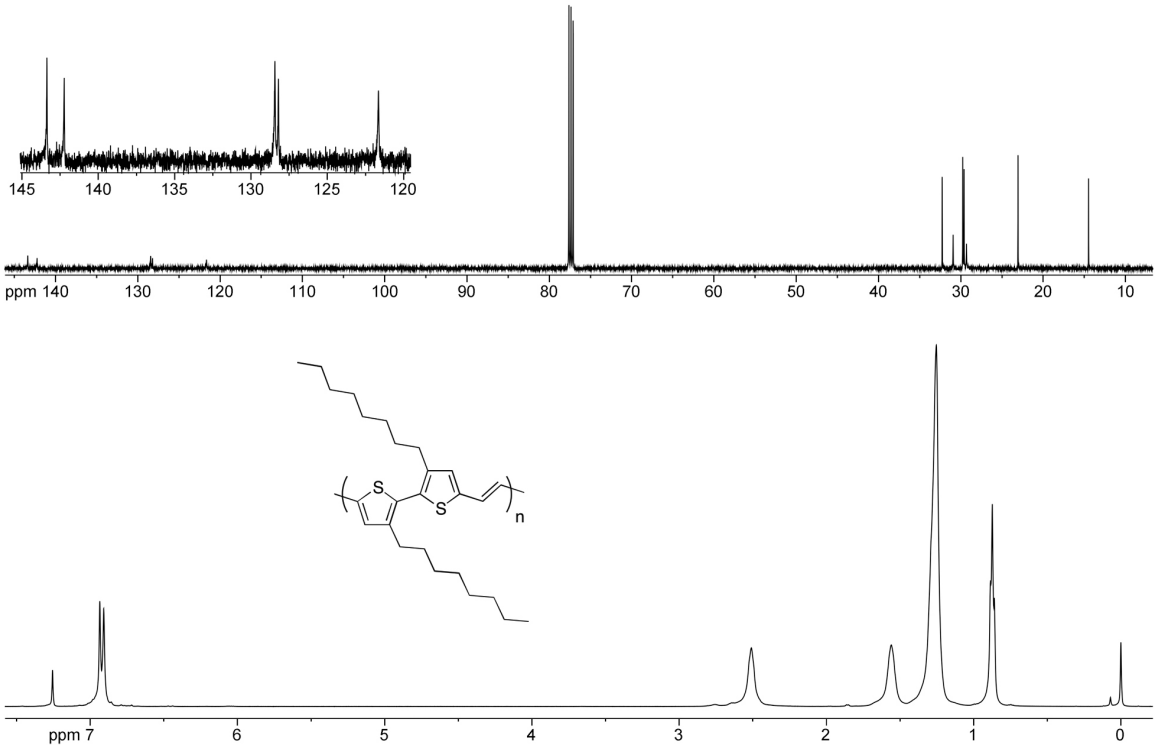

Figure 5.38
^{13}C and ^{1}H NMR spectra of **iiPTTV**.

ooPTTV. 8 (250 mg, 0.43 mmol, *Z*:*E* = 83:17) was dissolved in TCB (4.5 mL). G3 (3.8 mg, 0.0043 mmol) in TCB (0.5 mL) was added and polymerized for 2 h before workup.

Isolated product as black solid (134 mg, 59 %). ^{1}H NMR (500 MHz, $CDCl_3$): δ_H (ppm) = 6.91 (m, 4H), 2.61 (m, 4H), 1.62 (m, 4H), 1.26 (bs, 36H), 0.87 (m, 6H). IR (solid) $\bar{\nu}_{max}$ (cm^{-1}): 2916, 2847, 1462, 921, 817, 721. Anal. calcd. for $C_{34}H_{54}S_2$: C 77.50, H 10.33, S 12.17; Found: C 76.68, H 10.10, S 11.79.

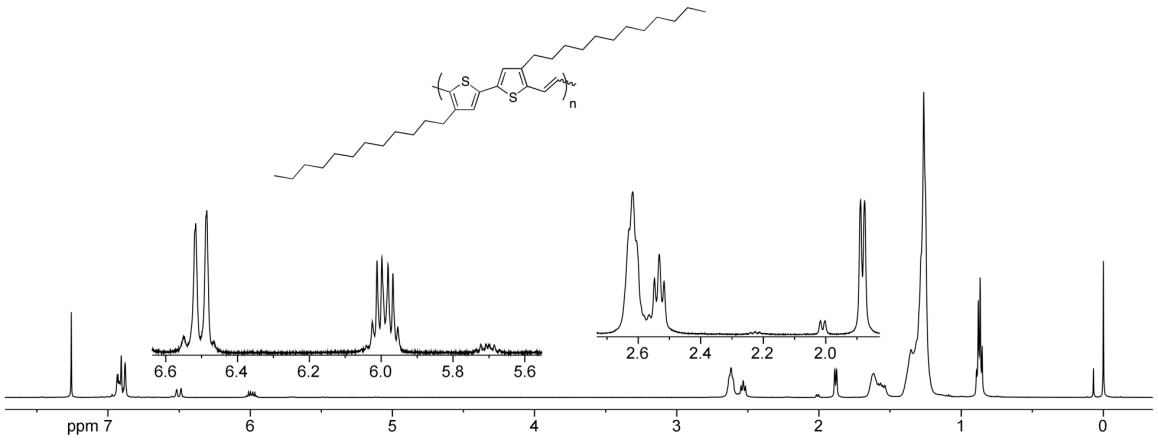

Figure 5.39

^{1}H NMR spectrum of **ooPTTV**.

ioPTTV. 13 (200 mg, 0.29 mmol, *Z*:*E* = 82:18) was dissolved in TCB (4.5 mL). G3 (2.6 mg, 0.0029 mmol) in TCB (0.5 mL) was added and polymerized for 24 h before workup. Isolated product as a black solid (175 mg, 95%). ^{1}H NMR (500 MHz, $CDCl_3$): δ_H (ppm) = 6.90 (m, 4H), 2.76 (bs, 2H), 2.66 (bs, 2H), 1.65 (bs, 4H), 1.25 (bs, 52H), 0.87 (t, J = 6.6, 6H). IR (solid) $\bar{\nu}_{max}$ (cm^{-1}): 2916, 2848, 1465, 924, 827, 720. Anal. calcd. for $C_{42}H_{70}S_2$: C 78.93, H 11.04, S 10.03; Found: C 78.75, H 10.81, S 10.15.

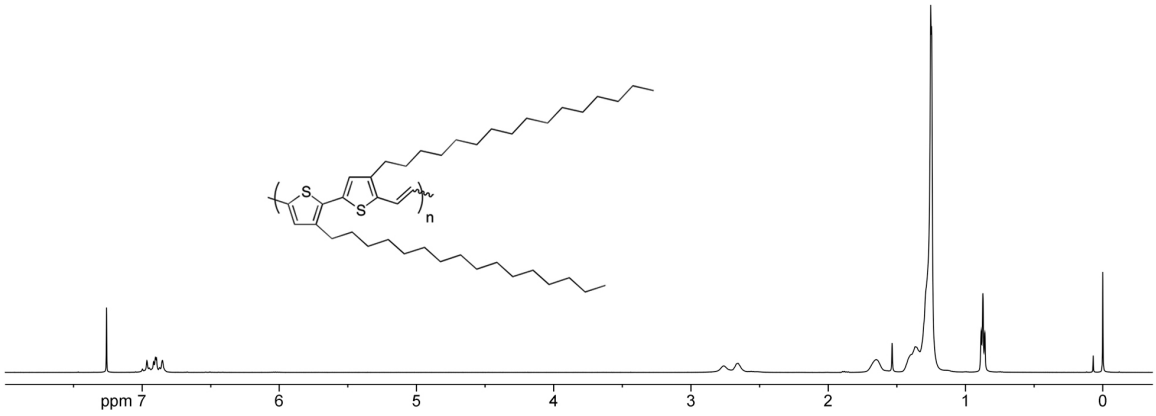

Figure 5.40

^{1}H NMR spectrum of **ioPTTV**.

PTTTV. 16 (250 mg, 0.32 mmol, *Z*:*E* = 80:20) was dissolved in TCB (4.5 mL).G3 (2.8 mg, 0.0032 mmol) in TCB (0.5 mL) was added and polymerized for 50 h before workup. Isolated product as a black solid (225 mg, 97%). ^{1}H NMR (500 MHz, $CDCl_3$): δ_H (ppm) = 7.09 (s, 2H), 6.91 (bs, 2H), 6.87 (bs, 2H), 2.76 (bs, 4H), 1.67 (bs, 4H), 1.25 (bs, 52H), 0.87 (t, *J* = 6.9, 6H). ^{13}C NMR (125 MHz, $CDCl_3$): δ_C (ppm) = 140.4, 136.4, 130.07, 130.00, 126.2, 121.5, 32.3, 30.10, 30.04, 29.7, 23.1, 14.5. IR (solid) $\bar{\nu}_{max}$ (cm^{-1}): 2917, 2849, 1465, 925, 829, 720. Anal. calcd. for $C_{42}H_{70}S_2$: C 76.70, H 10.06, S 13.34; Found: C 75.89, H 10.07, S 12.98.

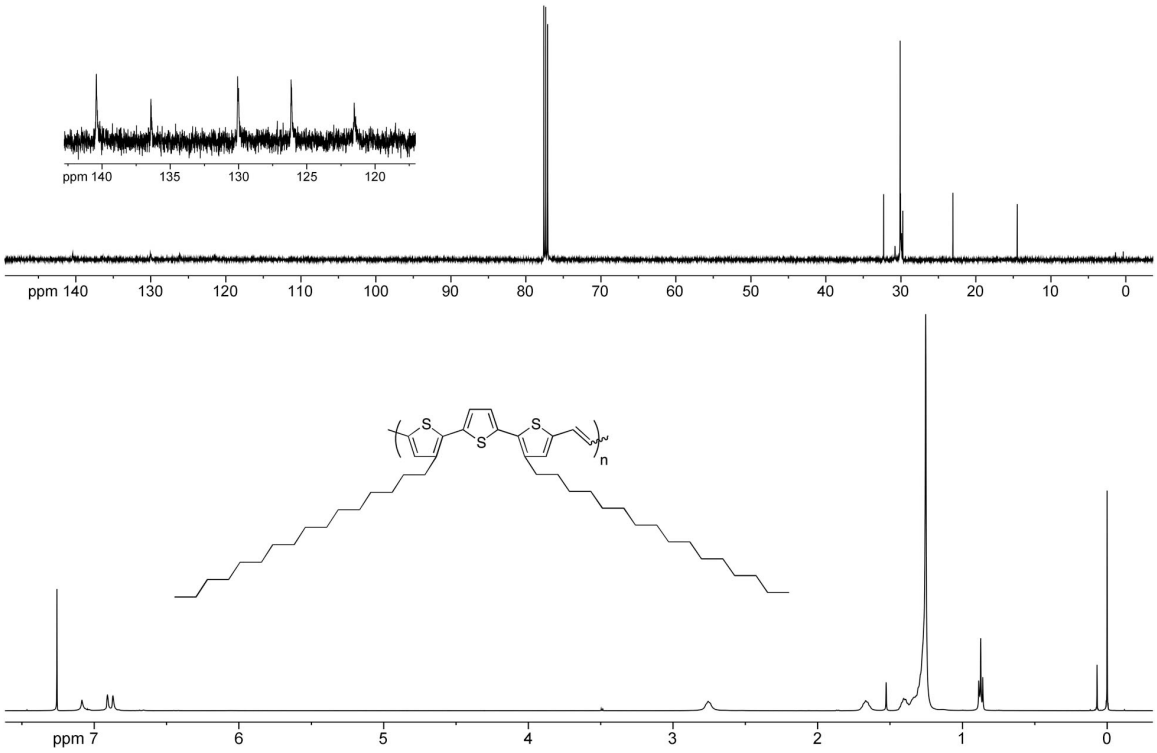

Figure 5.41
^{13}C and ^{1}H NMR spectra of **PTTTV**.

5.5 References

[1] Thompson, B. C.; Fréchet, J. M. J. *Angew. Chem., Int. Ed.* **2008**, *47*, 58–77.

[2] Cheng, Y.-J.; Yang, S.-H.; Hsu, C.-S. *Chem. Rev.* **2009**, *109*, 5868–5923.

[3] Mitschke, U.; Bäuerle, P. *J. Mater. Chem.* **2000**, *10*, 1471–1507.

[4] Zaumseil, J.; Sirringhaus, H. *Chem. Rev.* **2007**, *107*, 1296–1323.

[5] Kossmehl, V. G.; Härtel, M.; Manecke, G. *Makromol. Chem.* **1970**, *131*, 15–54.

[6] Brassett, A. J.; Colaneri, N. F.; Bradley, D. D. C.; Lawrence, R. A.; Friend, R. H.; Murata, H.; Tokito, S.; Tsutsui, T.; Saito, S. *Phys. Rev. B* **1990**, *41*, 10586–10594.

[7] Olejnik, E.; Pandit, B.; Basel, T.; Lafalce, E.; Sheng, C.-X.; Zhang, C.; Jiang, X.; Vardeny, Z. *Phys. Rev. B* **2012**, *85*, 235201.

[8] Xu, B.; Holdcroft, S. *Macromolecules* **1993**, *26*, 4457–4460.

[9] Li, Y.; Vamvounis, G.; Holdcroft, S. *Macromolecules* **2002**, *35*, 6900–6906.

[10] Cook, S.; Furube, A.; Katoh, R. *Energ. Environ. Sci.* **2008**, *1*, 294–299.

[11] Chen, J.; Cao, Y. *Acc. Chem. Res.* **2009**, *42*, 1709–1718.

[12] Li, Y. *Acc. Chem. Res.* **2012**, *45*, 723–733.

[13] Huo, L.; Chen, T. L.; Zhou, Y.; Hou, J.; Chen, H.-Y.; Yang, Y.; Li, Y. *Macromolecules* **2009**, *42*, 4377–4380.

[14] Lu, C.; Wu, H. C.; Chiu, Y. C.; Lee, W. Y.; Chen, W. C. *Macromolecules* **2012**, *45*, 3047–3056.

[15] Qin, Y.; Hillmyer, M. A. *Macromolecules* **2009**, *42*, 6429–6432.

[16] Speros, J. C.; Paulsen, B. D.; White, S. P.; Wu, Y.; Jackson, E. A.; Slowinski, B. S.; Frisbie, C. D.; Hillmyer, M. A. *Macromolecules* **2012**, *45*, 2190–2199.

[17] Speros, J. C.; Paulsen, B. D.; Slowinski, B. S.; Frisbie, C. D.; Hillmyer, M. A. *ACS Macro Lett.* **2012**, 986–990.

[18] Lowe, J.; Bartels, C.; Holdcroft, S. *Can. Journ. Chem* **1998**, *76*, 1524–1529.

[19] Zhou, H. X.; Yang, L. Q.; Xiao, S. Q.; Liu, S. B.; You, W. *Macromolecules* **2010**, *43*, 811–820.

[20] Biniek, L.; Fall, S.; Chochos, C. L.; Anokhin, D. V.; Ivanov, D. A.; Leclerc, N.; Lévêque, P.; Heiser, T. *Macromolecules* **2010**, *43*, 9779–9786.

[21] El-Shehawy, A. A.; Abdo, N. I.; El-Barbary, A. A.; Lee, J.-S. *Eur. J. Org. Chem.* **2011**, 4841–4852.

[22] Shi, Q.; Fan, H.; Liu, Y.; Chen, J.; Ma, L.; Hu, W.; Shuai, Z.; Li, Y.; Zhan, X. *Macromolecules* **2011**, *44*, 4230–4240.

[23] Massip, S.; Oberhumer, P. M.; Tu, G.; Albert-Seifried, S.; Huck, W. T. S.; Friend, R. H.; Greenham, N. C. *J. Phys. Chem. C* **2011**, *115*, 25046–25055.

[24] Zhang, Z.-G.; Min, J.; Zhang, S.; Zhang, J.; Zhang, M.; Li, Y. *Chem. Commun.* **2011**, *47*, 9474–9476.

[25] Lee, S. K.; Cho, S.; Tong, M.; Hwa Seo, J.; Heeger, A. J. *J. Polym. Sci., Polym. Chem.* **2011**, *49*, 1821–1829.

[26] Balan, B.; Vijayakumar, C.; Saeki, A.; Koizumi, Y.; Seki, S. *Macromolecules* **2012**, *45*, 2709–2719.

[27] Xu, J.; Ng, S. C.; Chan, H. S. O. *Tetrahedron Lett.* **2001**, *42*, 5327–5329.

[28] Guo, X.; Ortiz, R. P.; Zheng, Y.; Hu, Y.; Noh, Y.-Y.; Baeg, K.-J.; Facchetti, A.; Marks, T. J. *J. Am. Chem. Soc.* **2011**, *133*, 1405–1418.

[29] Kong, H.; Chung, D. S.; Kang, I.-N.; Lim, E.; Jung, Y. K.; Park, J.-H.; Park, C. E.; Shim, H.-K. *Bull. Korean Chem. Soc.* **2007**, *28*, 1945–1950.

[30] Gallazzi, M.; Bertarelli, C.; Montoneri, E. *Synth. Met.* **2002**, *128*, 91–95.

[31] Patel, J.; Mujcinovic, S.; Jackson, W. R.; Robinson, A. J.; Serelis, A. K.; Such, C. *Green Chem.* **2006**, *8*, 450–454.

[32] Love, J. A.; Morgan, J. P.; Trnka, T. M.; Grubbs, R. H. *Angew. Chem., Int. Ed.* **2002**, *41*, 4035–4037.

[33] Catellani, M.; Luzzati, S.; Musco, A.; Speroni, F. *Synth. Met.* **1994**, *62*, 223–228.

[34] Toyoshima, R.; Akagi, K.; Shirakawa, H. *Synth. Met.* **1997**, *84*, 431–432.

[35] Kokubo, H.; Sato, T.; Yamamoto, T. *Macromolecules* **2006**, *39*, 3959–3963.

[36] Yamamoto, T.; Kumagai, A.; Kokubo, H.; Nakamura, Y. *Bull. Chem. Soc. Jpn.* **2011**, *84*, 1291–1293.

[37] Liu, J.; Loewe, R. S.; McCullough, R. D. *Macromolecules* **1999**, *32*, 5777–5785.

[38] Hiorns, R. C.; de Bettignies, R.; Leroy, J.; Bailly, S.; Firon, M.; Sentein, C.; Khoukh, A.; Preud'homme, H.; Dagron-Lartigau, C. *Adv. Funct. Mater.* **2006**, *16*, 2263–2273.

[39] Wong, M.; Hollinger, J.; Kozycz, L. M.; McCormick, T. M.; Lu, Y.; Burns, D. C.; Seferos, D. S. *ACS Macro Lett.* **2012**, *1*, 1266–1269.

[40] Wagener, K. B.; Boncella, J. M.; Nel, J. G. *Macromolecules* **1991**, *24*, 2649–2657.

[41] Opper, K.; Wagener, K. *J. Polym. Sci., Polym. Chem.* **2011**, *49*, 821–831.

[42] Pretsch, E.; Bühlmann, P.; Affolter, C. *Structure Determination of Organic Compounds: Tables of Spectral Data*; Springer: Heidelberg, 2000; 248–251.

[43] Pavia, D. L.; Lampman, G. M.; Kriz, G. S. *Introduction to Spectroscopy: A Guide for Students of Organic Chemistry*; Brooks/Cole: United States, 2001; 39–40.

[44] He, M.; Leslie, T. M.; Sinicropi, J. A. *Chem. Mater.* **2002**, *14*, 4662–4668.

[45] Kim, J.; Lim, B.; Baeg, K.-J.; Noh, Y.-Y.; Khim, D.; Jeong, H.-G.; Yun, J.-M.; Kim, D.-Y. *Chem. Mater.* **2011**, *23*, 4663–4665.

[46] Theander, M.; Inganäs, O.; Mammo, W.; Olinga, T.; Svensson, M.; Andersson, M. R. *J. Phys. Chem. B* **1999**, *103*, 7771–7780.

[47] Roncali, J. *Chem. Rev.* **1997**, *97*, 173–206.

[48] Frisch, M. J.; Trucks, G. W.; Schlegel, H. B.; Scuseria, G. E.; Robb, M. A.; Cheeseman, J. R.; Scalmani, G.; Barone, V.; Mennucci, B.; Petersson, G. A.; Nakatsuji, H.; Caricato, M.; Li, X.; Hratchian, H. P.; Izmaylov, A. F.; Bloino, J.; Zheng, G.; Sonnenberg, J. L.; Hada, M.; Ehara, M.; Toyota, K.; Fukuda, R.; Hasegawa, J.; Ishida, M.; Nakajima, T.; Honda, Y.; Kitao, O.; Nakai, H.; Vreven, T.; Montgomery, J. A.; Peralta, J. E.; Ogliaro, F.; Bearpark, M.; Heyd, J. J.; Brothers, E.; Kudin, K. N.; Staroverov, V. N.; Kobayashi, R.; Normand, J.; Raghavachari, K.; Rendell, A.; Burant, J. C.; Iyengar, S. S.; Tomasi, J.; Cossi, M.; Rega, N.; Millam, J. M.; Klene, M.; Knox, J. E.; Cross, J. B.; Bakken, V.; Adamo, C.; Jaramillo, J.; Gomperts, R.; Stratmann, R. E.; Yazyev, O.; Austin, A. J.; Cammi, R.; Pomelli, C.; Ochterski, J. W.; Martin, R. L.; Morokuma, K.; Zakrzewski, V. G.; Voth, G. A.; Salvador, P.; Dannenberg, J. J.; Dapprich, S.; Daniels, A. D.; Farkas, Ö.; Foresman, J. B.; Ortiz, J. V.; Cioslowski, J.; Fox, D. J. *Gaussian 09, Revision A.02*; Gaussian, Inc.: Wallingford, CT, 2010.

[49] Zhao, Y.; Truhlar, D. G. *Theor. Chem. Acc.* **2008**, *120*, 215–241.

[50] Hehre, W. J.; Radom, L.; Schleyer, P. v. R.; Pople, J. A. *Ab Initio Molecular Orbital Theory*; Wiley: New York, 1986.

[51] Kim, Y.; Cook, S.; Tuladhar, S. M.; Choulis, S. A.; Nelson, J.; Durrant, J. R.; Bradley, D. D. C.; Giles, M.; Mcculloch, I.; Ha, C. S.; Ree, M. *Nat. Mater.* **2006**, *5*, 197–203.

[52] Cardona, C. M.; Li, W.; Kaifer, A. E.; Stockdale, D.; Bazan, G. C. *Adv. Mater.* **2011**, *23*, 2367–2371.

[53] Jiang, X. Q.; Patil, R.; Harima, Y.; Ohshita, J.; Kunai, A. *J. Phys. Chem. B* **2005**, *109*, 221–229.

[54] Ko, S.; Hoke, E. T.; Pandey, L.; Hong, S.; Mondal, R.; Risko, C.; Yi, Y.; Noriega, R.; McGehee, M. D.; Brédas, J.-L.; Salleo, A.; Bao, Z. *J. Am. Chem. Soc.* **2012**, *134*, 5222–5232.

[55] Stevens, D. M.; Speros, J. C.; Hillmyer, M. A.; Frisbie, C. D. *J. Phys. Chem. C* **2011**, *115*, 20806–20816.

[56] Drake, J. M.; Lesiecki, M. L.; Camaioni, D. M. *Chem. Phys. Lett.* **1985**, *113*, 530–534.

[57] Zhao, Y.; Truhlar, D. G. *Acc. Chem. Res.* **2008**, *41*, 157-167.

[58] Zhao, Y.; Truhlar, D. G. *J. Chem. Theory Comput.* **2009**, *5*, 324–333.

[59] Biniek, L.; Chochos, C. L.; Hadziioannou, G.; Leclerc, N.; Lévêque, P.; Heiser, T. *Macromol. Rapid. Commun.* **2010**, *31*, 651–656.

[60] Khor, E.; Ng, S. C.; Li, H. C.; Chai, S. *Heterocycles* **1991**, *32*, 1805–1812.

[61] Xu, J.; Ng, S. C.; Chan, H. S. O. *Tetrahedron Lett.* **2001**, *42*, 5327–5329.

Bibliography

[1] Akcelrud, L. *Prog. Polym. Sci.* **2003**, *28*, 875–962.

[2] Alam, M. M.; Jenekhe, S. A. *Chem. Mater.* **2004**, *16*, 4647–4656.

[3] Alvarez, R.; Gandini, A.; Martinez, R. *J. Polym. Sci., Polym. Lett.* **1975**, *13*, 385–390.

[4] Anglin, T. C.; Speros, J. C.; Massari, A. M. *J. Phys. Chem. C* **2011**, *115*, 16027–16036.

[5] Anthony, J. E.; Facchetti, A.; Heeney, M.; Marder, S. R.; Zhan, X. W. *Adv. Mater.* **2010**, *22*, 3876–3892.

[6] Armstrong, N. R.; Veneman, P. A.; Ratcliff, E.; Placencia, D.; Brumbach, M. *Acc. Chem. Res.* **2009**, *42*, 1748–1757.

[7] Aso, C.; Tanaka, Y. *Kobunshi Kogaku* **1964**, *21*, 373–377.

[8] Babudri, F.; Cicco, S. R.; Farinola, G. M.; Naso, F.; Bolognesi, A.; Porzio, W. *Macromol. Rapid Comm.* **1996**, *17*, 905–911.

[9] Backer, S. A.; Sivula, K.; Kavulak, D. F.; Fréchet, J. M. J. *Chem. Mater.* **2007**, *19*, 2927–2929.

[10] Balan, B.; Vijayakumar, C.; Saeki, A.; Koizumi, Y.; Seki, S. *Macromolecules* **2012**, *45*, 2709–2719.

[11] Ballantyne, A. M.; Chen, L.; Dane, J.; Hammant, T.; Braun, F. M.; Heeney, M.; Duffy, W.; McCulloch, I.; Bradley, D. D. C.; Nelson, J. *Adv. Funct. Mater.* **2008**, *18*, 2373–2380.

[12] Banishoeib, F.; Henckens, A.; Fourier, S.; Vanhooyland, G.; Breselge, M.; Manca, J.; Cleij, T. J.; Lutsen, L.; Vanderzande, D.; Nguyen, L. H.; Neugebauer, H.; Sariciftci, N. S. *Thin Solid Films* **2008**, *516*, 3978–3988.

[13] Baughman, T. W.; Wagener, K. B. *Adv. Polym. Sci.* **2005**, *176*, 1–42.

[14] Benoit, D.; Harth, E.; Fox, P.; Waymouth, R. M.; Hawker, C. J. *Macromolecules* **2000**, *33*, 363–370.

[15] Biagini, S. C. G.; Gareth Davies, R.; Gibson, V. C.; Giles, M. R.; Marshall, E. L.; North, M. *Polymer* **2001**, *42*, 6669–6671.

[16] Bian, L.; Zhu, E.; Tang, J.; Tang, W.; Zhang, F. *Prog. Polym. Sci.* **2012**, *37*, 1292–1331.

[17] Bielawski, C. W.; Grubbs, R. H. *Angew. Chem., Int. Ed.* **2000**, *39*, 2903–2906.

[18] Biniek, L.; Chochos, C. L.; Hadziioannou, G.; Leclerc, N.; Lévêque, P.; Heiser, T. *Macromol. Rapid. Commun.* **2010**, *31*, 651–656.

[19] Biniek, L.; Fall, S.; Chochos, C. L.; Anokhin, D. V.; Ivanov, D. A.; Leclerc, N.; Lévêque, P.; Heiser, T. *Macromolecules* **2010**, *43*, 9779–9786.

[20] Bloom, D. E. *Science* **2011**, *333*, 562–569.

[21] Blouin, N.; Michaud, A.; Leclerc, M. *Adv. Mater.* **2007**, *19*, 2295-2300.

[22] Boudouris, B. W.; Frisbie, C. D.; Hillmyer, M. A. *Macromolecules* **2008**, *41*, 67–75.

[23] Brabec, C. J.; Cravino, A.; Meissner, D.; Sariciftci, N. S.; Fromherz, T.; Rispens, M. T.; Sanchez, L.; Hummelen, J. C. *Adv. Funct. Mater.* **2001**, *11*, 374–380.

[24] Brabec, C. J.; Sariciftci, N. S.; Hummelen, J. C. *Adv. Funct. Mater.* **2001**, *11*, 15–26.

[25] Brassett, A. J.; Colaneri, N. F.; Bradley, D. D. C.; Lawrence, R. A.; Friend, R. H.; Murata, H.; Tokito, S.; Tsutsui, T.; Saito, S. *Phys. Rev. B* **1990**, *41*, 10586–10594.

[26] Braunecker, W. A.; Matyjaszewski, K. *Prog. Polym. Sci.* **2007**, *32*, 93–146.

[27] Brédas, J.-L.; Heeger, A. J.; Wudl, F. *J. Chem. Phys.* **1986**, *85*, 4673–4678.

[28] Brédas, J.-L.; Norton, J. E.; Cornil, J.; Coropceanu, V. *Acc. Chem. Res.* **2009**, *42*, 1691–1699.

[29] Burkhart, B.; Khlyabich, P. P.; Canak, T. C.; LaJoie, T. W.; Thompson, B. C. *Macromolecules* **2011**, *44*, 1242–1246.

[30] Burkhart, B.; Khlyabich, P. P.; Canak, T. C.; LaJoie, T. W.; Thompson, B. C. *Macromolecules* **2011**, *44*, 1242–1246.

[31] Burkhart, B.; Khlyabich, P. P.; Thompson, B. C. *ACS Macro Lett.* **2012**, *1*, 660-666.

[32] Burkhart, B.; Khlyabich, P. P.; Thompson, B. C. *Macromolecules* **2012**, *45*, 3740–3748.

[33] Burroughes, J. H.; Bradley, D. D. C.; Brown, A. R.; Marks, R. N.; Mackay, K.; Friend, R. H.; Burns, P. L.; Holmes, A. B. *Nature* **1990**, *347*, 539–541.

[34] Cardona, C. M.; Li, W.; Kaifer, A. E.; Stockdale, D.; Bazan, G. C. *Adv. Mater.* **2011**, *23*, 2367–2371.

[35] Carsten, B.; He, F.; Son, H. J.; Xu, T.; Yu, L. *Chem. Rev.* **2011**, *111*, 1493–1528.

[36] Catellani, M.; Luzzati, S.; Musco, A.; Speroni, F. *Synth. Met.* **1994**, *62*, 223–228.

[37] Chang, J.-F.; Clark, J.; Zhao, N.; Sirringhaus, H.; Breiby, D. W.; Andreasen, J. W.; Nielsen, M. M.; Giles, M.; Heeney, M.; McCulloch, I. *Phys. Rev. B* **2006**, *74*, 115318.

[38] Chang, S.-C.; Liu, J.; Bharathan, J.; Yang, Y.; Onohara, J.; Kido, J. *Adv. Mater.* **1999**, *11*, 734–737.

[39] Chen, C.-H.; Hsieh, C.-H.; Dubosc, M.; Cheng, Y.-J.; Hsu, C.-S. *Macromolecules* **2010**, *43*, 697–708.

[40] Chen, H.-C.; Chen, Y.-H.; Liu, C.-C.; Chien, Y.-C.; Chou, S.-W.; Chou, P.-T. *Chem. Mater.* **2012**, *24*, 4766–4772.

[41] Chen, H.-Y.; Hou, J.; Zhang, S.; Liang, Y.; Yang, G.; Yang, Y.; Yu, L.; Wu, Y.; Li, G. *Nat. Photonics* **2009**, *3*, 649–653.

[42] Chen, J.; Cao, Y. *Acc. Chem. Res.* **2009**, *42*, 1709–1718.

[43] Chen, T.-A.; Rieke, R. D. *J. Am. Chem. Soc.* **1992**, *114*, 10087–10088.

[44] Chen, X.; Schulz, G. L.; Han, X.; Zhou, Z.; Holdcroft, S. *J. Phys. Chem. C.* **2009**, *113*, 8505–8512.

[45] Cheng, Y.-J.; Yang, S.-H.; Hsu, C.-S. *Chem. Rev.* **2009**, *109*, 5868–5923.

[46] Chu, T.-Y.; Lu, J.; Beaupré, S.; Zhang, Y.; Pouliot, J.-R.; Wakim, S.; Zhou, J.; Leclerc, M.; Li, Z.; Ding, J.; Tao, Y. *J. Am. Chem. Soc.* **2011**, *133*, 4250–4253.

[47] Chu, T.-Y.; Lu, J.; Beaupré, S.; Zhang, Y.; Pouliot, J.-R.; Wakim, S.; Zhou, J.; Leclerc, M.; Li, Z.; Ding, J.; Tao, Y. *J. Am. Chem. Soc.* **2011**, *133*, 4250–4253.

[48] Clark, J.; Silva, C.; Friend, R. H.; Spano, F. C. *Phys. Rev. Lett.* **2007**, *98*, 206406.

[49] Clayden, J. *Tetrahedron* **2004**, *60*, 4335–4335.

[50] Coffin, R. C.; Peet, J.; Rogers, J.; Bazan, G. C. *Nature Chem.* **2009**, *1*, 657–661.

[51] Cohen, M. L. *Nature* **2000**, *406*, 762–767.

[52] Cook, S.; Furube, A.; Katoh, R. *Energ. Environ. Sci.* **2008**, *1*, 294–299.

[53] Cornelissen, J. J. L. M.; Peeters, E.; Janssen, R. A. J.; Meijer, E. W. *Acta. Polym.* **1998**, *49*, 471–476.

[54] Coropceanu, V.; Cornil, J.; da Silva Filho, D. A.; Olivier, Y.; Silbey, R.; Brédas, J.-L. *Chem. Rev.* **2007**, *107*, 926–952.

[55] Davey, A. P.; Drury, A.; Maier, S.; Byrne, H. J.; Blau, W. J. *Synth. Met.* **1999**, *103*, 2478–2479.

[56] Dechy-Cabaret, O.; Martin-Vaca, B.; Bourissou, D. *Chem. Rev.* **2004**, *104*, 6147–6176.

[57] Delgado, P. A.; Liu, D. Y.; Kean, Z.; Wagener, K. B. *Macromolecules* **2011**, *44*, 9529–9532.

[58] Dennler, G.; Scharber, M. C.; Brabec, C. J. *Adv. Mater.* **2009**, *21*, 1323–1338.

[59] Dierschke, F.; Grimsdale, A. C.; Müllen, K. *Synthesis* **2003**, 2470–2472.

[60] Diliën, H.; Palmaerts, A.; Lenes, M.; de Boer, B.; Blom, P.; Cleij, T. J.; Lutsen, L.; Vanderzande, D. *Macromolecules* **2010**, *43*, 10231–10240.

[61] Dillingham, K. A. PhD. Dissertation, Lancaster University, 1995.

[62] Dou, L.; You, J.; Yang, J.; Chen, C.-C.; He, Y.; Murase, S.; Moriarty, T.; Emery, K.; Li, G.; Yang, Y. **2012**, 1-6.

[63] Drake, J. M.; Lesiecki, M. L.; Camaioni, D. M. *Chem. Phys. Lett.* **1985**, *113*, 530–534.

[64] Dudgeon, D.; Arthington, A. H.; Gessner, M. O.; Kawabata, Z.-I.; Knowler, D. J.; Lévêque, C.; Naiman, R. J.; Prieur-Richard, A.-H.; Soto, D.; Stiassny, M. L. J.; Sullivan, C. A. *Biol. Rev.* **2006**, *81*, 163–182.

[65] Duffield, J. J.; Pettit, G. R. *J. Nat. Prod.* **2001**, *64*, 472–479.

[66] Dyer, A. L.; Thompson, E. J.; Reynolds, J. R. *ACS Appl. Mater. Interfaces* **2011**, *3*, 1787–1785.

[67] El-Shehawy, A. A.; Abdo, N. I.; El-Barbary, A. A.; Lee, J.-S. *Eur. J. Org. Chem.* **2011**, 4841–4852.

[68] Elsenbaumer, R. L.; Jen, K. Y.; Oboodi, R. *Synth. Met.* **1986**, *15*, 169–174.

[69] Eo, Y. S.; Rhee, H. W.; Chin, B. D.; Yu, J.-W. *Synth. Met.* **2009**, *159*, 1910–1913.

[70] Flook, M. M.; Ng, V. W. L.; Schrock, R. R. *J. Am. Chem. Soc.* **2011**, *133*, 1784–1786.

[71] Foley, J. A.; Ramankutty, N.; Brauman, K. A.; Cassidy, E. S.; Gerber, J. S.; Johnston, M.; Mueller, N. D.; O'Connell, C.; Ray, D. K.; West, P. C.; Balzer, C.; Bennett, E. M.; Carpenter, S. R.; Hill, J.; Monfreda, C.; Polasky, S.; Rockström, J.; Sheehan, J.; Siebert, S.; Tilman, D.; Zaks, D. P. M. *Nature* **2011**, *478*, 337–342.

[72] Forrest, S. R. *MRS Bull.* **2005**, *30*, 28-32.

[73] Forrest, S. R. *Nature* **2004**, *428*, 911–918.

[74] Fox, H. H.; Schrock, R. R.; O'Dell, R. *Organometallics* **1994**, *13*, 635–639.

[75] Friend, R. H.; Gymer, R. W.; Holmes, A. B.; Burroughes, J. H.; Marks, R. N.; Taliani, C.; Bradley, D. D. C.; Dos Santos, D. A.; Brédas, J. L.; Lögdlund, M.; Salaneck, W. R. *Nature* **1999**, *397*, 121–128.

[76] Frisch, M. J.; Trucks, G. W.; Schlegel, H. B.; Scuseria, G. E.; Robb, M. A.; Cheeseman, J. R.; Scalmani, G.; Barone, V.; Mennucci, B.; Petersson, G. A.; Nakatsuji, H.; Caricato, M.; Li, X.; Hratchian, H. P.; Izmaylov, A. F.; Bloino, J.; Zheng, G.; Sonnenberg, J. L.; Hada, M.; Ehara, M.; Toyota, K.; Fukuda, R.; Hasegawa, J.; Ishida, M.; Nakajima, T.; Honda, Y.; Kitao, O.; Nakai, H.; Vreven, T.; Montgomery, J. A.; Peralta, J. E.; Ogliaro, F.; Bearpark, M.; Heyd, J. J.; Brothers, E.; Kudin, K. N.; Staroverov, V. N.; Kobayashi, R.; Normand, J.; Raghavachari, K.; Rendell, A.; Burant, J. C.; Iyengar, S. S.; Tomasi, J.; Cossi, M.; Rega, N.; Millam, J. M.; Klene, M.; Knox, J. E.; Cross, J. B.; Bakken, V.; Adamo, C.; Jaramillo, J.; Gomperts, R.; Stratmann, R. E.; Yazyev, O.; Austin, A. J.; Cammi, R.; Pomelli, C.; Ochterski, J. W.; Martin, R. L.; Morokuma, K.; Zakrzewski, V. G.; Voth, G. A.; Salvador, P.; Dannenberg, J. J.; Dapprich, S.; Daniels, A. D.; Farkas, Ö.; Foresman, J. B.; Ortiz, J. V.; Cioslowski, J.; Fox, D. J. *Gaussian 09, Revision A.02*; Gaussian, Inc.: Wallingford, CT, 2010.

[77] Gallazzi, M.; Bertarelli, C.; Montoneri, E. *Synth. Met.* **2002**, *128*, 91–95.

[78] Gandini, A. *Green Chem.* **2011**, *13*, 1061–1083.

[79] Gandini, A. *Macromolecules* **2008**, *41*, 9491–9504.

[80] Gandini, A.; Belgacem, M. *Prog. Polym. Sci.* **1997**, *22*, 1203–1379.

[81] Gao, D.; Hollinger, J.; Seferos, D. S. *ACS Nano* **2012**, *6*, 7114–7121.

[82] Ge, J.; He, M.; Qiu, F.; Yang, Y. *Macromolecules* **2010**, *43*, 6422–6428.

[83] Gilch, H. G.; Wheelwright, W. L. *J. Polym. Sci., Polym. Chem.* **1966**, *4*, 1337–1349.

[84] Girotto, C.; Cheyns, D.; Aernouts, T.; Banishoeib, F.; Lutsen, L.; Cleij, T. J.; Vanderzande, D.; Genoe, J.; Poortmans, J.; Heremans, P. *Org. Electron.* **2008**, *9*, 740–746.

[85] Goh, C.; Kline, R. J.; McGehee, M. D.; Kadnikova, E. N.; Fréchet, J. M. J. *Appl. Phys. Lett.* **2005**, *86*, 122110.

[86] Gramlich, W. M.; Hillmyer, M. A. *Polym. Chem.* **2011**, *2*, 2062–2067.

[87] Gregg, B. A. *J. Phys. Chem. B* **2003**, *107*, 4688–4698.

[88] Gregg, B. A. *MRS Bull.* **2005**, *30*, 20–22.

[89] Gregg, B. A.; Hanna, M. C. *J. Appl. Phys.* **2003**, *93*, 3605–3614.

[90] Grubbs, R. H. *Tetrahedron* **2004**, *60*, 7117–7140.

[91] Guillerez, S.; Bidan, G. *Synth. Met.* **1998**, *93*, 123–126.

[92] Günes, S.; Neugebauer, H.; Sariciftci, N. S. *Chem. Rev.* **2007**, *107*, 1324–1338.

[93] Guo, X.; Ortiz, R. P.; Zheng, Y.; Hu, Y.; Noh, Y.-Y.; Baeg, K.-J.; Facchetti, A.; Marks, T. J. *J. Am. Chem. Soc.* **2011**, *133*, 1405–1418.

[94] Gupta, A. P.; Kumar, V. *Eur. Polym. J.* **2007**, *43*, 4053–4074.

[95] Gürbüz, E. I.; Gallo, J. M. R.; Alonso, D. M.; Wettstein, S. G.; Lim, W. Y.; Dumesic, J. A. *Angew. Chem., Int. Ed.* **2013**, *52*, 1270–1274.

[96] Hagfeldt, A.; Boschloo, G.; Sun, L.; Kloo, L.; Pettersson, H. *Chem. Rev.* **2010**, *110*, 6595–6663.

[97] Hamilton, R.; Bailey, C.; Duffy, W.; Heeney, M.; Shkunov, M.; Sparrowe, D.; Tierney, S.; McCulloch, I.; Kline, R. J.; DeLongchamp, D. M.; Chabinyc, M. *Proc. SPIE* **2006**, *6336*, 633611.

[98] Haugeneder, A.; Neges, M.; Kallinger, C.; Spirkl, W.; Lemmer, U.; Feldmann, J.; Scherf, U.; Harth, E.; Gügel, A.; Müllen, K. *Phys. Rev. B* **1999**, *59*, 15346–15351.

[99] Haukaas, M. H.; O'Doherty, G. A. *Org. Lett.* **2001**, *3*, 401–404.

[100] Havinga, E. E.; ten Hoeve, W.; Wynberg, H. *Synth. Met.* **1993**, *55*, 299–306.

[101] He, M.; Leslie, T. M.; Sinicropi, J. A. *Chem. Mater.* **2002**, *14*, 4662–4668.

[102] He, Y.; Zhao, G.; Min, J.; Zhang, M.; Li, Y. *Polymer* **2009**, *50*, 5055-5058.

[103] He, Z.; Zhong, C.; Huang, X.; Wong, W.-Y.; Wu, H.; Chen, L.; Su, S.; Cao, Y. *Adv. Mater.* **2011**, *23*, 4636–4643.

[104] He, Z.; Zhong, C.; Su, S.; Xu, M.; Wu, H.; Cao, Y. *Nat. Photonics* **2012**, *6*, 591–595.

[105] Heath, W. H.; Palmieri, F.; Adams, J. R.; Long, B. K.; Chute, J.; Holcombe, T. W.; Zieren, S.; Truitt, M. J.; White, J. L.; Willson, C. G. *Macromolecules* **2008**, *41*, 719–726.

[106] Heeger, A. J. *Angew. Chem., Int. Ed.* **2001**, *40*, 2591–2611.

[107] Heeger, A. J. *Chem. Soc. Rev.* **2010**, *39*, 2354–2371.

[108] Hehre, W. J.; Radom, L.; Schleyer, P. v. R.; Pople, J. A. *Ab Initio Molecular Orbital Theory*; Wiley: New York, 1986.

[109] Helgesen, M.; Søndergaard, R.; Krebs, F. C. *J. Mater. Chem.* **2010**, *20*, 36–60.

[110] Henckens, A.; Duyssens, I.; Lutsen, L.; Vanderzande, D.; Cleij, T. J. *Polymer* **2006**, *47*, 123–131.

[111] Hiorns, R. C.; de Bettignies, R.; Leroy, J.; Bailly, S.; Firon, M.; Sentein, C.; Khoukh, A.; Preud'homme, H.; Dagron-Lartigau, C. *Adv. Funct. Mater.* **2006**, *16*, 2263–2273.

[112] Hiromasa, S. Preparation of Vinylfurans and Purification by Steam Distillation JP 2010235545, 2010.

[113] Hoeben, F. J. M.; Jonkheijm, P.; Meijer, E. W.; Schenning, A. P. H. J. *Chem. Rev.* **2005**, *105*, 1491–1546.

[114] Höhne, S.; Spange, S. *Macromol. Chem. Phys.* **2003**, *204*, 841–849.

[115] Holdcroft, S. *J. Polym. Sci., Polym. Phys.* **1991**, *29*, 1585–1588.

[116] Hopkinson, P. E.; Staniec, P. A.; Pearson, A. J.; Dunbar, A. D. F.; Wang, T.; Ryan, A. J.; Jones, R. A. L.; Lidzey, D. G.; Donald, A. M. *Macromolecules* **2011**, *44*, 2908–2917.

[117] Horie, M.; Shen, I.-W.; Tuladhar, S. M.; Leventis, H.; Haque, S. A.; Nelson, J.; Saunders, B. R.; Turner, M. L. *Polymer* **2010**, *51*, 1541–1547.

[118] Huang, J.-H.; Chen, F.-C.; Chen, C.-L.; Huang, A. T.; Hsiao, Y.-S.; Teng, C.-M.; Yen, F.-W.; Chen, P.; Chu, C.-W. *Org. Electron.* **2011**, *12*, 1755–1762.

[119] Huitema, H. E. A.; Gelinck, G. H.; van der Putten, J. B. P. H.; Kuijk, K. E.; Hart, C. M.; Cantatore, E.; Herwig, P. T.; van Breemen, A. J. J. M.; de Leeuw, D. M. *Nature* **2001**, *414*, 599.

[120] Hultgren, V. M.; Mariotti, A. W. A.; Bond, A. M.; Wedd, A. G. *Anal. Chem.* **2002**, *74*, 3151–3156.

[121] Huo, L.; Chen, T. L.; Zhou, Y.; Hou, J.; Chen, H.-Y.; Yang, Y.; Li, Y. *Macromolecules* **2009**, *42*, 4377–4380.

[122] Huong Nguyen, L.; Günes, S.; Neugebauer, H.; Serdar Sariciftci, N.; Banishoeib, F.; Henckens, A.; Cleij, T.; Lutsen, L.; Vanderzande, D. *Sol. Energy Mater. Sol. Cells* **2006**, *90*, 2815–2828.

[123] Inganäs, O.; Salaneck, W. R.; Österholm, J. E.; Laakso, J. *Synth. Met.* **1988**, *22*, 395–406.

[124] Iovu, M. C.; Jeffries-El, M.; Sheina, E. E.; Cooper, J. R.; McCullough, R. D. *Polymer* **2005**, *46*, 8582–8586.

[125] Iovu, M. C.; Sheina, E. E.; Gil, R. R.; McCullough, R. D. *Macromolecules* **2005**, *38*, 8649–8656.

[126] Iraqi, A.; Barker, G. W. *J. Mater. Chem.* **1998**, *8*, 25–29.

[127] Ito, T.; Shirakawa, H.; Ikeda, S.; *J. Polym. Sci. Chem. Ed.* **1974**, *12*, 11.

[128] Jackson, R. B.; Carpenter, S. R.; Dahm, C. N.; McKnight, D. M.; Naiman, R. J.; Postel, S. L.; Running, S. W. *Ecol. Appl.* **2001**, *11*, 1027–1045.

[129] Janietz, S.; Bradley, D. D. C.; Grell, M.; Giebeler, C.; Inbasekaran, M.; Woo, E. P. *Appl. Phys. Lett.* **1998**, *73*, 2453–2455.

[130] Janssen, R. A. J.; Nelson, J. *Adv. Mater.* **2012**, *25*, 1847–1858.

[131] Jeffries-El, M.; Sauvé, G.; McCullough, R. D. *Macromolecules* **2005**, *38*, 10346–10352.

[132] Jen, K.-Y.; Maxfield, M.; Shacklette, L. W.; Elsenbaumer, R. L. *J. Chem. Soc., Chem. Commun.* **1987**, 309-311.

[133] Jenekhe, S. A.; Lu, L.; Alam, M. M. *Macromolecules* **2001**, *34*, 7315–7324.

[134] Jenekhe, S. A.; Yi, S. *Appl. Phys. Lett.* **2000**, *77*, 2635–2637.

[135] Jestin, I.; Frere, P.; Mercier, N.; Levillain, E.; Stievenard, D.; Roncali, J. *Journal of the American Chemical Society* **1998**, *120*, 8150–8158.

[136] Jiang, X. Q.; Patil, R.; Harima, Y.; Ohshita, J.; Kunai, A. *J. Phys. Chem. B* **2005**, *109*, 221–229.

[137] Jones, K. E.; Patel, N. G.; Levy, M. A.; Storeygard, A.; Balk, D.; Gittleman, J. L.; Daszak, P. *Nature* **2008**, *451*, 990–993.

[138] Jørgensen, M.; Norrman, K.; Krebs, F. C. *Sol. Energ. Mater. Sol. C.* **2008**, *92*, 686–714.

[139] Junkers, T.; Vandenbergh, J.; Adriaensens, P.; Lutsen, L.; Vanderzande, D. *Polym. Chem.* **2012**, *3*, 275–285.

[140] Kaltenbrunner, M.; White, M. S.; Glowacki, E. D.; Sekitani, T.; Someya, T.; Sariciftci, N. S.; Bauer, S. *Nature Commun.* **2012**, *3*, 1–7.

[141] Kappe, C. O.; Murphree, S. S.; Padwa, A. *Tetrahedron* **1997**, *53*, 14179–14233.

[142] Karinen, R.; Vilonen, K.; Niemela, M. *ChemSusChem* **2011**, *4*, 1002–1016.

[143] Katritzky, A. R.; Karelson, M.; Sild, S.; Krygowski, T. M.; Jug, K. *J. Org. Chem.* **1998**, *63*, 5228–5231.

[144] Katz, H. E.; Bao, Z.; Gilat, S. L. *Acc. Chem. Res.* **2001**, *34*, 359–369.

[145] Keitz, B. K.; Endo, K.; Patel, P. R.; Herbert, M. B.; Grubbs, R. H. *J. Am. Chem. Soc.* **2011**, *134*, 693–699.

[146] Keitz, B. K.; Fedorov, A.; Grubbs, R. H. *J. Am. Chem. Soc.* **2012**, *134*, 2040–2043.

[147] Khlyabich, P. P.; Burkhart, B.; Ng, C. F.; Thompson, B. C. *Macromolecules* **2011**, *44*, 5079–5084.

[148] Khor, E.; Ng, S. C.; Li, H. C.; Chai, S. *Heterocycles* **1991**, *32*, 1805–1812.

[149] Kim, J. Y.; Frisbie, C. D. *J. Phys. Chem. C* **2008**, *112*, 17726–17736.

[150] Kim, J. Y.; Qin, Y.; Stevens, D. M.; Kalihari, V.; Hillmyer, M. A.; Frisbie, C. D. *J. Phys. Chem. C* **2009**, *113*, 21928–21936.

[151] Kim, J. Y.; Qin, Y.; Stevens, D. M.; Ugurlu, O.; Kalihari, V.; Hillmyer, M. A.; Frisbie, C. D. *J. Phys. Chem. C* **2009**, *113*, 10790–10797.

[152] Kim, J.; Lim, B.; Baeg, K.-J.; Noh, Y.-Y.; Khim, D.; Jeong, H.-G.; Yun, J.-M.; Kim, D.-Y. *Chem. Mater.* **2011**, *23*, 4663–4665.

[153] Kim, Y.; Cook, S.; Choulis, S. A.; Nelson, J.; Durrant, J. R.; Bradley, D. D. C. *Chem. Mater.* **2004**, *16*, 4812–4818.

[154] Kim, Y.; Cook, S.; Tuladhar, S. M.; Choulis, S. A.; Nelson, J.; Durrant, J. R.; Bradley, D. D. C.; Giles, M.; McCulloch, I.; Ha, C.-S.; Ree, M. *Nat. Mater.* **2006**, *5*, 197–203.

[155] King, R. R.; Law, D. C.; Edmondson, C. M.; Fetzer, C. M.; Kinsey, G. S.; Yoon, H.; Sherif, R. A.; Karam, N. H. *Appl. Phys. Lett.* **2007**, *90*, 183516.

[156] Klavetter, F. L.; Grubbs, R. H. *J. Am. Chem. Soc.* **1988**, *110*, 7807–7813.

[157] Kline, R. J.; McGehee, M. D.; Kadnikova, E. N.; Liu, J.; Fréchet, J. M. J.; Toney, M. F. *Macromolecules* **2005**, *38*, 3312–3319.

[158] Kline, R. J.; McGehee, M. D.; Kadnikova, E. N.; Liu, J.; Fréchet, J. M. J. *Adv. Mater.* **2003**, *15*, 1519–1522.

[159] Ko, S.; Hoke, E. T.; Pandey, L.; Hong, S.; Mondal, R.; Risko, C.; Yi, Y.; Noriega, R.; McGehee, M. D.; Brédas, J.-L.; Salleo, A.; Bao, Z. *J. Am. Chem. Soc.* **2012**, *134*, 5222–5232.

[160] Kobayashi, S.; Pitet, L. M.; Hillmyer, M. A. *J. Am. Chem. Soc.* **2011**, *133*, 5794–5797.

[161] Kobayashi, T. *Pure Appl. Chem.* **1995**, *67*, 387–400.

[162] Koch, N. *ChemPhysChem* **2007**, *8*, 1438–1455.

[163] Kokubo, H.; Sato, T.; Yamamoto, T. *Macromolecules* **2006**, *39*, 3959–3963.

[164] Kong, H.; Chung, D. S.; Kang, I.-N.; Lim, E.; Jung, Y. K.; Park, J.-H.; Park, C. E.; Shim, H.-K. *Bull. Korean Chem. Soc.* **2007**, *28*, 1945–1950.

[165] Kopelman, P. G. *Nature* **2000**, *404*, 635–643.

[166] Kossmehl, G.; Härtel, M.; Manecke, G. *Makromolekul. Chem.* **1970**, *131*, 15–54.

[167] Kreyenschmidt, M.; Klaerner, G.; Fuhrer, T.; Ashenhurst, J.; Karg, S.; Chen, W. D.; Lee, V. Y.; Scott, J. C.; Miller, R. D. *Macromolecules* **1998**, *31*, 1099–1103.

[168] Kroon, R.; Lenes, M.; Hummelen, J. C.; Blom, P. W. M.; de Boer, B. *Polym. Rev.* **2008**, *48*, 531–582.

[169] Kumar, P.; Chand, S. *Prog. Photovoltaics* **2012**, *20*, 377–415.

[170] Lam, J. W. Y.; Tang, B. Z. *Acc. Chem. Res.* **2005**, *38*, 745–754.

[171] Lee, J.-I.; Klaerner, G.; Davey, M. H.; Miller, R. D. *Synth. Met.* **1999**, *102*, 1087–1088.

[172] Lee, S. K.; Cho, S.; Tong, M.; Hwa Seo, J.; Heeger, A. J. *J. Polym. Sci., Polym. Chem.* **2011**, *49*, 1821–1829.

[173] Lee, Y.-B.; Shim, H.-K.; Ko, S.-W. *Macromol. Rapid Comm.* **2003**, *24*, 522–526.

[174] Lehman Jr., S. E.; Wagener, K. B. In *Handbook of Metathesis*; Grubbs, R. H., Ed., Wiley-VCH Verlag GmbH & Co.: Weinheim, 2003; Vol. 3.

[175] Lehman, S. E.; Wagener, K. B. *Macromolecules* **2002**, *35*, 48–53.

[176] Lewis, N. S. *MRS Bull.* **2007**, *32*, 808–820.

[177] Lewis, N. S.; Nocera, D. G. *Proc. Natl. Acad. Sci. USA* **2006**, *103*, 15729–15735.

[178] Li, G.; Zhu, R.; Yang, Y. *Nat. Photonics* **2012**, *6*, 153–161.

[179] Li, J. L.; Dierschke, F.; Wu, J. S.; Grimsdale, A. C.; Müllen, K. *J. Mater. Chem.* **2006**, *16*, 96–100.

[180] Li, J.; Ong, K.-H.; Sonar, P.; Lim, S.-L.; Ng, G.-M.; Wong, H.-K.; Tan, H.-S.; Chen, Z.-K. *Polym. Chem.* **2013**, *4*, 804–811.

[181] Li, Y. *Acc. Chem. Res.* **2012**, *45*, 723–733.

[182] Li, Y.; Vamvounis, G.; Holdcroft, S. *Macromolecules* **2002**, *35*, 6900–6906.

[183] Liang, Y.; Xu, Z.; Xia, J.; Tsai, S.-T.; Wu, Y.; Li, G.; Ray, C.; Yu, L. *Adv. Mater.* **2010**, *22*, E135-E138.

[184] Lim, J.-C.; Suzuki, M.; Saegusa, T. *Polym. Bull.* **1993**, *31*, 651–658.

[185] Liu, J.; Loewe, R. S.; McCullough, R. D. *Macromolecules* **1999**, *32*, 5777–5785.

[186] Liu, J.; Sheina, E.; Kowalewski, T.; McCullough, R. D. *Angew. Chem. Int. Ed.* **2002**, *41*, 329–332.

[187] Locke, J. R.; McNeil, A. J. *Macromolecules* **2010**, *43*, 8709–8710.

[188] Loewe, R. S.; Khersonsky, S. M.; McCullough, R. D. *Adv. Mater.* **1999**, *11*, 250–253.

[189] Loewe, R. S.; McCullough, R. D. *Chem. Mater.* **2000**, *12*, 3214–3221.

[190] Logothetidis, S. *Mater. Sci. Eng. B-Adv.* **2008**, *152*, 96–104.

[191] Lombardo, L. *Tetrahedron Lett.* **1982**, *23*, 4293–4296.

[192] Louwet, F.; Vanderzande, D.; Gelan, J. *Synth. Met.* **1992**, *52*, 125–130.

[193] Love, J. A.; Morgan, J. P.; Trnka, T. M.; Grubbs, R. H. *Angew. Chem. Int. Ed.* **2002**, *41*, 4035–4037.

[194] Lowe, J.; Bartels, C.; Holdcroft, S. *Can. Journ. Chem.* **1998**, *76*, 1524–1529.

[195] Ltaief, A.; Bouazizi, A.; Davenas, J. *Materials* **2009**, *2*, 710–718.

[196] Lu, C.; Wu, H. C.; Chiu, Y. C.; Lee, W. Y.; Chen, W. C. *Macromolecules* **2012**, *45*, 3047–3056

[197] Ma, W.; Kim, J. Y.; Lee, K.; Heeger, A. J. *Macromol. Rapid Commun.* **2007**, *28*, 1776–1780.

[198] Ma, W.; Yang, C.; Gong, X.; Lee, K.; Heeger, A. J. *Adv. Funct. Mater.* **2005**, *15*, 1617–1622.

[199] Ma, W.; Yang, C.; Heeger, A. J. *Adv. Mater.* **2007**, *19*, 1387–1390.

[200] MacDiarmid, A. G. *Angew. Chem. Int. Ed.* **2001**, *40*, 2581–2590.

[201] Malmqvist, B.; Rundle, S. *Environ. Conserv.* **2002**, *29*, 134–153.

[202] Mamman, A. S.; Lee, J.-M.; Kim, Y.-C.; Hwang, I. T.; Park, N.-J.; Hwang, Y. K.; Chang, J.-S.; Hwang, J.-S. *Biofuel. Bioprod. Bior.* **2008**, *2*, 438–454.

[203] Manceau, M.; Angmo, D.; Jørgensen, M.; Krebs, F. C. *Organic Electronics* **2011**, *12*, 566–574.

[204] Massip, S.; Oberhumer, P. M.; Tu, G.; Albert-Seifried, S.; Huck, W. T. S.; Friend, R. H.; Greenham, N. C. *J. Phys. Chem. C* **2011**, *115*, 25046–25055.

[205] Mathers, R. T. *J. Polym. Sci., Polym. Chem.* **2012**, *50*, 1–15.

[206] McCullough, R. D.; Lowe, R. D. *J. Chem. Soc. Chem. Comm.* **1992**, 70–72.

[207] McCullough, R. D.; Lowe, R. D.; Jayaraman, M.; Anderson, D. L. *J. Org. Chem.* **1993**, *58*, 904–912.

[208] McQuade, D. T.; Pullen, A. E.; Swager, T. M. *Chem. Rev.* **2000**, *100*, 2537–2574.

[209] Meek, S. J.; O'Brien, R. V.; Llaveria, J.; Schrock, R. R.; Hoveyda, A. H. *Nature* **2011**, *471*, 461–466.

[210] Mercier, L. G.; Leclerc, M. *Acc. Chem. Res.* **2013**, DOI: 10.1021/ar3003305.

[211] Métivaud, V.; Lefèvre, A.; Ventolà, L.; Négrier, P.; Moreno, E.; Calvet, T.; Mondieig, D.; Cuevas-Diarte, M. A. *Chem. Mater.* **2005**, *17*, 3302–3310.

[212] Miao, Y.-J.; Bazan, G. C. *Macromolecules* **1997**, *30*, 7414–7418.

[213] Miller, N. C.; Gysel, R.; Miller, C. E.; Verploegen, E.; Beiley, Z.; Heeney, M.; McCulloch, I.; Bao, Z. N.; Toney, M. F.; McGehee, M. D. *J. Polym. Sci., Polym. Phys.* **2011**, *49*, 499–503.

[214] Mishra, A.; Bäuerle, P. *Angew. Chem. Int. Ed.* **2012**, *51*, 2020–2067.

[215] Mitschke, U.; Bäuerle, P. *J. Mater. Chem.* **2000**, *10*, 1471–1507.

[216] Moet, D. J. D.; Lenes, M.; Kotlarski, J. D.; Veenstra, S. C.; Sweelssen, J.; Koetse, M. M.; de Boer, B.; Blom, P. W. M. *Org. Electron.* **2009**, *10*, 1275–1281.

[217] Mohanty, A. K.; Misra, M.; Hinrichsen, G. *Macromol. Mater. Eng.* **2000**, *276/277*, 1–24.

[218] Moughton, A. O.; Sagawa, T.; Gramlich, W. M.; Seo, M.; Lodge, T. P.; Hillmyer, M. A. *Polym. Chem.* **2013**, *4*, 166–173.

[219] Müller, C.; Bergqvist, J.; Vandewal, K.; Tvingstedt, K. Anselmo, A. S.; Magnusson, R.; Alonso, M. I.; Moons, E.; Arwin, H.; Campoy-Quiles, M.; Inganäs, O. *J. Mater. Chem.* **2011**, *21*, 10676–10684.

[220] Müller, C.; Ferenczi, T. A. M.; Campoy-Quiles, M.; Frost, J. M.; Bradley, D. D. C.; Smith, P.; Stingelin-Stutzmann, N.; Nelson, J. *Adv. Mater.* **2008**, *20*, 3510–3515.

[221] Müller, C.; Wang, E.; Andersson, L. M.; Tvingstedt, K.; Zhou, Y.; Andersson, M. R.; Inganäs, O. *Adv. Funct. Mater.* **2010**, *20*, 2124–2131.

[222] Natta, G.; Mazzanti, G.; Corradini, P. *Atti. Acad. Nazl. Lincei, Rend. Classe Sci. Fis. Mat. Nat.* **1958**, *25*, 3.

[223] Nguyen, L. H.; Günes, S.; Neugebauer, H.; Sariciftci, N. S; Banishoeib, F.; Henckens, A.; Cleij, T.; Lutsen, L.; Vanderzande, D. *Sol. Energ. Mater. Sol. C.* **2006**, *90*, 2815–2828.

[224] Nguyen, L. H.; Hoppe, H.; Erb, T.; Günes, S.; Gobsch, G.; Sariciftci, N. S. *Adv. Funct. Mater.* **2007**, *17*, 1071–1078.

[225] Nielsen, C. B.; Ashraf, R. S.; Schroeder, B. C.; D'Angelo, P.; Watkins, S. E.; Song, K.; Anthopoulos, T. D.; McCulloch, I. *Chem. Commun.* **2012**, *48*, 5832–5834.

[226] Nomura, K.; Miyamoto, Y.; Morimoto, H.; Geerts, Y. *J. Polym. Sci., Polym. Chem.* **2005**, *43*, 6166–6177.

[227] Nomura, K.; Morimoto, H.; Imanishi, Y.; Ramhani, Z.; Geerts, Y. *J. Polym. Sci., Polym. Chem.* **2001**, *39*, 2463–2470.

[228] Normile, D. *Science* **2012**, *336*, 1220–1221.

[229] Nunzi, J. M. *CR Phys.* **2002**, *3*, 523–542.

[230] O'Regan, B.; Grätzel, M. *Nature* **1991**, *353*, 737–740.

[231] Occhipinti, G.; Hansen, F. R.; Törnroos, K. W.; Jensen, V. R. *J. Am. Chem. Soc.* **2013**, *135*, 3331–3334.

[232] Odian, G. *Principles of Polymerization,* 4th ed.; John Wiley & Sons, Inc.: Hoboken, NJ, 2004.

[233] Ohkita, H.; Cook, S.; Astuti, Y.; Duffy, W.; Tierney, S.; Zhang, W.; Heeney, M.; McCulloch, I.; Nelson, J.; Bradley, D. D. C.; Durrant, J. R. *J. Am. Chem. Soc.* **2008**, *130*, 3030–3042.

[234] Okada, M. *Prog. Polym. Sci.* **2002**, *27*, 87–133.

[235] Olejnik, E.; Pandit, B.; Basel, T.; Lafalce, E.; Sheng, C.-X.; Zhang, C.; Jiang, X.; Vardeny, Z. *Phys. Rev. B* **2012**, *85*, 235201.

[236] Onoda, M.; Morita, S.; Iwasa, T.; Nakayama, H.; Yoshino, K. *J. Chem. Phys.* **1991**, *95*, 8584–8591.

[237] Opper, K.; Wagener, K. *J. Polym. Sci., Polym. Chem.* **2011**, *49*, 821–831.

[238] Osaka, I.; McCullough, R. D. *Acc. Chem. Res.* **2008**, *41*, 1202–1214.

[239] Padinger, F.; Rittberger, R. S.; Sariciftci, N. S. *Adv. Funct. Mater.* **2003**, *13*, 85–88.

[240] Park, K.; Levon, K. *Macromolecules* **1997**, *30*, 3175–3183.

[241] Park, S. H.; Roy, A.; Beaupré, S.; Cho, S.; Coates, N.; Moon, J. S.; Moses, D.; Leclerc, M.; Lee, K.; Heeger, A. J. *Nat. Photonics* **2009**, *3*, 297–302.

[242] Parker, I. D. *J. Appl. Phys.* **1994**, *75*, 1656–1666.

[243] Parkin, D. M.; Bray, F.; Ferlay, J.; Pisani, P. *CA-Cancer J. Clin.* **2005**, *55*, 74–108.

[245] Parlak, E. A. *Sol. Energ. Mater. Sol. C.* **2012**, *100*, 174–184.

[246] Patel, J.; Mujcinovic, S.; Jackson, W. R.; Robinson, A. J.; Serelis, A. K.; Such, C. *Green Chem.* **2006**, *8*, 450–454.

[247] Paulsen, B. D.; Frisbie, C. D. *J. Phys. Chem. C* **2012**, *116*, 3132–3141.

[248] Pavia, D. L.; Lampman, G. M.; Kriz, G. S. *Introduction to Spectroscopy: A Guide for Students of Organic Chemistry*; Brooks/Cole: United States, 2001; 39–40.

[249] Peet, J.; Heeger, A. J.; Bazan, G. C. *Acc. Chem. Res.* **2009**, *42*, 1700–1708.

[250] Peierls, R. E. *Quantum Theory of Solids*; Oxford University Press: London, 1955.

[251] Peumans, P.; Bulovic, V.; Forrest, S. R. *Appl. Phys. Lett.* **2000**, *76*, 2650–2652.

[252] Photovoltaic Research: Measurements & Characterization. National Renewable Energy Laboratory. www.nrel.gov/pv/measurements/current_vs_voltage.html (accessed May 2013).

[253] Pivrikas, A.; Neugebauer, H.; Sariciftci, N. S. *Sol. Energy* **2011**, *85*, 1226–1237.

[254] Pretsch, E.; Bühlmann, P.; Affolter, C. *Structure Determination of Organic Compounds: Tables of Spectral Data*; Springer: Heidelberg, 2000; 248–251.

[255] Price, S. C.; Stuart, A. C.; Yang, L.; Zhou, H.; You, W. *J. Am. Chem. Soc.* **2011**, *133*, 4625–4631.

[256] Qin, Y.; Hillmyer, M. A. *Macromolecules* **2009**, *42*, 6429–6432.

[257] Radano, C. P.; Scherman, O. A.; Stingelin-Stutzmann, N.; Müller, C.; Breiby, D. W.; Smith, P.; Janssen, R. A. J.; Meijer, E. W. *J. Am. Chem. Soc.* **2005**, *127*, 12502–12503.

[258] Ragauskas, A. J.; Williams, C. K.; Davison, B. H.; Britovsek, G.; Cairney, J.; Eckert, C. A.; Frederick Jr., W. J.; Hallett, J. P.; Leak, D. J.; Liotta, C. L.;

Mielenz, J. R.; Murphy, R.; Templer, R.; Tschaplinski, T. *Science* **2006**, *311*, 484–489.

[259] Roncali, J. *Acc. Chem. Res.* **2000**, *33*, 147–156.

[260] Roncali, J. *Acc. Chem. Res.* **2009**, *42*, 1719–1730.

[261] Roncali, J. *Chem. Rev.* **1992**, *92*, 711–738.

[262] Roncali, J. *Chem. Rev.* **1997**, *97*, 173–206.

[263] Roncali, J. *Macromol. Rapid Comm.* **2007**, *28*, 1761–1775.

[264] Rostalski, J.; Meissner, D. *Sol. Energ. Mater. Sol. C.* **2000**, *61*, 87–95.

[265] Rudenko, A. E.; Wiley, C. A.; Stone, S. M.; Tannaci, J. F.; Thompson, B. C. *J. Polym. Sci., Polym. Chem.* **2012**, *50*, 3691–3697.

[266] Sakamoto, J.; Rehahn, M.; Wegner, G.; Schlüter, A. D. *Macromol. Rapid. Commun.* **2009**, *30*, 653–687.

[267] Salaneck, W. R.; Inganäs, O.; Themans, B.; Nilsson, J. O.; Sjögren, B.; H Österholm, J. E.; Brédas, J. L.; Svensson, S. *J. Chem. Phys.* **1988**, *89*, 4613–4619.

[268] Sariciftci, N. S.; Braun, D.; Zhang, C.; Srdanov, V. I.; Heeger, A. J.; Stucky, G.; Wudl, F. *Appl. Phys. Lett.* **1993**, *62*, 585–587.

[269] Scharber, S. C.; Muhlbacher, D.; Koppe, M.; Denk, P.; Waldauf, C.; Heeger, A. J.; Brabec, C. J. *Adv. Mater.* **2006**, *18*, 789–794.

[270] Scheffran, J.; Brzoska, M.; Kominek, J.; Link, P. M.; Schilling, J. *Science* **2012**, *336*, 869–871.

[271] Scherman, O. A.; Grubbs, R. H. *Synth. Met.* **2002**, *124*, 431–434.

[272] Scherman, O. A.; Rutenberg, I. M.; Grubbs, R. H. *J. Am. Chem. Soc.* **2003**, *125*, 8515–8522.

[273] Schilinsky, P.; Asawapirom, U.; Scherf, U.; Biele, M.; Brabec, C. J. *Chem. Mater.* **2005**, *17*, 2175–2180.

[274] Scholl, M.; Ding, S.; Lee, C. W.; Grubbs, R. H. *Org. Lett.* **1999**, *1*, 953–956.

[275] Segalman, R. A.; McCulloch, B.; Kirmayer, S.; Urban, J. J. *Macromolecules* **2009**, *42*, 9205–9216.

[276] Segura, J. L. *Acta Polym.* **1998**, *49*, 319–344.

[277] Seo, M.; Hillmyer, M. A. *Science* **2012**, *336*, 1422–1425.

[278] Service, R. F. *Science* **2011**, *332*, 293.

[279] Shaheen, S. E.; Ginley, D. S.; Jabbour, G. E. *MRS Bull.* **2005**, *30*, 10–19.

[280] Shaheen, S. E.; Radspinner, R.; Peyghambarian, N.; Jabbour, G. E. *Appl. Phys. Lett.* **2001**, *79*, 2996–2998.

[281] Shaheen, S.; Brabec, C.; Sariciftci, N. S.; Padinger, F.; Fromherz, T.; Hummelen, J. C. *Appl. Phys. Lett.* **2001**, *78*, 841–843.

[282] Shi, Q.; Fan, H.; Liu, Y.; Chen, J.; Ma, L.; Hu, W.; Shuai, Z.; Li, Y.; Zhan, X. *Macromolecules* **2011**, *44*, 4230–4240.

[283] Shiddiky, M. J. A.; Torriero, A. A. J.; Zhao, C.; Burgar, I.; Kennedy, G.; Bond, A. M. *J. Am. Chem. Soc.* **2009**, *131*, 7976–7989.

[284] Sirringhaus, H.; Brown, P. J.; Friend, R. H.; Nielsen, M. M.; Bechgaard, K.; Langeveld-Voss, B. M. W.; Spiering, A. J. H.; Janssen, R. A. J.; Meijer, E. W.; Herwig, P.; de Leeuw, D. M. *Nature* **1999**, *401*, 685–688.

[285] Small, C. E.; Chen, S.; Subbiah, J.; Amb, C. M.; Tsang, S.-W.; Lai, T.-H.; Reynolds, J. R.; So, F. *Nat. Photonics* **2011**, 1-6.

[286] Smith, A. P.; Smith, R. R.; Taylor, B. E.; Durstock, M. F. *Chem. Mater.* **2004**, *16*, 4687–4692.

[287] Solar Energy Technologies Program. National Renewable Energy Laboratory. http://www.nrel.gov/docs/fy04osti/33875.pdf (accessed May 2013).

[288] Sommer-Larsen, P.; Jørgensen, M.; Søndergaard, R. R.; Hösel, M.; Krebs, F. C. *Energy Technol.* **2013**, *1*, 15–19.

[289] Son, S.; Dodabalapur, A.; Lovinger, A. J.; Galvin, M. E. *Science* **1995**, *269*, 376–378.

[290] Song, C. E.; Kang, I.-N.; Kim, J.-H.; Hwang, D.-H.; Lee, J.-C.; Ahn, T.; Shin, W. S.; Moon, S.-J.; Lee, S. K. *J. Polym. Sci., Polym. Chem.* **2013**, *15*, 1512–1519.

[291] Song, I. Y.; Kim, J.; Im, M. J.; Moon, B. J.; Park, T. *Macromolecules* **2012**, *45*, 5058–5068.

[292] Speros, J. C.; Paulsen, B. D.; Slowinski, B. S.; Frisbie, C. D.; Hillmyer, M. A. *ACS Macro Lett.* **2012**, *1*, 986-990.

[293] Speros, J. C.; Paulsen, B. D.; White, S. P.; Wu, Y.; Jackson, E. A.; Slowinski, B. S.; Frisbie, C. D.; Hillmyer, M. A. *Macromolecules* **2012**, *45*, 2190-2199.

[294] Spring, A. M.; Yu, C.-Y.; Horie, M.; Turner, M. L. *Chem. Commun.* **2009**, 2676–2678.

[295] Stevens, D. M.; Speros, J. C.; Hillmyer, M. A.; Frisbie, C. D. *J. Phys. Chem. C* **2011**, *115*, 20806–20816.

[296] Stuart, A. C.; Tumbleston, J. R.; Zhou, H. X.; Li, W. T.; Liu, S. B.; Ade, H.; You, W. *J. Am. Chem. Soc.* **2013**, *135*, 1806–1815.

[297] Stübinger, T.; Brütting, W. *J. Appl. Phys.* **2001**, *90*, 3632–3641.

[298] Sugimoto, R.; Taketa, S.; Gu, H. B.; Yoshino, K. *Chem. Express* **1986**, *1*, 635–638.

[299] Sun, S.-S.; Sariciftci, N. S. *Organic Photovoltaics*; Taylor & Francis: Boca Raton, FL, 2005.

[300] Sun, Y.; Welch, G. C.; Leong, W. L.; Takacs, C. J.; Bazan, G. C.; Heeger, A. J. *Nat. Mater.* **2011**, *11*, 44–48.

[301] Sworen, J. C.; Smith, J. A.; Wagener, K. B.; Baugh, L. S.; Rucker, S. P. *J. Am. Chem. Soc.* **2003**, *125*, 2228–2240.

[302] Tang, C. W. *Appl. Phys. Lett.* **1986**, *48*, 183–185.

[303] Tao, D.; Wagener, K. B. *Macromolecules* **1994**, *27*, 1281–1283.

[304] The Nobel Prize in Chemistry 2000. Nobel Prize site. www.nobelprize.org/nobel_prizes/chemistry/laureates/2000/ (accessed May 2013).

[305] Theander, M.; Inganäs, O.; Mammo, W.; Olinga, T.; Svensson, M.; Andersson, M. R. *J. Phys. Chem. B* **1999**, *103*, 7771–7780.

[306] Theander, M.; Yartsev, A.; Zigmantas, D.; Sundström, V.; Mammo, W.; Andersson, M. R.; Inganäs, O. *Phys. Rev. B* **2000**, *61*, 12957–12963.

[307] Thompson, B. C.; Fréchet, J. M. J. *Angew. Chem. Int. Ed.* **2008**, *47*, 58–77.

[308] Tilman, D.; Cassman, K. G.; Matson, P. A.; Naylor, R.; Polasky, S. *Nature* **2002**, *418*, 671–677.

[309] Tong, M.; Cho, S.; Rogers, J. T.; Schmidt, K.; Hsu, B. B. Y.; Moses, D.; Coffin, R. C.; Kramer, E. J.; Bazan, G. C.; Heeger, A. J. *Adv. Funct. Mater.* **2010**, *20*, 3959–3965.

[310] Toyoshima, R.; Akagi, K.; Shirakawa, H. *Synth. Met.* **1997**, *84*, 431–432.

[311] Trnka, T. M.; Grubbs, R. H. *Acc. Chem. Res.* **2001**, *34*, 18–29.

[312] Tsuie, B.; Wagener, K. B.; Reynolds, J. R. *Polym. Preprints* **1999**, *40*, 790.

[313] Tsuzuki, T.; Shirota, Y.; Rostalski, J. K.; Meissner, D. *Sol. Energ. Mat. Sol. C.* **2000**, *61*, 1–8.

[314] Tvingstedt, K.; Vandewal, K.; Gadisa, A.; Zhang, F.; Manca, J.; Inganäs, O. *J. Am. Chem. Soc.* **2009**, *131*, 11819–11824.

[315] van der Poll, T. S.; Love, J. A.; Nguyen, T.-Q.; Bazan, G. C. *Adv. Mater.* **2012**, *24*, 3646–3649.

[316] Veldman, D.; İpek, Ö.; Meskers, S. C. J.; Sweelssen, J.; Koetse, M. M.; Veenstra, S. C.; Kroon, J. M.; van Bavel, S. S.; Loos, J.; Janssen, R. A. J. *J. Am. Chem. Soc.* **2008**, *130*, 7721–7735.

[317] Veldman, D.; Meskers, S. C. J.; Janssen, R. A. J. *Adv. Funct. Mater.* **2009**, *19*, 1939–1948.

[318] Vennestrøm, P. N. R.; Osmundsen, C. M.; Christensen, C. H.; Taarning, E. *Angew. Chem., Int. Ed.* **2011**, *50*, 2–10.

[319] Verploegen, E.; Mondal, R.; Bettinger, C. J.; Sok, S.; Toney, M. F.; Bao, Z. A. *Adv. Funct. Mater.* **2010**, *20*, 3519–3529.

[320] Wagener, K. B.; Boncella, J. M.; Nel, J. G. *Macromolecules* **1991**, *24*, 2649–2657.

[321] Wagener, K.; Brzezinska, K.; Anderson, J. D.; Dilocker, S. *J. Polym. Sci., Polym. Chem.* **1997**, *35*, 3441–3449.

[322] Wan, M.; Wu, W.; Sang, G.; Zou, Y.; Liu, Y.; Li, Y. *J. Polym. Sci., Polym. Chem.* **2009**, *47*, 4028–4036.

[323] Wang, W.; Xu, J.; Lai, Y.-H.; Wang, F. *Macromolecules* **2004**, *37*, 3546–3553.

[324] Weerts, P. A.; van der Loos, J. L. M.; German, A. L. *Makromol. Chem.* **1990**, *191*, 2615–2630.

[325] Wen, S.; Pei, J.; Li, P.; Zhou, Y.; Cheng, W.; Dong, Q.; Li, Z.; Tian, W. *J. Polym. Sci., Polym. Chem.* **2011**, *49*, 2715–2724.

[326] Wessling, R. A. *J. Polym. Sci., Polym. Sym.* **1985**, 55–66.

[327] Wienk, M. M.; Kroon, J. M.; Verhees, W. J. H.; Knol, J.; Hummelen, J. C.; van Hal, P. A.; Janssen, R. A. J. *Angew. Chem. Int. Ed.* **2003**, *42*, 3371–3375.

[328] Williams, C. K.; Hillmyer, M. A. *Polym. Rev.* **2008**, *48*, 1–10.

[329] Williams, R. *J. Chem. Phys.* **1960**, *32*, 1505–1514.

[330] Winder, C.; Sariciftci, N. S. *J. Mater. Chem.* **2004**, *14*, 1077–1086.

[331] Winograd, I. J.; Roseboom Jr., E. H. *Science* **2008**, *320*, 1426–1427.

[332] Wong, M.; Hollinger, J.; Kozycz, L. M.; McCormick, T. M.; Lu, Y.; Burns, D. C.; Seferos, D. S. *ACS Macro Lett.* **2012**, *1*, 1266–1269.

[333] Wu, D.; Xu, F.; Sun, B.; Fu, R.; He, H.; Matyjaszewski, K. *Chem. Rev.* **2012**, *112*, 3959–4015.

[334] Wudl, F. *Acc. Chem. Res.* **1992**, *25*, 157–161.

[335] Xu, B.; Holdcroft, S. *Macromolecules* **1993**, *26*, 4457–4460.

[336] Xu, J.; Ng, S. C.; Chan, H. S. O. *Tetrahedron Lett.* **2001**, *42*, 5327–5329.

[337] Xue, J.; Uchida, S.; Rand, B. P.; Forrest, S. R. *Appl. Phys. Lett.* **2004**, *85*, 5757–5759.

[338] Xue, J.; Uchida, S.; Rand, B. P.; Forrest, S. R. *Appl. Phys. Lett.* **2004**, *84*, 3013–3015.

[339] Yamada, S.; Tokito, S.; Tsutsui, T.; Saito, S. *J. Chem. Soc., Chem. Commun.* **1987**, 1448–1449.

[340] Yamamoto, N.; Ito, R.; Geerts, Y.; Nomura, K. *Macromolecules* **2009**, *42*, 5104–5111.

[341] Yamamoto, T.; Kumagai, A.; Kokubo, H.; Nakamura, Y. *Bull. Chem. Soc. Jpn.* **2011**, *84*, 1291–1293.

[342] Yamamoto, T.; Sanechika, K.; Yamamoto, A. *J. Polym. Sci., Polym. Lett.* **1980**, *18*, 9–12.

[343] Yang, X.; Loos, J. *Macromolecules* **2007**, *40*, 1353–1362.

[344] Yin, J.; Ge, Z. S.; Liu, H.; Liu, S. *J. Polym. Sci., Polym. Chem* **2009**, *47*, 2608–2619.

[345] Yin, L.; Dalsin, M. C.; Sizovs, A.; Reineke, T. M.; Hillmyer, M. A. *Macromolecules* **2012**, *45*, 4322–4332.

[346] Yu, C.-Y.; Horie, M.; Spring, A. M.; Tremel, K.; Turner, M. L. *Macromolecules* **2010**, *43*, 222–232.

[347] Yu, C.-Y.; Kingsley, J. W.; Lidzey, D. G.; Turner, M. L. *Macromol. Rapid Comm.* **2009**, *30*, 1889–1892.

[348] Yu, C.-Y.; Turner, M. L. *Angew. Chem. Int. Ed.* **2006**, *45*, 7797–7800.

[349] Yu, G.; Gao, J.; Hummelen, J. C.; Wudl, F.; Heeger, A. J. *Science* **1995**, *270*, 1789–1791.

[350] Zaumseil, J.; Sirringhaus, H. *Chem. Rev.* **2007**, *107*, 1296–1323.

[351] Zen, A.; Pflaum, J.; Hirschmann, S.; Zhuang, W.; Jaiser, F.; Asawapirom, U.; Rabe, J. P.; Scherf, U.; Neher, D. *Adv. Funct. Mater.* **2004**, *14*, 757–764.

[352] Zhang, C.; Sun, J.; Li, R.; Sun, S.-S.; Lafalce, E.; Jiang, X. *Macromolecules* **2011**, *44*, 6389–6396.

[353] Zhang, J.; Matta, M. E.; Martinez, H.; Hillmyer, M. A. *Macromolecules* **2013**, *46*, 2535–2543.

[354] Zhang, W.; Kraft, S.; Moore, J. S. *J. Am. Chem. Soc.* **2004**, *126*, 329–335.

[355] Zhang, X.; Richter, L. J.; DeLongchamp, D. M.; Kline, R. J.; Hammond, M. R.; McCulloch, I.; Heeney, M.; Ashraf, R. S.; Smith, J. N.; Anthopoulos, T. D.; Schroeder, B.; Geerts, Y. H.; Fischer, D. A.; Toney, M. F. *J. Am. Chem. Soc.* **2011**, *133*, 15073–15084.

[356] Zhang, Z.-G.; Min, J.; Zhang, S.; Zhang, J.; Zhang, M.; Li, Y. *Chem. Commun.* **2011**, *47*, 9474–9476.

[357] Zhao, J.; Bertho, S.; Vandenbergh, J.; Van Assche, G.; Manca, J.; Vanderzande, D.; Yin, X.; Shi, J.; Cleij, T.; Lutsen, L.; Van Mele, B. *Phys. Chem. Chem. Phys.* **2011**, *13*, 12285–12292.

[358] Zhao, J.; Swinnen, A.; Van Assche, G.; Manca, J.; Vanderzande, D.; Mele, B. V. *J. Phys. Chem. B* **2009**, *113*, 1587–1591.

[359] Zhao, Y.; Truhlar, D. G. *Acc. Chem. Res.* **2008**, *41*, 157-167.

[360] Zhao, Y.; Truhlar, D. G. *J. Chem. Theory Comput.* **2009**, *5*, 324–333.

[361] Zhao, Y.; Truhlar, D. G. *Theor. Chem. Acc.* **2008**, *120*, 215–241.

[362] Zhou, E.; Tan, Z.; Yang, Y.; Huo, L.; Zou, Y.; Yang, C.; Li, Y. *Macromolecules* **2007**, *40*, 1831–1837.

[363] Zhou, H. X.; Yang, L. Q.; Xiao, S. Q.; Liu, S. B.; You, W. *Macromolecules* **2010**, *43*, 811–820.

[364] Zhou, H.; Yang, L.; Stuart, A. C.; Price, S. C.; Liu, S.; You, W. *Angew. Chem. Int. Ed.* **2011**, *50*, 2995–2998.

[365] Zhou, H.; Zhang, Y.; Seifter, J.; Collins, S. D.; Luo, C.; Bazan, G. C.; Nguyen, T.-Q.; Heeger, A. J. *Adv. Mater.* **2013**, *25*, 1646-1652.

Appendix A

Characterization

This appendix summarizes the common techniques employed for the characterization of materials discussed in this dissertation.

A.1 Nuclear Magnetic Resonance Spectroscopy

Nuclear magnetic resonance (NMR) spectra were obtained in boro-silicate glass tubes (Wilmad-LabGlass 528-PP or 507-PP) with the sample at a concentration of 5–30 mg mL^{-1} in deuterated solvent. Solvents were chosen to ensure homogeneous solutions and all spectra were collected at room temperature.

All NMR spectra were collected on one of three instruments: Varian Inova 300 MHz, Varian Inova 500 MHz (^{13}C 125 MHz), or Bruker Avance III 500 MHz (^{13}C 125 MHz). Spectral resonances were referenced to either trace hydrogenous signals from the deuterated solvent or to an internal standard (Table A.1).

Table A.1
Characteristics Deuterated NMR Solvents

Solvent/Standard	^{1}H signal (ppm)	^{13}C signal (ppm)
chloroform ($CDCl_3$)	7.26	77.36
dimethylsulfoxide (DMSO)	2.50	39.52
tetramethylsilane (TMS)[a]	0.00	–

[a]Used as an internal standard in $CDCl_3$

A.2 Infrared Spectroscopy

Infrared (IR) spectroscopy was performed on pristine samples with a Bruker Alpha-P Platinum FT-IR spectrometer equipped with a platinum attenuated total reflectance (ATR) sampling module hosting a diamond crystal (single bounce). The software used for data collection and workup was OPUS 7.0.

A.3 Ultraviolet–Visible Spectroscopy

Ultraviolet–visible (UV–vis) spectroscopy was performed using a Spectronic Genesys 5 spectrometer over a wavelength range of 300–1000 nm. Solution and solid-state (film) absorption spectra were collected for each polymer. Solutions were prepared in chloroform (ca. 1×10^{-5} M, repeat unit basis) and measured in a 1 cm quartz cuvette. Polymer films were prepared by spin coating on glass microscope slides (10 mg mL^{-1} $CHCl_3$, 1500 rpm, 40 s) and were measured after solvent evaporation. Reference samples (solution = pure $CHCl_3$, film = clean glass slide) were used prior to analysis.

A.4 Elemental Analysis

Elemental analysis was performed by Atlantic Microlab, Inc. Samples were analyzed for carbon, hydrogen, oxygen, nitrogen, sulfur, and bromine content using combustion coupled with thermal conductivity detection. Samples were sent to:

6180 Atlantic Blvd. Suite M
Norcross, GA 30071
Tel. 770.242.0082
Fax. 770.242.0236

A.5 Mass Spectrometry

High resolution mass spectrometry (MS) was performed on a Finnigan MAT 95 mass spectrometer operating in electron impact (EI) mode. Samples were introduced

directly using a solid probe. Gas chromatography–mass spectrometry (GCMS) was performed on the same instrument. In this case samples were introduced and separated using a Hewlett-Packard Series II Model 5890 gas chromatograph. Samples were prepared in dichloromethane (ca. 20 mM) and introduced via microsyringe (ca. 1 μL). The typical ramp program applied involved heating from 50 to 300 °C at 15 °C min^{-1}.

A.6 Size-Exclusion Chromatography

Size-exclusion chromatography (SEC) was used to determine the relative sizes (i.e., molecular weights) of all soluble polymeric species. SEC measurements were performed on two separate instruments depending on polymer solubility and intended analysis.

The primary SEC employed was a Hewlett-Packard (Agilent Technologies) 1100 Series liquid chromatograph equipped with a refractive index detector (Hewlett-Packard 1047A). Polymers were separated using three PlGel 5 μm Mixed-C (Polymer Laboratories) columns with pore sizes of 500, 1×10^3, and 1×10^4 Å. The mobile phase was chloroform (1 mL min^{-1}, 35 °C) and polymer solutions were prepared at concentrations of ca. 1 mg mL^{-1}. The refractive index detector was calibrated using polystyrene standards (Polymer Laboratories) allowing for calculation of relative molecular weight data.

The second SEC employed was an Agilent 1260 Infinity liquid chromatograph equipped with an Agilent 1260 Infinity Variable Wavelength Detector (254 nm), a Wyatt DAWN Heleos II multi-angle (18 angles) light scattering detector, and a Wyatt OPTILAB T-rEX refractive index detector. Polymers were separated using three Waters Styragel 5 μm columns (HR6, HR4, HR1). The mobile phase was tetrahydrofuran (1 mL min^{-1}, 25 °C) and polymer solutions were prepared at concentrations of ca. 2–4 mg mL^{-1}. The refractive index and UV detectors were calibrated with polystyrene standards (Agilent Technologies), while the light scattering detector allowed for determination of absolute weight-average molecular weight (M_w).

A.7 Differential Scanning Calorimetry

Differential scanning calorimetry (DSC) was used to assess the thermal behavior (melting, crystallization, and glass transition temperatures) of polymer samples. DSC measurements were recorded on one of two instruments. A typical experiment involved heating in a nitrogen atmosphere from ca. 40 °C to ca. 230 °C at 10 °C min^{-1} to erase thermal history. The sample was then cooled to ca. -30 °C at 10 °C min^{-1} before heating again to ca. 230 °C at 10 °C min^{-1}. Analysis was performed on first cooling and second heating sweeps.

The primary DSC was a TA Instruments Discovery DSC equipped with a refrigerated cooling system (RCS90). The instrument was calibrated with indium and had a working range of -90 to 400 °C. Samples were prepared in aluminum Tzero (standard or hermetic) sample containers (1–10 mg).

The second DSC was a TA Instruments Q1000 equipped with a liquid nitrogen cooling accessory (LNCS). The instrument was calibrated with indium and had a working range of -180 to 550 °C. Samples were prepared in hermetically-sealed aluminum sample containers (5–15 mg).

A.8 Thermogravimetric Analysis

Thermogravimetric analysis (TGA) was used to assess the decomposition temperature (T_d, temperature at 5% weight loss) of select polymers. The instrument employed was a PerkinElmer Pyris Diamond TG/DTA 6300. Samples (2–5 mg) were prepared in aluminum pans and heated from 50 to 550 °C at 10 °C min^{-1} in a nitrogen or air (80% N_2, 20% O_2) atmosphere.

A.9 Wide Angle X-ray Scattering

Wide angle X-ray scattering (WAXS) was used to elucidate the semicrystalline nature of select polymers. Two different instruments were employed depending on the analysis required.

The first diffractometer, a Bruker-AXS Microdiffractometer, was employed for analysis of polymer thin films. The instrument used a 2.2 kW sealed Cu X-ray source (λ = 1.54 Å) and employed a charge-coupled device (CCD) Hi-Star 2-D area detector. Samples were prepared by drop coating a concentrated polymer solution ($CHCl_3$, 10–20 mg mL^{-1}) on cleaned glass slides. After solvent evaporation polymer films were pealed from the substrate and fixed to a quartz substrate using a small amount of vacuum grease. These samples were mounted in the diffractometer and patterns were collected from ca. 2-30° (2θ). Values were converted to the magnitude of the principle scattering momentum vector ($q = (4\pi/\lambda)\sin(\theta/2)$) and domain spacing was determined ($d = 2\pi/q$).

The second diffractometer, a Bruker-AXS D8 Advance, was employed for temperature-dependent analysis of powdered polymer samples. The instrument employed a Cu X-ray source (λ = 1.54 Å), an Anton-Paar CHC cryo and humidity stage, and a Bruker Lynx-eye position sensitive detector. Samples were ground with a mortar and pestle before adding to the sample stage. Patterns were collected from 5–40° (2θ) at temperatures ranging from 30–200 °C. Polymers were allowed to equilibrate at the desired temperature for 10 minutes before analysis. Domain spacing was determined as described above.

A.10 Cyclic Voltammetry

Cyclic voltammetry (CV) was employed to understand the redox behavior of select polymers. Two different CV methods were used depending on the desired analysis.

The first method was performed using a Pine Instruments bipotentiostat with an analog-to-digital converter (LabJack) to record data. The electrochemical cell consisted of a Pt wire counter electrode, Ag/AgCl reference electrode, and an Au-coated Si working electrode. Polymers were spin coated onto the working electrode from a 1,2-dichlorobenzene solution, and voltammograms were recorded in acetonitrile with 0.1 M $[Bu_4N][PF_6]$ as the supporting electrolyte at a scan rate of 20 mV s^{-1}. The HOMO level was estimated from the oxidation onset relative to ferrocene (E_{fer} = 0.45 V vs. Ag/AgCl) using the equation: $E_{HOMO} = -q(E_{ox,\ onset\ vs.\ fer} + 4.8)$.

The second method was performed using a Pine Instruments AFRDE5 bipotentiostat with an analog-to-digital converter (LabJack) to record data. The electrochemical cell consisted of a 1 mL Teflon chamber with a Pt mesh counter electrode, an Ag wire quasi-reference electrode, and an Au-coated Si working electrode. Polymers were spin coated onto the working electrode, and the cell was assembled in an inert atmosphere glovebox. Voltammograms were recorded in an ionic liquid (1-butyl-1-methylpyrrolidinium bis(trifluoromethylsulfonyl)imide [P14][TFSI]) electrolyte medium. The HOMO level was estimated from the oxidation onset relative to cobaltocenium hexafluorophosphate ($CcPF_6$) using the equation: $E_{HOMO} = -q(E_{ox,\ onset\ vs.\ Cc\pm} + 3.75)$.

A.11 Device Characterization

Thin film transistors and solar cells were fabricated and tested using select polymers.

Bottom gate bottom contact geometry transistors were fabricated on doped Si wafers with 3000 Å of thermally grown oxide. Gold source-drain contacts, ca. 250 Å as measured by profilometry and quartz crystal microbalance, were deposited via electron beam evaporation (Temescal) of a 25 Å chromium adhesion layer and 225 Å gold layer, and patterned via the lift-off technique. Substrates were cleaned with successive acetone, methanol, and isopropyl alcohol sonications followed by an UV/O_3 exposure. In a N_2

glove box, polymer active layers were spin-coated from 10 mg mL^{-1} 1,2-dichlorobenzene or chloroform solutions at 2000 rpm, and heated on a hot plate to drive off residual solvent. Transistors were tested in Desert Cryogenics vacuum probe station at room temperature housed within a N_2 glovebox. Output and transfer curves were collected with Keithly 236, 237, and 6517A source meters controlled by customized LabView code.

Photovoltaic devices were fabricated on patterned indium tin oxide (ITO) coated glass substrates (Delta Technologies, Stillwater, MN, sheet resistance 8–12 ohms sq^{-1}), cleaned with successive acetone, methanol, and isopropyl alcohol sonications followed by an UV/O_3 exposure. PEDOT:PSS was spin-coated from a filtered water suspension twice at 4000 rpm, forming ca. 30–40 nm films as measured by profilometry (KLA Tencor P-10). Coated substrates were then transferred to nitrogen atmosphere glovebox (all remaining steps in glovebox) and annealed at elevated temperature for 10 minutes. PTV:PCBM active layers were spin-coated from 1,2-dichlorobenzene solutions, varying spin speed and concentration to control active layer thickness. Wet spun devices were placed in covered Petri dishes to slowly dry. Aluminum cathodes, ca. 100 nm as measured by profilometry and quartz crystal microbalance, were formed via thermal evaporation at a rate of 2-3 Å min^{-1}. Silver paste was applied to the anode and cathode contact pads facilitating ohmic contact with the testing apparatus. PV current-voltage characteristics were collected using an Agilent 4155C Semiconductor Parameter Analyzer, under dark conditions and simulated solar illumination using a 150 W Xe-arc lamp (Oriel) with an AM 1.5 G filter, attenuated to 100 mW cm^{-2}. External quantum efficiency spectra were obtained using a monochromator (Cornerstone 130 1/8 m) equipped with gratings and filters (Newport Corp.) in conjunction with a SRB 10 DSP lock-in amplifier (Stanford Research Systems) controlled by customized LabView code.

Appendix B

Assorted Conjugated Polymer Syntheses

This appendix describes the synthesis of conjugated polymer systems, which were prepared to address a variety of concepts including: fundamental organic electronic device behavior, polymer regioregularity, alkyl functionalization, electron-withdrawing/donating substituent effects, and crosslinked conjugated polymer networks. The synthesis and characterization of all small molecules and polymers is described.

B.1 Polythiophenes

B.1.1 Motivation

Regioregular polythiophenes are perhaps the most studied of conjugated polymers (CPs).[1] Consequently, the synthesis of these materials has been highly refined,[2] and they have found their way into a variety of fundamental conjugated polymer studies. Understanding polythiophene charge transport at interfaces will aid in the design of high performance organic electronics. With that in mind, regioregular poly(3-hexylthiophene-d_{13}) (P1) was prepared for ultrafast infrared spectroscopy studies (Scheme B.1).[3] Deuteration of the hexyl side chain was necessary in order to prevent interference from C–H stretching vibrations. Additionally, researchers have sought to understand the effect of alkyl side chain length on polythiophene performance in organic solar cells (OSCs). Therefore, poly(3-hexadecylthiophene) (P2) was synthesized for systematic studies of polythiophene alkyl chain length (Scheme B.1).[4]

Scheme B.1

Polythiophene synthesis.

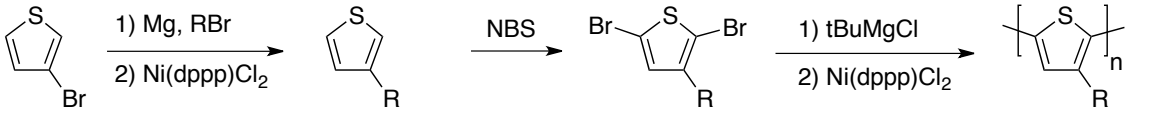

B.1.2 Synthetic Details

3-Hexylthiophene-d_{13} (1). A 250 mL 3-neck round bottom flask was equipped with a magnetic stirring bar, reflux condenser, glass stopcock, liquid addition funnel, and two rubber septa. Magnesium turnings (1.4 g, 58.5 mmol) were added, and the apparatus was

flame dried under vacuum. Anhydrous THF (75 mL) was added via cannula, and 1,2-dibromoethane (0.15 mL) was added via syringe. 1-Bromohexane-d_{13} (5.0 g, 28.1 mmol) was added to the addition funnel via syringe along with anhydrous THF (10 mL). This solution was added to the Mg suspension over the course of 20 min and stirred under argon for 2 h. A second 250 mL round bottom flask was equipped with a magnetic stirring bar and flame dried before adding 3-bromothiophene (2.2 mL, 23.4 mmol), [bis(diphenylphosphino)propane]dichloronickel(II) (Ni(dppp)Cl_2, 253 mg, 0.47 mmol), and anhydrous THF (20 mL). The red heterogeneous solution was cooled to 0 °C before adding the Grignard solution via cannula. The reaction was allowed to warm to room temperature and stirred under argon for 17 h. The reaction was quenched by the addition of 1 M NH_4HCO_3 (50 mL) and extracted with diethyl ether (2 × 75 mL). The combined organics were washed with water, saturated $NaHCO_3$, and brine (50 mL each) before drying over Na_2SO_4. The solvent was removed by rotary evaporation and the resultant brown oil was distilled under vacuum to afford product as a clear liquid (3.65 g, 87%). ^{1}H NMR (300 MHz, $CDCl_3$): δ_H = 7.27 (d, *J* = 5.0 Hz, 2H), 7.24 (dd, *J* = 3.2, 1.4 Hz, 2H), 7.02 (dd, *J* = 5.0, 1.3 Hz, 2H). Anal. calcd: C 66.22, H 8.89, S 17.68; Found: C 66.40, H 9.19, S 16.37.

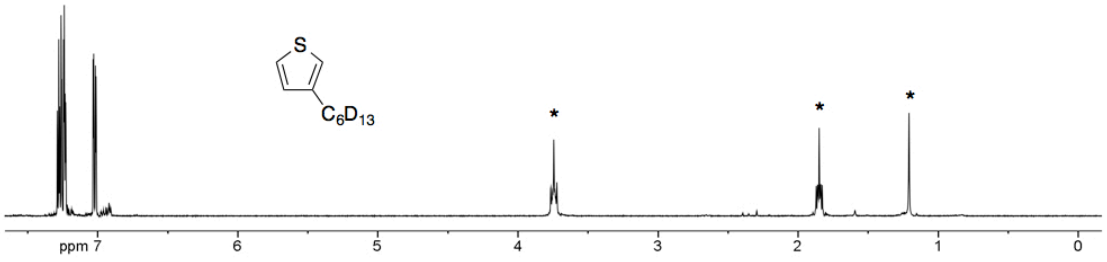

Figure B.1
^{1}H NMR spectrum of **1**. Asterisks mark solvents and other non-product peaks.

3-Hexadecylthiophene (2). A 1 L 3-neck round bottom flask was equipped with a magnetic stirring bar, reflux condenser, glass stopcock, liquid addition funnel, and two rubber septa. Magnesium turnings (12.9 g, 533 mmol) were added, and the apparatus was

flame dried under vacuum. Anhydrous THF (300 mL) was added via cannula, and 1,2-dibromoethane (1 mL) was added via syringe. 1-Bromohexadecane (78 g, 256 mmol) was added to the addition funnel via syringe along with anhydrous THF (75 mL). This solution was added to the Mg suspension over the course of 1 h and stirred under argon for 2 h. A second 1 L round bottom flask was equipped with a magnetic stirring bar and flame dried before adding 3-bromothiophene (20 mL, 213 mmol), Ni(dppp)Cl_2 (2.3 g, 4.3 mmol), and anhydrous THF (100 mL). The red heterogeneous solution was cooled to 0 °C before adding the Grignard solution via cannula. The reaction was allowed to warm to room temperature and stirred under argon for 18 h. The reaction was quenched by the addition of 1 M NH_4HCO_3 (150 mL) and extracted with diethyl ether (3 × 100 mL). The combined organics were washed with water, saturated $NaHCO_3$, and brine (150 mL each) before drying over Na_2SO_4. The solvent was removed by rotary evaporation and the resultant brown residue was dissolved in minimal THF and precipitated into methanol (0 °C) to afford product as an off-white solid, which was collected by vacuum filtration (45.7 g, 70%). ^{1}H NMR (300 MHz, $CDCl_3$): δ_H = 7.23 (dd, J = 4.9, 3.0 Hz, 1H), 6.94–6.91 (m, 2H), 2.62 (t, J = 7.7 Hz, 2H), 1.61 (quintet, J = 7.4 Hz, 2H), 1.25 (s, 26H), 0.88 (t, J = 6.6 Hz, 3H). ^{13}C NMR (125 MHz, $CDCl_3$): δ_C = 143.5, 128.5, 125.2, 119.9, 32.6, 30.8, 30.5, 29.9, 29.8, 29.7, 29.6 (2), 22.9, 14.4. HRGC-MS (EI): $M_{calcd.}$ = 308.2538, M_{found} = 308.2555. Anal. calcd. for $C_{20}H_{36}S$: C 77.85, H 11.76, S 10.39; Found: C 78.64, H 11.96, S 9.23.

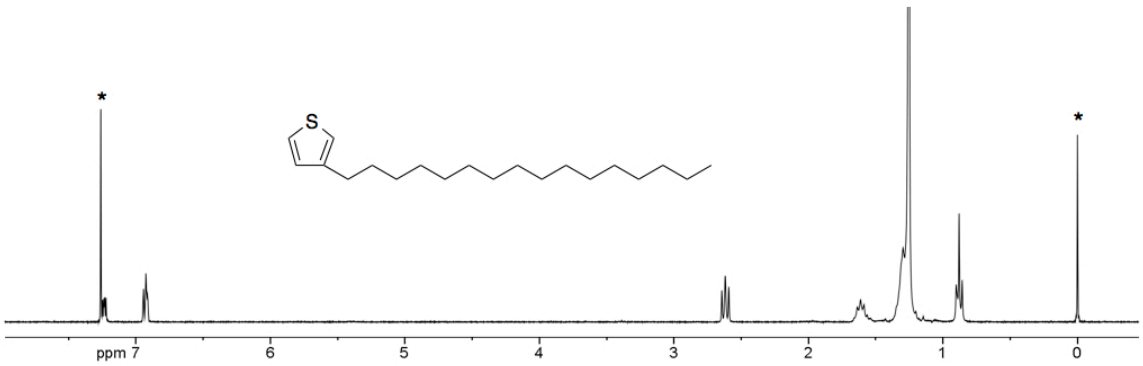

Figure B.2
^{1}H NMR spectrum of **2**. Asterisks mark solvents and other non-product peaks.

2,5-Dibromo-3-hexylthiophene-d_{13} (3). A 100 mL round bottom flask was equipped with a magnetic stirring bar before adding **1** (3.3 g, 18.1 mmol) and THF (75 mL). The solution was cooled to 0 °C before adding recrystallized N-bromosuccinimide (NBS, 6.6 g, 37.1 mmol). The reaction was allowed to warm to room temperature and stirred in the dark under argon for 72 h. The reaction was quenched by the addition of 1 M $NaHSO_3$ (25 mL) and extracted with diethyl ether (2 × 50 mL). The combined organics were washed with water and brine (50 mL each) before drying over Na_2SO_4. The solvent was removed by rotary evaporation to afford product as a yellow oil (5.0 g, 81%). ^{1}H NMR (300 MHz, $CDCl_3$): δ_H = 6.70 (s, 1H). $M_{calcd.}$ = 308.2538, M_{found} = 308.2555. Anal. calcd: C 35.41, H 4.16, Br 47.12, S 9.45; Found: C 36.72, H 4.35, Br 46.89, S 9.37.

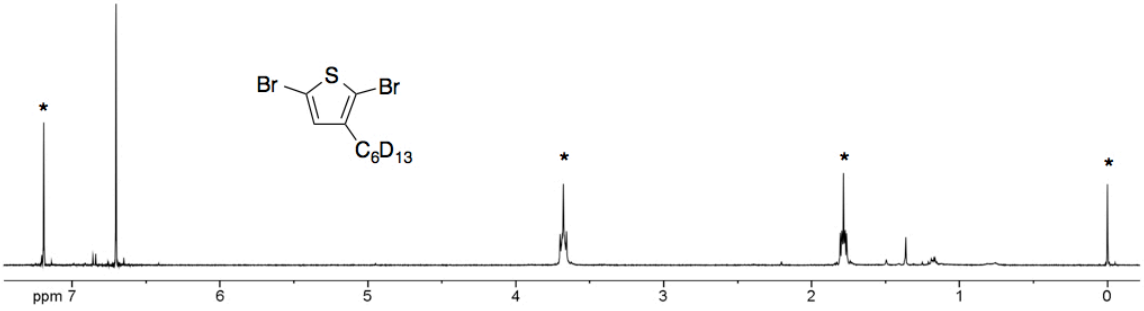

Figure B.3
^{1}H NMR spectrum of **3**. Asterisks mark solvents and other non-product peaks.

2,5-Dibromo-3-hexadecylthiophene (4). A 500 mL round bottom flask was equipped with a magnetic stirring bar before adding **2** (13.2 g, 42.9 mmol) and THF (300 mL). The solution was cooled to 0 °C before adding recrystallized NBS (15.6 g, 87.9 mmol). The reaction was allowed to warm to room temperature and stirred in the dark under argon for 48 h. The reaction was quenched by the addition of 1 M $NaHSO_3$ (50 mL) and extracted with diethyl ether (2 × 100 mL). The combined organics were washed with water, 0.2 M HCl, and brine (150 mL each) before drying over $MgSO_4$. The solvent was

removed by rotary evaporation, and the residual succinimide was removed by dissolving the product mixture in hexanes and passing through a plug of silica gel. The hexanes were removed by rotary evaporation to afford product, which was further purified by recrystallization from 1:9 THF/methanol (18.3 g, 91%). ^{1}H NMR (300 MHz, $CDCl_3$): δ_H = 6.77 (s, 1H), 2.50 (t, *J* = 7.6 Hz, 2H), 1.53 (s, 2H), 1.25 (s, 26H), 0.88 (t, *J* = 6.7 Hz, 3H). ^{13}C NMR (125 MHz, $CDCl_3$): δ_C = 143.3, 131.3, 110.6, 108.2, 32.3, 30.06, 30.02, 29.99, 29.92, 29.88, 29.82, 29.73, 29.72, 29.5, 23.1, 14.5. Anal. calcd. for $C_{20}H_{34}Br_2S$: C 51.51, H 7.35, Br 34.27, S 6.88; Found: C 53.47, H 7.73, Br 32.39, S 6.41.

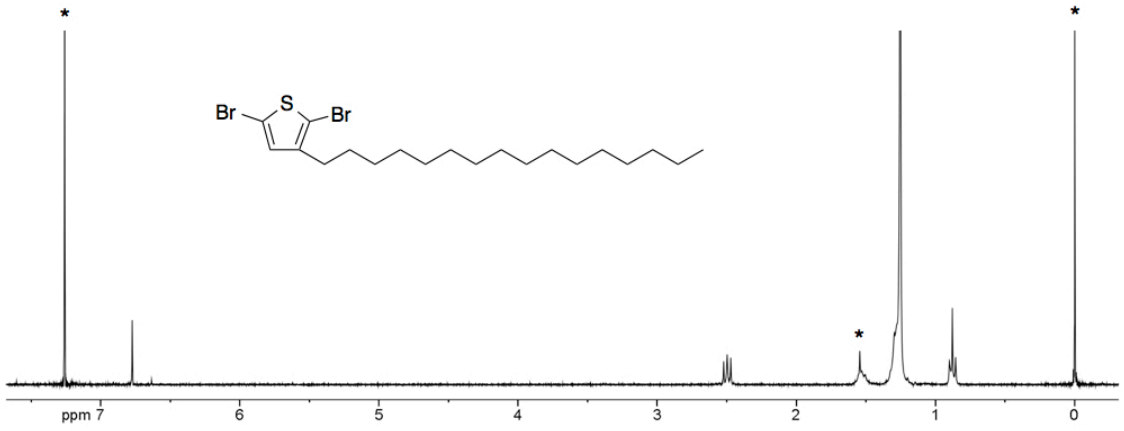

Figure B.4
^{1}H NMR spectrum of **4**. Asterisks mark solvents and other non-product peaks.

Poly(3-hexylthiophene-d_{13}) (P1). A 250 mL 3-neck round bottom flask was equipped with a magnetic stirring bar, reflux condenser, glass stopcock, and two rubber septa. The apparatus was flame dried under vacuum before adding **3** (4.6 g, 13.6 mmol) and anhydrous THF (150 mL). *tert*-Butylmagnesium chloride (2 M in diethyl ether, 6.8 mL, 13.6 mmol) was added via syringe, and the solution was refluxed for 90 minutes. The solution was cooled to room temperature before adding $Ni(dppp)Cl_2$ (5.1 mg, 0.0095 mmol) as a solid under argon flow. The polymerization was quenched after 45 min by the addition of 5 M HCl (5 mL). The solution was precipitated into methanol (750 mL) and filtered to collect the crude polymer, which was further purified by Soxhlet extraction

with methanol, hexanes, and chloroform. The chloroform fraction was concentrated by rotary evaporation to afford pure polymer (0.41 g, 17%). ^{1}H NMR (500 MHz, $CDCl_3$): δ_H = 6.98 (s, 1H). SEC ($CHCl_3$, 1 mL min^{-1}, RI): M_n = 59 kg mol^{-1}, M_w = 74 kg mol^{-1}, $Đ$ = 1.25. Anal. calcd: C 66.96, H 7.87, S 17.88; Found: C 67.45, H 8.01, S 16.95.

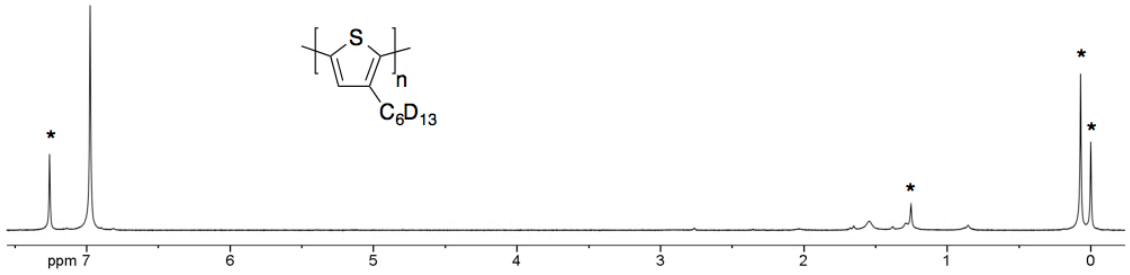

Figure B.5
^{1}H NMR spectrum of **P1**. Asterisks mark solvents and other non-product peaks.

Poly(3-hexadecylthiophene) (P2). A 250 mL 3-neck round bottom flask was equipped with a magnetic stirring bar, reflux condenser, glass stopcock, and two rubber septa. The apparatus was flame dried under vacuum before adding **4** (5.0 g, 10.7 mmol) and anhydrous THF (200 mL). *tert*-Butylmagnesium chloride (2 M in diethyl ether, 5.4 mL, 10.7 mmol) was added via syringe, and the solution was refluxed for 90 minutes. The solution was cooled to room temperature before adding Ni(dppp)Cl_2 (35 mg, 0.064 mmol) as a solid under argon flow. The polymerization was quenched after 45 min by the addition of 5 M HCl (5 mL). The solution was precipitated into methanol (600 mL) and filtered to collect the crude polymer, which was further purified by Soxhlet extraction with methanol, hexanes, and chloroform. The chloroform fraction was precipitated into methanol (300 mL), and the polymer was collected by vacuum filtration (1.25 g, 38%). ^{1}H NMR (500 MHz, $CDCl_3$): δ_H = 6.97 (s, 1H), 2.80 (t, J = 7.2 Hz, 2H), 1.70 (quintet, J = 6.8 Hz, 2H), 1.42 (quintet, J = 7.6 Hz, 2H), 1.35 (quintet, J = 7.4 Hz, 2H), 1.29 (s, 22H), 0.87 (t, J = 5.3 Hz, 3H). SEC ($CHCl_3$, 1 mL min^{-1}, RI): M_n = 25 kg mol^{-1}, M_w = 30 kg mol^{-1}, $Đ$ = 1.20.

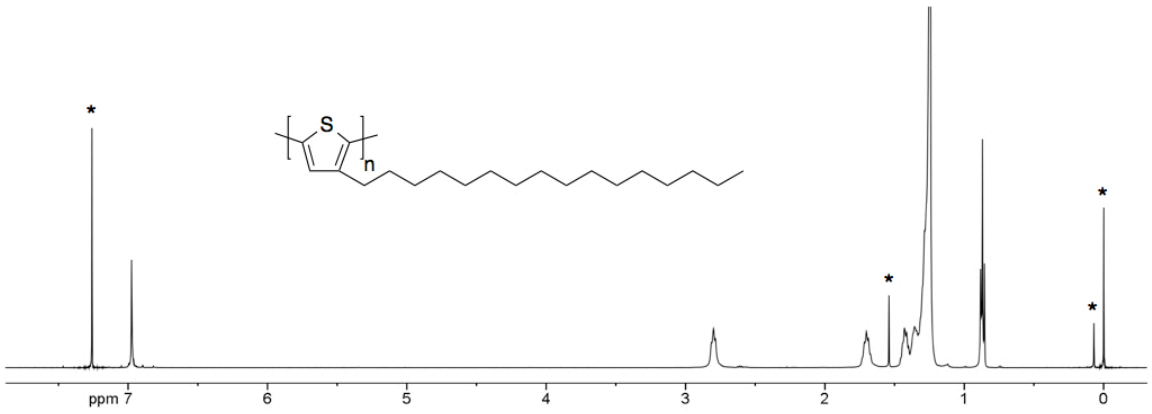

Figure B.6
^{1}H NMR spectrum of **P2**. Asterisks mark solvents and other non-product peaks.

B.2 PTVs: Regioregularity and Branched Alkyl Chains

B.2.1 Motivation

Poly(thienylene vinylenes) (PTVs) achieve a lower band gap (i.e., increased conjugation length) than polythiophenes because the olefin moiety allows for a more planar polymer backbone.[5] However, increased planarity typically leads to greater π-stacking and reduced solubility. Therefore, branched alkyl chains are often employed to improve solubility without sacrificing conjugation length.[6] This concept was applied to PTVs (P3, Scheme B.2). Although polymers were successfully prepared, the steric bulk of the branched alkyl group (i.e., 2-ethylhexyl) prevented realization of high molar mass making this polymer a poor candidate for solar cells. Regioregular polythiophenes are known to perform better in OSCs than their regiorandom counterparts. Therefore, symmetric PTV monomers with linear (P4) and branched (P5) alkyl chains were prepared and polymerized (Scheme B.2). Due to enhanced backbone planarity, both P5 and P6 were poorly soluble making them poor candidates for OSC applications. Finally,

the concepts of regioregularity and branched alkyl chains were combined into a simplified polymer (P6), but steric hindrance prevented the achievement of substantial molar mass.

Scheme B.2

Branched alkyl chain and regioregular PTV synthesis.

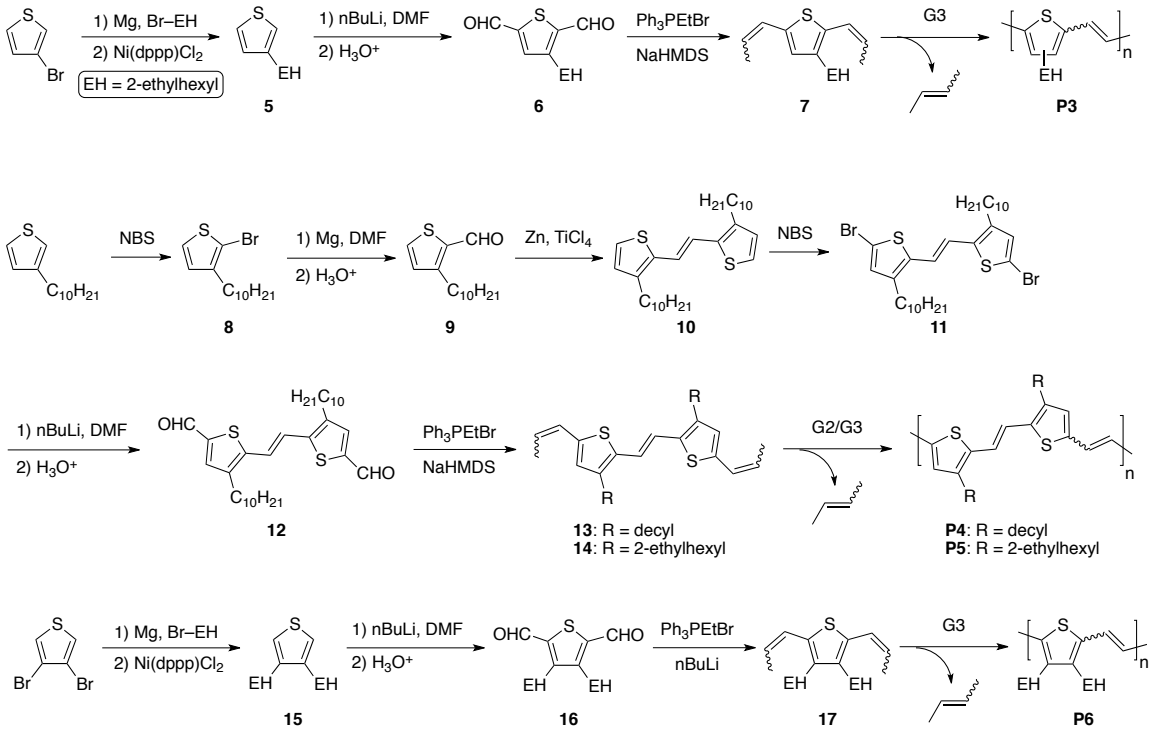

B.2.2 Synthetic Details

3-(2-Ethylhexyl)thiophene (5). A 1 L 3-neck round bottom flask was equipped with a magnetic stirring bar, reflux condenser, glass stopcock, liquid addition funnel, and two rubber septa. Magnesium turnings (19.5 g, 801 mmol) were added, and the apparatus was flame dried under vacuum. Anhydrous THF (300 mL) was added via cannula, and 1,2-dibromoethane (1 mL) was added via syringe. 2-Ethylhexylbromide (68.3 mL, 384 mmol) was added to the addition funnel via syringe along with anhydrous THF (75 mL). This solution was added to the Mg suspension over the course of 1 h and stirred under

argon for 3 h. A second 1 L round bottom flask was equipped with a magnetic stirring bar and flame dried before adding 3-bromothiophene (30.0 mL, 320 mmol), Ni(dppp)Cl_2 (3.5 g, 6.4 mmol), and anhydrous THF (100 mL). The red heterogeneous solution was cooled to 0 ˚C before adding the Grignard solution via cannula. The reaction was allowed to warm to room temperature and stirred under argon for 18 h. The reaction was quenched by the addition of 1.5 M NH_4HCO_3 (150 mL) and extracted with diethyl ether (3 × 100 mL). The combined organics were washed with water, saturated $NaHCO_3$, and brine (100 mL each) before drying over Na_2SO_4. The solvent was removed by rotary evaporation, and the resultant brown oil was distilled under vacuum to afford product as a light yellow liquid (48.0 g, 76%). ^{1}H NMR (300 MHz, $CDCl_3$): δ_H = 7.19 (dd, *J* = 4.9, 2.9 Hz, 1H), 6.90–6.86 (m, 2H), 2.55 (d, *J* = 6.9 Hz, 2H), 1.54 (dt, *J* = 12.4, 6.2 Hz, 1H), 1.33–1.19 (m, 8H), 0.91–0.81 (m, 6H). Anal. calcd. for $C_{12}H_{20}S$: C 73.40, H 10.27, S 16.33; Found: C 73.32, H 10.46, S 16.05.

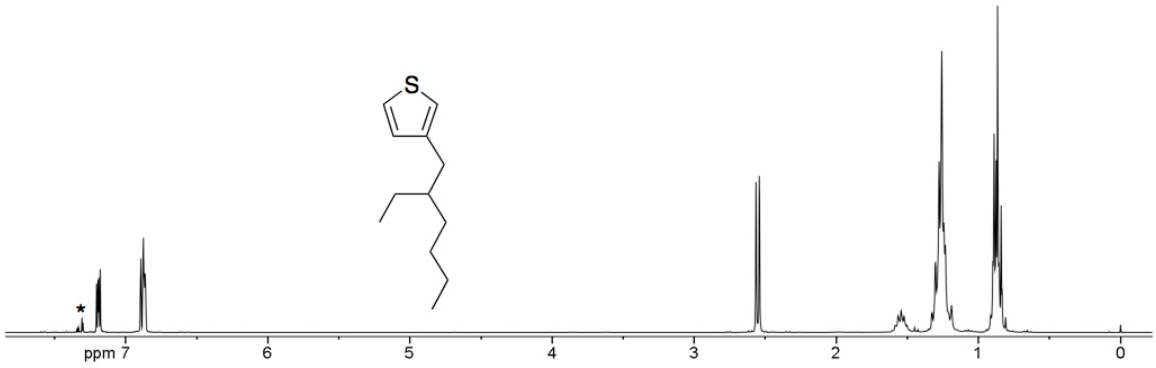

Figure B.7
^{1}H NMR spectrum of **5**. Asterisks mark solvents and other non-product peaks.

3-(2-Ethylhexyl)thiophene-2,5-dicarbaldehyde (6). A 3-neck 1 L round bottom flask was equipped with a magnetic stirring bar, reflux condenser, glass stopcock, liquid addition funnel, and two rubber septa. The apparatus was flame dried under vacuum before adding **5** (30.0 g, 153 mmol) via syringe. Anhydrous hexanes (400 mL) were cannulated into the flask followed by distilled N,N,N',N'-tetramethylethylenediamine

(TMEDA, 57.3 mL, 382 mmol). *n*-Butyllithium (2.5 M in hexanes, 153 mL, 382 mmol) was added to the solution dropwise from the addition funnel. Following addition, the reaction was refluxed for 1 h before adding anhydrous THF (300 mL) and cooling to 0 °C. Dimethylformamide (DMF, 47.2 mL, 611 mmol) was added via syringe, and the reaction was allowed to warm to room temperature while stirring under argon for 18 h. The reaction was quenched by the addition of 3 M HCl (225 mL) and extracted with diethyl ether (2 × 100 mL). The combined organics were washed with 1 M HCl (300 mL) and brine (100 mL) before drying over Na_2SO_4. The solvent was removed by rotary evaporation, and the resultant brown oil was distilled under vacuum to afford product as an orange oil (18.4 g, 48%). ^{1}H NMR (300 MHz, $CDCl_3$): δ_H = 10.13 (s, 1H), 9.98 (s, 1H), 7.62 (s, 1H), 2.92 (d, *J* = 7.2 Hz, 2H), 1.64 (dt, *J* = 12.0, 6.0 Hz, 1H), 1.39–1.23 (m, 8H), 0.93-0.86 (m, 6H).

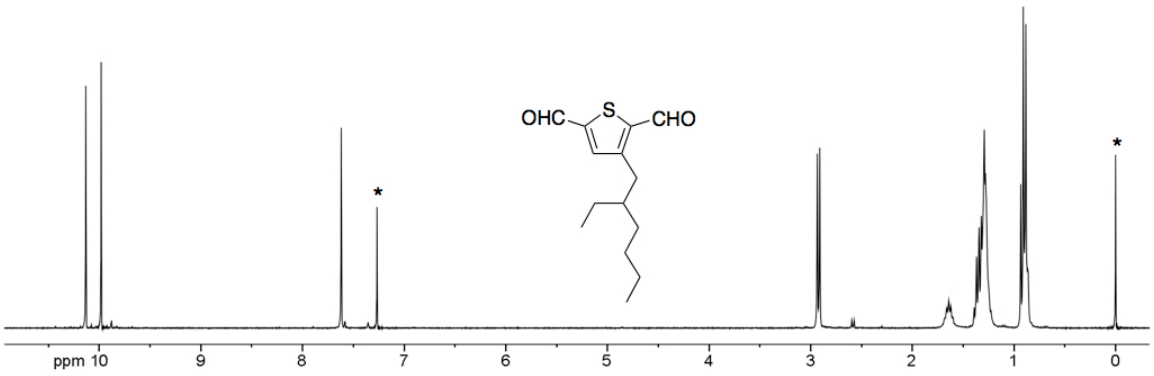

Figure B.8
^{1}H NMR spectrum of **6**. Asterisks mark solvents and other non-product peaks.

2,5-Dipropenyl-3-(2-ethylhexyl)thiophene (7). A 1 L 3-neck round bottom flask was equipped with a magnetic stirring bar, reflux condenser, glass stopcock, and two rubber septa. The apparatus was flame dried under vacuum before adding (ethyl)triphenylphosphonium bromide (59.6 g, 160 mmol) and sodium bis(trimethylsilyl)amide (29.4 g, 160 mmol). The solids were dried under vacuum for 1 h before adding anhydrous hexanes (400 mL) via cannula. The suspension was refluxed for

1 h at which point the orange-red Wittig reagent was formed. The reaction was cooled to -78 ˚C and stirring was suspended. The solids were allowed to settle out, and the hexanes were removed via cannula. This washing procedure was performed twice more with 200 mL of hexanes. The remaining solids were dried under vacuum. Meanwhile, a second 1 L round bottom flask was equipped with a magnetic stirring bar and flame dried. **6** (18.4 g, 73 mmol) and anhydrous THF (100 mL) were added. The solution was sealed with a septum and cooled to 0 ˚C under argon. Anhydrous THF (350 mL) was added to dissolve the solid Wittig reagent, which was then cannulated (taking care to leave NaBr salt behind) into the cooled dicarbaldehyde solution. The reaction was stirred for 16 h under argon. The solution was filtered to remove most of the $Ph_3P{=}O$. The filtrate was subjected to rotary evaporation, and the resultant brown residue was washed thoroughly with hexanes before passing through a plug of silica gel. The hexanes were removed by rotary evaporation and the resultant oil was distilled under vacuum to give pure product as a light yellow oil (16.8 g, 83%). *E*:*Z* = 30:70. ^{1}H NMR (300 MHz, $CDCl_3$): δ_H = 6.73–6.60 (m, 1H), 6.55–6.42 (m, 2H), 6.10–5.60 (m, 2H), 2.49–2.43 (m, 2H), 2.01–1.82 (m, 6H), 1.55–1.48 (m, 1H), 1.33–1.20 (m, 8H), 0.89–0.82 (m, 6H). Anal. calcd. for $C_{18}H_{28}S$: C 78.19, H 10.21, S 11.60; Found: C 78.47, H 10.31, S 11.35.

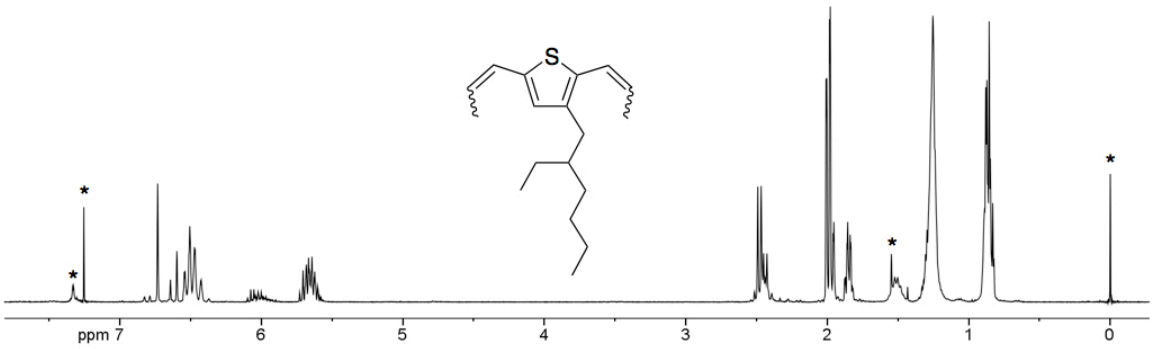

Figure B.9
^{1}H NMR spectrum of **7**. Asterisks mark solvents and other non-product peaks.

Poly(3-(2-ethylhexyl)thienylene vinylene) (P3). In an apparatus like that shown in Figure 2.24, **8** (1.0 g, 3.6 mmol) was dissolved in 1,2,4-trichlorobenzene (TCB, 15 mL). The solution was degassed under vacuum for 30 min before adding G3 (32 mg, 0.036 mmol) in TCB (1 mL). The reaction was refluxed under vacuum at 80 °C for 24 h before precipitating into acetone (400 mL). The precipitate was collected by vacuum filtration and purified by Soxhlet extraction with acetone. The polymer was extracted into chloroform, concentrated, and precipitated a second time before filtering and drying under vacuum. The polymer was isolated as black solid (0.60 g, 76%). ^{1}H NMR (500 MHz, $CDCl_3$): δ_H = 6.98–6.86 (m, 2H), 6.74 (s, 1H), 2.54 (s, 2H), 1.55 (s, 1H), 1.34 (s, 8H), 0.93 (s, 6H). SEC ($CHCl_3$, 1 mL min^{-1}, RI): M_n = 11 kg mol^{-1}, M_w = 21 kg mol^{-1}, $Đ$ = 1.90. Anal. calcd. for $C_{14}H_{20}S$: C 76.30, H 9.15, S 14.55; Found: C 74.63, H 9.15, S 13.98.

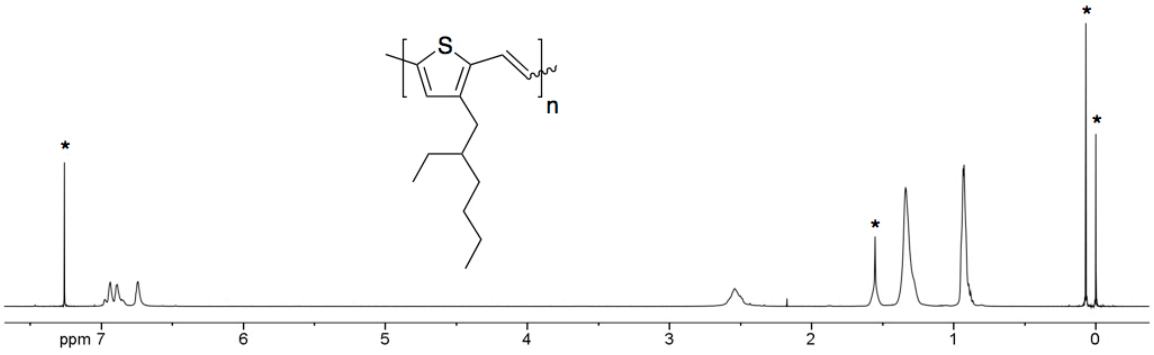

Figure B.10
^{1}H NMR spectrum of **P3**. Asterisks mark solvents and other non-product peaks.

2-Bromo-3-decylthiophene (8). A 500 mL round bottom flask was equipped with a magnetic stirring bar before adding 3-decylthiophene (30.0 g, 116 mmol) and THF (300 mL). The solution was cooled to 0 °C before adding recrystallized NBS (21.7 g, 122 mmol). The reaction was sealed under argon and allowed to warm to room temperature where it was stirred in the dark for 48 h. The reaction was quenched with 1 M $NaHSO_3$ (100 mL) and extracted with diethyl ether (2 × 100 mL). The combined organics were

washed with water, 1 M HCl, and brine (100 mL each) before drying over Na_2SO_4. The solvent was removed by rotary evaporation, and the product was used without further purification (34 g, 97%). ^{1}H NMR (300 MHz, $CDCl_3$): δ_H = 7.18 (d, *J* = 5.6 Hz, 1H), 6.79 (d, *J* = 5.6 Hz, 1H), 2.55 (t, *J* = 7.7 Hz, 2H), 1.57 (quintet, *J* = 7.4 Hz, 2H), 1.31–1.26 (m, 14H), 0.88 (t, *J* = 6.7 Hz, 3H).

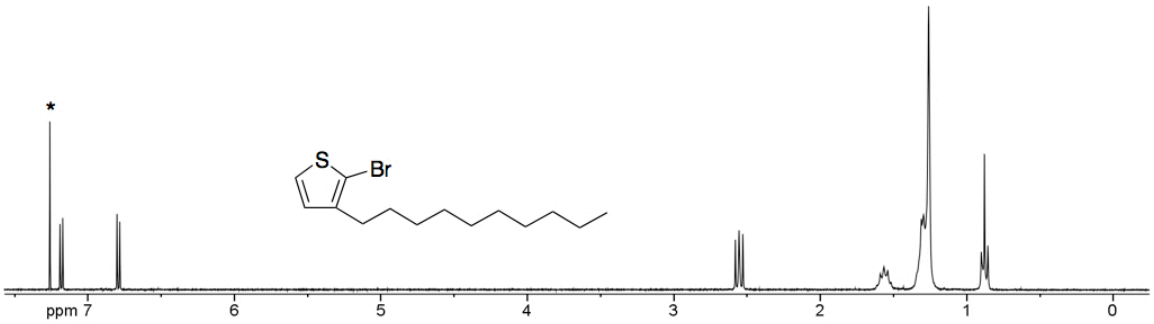

Figure B.11
^{1}H NMR spectrum of **8**. Asterisks mark solvents and other non-product peaks.

3-Decylthiophene-2-carbaldehyde (9). A 3-neck 500 mL round bottom flask was equipped with a magnetic stirring bar, reflux condenser, liquid addition funnel, glass stopcock, and two rubber septa. Magnesium turnings (4.3 g, 178 mmol) were added and the apparatus was flame dried under vacuum. Anhydrous THF (300 mL) was added via cannula followed by 1,2-dibromoethane (1 mL) via syringe. **8** (21.6 g, 71 mmol) and anhydrous THF (40 mL) were added to the addition funnel. This solution was added dropwise to the Mg suspension over the course of 30 min. The reaction was stirred at 60 ˚C for 90 min before cooling to -78 ˚C. Anhydrous DMF (13.7 mL, 178 mmol) was slowly added, and the solution was allowed to warm to room temperature while stirring under argon for 17 h. The reaction mixture was quenched with 1 M HCl (180 mL) and extracted with diethyl ether (3 × 100 mL). The combined organics were washed with water and brine (100 mL each) before drying over $MgSO_4$. The solvent was removed by rotary evaporation to yield product as a light brown oil (17.3 g, 97%). ^{1}H NMR (500

MHz, $CDCl_3$): δ_H = 10.04 (s, 1H), 7.64 (d, *J* = 4.9 Hz, 1H), 7.01 (d, *J* = 5.0 Hz, 1H), 2.96 (t, *J* = 7.7 Hz, 2H), 1.67 (dt, *J* = 14.8, 7.5 Hz, 2H), 1.35–1.26 (m, 14H), 0.88 (t, *J* = 7.0 Hz, 3H).

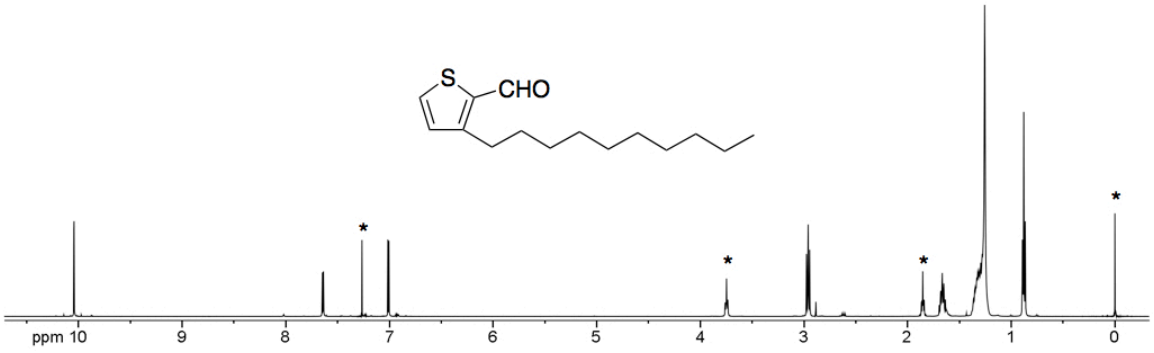

Figure B.12
^{1}H NMR spectrum of **9**. Asterisks mark solvents and other non-product peaks.

(*E*)-1,2-Bis(3-decylthiophen-2-yl)ethane (10). A 2-neck 500 mL round bottom flask was equipped with a magnetic stirring bar, reflux condenser, glass stopcock, and rubber septum. Zinc dust (65.4 g, 202 mmol) was added and the apparatus was flame dried under vacuum. Anhydrous THF (150 mL) was added via cannula and the solution was cooled to 0 °C. Titanium(IV) chloride (11.1 mL, 101 mmol) was *slowly* added via syringe. Caution: HCl forms. Following addition the reaction mixture was refluxed for 1 h at which point a dark gray/blue slurry had formed. The slurry was cooled to 0 °C before adding **9** (17.0 g, 67 mmol) and triethylamine (18.8 mL, 135 mmol) as a solution in anhydrous THF (50 mL) via cannula. The reaction was refluxed for 16 h under argon and quenched with saturated $NaHCO_3$ (500 mL). The solution was filtered through a pad of celite and extracted with diethyl ether (4 × 100 mL). The combined organics were washed with water, brine, and 10 wt% NH_4OH (100 mL each) before drying over $MgSO_4$. The solvent was removed by rotary evaporation to afford product as an orange oil, which crystallized on standing (15.7 g, 99%). ^{1}H NMR (500 MHz, $CDCl_3$): δ_H =

7.07 (d, *J* = 5.1 Hz, 2H), 6.99 (s, 2H), 6.84 (d, *J* = 5.1 Hz, 2H), 2.65 (t, *J* = 7.7 Hz, 4H), 1.60 (dt, *J* = 14.9, 7.5 Hz, 4H), 1.32–1.26 (m, 28H), 0.87 (t, *J* = 7.0 Hz, 6H).

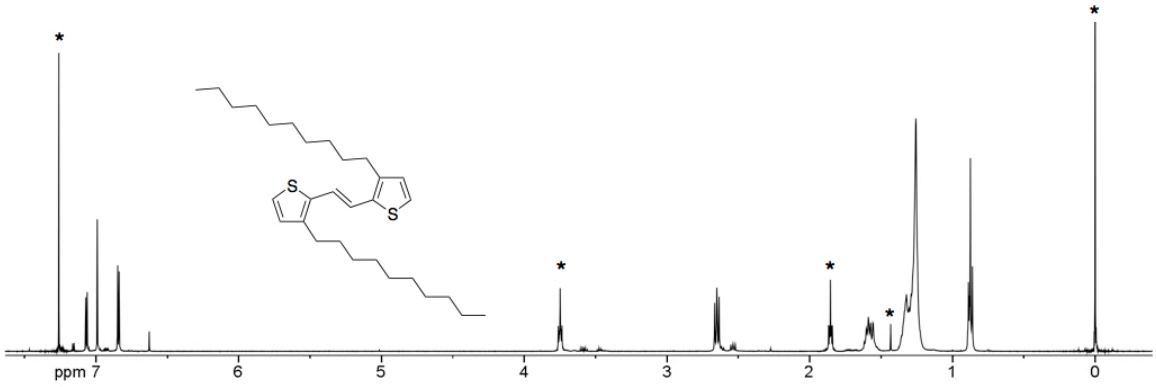

Figure B.13
^{1}H NMR spectrum of **10**. Asterisks mark solvents and other non-product peaks.

(*E*)-1,2-Bis(5-bromo-3-decylthiophen-2-yl)ethane (11). A 500 mL round bottom flask was equipped with a magnetic stirring bar before adding **10** (16.0 g, 34 mmol) and THF (200 mL). The solution was cooled to 0 °C before adding recrystallized NBS (12.3 g, 69 mmol). The reaction was sealed under argon and allowed to warm to room temperature where it was stirred in the dark for 48 h. The reaction was quenched with 1 M $NaHSO_3$ (75 mL) and extracted with diethyl ether (2 × 100 mL). The combined organics were washed with water and brine (100 mL each) before drying over $MgSO_4$. The solvent was removed by rotary evaporation to yield an orange/brown oil. The oil was dissolved in 1:1 THF/methanol (200 mL) and allowed to crystallize at -20 °C for 2 h. The product was obtained by vacuum filtration as a yellow crystalline solid (12.7 g, 60%). ^{1}H NMR (500 MHz, $CDCl_3$): δ_H = 6.80 (s, 2H), 6.76 (s, 2H), 2.56 (t, *J* = 7.6 Hz, 4H), 1.56–1.51 (m, 4H), 1.31–1.26 (m, 28H), 0.88 (t, *J* = 7.0 Hz, 6H).

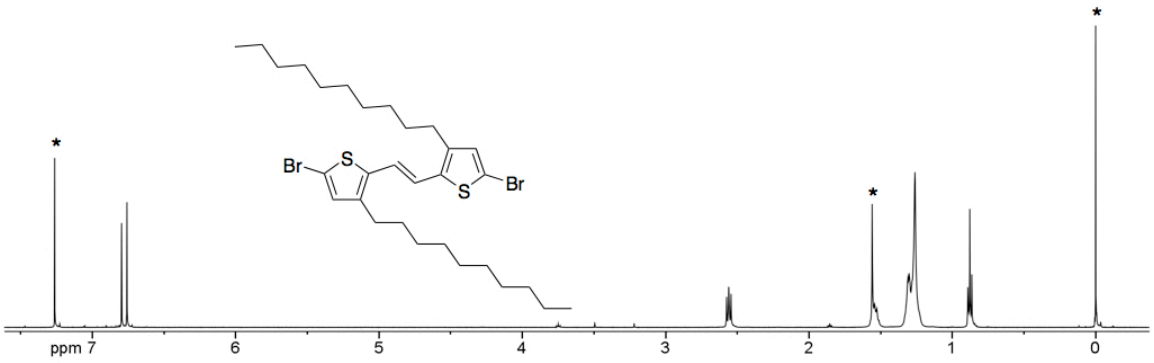

Figure B.14
^{1}H NMR spectrum of **11**. Asterisks mark solvents and other non-product peaks.

(*E*)-1,2-Bis(5-carbaldehyde-3-decylthiophen-2-yl)ethane (12). A 250 mL reaction flask was equipped with a magnetic stirring bar and flame dried before adding **11** (16.5 g, 26 mmol). The solid was dried under vacuum before adding anhydrous THF (300 mL) via cannula. The solution was cooled to 0 °C before *slowly* adding *n*-butyllithium (2.5 M in hexanes, 36.7 mL, 92 mmol) via syringe. The reaction turned deep red and was stirred under argon at 0 °C for 1 h. Anhydrous DMF (8.1 mL, 105 mmol) was added via syringe, and the reaction was allowed to warm to room temperature while stirring under argon for 18 h. The reaction was quenched by the addition of 1 M HCl (105 mL) and extracted with diethyl ether (150 mL). The organics were washed with water and brine (150 mL each) before drying over Na_2SO_4. The solvent was removed by rotary evaporation to afford product as an orange solid (12.5 g, 90%). Used without further purification. ^{1}H NMR (500 MHz, $CDCl_3$): δ_H = 9.84 (s, 2H), 7.26 (s, 2H), 7.22 (s, 2H), 2.69 (t, *J* = 7.7 Hz, 4H), 1.63 (dt, *J* = 14.8, 7.5 Hz, 4H), 1.34–1.26 (m, 28H), 0.89–0.86 (m, 6H).

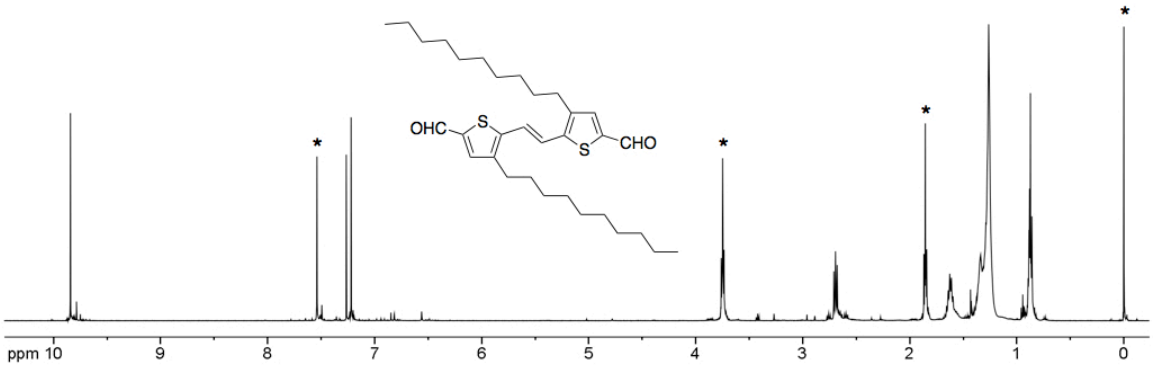

Figure B.15
^{1}H NMR spectrum of **12**. Asterisks mark solvents and other non-product peaks.

(*E*)-1,2-Bis(5-propenyl-3-decylthiophen-2-yl)ethane (13). A 1 L 3-neck round bottom flask was equipped with a magnetic stirring bar, reflux condenser, glass stopcock, and two rubber septa. The apparatus was flame dried under vacuum before adding (ethyl)triphenylphosphonium bromide (32.0 g, 86 mmol) and sodium bis(trimethylsilyl)amide (15.8 g, 86 mmol). The solids were dried under vacuum for 1 h before adding anhydrous hexanes (500 mL) via cannula. The suspension was refluxed for 1 h at which point the orange-red Wittig reagent was formed. The reaction was cooled to -78 °C and stirring was suspended. The solids were allowed to settle out, and the hexanes were removed via cannula. This washing procedure was performed once more with 200 mL of hexanes. The remaining solids were dried under vacuum. A second 1 L round bottom flask was equipped with a magnetic stirring bar and flame dried. **12** (15.2 g, 29 mmol) and anhydrous THF (250 mL) were added. The solution was sealed with a septum and cooled to -78 °C under argon. Anhydrous THF (350 mL) was added to dissolve the solid Wittig reagent, which was then cannulated (taking care to leave NaBr salt behind) into the cooled dicarbaldehyde solution. The reaction was stirred for 16 h under argon. The reaction solution was then concentrated by rotary evaporation and the resultant brown residue was stirred vigorously in hexanes before filtering to remove $Ph_3P{=}O$. The filtrate was concentrated by rotary evaporation and purified by column

chromatography with hexanes. The resultant orange oil was crystallized from 1:1 THF/methanol (150 mL) to afford product as an orange crystalline solid (6.7 g, 42%). *E*:*Z* = 25:75. ^{1}H NMR (500 MHz, $CDCl_3$): δ_H = 6.86 (s, 2H), 6.58 (s, 2H), 6.43 (dd, *J* = 15.6, 1.3 Hz, 2H), 6.03 (dq, *J* = 15.0, 7.3 Hz, 2H), 2.56 (t, *J* = 7.6 Hz, 4H), 2.01 (dd, *J* = 7.4, 1.7 Hz, 1H), 1.85 (dd, *J* = 6.8, 1.7 Hz, 5H), 1.55 (m, 4H), 1.31–1.26 (m, 28H), 0.87 (t, *J* = 7.0 Hz, 6H).

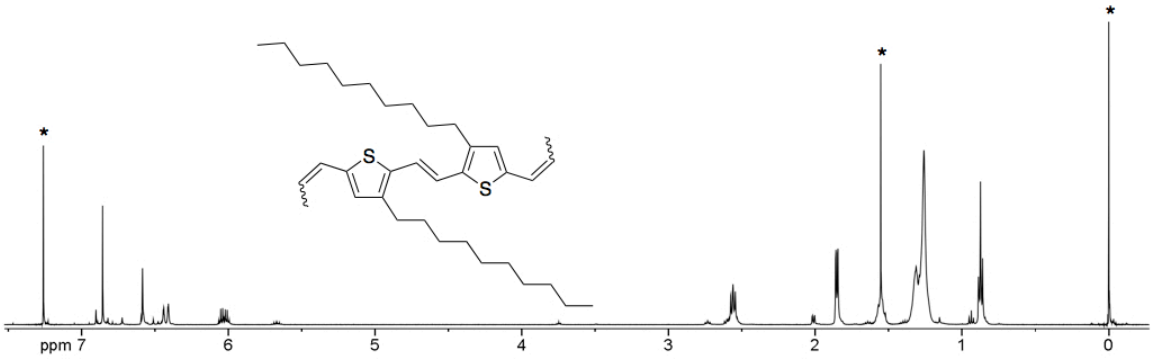

Figure B.16
^{1}H NMR spectrum of **13**. Asterisks mark solvents and other non-product peaks.

(*E*)-1,2-Bis(5-propenyl-3-(2-ethylhexyl)thiophen-2-yl)ethane (14). This compound was prepared in the same manner as **13** by Yang Qin. Compound isolated as bright orange crystalline solid (9.0 g, 48%).

P4. In an apparatus like that shown in Figure 2.24, **13** (1.0 g, 1.8 mmol) was dissolved in TCB (15 mL). The solution was degassed under vacuum for 30 min before adding G2 (15 mg, 0.018 mmol) in toluene (1 mL). The reaction was refluxed under vacuum at 70 °C for 24 h before adding another 15 mg of G2 and increasing the temperature to 80 °C. After an additional 24 h the polymer was precipitated into acetone (300 mL). The precipitate was collected by vacuum filtration and purified by Soxhlet extraction with acetone and chloroform. The chloroform fraction was concentrated by rotary evaporation, and precipitated into acetone before filtering and drying under vacuum. The polymer was

isolated as black solid (0.60 g, 76%). ^{1}H NMR (500 MHz, $CDCl_3$): δ_H = 6.98–6.69 (m, 6H), 6.44 (d, *J* = 15.4 Hz, end group), 6.05 (dq, *J* = 15.0, 7.2 Hz, end group), 2.61 (d, *J* = 7.1 Hz, 4H), 1.87 (d, *J* = 6.7 Hz, end group), 1.60–1.56 (m, 4H), 1.31 (bs, 28H), 0.88 (t, *J* = 6.1 Hz, 6H). SEC ($CHCl_3$, 1 mL min^{-1}, RI): M_n = 4.6 kg mol^{-1}, M_w = 7.4 kg mol^{-1}, $Đ$ = 1.61. Anal. calcd. for $C_{32}H_{48}S_2$: C 77.36, H 9.74, S 12.91; Found: C 74.67, H 9.40, S 11.56.

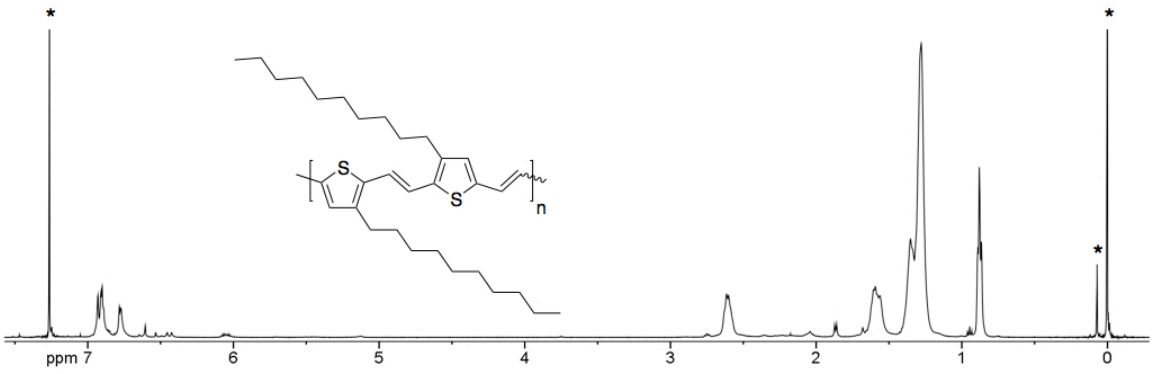

Figure B.17
^{1}H NMR spectrum of **P4**. Asterisks mark solvents and other non-product peaks.

P5. In an apparatus like that shown in Figure 2.24, **14** (1.0 g, 2.0 mmol) was dissolved in TCB (15 mL). The solution was degassed under vacuum for 30 min before adding G3 (18 mg, 0.020 mmol) in toluene (1 mL). The reaction was refluxed under vacuum at 80 °C for 24 h before precipitating into acetone (400 mL). The precipitate was collected by vacuum filtration and purified by Soxhlet extraction with acetone and chloroform. All polymer remained in the Soxhlet thimble and was isolated as black insoluble solid (0.72 g, 81%). Anal. calcd. for $C_{28}H_{40}S_2$: C 76.30, H 9.15, S 14.55; Found: C 76.40, H 9.21, S 14.31.

3,4-Bis(2-ethylhexyl)thiophene (15). A 3-neck 100 mL round bottom flask was equipped with a magnetic stirring bar, reflux condenser, glass stopcock, liquid addition funnel, and

2 rubber septa. Magnesium turnings (1.2 g, 50 mmol) were added and the apparatus was flame dried under vacuum. Anhydrous diethyl ether (10 mL) was added to the Mg and the liquid addition funnel. 2-ethylhexylbromide (7.7 mL, 44 mmol) was added to the addition funnel and the resulting solution was added dropwise to the Mg suspension over the course of 1 h. The reaction was stirred for an additional 1 h. Meanwhile, a 100 mL round bottom flask was equipped with a magnetic stirring bar and flame dried before adding 3,4-dibromothiophene (2.3 mL, 21 mmol), Ni(dppp)Cl_2 (112 mg, 0.21 mmol), and anhydrous diethyl ether (20 mL). The red suspension was cooled to 0 °C before adding the Grignard solution via cannula. The reaction was allowed to warm to room temperature while stirring under argon for 18 h. The reaction was quenched with 1 M HCl (10 mL) and poured into water (100 mL). The mixture was extracted with diethyl ether (3 × 100 mL) and the combined organics were washed with water and brine (100 mL each). The solution was dried over Na_2SO_4 and the solvent was removed by rotary evaporation. Pure product was obtained as a light yellow oil after vacuum distillation (4.7 g, 73%). ^{1}H NMR (300 MHz, $CDCl_3$): δ_H = 6.85 (s, 2H), 2.43 (d, *J* = 7.1 Hz, 4H), 1.54 (quintet, *J* = 8.4 Hz, 2H), 1.35–1.18 (m, 16H), 0.91–0.81 (m, 12H).

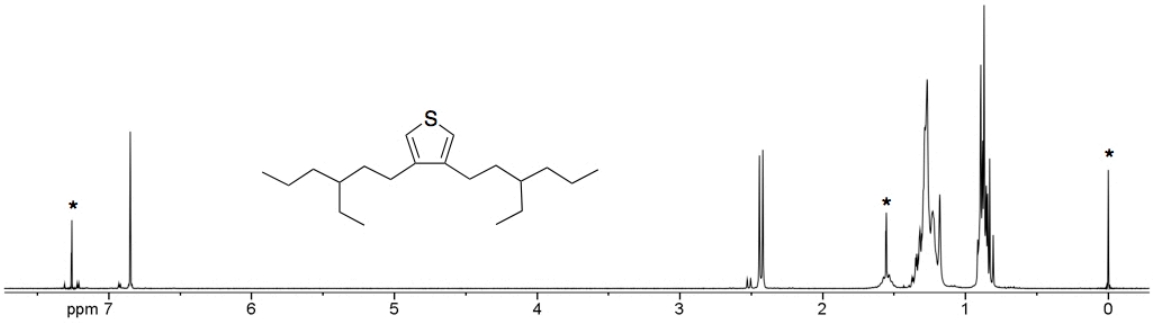

Figure B.18
^{1}H NMR spectrum of **15**. Asterisks mark solvents and other non-product peaks.

3,4-Bis(2-ethylhexyl)thiophene-2,5-dicarbaldehyde (16). A 3-neck 250 mL round bottom flask was equipped with a magnetic stirring bar, reflux condenser, glass stopcock, liquid addition funnel, and two rubber septa. The apparatus was flame dried under

vacuum before adding **15** (4.7 g, 15 mmol), TMEDA (5.7 mL, 38 mmol), and anhydrous hexanes (100 mL). *n*-Butyllithium (2.5 M in hexanes, 15.2 mL, 38 mmol) was *slowly* added dropwise via addition funnel. After addition the reaction was refluxed for 1 h and cooled to 0 °C. Anhydrous DMF (4.7 mL, 61 mmol) was added and the reaction was allowed to warm to room temperature while stirring under argon for 17 h. The reaction was quenched by the addition of 4 M HCl (20 mL) and extracted with diethyl ether (3 × 50 mL). The combined organics were washed with 1 M HCl and brine (50 mL each) before drying over Na_2SO_4. The solvent was removed by rotary evaporation to afford a brown oil, which was purified by column chromatography with 1:4 ethyl acetate/hexanes (3.8 g, 69%). ^{1}H NMR (300 MHz, $CDCl_3$): δ_H = 10.11 (s, 2H), 2.85 (d, *J* = 7.3 Hz, 4H), 1.51 (dt, *J* = 12.4, 6.3 Hz, 2H), 1.36–1.19 (m, 16H), 0.89 (q, *J* = 7.4 Hz, 12H).

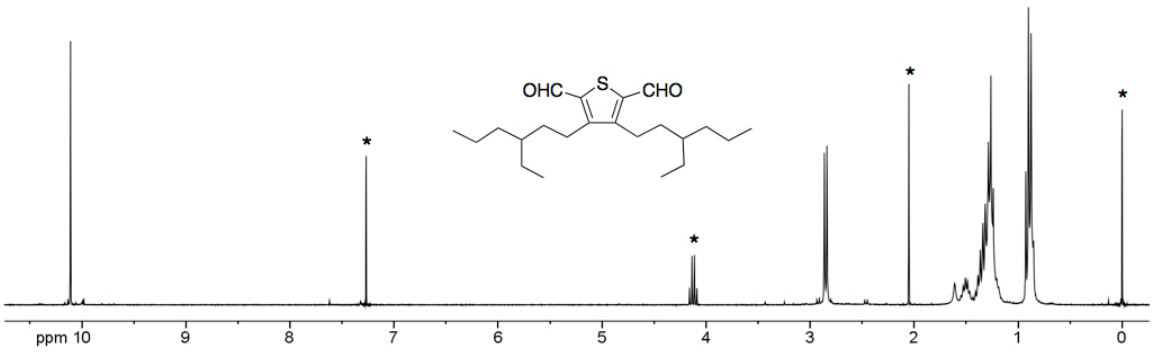

Figure B.19
^{1}H NMR spectrum of **16**. Asterisks mark solvents and other non-product peaks.

3,4-Bis(2-ethylhexyl)thiophene-2,5-dicarbaldehyde (17). A 100 mL reaction flask was equipped with a magnetic stirring bar and rubber septum before flame drying under vacuum. (Ethyl)triphenylphosphonium bromide (7.9 g, 21 mmol) was added and dried under vacuum before adding anhydrous THF (50 mL) via cannula. The suspension was cooled to 0 °C before adding *n*-butyllithium (2.5 M in hexanes, 8.5 mL, 21 mmol). The reaction was stirred for 30 min to form the Wittig reagent. **16** (3.7 g, 10 mmol) was added as a solution in anhydrous THF (15 mL). The reaction was allowed to warm to

room temperature while stirring under argon for 18 h. The reaction was concentrated by rotary evaporation and the residue was dissolved in 1:1 diethyl ether/hexanes (200 mL) and flushed through a plug of silica gel. This procedure was repeated once more with 1:1 ether/hexanes and then with pure hexanes to afford product as a yellow/orange oil (3.2 g, 82%). *E*:*Z* = 45:55. ^{1}H NMR (300 MHz, $CDCl_3$): δ_H = 6.56–6.44 (m, 2H), 6.07–5.89 (m, 1H), 5.64 (tq, *J* = 10.9, 7.3 Hz, 1H), 2.49–2.37 (m, 4H), 1.99 (t, *J* = 6.9 Hz, 3H), 1.86 (t, *J* = 5.6 Hz, 3H), 1.43 (quintet, *J* = 5.3 Hz, 2H), 1.26 (s, 16H), 0.86 (t, *J* = 4.0 Hz, 12H). Anal. calcd. for $C_{26}H_{44}S$: C 80.34, H 11.41, S 8.25; Found: C 80.34, H 11.45, S 8.19.

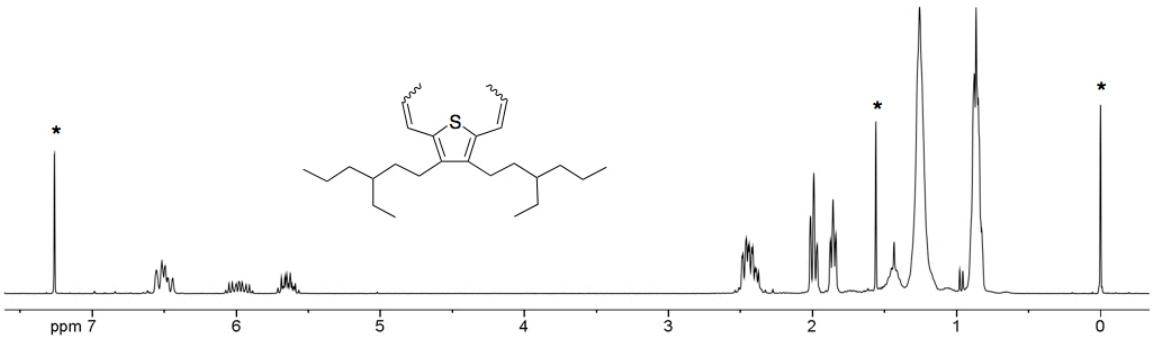

Figure B.20
^{1}H NMR spectrum of **17**. Asterisks mark solvents and other non-product peaks.

Poly(3,4-bis(2-ethylhexyl)thienylene vinylene) (P6). In an apparatus like that shown in Figure 2.24, **17** (0.5 g, 1.3 mmol) was dissolved in TCB (7 mL). The solution was degassed under vacuum for 30 min before adding G3 (9 mg, 0.013 mmol) in TCB (1 mL). The reaction was refluxed under vacuum at 80 °C for 24 h before adding another 9 mg of G3. After an additional 24 h another 9 mg of G3 was added. After 72 h total, the TCB was removed by vacuum distillation. The polymer residue was dissolved in hexanes and precipitated into methanol (0 °C). The precipitation procedure was repeated to afford the product polymer (0.42 g, 98%). ^{1}H NMR (500 MHz, $CDCl_3$): δ_H = 6.98 (s,

2H), 2.53 (s, 4H), 1.49 (s, 2H), 1.31 (s, 16H), 0.96–0.88 (m, 12H). SEC ($CHCl_3$, 1 mL min^{-1}, RI): M_n = 4.1 kg mol^{-1}, M_w = 7.9 kg mol^{-1}, $Đ$ = 1.93.

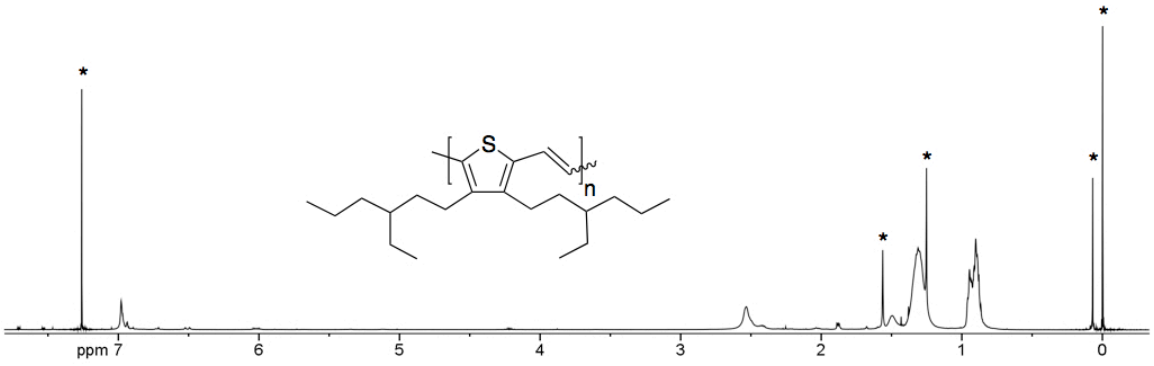

Figure B.21
^{1}H NMR spectrum of **P6**. Asterisks mark solvents and other non-product peaks.

B.3 PTVs: Substituent Effects

B.3.1 Motivation

Non-alkyl substituent groups have been shown to have a profound impact on CP behavior by changing the electronic structure of the polymer scaffold.[7] Therefore, PTVs with electron-withdrawing (Scheme B.3) and electron-donating (Scheme B.4) substituents were prepared in an effort to understand these effects. Attempts to prepare P8 and P9 by ADMET polymerization failed. Therefore, palladium-catalyzed Stille coupling was employed to generate these materials.

Scheme B.3

Synthesis of PTVs with electron-withdrawing functionalities.

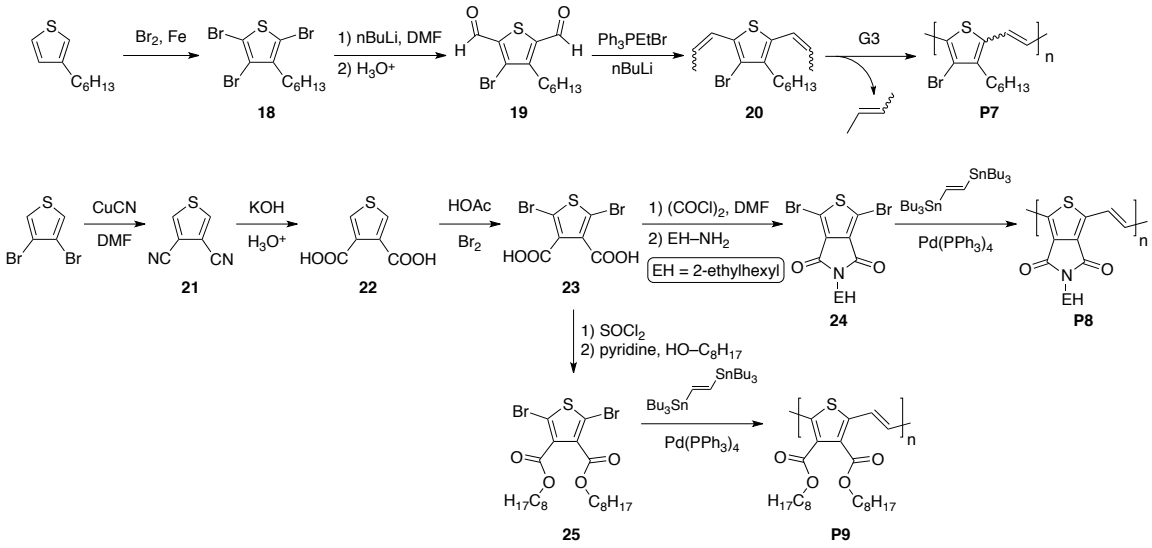

Scheme B.4

Synthesis of PTVs with electron-donating functionalities.

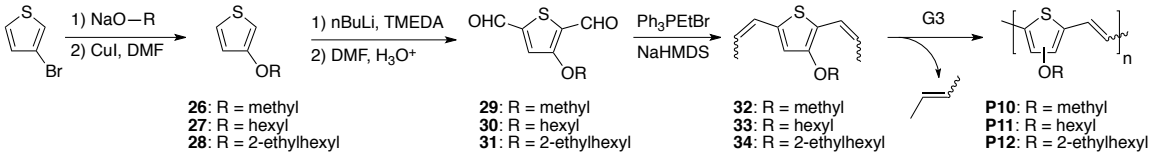

B.3.2 Synthetic Details

2,3,5-Tribromo-4-hexylthiophene (18). A 2-neck 500 mL round bottom flask was equipped with a magnetic stirring bar, liquid addition funnel, and two rubber septa. Iron powder (0.66 g, 12 mmol) was added and the apparatus was flame dried under a nitrogen flow. Anhydrous chloroform (200 mL) was added via cannula and 3-hexylthiophene (21.4 mL, 119 mmol) was added via syringe. Bromine (18.9 mL, 369 mmol) was *slowly* added to the reaction solution via the addition funnel. Note: Care must be taken to

properly vent the reaction. The reaction was stirred for 3 h before neutralizing with water (40 mL) and 2 M NaOH (125 mL). The solution was extracted with methylene chloride (2 × 75 mL), and the combined organics were washed with saturated $Na_2S_2O_3 \cdot H_2O$ (100 mL). The solution was dried over Na_2SO_4 before removing the solvent via rotary evaporation. The resulting dark orange oil was dried under high vacuum (45.3 g, 94%). ^{1}H NMR (300 MHz, $CDCl_3$): δ_H = 2.64 (t, *J* = 7.5 Hz, 2H), 1.50 (dt, *J* = 15.2, 7.5 Hz, 2H), 1.40–1.31 (m, 6H), 0.89 (t, *J* = 6.7 Hz, 3H).

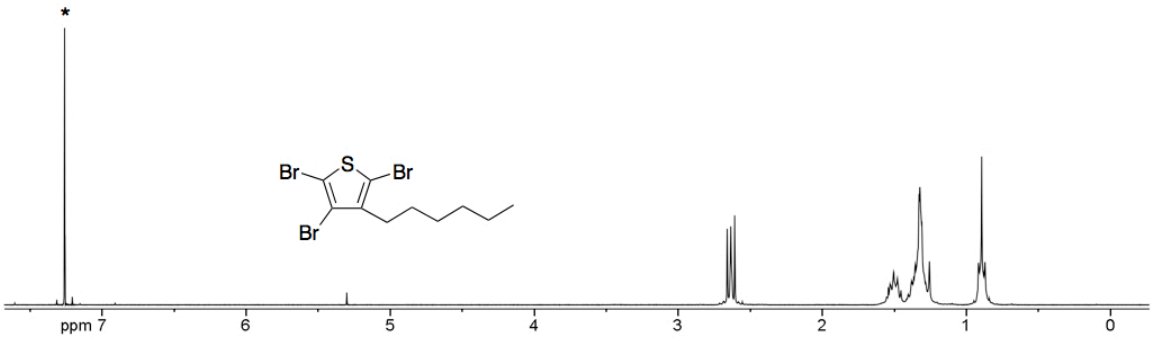

Figure B.22
^{1}H NMR spectrum of **18**. Asterisks mark solvents and other non-product peaks.

3-Bromo-4-hexylthiophene-2,5-dicarbaldehyde (19). A 3-neck 500 mL round bottom flask was equipped with a magnetic stirring bar, thermometer, liquid addition funnel, and two rubber septa. The apparatus was flame dried under a rapid nitrogen flow before adding **18** (15.0 g, 37 mmol) and anhydrous THF (200 mL). The solution was cooled to -65 °C, and *n*-butyllithium (2.5 M in hexanes, 30.0 mL, 74 mmol) was *slowly* added dropwise via addition funnel taking care not to exceed -60 °C. The reaction was stirred at -65 °C for an additional 30 min. 1-Formylpiperidine (9.2 mL, 83 mmol) was added, and the solution was allowed to slowly warm to room temperature while stirring under argon for 15 h. The reaction was cooled to 0 °C before *slowly* adding 6 M HCl (100 mL) via addition funnel. The mixture was separated, and the aqueous phase was extracted with diethyl ether (2 × 75 mL). The combined organics were washed with water (100 mL) and

dried over Na_2SO_4. The solvent was removed by rotary evaporation, and the resulting orange/brown oil was dissolved in hexanes. The hexanes solution was cooled to -78 °C and the product precipitated as a light brown solid (5.5 g, 49%). ^{1}H NMR (300 MHz, $CDCl_3$): δ_H = 10.12 (s, 1H), 10.10 (s, 1H), 3.03 (t, *J* = 7.8 Hz, 2H), 1.64 (dt, *J* = 15.3, 7.6 Hz, 2H), 1.44–1.30 (m, 6H), 0.90 (t, *J* = 6.9 Hz, 3H).

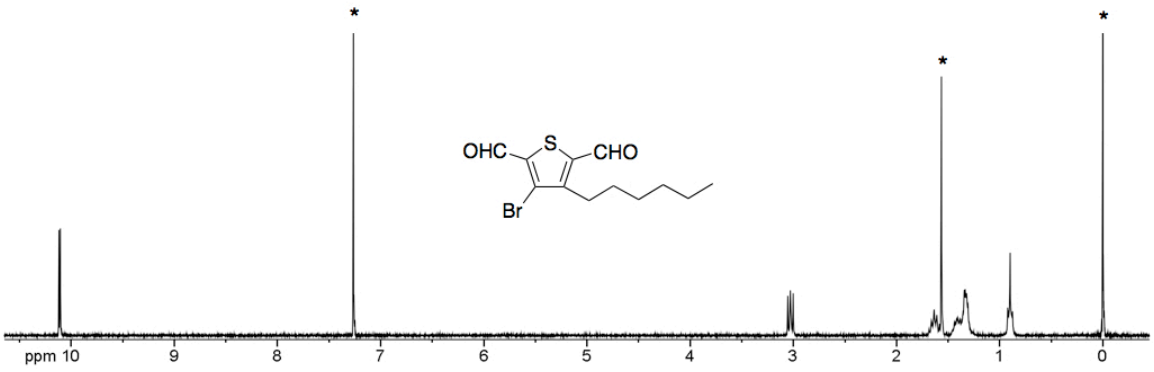

Figure B.23
^{1}H NMR spectrum of **19**. Asterisks mark solvents and other non-product peaks.

3-Bromo-4-hexylthiophene-2,5-dipropenyl (20). A 2-neck 100 mL round bottom flask was equipped with a magnetic stirring bar, glass stopcock, and rubber septum. The apparatus was flame dried under vacuum before adding (ethyl)triphenylphosphonium bromide (4.9 g, 13 mmol) and anhydrous THF (40 mL). The solution was cooled to 0 °C before adding *n*-butyllithium (2.5 M in hexanes, 5.3 mL, 13 mmol) via syringe. The reaction was stirred for 30 min before adding **19** (2.0 g, 6.6 mmol) in anhydrous THF (10 mL). The reaction was allowed to warm to room temperature while stirring under argon for 19 h. The reaction was concentrated by rotary evaporation and the resulting brown residue was dissolved in 1:1 diethyl ether/hexane (150 mL). This solution was passed through a silica gel column. This purification procedure was repeated once more with ether/hexanes and then with pure hexanes to afford product as a yellow oil (1.25 g, 58%). *E*:*Z* = 45:55. ^{1}H NMR (300 MHz, $CDCl_3$): δ_H = 6.69–6.44 (m, 2H), 6.20–5.68

(m, 2H), 2.67–2.54 (m, 2H), 2.02–1.86 (m, 6H), 1.52–1.43 (m, 2H), 1.31–1.26 (m, 6H), 0.88 (d, J = 13.1 Hz, 3H).

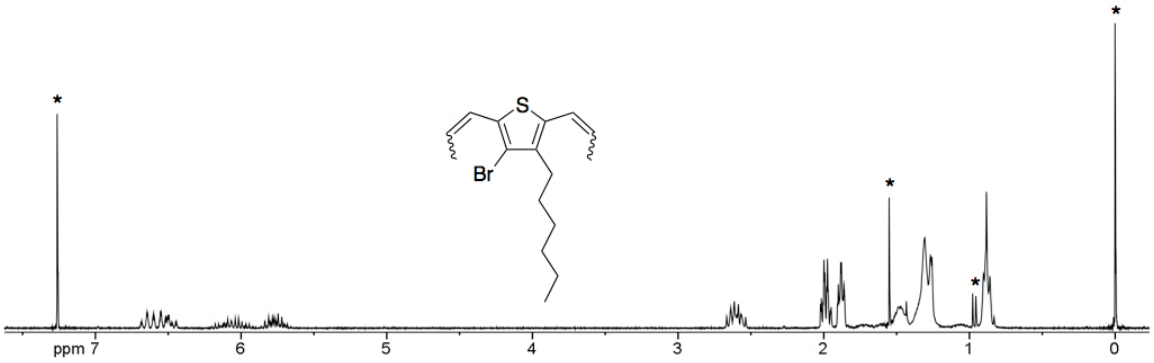

Figure B.24
^{1}H NMR spectrum of **20**. Asterisks mark solvents and other non-product peaks.

Poly(3-bromo-4-hexylthienylene vinylene) (P7). In an apparatus like that shown in Figure 2.24, **20** (0.5 g, 1.5 mmol) was dissolved in TCB (7 mL). The solution was degassed under vacuum for 30 min before adding G3 (14 mg, 0.015 mmol) in TCB (0.5 mL). The reaction was refluxed under vacuum at 80 °C for 24 h before precipitating into acetone (0 °C, 200 mL). The polymer was collected by filtration and purified by Soxhlet extraction with acetone and chloroform. Isolated the product as a black solid (0.36 g, 87%). Most of the polymer was insoluble, but enough soluble material was isolated for NMR and SEC analysis. ^{1}H NMR (500 MHz, $CDCl_3$): δ_H = 7.07–6.87 (m, 2H), 2.65 (s, 2H), 1.55 (s, 2H), 1.36 (s, 6H), 0.93 (s, 3H). SEC ($CHCl_3$, 1 mL min^{-1}, RI): M_n = 2.5 kg mol^{-1}, M_w = 3.3 kg mol^{-1}, $Đ$ = 1.30. Anal. calcd. for $C_{12}H_{15}BrS$: C 53.14, H 5.57, Br 29.46, S 11.82; Found: C 53.86, H 5.71, Br 28.89, S 11.48.

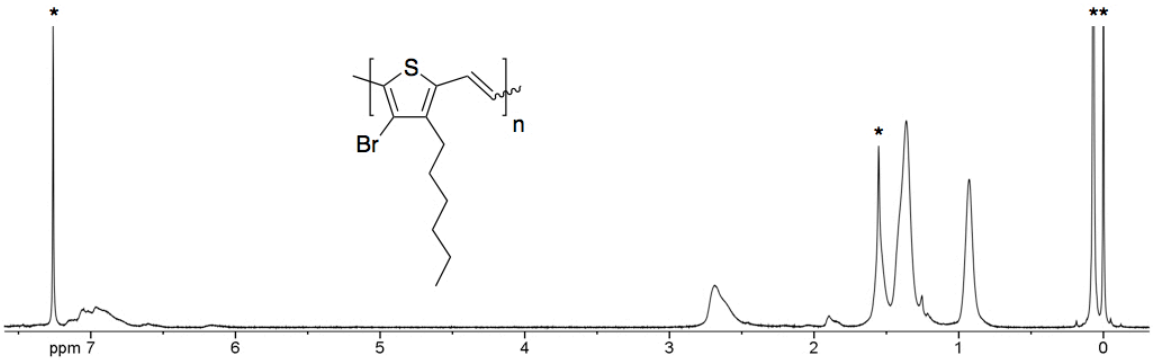

Figure B.25
^{1}H NMR spectrum of **P7**. Asterisks mark solvents and other non-product peaks.

Thiophene-3,4-dicarbonitrile (21). A 2-neck 50 mL round bottom flask was equipped with a magnetic stirring bar, reflux condenser, glass stopcock, and rubber septum. The apparatus was flame dried under vacuum, and 3,4-dibromothiophene (10.0 g, 41 mmol) was added. Copper(I) cyanide (9.3 g, 103 mmol) was added followed by anhydrous DMF (25 mL). The solution was refluxed under argon for 3 h and poured into a solution of iron(III) chloride (23.5 g, 145 mmol) and 2 M HCl (50 mL). This solution was stirred at 70 ˚C for 30 min before cooling to room temperature and extracting with methylene chloride (3 × 100 mL). The combined organics were washed with 6 M HCl, water, saturated $NaHCO_3$, and brine (100 mL each) before drying over Na_2SO_4. The solvent was removed by rotary evaporation, and the resultant residue was purified by vacuum sublimation at 110 ˚C to afford product as a white solid (4.4 g, 80%). ^{1}H NMR (300 MHz, $CDCl_3$): δ_H = 8.07 (s, 2H).

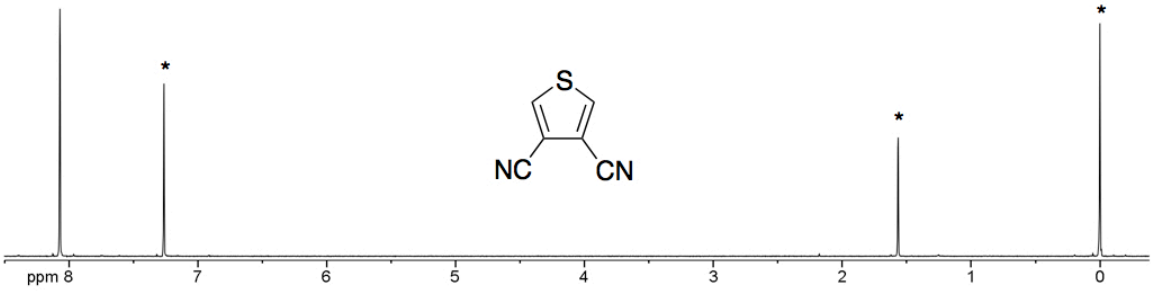

Figure B.26
^{1}H NMR spectrum of **21**. Asterisks mark solvents and other non-product peaks.

Thiophene-3,4-dicarboxylic acid (22). To a 100 mL round bottom flask **21** (4.4 g, 33 mmol), potassium hydroxide (12.0 g, 213 mmol), ethylene glycol (50 mL), and magnetic stirring bar were added. The flask was equipped with a reflux condenser and glass stopcock before refluxing for 4 h. The reaction was allowed to cool at which point a white precipitate formed. The reaction was poured into water (200 mL) and extracted with diethyl ether (100 mL). The aqueous portion was acidified with excess HCl, and the resultant precipitate was collected by vacuum filtration and dissolved in diethyl ether (200 mL). The acidified filtrate was also extracted with diethyl ether (3 × 50 mL). The combined ethereal portions were dried over Na_2SO_4 before removing the solvent by rotary evaporation to afford product as a pinkish solid. Trace ethylene glycol was removed under vacuum (4.9 g, 88%). ^{1}H NMR (500 MHz, DMSO-d_6): δ_H = 8.15 (s, 2H).

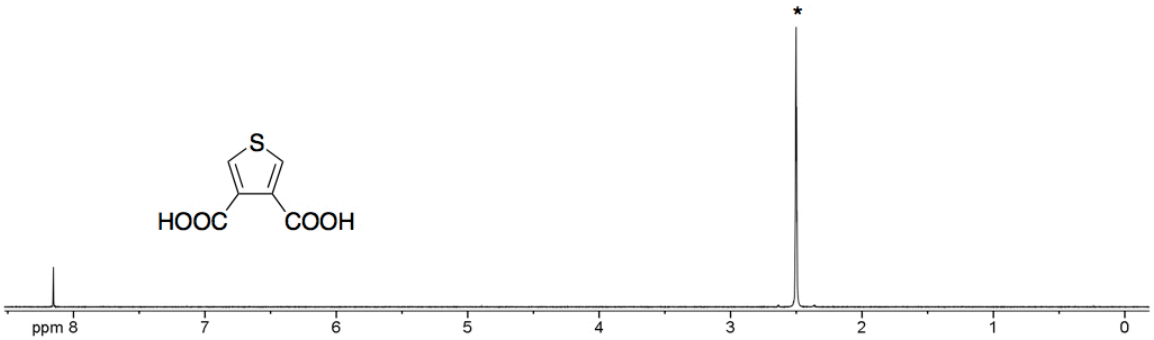

Figure B.27
^{1}H NMR spectrum of **22**. Asterisks mark solvents and other non-product peaks.

2,5-Dibromothiophene-3,4-dicarboxylic acid (23). A 50 mL round bottom flask was equipped with a magnetic stirring bar before adding **22** (1.25 g, 7.3 mmol) and glacial acetic acid (13 mL). The flask was sealed under argon with a septum before *slowly* adding bromine (2.2 mL, 44 mmol) via syringe. Caution: care must be taken to properly vent the system. Following addition the reaction was allowed to stir under argon at room temperature for 20 h. The reaction was quenched by pouring into saturated $NaHSO_4$ (100 mL), and saturated $NaHSO_3$ (25 mL) was added to remove residual bromine. The heterogeneous solution was cooled on an ice bath and filtered to afford product as an off-white crystalline solid (1.9 g, 81%). ^{13}C NMR (125 MHz, DMSO-d_6): δ_C = 162.6, 135.2, 114.5.

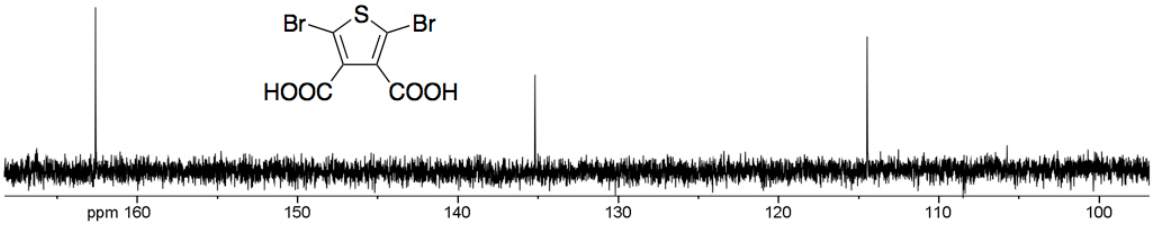

Figure B.28

^{13}C NMR spectrum of **23**.

1,3-Dibromo-5-(2-ethylhexyl)-4*H*-thieno[3,4-*c*]pyrrole-4,6(5*H*)-dione (24). A 2-neck 250 mL round bottom flask was equipped with a magnetic stirring bar, reflux condenser, and two rubber septa. The apparatus was flame dried under nitrogen flow before adding **23** (1.9 g, 5.8 mmol), 1 drop of anhydrous DMF (catalyst), and benzene (100 mL). Oxalyl chloride (2.0 mL, 23 mmol) was *slowly* added via syringe. Caution: care must be taken to properly vent the system as CO_2 and CO violently form. Once bubbling subsided the reaction was refluxed for 1 h before cooling to room temperature. The solvent was removed by rotary evaporation to yield the diacid chloride (1.9 g, 5.2 mmol), which was immediately added to a flame dried 10 mL round bottom flask. The flask was

sealed with a rubber septum and purged with argon before *slowly* adding 2-ethylhexylamine (0.85 mL, 5.2 mmol). Caution: HCl forms. Following addition the reaction was heated to 140 °C and stirred for 18 h. The resulting brown solid was dissolved in ethyl acetate and washed with saturated $NaHCO_3$ (100 mL) and dried over Na_2SO_4. The solvent was removed by rotary evaporation, and the resultant solid was subjected to column chromatography with 1:9 ethyl acetate/hexanes. The resulting yellow crystalline solid was further purified by recrystallization from ethanol (1.9 g, 86%). ^{1}H NMR (500 MHz, $CDCl_3$): δ_H = 3.49 (d, *J* = 6.9 Hz, 2H), 1.77 (dquintet, *J* = 12.5, 6.3 Hz, 1H), 1.34–1.25 (m, 8H), 0.92-0.88 (m, 6H). Anal. calcd. for $C_{14}H_{17}Br_2NO_2S$: C 39.74, H 4.05, Br 37.77, N 3.31, O 7.56, S 7.58; Found: C 40.31, H 4.08, Br 36.40, N 3.33, O 7.46, S 7.85.

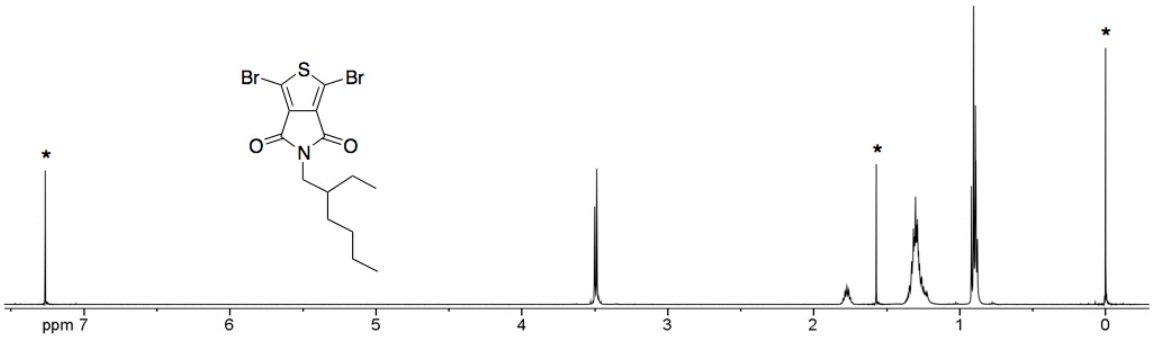

Figure B.29
^{1}H NMR spectrum of **24**. Asterisks mark solvents and other non-product peaks.

P8. A 5 mL Schlenk tube was equipped with a magnetic stirring bar and flame dried under vacuum before adding **24** (100 mg, 0.24 mmol). The tube was sealed and brought into an inert atmosphere glovebox where degassed anhydrous toluene (4 mL), (*E*)-1,2-bis(tributylstannyl)ethane (0.13 mL, 0.24 mmol), and tetrakis(triphenylphosphine)palladium(0) (17 mg, 0.015 mmol) were added. The flask was removed from the glovebox and heated to 110 °C for 72 h. The solution was precipitated into methanol. The polymer precipitate was collected by filtration and

purified by Soxhlet extraction with methanol, hexanes, and chloroform. The chloroform fraction was concentrated by rotary evaporation to afford the product polymer as a dark solid (48 mg, 69%). ^{1}H NMR (500 MHz, $CDCl_3$): δ_H = 7.85–7.47 (m, 2H), 3.56 (s, 2H), 1.85 (s, 1H), 1.41–1.25 (m, 8H), 0.92 (t, J = 7.2 Hz, 6H). SEC ($CHCl_3$, 1 mL min^{-1}, RI): M_n = 5 kg mol^{-1}, M_w = 10 kg mol^{-1}, $Đ$ = 2.00.

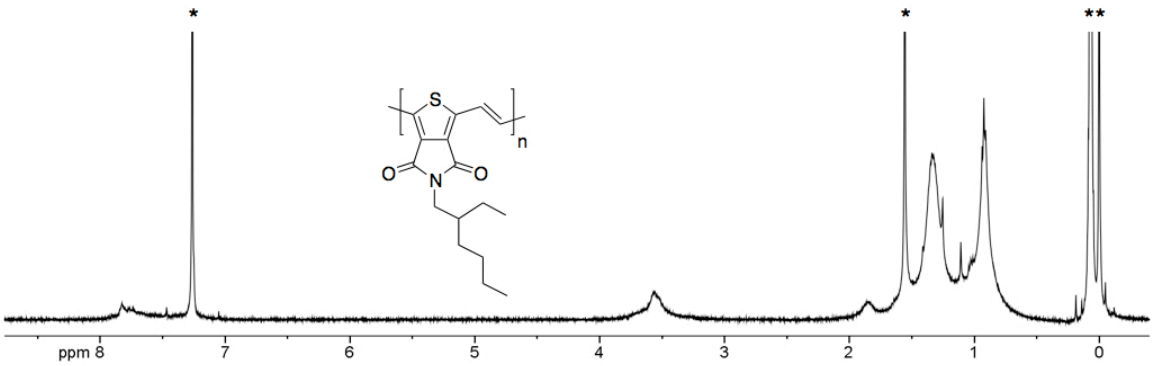

Figure B.30
^{1}H NMR spectrum of **P8**. Asterisks mark solvents and other non-product peaks.

Dioctyl-2,5-dibromothiophene-3,4-dicarboxylate (25). 23 (0.5 g, 1.5 mmol) and thionyl chloride (11 mL, 151 mmol) were refluxed for 6 h before removing the excess thionyl chloride under vacuum. A mixture of 1-octanol (2.0 g, 15 mmol) and pyridine (3 mL) was *slowly* added to the diacid chloride. The reaction was stirred for 6 h at 80 °C before cooling and pouring into a mixture of ice (20 g) and 1 M HCl (20 mL). The mixture was extracted with diethyl ether (4 × 50 mL), and the combined organics were washed with saturated $NaHCO_3$ (3 × 50 mL) before drying over Na_2SO_4. The product was isolated as a light yellow solid by column chromatography with 1:4 ethyl acetate/hexanes (0.5 g, 60%). ^{1}H NMR (500 MHz, $CDCl_3$): δ_H = 4.28 (t, J = 6.7 Hz, 4H), 1.71 (dt, J = 14.6, 7.1 Hz, 4H), 1.40 (dt, J = 15.4, 7.7 Hz, 4H), 1.29 (dt, J = 15.0, 7.7 Hz, 18H), 0.88 (td, J = 7.2, 2.9 Hz, 7H). ^{13}C NMR (125 MHz, $CDCl_3$): δ_C = 161.9, 134.2, 115.9, 66.6, 32.1, 29.52, 29.51, 28.8, 26.2, 23.0, 14.4.

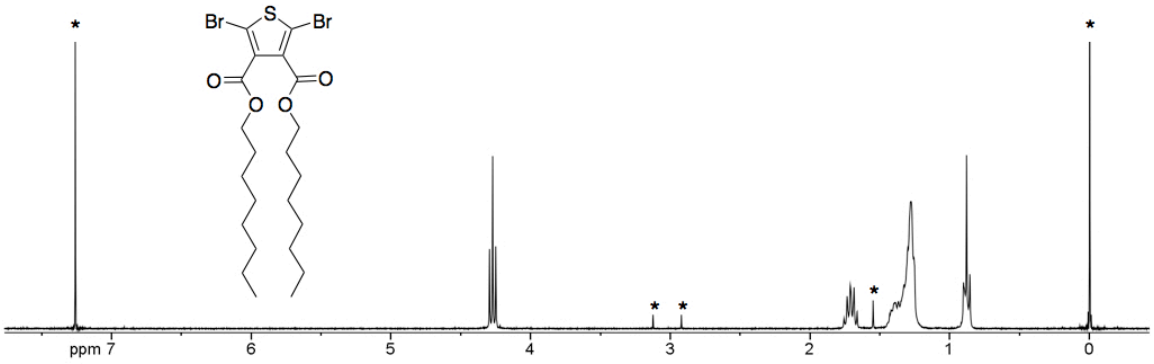

Figure B.31
^{1}H NMR spectrum of **25**. Asterisks mark solvents and other non-product peaks.

P9. A 5 mL Schlenk tube was equipped with a magnetic stirring bar and flame dried under vacuum before adding **25** (100 mg, 0.18 mmol). The tube was sealed and brought into an inert atmosphere glovebox where degassed anhydrous toluene (1 mL), (*E*)-1,2-bis(tributylstannyl)ethane (95 μL, 0.18 mmol), and tetrakis(triphenylphosphine)palladium(0) (2.0 mg, 0.0018 mmol) were added. The flask was removed from the glovebox and heated to 110 °C for 48 h. The solution was precipitated into methanol. The polymer precipitate was collected by filtration and purified by Soxhlet extraction with methanol and chloroform. The chloroform fraction was concentrated by rotary evaporation to afford the product polymer as a dark solid (70 mg, 93%). ^{1}H NMR (500 MHz, $CDCl_3$): δ_H = 7.72–7.47 (m, 2H), 4.32–4.20 (m, 4H), 1.75–1.74 (m, 4H), 1.52–1.23 (m, 20H), 0.94–0.84 (m, 6H). SEC ($CHCl_3$, 1 mL min^{-1}, RI): M_n = 5 kg mol^{-1}, M_w = 8 kg mol^{-1}, $Đ$ = 1.60.

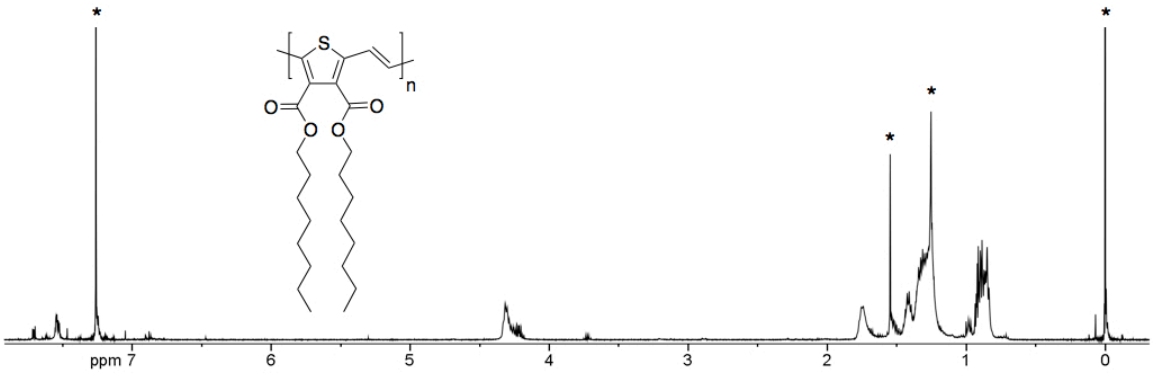

Figure B.32
^{1}H NMR spectrum of **P9**. Asterisks mark solvents and other non-product peaks.

General synthesis procedure for 26–28. To a flame dried round bottom flask was added the appropriate alcohol (at least 10 molar equivalents), sodium chunks (1.4 molar equivalents), and a magnetic stirring bar. The flask was sealed under argon with a rubber septum and stirred until all sodium dissolved (alkoxide formation). Warming the solution was often necessary. The residual alcohol was distilled under vacuum before adding anhydrous DMF and heating to 110 °C. 3-Bromothiophene (1.0 molar equivalent) and copper(I) iodide (0.20 molar equivalents) were then added, and the reaction was stirred under argon for 18 h at 110 °C. A copper mirror was often observed and was indicative of reaction. The reaction was quenched with 1 M NH_4Cl and extracted with hexanes. The combined organics were washed thoroughly with water. The solvent was removed by rotary evaporation, and residuals (alcohol and DMF) were removed by vacuum distillation. The product was further purified by vacuum distillation or column chromatography with hexanes.

3-(Methyloxy)thiophene (26). Product was isolated as a clear liquid after vacuum distillation (4.9 g, 70%). ^{1}H NMR (300 MHz, $CDCl_3$): δ_H = 7.21 (dd, J = 5.2, 3.1 Hz,

1H), 6.79 (dd, *J* = 5.2, 1.6 Hz, 1H), 6.28 (dd, *J* = 3.1, 1.6 Hz, 1H), 3.83 (s, 3H). ^{13}C NMR (75 MHz, $CDCl_3$): δ_C = 159.0, 125.1, 119.5, 96.8, 57.6.

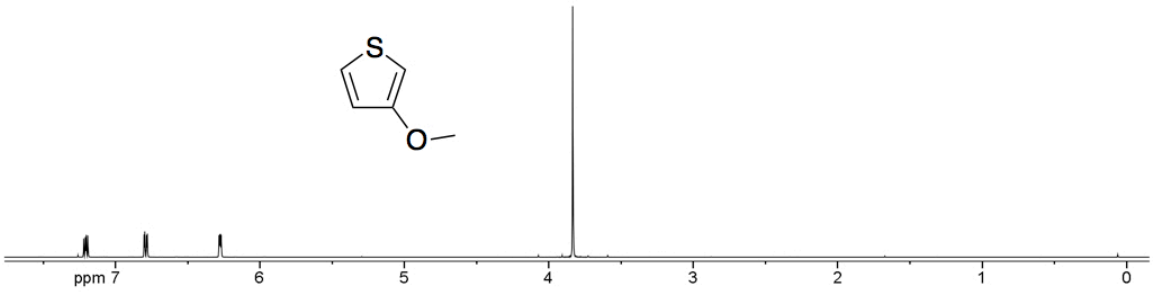

Figure B.33

^{1}H NMR spectrum of **26**.

3-(Hexyloxy)thiophene (27). Product was isolated as a yellow liquid after vacuum distillation (34.4 g, 70%). ^{1}H NMR (500 MHz, $CDCl_3$): δ_H = 7.17 (dd, *J* = 5.3, 3.1 Hz, 1H), 6.75 (dd, *J* = 5.2, 1.5 Hz, 1H), 6.22 (dd, *J* = 3.1, 1.5 Hz, 1H), 3.94 (t, *J* = 6.6 Hz, 2H), 1.77 (dt, *J* = 14.7, 7.1 Hz, 2H), 1.45 (quintet, *J* = 7.5 Hz, 2H), 1.34–1.32 (m, 4H), 0.90 (t, *J* = 7.0 Hz, 3H).

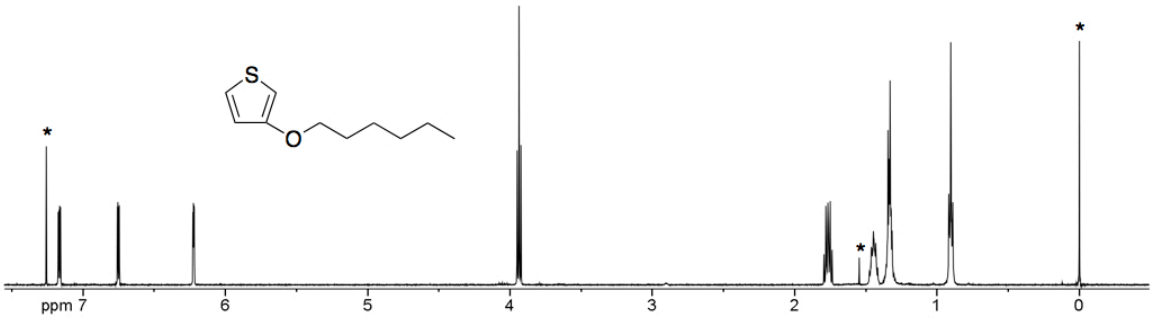

Figure B.34

^{1}H NMR spectrum of **27**. Asterisks mark solvents and other non-product peaks.

3-((2-Ethylhexyl)oxy)thiophene (28). Product was isolated as a yellow oil after column chromatography (5.6 g, 86%). ^{1}H NMR (300 MHz, $CDCl_3$): δ_H = 7.16 (dd, *J* = 5.2, 3.1 Hz, 1H), 6.75 (dd, *J* = 5.2, 1.5 Hz, 1H), 6.22 (dd, *J* = 3.1, 1.5 Hz, 1H), 3.83 (d, *J* = 5.8

Hz, 2H), 1.70 (dt, J = 12.1, 6.0 Hz, 1H), 1.52–1.26 (m, 8H), 0.95–0.88 (m, 6H). ^{13}C NMR (125 MHz, $CDCl_3$): δ_C = 158.6, 124.7, 119.9, 97.0, 73.0, 39.7, 30.8, 29.4, 24.2, 23.4, 14.4, 11.4.

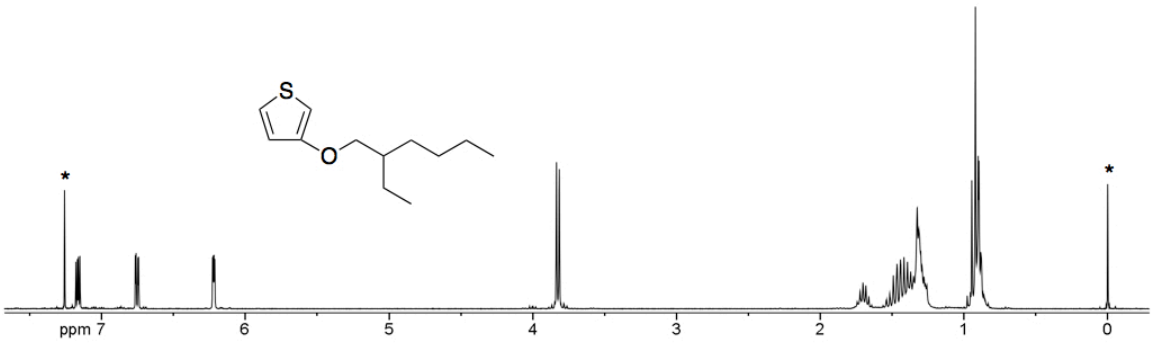

Figure B.35
^{1}H NMR spectrum of **28**. Asterisks mark solvents and other non-product peaks.

General synthesis procedure for 29–31. A 3-neck round bottom flask was equipped with a magnetic stirring bar, reflux condenser, glass stopcock, liquid addition funnel, and two rubber septa. The flask was flame dried under vacuum before adding the alkoxy thiophene (**26–28**, 1.0 molar equivalent), TMEDA (2.5 molar equivalents), and anhydrous hexanes. *n*-Butyllithium (2.5 M in hexanes, 2.5 molar equivalants) was added dropwise to the solution via addition funnel. The solution was refluxed for 1 h before adding anhydrous THF and cooling to 0 °C. Anhydrous DMF (4.0 molar equivalents) was added and the reaction was allowed to warm to room temperature while stirring under argon for 18 h. The reaction was quenched by the addition of 1 M HCl and extracted with diethyl ether. The combined organics were washed with water and brine and the solvent was removed by rotary evaporation. The resulting residue was purified by column chromatography with hexanes→methylene chloride to yield product.

3-(Methyloxy)thiophene-2,5-dicarbaldehyde (29). Product was isolated as an orange solid (2.8 g, 42%). ^{1}H NMR (300 MHz, $CDCl_3$): δ_H = 10.12 (s, 1H), 9.91 (s, 1H), 7.52 (s, 1H), 4.05 (s, 3H).

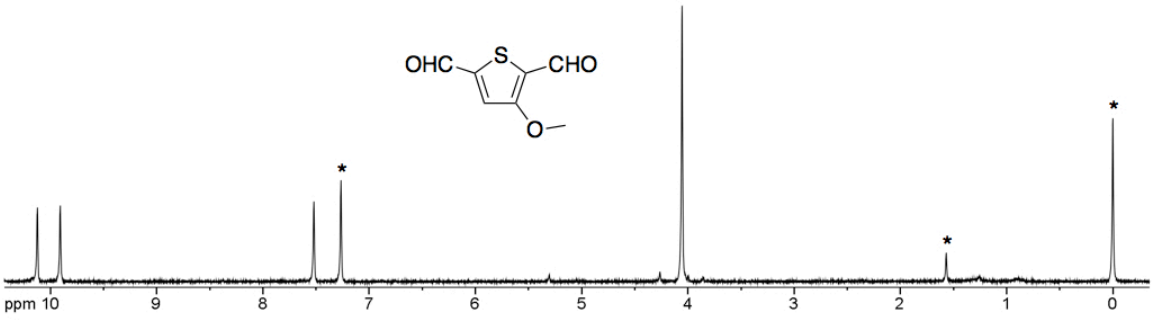

Figure B.36
^{1}H NMR spectrum of **29**. Asterisks mark solvents and other non-product peaks.

3-(Hexyloxy)thiophene-2,5-dicarbaldehyde (30). Product was isolated as yellow solid (14.2 g, 73%). ^{1}H NMR (500 MHz, $CDCl_3$): δ_H = 10.14 (s, 1H), 9.89 (s, 1H), 7.49 (s, 1H), 4.20 (t, *J* = 6.5 Hz, 2H), 1.85 (dt, *J* = 14.7, 7.1 Hz, 2H), 1.48 (quintet, *J* = 7.5 Hz, 2H), 1.39–1.32 (m, 4H), 0.92 (t, *J* = 7.1 Hz, 3H).

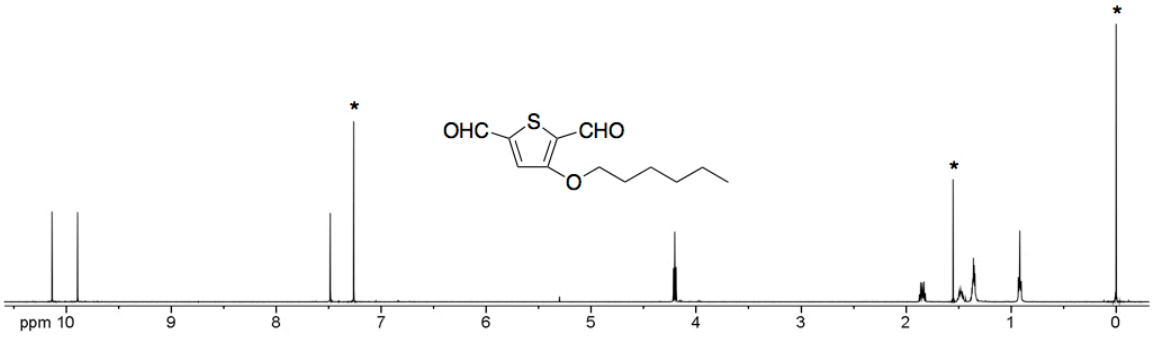

Figure B.37
^{1}H NMR spectrum of **30**. Asterisks mark solvents and other non-product peaks.

3-((2-Ethylhexyl)oxy)thiophene-2,5-dicarbaldehyde (31). Product was isolated as a brown oil (4.4 g, 70%). ^{1}H NMR (300 MHz, $CDCl_3$): δ_H = 10.13 (s, 1H), 9.90 (s, 1H), 7.50 (s, 1H), 4.10 (d, *J* = 5.7 Hz, 2H), 1.79 (dquintet, *J* = 12.2, 6.1 Hz, 1H), 1.55–1.26

(m, 8H), 0.98–0.89 (m, 6H). ^{13}C NMR (125 MHz, $CDCl_3$): δ_C = 182.9, 182.2, 163.5, 146.6, 127.5, 121.5, 74.9, 39.4, 30.3, 29.0, 23.7, 23.0, 14.1, 11.1.

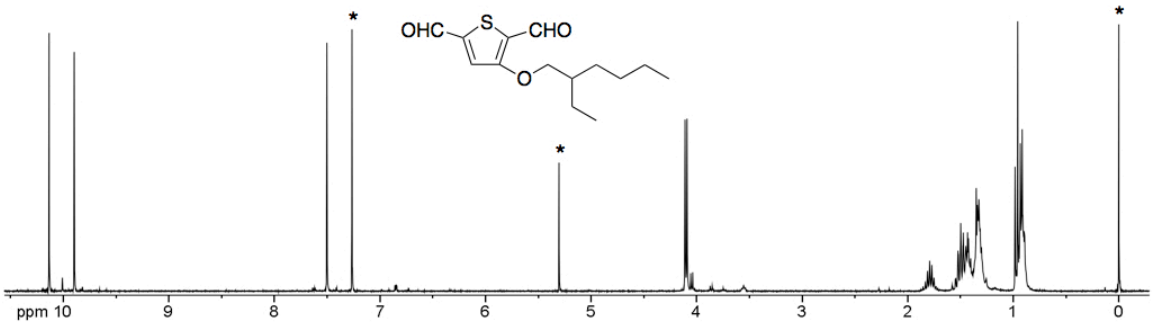

Figure B.38
^{1}H NMR spectrum of **31**. Asterisks mark solvents and other non-product peaks.

General synthesis procedure for 32–34. A 2-neck round bottom flask was equipped with a magnetic stirring bar, reflux condenser, glass stopcock, and rubber septum. The flask was flame dried under vacuum before adding (ethyl)triphenylphosphonium bromide (2.1 molar equivalents) and sodium bis(trimethylsilyl)amide (2.1 molar equivalents). The solids were dried under vacuum for 30 min before adding anhydrous hexanes. The heterogeneous reaction mixture was refluxed for 1 h to form the Wittig reagent. The solution was cooled to -78 °C and the solids were allowed to settle. The hexanes were decanted away using a cannula. Fresh hexanes were added for a second wash before drying the solids under vacuum and dissolving in anhydrous THF. Meanwhile, a second flame dried round bottom flask was equipped with a magnetic stirring bar before adding dialdehyde (**29–31**, 1.0 molar equivalent) and anhydrous THF. This solution was cooled to 0 °C before adding the Wittig solution via cannula. After stirring for 1 h the reaction solution was filtered to remove $Ph_3P{=}O$. The filtrate was concentrated, dissolved in 1:9 diethyl ether/hexanes, and passed through a plug silica gel. The silica gel purification was repeated with hexanes to afford product.

3-(Methyloxy)thiophene-2,5-dipropenyl (32). Isolated product as a light yellow oil after vacuum distillation (2.2 g, 96%). *E*:*Z* = 23:77. ^{1}H NMR (500 MHz, $CDCl_3$): δ_H = 6.70, 6.59 (s, 1H), 6.63–6.37 (m, 2H), 6.09–5.48 (m, 2H), 3.83–3.77 (m, 3H), 2.00–1.82 (m, 6H). ^{13}C NMR (125 MHz, $CDCl_3$): δ_C = 154.8, 139.8, 138.1, 125.43, 125.23, 125.0, 124.8, 123.59, 123.50, 123.32, 122.2, 121.8, 121.1, 119.41, 119.39, 118.7, 116.5, 115.4, 112.8, 58.93, 58.91, 18.6, 15.64, 15.50.

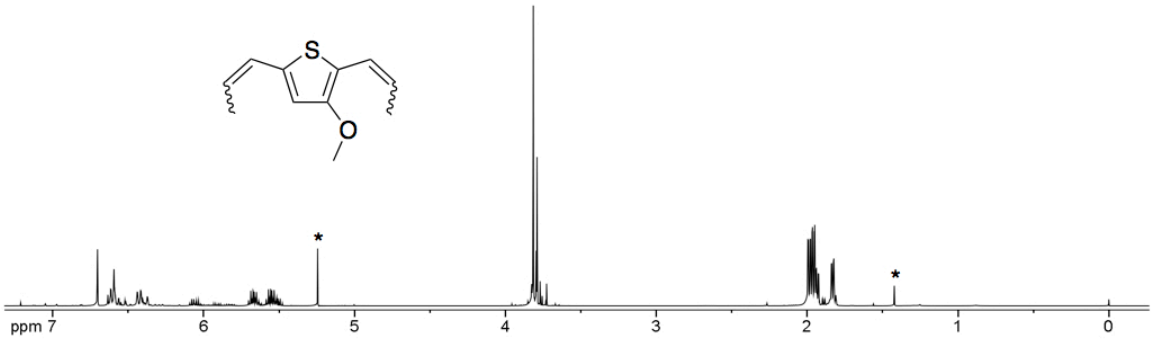

Figure B.39
^{1}H NMR spectrum of **32**. Asterisks mark solvents and other non-product peaks.

3-(Hexyloxy)thiophene-2,5-dipropenyl (33). Isolated product as a yellow oil (8.5 g, 54%). *E*:*Z* = 23:77. ^{1}H NMR (500 MHz, $CDCl_3$): δ_H = 6.71, 6.60 (s, 1H), 6.64–6.39 (m, 2H), 6.11–5.48 (m, 2H), 4.00–3.92 (m, 2H), 2.01–1.84 (m, 6H), 1.77–1.69 (m, 2H), 1.47–1.41 (m, 2H), 1.34–1.26 (m, 4H), 0.90 (t, *J* = 6.9 Hz, 3H).

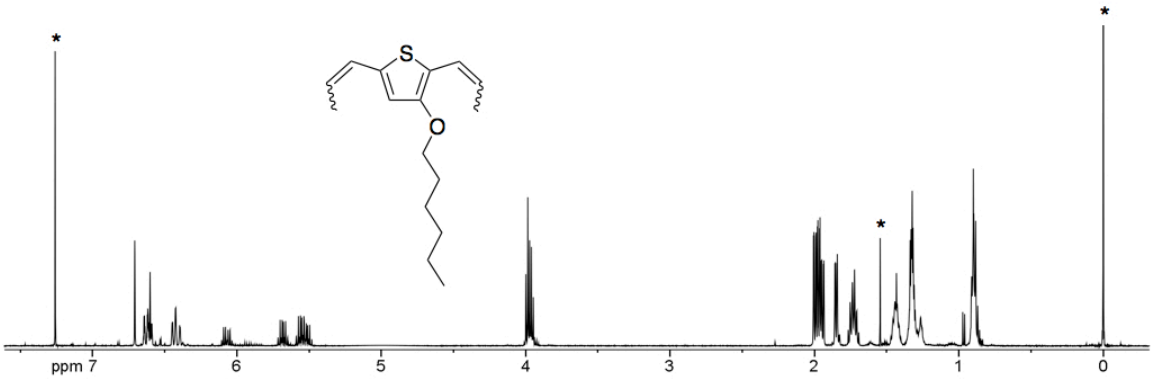

Figure B.40

^{1}H NMR spectrum of **33**. Asterisks mark solvents and other non-product peaks.

3-((2-Ethylhexyl)oxy)thiophene-2,5-dipropenyl (34). Isolated product as a yellow oil after column chromatography (3.1 g, 70%). *E*:*Z* = 30:70. ^{1}H NMR (500 MHz, $CDCl_3$): δ_H = 6.71, 6.61 (s, 1H), 6.65–6.34 (m, 2H), 6.11–5.47 (m, 2H), 3.90–3.83 (m, 2H), 2.01–1.83 (m, 6H), 1.68 (dq, *J* = 12.5, 6.3 Hz, 1H), 1.54–1.25 (m, 8H), 0.94–0.89 (m, 6H). ^{13}C NMR (125 MHz, $CDCl_3$): δ_C = 154.5, 152.8, 139.7, 138.0, 125.29, 125.12, 125.04, 124.94, 124.89, 123.70, 123.61, 123.0, 121.7, 121.36, 121.30, 119.72, 119.70, 119.2, 117.5, 116.3, 113.7, 74.3, 40.1, 30.79, 30.77, 29.42, 29.40, 24.16, 24.14, 23.4, 18.6, 15.72, 15.55, 14.4, 11.4.

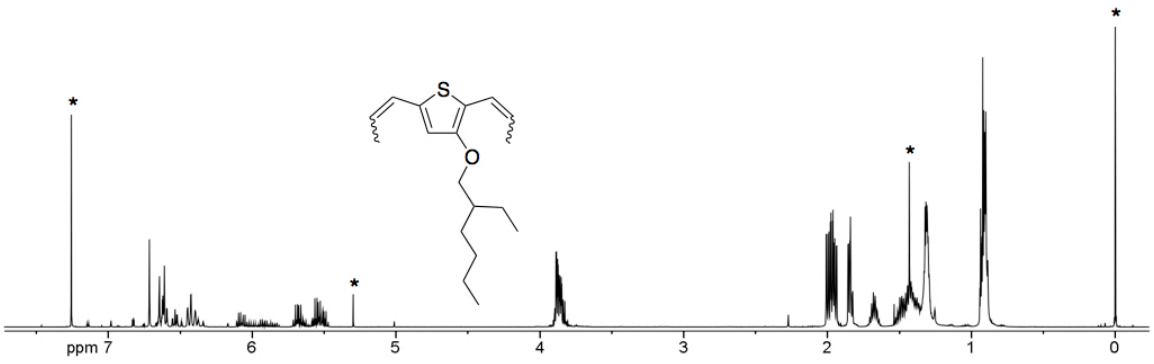

Figure B.41
^{1}H NMR spectrum of **34**. Asterisks mark solvents and other non-product peaks.

General polymerization procedure for P10–P12. In an apparatus like that shown in Figure 2.24, **32–34** (1.0 molar equivalent) was dissolved in TCB (5–7 mL). The solution was degassed under vacuum for 30 min before adding G3 (0.01 molar equivalents) in TCB (0.5 mL). The reaction was refluxed under vacuum at 80 °C for 24–48 h before precipitating into a non-solvent (acetone or methanol). The polymer was purified by Soxhlet extraction with the same non-solvent before extracting into chloroform. The chloroform fraction was concentrated by rotary evaporation to afford polymer as a dark solid.

Poly(3-(methyloxy)thienylene vinylene) (P10). Polymer was isolated as a black insoluble material (170 mg, 47%).

Poly(3-(hexyloxy)thienylene vinylene) (P11). Polymer was isolated as a black material (120 mg, 60%). ^{1}H NMR (500 MHz, $CDCl_3$): δ_H = 7.03–6.66 (m, 3H), 4.03 (s, 2H), 1.80 (s, 2H), 1.49 (s, 2H), 1.38 (s, 4H), 0.94 (s, 3H). SEC ($CHCl_3$, 1 mL min^{-1}, RI): M_n = 2.6 kg mol^{-1}, M_w = 2.9 kg mol^{-1}, $Đ$ = 1.13.

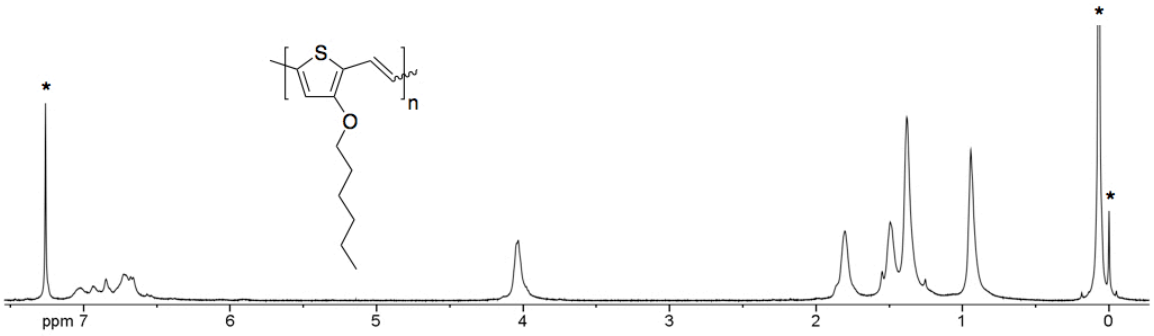

Figure B.42
^{1}H NMR spectrum of **P11**. Asterisks mark solvents and other non-product peaks.

Poly(3-((2-ethylhexyl)oxy)thienylene vinylene) (P12). Polymer was isolated as a black sticky material (260 mg, 65%). ^{1}H NMR (500 MHz, $CDCl_3$): δ_H = 7.03–6.67 (m, 3H), 3.94 (s, 2H), 1.76 (s, 1H), 1.53–1.36 (m, 8H), 0.98–0.94 (m, 6H). SEC ($CHCl_3$, 1 mL min^{-1}, RI): M_n = 2.3 kg mol^{-1}, M_w = 2.9 kg mol^{-1}, $Đ$ = 1.26. Anal. calcd. for $C_{14}H_{20}OS$: C 71.14, H 8.53, O 6.77, S 13.57; Found: C 70.45, H 8.42, O 6.93, S 13.01.

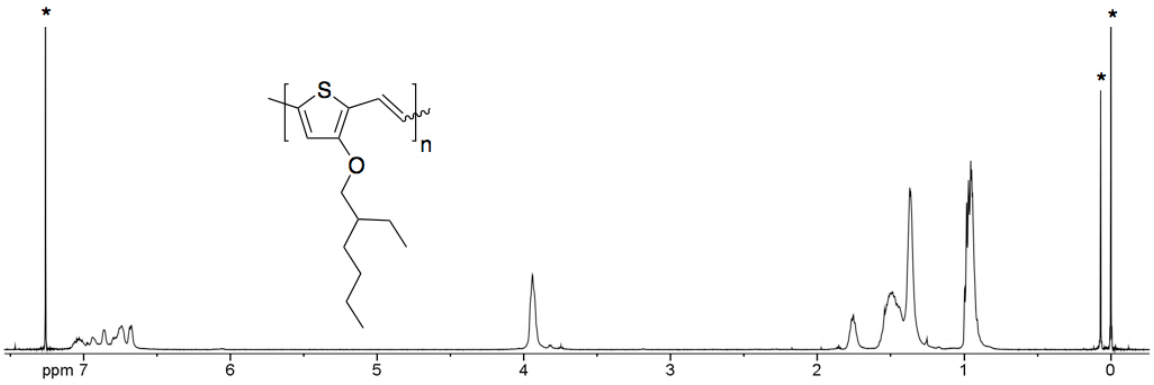

Figure B.43
^{1}H NMR spectrum of **P12**. Asterisks mark solvents and other non-product peaks.

B.4 Crosslinked Conjugated Polymers

B.4.1 Motivation

Porous polymers are an interesting class of materials, which find use in myriad applications including gas storage, gas separation, catalysis, and sensors.[8] A subset of this class of polymers includes conjugated microporous polymers (CMPs). Although many examples of CMP synthesis exist,[8] no one has employed ADMET in CMP synthesis. We explored this possibility (Scheme B.5). Unfortunately, the prepared polymers (P13–P15) demonstrated no significant porosity by nitrogen sorption analysis. However, the monomers may potentially find use in other porous polymer methodologies.[9]

Scheme B.5

ADMET synthesis of crosslinked conjugated polymers.

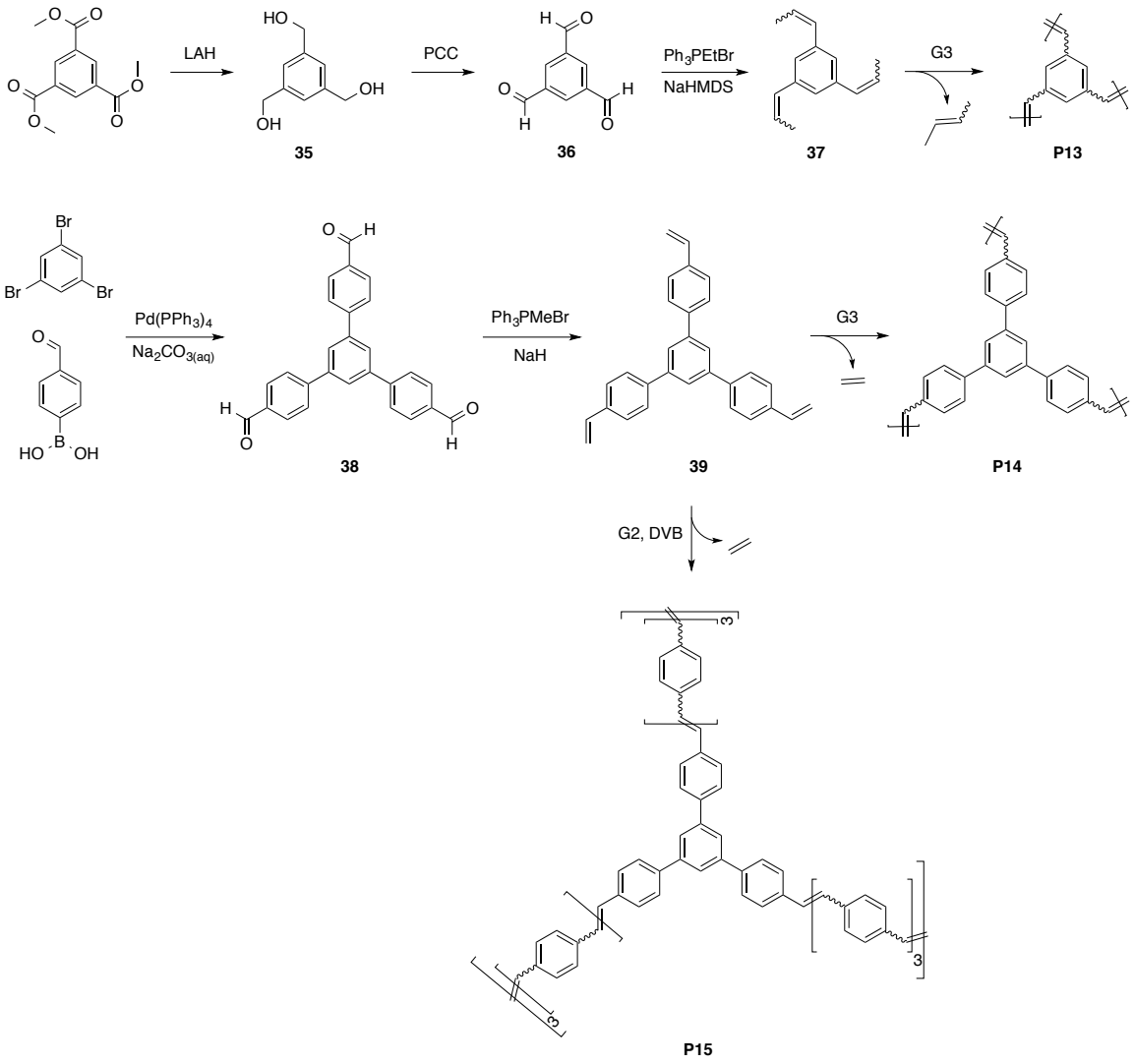

B.4.2 Synthetic Details

Benzene-1,3,5-triyltrimethanol (35). A 2-neck 500 mL round bottom flask was equipped with a magnetic stirring bar, liquid addition funnel, and two rubber septa. The apparatus was flame dried under vacuum and lithium aluminum hydride (LAH, 7.5 g,

197 mmol) was added as a solid under argon purge. This solid was purged with argon for 10 minutes before adding anhydrous THF (250 mL) via cannula and cooling to 0 °C. A solution of trimethyl 1,3,5-benzenetricarboxylate (12.4 g, 49 mmol) in anhydrous THF (125 mL) was added to the liquid addition funnel via cannula. The solution was added dropwise to the LAH suspension over the course of 1 h. The reaction was stirred for 30 min at 0 °C and quenched at room temperature by the careful addition of water (7.5 g), 10 wt% NaOH (15 g), and water (21 g). The mixture was filtered through a pad of celite and washed with THF (3 × 40 mL). The solvent was removed by rotary evaporation to yield product as a white solid (7.55 g, 91%). Used without further purification. ^{1}H NMR (500 MHz, DMSO-d_6): δ_H = 7.16 (s, 3H), 5.19 (t, J = 5.7 Hz, 3H), 4.51 (d, J = 5.7 Hz, 6H). ^{13}C NMR (125 MHz, DMSO-d_6): δ_C = 142.1, 123.0, 63.1. HRGC-MS (EI): M_{calcd} = 168.0786, M_{found} = 168.0780. Anal. calcd. for $C_9H_{12}O_3$: C 64.27, H 7.19, O 28.54; Found: C 64.00, H 7.16, O 28.70.

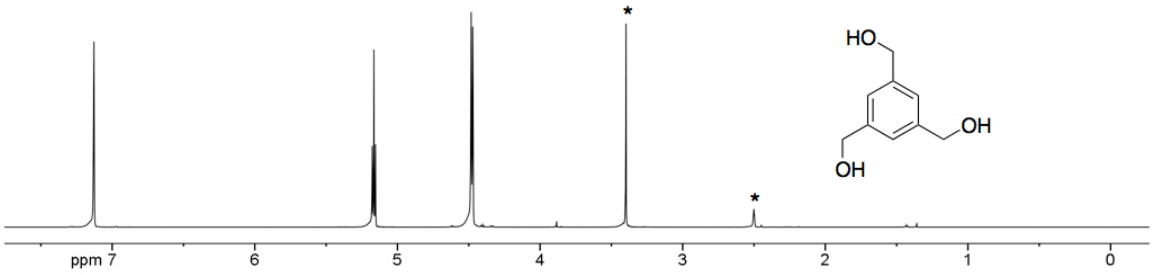

Figure B.44
^{1}H NMR spectrum of **35**. Asterisks mark solvents and other non-product peaks.

Benzene-1,3,5-tricarbaldehyde (36). To a 1 L round bottom flask equipped with a magnetic stir bar was added pyridinium chlorochromate (PCC, 26.8 g, 124 mmol), celite (20 g), and methylene chloride (500 mL). The flask was sealed under argon and stirred for 5 min before adding **35** (5.0 g, 30 mmol) as a solid. The orange heterogeneous solution became dark brown after 15 min, and the reaction was stirred for 18 h. Diethyl ether (100 mL) was added and stirred for 30 min before filtering through a pad of celite.

The celite was washed thoroughly with methylene chloride (500 mL). The filtrate was concentrated by rotary evaporation, and the resulting residue was purified by column chromatography with methylene chloride to yield a white solid (3.75 g, 78%). ^{1}H NMR (500 MHz, DMSO-d_6): δ_H = 10.24 (s, 3H), 8.71 (s, 3H). ^{13}C NMR (125 MHz, DMSO-d_6): δ_C = 192.1, 137.4, 134.5. HRGC-MS (EI): $M_{calcd.}$ = 162.0317, M_{found} = 162.0312. Anal. calcd. for $C_9H_6O_3$: C 66.67, H 3.73, O 29.60; Found: C 66.41, H 3.77, O 29.86.

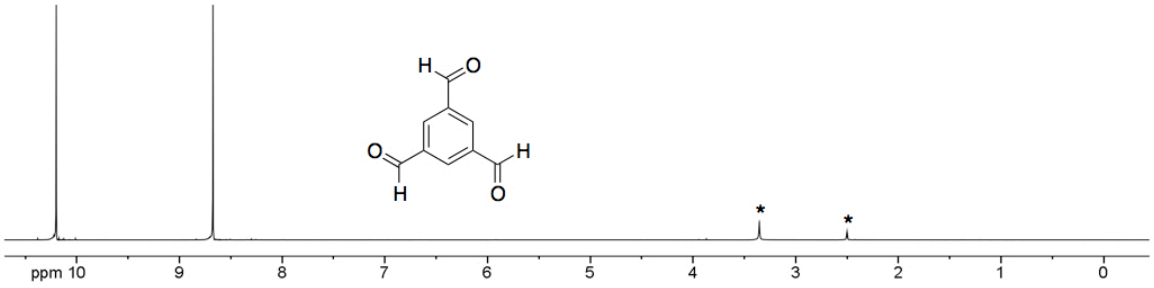

Figure B.45
^{1}H NMR spectrum of **36**. Asterisks mark solvents and other non-product peaks.

Benzene-1,3,5-tripropenyl (37). A 2-neck 250 mL round bottom flask was equipped with a magnetic stirring bar, reflux condenser, glass stopcock, and rubber septum. The apparatus was flame dried under vacuum and sodium bis(trimethylsilyl)amide (11.3 g, 62 mmol) and (ethyl)triphenylphosphonium bromide (22.9 g, 62 mmol) were added under argon purge. Solid mixture was dried under vacuum for 30 min. A second flame dried 500 mL round bottom flask was equipped with a magnetic stirring bar and rubber septum before adding **36** (2.0 g, 12 mmol) and anhydrous THF (130 mL). Cannulated anhydrous hexanes (150 mL) into 2-neck flask and refluxed for 1 h to form the Wittig reagent. The reaction was cooled to -78 °C and the excess hexanes were removed from the precipitate via cannula. The washing procedure was repeated with anhydrous hexanes (100 mL). The residual hexanes were removed under vacuum and anhydrous THF (100 mL) was added at room temperature. The Wittig solution was transferred via cannula to

the second flask. After stirring for 1 h under argon the solvent was removed by rotary evaporation. The product was purified by column chromatography with hexanes to yield a colorless liquid (0.5 g, 82%). *E*:*Z* = 16:86. ^{1}H NMR (300 MHz, $CDCl_3$): δ_H = 7.09 (s, 3H), 6.45–6.36 (m, 3H), 6.27–5.72 (m, 3H), 1.92–1.85 (m, 9H). ^{13}C NMR (75 MHz, $CDCl_3$): δ_C = 137.5, 131.3, 130.2, 128.1, 127.8, 127.1, 126.0, 124.9, 18.8, 15.0. HRGC-MS (EI): $M_{Calcd.}$ = 198.1409, M_{Found} = 198.1392. Anal. calcd. for $C_{15}H_{18}$: C 90.85, H 9.15; Found: C 90.26, H 9.39.

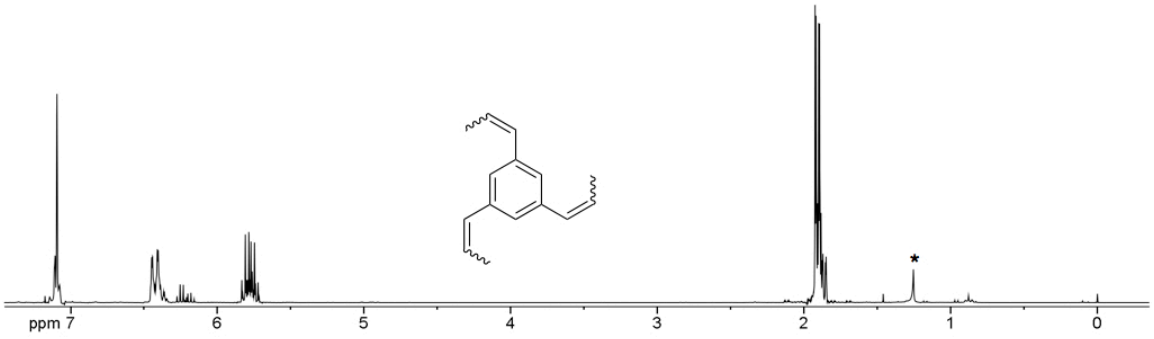

Figure B.46
^{1}H NMR spectrum of **37**. Asterisks mark solvents and other non-product peaks.

P13. A 2-neck 5 mL round bottom flask was equipped with a magnetic stirring bar, reflux condenser, glass stopcock, and rubber septum. The apparatus was flame dried under vacuum before adding **37** (50 mg, 0.25 mmol) and TCB (2 mL). The solution was degassed by freeze-pump-thaw before adding G3 (2.2 mg, 0.0025 mmol) in TCB (0.25 mL). The reaction was refluxed at 80 °C under vacuum for 3 h at which point an insoluble material had formed. The light brown product was collected by vacuum filtration and rinsed thoroughly with chloroform before drying under vacuum (25 mg, 66%).

5'-(4-formylphenyl)-[1,1':3',1''-terphenyl]-4,4''-dicarbaldehyde (38). A 3-neck 1 L round bottom flask was equipped with a magnetic stirring bar, glass stopcock, reflux

condenser, and two rubber septa. 1,3,5-Tribromobenzene (5.0 g, 16 mmol), 4-formylphenylboronic acid (9.5 g, 64 mmol), 1:1 THF/toluene (500 mL), and 15 wt% Na_2CO_3 (70 mL) were added. The solution was degassed with argon for 75 min before adding tetrakis(triphenylphosphine)palladium(0) (1.8 g, 1.6 mmol) in one portion. The solution was refluxed (80 °C) for 17 h at which point TLC confirmed product formation. The reaction was poured into water (500 mL) and extracted with methylene chloride (2 × 500 mL). The combined organics were washed with water and brine (500 mL) each and dried over Na_2SO_4. The solvent was removed by rotary evaporation, and the residue was recrystallized from 1:1 hexanes/THF to afford product as off-white needles (3.8 g, 61%). ^{1}H NMR (300 MHz, $CDCl_3$): δ_H = 10.11 (s, 3H), 8.03 (d, *J* = 8.1 Hz, 6H), 7.91 (d, *J* = 6.5 Hz, 6H), 7.87 (s, 3H).

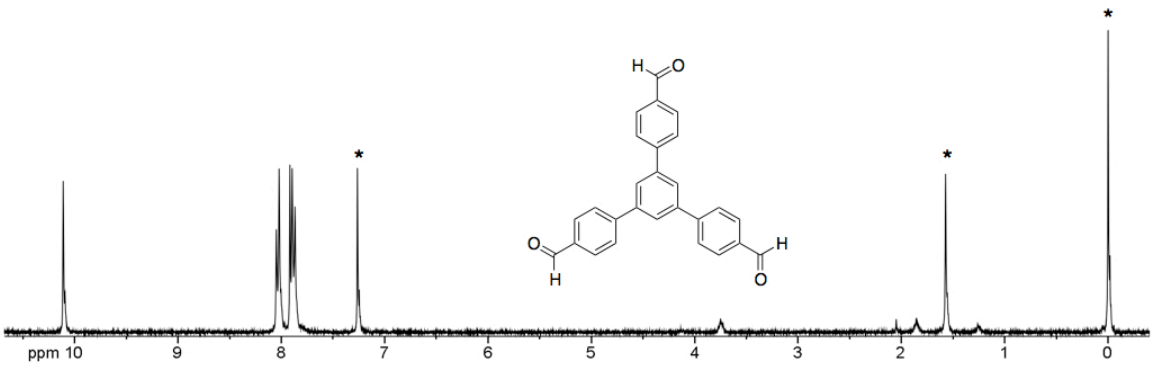

Figure B.47
^{1}H NMR spectrum of **38**. Asterisks mark solvents and other non-product peaks.

4,4''-Divinyl-5'-(4-vinylphenyl)-1,1':3',1''-terphenyl (39). A 2-neck 50 mL round bottom flask was equipped with a magnetic stirring bar and two rubber septa. The apparatus was flame dried under argon flow before adding **38** (0.5 g, 1.3 mmol) and anhydrous THF (25 mL). The solution was warmed to dissolve **38** before adding methyltriphenylphosphonium bromide (2.7 g, 7.4 mmol) and sodium hydride (60 wt% dispersion in mineral oil, 0.5 g, 12.8 mmol). The reaction was stirred at room temperature under argon for 48 h. The reaction was filtered through a pad of celite and

rinsed with THF. The filtrate was concentrated by rotary evaporation, and the resulting residue was dissolved in methylene chloride and passed through two consecutive silica gel columns. The product was obtained as off-white needles after recrystallization from 95:5 hexanes/THF (0.40 g, 82%). ^{1}H NMR (500 MHz, $CDCl_3$): δ_H = 7.78 (s, 3H), 7.67 (d, *J* = 8.1 Hz, 6H), 7.53 (d, *J* = 8.1 Hz, 6H), 6.78 (dd, *J* = 17.6, 10.8 Hz, 3H), 5.82 (d, *J* = 17.6 Hz, 3H), 5.30 (d, *J* = 10.9 Hz, 3H). ^{13}C NMR (125 MHz, $CDCl_3$): δ_C = 142.3, 140.8, 137.3, 136.7, 127.8, 127.1, 125.1, 114.5.

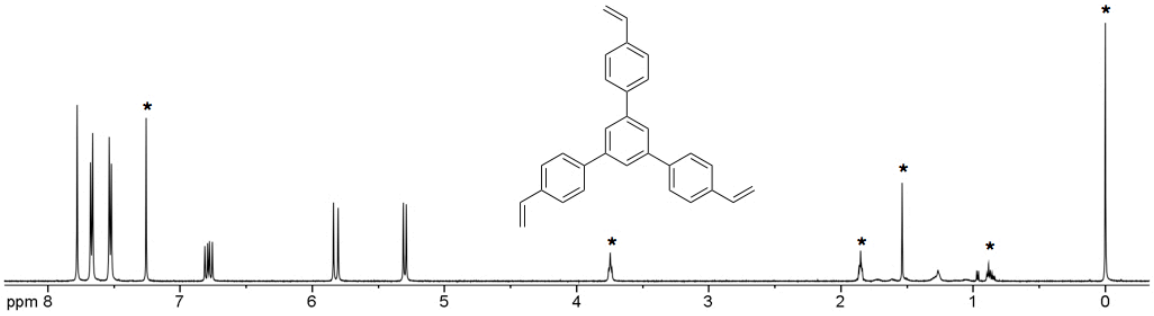

Figure B.48
^{1}H NMR spectrum of **39**. Asterisks mark solvents and other non-product peaks.

P14. In an apparatus like that shown in Figure 2.24, **39** (100 mg, 0.26 mmol) was dissolved in TCB (5 mL). The solution was degassed under vacuum for 30 min before adding G3 (2.3 mg, 0.0026 mmol) in TCB (0.5 mL). The reaction was refluxed under vacuum at 80 °C for 15 h at which point an insoluble material had formed. The reaction was quenched by addition of ethyl vinyl ether (0.25 mL) and methanol (10 mL). The solids were purified by Soxhlet extraction with methanol and chloroform to afford the product polymer as an off-white insoluble material (63 mg, 71%).

P15. 39 (100 mg, 0.26 mmol) and divinylbenzene (0.42 mL, 2.3 mmol) were added to a 4 mL scintillation vial. After a homogeneous solution was achieved, G2 (2.2 mg, 0.0026 mmol) was added. The red solution was sealed with a septum and purged with argon while heating to 80 °C. After 5 min the red solution had become a yellow solid. The

reaction was placed under vacuum for 20 h. The bright yellow insoluble solid was removed and purified by Soxhlet extraction with chloroform (230 mg, 56%).

B.5 References

[1] Roncali, J. *Chem. Rev.* **1992**, *92,* 711–738.

[2] Osaka, I.; McCullough, R. D. *Acc. Chem. Res.* **2008**, *41*, 1202–1214.

[3] Anglin, T. C.; Speros, J. C.; Massari, A. M. *J. Phys. Chem. C* **2011**, *115*, 16027–16036.

[4] Stevens, D. M.; Speros, J. C.; Hillmyer, M. A.; Frisbie, C. D. *J. Phys. Chem. C* **2011**, *115*, 20806–20816.

[5] Roncali, J. *Macromol. Rapid Comm.* **2007**, *28*, 1761–1775.

[6] Zhang, X.; Richter, L. J.; DeLongchamp, D. M.; Kline, R. J.; Hammond, M. R.; McCulloch, I.; Heeney, M.; Ashraf, R. S.; Smith, J. N.; Anthopoulos, T. D.; Schroeder, B.; Geerts, Y. H.; Fischer, D. A.; Toney, M. F. *J. Am. Chem. Soc.* **2011**, *133*, 15073–15084.

[7] Li, Y. *Acc. Chem. Res.* **2012**, *45*, 723–733.

[8] Wu, D.; Xu, F.; Sun, B.; Fu, R.; He, H.; Matyjaszewski, K. *Chem. Rev.* **2012**, *112*, 3959–4015.

[9] Seo, M.; Hillmyer, M. A. *Science* **2012**, *336*, 1422–1425.

Appendix C

Poly(vinyl furans) from Renewable Feedstocks

This appendix describes the synthesis of two vinylfuran monomers from abundant naturally-derived furfurals. The vinylfuran monomers were polymerized using common emulsion polymerization techniques. Copolymerization with styrene and post-polymerization Diels-Alder chemistry was explored as a means of demonstrating monomer versatility and imparting useful functionality. Additional applications for this monomer and polymer system are also discussed.

C.1 Introduction

It is well known that most commercially relevant polymers (plastics) are ultimately derived from fossil fuel feedstocks. However, these resources are not boundless, and scientists have begun to seek out renewable sources for the preparation of polymeric materials.[1-3] Along these lines, two approaches have been taken. The first involves the preparation of traditionally non-renewable monomers and polymers from renewable feedstocks.[4] The second focuses on integrating biodegradability in addition to renewability (i.e., sustainable polymers).[5,6] Polylactide (PLA) is perhaps the most well-known sustainable polymer (Scheme C.1).[7,8] PLA is typically sourced from plant polysaccharides, which are subjected to bacterial fermentation to yield lactic acid. The lactic acid can be polymerized directly under polycondensation conditions to give low molecular weight PLA. Alternatively, thermal cracking of this PLA yields lactide (the cyclic dimer of lactic acid), which can be polymerized to high molar mass using a variety of ring-opening polymerization (ROP) techniques.[9] Although PLA finds use in food packaging and as fibers, its brittleness has limited it to niche applications. As a result, there still exists a need for renewable and/or sustainable polymers with a broader range of applications.

Scheme C.1

PLA synthesis.

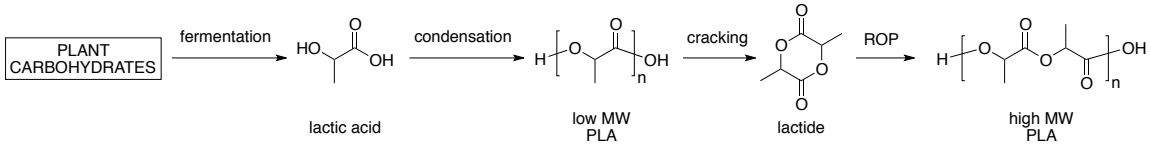

Furfural is a small molecule that finds principal use in resin technology. Approximately 250,000 tons of furfural are produced each year from the acidic hydrolysis of hemicellulose (found in all lignocellulosic feedstocks) followed by the acidic dehydration of xylose (Scheme C.2).[10] Although this method of production is effective, it employs corrosive mineral acids, which are a both a health and environmental concern. Additionally, yields are typically less than 60%.[11] Gürbüz and coworkers recently increased this yield to over 80% by employing solid acid catalysts and γ-valerolactone as a solvent.[12] They also used the same technique to convert glucose to furfural. Given the large amount of furfural produced annually, we identified this as a promising feedstock for monomer synthesis and subsequent polymerization.

Scheme C.2

Furfural production.

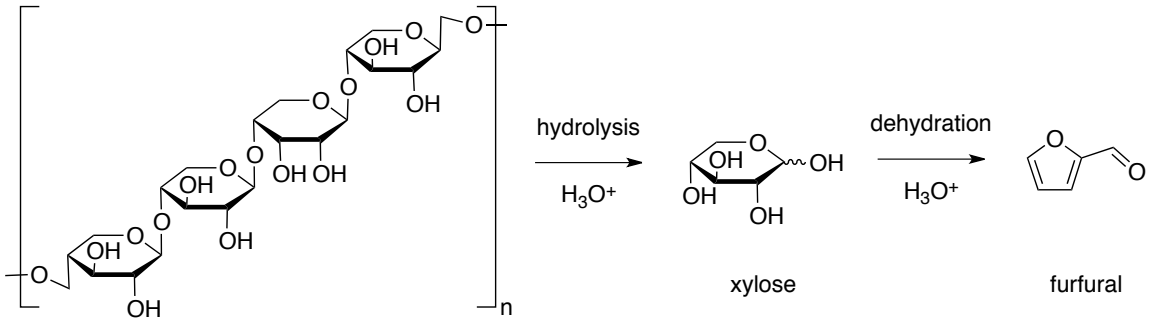

Hemicellulose

2-vinylfuran is the furan version of styrene, which suggests heavy investigation into its polymerization. In fact, radical and emulsion polymerization attempts date back to ca. 1960.[13] However, radical attempts were found to give low molar mass presumably due to radical trapping by the furan ring. This is likely the result of poor furan aromaticity, which leaves electrons free for additional chemistry.[14] Consequently, poly(2-vinylfuran) (PVF) is known to be particularly susceptibly to oxidation and crosslinking when exposed to the atmosphere. Emulsion polymerization attempts, where the radical concentration is low (ca. one radical per active micelle), have been demonstrated to achieve both high

PVF yields and molar masses.[15] Cationic polymerization of 2-vinylfuran has also been reported.[16,17]

The remainder of this appendix will discuss (i) the preparation of two vinyl furan monomers, (ii) homo- and copolymerization using emulsion techniques, and (iii) post-polymerization functionalization of the polymer scaffold using Diels-Alder Chemistry.

C.2 Results and Discussion

C.2.1 Monomer Synthesis

2-vinylfuran and 2-methyl-5-vinylfuran were prepared by treating furfural or 5-methylfurfural with the Grignard reagent formed from chloromethyltrimethylsilane. The resulting secondary alcohols were reacted with HCl to generate 2-vinylfuran and 2-methyl-5-vinylfuran as clear liquids in 51 and 70% yield, respectively (Scheme C.3a).[18] Although ^{1}H NMR analysis confirmed clean monomers (Figure C.1), there was one unknown resonance at 0.07 ppm (indicative of a silicon-based compound). Using gas chromatography–mass spectrometry (GC-MS) the compound was identified as hexamethyldisilane. This byproduct has a boiling point similar to the vinylfurans (ca. 110 °C), which explains why additional purification efforts (i.e., distillation) ultimately failed. Therefore, despite the potentially negative effects of hexamethyldisilane, these monomers were used as is for the polymerizations described in Section C.2.2.

Scheme C.3

Vinylfuran synthesis.

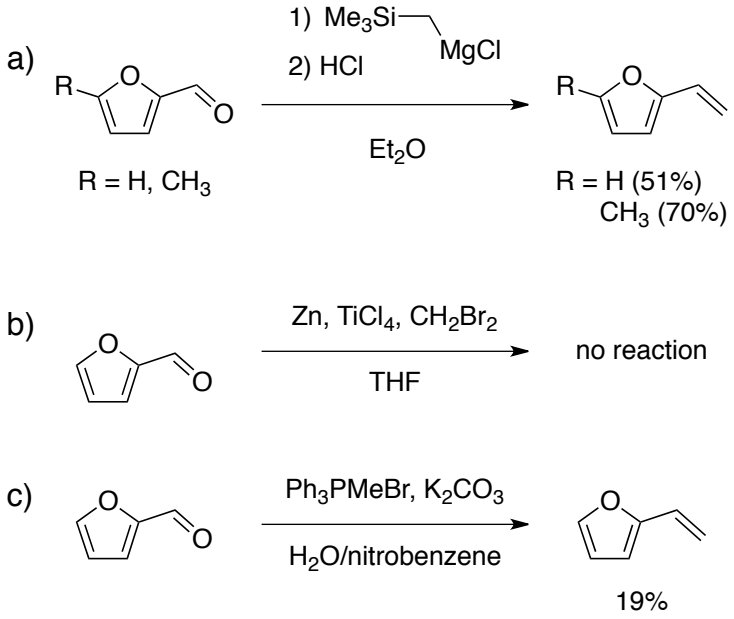

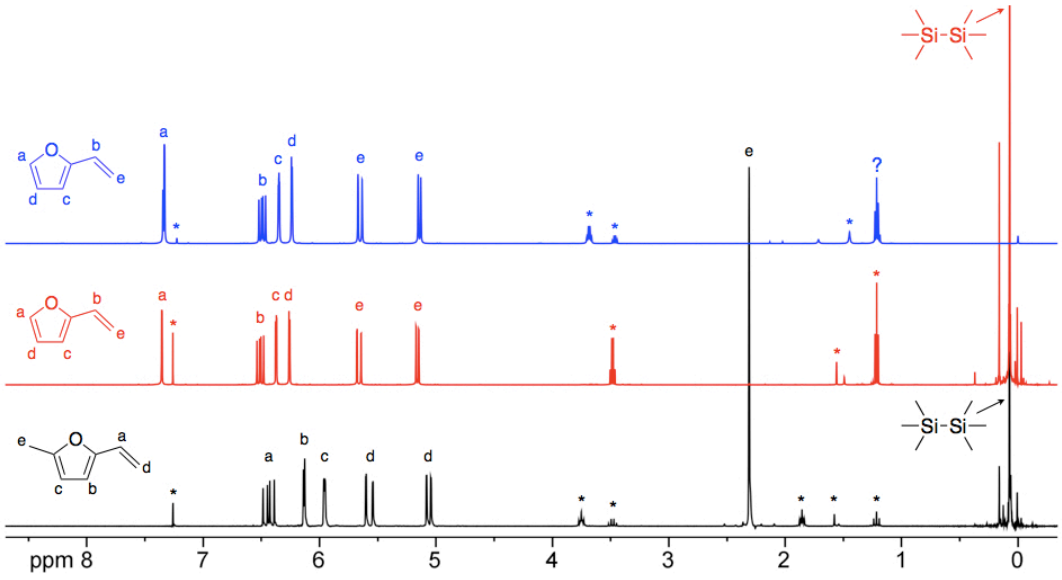

Figure C.1

^{1}H NMR spectra of vinylfurans. 2-Methyl-5-vinylfuran (black) and 2-vinylfuran (red) prepared by Grignard route. 2-vinylfuran (blue) prepared by Wittig route. Asterisks mark solvent peaks.

Two additional methods for the preparation of 2-vinylfuran were explored in an effort to isolate contaminant-free monomer. The first involved treating furfural under Lombardo methylenation conditions,[19] and resulted in no product formation (Scheme C.3b). A second synthesis employing methyltriphenylphosphonium bromide, potassium carbonate, nitrobenzene, and water (i.e., Wittig reaction) was discovered in the patent literature.[20] This reaction resulted in the successful preparation of high purity 2-vinylfuran in 19% yield (Scheme C.3c) and required less time and less expensive reagents compared to the first synthesis (Scheme C.3a). Consequently, after optimization, this should be considered the preferable means of 2-vinylfuran preparation. See Section C.4.2 for complete synthetic details.

C.2.2 Homopolymer Synthesis and Characterization

The only successful polymerizations of vinyl furan have been accomplished under emulsion or cationic conditions. Therefore, we first sought to prepare poly(vinylfurans) using more contemporary polymerization techniques (Scheme C.4). The benefits of these methodologies include low dispersity and end-functionalization, neither of which has been demonstrated for poly(vinylfurans). Anionic polymerization was attempted with each monomer (Scheme C.4a). Although the monomers did not decompose under anionic conditions, no evidence of polymerization was observed. Controlled radical polymerization (CRP) techniques were considered because of their intrinsically low radical concentrations during polymerization.[21] Atom transfer radical polymerization (ATRP) was the first CRP attempted (Scheme C.4b), and also resulted in no polymerization. Using a rather exotic α-hydrido nitroxide compound Benoit and coworkers reported the facile nitroxide-mediated polymerization (NMP) of 1,3-dienes.[22] The poor aromaticity of 2-vinylfuran makes for a fair comparison to dienes. Therefore, we hypothesized that these reaction conditions would result in the successful polymerization of 2-methyl-5-vinylfuran (Scheme C.4c). This was confirmed when poly(2-methyl-5-vinylfuran) (PVMF) was isolated as an off-white polymeric material after workup (M_n = 7.9 kg/mol, M_w = 11.1 kg/mol, $Đ$ = 1.40). However, due to a low yield (30%) and the costly nitroxide ($280/g, Sigma-Aldrich) this polymerization route was not pursued further.

Scheme C.4

Controlled polymerization attempts.

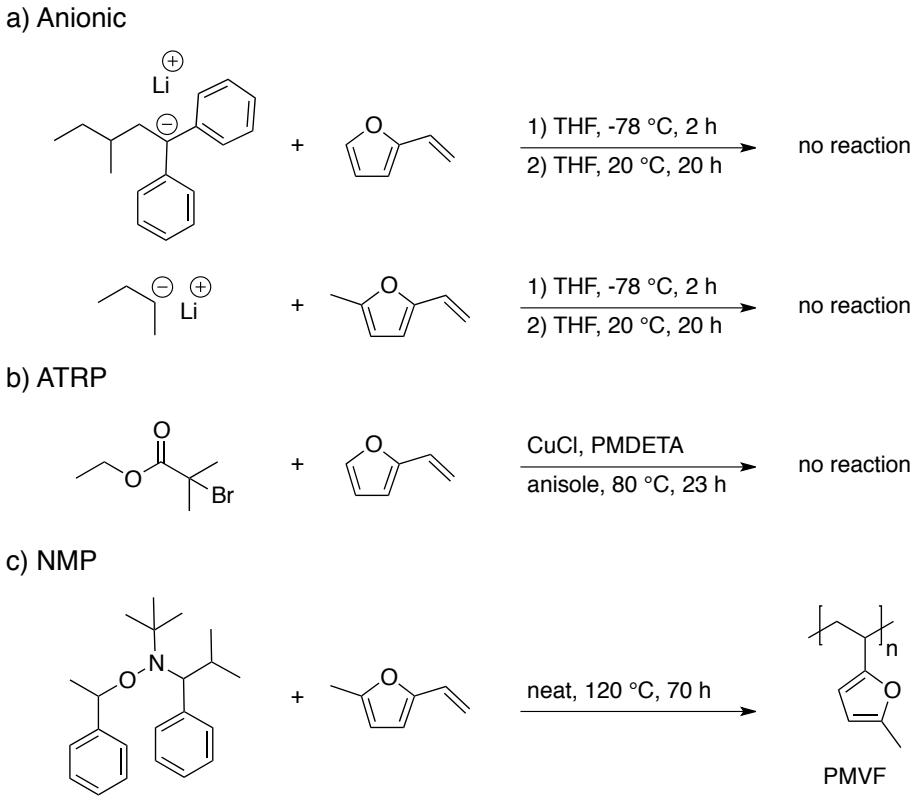

Our most successful polymerizations of 2-vinylfuran and 5-methyl-2-vinylfuran were accomplished using common emulsion techniques for the polymerization of butadiene.[23] Degassed vinylfurans were emulsified by rapid stirring in degassed H_2O with sodium dodecylsulfate (SDS), potassium carbonate, and potassium persulfate. Dodecanethiol was added as a chain transfer agent before sealing the reaction solution under argon and heating to 70 °C for 16–24 hours (Scheme C.5). The polymers were collected by precipitation in cold methanol and dried under vacuum. To prevent oxidative degradation polymers were also stored under vacuum in the dark. Each polymer was characterized by ^{1}H NMR spectroscopy (Figure C.2), size exclusion chromatography (SEC), and differential scanning calorimetry (DSC) (Table C.1).

Scheme C.5

Emulsion polymerization of vinylfurans.

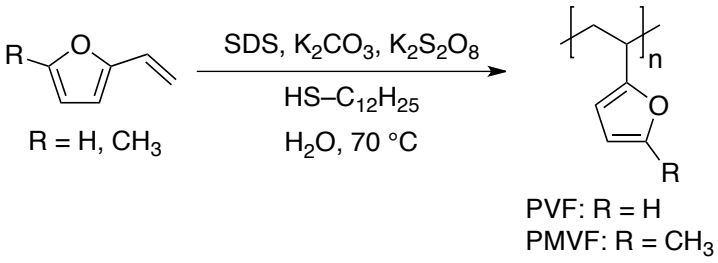

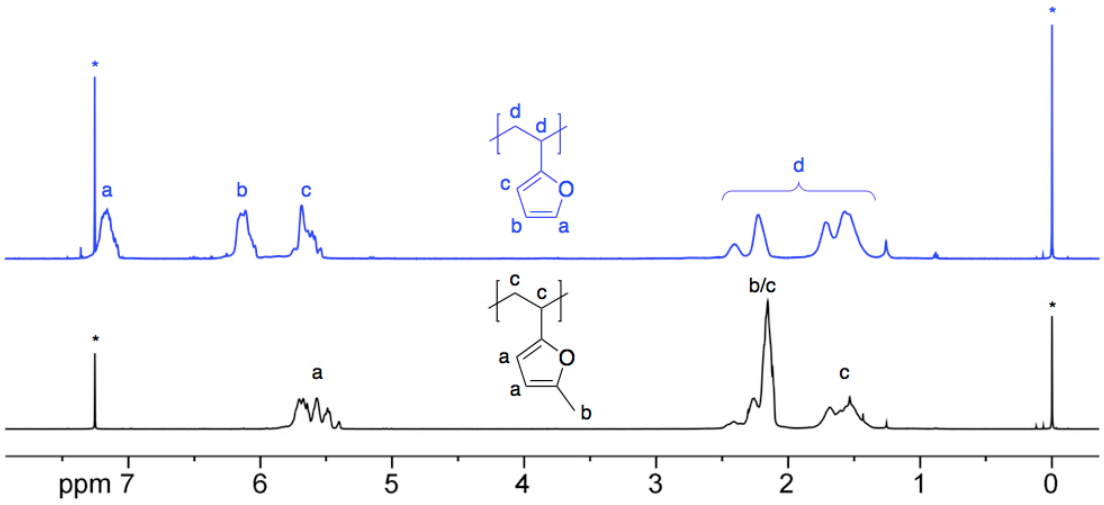

Figure C.2

^{1}H NMR spectra of PMVF (black) and PVF (blue). Asterisks mark solvent and reference peaks.

All polymers were isolated in respectable yields and molar masses (M_n and M_w). Dispersity ($Đ$) values were high, which was expected considering the nature of free-radical polymerization. However, it is worth noting that the highest purity 2-vinylfuran (Entry 5, Table C.1) gave the highest yield, twice the molecular weight, and the lowest $Đ$. This suggests that the hexamethyldisilane impurity retards polymerization in some way.

Owing to their oxidative instability, crosslinking was observed for both PVF and PMVF (Table C.1) if not properly stored. DSC analysis confirmed PVF and PMVF to be amorphous with glass transition temperatures (T_g) of approximately 50 and 35 °C, respectively (Figure C.3).

Table C.1
Homopolymerization data.

Entry	Polymer	t (h)	Yield (%)	M_n[a] (kg/mol)	M_w[a] (kg/mol)	$Đ$[a]	T_g (°C)
1	PVF[b]	24	57	10	127	12.7	49
2	PVF[b]	23	28	26	167	6.4	50
3	PVF[b]	24	22	28	140	5.0	49
4	PVF[b]	23	19	–[d]	–[d]	–[d]	52
5	PVF[c]	16	59	56	225	4.0	49
6	PMVF	21	30	26	70	2.7	36
7	PMVF	21	36	–[d]	–[d]	–[d]	53[e]
8	PMVF	24	40	22	62	2.8	34

[a]Determined by SEC (RI) in THF versus polystyrene standards. [b]Monomer prepared by method detailed in Scheme C.3a. [c]Monomer prepared by method detailed in Scheme C.3c. [d]Polymer crosslinked before SEC analysis could be performed. [e]T_g likely high due to crosslinking.

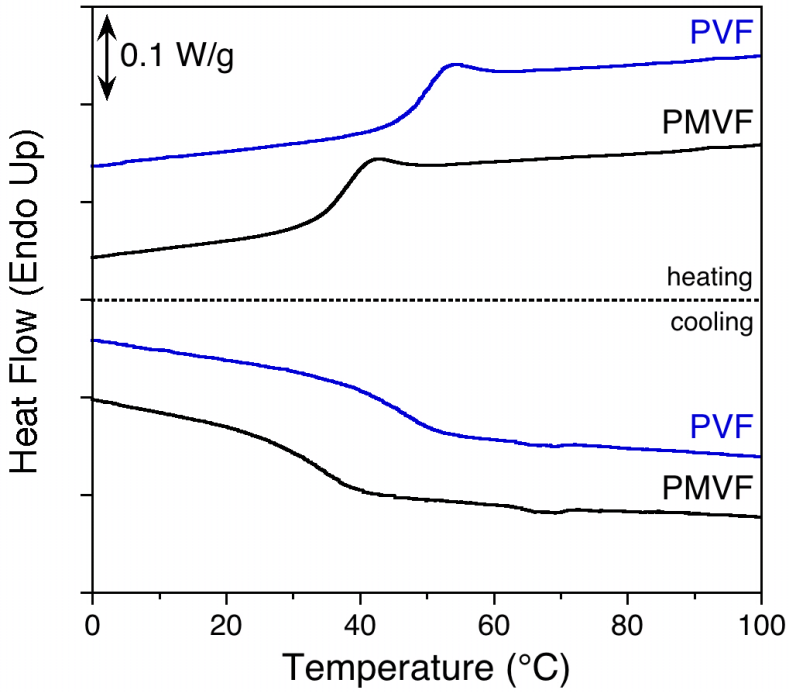

Figure C.3
DSC thermograms of PVF and PMVF.

Although the 2-methyl-5-vinylfuran monomer could be prepared in greater yields than its non-methylated counterpart, the polymerization yield was consistently lower. Additionally, owing to its derivation from rhamnose (a less common sugar), the 5-methylfurfural starting material is far less abundant than furfural.[3] Therefore, PMVF was not investigated beyond its initial preparation.

C.2.3 PS-co-PVF Synthesis and Characterization

In an effort to further demonstrate the utility of emulsion polymerization 2-vinylfuran was copolymerized with styrene (Scheme C.6). The resulting polystyrene-poly(2-vinylfuran) (PS-co-PVF) copolymers were characterized by ^{1}H NMR spectroscopy (Figure C.4).

Scheme C.6

PS-co-PVF synthesis.

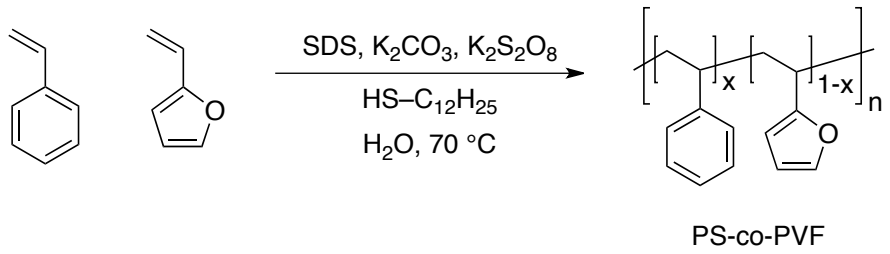

PS-co-PVF

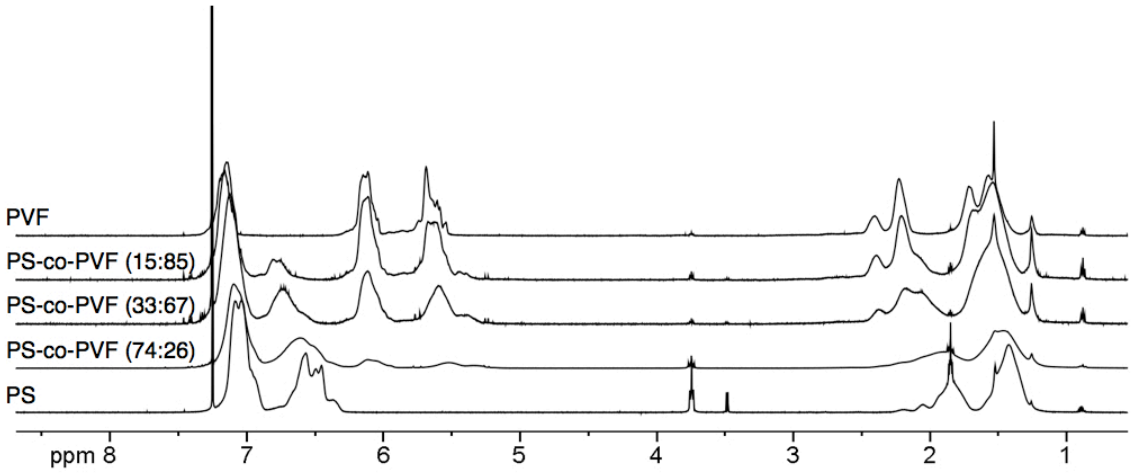

Figure C.4

^{1}H NMR spectra of PS, PS-co-PVF copolymer, and PVF.

From NMR, monomer composition in the copolymers was quantified and found to deviate from feed ratio values (Table C.2). This difference could be a manifestation of differences in monomer reactivity ratios (r). Therefore we fit the composition data using the nonlinear method,[24] $F_1 = (r_1f_1^2 + f_1f_2)/(r_1f_1^2 + 2f_1f_2 + r_2f_2^2)$, and determined $r_1 = 0.78 \pm 0.14$, $r_2 = 0.33 \pm 0.07$, as shown in Figure C.5. This data varies from literature, which gives values of 1.9 and 0.25 for r_1 and r_2, respectively.[25] This could be due to the fact that the polymerizations in this analysis were run to conversions much higher than

appropriate for reactivity ratio analysis.[26] Additionally, the hexamethyldisilane contaminant in 2-vinylfuran could have impacted polymerization kinetics, which would cause deviations in reactivity ratios.

Table C.2
PS-co-PVF data.

S:VF (feed)	S:VF[a] (copolymer)	t (h)	Yield (%)	M_n[b] (kg/mol)	M_w[b] (kg/mol)	$Đ$[b]	T_g (°C)
100:0	100:0	22	92	40	327	8.2	99
75:25	74:26	17	99	24	196	8.2	83
50:50	33:67	16	41	27	118	4.4	52
25:75	15:85	16	28	20	62	3.2	48
0:100	0:100	23	28	26	167	6.4	50

[a]Determined by ^{1}H NMR analysis. [b]Determined by SEC (RI) in THF versus polystyrene standards.

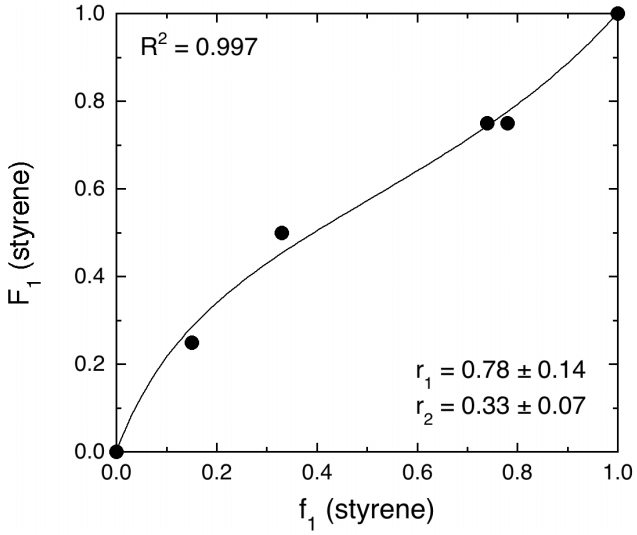

Figure C.5
Non-linear fit, $F_1 = (r_1f_1^2 + f_1f_2)/(r_1f_1^2 + 2f_1f_2 + r_2f_2^2)$, of data shown in Table C.2 to determine the reactivity ratios between styrene (monomer 1) and 2-vinylfuran (monomer 2) in free-radical emulsion polymerizations at 70 °C.

C.2.4 Post-Polymerization Diels-Alder Chemistry

Diels-Alder chemistry allows for the rapid and straightforward preparation of a tremendous range of compounds. Furan is a commonly employed diene in Diels-Alder chemistry and was one of the first reagents utilized at the advent of this chemical technique.[27] Upon preparation of PVF, we postulated that treating the homopolymer with various dienophiles would generate a functionalized backbone (Scheme C.8). In essence, the PVF homopolymer could be tailored to a variety of applications ranging from tuned solubility to macromolecular initiation of graft polymers (i.e., grafting from).

Scheme C.8

Post-polymerization Diels-Alder functionalization.

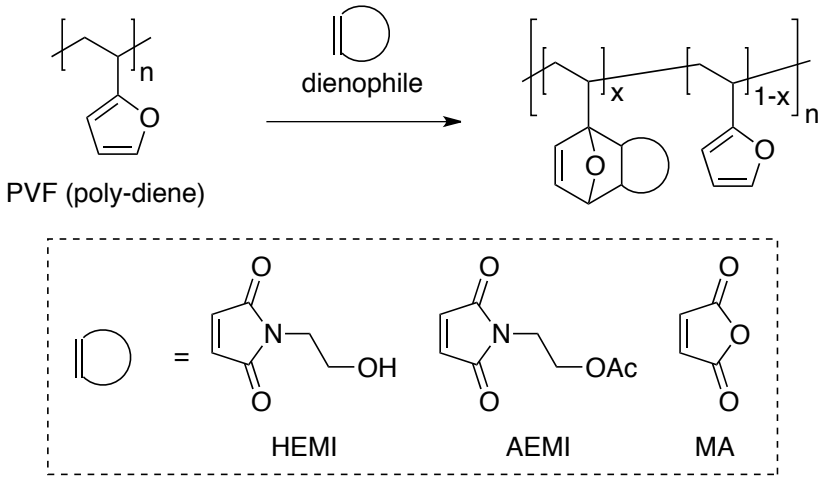

Three dienophiles were employed to test the plausibility of this post-polymerization approach. 1-(2-Hydroxyethyl)-maleimide (HEMI) and 1-(2-acetoxyethyl)-maleimide (AEMI) were prepared according to previous literature reports.[28,29] Maleic anhydride (MA) was recrystallized from chloroform before use. HEMI was chosen as a means to change PVF solubility and to provide an initiating moiety for ROP of lactide.[30] AEMI

was chosen as a less polar counterpart to HEMI (i.e., enhanced solubility in non-polar solvents).[31] Finally, MA was chosen as it is a common dienophile for Diels-Alder with furan. The general procedure involved dissolving the polymer (diene) and dienophile in a suitable solvent, degassing three times via the freeze-pump-thaw method, and stirring at a specified temperature and time (Table C.3). In all cases the product polymer was isolated by precipitation from methanol and dried under vacuum.

Table C.3
PVF-dienophile data.

Dienophile	D_f/D_p[a] (mol %)	t (h)	T (°C)	Solvent	M_n[b] (kg/mol)	$Đ$[b]	$\nu_{C=O}$[c] (cm^{-1})
HEMI	150/–[d]	22	110	toluene	–[d]	–[d]	1694
HEMI	25/–[d]	16	110	toluene	–[d]	–[d]	1695
HEMI	5/5	18	110	toluene	34	4.8	1700
AEMI	105/–[d]	19	60	toluene	–[d]	–[d]	1739, 1697
AEMI	5/6	18	110	toluene	29	4.6	1744, 1704
MA	100/–[d]	68	80	dioxane	–[d]	–[d]	1846, 1776
MA	100/9	22	60	THF	8	3.5	1861, 1780
MA	100/3	48	25	THF	22	3.1	1863, 1781

[a]Dienophile in feed versus dienophile in product (^{1}H NMR). [b]Determined by SEC (RI) in THF versus polystyrene standards. [c]Carbonyl stretching values determined from ATR-IR. [d]Polymer was insoluble preventing NMR and SEC analysis.

Initial attempts to functionalize the PVF backbone (x = 1 or 0.25, Scheme C.8) with HEMI resulted in completely intractable polymers. Although oxidative crosslinking is a potential explanation for this insolubility, it is more likely that the large number of alkoxy functionalities introduced dramatically altered PVF solubility. Also, when targeting lower levels of functionality (x = 0.05) complete consumption of the dienophile was observed by NMR spectroscopy, and the resulting polymer was completely soluble. Indicative of successful functionalization, the polymer molar mass determined from SEC was slightly higher than the parent polymer. Regardless of solubility, attenuated total reflectance-

infrared (ATR-IR) spectroscopy was helpful in confirming both the presence and relative amounts of maleimide in the polymer backbone (Figure C.6).

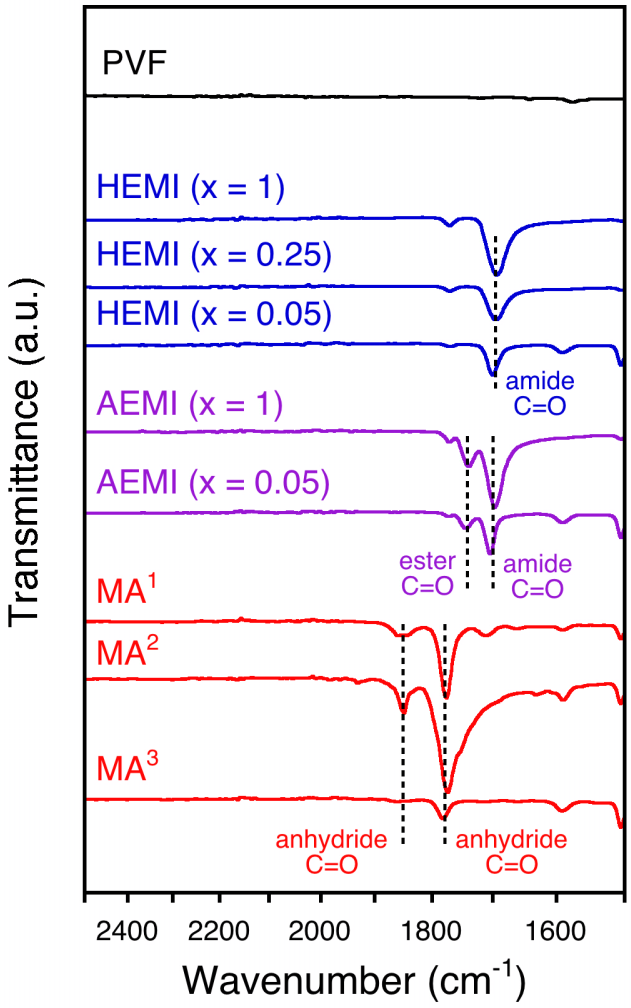

Figure C.6
ATR-IR spectra of PVF (black), PVF-HEMI (blue), PVF-AEMI (purple), and PVF-MA (red). The superscript on MA refers to the Table C.3 entries in descending order (e.g., MA^1 is the first entry).

PVF functionalization with AEMI behaved similarly to attempts with HEMI. Although the reduced polarity of the acetoxy group was thought to aid in solubility, targeting complete functionality (x = 1) resulted in an insoluble material. However, a

reduced functionality (x = 0.05) was easily achieved and characterized by NMR and SEC. Again, in both cases ATR-IR showed the presence of maleimide and acetoxy carbonyls (Figure C.6).

Diels-Alder reactions employing MA were successful as determined by NMR, but achievement of desired functionality was difficult. For instance, at low temperatures in THF, targeted functionalities of 1 resulted in true values of 0.03 and 0.09. Increasing the time, temperature, and performing the reaction in 1,4-dioxane resulted in an insoluble material. SEC data of the soluble materials indicated increased molar masses compared to the parent polymer, but these values did not correlate well with observed functionalities. In all cases, ATR-IR demonstrated dual carbonyl stretches characteristic of anhydrides (Figure C.6).

From this set of experiments one primary conclusion can be drawn. Functionalizing the PVF scaffold through Diels-Alder chemistry is possible. However, successful functionalization and subsequent characterization can only be realized at low dienophile levels. This suggests that PVF would be suitable for graft copolymer strategies, but completely functionalized PVF scaffolds would only be useful where the product polymer requires no additional solution processing.

C.3 Conclusions and Future Directions

This appendix demonstrated the synthesis and successful polymerization of two vinylfuran monomers. Although successful vinylfuran polymerization has been demonstrated before, thorough characterization is not present in the literature. The present work resolves this deficiency by reporting ^{1}H NMR, SEC, DSC, and ATR-IR data. In addition, the successful copolymerization with styrene and functionalization via Diels-Alder chemistry served to highlight the versatility of this renewably-sourced polymer system.

Despite preparing these often challenging polymers in appreciable yields and molar masses, more must be done if these materials are to find application. First, the oxidative instability of both PVF and PMVF needs to be addressed. In order to prevent this degradation and subsequent crosslinking, the diene moiety of the polymer repeat unit must be removed. Complete functionalization by Diels-Alder remains one way to approach this problem. However, a dienophile must be chosen that is both highly reactive and results in a soluble polymer. One possibility is maleic acid, which could give rise to a water-soluble polymer. Hydrogenation represents a more straightforward approach to enhancing polymer stability. In addition, it would give rise to poly(2-vinyltetrahydrofuran), a completely new material to polymer chemistry. We have attempted hydrogenation under both heterogeneous and homogeneous conditions and have so far been unsuccessful. However, many conditions and catalysts still remain untested.

Graft copolymerization also represents a way to prepare unique macromolecules from PVF. Therefore, future efforts will focus on using HEMI-functionalized PVF (x ~ 0.05) as the macromolecular initiator for lactide polymerization. Additionally, a bromine-functionalized dienophile would prove useful for graft copolymerization of various vinyl monomers (e.g., styrene) by ATRP. Finally, one might imagine deliberately crosslinking the PVF backbone by performing ring opening metathesis polymerization (ROMP) on the MA functionalized PVF. Scheme C.9 summarizes the future directions for poly(vinylfurans).

Scheme C.9

Summary of future directions.

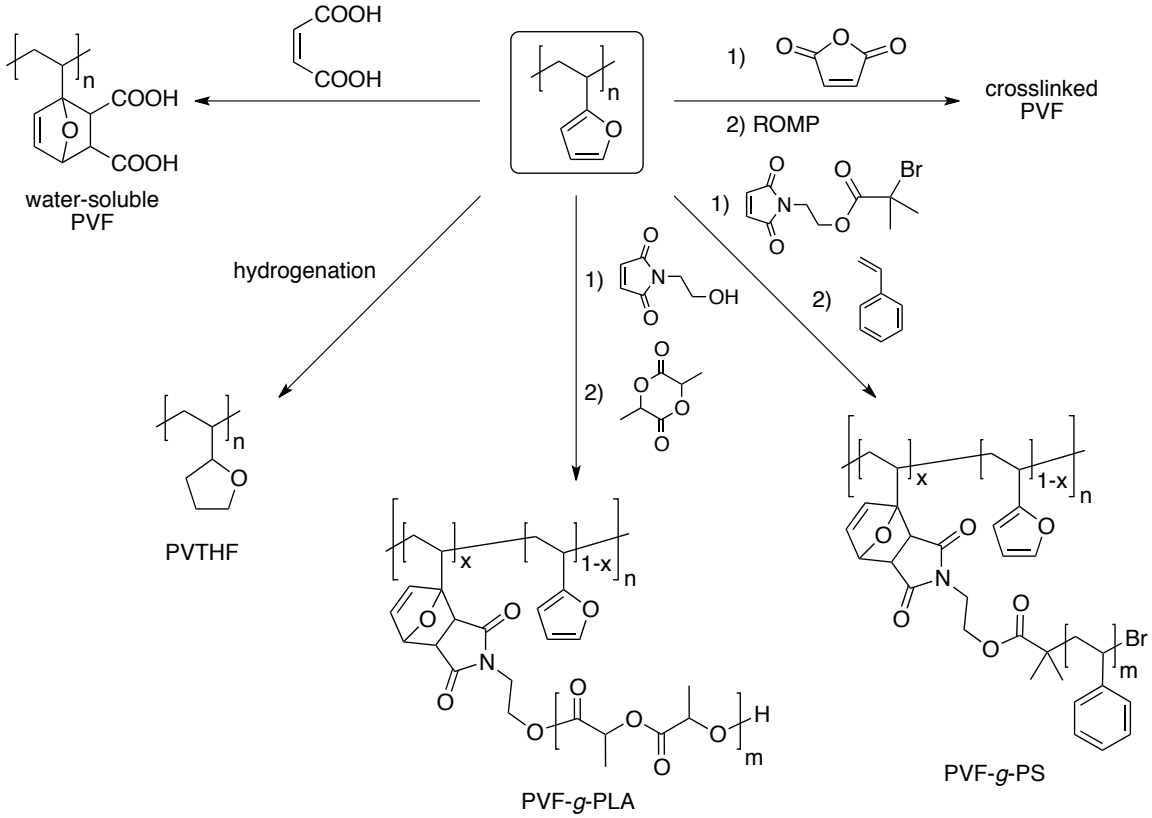

C.4 Experimental Details

C.4.1 Materials and Methods

All solvents and reagents were purchased and used as received unless otherwise noted. Furfural and 5-methylfurfural (Aldrich) were purified by distilling over sodium carbonate and stored under argon in the dark at -20 °C. Styrene and furan were purified immediately before use by passage through neutral alumina. All reactions were run under

argon or vacuum using standard Schlenk techniques. A complete description of the characterization techniques employed is available in Appendix A.

C.4.2 Synthetic Details

2-Vinylfuran (Grignard Method). A 3-neck round bottom flask was equipped with a magnetic stirring bar, reflux condenser, and addition funnel. Magnesium turnings (8.2 g, 338 mmol) were added and the apparatus was sealed with rubber septa before flame drying under an argon purge. Anhydrous diethyl ether (150 mL) and chloromethyltrimethylsilane (38.8 mL, 278 mmol) were transferred to the addition funnel via cannula and syringe, respectively. The apparatus was placed in an ice bath while the ether solution was slowly added to the magnesium turnings. Following addition, the reaction was refluxed for 1 h to form the Grignard reagent. The reaction was then cooled to 0 ˚C before furfural (20.0 mL, 242 mmol) was added in a solution of anhydrous diethyl ether (150 mL) via addition funnel. The reaction was warmed to room temperature and stirred under argon for 18 h. The reaction was poured into saturated NH_4Cl solution (300 mL) before extracting with diethyl ether (200 mL). The combined organics were washed with saturated $NaHCO_3$ and brine (100 mL each). Most of the diethyl ether was removed by rotary evaporation leaving a solution of 1-(2′-Furyl)-2-(trimethylsilyl)-ethanol. While stirring rapidly, 1 M HCl (60 mL) was added to the alcohol intermediate. The solution warmed and was stirred under argon for 1 h. The phases were separated and the aqueous phase was washed with diethyl ether (100 mL). The combined organics were washed with brine and dried over Na_2SO_4. The diethyl ether was removed by careful rotary evaporation (no heat), and the product was purified by distilling twice under an atmosphere of argon (clear liquid, 11.6 g, 51%). ^{1}H NMR (500 MHz, $CDCl_3$): δ_H = 7.35 (d, J = 1.5 Hz, 1H), 6.51 (dd, J = 17.5, 11.3 Hz, 1H), 6.37

(dd, *J* = 3.3, 1.8 Hz, 1H), 6.26 (d, *J* = 3.3 Hz, 1H), 5.66 (dd, *J* = 17.5, 1.3 Hz, 1H), 5.16 (dd, *J* = 11.3, 1.3 Hz, 1H).

2-Vinylfuran (Wittig Method). Furfural (8.6 mL, 104 mmol), methyltriphenylphosphonium bromide (39.0 g, 109 mmol), potassium carbonate (56.1 g, 406 mmol), water (2 mL), nitrobenzene (100 mL), and a magnetic stirring bar were added to a 500 mL Erlenmeyer flask. The flask was sealed with a rubber septum, placed under an argon atmosphere, and stirred at 90 °C for 3 h. The reaction was cooled to room temperature and filtered to remove the solids. The filtrate was carefully distilled under argon. The first fraction contained a mixture of product and nitrobenzene. This was distilled a second time to yield product as a slightly yellow liquid (1.9 g, 19%). ^{1}H NMR (500 MHz, $CDCl_3$): δ_H = 7.37 (s, 1H), 6.53 (dd, *J* = 17.5, 11.3 Hz, 1H), 6.38 (dd, *J* = 3.1, 1.9 Hz, 1H), 6.27 (d, *J* = 3.2 Hz, 1H), 5.69 (d, *J* = 17.5 Hz, 1H), 5.18 (d, *J* = 11.3 Hz, 1H).

2-Methyl-5-vinylfuran (Grignard Method). This compound was prepared following the same procedure for 2-vinylfuran (clear liquid, 14.2 g, 70%). ^{1}H NMR (300 MHz, $CDCl_3$): δ_H = 6.44 (dd, *J* = 17.5, 11.3 Hz, 1H), 6.13 (d, *J* = 3.1 Hz, 1H), 5.96 (dd, *J* = 3.1, 0.9 Hz, 1H), 5.57 (dd, *J* = 17.5, 1.2 Hz, 1H), 5.06 (dd, *J* = 11.3, 1.3 Hz, 1H), 2.31 (s, 3H).

General Emulsion Polymerization Procedure. An oven-dried Schlenk tube (5, 25, or 50 mL) was equipped with a magnetic stirring bar before adding sodium dodecylsulfate (SDS, 0.027 molar equivalents), potassium persulfate (0.0025 molar equivalents), and potassium carbonate (0.013 molar equivalents). The solids were degassed by an argon purge before adding degassed water (ca. 10 molar equivalents). The mixture was stirred rapidly to generate a homogeneous solution before adding degassed vinylfuran (1 molar

equivalent) and dodecanethiol (0.0033 molar equivalents) via syringe. The tube was sealed under argon and stirred rapidly at 70 ˚C for 16–24 h. The polymerization was quenched by precipitation into a 10-fold excess of methanol. The product polymer (white solid) was dried and stored under vacuum in the dark.

PVF. Highest yielding reaction gave 0.83 g (59%) of polymer. Largest scale reaction gave 4.4 g (57%) of polymer. ^{1}H NMR (500 MHz, $CDCl_3$): δ_H = 7.20–7.09 (m, 1H), 6.15–6.04 (m, 1H), 5.75–5.55 (m, 1H), 2.42–2.22 (m, 1H), 1.72–1.43 (m, 2H). Anal. calcd. for C_6H_6O: C 76.57, H 6.43; Found: C 76.54, H 6.48.

PMVF. 3.2 g (40%) of polymer was isolated. ^{1}H NMR (500 MHz, $CDCl_3$): δ_H = 5.71–5.41 (m, 2H), 2.42–2.12 (m, 4H), 1.69–1.44 (m, 2H).

General Copolymerization (PS-co-PVF) Procedure. The same procedure employed for PVF and PMVF synthesis and workup was followed. The molar equivalents for SDS, potassium persulfate, potassium carbonate, and dodecanethiol were all the same. However, styrene and 2-vinylfuran amounts were chosen such that the sum was 1 molar equivalent. Polymerizations proceeded at 70 ˚C under argon for 16–22 h. Following polymerization the reaction solution was precipitated into methanol as before. However, in all cases polymer solids remained in the Schlenk tube. These were dissolved in minimal THF and precipitated into methanol. Polymers were collected by filtration and dried under vacuum. Copolymer compositions were determined by ^{1}H NMR analysis.

Scheme C.8

Synthesis of HEMI and AEMI dienophiles.

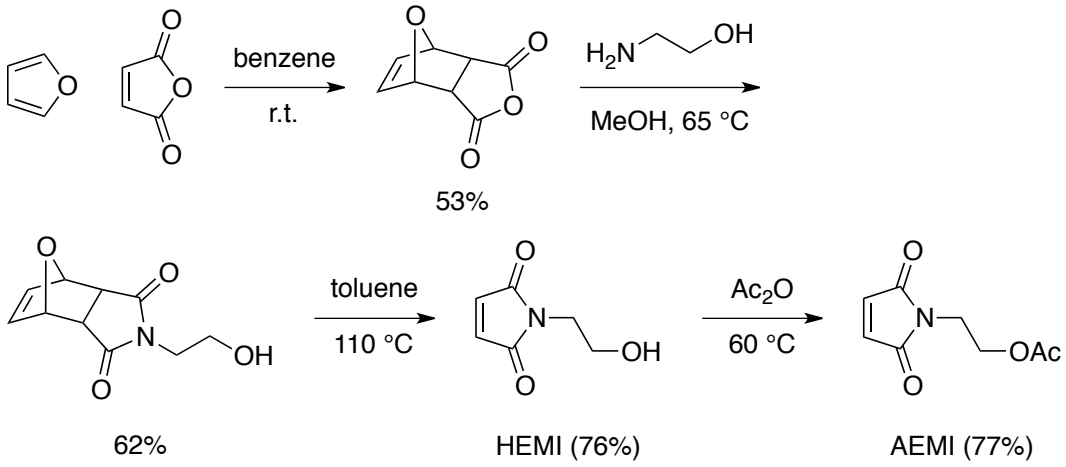

4,10-Dioxatricyclo[5.2.1.0^{2,6}]dec-8-ene-3,5-dione. A 500 mL round bottom flask was flame dried under a stream of nitrogen. A magnetic stirring bar, maleic anhydride (40.0 g, 408 mmol), furan (30.0 mL, 413 mmol), and benzene (200 mL) were added. The flask was sealed with a rubber septum and stirred at room temperature for 19 h under argon. The product precipitated from solution, was collected by vacuum filtration, and was washed with diethyl ether (2 × 50 mL). The product (35.6 g, 53%) was pure *exo* isomer by ^{1}H NMR analysis and was used without further purification. ^{1}H NMR (500 MHz, DMSO-d_6): δ_H = 6.58 (s, 2H), 5.35 (s, 2H), 3.31 (s, 2H). ^{13}C NMR (125 MHz, DMSO-d_6): δ_C = 171.5, 136.8, 81.6, 49.1.

4-(2-Hydroxy-ethyl)-10-oxa-4-aza-tricyclo[5.2.1.0^{2,6}]-dec-8-ene-3,5-dione. A 2-neck 250 mL round bottom flask was equipped with a magnetic stirring bar, reflux condenser, and two rubber septa. The apparatus was flame dried under an argon purge before adding 4,10-dioxatricyclo[5.2.1.0^{2,6}]dec-8-ene-3,5-dione (20.0 g, 120 mmol) and 40 mL

anhydrous methanol. Ethanolamine (7.3 mL, 120 mmol) was slowly added via syringe (heat evolved). The reaction was refluxed for 24 h before removing from heat. The product was allowed to crystallize from the reaction solvent at room temperature over the course of 36 h. The product was isolated by vacuum filtration as a white crystalline solid (15.6 g, 62%). ^{1}H NMR (500 MHz, DMSO-d_6): δ_H = 6.55 (s, 2H), 5.12 (s, 2H), 4.77 (s, 1H), 3.42 (s, 4H), 2.92 (s, 2H). ^{13}C NMR (125 MHz, DMSO-d_6): δ_C = 176.5, 136.5, 80.3, 57.3, 47.2, 40.6.

1-(2-Hydroxyethyl)-maleimide (HEMI). A 250 mL round bottom flask was equipped with a magnetic stirring bar. 4-(2-Hydroxy-ethyl)-10-oxa-4-aza-tricyclo[5.2.1.0^{2,6}]-dec-8-ene-3,5-dione (10.0 g, 47.8 mmol) and toluene (100 mL) were added before attaching a vigreaux condenser. The reaction was refluxed open to the atmosphere for 20 h. The solution was then hot filtered and slowly cooled to 0 °C to facilitate crystallization. The product was isolated by vacuum filtration as an off-white solid (5.1 g, 76%). ^{1}H NMR (300 MHz, DMSO-d_6): δ_H = 7.01 (s, 2H), 4.79 (s, 1H), 3.45 (s, 4H). ^{13}C NMR (75 MHz, DMSO-d_6): δ_C = 171.1, 134.5, 57.9, 40.0.

1-(2-Acetoxyethyl)-maleimide (AEMI). A 25 mL round bottom flask was equipped with a magnetic stirring bar before adding HEMI (0.5 g, 3.5 mmol) and acetic anhydride (10 mL). A vigreaux condenser was attached, and the reaction was stirred open to the atmosphere at 60 °C for 4 h. The excess acetic anhydride was removed by vacuum distillation. The remaining residue was dissolved in acetone/diethyl ether (1:5, 15 mL) and slowly cooled to precipitate the product as an off-white solid. The product was collected by vacuum filtration (0.5 g, 77%). ^{1}H NMR (500 MHz, $CDCl_3$): δ_H = 6.73 (s, 2H), 4.22 (t, J = 5.3 Hz, 2H), 3.80 (t, J = 5.3 Hz, 2H), 2.02 (s, 3H).

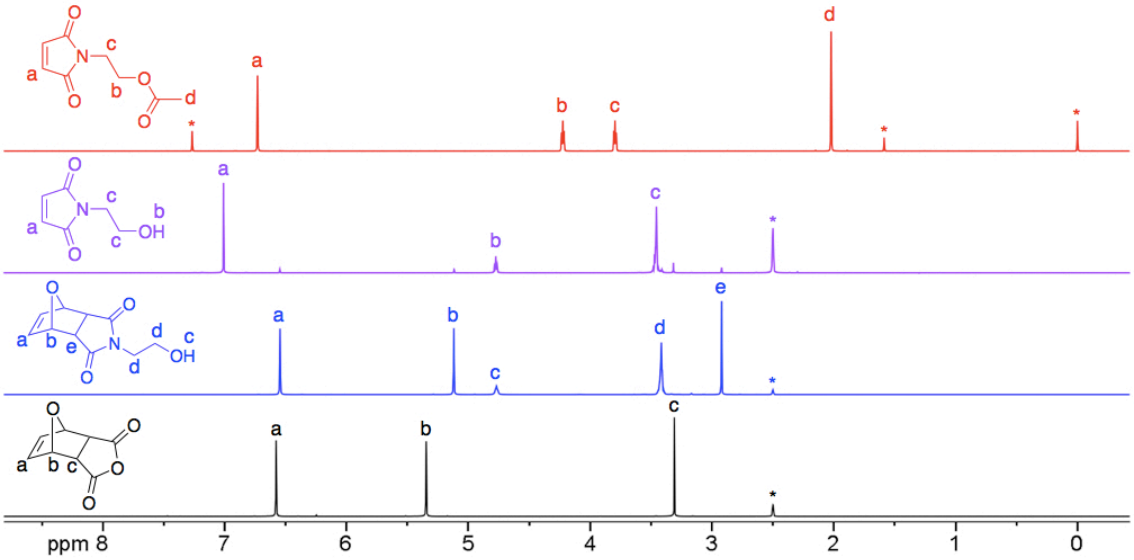

Figure C.6
^{1}H NMR spectra of 4,10-dioxatricyclo[5.2.1.0^{2,6}]dec-8-ene-3,5-dione (black), 4-(2-hydroxy-ethyl)-10-oxa-4-aza-tricyclo[5.2.1.0^{2,6}]-dec-8-ene-3,5-dione (blue), HEMI (purple), and AEMI (red). Asterisks mark solvent and reference peaks.

General Diels-Alder Functionalization Procedure. The diene (PVF) and selected amount of dienophile (HEMI, AEMI, or MA) were dissolved in solvent (toluene, 1,4-dioxane, or THF) to achieve a concentration of approximately 0.3 M. The solution was degassed by three freeze-pump-thaw cycles, sealed under argon, and heated to the desired temperature for the desired time. The product polymer was precipitated into methanol (10–20 fold excess) and collected by vacuum filtration before drying under high vacuum.

C.5 References

[1] Gandini, A. *Macromolecules* **2008**, *41*, 9491–9504.

[2] Vennestrøm, P. N. R.; Osmundsen, C. M.; Christensen, C. H.; Taarning, E. *Angew. Chem., Int. Ed.* **2011**, *50*, 2–10.

[3] Gandini, A. *Green Chem.* **2011**, *13*, 1061–1083.

[4] Mathers, R. T. *J. Polym. Sci., Polym. Chem.* **2012**, *50*, 1–15.

[5] Mohanty, A. K.; Misra, M.; Hinrichsen, G. *Macromol. Mater. Eng.* **2000**, *276/277*, 1–24.

[6] Okada, M. *Prog. Polym. Sci.* **2002**, *27*, 87–133.

[7] Gupta, A. P.; Kumar, V. *Eur. Polym. J.* **2007**, *43*, 4053–4074.

[8] Williams, C. K.; Hillmyer, M. A. *Polym. Rev.* **2008**, *48*, 1–10.

[9] Dechy-Cabaret, O.; Martin-Vaca, B.; Bourissou, D. *Chem. Rev.* **2004**, *104*, 6147–6176.

[10] Mamman, A. S.; Lee, J.-M.; Kim, Y.-C.; Hwang, I. T.; Park, N.-J.; Hwang, Y. K.; Chang, J.-S.; Hwang, J.-S. *Biofuel. Bioprod. Bior.* **2008**, *2*, 438–454.

[11] Karinen, R.; Vilonen, K.; Niemela, M. *ChemSusChem* **2011**, *4*, 1002–1016.

[12] Gürbüz, E. I.; Gallo, J. M. R.; Alonso, D. M.; Wettstein, S. G.; Lim, W. Y.; Dumesic, J. A. *Angew. Chem., Int. Ed.* **2013**, *52*, 1270–1274.

[13] Gandini, A.; Belgacem, M. *Prog. Polym. Sci.* **1997**, *22*, 1203–1379.

[14] Katritzky, A. R.; Karelson, M.; Sild, S.; Krygowski, T. M.; Jug, K. *J. Org. Chem.* **1998**, *63*, 5228–5231.

[15] Dillingham, K. A. PhD. Dissertation, Lancaster University, 1995.

[16] Alvarez, R.; Gandini, A.; Martinez, R. *J. Polym. Sci., Polym. Lett.* **1975**, *13*, 385–390.

[17] Höhne, S.; Spange, S. *Macromol. Chem. Phys.* **2003**, *204*, 841–849.

[18] Haukaas, M. H.; O'Doherty, G. A. *Org. Lett.* **2001**, *3*, 401–404.

[19] Lombardo, L. *Tetrahedron Lett.* **1982**, *23*, 4293–4296.

[20] Hiromasa, S. Preparation of Vinylfurans and Purification by Steam Distillation JP 2010235545, 2010.

[21] Braunecker, W. A.; Matyjaszewski, K. *Prog. Polym. Sci.* **2007**, *32*, 93–146.

[22] Benoit, D.; Harth, E.; Fox, P.; Waymouth, R. M.; Hawker, C. J. *Macromolecules* **2000**, *33*, 363–370.

[23] Weerts, P. A.; van der Loos, J. L. M.; German, A. L. *Makromol. Chem.* **1990**, *191*, 2615–2630.

[24] Odian, G. *Principles of Polymerization,* 4th ed.; John Wiley & Sons, Inc.: Hoboken, NJ, 2004.

[25] Aso, C.; Tanaka, Y. *Kobunshi Kogaku* **1964**, *21*, 373–377.

[26] Yin, L.; Dalsin, M. C.; Sizovs, A.; Reineke, T. M.; Hillmyer, M. A. *Macromolecules* **2012**, *45*, 4322–4332.

[27] Kappe, C. O.; Murphree, S. S.; Padwa, A. *Tetrahedron* **1997**, *53*, 14179–14233.

[28] Heath, W. H.; Palmieri, F.; Adams, J. R.; Long, B. K.; Chute, J.; Holcombe, T. W.; Zieren, S.; Truitt, M. J.; White, J. L.; Willson, C. G. *Macromolecules* **2008**, *41*, 719–726.

[29] Yin, J.; Ge, Z. S.; Liu, H.; Liu, S. *J. Polym. Sci., Polym. Chem* **2009**, *47*, 2608–2619.

[30] Gramlich, W. M.; Hillmyer, M. A. *Polym. Chem.* **2011**, *2*, 2062–2067.

[31] Moughton, A. O.; Sagawa, T.; Gramlich, W. M.; Seo, M.; Lodge, T. P.; Hillmyer, M. A. *Polym. Chem.* **2013**, *4*, 166–173.